THE PHYSICAL REVIEW

VOLUME 92 Second Series NUMBER 5

DECEMBER 1, 1953

Published for the

AMERICAN PHYSICAL SOCIETY

by the

AMERICAN INSTITUTE OF PHYSICS

Incorporated

LANCASTER, PA., AND NEW YORK, N. Y.

THE
PHYSICAL REVIEW

A journal of experimental and theoretical physics established by E. L. Nichols in 1893

SECOND SERIES, VOL. 92, NO. 5 DECEMBER 1, 1953

Origin of the *E* Layer of the Ionosphere*

ERNEST BAUER, *Mathematics Research Group, New York, University, New York, New York*

AND

TA-YOU WU, *Division of Physics, National Research Council, Ottawa, Canada*

(Received August 27, 1953)

The electron concentration in the *E* layer has been calculated as a function of height according to the theory of the pre-ionization of molecular oxygen by the sun's radiation (Nicolet) and subsequent dissociative recombination (Bates and Massey). The calculations are based on the recent work of Moses and Wu on the distribution of molecular and atomic oxygen in the atom-molecule transition region. It is shown that both the observed height and the value of the peak electron density can be accounted for satisfactorily. We also examine the photo-ionization of atomic oxygen which leads to a peak in the region of the F_1 layer, but it does not seem possible to explain the observed effective recombination coefficient for the F_1 layer on the basis of a theory involving atomic and molecular oxygen alone.

I. INTRODUCTION

SINCE the proposal by Chapman of the theory of formation of ionized layers in the upper atmosphere by solar radiation, many attempts have been made to account for the observed properties of the various layers.[1] Recently it has been suggested rather more definitely than before that the *E* and F_1 layers arise mainly from the ionization of oxygen molecules and atoms, respectively.[2] The arguments for these identifications are the following.

(1) It is generally believed, on the basis of many theoretical studies, that the oxygen molecules in the upper atmosphere are dissociated into atoms by solar radiation, and that this dissociation takes place in a fairly sharp transition region, a few kilometers thick, which lies between 90 and 110 km. The details depend on the particular assumptions in the theory of the dissociation-recombination region. The *E* layer is known to be situated at an altitude of about 100 km,[1] and on account of the dissociation there are very few oxygen molecules present above *E*-layer altitudes.

(2) Of the various known chief constituents of the upper atmosphere, O, O_2, N, N_2, the oxygen molecule has the lowest ionization potential (12.2 ev, corresponding to a threshold wavelength of 1010A). Hence only the radiations necessary to ionize O_2 (wavelengths immediately below 1010A) are not absorbed by the overlying layers of the other constituents, and are thus able to penetrate down to the altitude of the *E* layer.

(3) On the other hand, the oxygen atoms extend to much greater heights than oxygen molecules, and it seems an attractive theory to identify the F_1 layer with the first ionization of the oxygen atom.

There are, however, difficulties in the above simple theory. The first of these is that the observed absorption cross section σ_2 leading to the ionization of O_2 in the first ionization limit (12.2 ev),

$$O_2+h\nu\rightarrow O_2^++e, \quad \sigma_2\sim 10^{-19}\ \text{cm}^2,^{3} \qquad (1)$$

is much too small to account for the observed height of the maximum electron density on the basis of the Chapman theory. It has been suggested by Nicolet[4] that this difficulty can be overcome by assuming that the O_2 absorbs radiation of wavelengths below 1010A in transitions not leading to O_2^+ directly, but to excited states of O_2 that lie in the continuum above the first ionization limit of O_2 and converge to the second

* This work was supported in part by contract with the U. S. Air Force through sponsorship of the Geophysics Research Directorate of the Air Force Cambridge Research Center, Air Research and Development Command.

[1] See S. K. Mitra, *The Upper Atmosphere* (The Royal Asiatic Society of Bengal, Calcutta, 1952), pp. 290–291.

[2] D. R. Bates and H. S. W. Massey, Proc. Roy. Soc. (London) **A187**, 261 (1946); **A192**, 1 (1947); H. S. W. Massey, Phil. Mag. Supplement **1**, 395 (1952), Sec. 5.

[3] Watanabe, Marmo, and Inn, Phys. Rev. **90**, 155 (1953).

[4] M. Nicolet, Inst. Roy. Météorol. Belgique, Mem. **19** (1945).

ionization limit of O_2 (i.e., to an excited state of O_2^+). The oxygen molecules in these excited states are in a condition for auto-ionization, so that the ionization of O_2 consists of two successive processes:

$$O_2+h\nu\rightarrow O_2^*, \quad \lambda<1010\text{A}, \quad \sigma^*, \tag{2}$$

$$O_2^*\rightarrow O_2^+ + e, \quad p. \tag{3}$$

This suggestion is plausible, as the spectrum of O_2 has strong absorption bands in the region 910–1010A (corresponding to 13.5–12.2 ev).[5] The cross section σ^* of the process (2) is not known, although a value of 4×10^{-17} cm^2 has been postulated arbitrarily;[4] and the transition probability p per sec of the radiationless process (3) is also unknown. Let the transition probability per second (Einstein A coefficient) for the reverse process of (2) be denoted by A. Then the fraction of O_2^* produced by (2) which undergoes the auto-ionization process (3) is $p/(p+A)$, and the effective absorption cross section for O, leading to O_2^+ and e is

$$\sigma_2^{\text{eff}}=\frac{p}{p+A}\sigma^*+\sigma_2. \tag{4}$$

While p is not known, it seems that $p<A$, or the absorption bands in (2) would have appeared diffuse by auto-ionization. In the present work we have tried a number of values of σ_2^{eff} which correspond to plausible values of σ^*, p, A, and shall show that values of σ_2^{eff} in this range are capable of accounting for the E layer, when used in conjunction with the other data.

The second difficulty of the theory of the E and F_1 layers is that the observed recombination coefficients α for the E and F_1 layers have the values 10^{-8} and 4×10^{-9} cm^3 sec^{-1}, respectively; these values are much larger than the coefficients for radiative recombination that can be deduced from the photo-ionization cross section:[3,6]

$$O_2^++e\rightarrow O_2+h\nu, \quad \alpha_{r2}\sim10^{-14}\text{ cm}^3\text{ sec}^{-1}; \tag{5}$$

$$O^++e\rightarrow O+h\nu, \quad \alpha_{r1}\sim5\times10^{-13}\text{ cm}^3\text{ sec}^{-1}. \tag{6}$$

It has been suggested[2] that, instead of (5), the O_2^+ recombine with electrons by the following "dissociative" recombination leading to two oxygen atoms in excited states:

$$O_2^++e\rightarrow O'+O'', \quad \alpha_d\sim10^{-8}\text{ cm}^3\text{ sec}^{-1}; \tag{7}$$

and that O^+ and electrons recombine by the two-stage process of a charge transfer

$$O^++O_2\rightarrow O+O_2^+, \quad \gamma\sim10^{-12}\text{ cm}^3\text{ sec}^{-1}, \tag{8}$$

followed by (7). The values of the coefficients α_d and γ are not known either experimentally or theoretically; the values given above are assumed on plausibility considerations to account for the observed α for the E and F_1 layers.[6a]

Partly on account of the above-mentioned difficulty connected with the absorption cross section σ_2, another theory for the production of the E layer has been proposed recently by Hoyle and Bates.[7] They suggest that the ionization is produced by x-rays of about 300 ev emitted from the solar corona. While it certainly seems possible to arrive at any desired rate of ion production and depth of penetration by assuming x-ray quanta of various energies and intensities, this mode of ionized layer formation cannot be taken seriously on account of the following difficulty. The important data characterizing any ionized layer are the maximum electron density, the height of the maximum, and the effective recombination coefficient. The ionization due to x-rays will always be general rather than selective, in the sense that all atoms and molecules at a given height will be ionized to the same extent on account of the high energy of the radiation. For example, between 100 and 150 km, say, the oxygen atoms and nitrogen molecules will be ionized together with the oxygen molecules. The effective recombination coefficient between the ions O^+, O_2^+, N_2^+, and the electrons will be an average of the coefficients for O^++e, O_2^++e, N_2^++e, weighted by their relative abundances. As the only plausible process that has a recombination coefficient as high as the observed 10^{-8} cm^3/sec is a dissociative recombination such as (7), and as the concentration of O atoms greatly outweighs that of O_2 molecules above about 100 km, it follows that the effective recombination coefficient of the ion mixture and the electrons must be very much smaller than the observed value. This has the consequence that it will not be possible to account for the observed recombination coefficient together with the observed maximum electron density and the height of the maximum. Thus one may conclude that while some ionization may be caused by some x-rays from the corona, yet this mode cannot play a major part in the formation of the E layer.

The purpose of the present work is to make a quantitative calculation of the electron densities resulting from the photo-ionization of molecular and atomic oxygen, on the basis of the recent work of Moses and Wu[8] on the distributions of O_2 and of O in and above the oxygen dissociation layer. While these distributions are not definitive on account of the lack of definite knowledge about the mechanism of association, they are, for each assumed model, soundly based on a "self-consistent" treatment, so that a calculation of the

[5] W. C. Price and G. Collins, Phys. Rev. **48**, 714 (1935).
[6] T. Yamanouchi and M. Kotani, Proc. Phys. Math. Soc. Japan **22**, 60 (1940).

[6a] The assumption $\alpha_d\sim10^{-8}$ cm^3 sec^{-1} has been made quite plausible by the observation of a similar coefficient for the process $He_2^++e\rightarrow He'+He''$ in the laboratory, by Biondi *et al.* See M. A. Biondi and T. Holstein, Phys. Rev. **82**, 962 (1951); Biondi, Phys. Rev. **83**, 1078 (1951).

[7] F. Hoyle and D. R. Bates, Terrestrial Magnetism and Atm. Elec. **53**, 51 (1948).

[8] H. E. Moses and T. Y. Wu, Phys. Rev. **87**, 628 (1952), for the "two-body" association model; and result [Phys. Rev. **91**, 1408 (1953)] for the "three-body" association model.

ionized layers on their basis should be satisfactory in the same sense of "self-consistency."[9]

In the following, the number of particles X per cm^3 will be denoted by $[X]$.

II. PHOTO-IONIZATION OF MOLECULAR OXYGEN AND THE E LAYER

Recently it has been assumed[10] that the E layer is the result of the photoionization of oxygen atoms, involving the processes (6), (8), and (7). It will be shown in the next section, however, that the contribution to the electron density in the E layer arising from oxygen atoms is extremely small, so that it is sufficient to assume here that the basic processes for the E-layer ionization are (2), (3), and (7).

The time rate of change of electron density is given by

$$\frac{d}{dt}[e]=q_2[O_2]-\alpha_d[O_2^+][e], \tag{9}$$

where q_2 is the number of photoionizations per second, and is given by

$$q_2(x)=\int_{\nu_2}^{\infty}d\nu\frac{c}{h\nu}\rho_\nu(x)\sigma_2^{\text{eff}}(\nu). \tag{10}$$

Here x is the altitude, $\sigma_2^{\text{eff}}(\nu)$ the effective cross section in (4), and $\rho_\nu(x)$, the energy density per unit frequency range at altitude x, is given by

$$\rho_\nu(x)=\rho_\nu(\infty)\exp\left\{-\sigma_2^{\text{eff}}(\nu)\int_x^{\infty}[O_2]dx\right\}, \tag{11}$$

where $\rho_\nu(\infty)$ is the corresponding density at the top of the atmosphere. We shall make the usual assumption that $\rho_\nu(\infty)$ is the density function of a blackbody at temperature $\theta=6000°$K, "diluted" by a factor W, $4\pi W$ being the solid angle subtended by the earth at the sun. As the spectral regions concerned lie at or below 1000A, it is sufficient to employ Wien's form for $\rho_\nu(\infty)$, so that

$$\rho_\nu(\infty)=\frac{8\pi W h\nu^3}{c^3}\exp(-\nu/\nu_s),\quad \nu_s=k\Theta/k, \tag{12}$$

$$W=5.4\times10^{-6}.$$

Also, on account of the rapid decrease of ρ_ν with increasing frequency ν in this region, we may replace $\sigma_2^{\text{eff}}(\nu)$ by a constant equal to the value at the threshold ν_2. Thus (10) becomes

$$q_2(x)=Q\exp\left\{-\sigma_2^{\text{eff}}\int_x^{\infty}[O_2]dx\right\}.$$

$$Q=\frac{8\pi W}{c^2}\sigma_2^{\text{eff}}\nu_s^3e^{-\xi_2}[\xi_2^2+2\xi_2+2], \tag{13}$$

where $\xi_2=\nu_2/\nu_s$.

The condition for the ionosphere to be electrically neutral is that

$$[O_2^+]=[e]. \tag{14}$$

In order that Eq. (9), with (14), agree with the empirical relation in which the observed recombination coefficient is $\alpha=10^{-8}$ cm^3 sec^{-1}, one assumes that

$$\alpha_d=\alpha=10^{-8}\text{ cm}^3\text{ sec}^{-1}. \tag{15}$$

The maximum electron density at noon, when

$$d[e]/dt=0$$

is given by

$$[e]^2=q_2(\text{noon})[O_2]/\alpha_d, \tag{16}$$

a relation which holds for any height x. Thus, to obtain $[e]$ as a function of x, we need to know $[O_2]$ as a function of x, both for the factor $[O_2]$ in (16), and for the integrated O_2-concentration that occurs in $q_2(x)$ from Eqs. (10) and (11).

Detailed calculations have been carried out in the present work for two of the models studied by Moses and Wu,[8] namely, their two-body recombination model with $T=300°$K, and their three-body recombination model with $T=300°$K and a three-body recombination coefficient $C=10^{-32}$ cm^6 sec^{-1}. Their other models (with different temperature distributions and other C values) give substantially similar results. The distributions of $[e]$ as a function of x for the three-body model, are given in Fig. 1 for various values of σ_2^{eff}, namely $\sigma_2^{\text{eff}}=1.8\times10^{-17}$, 0.9×10^{-17}, 0.45×10^{-17} cm^2. With the two-body model, the curves obtained reproduce those in Fig. 1 to within 10 percent in electron concentration, but are shifted by about 8 km to lower altitudes.

The absolute magnitudes of $[e]$ as given in Fig. 1 may be too large by as much as a factor of three, for the following reason. $[e]^2$ is proportional to the energy density of solar radiation of the appropriate frequency [see Eqs. (10)–(13), (16)]. The energy density used in the computations corresponds to 12.2 ev; at 13.5 ev it is smaller by a factor of ten. From the results of Price and Collins[5] it is seen that there is a number of absorption bands in this frequency range, and their relative importance in contributing to the pre-ionization of O_2 is obviously very hard to evaluate. When allowance is made for this fact we see that the observed peak value $[e]=1.5\times10^5$ cm^{-3} at a height of about 100 km can be accounted for on the basis of the ionization of oxygen molecules.

[9] D. C. Choudhury, Phys. Rev. **88**, 405 (1952), has calculated the absorption cross section σ_2^{eff} needed for (2) and (3) in order to account for the observed height of maximum electron density in the E layer according to the simple Chapman theory, on the basis of the earlier work of H. E. Moses and T.-Y. Wu, Phys. Rev. **83**, 109 (1951). It is preferable, however, to replace that treatment of Moses and Wu by their later work mentioned in reference 8.

[10] E. Gerjuoy and M. A. Biondi, J. Geophys. Research **58**, 295 (1953). We should like to thank these authors for letting us see their work before publication.

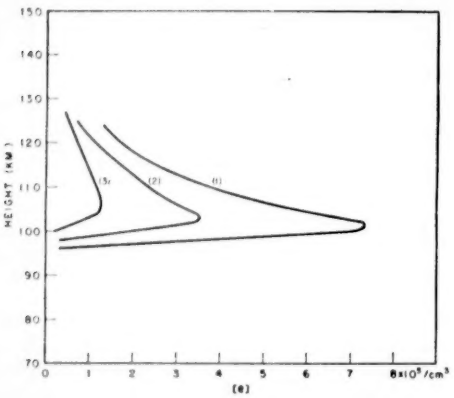

FIG. 1. Concentration of free electrons e in the E layer, resulting from the photoionization of molecular oxygen, for various values of the effective ionization cross section σ_2^{eff}. Curves (1), (2), and (3) correspond to $\sigma_2^{eff}=0.45\times10^{-17}$ cm², 0.9×10^{-17} cm², and 1.8×10^{-17} cm², respectively. The present curves result from the three-body model of Moses and Wu (reference 8), with $T=300°$K and $C=10^{-33}$ cm⁶ sec^{-1}; the two-body model gives very similar curves, but shifted to lower altitudes by 8 km.

III. IONIZATION OF ATOMIC OXYGEN AND THE F_1 LAYER

It is seen from the preceding section that for any reasonable distribution of molecular oxygen with height above the $O_2 \rightleftarrows O$ dissociation region, the contribution from O_2 to the electron density decreases very rapidly with height above the E layer, and is negligibly small at the height of the F_1 layer. On the other hand, the ionization of oxygen atoms is expected to give rise to an ionized layer with maximum electron density at greater altitudes than the E layer. In the following, we shall again calculate the height of maximum electron density due to the ionization of atomic oxygen on the basis of the distributions of atomic oxygen given by the two models of Moses and Wu. It will be shown that, despite the qualitative agreement with the observed data, a complete understanding of the F_1 layer is still lacking.

The F_1 layer is characterized by the following observed data:

Height of maximum electron density$\simeq$200 km.

Peak electron density $[e]\simeq 2.5\times10^5$ cm^{-3}. (17)

Recombination coefficient $\alpha=4\times10^{-9}$ cm³ sec^{-1}.

The ionization process considered here is the photoionization of oxygen atoms just beyond the first ionization limit:

$$O+h\nu\rightarrow O^+ + e;\ \lambda<910\text{A};\ \sigma_1=4.5\times10^{-18}\text{ cm}^2. \quad (18)$$

As was mentioned in Sec. I, the radiative recombination coefficient for the reverse process (6) is several orders of magnitude smaller than the observed α above. Hence, in any theory involving oxygen atoms and molecules alone, the only hope to account for the observed α is to assume that O^+ and e recombine through the two-stage process of charge transfer (8) followed by dissociative recombination (7). On this assumption the equations for the rate of change of $[e]$ and $[O^+]$ are

$$(d/dt)[e]=q_1(x)[O]-\alpha_d[O_2^+][e], \quad (19)$$

$$(d/dt)[O^+]=q_1(x)[O]-\gamma[O^+][O_2], \quad (20)$$

where $q_1(x)$ is similar to $q_2(x)$ of Eq. (10), but always with oxygen atoms instead of oxygen molecules, and with σ_1 instead of σ_2^{eff}, so that

$$q_1(x)=\int_{\nu_1}^{\infty} d\nu \frac{c}{h\nu}\rho_\nu(x)\sigma_1(x), \quad (21)$$

$$\rho_\nu(x)=\rho_\nu(\infty)\exp\left\{-\sigma_1(\nu)\int_x^\infty [O]dx\right\}. \quad (22)$$

The condition for the F_1-layer to be electrically neutral is

$$[O^+]+[O_2^+]=[e], \quad (23)$$

so that (19) becomes

$$\frac{d}{dt}[e]=q_1(x)[0]-\alpha_d\left\{1-\frac{[O^+]}{[e]}\right\}[e]^2 \quad (24)$$

at noon,

$$(d/dt)[e]=(d/dt)[O^+]=0;$$

and it can be shown by means of (19), (20), and (23) that the electron density is given by either of the following equivalent expressions:

$$[e]^2=\frac{q_1(\text{noon})[O]}{\alpha_d}\left\{1-\frac{q_1[O]}{\gamma[O_2][e]}\right\}^{-1}, \quad (25a)$$

$$=\frac{q_1(\text{noon})[O]}{\alpha_d\gamma[O_2]}\{\alpha_d[e]+\gamma[O_2]\}. \quad (25b)$$

At E-layer altitudes, $\gamma[O_2]\sim10^{-12}\times10^{13}$ sec^{-1}, and $\alpha_d[e]\sim10^{-8}\ 10^5$ sec^{-1}, so that the effective recombination coefficient

$$\alpha_d\gamma[O_2]/\{\alpha_d[e]+\gamma[O_2]\}$$

is practically α_d. Calculations of $q_1(x)[O](x)$ on the basis of the distributions of atomic oxygen in any of the models of Moses and Wu[8] (or of other authors for that matter) show that the contribution to $[e]$ from the photoionization of oxygen atoms is negligibly small in the E layer (see Table I). This seems to have eliminated atomic oxygen as an important source of electrons in the E layer.[10]

To calculate $[e]$ in (25) on the basis of the models of Moses and Wu,[8] one has to extend the concentrations of atomic and molecular oxygen given by Moses and Wu above the $O_2 \rightleftarrows O$ transition region. In these altitudes ($x>130$ km) the distribution of O is governed by diffusion rather than by dissociation-association. Instead of assuming an isothermal atmosphere, it is perhaps in better accord with empirical facts to assume

a linear temperature rise with height,

$$T(x)=T(x_E)+b(x-x_E), \tag{26}$$

where x_E is taken as some convenient point near the top of the E layer; the most reliable values of b that have been deduced are 2.15×10^{-5} deg K/cm for an atmosphere of variable molecular weight, or 5.53×10^{-5} for constant molecular weight of 28.966.[11]

For an atmosphere with the temperature distribution (26), the density of a species X varies as

$$[X]=[X]_E\left\{1+\frac{b(x-x_E)}{T(x_E)}\right\}^{-(1+M_X g/kb)}. \tag{27}$$

We shall calculate $[e]$ from the *empirical* relation

$$\alpha[e]^2=q_1(x)[O], \tag{28}$$

in which α has the constant empirical value 4×10^{-9} cm^3 sec^{-1}. The results of a number of models are given in Table I. It is seen that if one uses temperatures derived from the assumption of variable molecular weight [case (1) in the table], one arrives at results in passable agreement with the experimental data[1] (17), and one is tempted to identify the F_1 layer with the region of ionization of oxygen atoms.

The above result, however, is obtained by using the empirical relation (28) instead of (25). When the "theoretical" relation (25a) is employed for heights near the F_1 layer, one obtains the meaningless result that $[e]^2$ becomes negative as $q_1[O]$ becomes greater than $\gamma[O_2]e$. Alternatively, one may impose the empirical value 4×10^{-9} cm^3 sec^{-1} on the theoretical expression for α_{eff} in (25b):

$$\frac{\alpha_d\gamma[O_2]}{\alpha_d[e]+\gamma[O_2]}=4\times10^{-9}\text{ cm}^3\text{ sec}^{-1}, \tag{29}$$

and finds the necessary value for $[O_2]$:

$$[O_2]\sim\frac{2}{3}\frac{\alpha_d[e]}{\gamma}=\tfrac{2}{3}\times11^9\text{ cm}^{-3},$$

which corresponds to a *much lower* altitude than the F_1 layer.

The above difficulty is not resolved by including the radiative recombination (6) for the F_1 layer. In this case, an additional term $-\alpha_{r1}[O^+][e]$ is to be added to the right-hand side of Eqs. (19) and (20), and the maximum electron density at noon is given by

$$[e]^2=\frac{q_1[O]}{\alpha_d}\cdot\frac{\alpha_d[e]+\gamma[O_2]}{\alpha_{r1}[e]+\gamma[O_2]}, \tag{30}$$

instead of by (25). This relation obviously meets with the same difficulty as (25b). In fact, it can readily be shown by similar arguments that it is not possible to have a complete theory of the F_1 layer (especially of the observed value $\alpha=4\times10^{-9}$ cm^3 sec^{-1}) based on processes involving oxygen atoms and molecules alone, such as (2), (3), (5), (6), (7), (8), (18). The difficulty of accounting for the observed α for the F_1 layer lies in the smallness of the concentration of O_2 in that region, and the smallness of the radiative recombination coefficient α_{r1} of (6). The rapid decrease of $[O_2]$ with height above the E layer as a result of the dissociation of molecular oxygen into atoms renders such processes as (8) and (7) ineffective.

[11] The Rocket Panel, Phys. Rev. **88**, 1027 (1952).

TABLE I. Electron density due to the photo-ionization of atomic oxygen.

Data at the reference height x_E	Two-body model $T=300°$K		Three-body model $T=300°$K $C=10^{-32}$ cm^6 sec^{-1}	
x_E in km	97		105.5	
$[O]_E$ in cm^{-3}	3.86×10^{13}		4.3×10^{12}	
$[O_2]_E$ in cm^{-3}	2.32×10^{11}		1.67×10^{11}	
	(1)[a]	(2)[b]	(1)[a]	(2)[b]
height of maximum $[e]$ in km	220	305	170	190
α (empirical[c]) in cm^3 sec^{-1}	4×10^{-9}	8×10^{-11}	4×10^{-9}	4×10^{-9}
$[e]_{max}$ in cm^{-3}	1.5×10^5	6.6×10^5	1.7×10^5	1.3×10^5
$[e]$ at x_E in cm^{-3}	$\ll1$		~1	

[a] (1) refers to temperatures calculated by using variable molecular weight (see reference 11); thus in Eq. (26), $b=2.15\times10^{-5}$ deg K/cm.
[b] (2) refers to temperatures calculated for fixed molecular weight $M=28.966$ ($b=5.53\times10^{-5}$ deg K/cm). The effective molecular weight is certainly not constant at these altitudes, and thus (1) should be considerably more reliable than (2).
[c] See reference 1.

This difficulty of explaining the observed recombination coefficient of the F_1 layer in terms of oxygen-atom ionization is rather independent of the particular theory for the oxygen distribution employed in the calculation. Furthermore, the difficulty is not resolved by adding the contribution from the ionization of nitrogen molecules at the first ionization potential of 15.5 ev to the contribution from atomic oxygen.[2] Thus, on assuming

$$N_2+h\nu\rightarrow N_2^++e,\quad \sigma_N=10^{-17}\text{ cm}^2\text{ at }15.5\text{ ev}; \tag{31}$$

$$N_2^++e\rightarrow N'+N'',\quad \sigma_N=4\times10^{-9}\text{ cm}^3\text{ sec}^{-1}, \tag{32}$$

in addition to (18), (7), and (8), it can be shown that the maximum electron density at noon is given by

$$[e]^2=q_1[O]/\alpha_{r1}+q_N[N_2]/\alpha_N, \tag{33}$$

and the effective recombination coefficient is given by

$$\alpha_{r1}\left\{1+\frac{q_N[N_2]}{q_1[O]}\right\}\frac{[O^+]}{[e]}=\alpha_N\left\{1+\frac{q_1[O]}{q_N[N_2]}\right\}\frac{[N_2^+]}{[e]}.$$

Calculations of $q_N[N_2]$, $q_1[O]$ at the heights of the F_1 layer (200 km) based on the three-body association model of Moses and Wu[8] and on the assumption of a linear rise of temperature with altitude between 100 and 200 km, as in Eq. (26), show that

$$q_N[N_2]/q_1[O]\sim1/160\text{ at }200\text{ km}.$$

This means that at this height the contribution to the electron density comes predominantly from the oxygen atoms, and the rate of recombination is determined essentially by that between O^+ and electrons.

PHYSICAL REVIEW VOLUME 92, NUMBER 5 DECEMBER 1, 1953

Liquid Helium II: Bose-Einstein Condensation and Two-Fluid Model

P. R. ZILSEL

University of Connecticut, Storrs, Connecticut

(Received June 19, 1953)

The Bose-Einstein condensation mechanism is shown to be capable of accounting for the existence of separate hydrodynamic velocity fields for the normal and the superfluid, provided suitable assumptions are made with regard to the single-particle energy spectrum. We consider the effect on the microcanonical gas distribution of imposing a nonzero value of the total momentum **P**. For an ordinary gas the effect is trivial, the whole distribution being merely shifted in momentum space. However, in the case of a degenerate Bose gas whose single-particle energy spectrum has a sharp minimum (gap or cusp), only the excited part of the gas (normal fluid) participates in the imposed motion, the condensate (superfluid) remaining "frozen" in momentum space. This rigidity of the condensate in momentum space plays the same role as the rigidity of the superelectrons on imposition of a magnetic field in the London theory of superconductivity. **P** acts as an additional thermodynamic variable, states with $\mathbf{P}\neq 0$ being macroscopically metastable and corresponding to the existence of a relative velocity between normal and superfluid. The basic hydrodynamic assumption of the two-fluid model is thus reduced to an assumption concerning the form of an effective single-particle energy spectrum, and the parallelism between the theories of superconductivity and superfluidity is clearly exhibited. The present theory permits, in particular, the introduction of the mathematical form of Landau's phonon and "roton" spectra within the framework of the Bose-Einstein condensation picture. The statistical-thermodynamic formulas are derived and are shown to lead to characteristic two-fluid equations derived previously from a variational principle.

I. INTRODUCTION

THE characteristic properties of liquid helium, which distinguish it from all other fluids except the "electron gas" in superconductors, may be classified phenomenologically into two types.

(1) purely thermostatic equilibrium properties. The most significant are the stability of the liquid phase apparently down to absolute zero, and the λ transition within the liquid phase.

(2) the dynamic "superfluid" properties of the liquid below the λ transition (liquid helium II). These may be summarized by the statement that reversible—or, at least, almost reversible—transport processes exist within the liquid.

In contrast to the case of superconductivity, where the existence of strictly reversible transport processes (persistent currents) is definitely established, the stricly reversible character of the "superfluid" processes in He II is still to some extent a matter of dispute, since the persistence or decay of a current of neutral helium atoms is much more difficult to establish by direct observation than the persistence or decay of a current of charged electrons. Nevertheless, such experimental evidence, direct and indirect, as exists, as well as the very suggestive and probably quite fundamental parallelism with superconductivity[1]—about which more later—favors the assumption of strict reversibility under suitable conditions. We shall, moreover, attempt to show that, just as in the case of superconductivity, strict reversibility in the case of He II is less difficult to understand theoretically than the alternative assumption, which involves the necessity of explaining why dissipative interactions which are very strong in other fluids, including liquid helium I, should be extremely weak, though qualitatively present, in liquid helium II.

A successful molecular theory of liquid helium has to account simultaneously for both the thermostatic properties (1) and the dynamic properties (2), presumably on the basis of quantum statistical mechanics. Such a theory, again as in the case of superconductivity, does not yet exist. However, a basic point of view from which attempts at building such theories may proceed, has been expressed by London.[1] According to this point of view both superconductivity and superfluidity result from quantum statistical mechanisms producing condensation into a more or less rigid lattice in momentum space.

Attempts at developing this point of view into complete theories have led to a peculiar contrast between the status of the theory of superconductivity, on the one hand, and of liquid helium, on the other. In the case of superconductivity, the concept of a rigid lattice in momentum space leads almost directly to a generally satisfactory phenomenological theory of the dynamical properties of superconductors (the London theory). The question, however, of what is the mechanism producing this condensation of the electron fluid into a rigid lattice in momentum space, and thus, ultimately, the question of the statistical thermodynamics of the superconductive state and the phase transition into this state, is a very difficult one. Only quite recently has any real progress been made toward its solution.[2]

The situation with respect to liquid helium is almost exactly opposite. Here a mechanism which can account at least qualitatively for the condensation in momentum space, and thus for the existence of the λ transition, is provided by the Bose-Einstein condensation,[3] which predicts for an ideal Bose gas the existence of a transition temperature T_0 below which a finite fraction of all the molecules condenses progressively into the lowest

[1] See F. London, *Superfluids* (John Wiley and Sons, Inc., New York, 1950), Vol. I.

[2] H. Froehlich, Phys. Rev. **79**, 845 (1950); Proc. Phys. Soc. (London) **A64**, 129 (1951). J. Bardeen, Phys. Rev. **80**, 567 (1950); Revs. Modern Phys. **23**, 261 (1951).

[3] F. London, Nature **141**, 643 (1938); Phys. Rev. **54**, 947 (1938).

energy level. While liquid helium is not, of course, an ideal gas, there is good reason for believing that the qualitative features of the Bose-Einstein condensation remain valid for a liquid with such a large specific volume and such small intermolecular forces as liquid helium.[4] In particular, Guggenheim's smoothed potential model of a liquid[5] exhibits a Bose-Einstein condensation very similar to that of an ideal gas, except that the properties of the phase transition approach more closely to those actually observed in liquid helium.

While, however, the Bose-Einstein condensation has provided at least a qualitative understanding of the *thermostatic* properties of liquid helium, it has not, until now, served as a convincing basis for an understanding of the *two-fluid dynamic* properties. It is true that, historically, Tisza's development of the "two-fluid model",[6] which furnishes a generally successful phenomenological theory of the dynamic properties, sprang from ideas suggested by the Bose-Einstein condensation. With its division of the gas into two parts—the entropiless condensate in momentum space, and the remainder of the gas distributed statistically among the excited energy levels—the Bose-Einstein condensation indeed furnished a basis for *some* features of the two-fluid model. But the crucial hydrodynamic feature of the model, that is the existence of separate hydrodynamic velocity fields for the condensate (superfluid) and the excited part (normal fluid), appeared as a very questionable assumption which could be justified only *a posteriori* by the success of the model. It seemed to be necessary to assume a completely unintelligible absence of collisions between the atoms constituting the superfluid and those constituting the normal fluid, in order to account for the apparently frictionless flow of the two fluids relative to each other. At the same time, collisions are, of course, necessary to establish local thermal equilibrium within the liquid, without which the application of thermodynamic reasoning, a very essential feature of the two-fluid theory, would be quite without justification.

The key to the only way out of this dilemma would seem to be the hypothesis put forth by London, that, under given macroscopic boundary conditions, a state of relative motion between the normal and the superfluid is macroscopically metastable, in the same way as a supercurrent is macroscopically metastable in the presence of a given external magnetic field. This means that the superflow is truly reversible; it is maintained not by the absence of collisions, but—under the given conditions—is the thermodynamic equilibrium state established by the collisions.

It is the purpose of the present paper to show that, under suitable assumptions with regard to the single-particle energy spectrum, a degenerate Bose "gas" below its condensation temperature behaves in accordance with London's hypothesis. We shall see that the imposition of nonzero *total momentum* on the degenerate Bose gas plays here a role analogous to that of the imposition of a magnetic field in the London theory of superconductivity. If one calculates the microcanonical gas distribution under the condition of fixed (nonzero) total momentum as well as fixed total energy and number of particles, the equilibrium distribution turns out to involve relative motion between the condensate and the center of mass of the excited part of the gas.

In this way we find that the Bose-Einstein condensation mechanism can furnish at least a qualitative kinetic insight into the existence of two distinct hydrodynamic velocity fields, as well as into the thermostatic properties of liquid helium II. The general features of the two-fluid hydrodynamics can thus be put on a statistical basis within the framework of the Bose-Einstein condensation picture. This is significant especially in view of the apparent absence of superfluidity in pure $_2He^3$, which obeys Fermi-Dirac statistics. The present treatment, further, exhibits in a new light the parallelism between superfluidity and superconductivity.

The theory is still phenomenological in that it considers the liquid in a single-particle approximation, neglecting correlations between the molecules and considering intermolecular forces only to the extent that they are assumed to modify the effective single-particle energy spectrum. To obtain statistical results corresponding to the two-fluid behavior, it is further necessary to assume that this effective single-particle energy spectrum, as a function of the single-particle momentum, has a sharp minimum—either a cusp or a gap. In particular one may use, for example, the mathematical forms of Landau's phonon or "roton" spectrum.[7] The present treatment, further, is confined to a discussion of the *statistical* aspects of two-fluid theory. No attempt is made to solve the fundamental quantum mechanical problem concerning the dynamic behavior of the pure ground state of an ideal quantum liquid.

Some of the statistical-thermodynamic formulas of the present theory will be seen to be similar to some of those given by Landau,[7] and by Dingle[8] and Temperley[9] in further elaboration of Landau's approach. However the significance and interpretation of these equations will be very different.[10]

[4] F. London, *Superfluids*, Vol. 2 (to be published). See also R. P. Feynman, Phys. Rev. **90**, 1116 (1953).

[5] E. A. Guggenheim, Proc. Roy. Soc. (London) **A135**, 181 (1932).

[6] L. Tisza, Compt. rend. **207**, 1035 and 1186 (1938); Phys. Rev. **72**, 838 (1947).

[7] L. Landau, J. Phys. U.S.S.R. **5**, 71 (1941).

[8] R. B. Dingle, Phil. Mag. Supplement **1**, 111 (1952).

[9] H. N. V. Temperley, Proc. Phys. Soc. (London) **A65**, 490 (1952).

[10] It should perhaps be pointed out that, in adopting here the approach from the gas-like Bose-Einstein approximation, I do not wish to maintain that this is the best available approximation at all temperatures. It seems very likely from the experimental evidence that at the lowest temperatures (below about 0.6°K) the excitations in He II are better described by Landau's Debye-type phonon picture. There seems to be little doubt, however, that in the region of the λ transition and down to about 1°K the gas-like picture is more nearly adequate, and is the only one of the two which can account for the existence of the λ transition

II. PRELIMINARY THERMODYNAMIC CONSIDERATIONS

The thermodynamic system under discussion will be taken to be a *unit volume* of fluid. For a simple one-component system such as liquid helium (neglecting the irrelevant complication of a small admixture of the isotope $_2He^3$ in natural helium) the specification of a thermostatic equilibrium state requires two variables of state, for which we shall take the entropy S and the number of particles N in the unit volume. However, we wish to consider the effect on the system of imposing and adiabatically varying certain external conditions—which we may call, somewhat loosely, "boundary conditions." In the language of statistical mechanics, these boundary conditions correspond to constraints or inhibitions imposed on the assembly representing our thermodynamic system. The thermodynamic description of the system then requires at least one additional variable or parameter suitably specifying the effect of the imposed constraint. Without enquiring at the moment what the physical significance of this variable might be for the case we are interested in, we shall denote it by Y.

The First Law of Thermodynamics for reversible processes, including adiabatic changes in the imposed constraints, then reads

$$dE' = TdS + \mu dN + \varphi dY, \tag{2.1}$$

where $E'(S, N, Y)$ is the total energy. The temperature is given by

$$T = (\partial E'/\partial S)_{N,Y}, \tag{2.2}$$

the chemical potential by

$$\mu = (\partial E'/\partial N)_{S,Y}, \tag{2.3}$$

and the quantity φ is defined by

$$\varphi = (\partial E'/\partial Y)_{S,N}. \tag{2.4}$$

It is clear that the quantity φ must be such as to represent a generalized force and dY the corresponding infinitesimal displacement, so that $-\varphi dY$ is the infinitesimal work done by the system against the yielding constraint.

If, then, in the two-fluid model, the states of relative motion between the normal and the superfluid are metastable equilibrium states resulting from the application of suitable macroscopic constraints, it follows that the thermodynamic functions occurring in the two-fluid model must depend on at least one additional variable beside the usual two. In an earlier paper[11] it was found from a detailed analysis of the two-fluid hydrodynamics that such must indeed be the case, if both the requirements of reversibility of superflow and of conservation of total energy and momentum are to be met. The variable which appeared in that discussion was the *relative density of the normal fluid*, $x = \rho_n/\rho$, and it was shown that the *internal energy per gram* U depends on x through the relation

$$(\partial U/\partial x)_{s,\rho} = v^2/2, \tag{2.5}$$

so that

$$dU = Tds + (\mathfrak{P}/\rho^2)d\rho + (v^2/2)dx. \tag{2.6}$$

Here $s = S/\rho$ is the entropy per gram, $\mathfrak{P}$ is the pressure, and $\mathbf{v}$ is the relative velocity of the two fluids.[12]

The problem now before us is to determine whether it is possible to express the conditions responsible for the appearance of a relative velocity in liquid He II in terms of a physically meaningful statistical constraint on the distribution of a degenerate Bose gas, and what the nature of such a constraint might be. For this purpose it will be useful to consider the analogous situation in the London theory of superconductivity.

The physical constraint responsible for the appearance of a supercurrent is the application of a magnetic field, $\mathbf{H}$, and the term corresponding to our φdY in Eq. (2.1) is $(1/4\pi)\mathbf{H}\cdot d\mathbf{B}$, where $\mathbf{B}$ is the magnetic induction per unit volume. The electric current per superelectron is $-(e^2/mc)\mathbf{A}$. The vector potential $\mathbf{A}$ is determined in the present case by $\mathrm{curl}\mathbf{A} = \mathbf{h}$, $\mathrm{div}\mathbf{A} = 0$, where $\mathbf{h}$ is the local value of the magnetic field. These relations are not very useful for our purpose in their present form. They can, however, be re-expressed in such a way as to provide a clue to the corresponding situation in liquid helium.

The momentum of a charged particle in the presence of a magnetic field is given by

$$\mathbf{p}_i = m\mathbf{v}_i + (e/c)\mathbf{A}(\mathbf{r}_i),$$

and the corresponding electric current by

$$\mathbf{j}_i = e\mathbf{v}_i,$$

where $\mathbf{v}_i$ is the velocity of the particle. Consider now a gas of free electrons in statistical equilibrium. In the absence of a magnetic field both the total momentum

$$\mathbf{P} = \sum_i \mathbf{p}_i,$$

and the total current

$$\mathbf{J} = \sum_i \mathbf{j}_i,$$

will be zero. If a magnetic field is applied, however, the total current will classically[13] still be zero, but there will now be a total momentum given by

$$\mathbf{P} = \sum_i (e/c)\mathbf{A}(\mathbf{r}_i).$$

Thus, for a free electron gas, the application of a mag-

itself (see F. London, reference 4, and also H. N. V. Temperley, reference 9).

[11] P. R. Zilsel, Phys. Rev. **79**, 309 (1950).

[12] The treatment of x as a thermodynamic variable and, in particular, Eq. (2.5) has been criticized as inconsistent by H. N. V. Temperley, Proc. Phys. Soc. (London) **A64**, 105 (1951), and by Dingle (reference 8). We shall see, however, that both the treatment and the equation follow directly from the statistical considerations of the present paper. Moreover, Eq. (2.5) can easily be shown to follow from Dingle's own equation (116) when the latter is interpreted correctly.

[13] There is a small quantum effect, the Landau-Peierls diamagnetism, which is irrelevant to our present purpose.

netic field is equivalent to the imposition of a total momentum.

Now the basic assumption of the London theory is that in the superconducting state a finite fraction of the electron gas is "frozen" into a rigid lattice in momentum space, so that the momentum of this fraction is unaffected by the application of a weak magnetic field. Only the "normal" electrons then contribute to the net total momentum of the gas in the presence of a field; the average momentum of the superelectrons remains zero, and there results a supercurrent

$$\mathbf{J}_s = -\sum'(e^2/mc)\mathbf{A},$$

(the summation extending over the "super"-fraction of the electron gas).

Guided by the analogy between superconductivity and superfluidity we will, then, consider the effect of imposing a nonzero value of the total momentum on our system. The variable we have called Y will now be the total momentum $\mathbf{P}$ in the unit volume, and the quantity φ will be a velocity defined by the relation

$$\mathbf{v} = (\partial E'/\partial \mathbf{P})_{S,N}. \tag{2.7}$$

In this case Eq. (2.1) becomes

$$dE' = TdS + \mu dN + \mathbf{v}\cdot d\mathbf{P}, \tag{2.8}$$

the infinitesimal work done in increasing the momentum of the system being $\mathbf{v}\cdot d\mathbf{P}$. The Helmholtz free energy, defined as

$$F' = E' - ST, \tag{2.9}$$

satisfies the equation

$$d(F'/T) = -(E'/T^2)dT + (\mu/T)dN + \mathbf{v}\cdot d\mathbf{P}/T. \tag{2.10}$$

For a closed system the total momentum is a constant of the motion. Thus the state resulting from the imposition of a total momentum different from zero is not subject to internal dissipation into the absolute equilibrium state characterized by $\mathbf{P}=0$, but is indeed macroscopically metastable.

Note that, since the total momentum is an extensive variable, the chemical potential is no longer equal to the Gibbs potential per particle G'/N, where

$$G' = E' - ST + \mathfrak{P}\mathfrak{V}, \tag{2.11}$$

and the volume $\mathfrak{V}$ is unity in the present case. Instead we have

$$\mu = (G' - \mathbf{P}\cdot\mathbf{v})/N. \tag{2.12}$$

Of course, for an ordinary thermodynamic system the imposition of a total momentum is trivial. It results simply in the total system being put into motion, without significant effect on its statistical properties, and is equivalent to a Galilean coordinate transformation. The velocity $\mathbf{v}$, defined by Eq. (2.7), is then the resulting center-of-mass velocity of the system as a whole and satisfies the relation

$$\mathbf{P} = \rho\mathbf{v}. \tag{2.13}$$

We shall see in the next section, however, that in the case of a degenerate Bose gas with a suitably generalized energy spectrum, an effect can occur which is quite analogous to the "freezing" of the superelectrons in momentum space which is assumed by the London theory of superconductivity.

III. THE DEGENERATE BOSE GAS WITH FIXED TOTAL MOMENTUM

We proceed to derive the most probable distribution in a Bose gas with a generalized energy spectrum $\epsilon_j = \epsilon(\mathbf{p}_j)$, under the conditions of fixed total number of particles N, total energy E', and total momentum $\mathbf{P}$, that is,

$$\sum_j n_j = N, \quad \sum_j n_j\epsilon_j = E', \quad \sum_j n_j\mathbf{p}_j = \mathbf{P}. \tag{3.1}$$

The entropy corresponding to a given distribution (occupation numbers n_j) is[14]

$$S_D = \sum_j S_j = \sum_j k[g_j \ln(1+n_j/g_j) + n_j \ln(1+g_j/n_j)], \tag{3.2}$$

where g_j is the degeneracy of the j'th energy level.

The most probable distribution is the one for which S_D is a maximum subject to the restrictions (3.1). It is, then, determined by the condition that for all i

$$(\partial/\partial n_i)[S/k - \alpha\sum n_j - \beta\sum n_j\epsilon_j - \boldsymbol{\gamma}\cdot\sum n_j\mathbf{p}_j] = 0, \tag{3.3}$$

that is,

$$\ln(1+g_j/n_j) - \alpha - \beta\epsilon_j - \boldsymbol{\gamma}\cdot\mathbf{p}_j = 0. \tag{3.4}$$

Thus we have for the most probable occupation numbers

$$n_j = g_j/[\exp(\alpha+\beta\epsilon_j+\boldsymbol{\gamma}\cdot\mathbf{p}_j) - 1]. \tag{3.5}$$

This distribution differs from the usual one, determined without specifying the total momentum, only through the presence of the extra term $\boldsymbol{\gamma}\cdot\mathbf{p}_j$ in the exponent.[15]

The Lagrange multipliers α, β, $\boldsymbol{\gamma}$, are determined by the conditions (3.1). α and β have their usual significance,

$$k\alpha = -\mu/T, \tag{3.6}$$

$$k\beta = 1/T, \tag{3.7}$$

and $\boldsymbol{\gamma}$ is given by

$$k\boldsymbol{\gamma} = -\mathbf{v}/T, \tag{3.8}$$

where $\mathbf{v}$ is the velocity defined by the thermodynamic relation (2.7).

Equation (3.8) plus, incidentally, Eqs. (3.6) and (3.7) may be obtained quickly, though somewhat nonrigorously, by a slight extension of a method used by Mayer and Mayer:[14] we consider the gas as consisting of two parts, a particular energy level j and the remainder, denoted by r. For the most probable distribution the total entropy, $S = S_j + S_r$, is stationary under the transfer of

[14] See J. E. Mayer and M. G. Mayer, *Statistical Mechanics* (John Wiley and Sons, Inc., New York, 1940), p. 124.

[15] A similar result was obtained by Temperley (reference 9) for an assembly of Debye modes in connection with Landau's phonon model.

a small number of particles,

$$\delta n_j = -\delta n_r, \tag{i}$$

into the state j from the remainder of the gas. This transfer has to be such as to conserve not only the total number of particles, but also the total energy and momentum, so that we have, in addition to (i),

$$\delta E_r' = -\delta E_j' = -\epsilon_j \delta n_j; \quad \delta \mathbf{P}_r = -\delta \mathbf{P}_j = -\mathbf{p}_j \delta n_j. \tag{ii}$$

The condition that the entropy is stationary gives

$$0 = \delta S = (dS_j/dn_j - \delta S_r/\delta n_r)\delta n_j. \tag{iii}$$

From (3.4)

$$dS_j/dn_j = k \ln(1+g_j/n_j) = k\alpha + k\beta\epsilon_j + k\boldsymbol{\gamma}\cdot\mathbf{p}_j. \tag{iv}$$

To evaluate $\delta S_r/\delta n_r$ we assume that the part r is so nearly the whole system that we can apply to it the thermodynamic formulas valid for the gas as a whole. Thus

$$\delta S_r/\delta n_r = \partial S/\partial N + (\partial S/\partial E')\delta E_r'/\delta n_r + (\partial S/\partial \mathbf{P})\cdot\delta \mathbf{P}_r/\delta n_r. \tag{v}$$

Equating (iv) to (v), making use of the relations (ii) and the identity

$$(\partial S/\partial \mathbf{P})_{E',N} = -(\partial S/\partial E')_{\mathbf{P},N}(\partial E'/\partial \mathbf{P})_{S,N} = -\mathbf{v}/T, \tag{vi}$$

we obtain the desired result.

Equation (3.5) for the most probable distribution thus takes the form

$$n_j = g_j/\{\exp[(\epsilon_j - \mathbf{v}\cdot\mathbf{p}_j - \mu)/kT] - 1\}. \tag{3.9}$$

To consider the properties of this distribution function it is convenient to introduce a quantity ϵ_j', defined as

$$\epsilon_j' = \epsilon_j - \mathbf{v}\cdot\mathbf{p}_j. \tag{3.10}$$

The distribution (3.9) is the same function of ϵ' as the usual Bose distribution without imposed momentum is of ϵ. Condensation will set in at the temperature at which μ becomes virtually equal to the minimum value of ϵ', and the condensation will be into the energy level ϵ_0 determined by the condition that

$$\epsilon_0' = \epsilon_0 - \mathbf{v}\cdot\mathbf{p}_0 = \min(\epsilon'). \tag{3.11}$$

In general the identity of this level will, of course, depend on the value of $\mathbf{v}$, which means, ultimately, on the value of the imposed momentum.

Ideal-Gas Energy Spectrum

Consider in particular the case where the energy spectrum is that of an ordinary ideal gas,

$$\epsilon_j = p_j^2/2m.$$

In this case

$$\epsilon_j' = p_j^2/2m - \mathbf{v}\cdot\mathbf{p}_j = (1/2m)|\mathbf{p}_j - m\mathbf{v}|^2 - mv^2/2,$$

so that, by Eq. (3.11), the condensation occurs into the level

$$\epsilon_0 = mv^2/2$$

with momentum

$$\mathbf{p}_0 = m\mathbf{v}.$$

The effect of imposing a total momentum on the gas is, then, what we should expect for an ordinary system: the whole distribution in momentum space is merely shifted by the amount $m\mathbf{v}$. The total momentum is

$$\mathbf{P} = Nm\mathbf{v} = \rho\mathbf{v},$$

in agreement with Eq. (2.13), and the velocity $\mathbf{v}$ has the significance of the center-of-mass velocity of the gas as a whole.

Energy Spectrum with Cusp or Gap

If, on the other hand, the energy spectrum $\epsilon(\mathbf{p})$ is a monotonically increasing function of the magnitude of $\mathbf{p}$ with a finite slope at the origin, such as

$$\epsilon_j = c|\mathbf{p}_j| + c'p_j^2 + \cdots, \tag{a}$$

or, *a fortiori*, if there is a finite energy gap separating the state of zero momentum from the other levels, e.g.,

$$\epsilon_j = 0, \quad \mathbf{p}_j = 0; \quad \epsilon_j = p_j^2/2m + \Delta, \quad \mathbf{p}_j \neq 0, \tag{b}$$

the situation is quite different. For sufficiently small $\mathbf{v}$ the minimum of ϵ' remains at the level with zero momentum.

$$\epsilon_0 = \epsilon(\mathbf{p} = 0),$$

so that *with this type of energy spectrum, only the excited part of the gas contributes to the total imposed momentum.* We thus have, in this case, an actual model of a macroscopically metastable state involving relative motion between the excited part (normal fluid) and the condensed part (superfluid) of the gas. As long as a finite fraction of the gas is condensed into the level with zero momentum, that is as long as we remain below the condensation temperature, the ratio of the total momentum $\mathbf{P}$ to the velocity $\mathbf{v}$ is less than the total mass ρ in the unit volume of gas, since only the excited part of the gas is accelerated when the momentum is increased. If, following Landau,[7] we define the effective density of the normal fluid as this ratio of the total momentum to what is in his treatment the "drift velocity" of the excitations,

$$\mathbf{P} = \rho_n\mathbf{v} = \rho x\mathbf{v}, \tag{3.12}$$

the velocity $\mathbf{v}$ takes on the significance of the relative velocity between the normal and the superfluid.[16]

The distortion of the equilibrium distribution by the imposition of a total momentum is shown schematically in Fig. 1 for the case of the energy spectrum (b). In this particular case

$$\mathbf{P} = mN_e\mathbf{v},$$

so that, by (3.12),

$$\rho_n = mN_e,$$

where

$$N_e = N - n_0$$

is the number of excited particles. Note that N_e is an increasing

[16] The statistical formulas of Landau (reference 7) and Dingle (reference 8) refer to assemblies of "excitations" moving with a drift velocity $\mathbf{v}$ relative to an unspecified rest system. These authors assume that this rest system is the one in which the "ground state" of the liquid (superfluid) is at rest. But since the ground state is not part of their statistical system, it is not clear in their treatment whether $\mathbf{v}$ is in fact a relative velocity between the assembly of excitations and the superfluid.

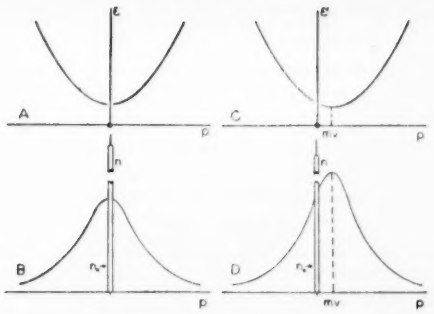

FIG. 1. Effect on the equilibrium distribution of imposing a total momentum on a degenerate ($T<T_0$) Bose gas, with energy spectrum $\epsilon_j=0$, for $\mathbf{p}_j=0$; $\epsilon_j=p_j^2/2m+\Delta$, for $\mathbf{p}_j\neq 0$ (schematic). A: energy spectrum as a function of $\mathbf{p}$; the circle at the origin indicates the lowest level. B: equilibrium distribution, n as a function of $\mathbf{p}$, for zero total momentum; the occupation number n_0 of the lowest level (condensate) is indicated schematically by the broken bar. C: quantity $\epsilon_j'=\epsilon_j-\mathbf{v}\cdot\mathbf{p}_j$, which governs the distribution for the case of nonzero total momentum. D: equilibrium distribution for nonzero total momentum. The average momentum of the excited particles is $m\mathbf{v}$, whereas the condensate (n_0) has zero momentum. The relative velocity between normal and superfluid is $\mathbf{v}$.

function of v^2. For the energy spectrum (b) the dependence is

$$N_\epsilon(v^2)=N_\epsilon(0)\exp[mv^2/2kT].$$

It should be noted that the conclusions of the preceding paragraphs are valid only for sufficiently small $\mathbf{v}$, since for any energy spectrum with finite slope or finite gap, a sufficiently large value of $\mathbf{v}$ will shift the minimum of ϵ' away from the state of zero momentum. In this way the notion of a critical velocity arises in the present considerations. A quantitative investigation of this and other detailed features which depend on the particular choice of the energy spectrum, may be left to a later time. It may be pointed out, however, that in particular the mathematical form of Landau's phonon or roton spectrum—the latter corresponding to our spectrum (b)—may be used in the present model, and that, in that case, our results are formally similar to those given by Landau,[7] even though the point of view is quite different.

We conclude this section by constructing the statistical equation for the Helmholtz Free Energy. For this purpose we introduce the function Q, which is the logarithm of the Grand Partition Function:

$$Q=\sum_j g_j\ln[1-\exp(-\alpha-\beta\epsilon_j-\boldsymbol{\gamma}\cdot\mathbf{p}_j)]. \quad (3.13)$$

Considered as a function of α, β, and $\boldsymbol{\gamma}$, Q has the following properties, as is easily verified:

$$\partial Q/\partial\alpha=N,\quad \partial Q/\partial\beta=E',\quad \partial Q/\partial\boldsymbol{\gamma}=\mathbf{P}. \quad (3.14)$$

The free energy F' is a function of T (or β), N, and $\mathbf{P}$, and can be obtained from Q essentially by a Legendre transformation. We shall verify that

$$\beta F'=Q-\alpha N-\boldsymbol{\gamma}\cdot\mathbf{P}. \quad (3.15)$$

Taking the differential of Eq. (3.15) and using (3.14), we have

$$d(\beta F')=E'd\beta-\alpha dN-\boldsymbol{\gamma}\cdot d\mathbf{P},$$

or, using Eqs. (3.6)–(3.8),

$$d(F'/T)=E'd(1/T)+(\mu/T)dN+(\mathbf{v}/T)\cdot d\mathbf{P},$$

which agrees with the thermodynamic equation (2.10), thus verifying (3.15) and, incidentally, the identifications (3.6)–(3.8) of the Lagrange multipliers α, β, and $\boldsymbol{\gamma}$.

We thus have explicitly for the Helmholtz Free Energy of a unit volume of the gas, as a function of the temperature, the number of particles, and the momentum, the following expression:[17]

$$F'=kT\sum_j g_j\ln\{1-\exp[(\mu+\mathbf{v}\cdot\mathbf{p}_j-\epsilon_j)/kT]\}+N\mu+\mathbf{v}\cdot\mathbf{P}. \quad (3.16)$$

IV. CONNECTION WITH THE TWO-FLUID MODEL. DISCUSSION

In discussing the thermo-hydrodynamics of the two-fluid model it is customary[18] to consider the total energy per unit volume, E, to consist of two parts: the hydrodynamic kinetic energy of the two fluids, and the "internal energy." Thus

$$E=\rho_n v_n^2/2+\rho_s v_s^2/2+\rho U, \quad (4.1)$$

where

$$\rho_n=x\rho,\quad \rho_s=(1-x)\rho, \quad (4.2)$$

are the densities of the normal and the superfluid, respectively, and $\mathbf{v}_n$ and $\mathbf{v}_s$ are their respective hydrodynamic velocities.

The energy E' considered in the preceding sections clearly corresponds neither to E nor to ρU: it is the total energy per unit volume in a coordinate system in which the condensate (superfluid) is at rest. To obtain the thermodynamic properties of E or of ρU, we have to transform to a coordinate system in which the superfluid has the velocity $\mathbf{v}_s$, that is a system moving with the velocity $-\mathbf{v}_s$ relative to the one for which the statistical formulas of the preceding section hold. The relation between E and E' is then found to be

$$E=E'+\rho v_s^2/2+\rho_n\mathbf{v}\cdot\mathbf{v}_s, \quad (4.3)$$

so that

$$\rho U=E'-\rho_n v^2/2. \quad (4.4)$$

Remembering the relation (3.12), whereby, in Eq. (2.8) for dE'

$$\mathbf{v}\cdot d\mathbf{P}=\mathbf{v}\cdot d(\rho x\mathbf{v})=xv^2d\rho+\rho v^2dx+\rho x dv^2/2,$$

we obtain from Eqs. (4.4) and (2.8)

$$dU=dE'/\rho-E'd\rho/\rho^2-d(xv^2)/2$$
$$=Tds+(ST+\rho xv^2-E'+N\mu)d\rho/\rho^2+(1/2)v^2dx. \quad (4.5)$$

[17] The corresponding formula given by Dingle [reference 8, Eq. (116)] for an assembly of excitations is obtained by a Galilean coordinate transformation involving a *fixed* velocity $\mathbf{v}$, and therefore omits the term $-\boldsymbol{\gamma}\cdot\mathbf{P}$ in the Legendre transformation (3.15). Hence Dingle's expression really stands for the function $F'-\mathbf{v}\cdot\mathbf{P}$, which accounts for its being a decreasing function of v^2.

[18] See, e.g., reference 11.

Substitution of the expression (2.12) for μ into (4.5) yields the characteristic equation (2.6) of the two-fluid model.

It will be well, in conclusion, to discuss briefly some questions relating to the physical significance of the formal statistical results we have obtained. We have seen that a degenerate Bose gas with a suitable energy spectrum exhibits the characteristic hydrodynamic property of the two-fluid model of liquid He II, that is the property of being able to sustain, under appropriate macroscopic conditions, a stable relative velocity between the condensed (superfluid) and the excited (normal) part of the gas. It is significant, however, that this result does not obtain for an *ideal gas* of helium atoms (energy spectrum $\epsilon=p^2/2m$), but requires the existence of an energy gap or, at least, a finite slope at the origin in the energy spectrum of an atom as a function of the magnitude of its momentum.

Now it is quite reasonable to expect that a single-particle approximation to the description of liquid helium would involve a spectrum of this type.[19] Such a single-particle approximation, or the smoothed potential model of a liquid,[5] for which the essential parts of the treatment in Sec. III are still valid, takes account of the interactions between the atoms in an approximate way by considering each atom to be moving in a potential obtained by averaging over the wave functions of all the other atoms. The energy spectrum of an atom in such a model therefore actually depends on the states of motion of all the atoms; it is a function of the statistical distribution. In our discussion we have assumed, however, that the single-particle energy spectrum is unaffected by the change in the distribution resulting from the imposition of a total momentum.

Quite apart, therefore, from the limitations of any model neglecting the correlations between the atoms in the description of a liquid, our results can be expected to have only limited qualitative validity as a basis for understanding the actual hydrodynamic properties of liquid He II. They will be valid only for situations in which the effective single-particle energy spectrum is not altered appreciably by the imposition of a total momentum on the fluid. We may expect that this will be the case if two conditions are met. First, the resultant relative velocity $\mathbf{v}$ must be sufficiently small, so that the distribution (3.9) is not greatly distorted by the presence of the $\mathbf{v}\cdot\mathbf{p}_j$ term. Second, the momentum must be imposed in such a way that not all the atoms are accelerated simultaneously, because otherwise one would expect the minimum of the single-particle energy spectrum to shift away from the state of zero momentum.

[19] A spectrum with a gap has been proposed by Bijl, deBoer, and Michels, Physica **8**, 655 (1941); and by Toda, Prog. Theoret. Phys. **6**, 458 (1951). See also Landau, reference 7.

The first of these conditions suggests that the reversibility of superflow will probably break down at considerably lower relative velocities than those one would deduce from the statistical considerations which assume a fixed energy spectrum. The second condition will bear a closer look at this time. In Sec. III we have assumed that the single-particle energy spectrum $\epsilon(\mathbf{p})$ has its sharp minimum at $\mathbf{p}=0$. However, the interactions between the atoms, which would be the cause of this sharp minimum, can depend only on *relative* momenta, so that in general we should expect the energy spectrum to be a function

$$\epsilon=\epsilon(|\mathbf{p}-\mathbf{p}_s|), \tag{4.6}$$

the particles of the condensate moving with a momentum $\mathbf{p}_s$. In this case the total momentum in the absence of a relative velocity $\mathbf{v}$ would be not zero, but $\mathbf{P}_0=N\mathbf{p}_s$. Clearly the treatment of Sec. III still holds for this case, a relative velocity resulting now from the imposition of a total momentum differing from $\mathbf{P}_0$. The application of forces which affect all the particles simultaneously, however, such as for example the force of gravity or body forces in general, would now be expected to result not in a relative velocity $\mathbf{v}$, but rather in a change of $\mathbf{p}_s$, that is, a shift in the minimum of the energy spectrum (4.6). On the other hand, "forces" which act statistically by collisions, such as viscous friction between layers of the fluid or between the fluid and a wall, will not affect the energy spectrum appreciably, but will instead lead to the emergence of a relative velocity between the condensate and the excited part of the fluid. This, then, is the kind of physical situation corresponding to the imposition of the statistical constraint of a total momentum (different from $\mathbf{P}_0$).

The behavior of $\mathbf{p}_s$ is presumably described by the equation of motion of the superfluid velocity $\mathbf{v}_s$ in the two-fluid model. The problem of a rigorous microscopic theory of this behavior is essentially the problem of a rigorous theory of the ground state of an ideal quantum liquid. It is, therefore, in the main a problem not of statistical mechanics but of pure quantum mechanics, and cannot be treated by the statistical methods of the present paper. It's complete solution must await the development of a theory of the pure quantum states of a liquid. We have seen, on the other hand, that the *statistical aspects* of the two-fluid hydrodynamics can be elucidated at least qualitatively within the framework of the Bose-Einstein condensation picture.

I am greatly indebted to Professor F. London for letting me see the manuscript of his forthcoming book before publication and for several valuable discussions. I am also indebted to Mr. H. M. Fried for assistance with some of the calculations, and to the Research Corporation for a financial grant.

Effect of the Surface on the Magnetic Properties of an Electron Gas

FRANK S. HAM
Harvard University, Cambridge, Massachusetts
(Received August 20, 1953)

The energy levels of free electrons confined to a finite cylindrical box with a uniform axial magnetic field are obtained by the WKB approximation and used to compute the magnetic susceptibility with Fermi statistics. The usual treatments which neglect the effects of the walls are shown to be justified for both the steady susceptibility and the de Haas van Alphen terms provided the radius of the box is sufficiently large. In the case of the oscillatory terms it is only necessary that the radius of the box exceed the classical orbit radius R_ϵ of an electron having the Fermi energy ζ in the magnetic field. However, there exists a surface correction to the steady susceptibility whose magnitude relative to the Landau value is $(\zeta/\beta H)^{\frac{1}{2}}(R_\epsilon/R)$. This surface correction, the existence of which has been previously pointed out by Osborne and Steele, and by Dingle, is shown to be extremely sensitive to the exact boundary conditions at the surface, including both the abruptness of the surface jump in potential and the height of the barrier relative to the Fermi energy. Indeed, the correction term can be either paramagnetic or diamagnetic depending on these details. The form of the WKB approximation appropriate to different boundary conditions is discussed, and a modification of Dingle's theory is presented which may be used to calculate approximately the susceptibility of the system for any value of the ratio R/R_ϵ when the boundary conditions are known.

I. INTRODUCTION

A NUMBER of papers[1–13] have been published in the last twenty years concerning the theory of the magnetic susceptibility of a system of free electrons or of electrons confined to a box, and a variety of elegant methods have been developed. It has not been altogether clear, however, to what extent the walls of the system could be neglected in some of these calculations, and the dependence of the susceptibility on the form of the wall potential has not been adequately investigated. Osborne,[7] Steele,[8] and Dingle,[3,4] have recently given calculations which take the walls into account, but they have arrived at different conclusions concerning the corrections to the susceptibility required by the finite size of the box. Since the walls play an essential role in a box of any size, it seems desirable to have a derivation which shows this explicitly. The author believes that the present treatment offers a clear picture of the physical situation as well as some new results concerning the dependence of the susceptibility upon the size of the box.

It is well known[14,15] that in classical physics the positive moment contributed by electrons that collide with the walls of the system exactly cancels the negative moment of electrons far from the walls. Van Vleck[5] and Teller[6] showed that a similar balancing occurs in quantum mechanics (with a nonzero resultant) and gave arguments to justify the value for the magnetic susceptibility obtained by Landau[9] from the free energy. However, Teller's argument was for an infinite plane wall, and Van Vleck's required the use of the old quantum mechanics, although the details of his arguments are very similar to those used in the present paper. It is not clear to what extent either justifies the more recent calculations by Landau[1] and others of the oscillatory de Haas van Alphen terms. The present work had its origin in an improved derivation for a cylindrical box which made clear this balancing of diamagnetic and paramagnetic states and obtained the usual results for the Landau steady susceptibility and the de Haas van Alphen oscillations provided the box was sufficiently large. It was then found that the WKB approximation could be used to calculate the energies of the electron states whose wave functions were appreciably distorted from free-electron form by the presence of the walls and that from these energies corrections to the total susceptibility could be obtained which were important for smaller boxes. This work was in qualitative agreement with that of Osborne[7] and Steele,[8] who predicted a "surface diamagnetism," and agreed with Dingle's work[4] in the size- and field-dependence of the corrections but disagreed in that Dingle predicted a paramagnetic correction of about one-third the magnitude of our result. We have found that this difference arises from our having determined the energy levels from that form of the WKB phase integral condition which is correct when the potential barrier at the surface rises slowly, whereas Dingle used the form correct when the barrier rises abruptly to infinite height. We have outlined a number of considerations which must determine the correct form of the WKB approximation when we know the form of the surface potential in a real

[1] D. Schoenberg, Proc. Roy. Soc. (London) **A170**, 341 (1939).
[2] E. H. Sondheimer and A. H. Wilson, Proc. Roy. Soc. (London) **A210**, 173 (1951).
[3] R. B. Dingle, Proc. Roy. Soc. (London) **A211**, 500, 517 (1952); **A212**, 38, 47 (1952).
[4] R. B. Dingle, Proc. Roy. Soc. (London) **A216**, 118 (1953).
[5] J. H. Van Vleck, *Theory of Electric and Magnetic Susceptibilities* (Oxford University Press, London, 1932), p. 353 ff.
[6] E. Teller, Z. Physik **67**, 311 (1931).
[7] M. F. M. Osborne, Phys. Rev. **88**, 438 (1952).
[8] M. C. Steele, Phys. Rev. **88**, 451 (1952).
[9] L. Landau, Z. Physik **64**, 629 (1930).
[10] C. G. Darwin, Proc. Cambridge Phil. Soc. **27**, 86 (1930).
[11] R. Peierls, Z. Physik **80**, 763 (1933); **81**, 186 (1933).
[12] M. Blackman, Proc. Roy. Soc. (London) **A166**, 1 (1938).
[13] A more complete bibliography is given in the papers by Dingle.
[14] J. H. Van Leeuwen, Dissertation, Leiden, 1919; Summary in J. phys. et radium **2**, 361 (1921).
[15] Reference 5, Chap. IV.

metal, but since we lack sufficiently detailed information concerning the surface potential we have not attempted to carry through a calculation for any model of a real metal. It appears that surface corrections of the general form predicted should result for any reasonable model, the numerical coefficient and sign depending on the details of the model. Before further calculation is done, it would be desirable to have experimental evidence at hand: if such surface corrections can be located, their sign and magnitude may be of great assistance in our selection of a model of the metal surface and our choice of the best form of the WKB approximation. If no such corrections can be found, we must seek a model that makes the surface effects too small for observation.

Unfortunately, much of the calculation that has gone into this work is too lengthy for publication here, so that frequently only results may be quoted. Most of the analysis has been made available elsewhere.[16]

II. METHODS OF CALCULATING THE MAGNETIC MOMENT

The usual procedure has been to calculate the magnetic moment M from the Helmholtz free energy F by the formula

$$M=-(\partial F/\partial H)_{T,V,N}, \tag{201}$$

where H is the absolute value of the uniform external magnetic field applied to the system, T the absolute temperature, V the volume of the system, and N the total number of electrons present. It is, however, evident that if the electrons are independent, except in so far as they obey the exclusion principle when Fermi statistics are used, then the moment of the system should also be given by the sum of the moments of the individual electron states weighted with the probability that the state is occupied.[5,7] Thus with Fermi statistics we should have

$$M=-\sum_i(\partial\epsilon_i(H)/\partial H)\times\{1+\exp[(\epsilon_i(H)-\zeta)/kT]\}^{-1}, \tag{2.2}$$

where k is the Boltzmann constant and $\epsilon_i(H)$ the energy of the state i, and where ζ is determined by the condition

$$N=\sum_i\{1+\exp[(\epsilon_i(H)-\zeta)/kT)\}^{-1}, \tag{2.3}$$

the sum being taken over all single electron states. On the other hand, the free energy is given by

$$F=N\zeta-kT\sum_i\ln\{1+\exp[(\zeta-\epsilon_i(H))/kT]\}, \tag{2.4}$$

and since by (2.3) $(\partial F/\partial\zeta)=0$, (2.1) and (2.2) give the same result, provided the limits of summation in (2.4) and the degeneracy of states with a common energy (if we should use the index i to label a collection of states with the same energy instead of a single state) do not depend on H.

However, for a system confined by a cylindrical box of cross section A with its axis parallel to the uniform magnetic field, the energies of states unperturbed by the walls are, if we neglect the moment due to spin,

$$\epsilon(n,k_z)=\hbar^2k_z^2/2m+(2n+1)\beta H,\quad n=0,1,2,\cdots, \tag{2.5}$$

where $e\hbar/2mc=\beta$ is the Bohr magneton, and the electronic wave function depends on the position coordinate z along the axis only through the factor $\exp(ik_zz)$. The degeneracy of each such (n,k_z) level is to first approximation[3,8] eHA/hc, if we neglect spin degeneracy. As remarked by Van Vleck[5] and Osborne,[7] if we use only these energy states (2.5) and this degeneracy in (2.2), we find a large negative total moment of magnitude greater than $N\beta$, whereas (2.4) and (2.1) yield the usual Landau result (for $\beta H\ll\zeta$)

$$M=-(4m\beta^2V/\hbar^2)(N\pi^2/9V)^{\frac{1}{3}}H=-N\beta^2H/2\zeta=-\tfrac{1}{3}n(\zeta)\beta^2H, \tag{2.6}$$

plus the periodic de Haas van Alphen terms. Here $n(\zeta)$ is the density of states (including spin degeneracy) in the energy scale at the Fermi level ζ, and the second expression shows (2.6) to be much less in magnitude than $N\beta$. Our first problem is, then, to show that the difference between these methods is removed when we include the positive moments of the boundary states in our summation (2.2).

III. THE BOUNDARY STATES IN THE WKB APPROXIMATION

We consider the Schrödinger equation satisfied by the wave function of a single electron state in a cylindrical box of length L and radius R with its axis parallel to the uniform magnetic field, in which we neglect all interaction between electrons

$$-(\hbar^2/2m)[(\partial^2\psi/\partial z^2)+r^{-2}(\partial^2\psi/\partial\phi^2)+r^{-1}(\partial/\partial r)(r\partial\psi/\partial r)]-i\beta H(\partial\psi/\partial\phi)+(e^2H^2/8mc^2)r^2\psi=E\psi, \tag{3.1}$$

for $r<R$, and the boundary condition $\psi(R)=0$. On separating in cylindrical coordinates, we put

$$\psi=f(r)\exp(ik_zz+is\phi),\qquad \epsilon'=E-(\hbar^2k_z^2/2m)-\beta Hs,\quad s=0,\pm1,\pm2,\cdots, \tag{3.2}$$

and get as the equation for $f(r)$

$$-(\hbar^2/2mr)(\partial/\partial r)(r\partial/\partial r)f(r)+[(\hbar^2s^2/2mr^2)+(e^2H^2r^2/8mc^2)]f(r)=\epsilon'f(r). \tag{3.3}$$

We now make the substitution $r=e^x$, $f(r)=g(x)$, which puts (3.3) in a form suitable for the WKB approxi-

[16] H. Brooks and F. S. Ham, Technical Report No. 169 of Cruft Laboratory, Harvard University, March 10, 1953. This report was published under contract with the Office of Naval Research and has been distributed to the usual recipients of the Cruft Laboratory Reports. The authors have a few extra copies which they will be glad to send upon request. This report has, moreover, been deposited as Document No. 4099 with the ADI Auxiliary Publications Project, Photoduplication Service, Library of Congress, Washington 25, D. C. A copy may be secured by citing the Document number and by remitting $7.50 for photoprints or $2.75 for 35-mm. microfilm. Advance payment is required. Make checks or money orders payable to: Chief, Photoduplication Service, Library of Congress.

mation,[17]

$$(\partial^2 g(x)/\partial x^2)+(2m/\hbar^2)[\epsilon' e^{2x}-(\hbar^2 s^2/2m) - (e^2H^2/8mc^2)e^{4x}]g(x)=0. \quad (3.4)$$

This determines ϵ' in terms of s and n through the phase integral condition (after transformation back to r)

$$\int_{r_1}^{r_2}\left[2m\left(\epsilon'-\frac{\hbar^2 s^2}{2mr^2}-\frac{e^2H^2r^2}{8mc^2}\right)\right]^{\frac{1}{2}}dr=(n+\tfrac{1}{2})h\pi, \quad (3.5)$$

where r_1 and r_2 are the two positive zeros of the quantity under the square root, provided $r_2<R$. This condition yields

$$\epsilon'=(2n+|s|+1)\beta H, \quad (3.6)$$

and the energies are given by (2.5). Electronic states with these energy values are not significantly distorted by the container from the free-electron form, and they will be referred to henceforth as "bulk states." If, however, $r_1<R<r_2$, then the upper limit of integration is R, and it is evident that for given n and s, ϵ' will be increased over the value (3.6).[18] These states are appreciably distorted by the wall and will be called "surface states." We note that the quantum numbers n, s, and k_z and the spin orientation completely specify a single state, which according to the exclusion principle can be occupied by no more than one electron.

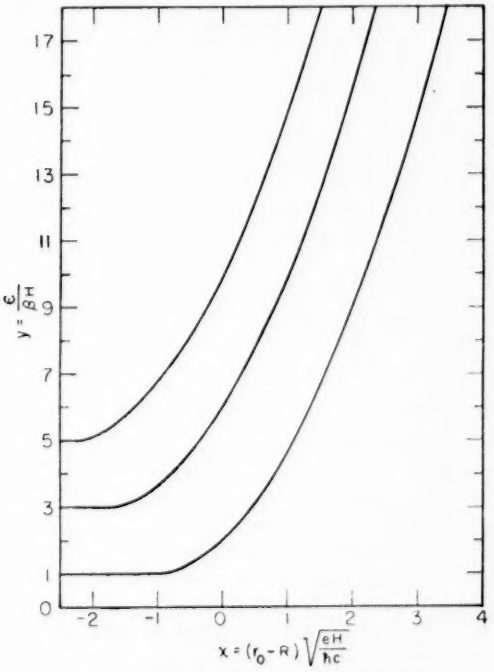

FIG. 1. Energy of surface states for $n=0, 1, 2$.

[17] R. E. Langer, Phys. Rev. **51**, 669 (1937).

[18] When the upper limit is R, the $(n+\frac{1}{2})$ in (3.5) is incorrect. For the present we will continue to use $(n+\frac{1}{2})$ here. The necessary corrections are discussed in Sec. IV.

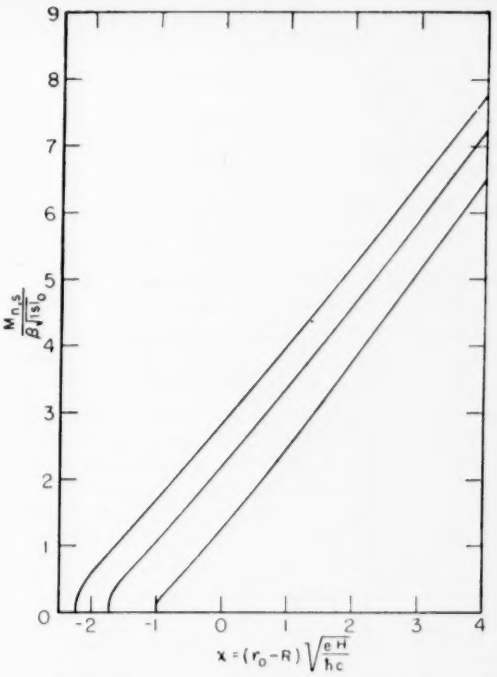

FIG. 2. Moment of surface states for $n=0, 1, 2$.

Evaluation of ϵ' in (3.5) for the surface states has been carried out, and the resulting "transverse energy" $\epsilon=E-\hbar^2k_z^2/2m$ is plotted in Fig. 1 for $n=0, 1, 2$. Details of this calculation may be found in reference 16 In plotting the figure we have changed the labeling o an electronic state from n, k_z, s to n, k_z, r_0, where $r_0=(2hc|s|/eH)^{\frac{1}{2}}$ is the radius at which the effective radial "potential" $v(r)=(\hbar^2s^2/2mr^2)+(e^2H^2r^2/8mc^2)$ appearing in (3.3) and (3.5) has its minimum. We notice that for a given n, states with r_0 smaller than a value depending on n and H are bulk states with energies given by (2.5).

The moment of a surface state is given by

$$M_{ns}=-(\partial\epsilon_{ns}/\partial H)_s =[-(\partial\epsilon_{ns}/\partial H)_{r_0}-(\partial\epsilon_{ns}/\partial r_0)_H(dr_0/dH)], \quad (3.7)$$

in which the second term is for surface states very much the larger. Since $(\partial\epsilon/\partial r_0)_H$ is positive, as is seen from Fig. 1, and (dr_0/dH) negative, the moment of a surface state is positive and very large compared to the moment of a bulk state. The relatively few surface states are thus able very nearly to cancel the large negative moment contributed by all the bulk states. M_{ns} is plotted in Fig. 2 for $n=0, 1, 2$. Here $|s|_0=eHA/hc$.

Calculation of the free energy and total moment using these surface states has been carried out for a container whose radius R is much larger than the classical orbit radius $R_c=(c/eH)(2m\zeta)^{\frac{1}{2}}$ of an electron moving in a plane perpendicular to the magnetic field

with energy equal to the Fermi energy ζ of the system. The details of the work are given in reference 16. The result shows that for $R \gg R_c$ the oscillatory part of the moment which accounts for the de Haas van Alphen effect for this model is correctly given by the usual formulas,[1-3] corrections being negligible. The steady part of the moment is found to be

$$M_s = -(0.02652)LR^2(2m/\hbar^2)^{\frac{1}{2}}\beta^{\frac{3}{2}}H\zeta^{\frac{1}{2}} - (0.02293)LR(2m/\hbar^2)\beta^{\frac{1}{2}}H^{-\frac{1}{2}}\zeta^{4/3}, \quad (3.8)$$

in which we neglect small temperature dependent corrections. The first term is the ordinary Landau moment, which dominates provided $R \gg (\zeta/\beta H)^{\frac{1}{2}}R_c$. The second term is a diamagnetic contribution due to the finite size of the container. Other corrections are very much smaller provided $R \gg R_c$. The numerical coefficients in (3.8) have been calculated for the simplified model of spinless electrons (for which no spin degeneracy exists). For a real electron gas we must multiply both terms in (3.8) by two to account for the twofold spin degeneracy of states even if we continue to neglect the contribution by the spin to the total moment. Inclusion of this moment further changes the coefficient of the first term in (3.8) from $2(-0.02652)$ to $4(0.02652)$—the usual Pauli paramagnetism. The second term is unchanged, spin corrections due to the surface states being small if $\zeta \gg \beta H$.

TABLE I. Numerical coefficient of the surface correction term [second term in Eq. (3.8) of text] for various values of the parameter α.

α	Coefficient
0.75	0.00763
0.70	−0.00047
0.65	−0.00770
0.60	−0.01378
0.55	−0.01896
0.50	−0.02293

The expression (3.8) for M_s agrees with the conclusion of Osborne and Steele that the system should show a surface diamagnetism which depends on container dimensions and magnetic field in the same way as the second term of (3.8). A surface correction of this form has also been predicted by Dingle,[4] but he has found that it should be paramagnetic. The origin of this discrepancy is discussed in the next section.

IV. CORRECTIONS FOR WALL THICKNESS

We remarked in a footnote[18] that for surface states the use of $(n+\frac{1}{2})$ in (3.5) is incorrect, yet we have used $(n+\frac{1}{2})$ in obtaining (3.8). The phase integral equation (3.5) with $(n+\frac{1}{2})$ is derived in WKB theory from the requirement that the phase of the oscillatory approximate wave function in the region between the turning points r_1 and r_2 be such that the wave function connects smoothly to a damped exponential in the classically forbidden regions beyond the turning points.[19] In the present problem we imagine our system bounded by a sharp, impenetrable wall at R—that is, we wish to impose the boundary condition $\psi(R)=0$. If the phase of the WKB wave function is chosen so that the wave function vanishes at one of the turning points, theory shows that $(n+\frac{3}{4})$ must replace $(n+\frac{1}{2})$ in (3.5); if the condition must be satisfied at both turning points, $(n+1)$ must be used, with $n=0, 1, 2, 3, \cdots$ as usual. This last form of (3.5) yields the correct eigenvalues for a one-dimensional electron in the potential $V(x)=0$ for $|x|<a$, $V(x)=\infty$ for $|x|>a$. The $(n+\frac{3}{4})$ form of (3.5) yields the exact eigenvalues for a similar problem with $V(x)=\infty$ for $x<0$, $V(x)=kx^2$ for $x>0$. Consequently, if we assume a sharp impenetrable wall in the present magnetic problem [$V(r)=0$ for $r<R$, $V(r)=\infty$ for $r>R$], then we should use $(n+\frac{3}{4})$ in (3.5) when calculating the energies of the surface states.

At first sight one would not expect this change to make much difference, since n is quite large for most of our electron states. However, we have calculated the magnetic moment by using the Poisson sum formula (Dingle I, Appendix) to carry out the sums over the quantum number n, and this formula depends critically on the choice between $(n+\frac{1}{2})$ and $(n+\frac{3}{4})$: with $(n+\frac{1}{2})$ we obtain (3.8); with $(n+\frac{3}{4})$ the correction term in (3.8) becomes paramagnetic. Specifically, the following form of the Poisson sum formula is readily proved:[16] if $0<\alpha<1$,

$$\sum_{n=0}^{\infty} f(n+\alpha) = \sum_{r=-\infty}^{\infty} e^{-2\pi i r\alpha}\int_0^{\infty} f(n)e^{2\pi i n r}dn. \quad (4.1)$$

In Table I we show the value of the coefficient of the second term in (3.8) obtained using various values of α. The value obtained using $\alpha=\frac{3}{4}$ agrees exactly with the coefficient of the leading term in Dingle's result for the surface correction (when our value is multiplied by two to include spin degeneracy).

Thus, the magnitude and sign of the surface corrections depend critically on the choice of α. The same is true of the value of the susceptibility at weak fields, $R \ll R_c$, calculated by Dingle,[4] for as may be seen from his derivation the coefficient of this term depends on the form of the Poisson sum exactly as does the coefficient of Table I. Using $\alpha=\frac{1}{2}$, we should thus obtain a paramagnetism roughly three times the magnitude of the diamagnetism Dingle reports.

For the idealized model using the sharp, impenetrable wall, there is no question but what we should use $\alpha=\frac{3}{4}$, as Dingle has done. However, for an approximate calculation of the susceptibility of the electrons in a real metal, the choice is not at all clear: the rise of potential at the wall is not infinitely sharp and is, moreover, of finite height, so that it is far from obvious that $\alpha=\frac{3}{4}$

[19] L. I. Schiff, *Quantum Mechanics* (McGraw-Hill Book Company, Inc., New York, 1949), p. 186.

is a good choice; yet the wall may be sufficiently sharp so that $\alpha=\frac{1}{2}$ is not sufficiently accurate.

To investigate the question of the best choice of α, we may compare the exact eigenvalues of certain one-dimensional problems with the eigenvalues obtained from a modified WKB phase integral in which α replaces the usual $\frac{1}{2}$ and is determined for each eigenstate such that the WKB eigenvalue agrees with the exact result. First, we consider the effect of having the surface potential barrier of finite height. For the potential

$$V(x)=\begin{cases}\infty, & x<-L\\ 0, & -L<x<0\\ W, & x>0\end{cases} \tag{4.2}$$

the wave function for $-L<x<0$ is, apart from a multiplicative constant, $\psi\sim\sin[k(x+L)]$, where

$$k=\hbar^{-1}(2mE)^{\frac{1}{2}},$$

and E is the energy eigenvalue. For $x>0$ and $E<W$, $\psi\sim e^{-\kappa x}$, $\kappa=\hbar^{-1}[2m(W-E)]^{\frac{1}{2}}$. The eigenvalue E is determined by equating the logarithmic derivatives $(1/\psi)(\partial\psi/\partial x)$ at $x=0$. This yields the equation for E:

$$k\cot(kL)=-\kappa. \tag{4.3}$$

For the WKB result we integrate

$$\int_{-L}^{0}(2mE)^{\frac{1}{2}}dx=(n+\alpha)h\pi, \quad n=0, 1, 2, \cdots \tag{4.4}$$

and obtain $kL=(n+\alpha)\pi$. We regard this as an equation for α, substitute it in (4.3), and obtain

$$\cot(\pi\alpha)=-\kappa/k=-[(W/E)-1]^{\frac{1}{2}}. \tag{4.5}$$

We thus obtain Table II. Here in addition to α we tabulate $\alpha'=\alpha-\frac{1}{4}$. In (4.2) the potential suffers an infinite jump at $x=-L$. Since in the problems mentioned earlier we reduce α by $\frac{1}{4}$ on replacing a sharp barrier by a slowly rising potential, it appears that α' would be a proper choice if in the potential (4.2) we made gradual the potential rise at $x=-L$.

We have also investigated the problem with the potential

$$V(x)=\begin{cases}\infty, & x<-L\\ 0, & -L<x<0.\\ \frac{1}{2}m\omega^2x^2, & x>0\end{cases} \tag{4.6}$$

The detailed calculations may be found in reference 16. The results are given in Table III.

Two other simple problems give further information concerning the proper choice of α in different situations. Table IV summarizes the results for the potential

$$V(x)=\begin{cases}W, & |x|>L/2\\ 0, & |x|<L/2\end{cases}, \tag{4.7}$$

and Table V summarizes those for

$$V(x)=\begin{cases}\frac{1}{2}m\omega^2x^2, & x>0\\ W, & x<0\end{cases}, \tag{4.8}$$

where $W\gg\hbar\omega$.

TABLE II. Tabulation[a] of the parameters α and α' for the one-dimensional potential $V(x)=\infty$, $x<-L$; $V(x)=0$, $-L<x<0$; $V(x)=W$, $x>0$, for various values of the ratio E/W.

E/W	α	α'
$\rightarrow 1$	$\rightarrow\frac{1}{2}$	$\rightarrow\frac{1}{4}$
$\frac{3}{4}$	$\frac{2}{3}$	5/12
$\frac{1}{2}$	$\frac{3}{4}$	$\frac{1}{2}$
$\frac{1}{4}$	$\frac{5}{6}$	7/12
$\rightarrow 0$	$\rightarrow 1$	$\rightarrow\frac{3}{4}$

[a] α is the parameter appearing in the WKB phase integral equation which brings the value of the energy eigenvalue E obtained by the WKB approximation into agreement with the exact value. Also $\alpha'=\alpha-\frac{1}{4}$.

The results of Tables II to V suggest the following behavior of α in the WKB evaluation of the eigenvalues of any differential equation which can be regarded as the Schrödinger equation for a one-dimensional electron confined by two potential barriers: if the barriers rise sharply and are of height W very much greater than the energy E of the eigenstate under consideration, then α is approximately unity; if one of the barriers is made to rise more gradually, α will be diminished somewhat, but it will not fall below roughly $\frac{3}{4}$; if the other barrier is similarly smoothed, α can be diminished further to about $\frac{1}{2}$; if the height W of one barrier is reduced so that E/W approaches unity, α will drop further by as much as about $\frac{1}{2}$; if the second barrier height is similarly reduced, α can drop by an additional $\frac{1}{2}$. The effect on α of making any one of these changes appears to be approximately independent of the other changes, so that the changes in α from these various alterations are roughly additive. It thus appears that if both barriers are gradual and if E/W is only slightly less than unity for both barriers, α can be as low as $-\frac{1}{2}$, provided, of course, that the eigenstate is not the one of lowest energy, since α must always be positive for this state to yield a positive zero-point energy.

In a real metal the energy difference between the Fermi level and the bottom of the conduction band is an appreciable fraction of the difference between the bottom of the band and the top of the surface barrier. We may crudely estimate the "sharpness" of the barrier in terms of Table III by representing the barrier by $\frac{1}{2}m\omega^2(r-R)^2$ and by defining ω in terms of the thickness of the wall region $(r'-R)$ and the Fermi energy ζ.

TABLE III. Tabulation of the parameter α for the one-dimensional potential $V(x)=\infty$, $x<-L$; $V(x)=0$, $-L<x<0$; $V(x)=\frac{1}{2}m\omega^2x^2$, $x>0$, for various values of the ratio $E/\hbar\omega$. For definition of α see footnote to Table II.

$E/\hbar\omega$	α
$\rightarrow\infty$	$\rightarrow\frac{3}{4}$
6	0.750
2	0.753
1	0.743
$\frac{1}{2}$	0.750
1/10	0.838
1/100	0.938
$\rightarrow 0$	$\rightarrow 1$

TABLE IV. Tabulation of the parameter α for the one-dimensional potential $V(x)=W$, $|x|>L/2$; $V(x)=0$, $|x|<L/2$, for various values of the ratio E/W. For definition of α see footnote to Table II.

E/W	α
$\to 1$	$\to 0$
$\frac{3}{4}$	$\frac{1}{3}$
$\frac{1}{2}$	$\frac{1}{2}$
$\frac{1}{4}$	$\frac{2}{3}$
$\to 0$	$\to 1$

Setting $\frac{1}{2}m\omega^2(r'-R)^2=\zeta$, we obtain

$$(\zeta/\hbar\omega)=\hbar^{-1}(r'-R)(\tfrac{1}{2}m\zeta)^{\frac{1}{2}}. \tag{4.9}$$

Using $\zeta\sim 10^{-12}$ erg, $(r'-R)\sim 10^{-8}$ cm, and the free-electron mass, we find $(\zeta/\hbar\psi)\sim 1/10$. From Table III we see that this gives us an intermediate value for α, especially since most occupied states have energies below ζ.

It appears from these considerations that for a given model of a real metal we might be able to satisfactorily estimate α as a function of the electron energy E. The calculation of the free energy and magnetic moment is not seriously complicated by the variation of α with E. A derivation based on Dingle's work is sketched in the Appendix, although no attempt is made to obtain a numerical result for any model. A numerical result will evidently depend on the details of the model chosen, and such a calculation would be of especial interest only when and if such size corrections to the susceptibility are located experimentally.

Finally we should remark that we obtain an additional term in the moment of the system if the wall potential is made gradual. To estimate this, we consider the potential

$$V(r)=\begin{cases}\frac{1}{2}m\omega^2(r-R)^2, & r\geqslant R\\ 0, & r\leqslant R\end{cases}. \tag{4.10}$$

Using the usual WKB analysis (see reference 16), we find that the ratio of this additional term to the usual surface term [the second term in (3.8)] is roughly $(eH/\omega mc)(\zeta/\beta H)^{\frac{1}{2}}$. Estimating ω from wall thickness as above, we find this to be about 10^{-2} or less for reasonable values of the parameters. We may thus infer that for any other form of wall potential confined to a sufficiently thin layer this contribution is negligible.

V. COMMENTS

The assumption has been tacitly made throughout this paper that the WKB approximation determines the energy eigenvalues with sufficient accuracy for the calculation of the surface corrections to the susceptibility. This assumption might be questioned in so far as it is well known that small errors in the eigenvalues can lead to a tremendous error in the calculated value of the susceptibility, and we have seen, moreover, that surface corrections depend critically in their numerical value and sign (though not in order of magnitude) on the choice of α in the WKB phase integral condition. However, the WKB calculation of the eigenvalues is very accurate when the quantum number n is large, as it is in the present problem for the vast majority of states. Moreover, although it is necessary to modify the WKB phase integral condition by choosing the value of $\alpha(E_p)$ appropriate to the given form of the surface potential, it appears from the one-dimensional problems studied above that this choice can be made in a consistent and predictable manner. It seems from these problems and from the procedure outlined in the appendix for calculating the susceptibility once $\alpha(E_p)$ is chosen that it should be possible to calculate the susceptibility for a given surface potential with accuracy of at least ten or twenty percent. Finally, it is reassuring that with the sharp, impenetrable wall $[\alpha(E_p)=\frac{3}{4}]$ Dingle has obtained the same results for small systems ($R\ll R_c$) using perturbation procedures with the exact zero-field wave functions[3] [Proc. Roy. Soc. (London) **A212**, 47 (1952)] that he has obtained with the WKB method.[4]

The author would like to express his sincere thanks to Professor Harvey Brooks for many stimulating discussions and valuable suggestions. This investigation was undertaken at Professor Brooks's suggestion, and the work reported in reference 16 was done in collaboration with him. The author would also like to thank Professor J. H. Van Vleck for reading the manuscript and discussing it with him, and Dr. M. F. M. Osborne and Dr. M. C. Steele for their comments.

APPENDIX

It is quite easy to modify Dingle's analysis[4] to take into account the variation of α with E. Instead of inquiring into the location of the zeros of the wave functions, as Dingle does, we determine the eigenvalues with the modified phase integral condition [from (3.5)]

$$n+1=1-\alpha(E_p)+\left(\frac{2m}{\pi^2\hbar^2}\right)^{\frac{1}{2}}\int_{r_1}^{r_2 \text{ or } R}\times\left[E_p-\beta Hs-\frac{\hbar^2s^2}{2mr^2}-\frac{e^2H^2r^2}{8mc^2}\right]^{\frac{1}{2}}dr. \tag{A1}$$

Here $E_p=E-\hbar^2k_z^2/2m$, the upper limit of integration is the smaller of r_2 or R, and the eigenvalues are determined by the condition that n be a positive integer or

TABLE V. Tabulation of the parameter α for the one-dimensional potential $V(x)=\frac{1}{2}m\omega^2x^2$, $x>0$; $V(x)=W$, $x<0$, for various values of the ratio E/W, where $\hbar\omega\ll W$. For definition of α see footnote to Table II.

E/W	α
$\to 1$	$\to \frac{1}{4}$
$\frac{1}{2}$	$\frac{1}{2}$
$\to 0$	$\to \frac{3}{4}$

zero. Temporarily confining our attention to two dimensions, as in Dingle's work, we find that the number of states with a given s, given spin orientation, and energies below any arbitrary value of E_p is the largest integer $[n+1]$ less than the quantity (in general not an integer) $(n+1)$ defined for that E_p by (A1). This is obtained from the Poisson sum formula exactly as in Dingle's analysis,

$$[n+1]=-\tfrac{1}{2}+\sum_{P=-\infty}^{\infty}\int_0^{(n+1)} e^{2\pi i\omega P}dx, \qquad \text{(A2)}$$

and $Z_p(E_p, H)$, the number of states in the two-dimensional system with energies below E_p, is then to sufficient accuracy obtained by inegrating over s and multiplying by two for spin degeneracy. We then follow Dingle exactly in transforming to three dimensions and obtaining $\int_0^E ZdE$.

When in (A1), for particular values of s and E_p, the larger turning point r_2 is less than R, the eigenstates with energies close to E_p are what Dingle calls "exponential states," or "bulk states" in our terminology. For these values of s and E_p, α is then $\frac{1}{2}$. For "surface states" or "trigonometrical states" (Dingle) for which which $r_1<R<r_2$, $\alpha(E_p)$ will depend on the form of the wall potential. It seems reasonable to assume that to sufficient accuracy it will depend only on E_p, and in particular not on s.

Evaluation of terms in $\int_0^E ZdE$ for exponential states is unchanged from Dingle's analysis. For the trig states, we replace Dingle's Eq. (3.4) by (A3), where we use his notation for ease of comparison except in replacing his $\sum_1^{P(E)}1$ by $[n+1]$, the same quantity,

$$[n+1]=\tfrac{1}{2}-\alpha(E_p)+\int_{x_-}^{\lambda}\frac{\{\eta^2x/\lambda-(l\pm x)^2\}^{\frac{1}{2}}}{2\pi x}dx + \sum_{P=-\infty}^{\infty}{}'\frac{\exp(2\pi iP[1-\alpha(E_p)])}{2\pi iP} \times\exp\left[2iP\int_{x_-}^{\lambda}\frac{\{\eta^2x/\lambda-(l\pm x)^2\}^{\frac{1}{2}}}{2x}dx\right]. \qquad \text{(A3)}$$

Dingle's calculations of the various integrals may now be used, and we obtain to replace his (3.19), (3.20), (3.21),

$$Z_p(E_p, H)=S'(E_p)(\eta\mp 2\lambda)^{\frac{1}{2}}/\eta^{\frac{1}{2}}, \qquad \text{(A4)}$$

$$S'(E_p)=(-\tfrac{1}{3})!S(E_p)/\pi(12)^{\frac{1}{2}}, \qquad \text{(A5)}$$

$$S(E_p)=2\sum_{P=1}^{\infty}P^{-5/3}\cos(2\pi P\alpha(E_p)+\pi/6). \qquad \text{(A6)}$$

The only change is thus to make S' and S dependent on E_p. Finally, defining $Q'(\eta)=S'(E)$, we obtain to replace Dingle's (3.22) and (3.23),

$$\int_0^E ZdE=-\frac{\pi h^2L\eta^{10/3}}{2mR^3}\mathbf{K}\left(\frac{2\lambda}{\eta},\eta\right), \qquad \text{(A7)}$$

$$-\tfrac{1}{2}\pi^2\mathbf{K}(a,\eta)=\int_0^1 Q'(\eta t)(t+a)^{\frac{1}{2}}t^{\frac{1}{2}}(1-t^2)^{\frac{1}{2}}dt + \int_a^1 Q'(\eta t)(t-a)^{\frac{1}{2}}t^{\frac{1}{2}}(1-t^2)^{\frac{1}{2}}dt. \qquad \text{(A8)}$$

We finally obtain for the low-temperature steady susceptibility [Dingle (6.5)] per unit volume

$$\chi=-(e^2R^{\frac{1}{2}}E_0^{\frac{1}{2}}/2^{\frac{1}{2}}m^{\frac{1}{2}}c^2h^{4/3})\{\mathbf{K}'(a,\eta_0)+\eta_0^{-\frac{1}{2}}\mathbf{J}'(a)\}, \qquad \text{(A9)}$$

where

$$\mathbf{K}'(a,\eta_0)=-(4/3\pi^2a)\left\{\int_0^1 Q'(\eta_0t)(t+a)^{-\frac{1}{2}}t^{\frac{1}{2}}(1-t^2)^{\frac{1}{2}}dt - \int_a^1 Q'(\eta_0t)(t-a)^{-\frac{1}{2}}t^{\frac{1}{2}}(1-t^2)^{\frac{1}{2}}dt\right\}. \qquad \text{(A10)}$$

The important oscillatory part of the susceptibility for $R>R_c$ is unchanged in this analysis since it arises from the exponential states alone. For $R\ll R_c$ the oscillatory susceptibility will depend on the choice of $\alpha(E_p)$.

Finally, we give in Table VI the values of $S(E)$ for various values of $\alpha(E)$.

TABLE VI. Tabulation of $S(E)$ as a function of the parameter $\alpha(E)$.[a] Values of $S(E)$ are in error by no more than 0.004.

$\alpha(E)$	$S(E)$	$\alpha(E)$	$S(E)$
0.00	3.678	0.50	−1.362
0.05	1.254	0.55	−1.126
0.10	0.204	0.60	−0.824
0.15	−0.496	0.65	−0.456
0.20	−0.986	0.70	−0.028
0.25	−1.312	0.75	0.456
0.30	−1.516	0.80	0.998
0.35	−1.608	0.85	1.592
0.40	−1.612	0.90	2.236
0.45	−1.522	0.95	2.934
		1.00	3.678

[a] $S(E)$ is defined in Eq. (A6) of the Appendix.

Magnetization in Nickel Ferrite-Aluminates and Nickel Ferrite-Gallates*†

LOUIS R. MAXWELL AND STANLEY J. PICKART
Naval Ordnance Laboratory, White Oak, Maryland
(Received August 25, 1953)

Trivalent aluminum and trivalent gallium have been substituted for trivalent iron in nickel ferrite $NiO \cdot Fe_2O_3$ to give the systems $NiO \cdot Fe_{2-t}Al_tO_3$ and $NiO \cdot Fe_{2-t}Ga_tO_3$, respectively, where t goes from 0 to 2. The materials, annealed and prepared in a powdered form, were homogeneous with the length of the edge of the unit cell decreasing linearly from 8.332A to 8.043A and 8.247A, for the aluminum and gallium substitution, respectively, as t varies from 0 to 2. In the case of the aluminum substitution, thermomagnetic curves were obtained of the types classified by Néel as Q; M_1, M_2, or P; and type R. The saturation magnetization extrapolated to 0°K (μ_0) for the nickel ferrite-aluminates decreases linearly with increase in t approaching zero in the region of $t=0.63$; for further increase in t, μ_0 increases to a maximum at about $t=1.0$ beyond which it decreases again to 0 at $t=2$. The increase in μ_0 is interpreted as an indication of a reversal in the direction of the resultant magnetization due to predominance of the magnetization of the ions on the A sites over those on the B sites. For the gallium substitution, the thermomagnetic curves follow the more conventional Q type with the appearance of the R-type curves for values of t from 0.63 to 1.5. As contrasted to the aluminates, the gallates show an increase in μ_0 with t, with a maximum developing in approximately the same region where the aluminates showed the crossover from B dominance to A dominance. The Curie temperatures decrease near-linearly with increase in t; the points for the aluminates and the gallates are so close together that they can be represented by one smooth curve. From an application of the Néel theory, it is indicated that the BB interaction is negative, both for the aluminates and the gallates, at least for values of t in the region 0.63 to 1.00.

I. INTRODUCTION

AN insight into the magnetic behavior of the ferrites can be gained by performing certain substitutions for the ferric ion. Michel and Pouillard[1] substituted Al^{3+} for Fe^{3+} in Fe_3O_4, and they found that both the Curie temperature and size of the unit cell decreased linearly with the amount of aluminum added until a point was reached where approximately one ion out of seven Fe^{3+} was replaced by one Al^{3+}; beyond this point, both the Curie temperature and size of unit cell remained constant. They concluded from this work that only a limited amount of aluminum can be held in solid solution with Fe_3O_4.

Thermomagnetic investigations of promoted, unreduced iron oxide catalysts were carried out by Maxwell, Smart, and Brunauer[2] on Fe_3O_4 containing up to about 35 mole percent of Al_2O_3. The Curie temperature remained constant with a reduction in the intensity of magnetization roughly proportional to the volume occupied by the Fe_3O_4 which indicated that the Al_2O_3 existed either as a separate phase or possibly in combination with FeO to form a ferrous aluminate.

Guillaud and Michel[3] have found a linear decrease in the saturation magnetic moment for magnetite with aluminum substituted until there was approximately 0.20 of an aluminum ion per molecule, presumably in solid solution. Although the authors state that their data is in agreement with the Néel theory,[4] the way in which this agreement is established is not clear because of the lack of sufficient information as to the distribution of the magnetic ions in the lattice.

The replacement of trivalent iron in Fe_3O_4 is complicated by the fact that the iron ion can go from the ferrous to ferric state rather easily by a simple transfer of an electron. It, therefore, is desirable to perform substitution experiments with a material having a more stable divalent ion.

Jones and Roberts[5] have carried out a series of substitutions of Fe^{3+} for Al^{3+} in magnesium ferrite ($MgO \cdot Fe_2O_3$). From thermomagnetic measurements they found that the saturation magnetization, at low temperature, decreased as Al^{3+} replaced Fe^{3+}, with a certain irregularity which they ascribed to heat treatment, until $MgAlFeO_4$ was reached which had a moment of about 0.3 Bohr magneton per molecule. The end points of this substitution series were investigated by neutron diffraction by Bacon and Roberts[6] who showed them to be

$$[Mg_{0.1}Fe_{0.9}]_A[Mg_{0.9}Fe_{1.1}]_BO_4$$

and

$$[Mg_{0.53}Fe_{0.47}]_A[Mg_{0.47}AlFe_{0.53}]_BO_4,$$

respectively, in agreement with the magnetic measurements and with earlier x-ray investigations by Greenwald[7] and Bertaut.[8]

Since the Al^{3+} ions apparently prefer to move into the B sites,[9] it is of interest to study such a substitution when the divalent ion has a magnetic moment as in the case of nickel ferrite ($NiO \cdot Fe_2O_3$). Because the nickel ferrite is inverted, we have a situation where

* This work was supported in part by the U. S. Office of Naval Research.
† Presented in part at the March Meeting (1953) of the American Physical Society [Phys. Rev. **91**, 206 (1953)].
[1] A. Michel and E. Pouillard, Compt. rend. **227**, 194 (1948).
[2] Maxwell, Smart, and Brunauer, J. Chem. Phys. **19**, 303 (1951).
[3] C. Guillaud and A. Michel, J. phys. et radium **12**, 65 (1951).
[4] L. Néel, Ann. phys. **3**, 137 (1948).
[5] G. O. Jones and F. F. Roberts, Proc. Phys. Soc. (London) **B65**, 390 (1952).
[6] G. E. Bacon and F. F. Roberts, Acta. Cryst. **6**, 57 (1953).
[7] Selma Greenwald, Naval Ordnance Laboratory Memorandum 10504, 1950 (unpublished).
[8] E. F. Bertaut, J. phys. et radium **12**, 252 (1951).
[9] E. J. W. Verwey and E. L. Heilmann, J. Chem. Phys. **15**, 174 (1947).

we expect that the aluminum ions will deplete the total magnetization arising from the ions in the B sites without a strong reduction in the intensity of magnetization of the ions in the A sites. As a result, a point should be reached where the intensity of magnetization of the magnetic ions on the B and A sites should be nearly equal and opposite so that the resultant magnetization of the material should approach zero—or similar to the antiferromagnetic state.

Trivalent gallium[10] has certain preferential tendencies for the tetrahedral interstices. It is listed by Verwey and Heilman[9] as one of the exceptions to a general rule laid down by them for the position of the trivalent and quadrivalent ions in accordance with the electrostatic requirements for minimum Coulomb energy. We will include in this paper the substitution of Ga^{3+} for Fe^{3+} in the nickel ferrite. The movement of Ga^{3+} to the tetrahedral interstices should mean an initial increase in the resultant magnetization. We, therefore, expect that in this substitution we would not reach a point where the magnetization from the B and A sites would be equal and opposite. An important point is the way in which Fe^{3+} and Ga^{3+} compete for the A sites.

II. PROCEDURE AND EXPERIMENTAL ARRANGEMENT

(a) Preparation of Materials

The materials used in this investigation are called the nickel ferrite-aluminates and nickel ferrite-gallates, defined by $NiO \cdot Fe_{2-t}Al_tO_3$ and $NiO \cdot Fe_{2-t}Ga_tO_3$, respectively. The parameter t was varied in steps ranging from 0 to 2, which covered the entire range from nickel ferrite to nickel aluminate ($NiO \cdot Al_2O_3$) and nickel gallate ($NiO \cdot Ga_2O_3$).

The substances were prepared following the procedures outlined by Harvey *et al.*,[11] using the oxides as the starting materials. The components were first mixed by the use of a ball mill containing a water slurry of the oxides. After the water was removed and the material ground in a mortar and pestle, it was heated to 1000°C for two hours, cooled, reworked, and heated a second time to 1000°C after the material has been passed through a 200-mesh sieve. The final heating carried the material up to a temperature of 1410°C for one hour. The cooling rate from this temperature was controlled, and in most instances was lowered at the rate of approximately 1° per minute. All of the heat treatments were carried out in air. It was found that platinum boats proved to be more suitable as containers for these materials than the usual oxide type boat.

(b) Intense Magnetic Field Solenoid

A high-current solenoid was constructed for this work to produce a field having a maximum strength of 8000 oersteds without using ferromagnetic materials. A diagrammatic sketch of the solenoid is shown in Fig. 1. The windings are 0.025-in. thick copper ribbons 0.875 in. in width wound concentrically with insulating glass cloth separating adjacent turns. The cooling was accomplished by inserting between each coil a circular water layer as illustrated in Fig. 1. An efficient labyrinth was devised so that the incoming cool water proceeded directly, after a few revolutions, to the inner diameter of the coil and then back out again, like a noninductive winding, to the exhaust without encountering any dead air pockets. The solenoid operates at a maximum current of 100 amperes at 300 volts.

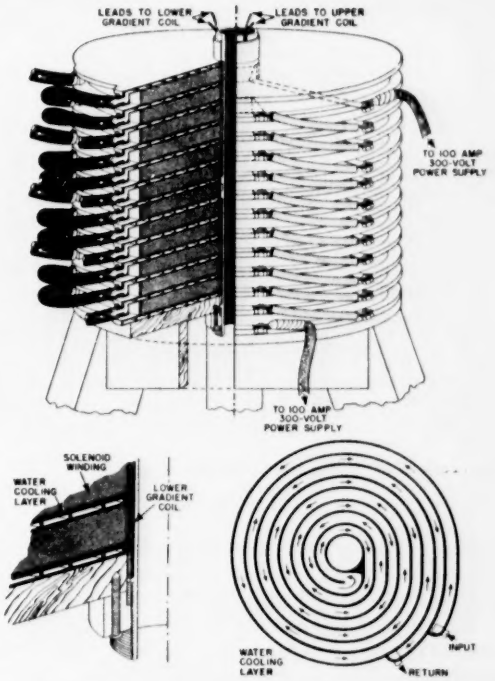

FIG. 1. Sketch of air core solenoid for producing intense magnetic fields. Dimensions of solenoid windings: length = 32.0 cm, inside diameter = 6.25 cm, outside diameter = 43.2 cm.

(c) Gradient Coils

A pair of opposing solenoid coils were mounted inside the large solenoid in such a way as to deliver at the center of the solenoid system a variable magnetic field gradient that is uniform over an appreciable volume. The nature of this gradient is illustrated in Fig. 2. It is seen that the resultant gradient is constant for a distance of 2 cm.

(d) The Method

We measure the intensity of magnetization of the specimen as a function of the applied field and the temperature of the material. This is accomplished by a

[10] F. Machatschki, Z. Krist. **82**, 348 (1932).
[11] Harvey, Hegyi, and Leverenz, R.C.A. Rev. **12**, 344 (1950).

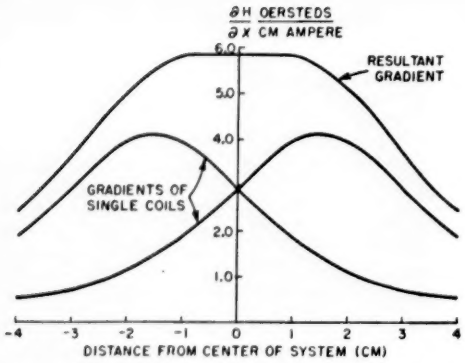

FIG. 2. Relationship between magnetic field gradient, produced by gradient coils (solenoid), as a function of distance. Distance between adjacent ends of coils = 3 cm; radius = 3 cm.

force method, using the following equation:

$$F = IV\partial H/\partial x, \tag{1}$$

where F is the force upon the specimen having an intensity of magnetization I, a volume V, in the presence of a magnetic field gradient of $\partial H/\partial x$.

We have, by this method, control of the force on the sample through the independent variation of the magnetic field and the magnetic-field gradient.

The way in which the force is measured is illustrated diagrammatically by Fig. 3. The specimen is suspended by a fine wire from a lever arrangement coupled to the winding of a Schaevitz differential transformer whose magnetic core is held in a fixed position. The output from this transformer varies linearly with the displacement of the winding with respect to the core at a usual sensitivity of 0.025 volt per 0.001-in. displacement. A recorder measures the signal output of the transformer. The force acting on the sample produces a small displacement of the transformer winding which appears as a deflection on the recorder. Although this is a deflection method, it is also, in effect, a null method because the displacements of the sample are so small—0.010-in. maximum for full-scale deflection—that over the region in which the specimen moves both the magnetic field and the gradient remain constant.

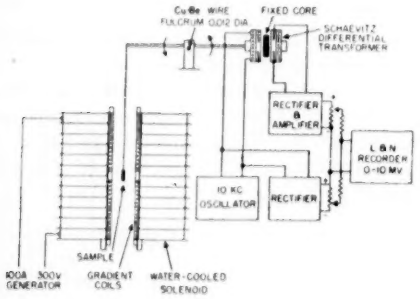

FIG. 3. Diagrammatic sketch of apparatus for measuring intrinsic magnetic moments.

The specimens were in a powdered form occupying a volume of 10 mm in length with a diameter of 1 mm. A piece of pure nickel (assumed to have a moment at 20°C of 0.57 Bohr magneton per atom)[12] of approximately the same size was used for calibration giving directly the deflections of the recorder in units of Bohr magnetons per molecule. The necessary furnaces and equipment for cooling the specimen are not shown in Fig. 3.

III. RESULTS

(a) Structure of Materials

Powder x-ray diffraction photographs showed, in all cases, a spinel structure whose length of edge of unit cell (a_0) varied in a linear fashion as shown by Fig. 4. The end points, corresponding to the nickel ferrite and nickel aluminate, are in essential agreement with previous values.[9] The size of the unit cell for all the intermediate points varied in a systematic manner. In no cases were there lines present due to the initial oxides that were used as starting materials.

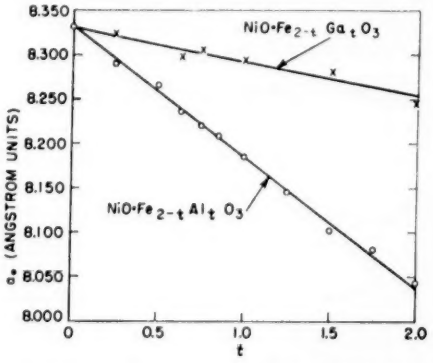

FIG. 4. Variation of unit cell size (a_0) with composition for $NiO \cdot Fe_{2-t}Al_tO_3$ and $NiO \cdot Fe_{2-t}Ga_tO_3$.

(b) Thermal Magnetization Data

The saturation magnetization (μ), sometimes called technical magnetization, was measured as a function of temperature, from liquid nitrogen temperature through the Curie temperature and beyond far enough to find any ferrimagnetism of the type predicted by Néel's N-type curve. The results are shown in Fig. 5 in a normalized form for both the aluminates and gallates; no N types were found in either series.

The way in which the saturation magnetization, extrapolated to absolute zero (μ_0), varies with the composition is shown in Fig. 6. Data are given for both quenched and annealed samples for both the aluminates and the gallates. The information on the aluminates has been expanded into three dimensions by a model

[12] R. M. Bozorth, *Ferromagnetism* (D. Van Nostrand Company, Inc., New York, 1951), p. 867.

illustrated in Fig. 7, which gives the relationship between the intensity of magnetization with respect to temperature and composition. The contour lines representing constant magnetization are illustrated for both positive and negative values.

The variation of Curie temperature with composition is illustrated in Fig. 8. The results for both of the systems studied can be represented by a single curve that departs slightly from linearity.

IV. DISCUSSION

The x-ray studies showed that the materials were in all cases homogeneous having the spinel structure. In the case of the aluminum substitutions the linear decrease in the size of the unit cell was expected since the trivalent radius of aluminum is 0.57A as compared to 0.67A the radius of Fe^{3+} as given by Goldschmidt. For the gallium substitution there was only a slight decrease with increasing amounts of gallium. This is explained by the fact that the radius of Ga^{3+} is very close to that of Fe^{3+}.

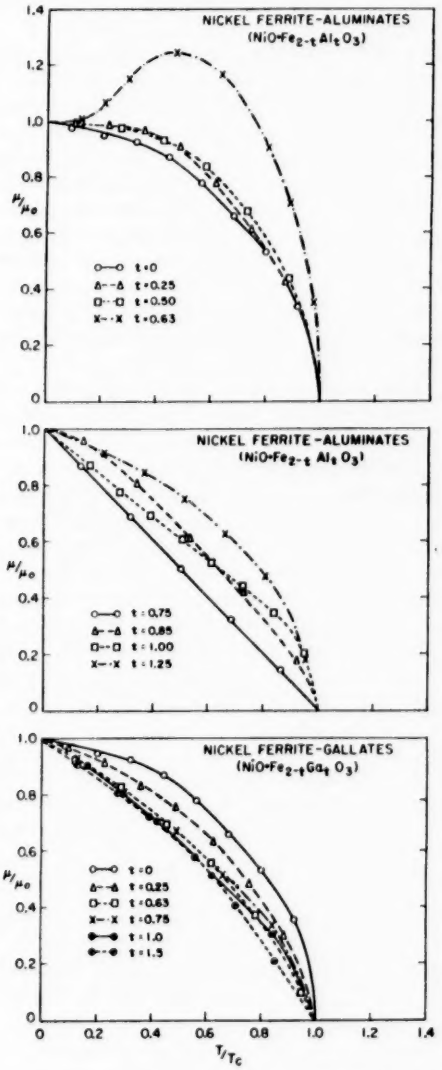

FIG. 5. Normalized thermomagnetization curves (annealed at 1°/min) for $NiO \cdot Fe_{2-t}Al_tO_3$ and $NiO \cdot Fe_{2-t}Ga_tO_3$.

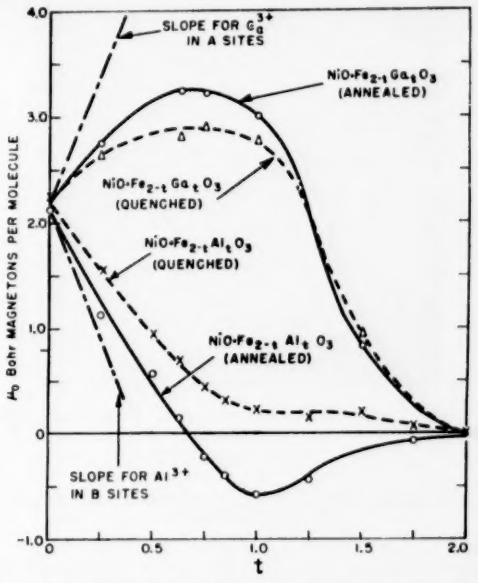

FIG. 6. Variation of μ_0 with composition for $NiO \cdot Fe_{2-t}Al_tO_3$ and $NiO \cdot Fe_{2-t}Ga_tO_3$ annealed at 1°/min, quenching carried out from 1410°C.

The thermomagnetization curves obtained for nickel ferrite-aluminate, as illustrated in Fig. 5, can be considered in terms of the Néel theory.[4] We have for the magnetizations M_a and M_b of the A and B lattice sites, respectively, for N magnetic ions (only one kind):

$$\begin{aligned} M_a &= \lambda N g\beta S B_S(g\beta S H_a/kT), \\ M_b &= \mu N g\beta S B_S(g\beta S H_b/kT), \end{aligned} \tag{2}$$

where λ and μ are the fraction of magnetic ions on the A and B sites, respectively; H_a and H_b are the effective fields acting on the magnetic ions in the A and B sites, respectively, which are expressed in terms of the molecular field coefficients (γ's) as

$$\begin{aligned} \mathbf{H}_a &= \mathbf{H}_0 + \gamma_{aa}\mathbf{M}_a - \gamma_{ab}\mathbf{M}_b, \\ \mathbf{H}_b &= \mathbf{H}_0 - \gamma_{ab}\mathbf{M}_a + \gamma_{bb}\mathbf{M}_b, \end{aligned} \tag{3}$$

where γ_{ij} is the Weiss molecular field coefficient for the interaction between the ions on the ith and jth sites. $B_S(\ )$ is the Brillouin function.

In the ferrimagnetic case we obtain the spontaneous magnetization ($H_0=0$) from Eqs. (2) and (3) in terms of the specific magnetization $\mathcal{y}_a$ and $\mathcal{y}_b$, given in terms

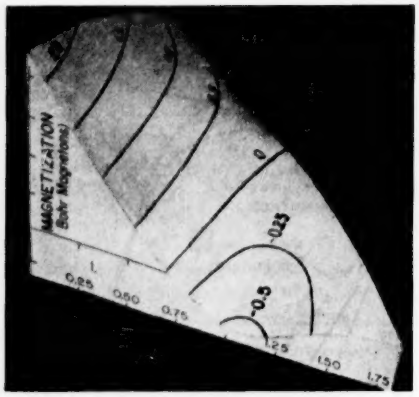

FIG. 7. Photograph of three dimensional model of the system nickel ferrite-aluminate. Temperature scale, not visible, starts from 0°K.

of the number of Bohr magnetons per molecule as

$$\begin{aligned} \mathcal{Y}_a &= B_S[(\tau/T)(\lambda\gamma_{aa}\mathcal{Y}_a - \mu\gamma_{ab}\mathcal{Y}_b)], \\ \mathcal{Y}_b &= B_S[(\tau/T)(-\lambda\gamma_{ab}\mathcal{Y}_a + \mu\gamma_{bb}\mathcal{Y}_b)], \end{aligned} \tag{4}$$

where $\tau = Ng^2\beta^2S^2/k$, with

$$\mathcal{Y}_a = M_a/\lambda Ng\beta S, \quad \mathcal{Y}_b = M_b/\mu Ng\beta S.$$

The net specific magnetization $\mathcal{Y}$ is given by

$$\mathcal{Y} = |\lambda\mathcal{Y}_a + \mu\mathcal{Y}_b|. \tag{5}$$

From this theory Néel has calculated $\mathcal{Y}$ as a function of the temperature and arranged the curves into various types according to their shapes. The classification is made in terms of the parameters α and β which are defined as follows:

$$\alpha = \gamma_{aa}/|\gamma_{ab}| \quad \beta = \gamma_{bb}/|\gamma_{ab}|.$$

The α's and β's give the strength and sign of the AA and BB interactions, respectively, in terms of the AB interaction.

In Fig. 5 we find certain types predicted by the above theory. In the case of the aluminates for t between 0 and 0.50, the curves follow the form we observed for ferromagnetic systems that are classified by Néel as Q curves. For $t=0$, we obtain a value of 2.20 Bohr magnetons per molecule for μ_0 in agreement with previous work.[13] When the amount of aluminum is increased by only a slight amount, to $t=0.63$, the magnetization increases with temperature like those curves predicted by Néel as his types M_1, M_2, or P. At $t=0.75$ the curve changes to nearly a straight line (Fig. 5) which holds approximately through to $t=1.00$. These curves are similar to those classified by Néel as type R which have been found to exist for zinc nickel ferrite and zinc manganese ferrite by Guillaud and Roux.[14] For greater amounts of aluminum, $t=1.25$, the curves return more nearly to the original form as for the nickel ferrite.

The increase in magnetization with increasing temperature found for the aluminates for $t=0.63$ is similar in shape to curves found by McGuire[15] for nickel chromite ($NiO \cdot Cr_2O_3$) and cobalt chromite ($CoO \cdot Cr_2O_3$).

In the present case, we have, instead of one type of magnetic ion, as developed by Néel, two of them which can occupy either or both the A or B sites; and, furthermore, one cannot assume that the g factor for a given magnetic ion will be the same in both the A and B sites. This imposes mathematical complexities, for Eqs. (2) through (5) would have to be modified accordingly before a detailed comparison with the theory could be accomplished. However, certain qualitative conclusions can be made.

Curves of the type R are represented on a β *vs* α plot by a restricted area whose position varies with the allowable values of λ and μ as shown by Fig. 9. We note that the area does not extend into positive values for β. This is the interpretation of the R-type curves for a system containing one kind of magnetic ion. We carry this interpretation to the present systems containing two kinds of magnetic ions on the assumption that they retain essentially the same features for the location of the R-type area on the β *vs* α plot (Fig. 9). This means that a negative BB interaction exists for those mixtures of the nickel ferrite-aluminate and nickel ferrite-gallate that give the R-type curves.

The R-type curves are constructed in Fig. 5 with a finite slope at absolute zero, although the lowest temperature at which these measurements were made was 75°K. Thermomagnetic measurements made on a zinc manganese ferrite (Ferroxcube III) by McGuire and Howard[16] at liquid helium temperature have shown a finite slope as the material is lowered in temperature to

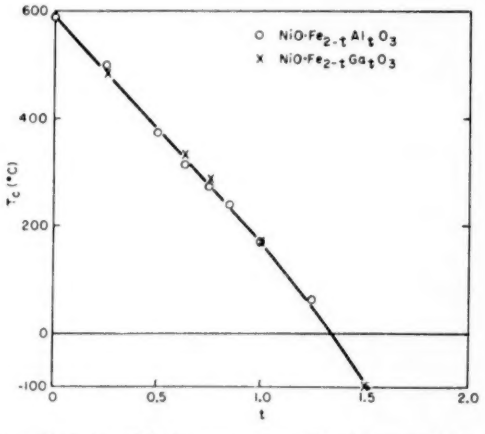

FIG. 8. Variation of Curie temperature (T_c) with composition for nickel ferrite-aluminates and nickel ferrite-gallates.

[13] See R. Pauthenet, Ann. phys. **7**, 710 (1952).
[14] C. Guillaud and M. Roux, Compt. rend. **229**, 1133 (1949); C. Guillaud, J. phys. et radium **12**, 239 (1951).
[15] T. R. McGuire (to be published).
[16] T. R. McGuire and L. N. Howard (to be published).

4°K. In view of the requirements of the third law of thermodynamics, we believe that in the region between 4°K and 0°K the curve for the zinc manganese ferrite bends over to zero slope at absolute zero. In the case of the present experiments, we are assuming that they also give a zero slope at absolute zero, with the departure from linearity occurring at a point near enough to 0°K as to give good values for the saturation magnetization by the methods used.

The way in which the saturation magnetization, extrapolated to absolute zero (μ_0), varies with composition, as shown by Fig. 6, indicates for the aluminates that the aluminum ions are going preferentially—but not entirely—into the B sites, thereby reducing the total magnetization as t varies from 0 to 0.63. For t from 0.75 to 2, μ_0 is plotted as negative, which gives a curve with no discontinuity in slope. At the crossover point we have found the situation where the magnetization of the ions in the A and B sites are equal in intensity but antiparallel. For greater amounts of aluminum, the magnetization from the A sites predominates; but as t increases further, the coupling weakens to that of a paramagnetic material at $t=2$. For the quenched samples, μ_0 decreases more slowly with increasing t in such a manner as to indicate that the B sites always predominate.

Gorter, Herbschleb, and Schulkes[17] have found data for the nickel ferrite-aluminate up to $t=1.0$ which is in agreement with our results shown in Fig. 6. The steepness of the curve as one approaches the crossover point depends upon the cooling rate—the less the rate, the steeper the curve until equilibrium is maintained throughout the cooling period. This fact was borne out by the work of Gorter, Herbschleb, and Schulkes[17] who were, we believe, the first to cool the material slowly enough to establish equilibrium conditions.

For the case of the gallates, starting from the nickel ferrite, the saturation moment increases indicating a preference of the gallium ions for the A sites, which results in a maximum at about the same place the aluminates pass through zero magnetization.

We find a Curie temperature of 590°C for the nickel ferrite (Fig. 8) without correcting for the effect of the applied field (4000 oersteds). This temperature is essentially in agreement with previous determinations.[18]

The Néel theory for the Curie temperature is expressed as follows:

$$T_c=\tfrac{1}{2}C\{\lambda\gamma_{aa}+\mu\gamma_{bb}+[(\lambda\gamma_{aa}-\mu\gamma_{bb})^2+4\lambda\mu\gamma_{ab}^2]^{\frac{1}{2}}\}, \quad (6)$$

where $C=Ng^2\beta^2S(S+1)/3k$. The way in which T_c varies with composition would be governed by changes in the coefficients λ and μ, after making certain modifications to allow for the fact that two separate magnetic ions are now involved as mentioned above. In view of this complexity, it is considered unlikely that a linear relationship would be observed. A slight departure from linearity for T_c has been found by Guillaud and Roux[14] for the zinc nickel ferrites as a function of the amount of zinc present.

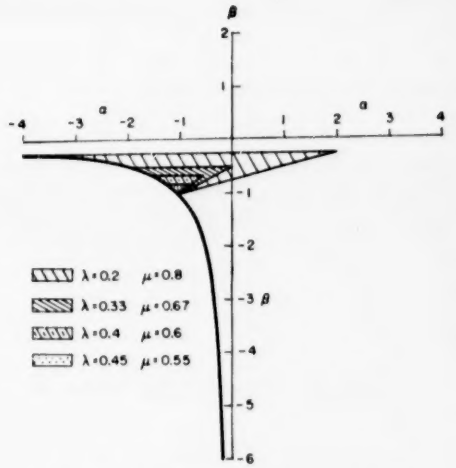

FIG. 9. Variation of Néel R-type area with magnetic ion distribution.

From the nature of our thermomagnetization curves, we observe that the exchange interactions, or the γ's, are certainly not identical for the aluminates and the gallates. It is, therefore, surprising that the Curie temperatures should be essentially the same, as a function of composition, for the aluminates and the gallates as shown in Fig. 8 in view of Eq. (6). Furthermore, one should expect a greater departure from linearity than we observe for the systems studied.

V. CONCLUSIONS

The substitution experiments replacing Fe^{3+} by Al^{3+} and Ga^{3+} furnish new significant facts concerning the magnetic behavior of ferrites as follows:

(a) Completely homogeneous nickel ferrite-aluminate and nickel ferrite-gallate systems can be prepared with a systematic linear variation in size of unit cell.

(b) The magnetic strength of the magnetic ions on the B and A sites can be varied relative to each other by the substitution of either Al^{3+} or Ga^{3+}, with a situation arising in the case of the aluminates where the magnetization on the B and A sites is equal and opposite.

(c) The case of the magnetization increasing with temperature, the Néel-type curves M_1, M_2, or P, is found for one of the nickel ferrite-aluminates ($t=0.63$).

(d) The R-type thermomagnetization curves predicted by Néel are found for certain nickel ferrite-aluminates and gallates.

(e) For the aluminates and gallates referred to in (d) above, it is concluded that the BB interaction is negative.

[17] Gorter, Herbschleb, and Schulkes (private communication).
[18] See Michel, Chaudron, and Bénard, J. phys. et radium **12**, 189 (1951).

(f) The Curie temperatures are found to depend upon the number of nonmagnetic ions substituted independent of the type and to follow nearly a linear decrease with increasing concentration of Al^{3+} or Ga^{3+}.

VI. ACKNOWLEDGMENT

The writers are indebted to Dr. J. Samuel Smart for his valuable discussions in regard to the Néel theory as it applies to the problem considered in this paper; to Dr. T. R. McGuire for his suggestion that we use nickel ferrite for this substitution work and his help in the design and construction of the magnetic solenoids; to Dr. Francis Bitter for suggesting the type of solenoid used for producing the intense magnetic fields; to Mr. R. W. Hall who assisted in the early phases of the work; and to Dr. Roald K. Wangsness for the idea of the three-dimensional model for studying these magnetic systems.

PHYSICAL REVIEW VOLUME 92, NUMBER 5 DECEMBER 1, 1953

An Augmented Plane-Wave Method for the Periodic Potential Problem. II*

M. M. Saffren and J. C. Slater
Massachusetts Institute of Technology, Cambridge, Massachusetts

(Received August 31, 1953)

It is shown that the augmented plane-wave method recently proposed can be given an alternative interpretation which leads to a much simpler analytical formulation. We join a plane wave of energy E_0 outside the spherical atoms continuously, but with a derivative which is discontinuous, to spherical solutions of Schrödinger's equation inside the spherical atoms, corresponding to an energy E, to be determined. We compute the expectation value of the energy for this combined wave function, consisting of contributions from the plane-wave region, the spherical atoms, and also a surface contribution from the surface of the sphere, since the discontinuous derivative is equivalent to an infinite Laplacian which integrates to a finite contribution over the sphere. We now regard E as a parameter, and vary it to make the expectation value of energy stationary. The resulting wave function is proved to be identical with that set up in Part (I). Furthermore, the energy E inside the spheres proves to be identical with the expectation value of the energy, so that our functions are exact solutions of Schrödinger's equation inside the sphere, but not outside the sphere, since the energy of the plane wave E_0 is different from E. However this discrepancy is just canceled in the expectation value of energy by the surface integral. The resulting formulas for energy and wave function are much more convenient to use then those in Part (I).

THIS note forms an extension to the paper by one of the authors,[1] outlining a method for fitting approximate solutions of a spherical Schrödinger equation within the atoms of a crystal onto a plane wave in the region between the atoms. The reader is assumed to be familiar with this paper, which we shall describe as (I). In Eq. (9) of (I) we have set up the expansion coefficients of the assumed function within the spherical atoms, corresponding to energy values given by Eq. (8) of (I). Both these equations contain infinite sums which would be hard to evaluate in practice. By noting the resemblance of these sums to the expansions of Green's functions in terms of eigenfunctions of Schrödinger's equation, it occurred to one of us (MMS) that these sums in Eqs. (8) and (9) could be rewritten in a closed form. In this note we state the resulting equations, and the simple physical interpretation which can be given them.

Outside the atoms, in a region whose potential energy is taken to be zero, we have a plane wave of propagation vector k, energy E_0. Let us now set up a solution of Schrödinger's equation inside the ith spherical atom, with energy E [so far undetermined, though later to be identified with the E of (I)]. We build up this solution from solutions of the Schrödinger equation for each l value, for the assumed E; let such a solution, regular at the origin of the ith atom, be $u_{il}(E;r)$. We can superpose such functions, with appropriate coefficients, to set up a function which is continuous with the plane wave at the surface of the sphere; in general, however, the derivative will be discontinuous at the surface. We can now compute the expectation value of the energy for the wave function consisting of the plane wave of energy E_0 outside the sphere, and the spherical solution of energy E inside the sphere. There will be contributions to the integral of the Hamiltonian function consisting of E_0 times the integral of the square of the amplitude of the plane wave outside the sphere, and E times the integral of the square of the spherical solution inside the sphere. These are not the only contributions, however: on account of the discontinuity of derivative on the surface of the sphere, the Laplacian, or kinetic energy, is infinite there, and integrates to a finite contribution over the surface of the sphere.

We can now show that the augmented plane-wave function as set up in (I) is just such a function as we have described, in which further the expectation value of the energy is identical with the value E for which we

* Work assisted by the U. S. Office of Naval Research.
[1] J. C. Slater, Phys. Rev. **92**, 603 (1953).

have a solution of Schrödinger's equation inside the sphere. In other words, our functions within the sphere are exact solutions of Schrödinger's equation, for an energy equal to the expectation value of the energy, and the discrepancy in expectation value of energy arising because the energy E_0 of the plane wave differs from E is exactly compensated by a contribution arising from the surface discontinuity. We can further show that if the value of E is varied, the expectation value of the energy is an extremum for just those values of E which we have just described, so that we can derive our functions from a variation principle, using E as the quantity to be varied.

It will be recognized that the method as described in this language has a close resemblance to that proposed in 1937 by one of the authors.[2] The difference is that in that earlier paper, the energy E of the solutions inside the spheres was carried as a parameter all through the calculation, including the secular equation involved in making a linear combination of augmented plane waves, and was finally constrained at the end of the calculation to equal the expectation value of energy for the linear combination of waves. This process proved in practice to be extremely difficult to carry out, and prevented the practical use of that method. The present method avoids this difficulty, and as will be apparent from the mathematical formulation to be presented, it is now very easy to get the energy values of the separate plane waves.

The statements which we have made about the present method can be easily verified, and lead to greatly simplified formulas to replace Eqs. (8) and (9) of (I). We proceed by expanding the functions $u_{il}(E;r)$ as series of the functions $u_{inl}(r)$ of (I). Those functions were solutions of the Schrödinger equation for such energies E_{inl} that the functions u_{inl} had the same logarithmic derivatives at the surface of the atomic sphere, $r=r_i$, as the corresponding spherical Bessel functions $j_l(kr)$ appearing in the expansion of the plane wave. The expansion coefficients c_{inl} in the expansion $u_{il}(E;r)=\sum(n)c_{inl}u_{inl}$ can be easily shown to be

$$c_{inl}=(2l+1)^{-1}4\pi r_i^2u_{inl}(r_i)u_{il}(E;r_i)(E_{inl}-E)^{-1}\times[d\ \ln u_{il}(E;r)/dr-d\ \ln j_l(kr)/dr]_{r=r_i}. \quad (1)$$

We can multiply these coefficients by $u_{inl}(r)$, and sum over n, obtaining a formula for $u_{il}(E;r)$. If we build up a sum of these functions inside the sphere, continuous with the plane wave outside, we have

$$a_0\exp(i\mathbf{k}\cdot\mathbf{R}_i)\sum(l)(2l+1)i^lP_l(\cos\theta)j_l(kr_i)\times u_{il}(E;r)[u_{il}(E;r_i)]^{-1}, \quad (2)$$

in the notation of (I). If we expand the functions $u_{il}(E;r)$ and $u_{il}(E;r_i)$ in terms of the u_{inl}'s, as described in Eq. (1), we can then immediately show that the expression (2) becomes identical with the wave function inside the sphere as derived in (I), which we find by multiplying the coefficients a_{inl} of Eq. (9) in (I) by the functions $u_{inl}(r)$, and summing over all values of n and l.

Next we consider the energy. It is immediately obvious how to compute the contributions of the plane wave, and of the spherical solutions, to the integral of the Hamiltonian operator over the wave function. As for the surface contribution, we note that the integral of the Laplacian kinetic energy operator over a thin spherical shell over which there is a discontinuity of normal derivative is $\int u[(du/dr)_1-(du/dr)_2]da$, where $(du/dr)_1$, $(du/dr)_2$, respectively, are the normal derivatives inside and outside the shell, and $\int da$ indicates integration over the surface of the sphere. Using this result, we find that the surface contribution to the integral of the energy can be written in the alternative forms:

$$a_0^*a_04\pi r_i^2\sum(l)(2l+1)j_l^2(kr_i)\times[d\ \ln u_{il}(E;r)/dr-d\ \ln j_l(kr)/dr]_{r=r_i} \quad (3)$$

or

$$a_0^*a_0\sum(l)(2l+1)^2j_l^2(kr_i)\times[\sum(n)u_{inl}^2(r_i)/(E_{inl}-E)]^{-1}. \quad (4)$$

The second term in the square bracket in (3) can be eliminated if we wish by using the relation $\sum(l)(2l+1)\times j_l(z)dj_l(z)/dz=0$, which can be proved from the properties of spherical Bessel functions.

When we add the three contributions to the energy integral, and use Eq. (10), (I), giving the normalization, we find that if we express everything in terms of the u_{inl}'s, our condition for the energy becomes identical with Eq. (8), (I). However, if we express the same thing in terms of the $u_{il}(E;r)$'s, we have the much simpler but equivalent formula

$$\Omega(E-E_0)=\sum(i,l)4\pi r_i^2(2l+1)j_l^2(kr_i)\times[d\ \ln u_{il}(E;r)/dr)]_{r=r_i}. \quad (5)$$

We can now use Eq. (5) to determine the energy E. This is a very simple formula to use, since we can plot the right side as a function of E, requiring only the logarithmic derivative of the function $u_{il}(E;r)$ on the surface of the sphere. This function has a resemblance to a cotangent curve, with an infinite number of branches. The intersections of this curve with the straight line $\Omega(E-E_0)$ give the required values of E. When these are determined the wave functions can be set up in terms of (2), and it is then a simple matter to calculate the matrix components of energy between different wave functions, required in setting up the secular equation for interaction of different augmented plane waves. Further properties of the method will be described later in connection with its application to specific cases.

It is interesting to see how the wave functions within the sphere, which were originally intended to join onto the plane wave continuously and with continuous derivative, have acquired a discontinuity of derivative

[2] J. C. Slater, Phys. Rev. **51**, 846 (1937).

at the surface of the sphere. Such a discontinuity is not present if we break off the series in n at a finite point, for each of the functions u_{inl} joins the plane wave with continuous slope. Superposition of the infinite number of functions introduces a discontinuity of slope, however, just as we know that a Fourier series can introduce such a discontinuity. The infinite series representation of the function inside the sphere cannot be differentiated at the surface of the sphere; its discontinuity of slope at the surface is related to the fact that it can be identified with a Green's function for Schrödinger's equation.

In the Appendix (the work of MMS), we shall show three things: that the slope of the function represented by the right side of Eq. (5) is always negative, verifying its resemblance to a cotangent curve, since it has asymptotes wherever one of the $u_{il}(E; r_i)$'s is zero, and goes monotonically from an infinite value at one asymptote to a negatively infinite value at the next; that our statement regarding the energy being an extremum as we vary E is true; and that the sums over n encountered in (I) are expressible in terms of Green's functions, the fact which led to the motivation of the present treatment, and which explains the discontinuity of slope.

APPENDIX

Let us define the quantity

$$\sum(i,l)4\pi r_i^2(2l+1)j_l^2(kr_i)[d\ \ln u_{il}(E;r)/dr]_{r=r_i}$$

as $f(E)$. It is this function which appears on the right side of Eq. (5). Comparison with Eq. (8), (I), shows that it can also be written in the form

$$f(E)=\sum(i,l)(2l+1)^2 j_l^2(kr_i) \times[\sum(n)u_{inl}^2(r_i)/(E_{inl}-E)]^{-1}.$$

Let us differentiate this expression with respect to E. Then we have

$$df/dE=-\sum(i,l)(2l+1)^2 j_l^2(kr_i) \times[\sum(n)u_{inl}^2(r_i)/(E_{inl}-E)^2] \times[\sum(n)u_{inl}^2(r_i)/(E_{inl}-E)]^{-2}. \quad (6)$$

Each term in (6) is a perfect square; thus we see that df/dE must be negative. Furthermore, by comparison with Eq. (10), (I), we can understand the significance of the quantity (6). That equation was the normalization relation; and we see that it can be written in the form

$$a_0^*a_0(-df/dE+\Omega)=1. \quad (7)$$

Hence we see that the contribution of the part of the wave function inside the spheres to the normalization equals $-a_0^*a_0 df/dE$, and the contribution of the plane wave is $a_0^*a_0\Omega$.

Next we can prove our theorem regarding the variation properties of the solution. Let us first set up the expectation value of the energy. The contribution of the spherical part of the solution is $a_0^*a_0(-Edf/dE)$, and of the plane wave $E_0a_0^*a_0\Omega$. From Eq. (3) or (4), the contribution of the surface discontinuity is $a_0^*a_0 f(E)$. If we write the total expectation value of energy, and eliminate $a_0^*a_0$ by use of (7), we have

$$\text{Energy}=(f-Edf/dE+E_0\Omega)(-df/dE+\Omega)^{-1}. \quad (8)$$

If we differentiate this expression with respect to E, denoting derivatives of f with respect to E by primes, the result is

$$f''[\Omega(E_0-E)+f](-f'+\Omega)^{-2}. \quad (9)$$

Our energy equation (5) is equivalent to setting $\Omega(E_0-E)+f=0$, so that we verify the statement that our procedure makes the expectation value of energy an extremum, when E is varied.

Finally we point out the relation between the series over n, which appear in Eqs. (8) and (9), (I), and in Eq. (4) of the present note, and Green's functions. For a given type of atom and for a given angular momentum we can subsume the two infinite series, taken over the index n, which appear in these equations, under the expression

$$(2l+1)G_{il}(x;\xi;E)/4\pi\xi x =\sum(n)u_{iml}(x)u_{inl}(\xi)/(E_{inl}-E). \quad (10)$$

This series is the expansion of a Green's function of the radial Schrödinger's equation in which the energy is to be regarded as a parameter. This Green's function $G_{il}(x;\xi;E)$ is determined through the condition that $G_{il}(x;\xi;E)/\xi x$ satisfy the same boundary conditions (for arbitrary ξ in the interval $(0, r_i)$ and for arbitrary energy) as do the u_{inl}.

As is well known, the Green's function is continuous with discontinuous slope at $x=\xi$. For the series we are interested in $\xi=r_i$ and $x=r$ is to the left of ξ. For these values, then, it can be shown that

$$G_{il}(r;r_i;E)=(r/r_i)u_{il}(E;r)[u_{il}(E;r_i)]^{-1} \times[d\ \ln u_{il}(E;r)/dr-d\ \ln j_l(kr)/dr]^{-1}. \quad (11)$$

The boundary condition at $r=r_i$ is satisfied by the value of $G_{il}(r;\xi;E)$ at $r=r_i$, and the slope of $G_{il}(r;\xi;E)$ taken with $r=r_i$ and ξ to the *right* of r. However, the function which represents our series takes on the slope of $G_{il}(r;\xi;E)$ with ξ to the *left* of r. Thus the series has the slope defined by $G_{il}'(r_i-0;r_i;E)$ which is different from $G_{il}'(r_i+0;r_i;E)$, which has the proper slope.

Electronic Energy Bands in Crystals*

THOMAS WAINWRIGHT AND GEORGE PARZEN
University of Notre Dame, Notre Dame, Indiana
(Received August 3, 1953)

In a previous paper, a variational principle was derived for the energy levels of a crystal. The variational principle was stated in terms of the Wannier functions of the crystal instead of the more usual Bloch waves. In this paper, the variational principle has been applied to two problems, to the one-dimensional cosine potential, and to the energy levels of the valence band of lithium. The method of forming the trial function is discussed. It was found more convenient to use the Wannier function in momentum space rather than in configuration space. In the lithium case, our results are compared with those obtained by the Wigner-Seitz spherical approximation.

I. INTRODUCTION

IN a previous paper[1] we have derived a variational principle for the energy levels of a crystal. The characteristic feature of this variational principle was that it was expressed in terms of the Wannier functions of the crystal instead of the more usual Bloch wave functions.[2] In this paper we will apply the variational principle to two problems. We shall treat the problem of an electron moving in a one-dimensional cosine potential. This problem has been treated in some detail by Slater,[3] and it is a problem for which the Wannier function has been explicitly calculated. We shall also calculate the energy levels of the valence band of lithium. This problem was chosen with the idea of testing the possible advantages of our method over other available methods. For this purpose, the choice of lithium has turned out to be not too fortunate. The reason for this is that for Li the method of orthogonalized plane waves, introduced by Herring,[4] seems to give quite good results with rather few parameters and our method is about equivalent in labor and accuracy to the method of OPW (abbreviation for orthogonalized plane waves) in this case. However, Li does serve very well as an illustration of the method and as an indication of which problems may find the method advantageous. We shall also compare our results with calculations based on the Wigner-Seitz spherical approximation.[5]

We would like to restate here our variational principle in the form that we have found most useful. All the properties of a particular energy band of a crystal are contained in a single function, the Wannier function, $U(x)$, of the band. From the Wannier function, we can compute the wave functions of the band according to the formula

$$\psi_k(x)=N^{-\frac{1}{2}}\sum_n \exp(ikx_n)U(x-x_n), \qquad (1.1)$$

where N is the total number of atoms in the lattice and x_n locates the atoms in the lattice. Having found $\psi_k(x)$, we can compute the energy levels $E(k)$ of the band by the equation

$$E(k)=\int dx\psi_k^*H\psi_k \Big/ \int dx\psi_k^*\psi_k, \qquad (1.2)$$

where H is the Hamiltonian of the crystal.

Thus from this point of view the entire problem is to calculate the Wannier function and we shall have all the information we require. To calculate the Wannier function we have the variational principle I, Eqs. (3.1) and (3.2). The Wannier function $U(x)$ is that function which minimizes the integral

$$I_0=\int dxU^*HU, \qquad (1.3a)$$

where U is restricted by the conditions

$$\int dxU^*U=1, \qquad (1.3b)$$

and

$$\int dxU^*D^nU=0, \quad n\neq 0. \qquad (1.3c)$$

The operator D^n is the displacement operator, $D^nf(x)=f(x+x_n)$.

In applying this variational principle it is difficult to find trial functions which satisfy all the side conditions (1.3c); that is, that $U(x)$ shall be orthogonal to $U(x-x_n)$ for all x_n different from zero. We shall therefore choose our trial function so that $U(x)$ and $U(x-x_n)$ are orthogonal for the smaller x_n, for the x_n to the nearest and next nearest neighbors say. For the larger x_n, the overlap between $U(x)$ and $U(x-x_n)$ becomes smaller as $U(x-x_n)$ is concentrated about the point x_n.

* Part of a thesis submitted in partial fulfillment of the requirements for the Ph.D. degree. This work was supported in part by the U. S. Office of Naval Research and the U. S. Atomic Energy Commission.

[1] G. Parzen, Phys. Rev. **89**, 237 (1953). This paper will be denoted by I. We shall use the same notation in the present paper. In describing general results we will use a one-dimensional notation, and we will go over to the three-dimensional notation when applying the general results to a particular problem.

[2] The same variational principle has also been derived by G. F. Koster, Phys. Rev. **89**, 67 (1953).

[3] J. C. Slater, Phys. Rev. **87**, 807 (1952).

[4] C. Herring, Phys. Rev. **57**, 1169 (1940).

[5] R. Parmenter, Phys. Rev. **86**, 552 (1952), has calculated the energy levels of Li using the method of OPW. However, as he did not use the Seitz potential and as his potential allowed him to compute only energy differences within the band, he was not able to make a complete comparison of his results with those based on the Wigner-Seitz spherical approximation.

The Wannier function $U(x)$ does not really fall off very rapidly as x becomes large. However the overlap between $U(x)$ and $U(x-x_n)$ seems to become smaller with increasing x_n more rapidly than the behavior of $U(x)$ would indicate. This is because $U(x)$ tends to have a node at the point x_n where $U(x-x_n)$ has its maximum.

Since in using the variational principle (1.3) for the Wannier function we shall not in general satisfy all the side conditions on $U(x)$, it would seem that we have thus lost one of the advantages of a variational principle, that our result for $E(k)$ will not be an upper bound for $E(k)$. This turns out not to be the case. If we take the Wannier function $U(x)$ that we calculate from the variational principle and calculate from it $\psi_k(x)$ according to Eq. (1.1), and then calculate the energy $E(k)$ according to Eq. (1.2), the $E(k)$ so calculated will still be an upper bound for the energy levels although the Wannier function we have used does not satisfy all the side conditions (1.3c).

This result may be understood as follows. Equation (1.2) is a variational principle for $E(k)$ and will give an upper bound on $E(k)$ provided $\psi_k(x)$ obeys the following two conditions. $\psi_k(x)$ must have the form of a Bloch wave, $\psi_k(x)=\exp(ikx)u(x)$, where $u(x)$ is periodic; this makes $\psi_k(x)$ orthogonal to all the other levels in the band in particular to those levels below the one being calculated. This requirement is guaranteed by the form of Eq. (1.1) without any restrictions on $U(x)$. The second condition is that $\psi_k(x)$ must be orthogonal to the wave functions of any lower band if there are any. This requirement is met if $U(x-x_n)$ is made orthogonal to the Wannier function of the lower band and the $U(x)$ we shall use shall be so constructed. Thus it is seen that it is not necessary for $U(x)$ to satisfy all the side conditions (1.3c) for Eq. (1.2) to give an upper bound for $E(k)$.

By substituting Eq. (1.1) into Eq. (1.2), we find the following variational result for $E(k)$ stated directly in terms of the Wannier function $U(x)$,

$$E(k)\leq\sum_s I_s \exp(ikx_s)/\sum_s \Delta_s \exp(ikx_s), \tag{1.4}$$

where

$$I_s=\int dx U^* H D^s U, \tag{1.5}$$

and

$$\Delta_s=\int dx U^* D^s U. \tag{1.6}$$

If our Wannier function $U(x)$ satisfied all the side conditions (1.3c), then we should have $\Delta_0=1$, $\Delta_s=0$ for $s\neq 0$. For the case of Li it turned out that enough of the side conditions were satisfied that Δ_s does have these values to the accuracy of the calculation.

We would like to remark that an important characteristic of the method is that it calculates the entire energy band and not each energy level separately. We must minimize just the one integral I_0 in contrast to, say, the method of OPW in which the energy integral must be minimized for each energy level that one desires to calculate.

II. APPLICATION TO THE COSINE POTENTIAL

In this section we will apply the variational principle to a one dimensional lattice; the atoms are located at the points $x_n=na$ and give rise to the potential

$$V(x)=V_0+2V_1\cos(k_1x), \tag{2.1}$$

where $k_1=2\pi/a$ defines the reciprocal lattice, and we make $V(0)=0$ by putting $V_1=-\frac{1}{2}V_0$.

We feel that this example may be instructive, as in choosing our trial functions we shall make certain assumptions as to the behavior of the Wannier function, which assumptions can be verified for the simple cosine potential.

We have adjusted the peak of the potential to correspond to the case which Slater[3] denotes by $s=1$. This corresponds to a weakly bound electron. For this problem we shall calculate the lowest band only and avoid the extra complications of the valence band.

In choosing our trial function, we have come to the conclusion that the Wannier function in momentum space is a considerably simpler function than the Wannier function in coordinate-space and has certain advantages which we will point out. Thus we will Fourier transform the Wannier function and introduce the function $b(k)$ defined by

$$U(x)=N^{-\frac{1}{2}}\sum_k b(k)\exp(ikx)/L^{\frac{1}{2}}, \tag{2.2}$$

where L is the length of the crystal.

In terms of $b(k)$ our side conditions (1.3b) and (1.3c) become

$$N^{-1}\sum_k |b(k)|^2\exp(ikx_s)=\delta_{s0}. \tag{2.3}$$

It is very often convenient not to have k range from $-\infty$ to $+\infty$, but to restrict k to varying over the lowest zone from $-\pi/a$ to $+\pi/a$. We can then write (2.3) as

$$N^{-1}\sum_{kn}|b(k-k_n)|^2\exp(ikx_s)=\delta_{s0}, \tag{2.4}$$

where it is understood that k ranges over the lowest zone only and we also sum over k_n, the vectors of the reciprocal lattice.

The integral we must minimize can be written in terms of $b(k)$ as

$$I_0=\frac{1}{N}\sum_{kn}\frac{\hbar^2}{2m}(k+k_n)^2|b(k+k_n)|^2 + \frac{1}{N}\sum_{knm}V_n b^*(k+k_n+k_m)b(k+k_m). \tag{2.5}$$

To evaluate $E(k)$ according to (1.2) we will need $\sum_s I_s \exp(ikx_s)$ which can be written

$$\sum_s I_s \exp(ikx_s)=\sum_n \frac{h^2}{2m}(k+k_n)^2|b(k+k_n)|^2 + \sum_{nm} V_n b^*(k+k_n+k_m)b(k+k_m). \quad (2.6)$$

The Wannier function in k space for the cosine potential has been considerably discussed by Slater.[3] We would just like to repeat here a few of his results. In Fig. 1 we have plotted the Wannier function in k space for the lowest band of a weakly bound electron, $s=1$, and for a strongly bound electron, $s=100$. It will be noted that for the weakly bound case, the Wannier function is different from zero only in the first few zones of k space. It is quite flat in the first zone and drops very sharply in the next zone. On the other hand the Wannier function of a strongly bound electron drops to zero very slowly and varies slightly within a zone.

For the valence bands the above behavior is complicated by the fact that the Wannier function must be orthogonal to the Wannier functions of the lower bands, which introduces further wiggles in the Wannier function. We shall see in the case of Li how the above behavior of the Wannier functions is maintained provided we subtract out the part that makes it orthogonal to the Wannier function of the lower band. This is the same trick as is used in the method of orthogonal plane waves by Herring.[4]

In this case, as we are calculating the lowest band, it is possible for us to construct a wave function that fulfills all the side conditions (2.3). Consider $b(k)$ in the lowest zone where k ranges from $-\pi/a$ to $+\pi/a$. In this region of k space, we can expand $b(k)$ in a Fourier series and write

$$b(k)=\sum_j a_{0,j}\exp(ikx_j). \quad (2.7)$$

We can break up k space into zones obtained by translating the lowest zone by k_n, and in each of these zones[6] express $b(k)$ as a Fourier series. Thus in the k_n zone,

$$b(k-k_n)=\sum_j a_{n,j}\exp(ikx_j). \quad (2.8)$$

In (2.8), and in all such similar formulas, k varies only over the lowest zone.

In terms of the new parameters $a_{n,j}$, our side conditions (2.4) become

$$\sum_j a_{n,j+s}{}^* a_{n,j}=\delta_{s0}, \quad (2.9)$$

where $a_{n,j}{}^*$ is the complex conjugate of $a_{n,j}$. It will be seen that it is possible to satisfy all the side conditions by just keeping a few of the parameters different from zero.

[6] We should like to point out that these zones are not identical with the Brillouin zones.

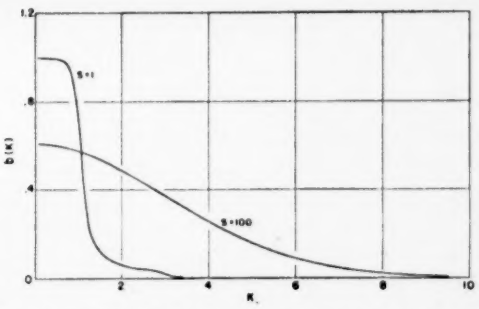

FIG. 1. The Wannier function for the lowest band of a weakly bound electron, $s=1$, and for a strongly bound electron, $s=100$, plotted in k space. k is measured in units of π/a. These curves are taken from Slater (reference 3).

We would like now to discuss a few of the simpler trial functions which arise from this Fourier series breakdown of the Wannier function in momentum space.

The simplest trial function is

$$b(k)=a_{0,0}, \quad (2.10)$$

and

$$b(k-k_n)=0 \quad k_n\neq 0,$$

where k ranges over just the lowest zone; that is, $b(k)$ is constant in the lowest zone and zero elsewhere.

For this trial function, the side conditions (2.7) reduce to $|a_{0,0}|^2=1$ and the parameter is fixed. This trial function is equivalent to the OPW method using just one plane wave.

A second trial function is

$$b(k)=a_{0,0}, \quad (2.11a)$$

$$b(k-k_{\pm 1})=a_{1,0}, \quad (2.11b)$$

and

$$b(k-k_n)=0, \text{ all other zones.} \quad (2.11c)$$

For this trial function, the side conditions (2.9) reduce to

$$|a_{0,0}|^2+2|a_{1,0}|^2=1. \quad (2.12)$$

Thus we have two parameters and just one condition, which leaves one parameter to vary.

A third trial function is

$$b(k)=a_{0,0}+a_{0,1}\exp(ikx_1) + a_{0,-1}\exp(ikx_{-1}), \quad (2.13a)$$

$$b(k-k_1)=a_{1,0}+a_{1,1}\exp(ikx_1) + a_{1,-1}\exp(ikx_{-1}), \quad (2.13b)$$

$$b(k-k_{-1})=a_{1,0}+a_{1,1}\exp(-ikx_1) + a_{1,-1}\exp(-ikx_{-1}), \quad (2.13c)$$

and

$$b(k-k_n)=0 \text{ all other zones.} \quad (2.13d)$$

To make $b(k)$ real, $a_{1,-1}=a_{1,1}{}^*$ and $a_{0,0}$ and $a_{1,0}$ are real. As $b(k)$ is even in the lowest zone $a_{0,1}$ is real. This leaves us with five parameters in (2.13). For this trial

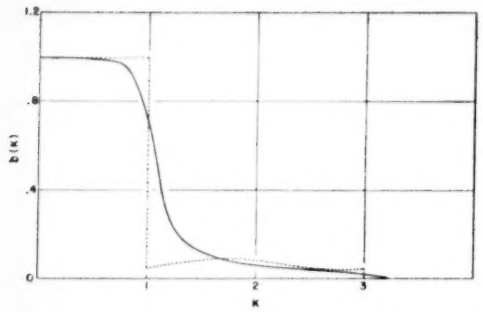

FIG. 2. Our calculated Wannier function compared with the exact Wannier function for the lowest band of cosine potential in the weakly bound $s=1$ case. The dashed curve is the calculated curve. k is measured in units of π/a.

function the side conditions become.

$$|a_{0,0}|^2+2|a_{1,0}|^2+2|a_{0,1}|^2+4|a_{1,1}|^2=1, \quad (2.14a)$$

$$a_{0,0}a_{0,1}+a_{1,0}(a_{1,1}+a_{1,-1})=0, \quad (2.14b)$$

and

$$a_{0,1}^2+a_{1,1}^2+a_{1,-1}^2=0. \quad (2.14c)$$

Thus we have five parameters and 3 conditions, leaving us two free parameters to vary.

This last trial function was used to compute the lowest band of the cosine potential for the weakly bound $s=1$ case.

In Fig. 2 we have compared the Wannier function we have calculated by minimizing I_0 using the trial function (2.13) with the exact Wannier function.[7]

In Fig. 3 we have plotted $E(k)$, which we calculated using the Wannier function found by minimizing I_0 and Eq. (1.4), and we have also plotted the exact $E(k)$. The agreement is good and our result is above the exact result as it should be. The agreement gets worse towards the top of the band, which seems to be a characteristic result of the method. This is probably due to the fact that the energy $E(k)$ near the top of the band becomes more sensitive to the behavior of $b(k)$ near the edge of the central zone.

We should remark that the method of orthogonalized plane waves using three plane waves and thus three parameters will give somewhat better results, particularly at the top of the band. This is due, in part, to the fact that in the OPW method we must minimize the energy integral for each energy level in the band we wish to find, whereas in the present method the minimizing process is carried out just once in for the entire band. Since I_0 can be shown to be the average energy level of the band, our results are probably best near the middle of the band.

We might add that for this one-dimensional problem the OPW method involves solving a third-order determinant, and minimizing the energy for each level in the band is no great hardship. Thus, for this problem, the OPW method seems the better. However in a problem where the number of parameters may become quite large, it seems to us that the present method may have considerable advantages.

[7] We would like to thank Dr. Slater for sending us a table of the exact Wannier function.

III. APPLICATION TO Li

For this calculation we used the Seitz potential[8] in order to be able to compare our results with those based on the Wigner-Seitz spherical approximation.

In this case we are calculating the valence band so our Wannier function must be orthogonal to the Wannier function of the lower 1s band.[9] Let $\varphi(r)$ be the 1s atomic wave function of the Seitz potential. If the 1s band is very narrow, then the atomic wave function is very nearly the Wannier function of the 1s band. We then write our Wannier function for the valence band as

$$U(\mathbf{r})=\mathcal{U}(\mathbf{r})-\sum_j c_j\varphi(\mathbf{r}-\mathbf{r}_j), \quad (3.1)$$

where $\mathbf{r}_j$, are the vectors of the lattice and the c_j are chosen so that $U(\mathbf{r})$ and $\varphi(\mathbf{r}-\mathbf{r}_j)$ are orthogonal. Thus

$$c_j=\int d\tau\varphi(\mathbf{r}-\mathbf{r}_j)\mathcal{U}(\mathbf{r}). \quad (3.2)$$

The c_j decrease with increasing $\mathbf{r}_j$ as the overlap between $\varphi(\mathbf{r}-\mathbf{r}_j)$ and $\mathcal{U}(\mathbf{r})$ gets smaller. For the case of Li, it was only necessary to include c_0, c_1, and c_2. c_1 is defined by (3.2), where $\mathbf{r}_1$ is the vector to one of the

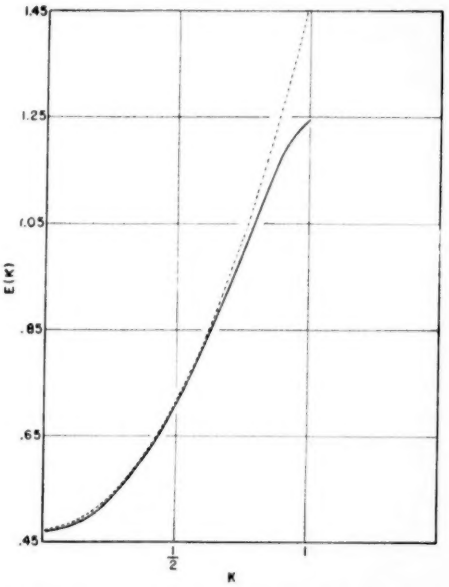

FIG. 3. The calculated $E(k)$ compared with the exact $E(K)$. The calculated curve is dashed. k is measured in units of π/a.

[8] F. Seitz, Phys. Rev. **47**, 400 (1935). We would like to thank Dr. C. Herring for sending us the corrected version of this potential.

[9] See reference 1.

nearest-neighbor atoms in the lattice and c_2 corresponds to a second-nearest neighbor.

We determined $\varphi(\mathbf{r})$ by numerical integration. The $1s$ level was found to have the energy[10] $E_{1s}=-5.352$ Ry.

In determining $\mathcal{U}(\mathbf{r})$, it seems more convenient to go over to momentum space as we did in the one-dimensional case. So we introduce the function $b(\mathbf{k})$ defined by

$$\mathcal{U}(\mathbf{r})=N^{-\frac{1}{2}}\sum_k b(k)\exp(i\mathbf{k}\cdot\mathbf{r})/\Omega^{\frac{1}{2}}, \tag{3.3}$$

where Ω is the volume of the crystal.

The integral we must minimize can now be written in terms of $b(\mathbf{k})$ as

$$I_0=\frac{1}{N}\sum_{\mathbf{kn}}\frac{\hbar^2}{2m}(\mathbf{k}+\mathbf{k}_n)^2|b(\mathbf{k}+\mathbf{k}_n)|^2 +\frac{1}{N}\sum_{\mathbf{knm}}V_n b^*(\mathbf{k}+\mathbf{k}_n+\mathbf{k}_m)b(\mathbf{k}+\mathbf{k}_m) -E_{1s}\sum_j|c_j|^2. \tag{3.4}$$

In (3.4) k ranges over the lowest zone in k-space; the sum over n or m is over $\mathbf{k}_n$ or $\mathbf{k}_m$, the vectors of the reciprocal lattice. The V_n are the Fourier coefficients of the potential,[11]

$$V(\mathbf{r})=\sum_n V_n\exp(i\mathbf{k}_n\cdot\mathbf{r}). \tag{3.5}$$

Our side conditions (1.3) now take the form

$$N^{-1}\sum_{\mathbf{kn}}|b(\mathbf{k}-\mathbf{k}_n)|^2-\sum_j|c_j|^2=1, \tag{3.6a}$$

and

$$N^{-1}\sum_{\mathbf{kn}}|b(\mathbf{k}-\mathbf{k}_n)|^2-\sum_j c_j^*c_{j+s}=0, \quad s\neq 0. \tag{3.6b}$$

We follow the same procedure as for the one-dimensional problem of breaking k space up into zones, and in each zone we expand $b(\mathbf{k})$ in a Fourier series. Thus we write in the $\mathbf{k}_n$ zone,

$$b(\mathbf{k}-\mathbf{k}_n)=\sum_j a_{n,j}\exp(i\mathbf{k}\cdot\mathbf{r}_j). \tag{3.7}$$

In terms of the new parameters $a_{n,j}$, our side conditions become

$$\sum_j a_{n,j+s}^*a_{n,j}-\sum c_{j+s}c_j=\delta_{s0}. \tag{3.8}$$

It is not easy in this case to satisfy all the side conditions (3.8) so we content ourselves with satisfying them for $\mathbf{r}_s=0$, for the $\mathbf{r}_s$ to the nearest neighbors and to the second-nearest neighbors.

In the trial function we used, we assumed $b(\mathbf{k})$ was different from zero only in the central zone of $\mathbf{k}$ space and in the 12 nearest-neighbor zones; and in each of these zones we expressed $b(\mathbf{k})$ as a Fourier series according to (3.7).

Our trial function was

$$b(\mathbf{k})=a_{0,0}+a_{0,1}\sum_{j'}\exp(i\mathbf{k}\cdot\mathbf{r}_{j'}), \tag{3.9a}$$

$$b(\mathbf{k}-\mathbf{k}_{n'})=a_{1,0}+a_{1,1}\sum_{j'}\exp(i\mathbf{k}\cdot\mathbf{r}_{j'}), \tag{3.9b}$$

and $b(\mathbf{k}-\mathbf{k}_n)=0$ in all other zones.

In (3.9) the $\mathbf{r}_{j'}$ are the 8 vectors to the 8 nearest neighbors in the lattice and the $\mathbf{k}_{n'}$ are the 12 vectors to the 12 nearest neighbors in the reciprocal lattice.

With this trial function, the side conditions become

$$a_{0,0}^2+12a_{1,0}^2+8a_{0,1}^2+96a_{1,1}^2=1+c_0^2+8c_1^2+6c_2^2, \tag{3.10a}$$

$$a_{0,1}a_{0,0}+12a_{1,0}a_{1,1}=c_0c_1+3c_1c_2 \tag{3.10b}$$

$$a_{0,1}^2+12a_{1,1}^2=\tfrac{1}{2}c_0c_2+c_1^2. \tag{3.10c}$$

These are just the side conditions up to the second-nearest neighbor, and we have neglected the c_j above c_2 which our results seem to justify. It is also necessary to compute c_0, c_1, and c_2 in terms of the $a_{n,j}$. This computation is done in Appendix I.

Subject to the side conditions (3.10) we must minimize the integral I_0 as given by (3.4). This integral can be written in terms of the $a_{n,j}$ as

$$\begin{aligned}I_0-E_{1s}=&a_{0,0}^2(\epsilon_0-E_{1s}+V_0)\\&+a_{0,1}^2 8(\epsilon-E_{1s}+V_0)\\&+a_{1,0}^2 12(\epsilon_0-E_{1s}+\hbar^2k_1^2/2m+V)\\&+a_{1,1}^2 96(\epsilon-E_{1s}+\hbar^2k_1^2/2m+V)\\&+a_{0,0}a_{0,1}16\epsilon_1+a_{0,0}a_{1,0}24V_1\\&+a_{1,1}a_{1,0}192\epsilon_1+a_{1,1}a_{0,1}192V_1.\end{aligned} \tag{3.11}$$

In (3.11) the ϵ_j are Fourier coefficients in the expansion for the $E(k)$ of a free particle,

$$\hbar^2k^2/2m=\sum_j\epsilon_j\exp(i\mathbf{k}\cdot\mathbf{r}_j). \tag{3.12}$$

The first five ϵ_j for a body-centered lattice are given in Appendix I. The quantity ϵ is defined as

$$\epsilon=\epsilon_0+3\epsilon_2+3\epsilon_3+\epsilon_6,$$

and

$$V=V_0+4V_1+2V_2+4V_3+V_4.$$

$\mathbf{k}_1$ is one of the vectors to a nearest neighbor in the reciprocal lattice.

For calculating $E(k)$ from (1.2) one needs $\sum_s I_s\times\exp(i\mathbf{k}\cdot\mathbf{r}_s)$, which can be written in terms of $b(\mathbf{k})$ as

$$\sum_s I_s\exp(i\mathbf{k}\cdot\mathbf{r}_s)=\sum_n\frac{\hbar^2}{2m}(\mathbf{k}+\mathbf{k}_n)^2|b(\mathbf{k}+\mathbf{k}_n)|^2 +\sum_{nm}V^n b^*(\mathbf{k}+\mathbf{k}_n+\mathbf{k}_m)b(\mathbf{k}+\mathbf{k}_m) -E_{1s}|\sum_s c_s\exp(i\mathbf{k}\cdot\mathbf{r}_s)|^2. \tag{3.13}$$

IV. RESULTS OF THE Li CALCULATION

In Table I, we have tabulated $E(k)$ in three directions in K space, the 100, 101, and 111 directions.

[10] It might be noted that the $1s$ wave function calculated here is not the true Li $1s$ wave function. It is the solution of the Seitz potential and has no direct physical significance.

[11] We found the V_n difficult to calculate for the Seitz potential, which is defined as spherically symmetric within each atomic polyhedron. This difficulty seems somewhat artificial to us, as the Seitz potential was devised with the idea of applying the Wigner-Seitz method for which it is convenient. We estimated the V_n as best as we could so that our results would be in error by at most 0.01 Rydberg.

TABLE I. The energy levels $E(k)$ for the valence band of Li as a function of k in the 100, 110, and 111 directions in k space. Atomic units are used.

100		110		111	
k	$E(k)$	k	$E(k)$	k	$E(k)$
0	−0.735	0	−0.735	0	−0.735
0.2	−0.703	0.2	−0.704	0.2	−0.704
0.4	−0.590	0.4	−0.596	0.4	−0.601
0.6	−0.371	0.6	−0.396	0.6	−0.415
0.8	−0.056	0.6816	−0.287	0.8	−0.135
0.9639	0.250			0.8348	−0.076

In Table II, we have compared several of our results with the corresponding results of previous calculations on Li. It might be noted that our result for the lowest level of the band $E(0)$ is −0.735 Ry, compared with −0.6635 Ry obtained by the Wigner-Seitz method and the value of −0.68 Ry obtained by Millman[12] using Slater's method. Since our result is obtained from a variational principle and it is the lower result, it is necessarily closer to the correct answer.

Our result for the width of the filled partition of the band is considerably larger than the Wigner-Seitz result. Soft x-ray measurements[13] indicate the width of the filled portion of the band to be 0.30±0.02 Ry.

It may be noted that though our values for $E(0)$ and ΔE differ by 0.07 Ry and 0.08 Ry from the Wigner-Seitz values, the results for the cohesive energy differ by only about 0.01 Ry/atom. The differences in $E(0)$ and ΔE cancel each other in computing the cohesive energy.

In conclusion, we think that in the case of Li our method has no advantages over the method of OPW and the two methods are about equivalent. However, for those cases where the method of OPW would require a large number of parameters, we feel our method may have some advantages. There is greater freedom in choosing the trial function and the number of undetermined parameters does not rise as quickly as it does in the OPW method. Also, our method treats the entire band at once and requires only one integral to be minimized, which should reduce the labor involved.

APPENDIX I

In this appendix we will calculate the c_j as defined by (3.2). More than one approach is possible. We chose to take advantage of the fact that the Wannier function of the 1s band is concentrated in a relatively small region compared to the size of the crystal cell. Let a_s be the radius of the 1s orbit and a the linear size of the crystal cell, then we shall find an expansion for c_j in powers of $(a_s/a)^2$. For lithium, a_s/a is about one-tenth.

In formula (3.2) for c_j, since $\mathcal{U}(\mathbf{r})$ varies slowly compared to $\varphi(\mathbf{r})$, we expand $\mathcal{U}(\mathbf{r})$ in a power series about $\mathbf{r}_j$ and obtain

$$c_j=\mathcal{U}(\mathbf{r}_j)\int d\tau\varphi(\mathbf{r})+\tfrac{1}{6}\nabla^2\mathcal{U}|_{r_j}\int d\tau\mathbf{r}^2\varphi(\mathbf{r})+\cdots. \quad \text{(A.1)}$$

Now replacing $\mathcal{U}(\mathbf{r})$ by its expression in terms of $b(\mathbf{k})$ and then in terms of the $a_{n,j}$, we get the result

$$c_j=\sum_n a_{n,j}(\alpha-k_n^2\beta^2)-\beta^2\sum_{n,s}a_{n,s}\epsilon_{s+j}, \quad \text{(A.2)}$$

TABLE II. $E(0)$ is the lowest level in the band; ΔE is the width of the filled portion of the band.

	$E(0)$ Ry	ΔE Ry	Cohesive energy kcal/mol	Effective mass m/m^*
Present method	−0.735	0.339	40.2	0.788
Wigner-Seitz[a]	−0.6635	0.258	35	0.727
Parmenter[b]		0.304		0.808

[a] The Wigner-Seitz type of approximation was first used by Seitz (reference 8) and was later improved by J. Bardeen [J. Chem. Phys. **6**, 367 (1938)] and by R. A. Silverman and W. Kohn [Phys. Rev. **80**, 912 (1950)].
[b] See reference 5.

where

$$\alpha=\Delta^{-3}\int d\tau\varphi(\mathbf{r}), \quad \text{(A.3)}$$

and

$$\beta^2=\tfrac{1}{6}\Delta^{-3}\int d\tau r^2\varphi(\mathbf{r}). \quad \text{(A.4)}$$

Δ is the size of the crystal cell. α and β were found by numerical integration. The ϵ_j are defined by (3.12). The first few ϵ_j for a body-centered lattice are, in units of h^2/ma^2,

$$\epsilon_0=3\pi^2/16, \qquad \epsilon_3=1/16,$$
$$\epsilon_1=-8/3\pi^2, \qquad \epsilon_4=8/45\pi^2,$$
$$\epsilon_2=-1/\pi^2, \qquad \epsilon_5=1/3\pi^2,$$

where a is one-half the edge of the cube that defines the body-centered lattice. $a=1.7246$ A^0 for Li.

[12] J. Millman, Phys. Rev. **47**, 286 (1935).
[13] H. W. B. Skinner, Repts. Progr. Phys. **5**, 257 (1938).

PHYSICAL REVIEW VOLUME 92, NUMBER 5 DECEMBER 1, 1953

Mechanism of Impurity Poisoning in the Luminescence of Zinc Sulfide Phosphors with Manganese Activator

RICHARD H. BUBE, SIMON LARACH, AND ROSS E. SHRADER
Radio Corporation of America, RCA Laboratories Division, Princeton, New Jersey

(Received August 28, 1953)

An investigation was made of the poisoning effects of iron, cobalt, and nickel impurity in cub.-ZnS:Mn phosphors. The parameters varied included: (1) proportion of manganese, (2) proportion of poison impurity, (3) photon energy of the exciting radiation, (4) intensity of the exciting radiation, and (5) operating temperature of the phosphor. Analysis of the results shows that the two most important poisoning mechanisms are: (1) dissipation by poison centers of energy absorbed by the host crystal before this energy has been used to excite activator centers, a mechanism relatively independent of the proportion of manganese and type of poison, and (2) dissipative interaction between activator and poison centers, a mechanism which depends strongly on the proportion of manganese and type of poison. The first mechanism predominates when the primary excitation is absorbed by the host crystal, whereas the second predominates when the activator centers are excited directly.

INTRODUCTION

THE poisoning of phosphors by the incorporation of small traces of certain impurities has been known for some time.[1] One of the authors[2] has reported detectable poisoning of the cathodoluminescence emission of cub.-ZnS:Ag phosphor by iron, cobalt, and nickel for 0.0001 percent of these impurities. The poisoning of zinc orthosilicate with manganese activator by iron impurity has been investigated by Nagy and Bodo.[3] Some of the poisoning effects of iron, cobalt, and nickel impurity in ZnS:Cu have been described by Arpiarian and Curie.[4]

There are at least three possible, essentially different, mechanisms for the poisoning effect of such impurities. (1) The centers formed by the poison impurity may be able to dissipate the energy absorbed by the host crystal, before this energy is transported to activator centers. (2) The centers formed by the poison impurity may interact with activator centers. The nature of this interaction will be discussed together with the experimental results of this paper. (3) The centers formed by the poison impurity may absorb either the exciting radiation or the luminescence emission and convert the energy nonradiatively.

In order to determine the relative importance of these three possible mechanisms, it is helpful to be able to selectively excite (1) by absorption by the host crystal, and (2) by absorption by activator centers directly. Luminescence associated with excitation by host-crystal absorption (hereafter called *HC* excitation) may be poisoned by any or all of the mechanisms mentioned above; luminescence associated with direct activator excitation (hereafter called *A* excitation) may be poisoned by only the last two mechanisms.

It has been reported[5] that the emission associated with manganese activator in ZnS:Mn phosphors can be excited (1) by host-crystal absorption, if the excitation energy is greater than 3.3 ev; or (2) by direct activator excitation, if the excitation energy is between 2.2 and 3.3 ev (four activator excitation peaks for ZnS:Mn being located at 2.45, 2.60, 2.87, and 3.12 ev).

This paper presents the results of measurements of the excitation efficiency of cub.-ZnS:Mn phosphors, as a function of both manganese and of poison (Fe, Co, and Ni) proportion. The results show that all three possible poisoning mechanisms are effective, their relative importance depending on the activator and poison proportions, and on the energy of the exciting radiation. Poisoning found for *A* excitation is primarily associated with interaction between poison and activator centers. Poisoning found for *HC* excitation is primarily associated with the dissipation by poison centers of the host-crystal energy before it has been transported to activator centers. Poisoning effects due to absorption by poison centers are important only for high proportions of poison impurity.

EXPERIMENTAL

Preparation of Materials

The phosphors used in this investigation were prepared from triple-purified, spectroscopically pure ZnS (RCA LM476). The proper proportions of manganese chloride and the chloride of the poison impurity were added with 2 percent of sodium chloride[6] as solutions in triple-distilled water. The phosphor mixes were dried at 110°C, and heated at 800°C for 20 minutes in a stationary atmosphere of purified nitrogen.

The use of an atmosphere of purified nitrogen is necessary to obtain reproducible results of excitation

[1] See, for example, H. W. Leverenz, *An Introduction to Luminescence of Solids* (John Wiley and Sons, Inc., New York, 1950), pp. 333–337.
[2] S. Larach, J. Chem. Phys. **18**, 896 (1950).
[3] E. Nagy and Z. Bodo, Acta Phys. Acad. Sci. Hung. **2**, 175 (1952).
[4] N. Arpiarian, Compt. rend. **233**, 387 (1951); N. Arpiarian and D. Curie, Compt. rend. **234**, 75 (1952).
[5] R. H. Bube, Phys. Rev. **90**, 70 (1953).
[6] All proportions are given in weight percent.

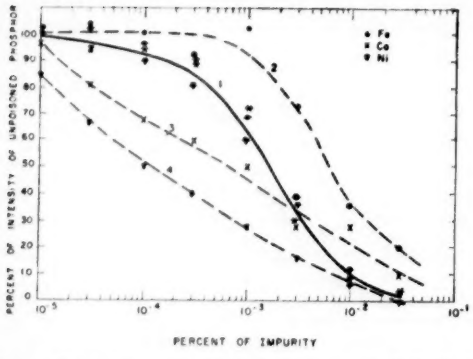

FIG. 1. The relative excitation efficiency of cub.-ZnS:Mn(1.0) phosphors as a function of various poison proportions. (1) Fe, Co, Ni impurity (experimental points with horizontal crossbar) for excitation by host-crystal absorption. (2) Fe impurity for activator excitation. (3) Co impurity for activator excitation. (4) Ni impurity for activator excitation.

efficiency for *A* excitation. The efficiency for *A* excitation is extremely sensitive to the presence of oxygen in the preparation atmosphere. Compared to a ZnS:Mn (1.0) phosphor prepared in purified nitrogen, a ZnS:Mn(1.0) phosphor prepared in an atmosphere of 88 percent nitrogen and 12 percent oxygen had 75 percent of the efficiency for *HC* excitation, but only 6 percent of the efficiency for *A* excitation. These results are similar to those previously reported,[5] which showed that the photoexcitation efficiency of ZnS:Mn phosphors, especially for radiation absorbed by the activator directly, is very dependent on whether the manganese is added as the chloride or the nitrate.

Measurements

The excitation source for the measurement of excitation spectra was a 500-mm Bausch and Lomb grating monochromator with incandescent light source. The emission of the phosphor was detected with a 1P21 phototube through a Corning 3480 filter. The photocurrent was passed through a Leeds and Northrup micromicroampere amplifier, and could be read directly or recorded on a Leeds and Northrup X-Y recorder.

Measurements of diffuse reflectivity were obtained with a multiple reflection method previously described,[6] using a $MgCO_3$ integrating sphere, and detecting the reflected light with a recording grating spectroradiometer, to be described in a future publication.

Measurements of luminescence emission intensity as a function of operating temperature were made with the apparatus described in previous investigations.[7] The excitation source was an incandescent lamp with Corning 5860 filter for host-crystal excitation, and with Wratten 47 and Farrand 4730A filters for activator excitation.

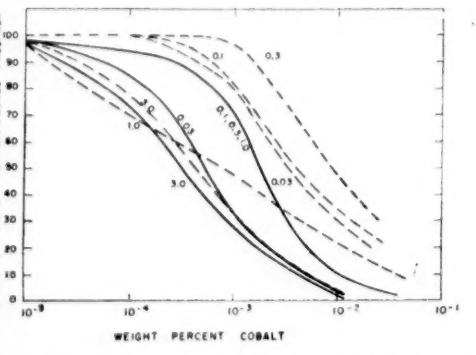

FIG. 2. The relative excitation efficiency of cub.-ZnS:Mn:Co phosphors as a function of the Co proportion, for various Mn proportions. Solid curves are for excitation by host-crystal absorption; dashed curves are for direct activator excitation. Numbers on the curves indicate the Mn proportion.

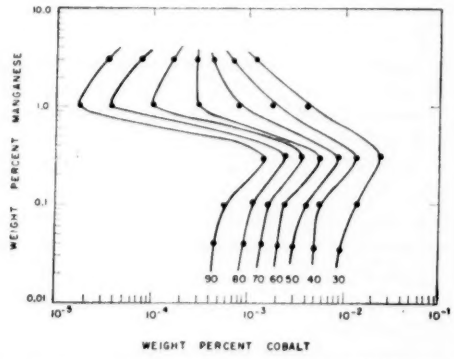

FIG. 3. Equal-poisoning contours for cub.-ZnS:Mn:Co phosphors as a function of Mn and Co proportions. The number below each curve is the percent of the intensity of the unpoisoned phosphor.

RESULTS

Excitation Efficiency as a Function of Mn and Poison Proportion

The data obtained from measurements of excitation efficiency are given in Figs. 1 through 5.[8] Figure 1 gives the relative excitation efficiency for cub.-ZnS:Mn(1.0) as a function of the proportion of Fe, Co, and Ni impurity. Experimental points are included in this figure to indicate the reliability of the data. Poisoning found for *HC* excitation is approximately the same for Fe, Co, and Ni; poisoning found for *A* excitation is markedly different for the different poisons.

Figure 2 gives the relative excitation efficiency for cub.-ZnS:Mn phosphors as a function of the proportion of Co, for proportions of Mn between 0.03 and 3 percent. Poisoning found for *HC* excitation is independent of the Mn proportion between 0.1 and 1.0 percent Mn; poisoning found for *A* excitation is markedly dependent on the Mn proportion over the same range. Figure 3

[7] R. H. Bube, Phys. Rev. **80**, 655 (1950).

[8] For these figures, *HC* excitation is by 3.65-ev ultraviolet; *A* excitation is by 2.60-ev light.

is a replot of Fig. 2, showing lines of equal poisoning as a function of Mn and Co proportions.

Figures 4 and 5 are the results for Fe impurity, equivalent to Figs. 2 and 3 for Co impurity. Again it is found that poisoning for *HC* excitation is independent of Mn proportion between 0.1 and 1.0 percent, whereas poisoning for *A* excitation is very dependent on the Mn proportion over this same range. A comparison of the equal-poisoning plots of Figs. 3 and 5 shows a similarity of contour between them. Fair quantitative agreement on poisoning is obtained if the poisoning for a phosphor with x-percent Mn by y-percent Fe is compared with the poisoning for a phosphor with $3x$-percent Mn by $(y/6)$-percent Co.

As detailed measurements have not been made for Ni as for Fe and Co impurity, but poisoning caused by Ni seems similar to poisoning caused by Co.

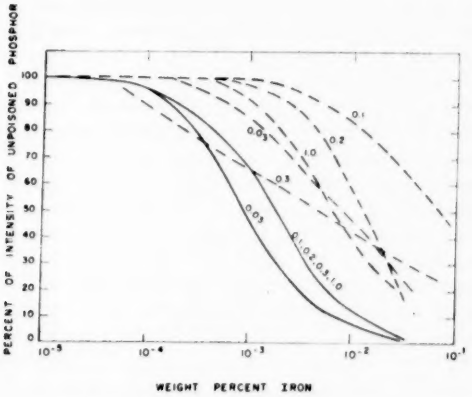

FIG. 4. The relative excitation efficiency of cub.-ZnS:Mn:Fe phosphors as a function of the Fe proportion, for various Mn proportions. Solid curves are for excitation by host-crystal absorption; dashed curves are for direct activator excitation. Numbers on the curves indicate the Mn proportion.

Reflectivity

Reflectivity spectra are given in Fig. 6 for phosphors without Mn and with 0.03 percent of each of the poison impurities, and for phosphors with 1.0-percent Mn and also 0.03 percent of each of the poison impurities. These spectra are compared with the reflectivity of a phosphor with 1.0-percent Mn only. It is found that (1) the absorption of phosphors containing Fe is very similar to that of phosphors containing Co, the absorption of phosphors with Fe or Co impurity being considerably less than for phosphors with Ni impurity; (2) the absorption by Fe or Co impurity in ZnS without Mn is small over most of the range of absorption by Mn centers; and (3) the absorption of ZnS:Mn phosphors in the range of absorption by Mn centers is increased by the incorporation of Fe, Co, or Ni.

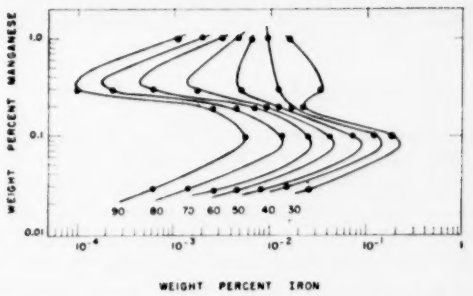

FIG. 5. Equal-poisoning contours for cub.-ZnS:Mn:Fe phosphors as a function of Mn and Fe proportions. The number below each curve is the percent of the intensity of the unpoisoned phosphor.

Poisoning as a Function of Excitation Energy

The data given in Figs. 1 through 5 for particular values of the excitation energy are equally valid for all other values of the excitation energy for the same type of excitation. If the exciting radiation has an energy less than about 2.9 ev, excitation is predominantly by activator absorption, and the variation of excitation efficiency with poison proportion is that found for *A* excitation. If the exciting radiation has an energy greater than about 3.2 ev, excitation is predominantly by host-crystal absorption, and the variation of excitation efficiency with poison proportion is that found for *HC* excitation.

The lack of dependence of excitation efficiency on excitation energy was checked particularly for cub.-ZnS:Mn(1.0):Ni phosphors since the absorption of these phosphors is a rapidly varying function of excitation energy in the range of Mn absorption. No

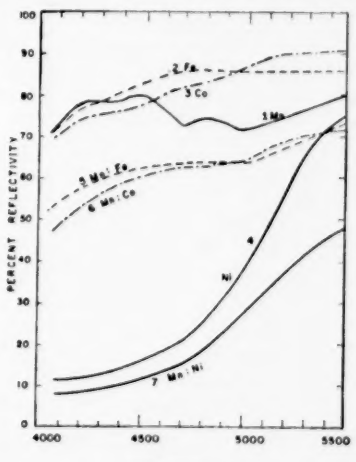

FIG. 6. Diffuse reflectivity spectra for cub.-ZnS phosphors with (1) 1.0 percent Mn; (2) 0.03 percent Fe; (3) 0.03 percent Co; (4) 0.03 percent Ni; (5) 1.0 percent Mn and 0.03 percent Fe; (6) 1.0 percent Mn and 0.03 percent Co; and (7) 1.0 percent Mn and 0.03 percent Ni.

difference in poisoning was found for excitation energies ranging from 2.25 to 2.7 ev (4600–5500A).

Poisoning and the Emission Spectrum

Because of the possibility that the emission spectrum of a ZnS:Mn phosphor might be altered if the poison impurity absorbed in the spectral region of the luminescence emission, emission spectra of cub.-ZnS:Mn(1.0):Ni(0.0003) (a phosphor with only 40 percent of the emission intensity of an unpoisoned cub.-ZnS:Mn(1.0) phosphor) were measured for excitation energies of 3.95 and 2.65 ev. (The path of the emission resulting from 2.65-ev excitation would be considerably longer in the material than the path of the emission excited by 3.95-ev ultraviolet.) No differences were found between the spectra of the emission obtained for this poisoned phosphor, which were the same as spectra obtained for an unpoisoned phosphor.

Emission Intensity as a Function of Excitation Intensity

In order to test the possible dependence of measurements of excitation efficiency on excitation intensity, measurements were made of the excitation efficiency of cub.-ZnS:Mn(0.3):Fe as a function of the Fe proportion for excitation intensities varying by a factor of fifty. The excitation intensity used for the data of Fig. 4 was intermediate in this range. No differences in poisoning were found, either for *HC* excitation or for *A* excitation.

As an additional check, the emission intensity of cub.-ZnS:Mn(1.0):Ni(0.001), cub.-ZnS:Mn(1.0):Co(0.003), cub.-ZnS:Mn(1.0):Fe(0.01), and cub.-ZnS:Mn(0.3):Co(0.01), were measured as a function of excitation intensity. A linear relationship between intensity and excitation intensity was found for excitation intensities varying by a factor of three thousand.

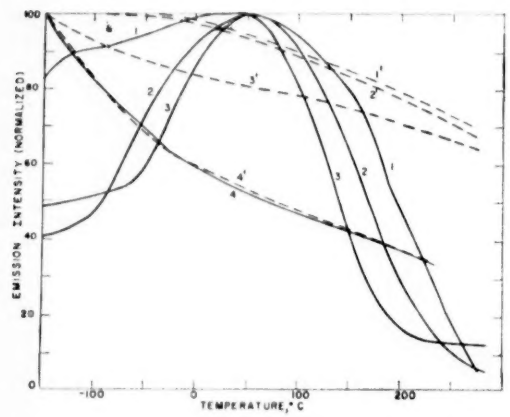

FIG. 7. Emission intensity of cub.-ZnS:Mn(1.0):Co phosphors as a function of operating temperature. Solid curves are for excitation by host-crystal absorption; dashed curves are for direct activator excitation. (1) and (1′) 0.00001 percent Co; (2) and (2′) 0.001 percent Co; (3) and (3′) 0.003 percent Co; (4) and (4′) 0.03 percent Co.

Emission Intensity as a Function of Temperature

Measurements of the emission intensity as a function of operating temperature were made for cub.-ZnS:Mn(1.0):Co phosphors for 0.00001, 0.001, 0.003, and 0.03 percent of Co, for both *HC* excitation and for *A* excitation. The data are given in Fig. 7. A marked difference in curve shape with type of excitation is found[8] for all but the most poisoned phosphor.

For *HC* excitation the emission intensity has a breakpoint at about 50°C. The location of this breakpoint does not change with poisoning at least until more than 70 percent of the unpoisoned phosphor's intensity has been lost; the rate of decrease of emission intensity with temperature past the breakpoint, however, increases with increased poisoning. (The variation of emission intensity with temperature below the breakpoint is probably due to the presence of traps and is characteristic of most sulfide phosphors.) When the phosphor has been severely poisoned, so that only 2 percent of the unpoisoned phosphor's intensity remains, the breakpoint lies below −150°C, and the variation of the emission intensity with temperature is identical for *HC* excitation and for *A* excitation.

For *A* excitation, a breakpoint of emission intensity is found at about −10°C for the unpoisoned phosphor, followed by a very slow decrease in intensity with increasing temperature. This breakpoint shifts to lower temperatures with increasing poisoning, lying below −150°C for phosphors which have lost 70 percent or more of the intensity of the unpoisoned phosphor.

DISCUSSION

Poisoning for Excitation by Host-Crystal Absorption

When excitation energy is absorbed by the host crystal, it must be transported by free electrons and holes, by excitons, or by some other mechanism, to activator centers before luminescence can occur. There are three principal points of the process at which the presence of poison centers can affect the luminescence efficiency: (1) the poison centers may interfere with the transport of energy to activator centers; (2) the poison centers may interact with activator centers to reduce or destroy their efficiency; and (3) poison centers may absorb the emission.

The data of Figs. 1, 2, and 4 show that poisoning for excitation by host-crystal absorption is independent of the Mn proportion between 0.1 and 1.0 percent, and of the particular poison used (Fe, Co, or Ni) over this same range of Mn proportion. These results indicate that both interaction and absorption by poison centers are relatively unimportant as poisoning mechanisms

for *HC* excitation over a wide range of Mn proportions. Interaction between poison centers and activator centers would be a function of both the Mn proportion and the particular poison used. The absorption of ZnS:Mn phosphors with Fe or Co impurity is considerably less in the region of the emission spectrum than the absorption of ZnS:Mn phosphors with Ni impurity, and hence poisoning by Ni impurity absorption would be larger than poisoning by Fe or Co impurity absorption. It is concluded, therefore, that poisoning found for *HC* excitation is associated primarily with the dissipation by poison centers of host-crystal energy before the transport of this energy to activator centers may be accomplished.

For low proportions of Mn, such as 0.03 percent shown in Figs. 2 and 4, an increase in poisoning may be associated with the increased distance between activator centers. The average path, over which energy absorbed by the host crystal must be transported to activator centers to produce luminescence, becomes longer, and an increased probability of dissipation by poison centers is introduced.

For high proportions of Mn, such as 3.0 percent shown in Fig. 2, the variation of excitation efficiency with poison proportion is the same for *HC* excitation as for *A* excitation. For these high Mn proportions, the poisoning effect of interaction between poison centers and activator centers is more important than the poisoning caused by the dissipation of host-crystal energy before this energy has been transported the relatively short distances to activator centers. The dominating factor is the effect of interaction on activator centers, and poisoning is not affected by the nature of the excitation.

The curves of emission intensity as a function of phosphor temperature given in Fig. 7 for *HC* excitation show that the incorporation of a poison increases the probability of the dissipation of host-crystal energy by thermal processes above the temperature breakpoint. When the phosphor is severely poisoned, it becomes improbable for host-crystal energy at any temperature where measurements were made to be transported over any appreciable distance in the crystal, and it is only the host-crystal energy which is absorbed in the immediate neighborhood of an activator center which may be utilized. The temperature variation of the emission intensity is then dependent upon the temperature variation of the efficiency of the activator center, as affected by interaction; curves of emission intensity *vs* temperature are the same for *HC* excitation as for *A* excitation (Fig. 7, curve 4). The beginning of this condition in less poisoned phosphors may be observed by comparing the variation of emission intensity at high temperatures for curves 1, 2, and 3 of Fig. 7. In these less poisoned phosphors, the dissipation of host-crystal energy at high temperatures is so large that once again the emission intensity for *HC* excitation varies with temperature in the same way as the emission intensity for *A* excitation.

Poisoning for Direct Activator Excitation

When the Mn activator centers are excited directly, electrons are raised to excited states of the Mn ions, but remain bound in the neighborhood of their parent ions. Poisoning by the incorporation of impurities may enter in three principal ways: (1) the poison centers may absorb the exciting radiation and thus decrease the density of excitation for activator centers; (2) the poison centers may interact with activator centers to reduce or destroy their efficiency; and (3) the poison centers may absorb the emission.

The fact that the absorption characteristics of Fe and Co impurities are similar to one another, but quite different from those of Ni impurity, whereas poisoning caused by Fe is quite different from that caused by Co or Ni, indicates that absorption effects play only a minor role in poisoning unless the poison impurities are present in very high proportions.

The dependence of poisoning for *A* excitation upon the proportion of Mn and the particular poison used indicates that an interaction between poison centers and activator centers is the principal poisoning mechanism.

Except for establishing the similarity between the complicated poisoning characteristics of Fe and Co impurity, the results of the present study have not led to date to an adequate explanation of the variation of poisoning with Mn proportion. For each poison impurity, all curves of excitation efficiency as a function of increasing log poison proportion show a relatively rapid decrease after some poison proportion, except for one proportion of Mn (1.0 percent Mn for Co and Ni, 0.3 percent Mn for Fe). For this critical proportion of Mn, which is also the proportion for which maximum poisoning is obtained for low poison proportions, the excitation efficiency is almost a linearly decreasing function of the log poison proportion.

The data, however, do allow conclusions to be drawn about the nature of the interaction between poison centers and activator centers. The interaction must (1) decrease the efficiency of an activator center by either affecting nonradiative processes within the center, or by dissipating the energy through a transfer from activator to poison center; (2) increase the absorption of radiation in the range of the Mn absorption by poisoned activator centers; and (3) prevent a poisoned activator center from being excited by acquisition of energy from the host crystal. The last effect of the interaction is indicated by the fact that a lower excitation efficiency may be found for *A* excitation than for *HC* excitation for the same impurity proportion. The increased absorption of incident radiation by poisoned activator centers would also play a part in producing this observed effect.

Exchange Potential in the Surface Region of a Free-Electron Metal*

HELLMUT J. JURETSCHKE
Polytechnic Institute of Brooklyn, Brooklyn, New York
(Received July 28, 1953)

The weighted average exchange charge and the average exchange potential proposed by Slater have been evaluated explicitly in the surface region of a free-electron gas bounded by an infinite barrier. It is found that in the surface the exchange hole ceases to accompany its electron and that the exchange potential beyond the surface is essentially that due to an exchange hole stationary in the surface region. This interpretation explains the failure of the statistical approximation to the exchange potential at low electron densities. At high densities, the statistical approximation agrees closely with the average exchange potential. In the surface region the normally spherically symmetrical exchange hole becomes distorted. This change of shape is discussed qualitatively for electrons in the immediate surface region and electrons very far from the surface of a distribution bounded by a finite low barrier. The exchange surface energy of this model of a metal surface is 96 ergs/cm^2 for an interior density equal to that of sodium.

I. INTRODUCTION

IF the Hartree-Fock equations for the best one-electron wave functions of electrons moving in the field of atomic nuclei are written in the standard form of one-electron Schrödinger equations, the potential energy term includes an exchange energy contribution which measures the effect of a spin-dependent repulsion between electrons.[1] As a result of this interaction, the density of all other electrons of like spin is reduced in the neighborhood of a given electron. The exchange potential is essentially the potential of this local deficiency of charge at the location of the electron under consideration.[2]

The general expression for the exchange potential for an electron represented by a wave function u_i and located at $\mathbf{r}$ is given by

$$-\frac{e^2}{u_i^*(\mathbf{r})u_i(\mathbf{r})}\sum_k \int d\mathbf{r}_1 \frac{u_i^*(\mathbf{r})u_k^*(\mathbf{r}_1)u_k(\mathbf{r})u_i(\mathbf{r}_1)}{|\mathbf{r}-\mathbf{r}_1|}, \quad (1)$$

where the summation includes all wave functions with spin parallel to u_i. The expression (1) cannot be readily evaluated except for very simple wave functions. In metals in which the ion cores are small and far apart the exchange potential is usually assumed to be the same as that of a free-electron gas of the proper average density, and is independent of position. The exchange potential of such a free-electron gas of density n, averaged over all electrons, has the value

$$-3e^2(3n/8\pi)^{\frac{1}{3}}. \quad (2)$$

It has often been pointed out that this is approximately the potential at the center of a uniformly charged sphere of density $n/2$ (i.e., one kind of spin only) and radius

$$r_0=(3/2\pi n)^{\frac{1}{3}}. \quad (3)$$

However, when there are large variations in the electron density, the exchange potential becomes a complicated function of position and cannot usually be represented in this simple descriptive manner. In this paper we investigate the behavior of the exchange potential in the region of rapidly changing electron density in the surface region of a free-electron metal. For this model some explicit calculations on exchange potentials and exchange charges can be carried out and can be used to illustrate the properties of these quantities in surface regions of electron distributions. Various approximations to the surface exchange potential are compared and discussed in terms of the physical interpretation of the exchange potential. In addition, the explicit calculations are applied to evaluate the exchange energy contribution to the surface energy of such a free-electron metal.

II. APPROXIMATIONS TO THE SURFACE EXCHANGE POTENTIAL

For use in a self-consistent calculation of the surface charge distribution of a free-electron metal, Bardeen[3] has evaluated the exact exchange potential (1) of a free-electron gas bounded by an infinite and a finite step barrier, at the position of the barrier. Since the two barriers of different height are located at different positions with respect to the charge distribution, this procedure yielded two points for the potential in the surface. The potential throughout the surface region was then constructed by connecting the two calculated points by a smooth line going over into the image potential far from the surface and into the constant value obtained from (2) in the interior. This potential is a slowly varying function of the electron wave vector. Figure 1 shows a typical potential derived by Bardeen, appropriate to the average potential for all electrons. Although the two calculated points are based on slightly different electron distributions, they are representative of the exchange potential variation in the surface. However, two points are not really sufficient to construct a

* This work has been supported by the U. S. Office of Naval Research.
[1] J. C. Slater and H. M. Krutter, Phys. Rev. **47**, 559 (1935).
[2] J. C. Slater, Revs. Modern Phys. **6**, 209 (1934).
[3] J. Bardeen, Phys. Rev. **49**, 653 (1936).

surface potential good everywhere in this region, and this method of construction suppresses the detailed dependence of the exchange potential on a particular electron distribution. In fact, Bardeen found that the final electron distribution self-consistent with respect to the fixed exchange potential differed only slightly from the distribution on which the exchange potential was based. However, it is unlikely that consideration of the minor variations in the exchange potential in the low-density region would affect his conclusions. In the regions of higher density these variations may introduce corrections.

Recently, Slater[4] has suggested a simplification of the Hartree-Fock equations such that all electrons move in a common exchange potential. This average potential is obtained by constructing the potential due to a weighted average exchange charge for all electrons. It is given by

$$-e^2\frac{\sum_{i,k}\int d\mathbf{r}_1\dfrac{u_i^*(\mathbf{r})u_i(\mathbf{r}_1)u_k^*(\mathbf{r}_1)u_k(\mathbf{r})}{|\mathbf{r}-\mathbf{r}_1|}}{\sum_i u_i^*(\mathbf{r})u_i(\mathbf{r})}. \tag{4}$$

This approximation assumes that the exchange holes for different electrons are not too different from each other, so that the dependence of the potential on the state of any one electron can be removed by substitution of the average value. For actual calculation Slater has proposed a further simplification of (4) which should be valid for slowly varying electron densities. The average exchange potential (4) is approximated by the average exchange potential of a free-electron gas of density equal to the electron density at the point in question. This is equivalent to making the density n in (2) a function of position; it corresponds, except for a numerical factor, to the Thomas-Fermi-Dirac statistical approximation. Figure 1 shows the exchange potential constructed in this manner from a distribution corresponding to a free-electron gas bounded by an infinite barrier. This electron distribution is shown in Fig. 2.

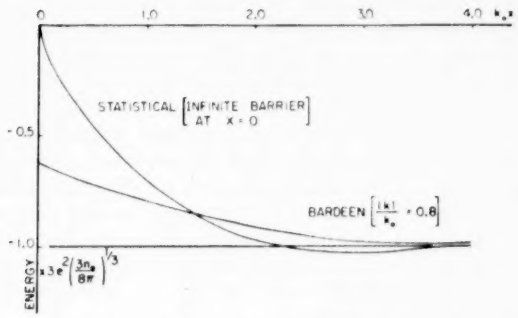

FIG. 1. Approximate exchange potentials in the surface of a free-electron metal.

[4] J. C. Slater, Phys. Rev. **81**, 385 (1951).

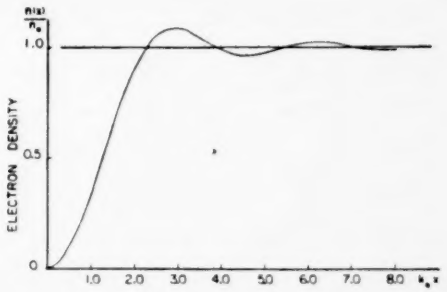

FIG. 2. Electron density distribution of free electrons bounded by an infinite barrier at $x=0$.

As to be expected, the statistical approximation is not reliable at low densities. In the regions of higher density it compares adequately with Bardeen's values. But in addition, it shows a dip in the region where the charge density has a maximum, which is not present in Bardeen's potential. The magnitude of this dip in the exchange potential will depend on the electron density, and it would be less pronounced for Bardeen's final charge distribution than for that used here. Nevertheless, this dip would reinforce the electrostatic dip in potential in the same region,[5] and a self-consistent computation of the surface charge density taking into account this variation of the exchange potential at high densities would result in a greater localization of electrons in the surface than found by Bardeen. The effective surface barrier would be more step-like and the surface would exhibit a lower electric double layer.

In the next section the Slater potential (4) will be evaluated exactly as a function of position for free electrons bounded by an infinite barrier. This allows on the one hand a comparison of the average potential with Bardeen's accurately computed points, and, on the other hand, an estimate of the accuracy of the statistical potential in regions of various electron densities and density gradients.

III. THE AVERAGE EXCHANGE POTENTIAL

Free electrons confined to the region $x>0$ by an infinite potential barrier at $x=0$ are represented by wave functions

$$u_k(x,y,z)=(2/L^3)^{\frac{1}{2}}\sin(k_x x)e^{i(k_y y+k_z z)}, \tag{5}$$

where $k_i=(2\pi/L)m_i$; m_y, m_z take on all integral values, while $m_x=\frac{1}{2}$, 1, $\frac{3}{2}$, 2, $\cdots$. The wave functions are normalized in a volume L^3. If $m=(m_x^2+m_y^2+m_z^2)^{\frac{1}{2}}$, all states (m_x, m_y, m_z) are doubly occupied by electrons up to a value $m_0=L(3n_0/8\pi)^{\frac{1}{2}}$ where n_0 is the electron density far from the surface. The maximum $|k|$ value is given by

$$k_0=2\pi(3n_0/8\pi)^{\frac{1}{2}}. \tag{6}$$

[5] See reference 3, Fig. 5.

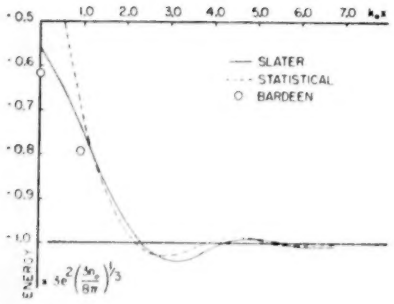

FIG. 3. Slater's exchange potential based on an average exchange charge. The statistical approximation to the exchange potential and Bardeen's calculated points are shown for comparison. The energy scale covers only half of the full range.

The electron density for one kind of spin occurring in the denominator of (4) is obtained directly from (5). It depends only on x, and in terms of $X=k_0x$ it can be written

$$\frac{n}{2}(X)=\frac{n_0}{2}\left(1-3\frac{\sin 2X}{(2X)^3}+3\frac{\cos 2X}{(2X)^2}\right). \tag{7}$$

n/n_0 is plotted in Fig. 2.

The numerator of (4) can be evaluated by first summing over i and k. By writing the $\sin(k_x x)$ as a sum of exponentials and rearranging the region of summation for k_x, the average exchange potential takes the form

$$-e^2\int\frac{d\tau_1}{r_1}\frac{\frac{1}{2}n_0}{n(k_0x)/n_0}\left\{3\frac{\sin(k_0r_1)-k_0r_1\cos(k_0r_1)}{(k_0r_1)^3}-3\frac{\sin(k_0r_2)-k_0r_2\cos(k_0r_2)}{(k_0r_2)^3}\right\}^2, \tag{8}$$

where $r_1^2=(x-x_1)^2+(y-y_1)^2+(z-z_1)^2$ and $r_2^2=(x+x_1)^2+(y-y_1)^2+(z-z_1)^2$. The effect of the barrier at $x=0$ is evident in the form of the average exchange charge contained in (8). It is made up of two terms. The normal term existing in a uniform charge distribution is modified by its image with respect to the barrier.

The remaining integrations in (8) must be carried out over half-space $x_1\geq 0$. The square of the first term in the bracket of (8), if integrated over all space, gives the normal exchange integral contribution. Hence there are three correction terms in the integration over half-space; the correction when the first term is limited to $x_1\geq 0$, and the two remaining terms in the square of the bracket of (8). Since these additional terms are appreciable only in the neighborhood of $X=0$, the limits of integration are $0\leq x_1\leq\infty$, $-\infty<y_1, z_1<\infty$. Without loss of generality, the expression (8) may be evaluated for electrons located at points on the x axis.

By very careful, lengthy but elementary integration, first over angles and then over r_1, and exact evaluation of limits, one obtains for the integral (8) the expression,

$$\frac{-3e^2(3n_0/8\pi)^{\frac{1}{3}}}{n(X)/n_0}\left\{1-[\tfrac{1}{2}\pi-\mathrm{Si}(4X)]\left(\frac{2X\cos 2X-\sin 2X}{4X^4}\right)-[\mathrm{Ci}(4X)-\log(4\gamma X)]\left(\frac{\cos 2X+2X\sin 2X}{4X^4}\right)-\left(\tfrac{1}{2}\pi-\mathrm{Si}(2X)-\frac{\cos 2X}{2X}\right)\left(\frac{2}{3X}-\frac{4X}{15}\right)+\frac{1}{X^4}\left(\frac{2}{5}\sin^2X-\frac{1}{48}\sin^2 2X\right)-\frac{1}{X^3}\left(\frac{7}{5}\sin 2X-\frac{1}{24}\sin 4X\right)+\frac{1}{X^2}\left(\frac{1}{12}+\frac{11}{15}\cos 2X+\frac{1}{6}\cos 4X\right)-\frac{1}{X}\frac{\sin 2X}{15}+\frac{2}{3X}[\mathrm{Si}(4X)-\mathrm{Si}(2X)]\right\}. \tag{9}$$

$\mathrm{Si}(X)$ and $\mathrm{Ci}(X)$ are the sine and cosine integrals as defined by Jahnke and Emde,[6] $\gamma=1.781$ is Euler's constant, and $X=k_0x$. The average exchange potential (9) has been graphed in Fig. 3. This figure also includes the statistical potential derived from expressions (2) and (7) and the two points calculated by Bardeen for $|k|/k_0=0.8$, which apply very closely to the average potential for all electrons.

At the position of the barrier, the average of Bardeen's potentials has dropped to $\pi^2/16$ of its value in the interior. The Slater potential (9) has decreased to 5/9 of its interior value at the same point. The difference arises because Slater's potential is based on a weighted average favoring electrons with high wave numbers which have low exchange potentials.

Throughout most of the immediate surface region, the Slater average potential agrees quite well with that constructed by Bardeen. However, in the region where the electron density has its first maximum, the average potential shows a dip very similar to that produced by the statistical potential. It is very likely that this dip is real and will also occur in the correct exchange potential (1) if the charge distribution exhibits a maximum. Farther away from the surface the average exchange potential agrees quite well with the statistical approximation. Both follow the charge density variations closely. It should be noted, however, that the exchange potential follows with a lag, and that it tends to emphasize regions of high density, and de-emphasize regions of lower density.

One can conclude from the comparison of the curves

[6] E. Jahnke and F. Emde, *Tables of Functions* (Dover Publications, New York, 1945), p. 1.

in Fig. 3 that the exchange potential (4) is a rather accurate description of the real average exchange potential at all densities. However, the additional simplification involved in the statistical approximation does not apply in the outer surface region. For the distribution used here, the statistical approximation becomes inaccurate when the density has dropped to about $\frac{1}{2}$ of its value in the interior.

IV. EXCHANGE CHARGE IN THE SURFACE

In Bardeen's calculation of a self-consistent surface potential the exchange potential is held fixed at the initially constructed values. Since the exchange potential is a slowly varying function in the surface region, its dependence on the actual charge distribution is probably not too critical. Nevertheless, it is of interest to understand the cause of the variation of the exchange potential in this region, in order to be able to predict possible effects of different electron distributions. For this purpose it is convenient to study the behavior of the exchange charge when the electron is in the surface region. In our model the exchange charge distribution is given by the expression contained in the integrand of (8),

$$e\frac{\frac{1}{2}n_0}{n(X)/n_0}\left\{3\frac{\sin R_1 - R_1\cos R_1}{R_1^3} - 3\frac{\sin R_2 - R_2\cos R_2}{R_2^3}\right\}^2. \quad (10)$$

In (10) all distances are measured in units of k_0^{-1}. R_1 is the distance from the location of the electron at (X, Y, Z) and R_2 is the distance from the image point $(-X, Y, Z)$.

Far from the surface ($X \gg 0$), only the first term in (10) is important, giving the usual exchange hole centered at the electron in question. In the surface interference between the first term and its image becomes important. As a result the exchange hole ceases to follow the electron exactly, but lags behind more and more as the electron moves into the surface. Figure 4 depicts the exchange charge density along a normal to the surface for various locations on the normal of the

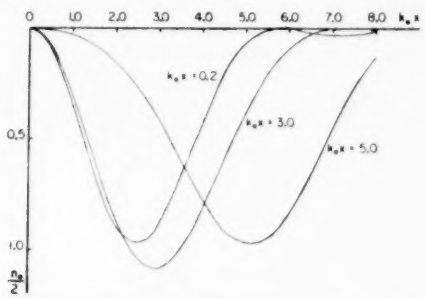

FIG. 4. Average exchange-hole density normal to the surface for various locations of an electron.

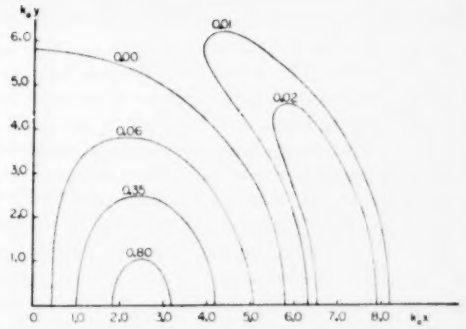

FIG. 5. Density contours of the average exchange hole associated with an electron at (0, 0). The surface is perpendicular to the x axis.

electron under consideration. The lag of the exchange hole is the cause of the shift of the peaks of the exchange potential with respect to the peaks of the electron density (and also of the statistical approximation) evident in Fig. 3. The interference of the two terms in (10) displaces the center of the exchange hole towards the interior of the metal. The explanation for the difference in response to peaks and valleys in the electron distribution of the statistical and the average exchange potential shown in Fig. 3 is not clear cut. One would expect in general that a potential based on an exchange hole following the actual charge density variations tends to average out local variations in density more than the statistical potential, which is based on an exchange hole in a uniform electron density. The higher peaks occurring in Slater's potential are probably due to the distortion of the exchange hole in the surface region.

As the electron moves into the surface the exchange hole is deformed in various ways. The hole becomes more compressed in the direction normal to the surface. Thus, the first zeros of (10) measured from the center of the hole approach the value given by (3). Figure 4 shows that in the cross section considered nearly all the electrons normally in the surface are displaced by the exchange hole, so that this cross section follows the density. In addition, the hole does not remain spherically symmetrical but flattens out in the surface region. Figure 5 is a plot of the density contours of the exchange hole for an electron at $x=0$. It should be noted that in spite of these distortions most of the exchange-hole charge remains close to the electron in question. In fact, for an electron at $x=0$ a hemisphere of radius $rk_0=6$ contains nearly as much charge as a sphere of the same radius around an electron in the interior.

The exchange potential in the surface can thus be described qualitatively by observing that as soon as the electron density decreases appreciably from its interior value the exchange hole tends to stay behind. In our model this occurs at about $k_0x=2.50$. This means that for all points beyond this limit the exchange

potential is not that for an electron in the center of the exchange hole, but for an electron some distance away from the center. The exchange hole can be approximated by a uniformly charged sphere of radius r_0. Since $k_0r_0=2.42$, an electron at $x=0$ is just about at the surface of the exchange hole. At that point its potential in the spherical charge distribution has decreased to $\frac{2}{3}$ of its maximum value. This is in good agreement with the potential found in expression (9). But such a description in terms of a uniform spherical charge distribution is only approximate. Actually, the exchange potential in Fig. 3 rises more rapidly than the corresponding potential of a uniformly charged sphere located at $k_0x=2.50$.

An infinite barrier is not suited for investigating the asymptotic behavior of the exchange hole, since the electron density decreases too rapidly. For this purpose it is convenient to study the exchange hole based on the wave functions proper to a finite step barrier which have been constructed by Bardeen. With these wave functions the approximate exchange hole distribution can be readily evaluated for electrons far beyond the barrier location, since the exponentially decaying wave functions in this region allow approximations in the summation over all occupied states. The result depends on the height of the barrier relative to the highest electron energy $\hbar^2k_0^2/2m$. If the relative barrier height is A, then for $A\gg1$ the potential seen at a distance k_0x_1 from the surface approaches asymptotically $e/|x_1|$, i.e., the exchange hole remains relatively concentrated in the surface. If $A\gtrsim1$, and the electron is not too far from the barrier, the exchange hole shows a behavior in the surface very similar to that already discussed above. But at points far away from the surface the exchange hole distribution is altered considerably. Thus, for $A\gtrsim1$, the exchange hole distribution along the x axis due to an electron at $-k_0x_1$, ($|k_0x_1|\gg1$) is approximately given by

$$\frac{n_0}{2}\frac{24(A-1)}{A(k_0x_1)^2}(\cos k_0x-(A-1)^{\frac{1}{2}}\sin k_0x)^2. \qquad (11)$$

In (11) all distances are measured from the position of the barrier. This expression is valid for $2(A-1)^{\frac{1}{2}}x\leq|x_1|$. For larger x the density oscillates with decreasing amplitude. Laterally the exchange hole is appreciable to distances up to $|x_1|^{\frac{1}{2}}$. Expression (11) shows that the single exchange hole is replaced by a series of disk-like charge distributions of equal magnitude, spaced at intervals of π/k_0 up to a distance about equal to the distance of the electron from the surface. The potential of this distribution is still essentially $e/|x_1|$, with a numerical factor smaller than unity for low barriers.

This appearance of the asymptotic exchange hole can be deduced from the general formula for the exchange hole in expression (4). Sums of the form $\sum_i u_i^*(\mathbf{r}_1)u_i(\mathbf{r})$, where $\mathbf{r}$ is inside the metal and $\mathbf{r}_1$ far away from the surface will be determined primarily by wave functions of high x wave numbers, and thus are asymptotically periodic in $\mathbf{r}$ with period $2\pi/k_0$. Similar behavior holds also true, although to smaller extent, for the exchange holes associated with the correct exchange potentials (1).

The basic reason why the exchange hole remains in the surface is clear; it must remove unit charge out of the existing charge distribution and thus must remain mostly in a rather dense region. Mathematically this is brought about by a correlation of phases of all wave functions in the surface region. Neither one of these two conditions is observed in the usual statistical approach to the exchange potential. Therefore, such an approach cannot lead to a good approximation in regions of low and rapidly changing charge density.

V. SURFACE EXCHANGE ENERGY

Expression (9), when multiplied by the local electron density, represents the exchange energy density in the surface region. A comparison of the energy obtained from (9), corresponding to a decaying electron density, with that of a uniform electron distribution will give the contribution to the exchange energy due to the existence of the surface. In determining surface energy contributions by such comparisons it is important to observe that (a) the density far from the surface must be the same for both distributions and (b) the comparison must be between equal total amounts of charge.[7] The charge distribution (7) on which (9) is based represents a deficit of $3\pi n_0/8k_0$ electrons per unit surface, in comparison with a uniform distribution up to the barrier.[8] If the energy based on expression (9) is corrected for this deficiency, the exchange energy per unit surface has a value $0.134e^2(3n_0/8\pi)$. This corresponds to 96 ergs/cm^2 for Na and compares closely with the value 75 ergs/cm^2 obtained by Huntington[8] directly from Bardeen's self-consistent potentials. Huntington's quoted value has been multiplied by $\frac{4}{5}$ to eliminate the contribution of the correlation energy.

[7] W. J. Swiatecki, Proc. Phys. Soc. (London) **64**, 226 (1951).
[8] H. B. Huntington, Phys. Rev. **81**, 1035 (1951).

Second-Order Elastic Deformation of Solids*

D. S. HUGHES AND J. L. KELLY†
Physics Department, University of Texas, Austin, Texas
(Received June 1, 1953)

Expressions for the velocities of elastic waves in stressed solids are derived using Murnaghan's theory of finite deformations and third-order terms in the energy. For isotropic materials, in addition to the Lamé constants λ and μ, three additional constants, l, m, and n, are required to describe the material.

By measuring the transmission time of elastic pulses through the material, the velocities of longitudinal and shear waves are determined as a function of applied stress. By subjecting the material to hydrostatic pressure as well as simple compression, it is found that seven functions of the three constants l, m, and n can be measured and thus numerical values calculated. Results are given for polystyrene, iron, and Pyrex glass.

INTRODUCTION

THE ordinary theory of elasticity is limited to infinitesimal deformations of perfectly elastic solids, i.e., solids in which the strains are functions only of the stresses and temperature. For such solids a strain-energy function exists. For many problems and materials this theory is adequate; however, under various conditions many ordinary solids are not adequately described by this theory. The failure may be ascribed to either one alone or a combination of two phenomena. First, the solid may be anelastic[1] or plastic. Second, the deformations may be so large that the infinitesimal theory is not accurate. Many attempts have been made to develop a theory of finite deformation. Cauchy derived some of the fundamental equations, and Love[2] made some advances in the subject. Brillouin[3] formulated elastic theory in tensor notation and derived some of the fundamental equations for finite deformations. Later[4] he extended this work and gave a complete formulation of the basic theory. This was later reviewed and somewhat condensed.[5] Murnaghan[6] developed the theory in a completely general tensor notation and later[7] rewrote this work in matrix notation. Biot[8] has developed a theory dealing particularly with the elasticity of pre-stressed solids and considered the effect of stress on wave propagation.[9]

A theory of finite deformations involves two departures from the infinitesimal theory. First, since the deformations are large, the final coordinates of a point are not interchangeable with the original coordinates as in the infinitesimal theory, and second, the expression of the strain energy in terms of the strains must be revised. Since the initial and final coordinates are no longer interchangeable, either may be taken as the independent variables. The initial coordinates as independent variables are called "Lagrangian coordinates," and the final coordinates as independent variables are called "Eulerian coordinates." The formulation in both systems was developed by Brillouin[4] and Murnaghan[6]; later Murnaghan[7] used the Lagrangian system exclusively.

For our experimental work, we need formulate the theory only under somewhat restricted conditions. Thus, rectangular cartesian coordinates will be used. The coordinates $(a_1\, a_2\, a_3)$ will designate the original position of a point in the body and $(x_1\, x_2\, x_3)$ the final position. The "Lagrangian" coordinates and general formulation of Murnaghan[7] will be used. We need consider only the special deformation given by

$$x_r = A_r a_r + U_r(a), \quad r = 1, 2, 3, \tag{1}$$

where the $U_r(a)$ are general functions of all the a's, but satisfy the condition

$$U_r(a) \ll A_r - 1.$$

Equation (1) then represents a general infinitesimal strain superimposed upon a homogeneous triaxial finite strain with the coordinate axes as principal axes. The "Lagrangian" strain components are then given by

$$\eta_{rs} = \alpha_r \delta_{rs} + A_r A_s e_{rs}, \tag{2}$$

where δ_{rs} is the Kronecker delta function,

$$\alpha_r = \tfrac{1}{2}(A_r^2 - 1),$$

and

$$e_{rs} = \tfrac{1}{2}(\partial U_r/\partial x_s + \partial U_s/\partial x_r). \tag{3}$$

The e_{rs} are the ordinary infinitesimal strains computed from a state of general triaxial finite strain given by the α_r. Our final equations for the strains are only accurate to terms involving the squares of the η_{rs}. Thus to obtain a consistent order of accuracy, we adopt the following rule for the stress equations:

* This work was supported by the U. S. Office of Naval Research and by research grants from the Shell Oil Company and the Humble Oil and Refining Company.
† Now at Murray Hill Laboratories of Bell Telephone Company, Inc., Murray Hill, New Jersey.
[1] C. M. Zener, *Elasticity and Anelasticity of Metals* (University of Chicago Press, Chicago, 1948).
[2] A. E. H. Love, *A Treatise on the Mathematical Theory of Elasticity* (Dover Publications, New York, 1944).
[3] Leon Brillouin, Ann. phys. **3**, 267 (1925).
[4] Leon Brillouin, Ann. phys. **4**, 328 (1925).
[5] Leon Brillouin, *Les Tenseurs* (Dover Publications, New York, 1946).
[6] T. D. Murnaghan, Am. J. Math. **59**, 235 (1937).
[7] T. D. Murnaghan, *Finite Deformation of an Elastic Solid* (John Wiley and Sons, Inc., New York, 1951).
[8] M. A. Biot, Z. angew. Math. Mech. **20**, 89 (1940).
[9] M. A. Biot, J. Appl. Phys. **11**, 522 (1940).

In terms not involving e_{rs} the first and second powers of α_r will be retained. In coefficients of e_{rs} only the first power of α_r will be retained. No terms involving e_{rs} to a higher power than the first will be retained.

It is most difficult in this subject to keep a strict level of accuracy and several apparent violations occur in the literature. With the above rule, Eq. (2) may be written

$$\eta_{rs}=\alpha_r\delta_{rs}+(1+\alpha_r+\alpha_s)e_{rs}. \tag{4}$$

For an isotropic body, the strain energy is a function only of the strain invariants, which we define by

$$\begin{aligned} I_1&=\delta_s{}^r\eta_{rs},\\ I_2&=(1/2!)\delta_{su}{}^{rt}\eta_{rs}\eta_{tu},\\ I_3&=(1/3!)\delta_{suw}{}^{rtv}\eta_{rs}\eta_{tu}\eta_{vw}, \end{aligned} \tag{5}$$

where the δ's are the general Kronecker delta functions. In terms of these invariants, the strain energy per unit mass can be written[7]

$$\phi=\tfrac{1}{2}(\lambda+2\mu)I_1{}^2-2\mu I_2+\tfrac{1}{3}(l+2m)I_1{}^3-2mI_1I_2+nI_3, \tag{6}$$

where λ and μ are ordinary Lamé constants and l, m, and n will be called the Murnaghan constants. Brillouin[4] gives an equivalent equation with invariants defined differently than Eq. (5); also, his strains are defined without the factor one half. Both Brillouin[4] and Murnaghan[7] included terms of zero and first order in their expressions. The zero order or constant has been omitted since only the derivative of Eq. (6) will be used. The inclusion of the first-order term which has the form of a constant times I_1 corresponds to referring the body to an initial state of hydrostatic strain. For our work we wish to refer the body to an initial unstrained state.

In our definition of the strain, we have included means of placing the body in any general prestrained state.

The density is given by

$$\rho=\rho_0/(1+2I_1+4I_2+8I_3),$$

where ρ_0 is the density at zero strain.

The stresses[7] are now given by

$$T_{rs}=T_{rs}{}^0+\textstyle\sum_{tu}C_{rstu}\partial U_t/\partial x_u, \tag{7}$$

where

$$\begin{aligned} T_{rs}{}^0&=[\lambda+(l-m-\lambda)\theta+(\lambda+m-\mu)\alpha_r]\theta\delta_{rs}\\ &\quad+2\mu(\alpha_r+2\alpha_r{}^2)\delta_{rs}+m\textstyle\sum_t\alpha_t{}^2\delta_{rs}+\tfrac{1}{2}n\sum_{tu}\delta_{stu}{}^{rtu}\alpha_t\alpha_u, \end{aligned} \tag{8}$$

$$\begin{aligned} C_{rstu}&=[\lambda+2(l-\lambda-m)\theta+2(\lambda+m)(\alpha_r+\alpha_t)-2\mu\alpha_r]\delta_{rs}\delta_{tu}\\ &\quad+[\mu+(\lambda+m-\mu)\theta+2\mu(\alpha_r+\alpha_s+\alpha_u)]\\ &\quad\times[\delta_{rt}\delta_{su}+\delta_{ru}\delta_{st}]+\tfrac{1}{2}n\textstyle\sum_v(\delta_{svt}{}^{rvu}+\delta_{srv}{}^{rvt})\alpha_v, \end{aligned} \tag{9}$$

and

$$\theta=\alpha_1+\alpha_2+\alpha_3. \tag{10}$$

Let us assume the U_r are given by the functions

$$U_r=F_r(\textstyle\sum_s N_sx_s-Vt).$$

The N_s are components of a unit vector and the U's thus represent a plane wave propagated in the direction N_s.

The velocity V is given by the solutions of

$$\mathrm{Det}\,|\textstyle\sum_{ru}C_{rstu}N_rN_u-V^2\delta_{st}|=0.$$

It should be noted that although the C_{rstu} do not satisfy the symmetry condition of similar constants in the infinitesimal theory this determinant is symmetric; therefore, there are three real solutions for V for any direction N_s and the particle velocities for the three solutions are orthogonal.

For our experimental results, we may consider only propagation along the x axis. The three solutions are then

$$\begin{aligned} \rho_0V_1{}^2&=\lambda+2\mu+(2l+\lambda)\theta+(4m+4\lambda+10\mu)\alpha_1,\\ \rho_0V_2{}^2&=\mu+(\lambda+m)\theta+4\mu\alpha_1+2\mu\alpha_2-\tfrac{1}{2}n\alpha_3,\\ \rho_0V_3{}^2&=\mu+(\lambda+m)\theta+4\mu\alpha_1+2\mu\alpha_3-\tfrac{1}{2}n\alpha_2. \end{aligned} \tag{11}$$

In order to specialize to the cases of hydrostatic pressure and simple axial stress it is sufficient to evaluate the α_r by means of the formulae of the linear theory which can be obtained from the linear approximation to the $T_0{}^{rs}$. We will designate the compressive stress applied along one of the three axes by T and hydrostatic pressure by P.

A second subscript on the V's will indicate the type of stress: 0 for hydrostatic pressure and x, y, z for axial compressive stress in the x, y, or z directions. Then setting $K_0=\lambda+\frac{2}{3}\mu$, the velocities are given by:

$$\begin{aligned} \rho_0V_{10}{}^2&=\lambda+2\mu-\frac{p}{3K_0}[6l+4m+7\lambda+10\mu],\\ \rho_0V_{20}{}^2&=\mu-\frac{P}{3K_0}[3m-\tfrac{1}{2}n+3\lambda+6\mu],\\ \rho_0V_{1x}{}^2&=\lambda+2\mu-\frac{T}{3K_0}\left[2l+\lambda+\frac{\lambda+\mu}{\mu}(4m+4\lambda+10\mu)\right].\\ \rho_0V_{2x}{}^2&=\mu-\frac{T}{3K_0}\left[m+\frac{\lambda n}{4\mu}+4\lambda+4\mu\right], \end{aligned} \tag{12}$$

$$\begin{aligned} \rho_0V_{1y}{}^2&=\lambda+2\mu-\frac{T}{3K_0}\left[2l-\frac{2\lambda}{\mu}(m+\lambda+2\mu)\right],\\ \rho_0V_{2y}{}^2&=\mu-\frac{T}{3K_0}\left[m+\frac{\lambda n}{4\mu}+\lambda+2\mu\right],\\ \rho_0V_{2z}{}^2&=\mu-\frac{T}{3K_0}\left[m-\frac{\lambda+\mu}{2\mu}n-2\lambda\right]. \end{aligned}$$

Measurements of any three of these velocities, excluding either V_{2x} or V_{2y}, as a function of stress allows the computation of l, m, and n. Any additional measurements give checks on the theory.

In the case of hydrostatic pressure, the entire second-order elastic behavior of the material may be described by two linear combinations of the Murnaghan constants. If $\alpha_1=\alpha_2=\alpha_3=\alpha$, the stress-strain relations (8) may be rewritten:

$$T_{rs}=P\delta_{rs}+LI_1\delta_{rs}+2Me_{rs}, \tag{13}$$

where

$$-P=(3\lambda+2\mu)\alpha+(9l+n-3\lambda-2\mu)\alpha^2,$$
$$L=\lambda+(6l-2m+n-2\lambda-2\mu)\alpha,$$
$$M=\mu+\tfrac{1}{2}(6m-n+6\lambda+6\mu)\alpha,$$
$$\bar{I}_1=\sum_r e_{rr}.$$

For small deviations about hydrostatic pressure, the material acts in every way like a solid with Lamé constants L, M, and bulk modulus K, where

$$K=L+M+\lambda+\tfrac{2}{3}\mu+(6l+\tfrac{2}{3}n)\alpha.$$

This same value of K may be found from the definition $K=-V\partial P/\partial V$.

EXPERIMENTAL PROCEDURE AND RESULTS

An experimental check of second-order elastic theory requires, in general, measurements of extreme accuracy. In static methods, the length or volume of a sample is measured as a function of stress. The elastic modulus is then the slope of the curve, stress *vs* change in length or volume. Infinitesimal elastic theory predicts this curve to be a straight line, whereas the second-order theory predicts it to be a parabola. Thus, in ordinary static methods the data must be accurate enough so that the second derivative of the stress *vs* length or volume can be computed. Professor Bridgman has measured the bulk modulus of many materials with such accuracy that the change of modulus with pressure is known with fair accuracy.

It is possible to measure the moduli by pulse transmission methods[10] with very good relative accuracy. The moduli measured in this way are first the adiabatic in place of the isothermal which are those desired for checking theory; second, since the measurements involve the transmission of high-frequency pulses, 2–5 megacycles, it is possible that the velocities are a function of frequency and thus the computed moduli are in error. We are certain that for the materials we have measured, this error is not more than about 4 percent, but its absolute value is for the present unknown. If the effect is no larger than this, its variation with stress is probably not important. Our best data on this point are the value presented in Table I comparing our measurements and Professor Bridgman's.

TABLE I. Elastic moduli and rates of changes with pressure; comparison with Bridgman.

	Present work	Bridgman
	Pyrex	
K_0	3.83×10^5 bars	3.320×10^5 bars[a]
dK/dP	-3.9 ± 1.0	-1.35
μ	2.75×10^5 bars	2.31×10^5 bars
dM/dP	-2.0 ± 14	-1.95
	Armco iron	
K_0	16.41×10^5 bars	17.12 bars[b]
dK/dP	2.7 ± 1.6	2.9
μ	8.18×10^5 bars	...
dM/dP	6.3 ± 1.0	...

[a] P. W. Bridgman, Proc. Am. Acad. Arts Sci. **63**, 401 (1929).
[b] Computed from revised values for iron as given in P. W. Bridgman's *Physics of High Pressure* (G. Bell and Sons, London 1949), p. 419.

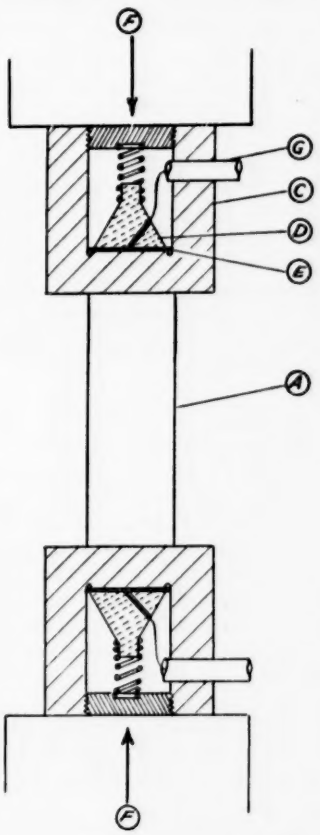

FIG. 1. Experimental arrangement for measuring V_{1z} and V_{2z} under anisotropic stress. A: material under investigation; C: crystal holder (hardened steel); D: teflon backing cone; E: quartz crystal; F: force exerted by hydraulic press; G: connecting cable.

In the foregoing theoretical development, seven different velocities were listed that could be measured experimentally. Two of these, V_{10} and V_{20}, are measured under hydrostatic pressure. The pulse method[11,12] works very well when the sample is under hydrostatic pressure. Using kerosene as a pressure fluid, the wave velocities as a function of hydrostatic pressure were measured up to 9000 bars.

[10] Hughes, Pondrom, and Mims, Phys. Rev. **75**, 1552 (1949).

[11] D. Lazarus, Phys. Rev. **76**, 545 (1949).
[12] Hughes, Blankenship, and Mims, J. Appl. Phys. **21**, 294 (1950).

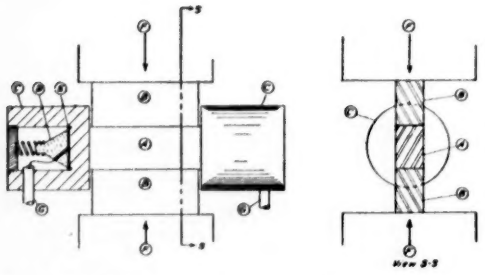

FIG. 2. Experimental arrangement for measuring V_{1y}, V_{2y}, and V_{2z}. A: material under investigation; B: same material for stress equalization; C: crystal holder (hardened steel) D: teflon backing cone; E: quartz crystal; F: force exerted by hydraulic press; G: connecting cable.

For measurements under anisotropic stress, the arrangements of Fig. 1 were used to measure V_{1x} and V_{2x} and the arrangement of Fig. 2 was used to measure V_{1y}, V_{2y}, and V_{2z}. In these measurements y-cut crystals were used to generate and detect the shear pulses. The anisotropic stress could not be carried very high without causing a permanent deformation of the sample.

According to the theory developed, there are four relations between the seven velocities. For polystyrene in which the changes are large and all velocities could be measured, an excellent check was obtained. With Pyrex only V_{10}, V_{20}, V_{1x}, and V_{2x} could be measured giving only one check which was, however, very good. With Armco iron, only V_{10}, V_{20}, and V_{1x} could be measured, thus providing a means of computing l, m, and n, but no check.

Table II presents values of λ, μ, l, m, and n computed from this data in units of bars. From Eq. (13) we may write

$$K(P)=L+\tfrac{2}{3}M=\lambda+\tfrac{2}{3}\mu-\frac{18l+2n}{3(3\lambda+2\mu)}$$

$$M(P)=\mu-\frac{6m-n+6\lambda+6\mu}{2(3\lambda+2\mu)}P. \qquad (14)$$

Thus the theory indicates that an isotropic material under hydrostatic pressure is still isotropic with a variable bulk and shear moduli. Since the development has been carried out to second-order terms in the stress-strain relation, the moduli are linear functions of the pressure. The velocities of longitudinal shear waves are given by

$$V_{10}^2=(L+2M)/\rho, \quad V_{20}^2=M/\rho. \qquad (15)$$

TABLE II. Lamé and Murnaghan constants (in bars$\times 10^6$).

Material	λ	μ	l	m	n
Poly-styrene	0.2889 ±0.0010	0.1381 ±0.0010	−1.89 ±0.32	−1.33 ±0.29	−1.00 ±0.14
Armco iron	11.00 ±0.04	8.20 ±0.10	−34.8 ±6.5	−103.0 ±7.0	+110. ±110
Pyrex	1.353 ±0.003	2.75 ±0.03	+1.4 ±4.0	+9.2 ±5.0	+42. ±35

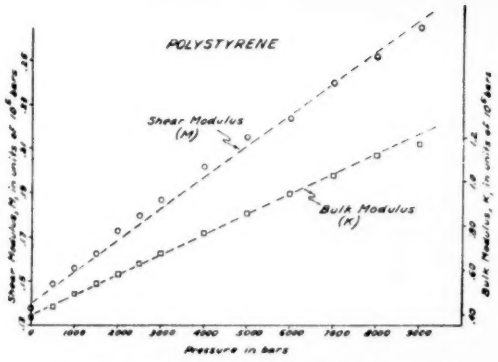

FIG. 3. Shear modulus M and bulk modulus K as a function of pressure for polystyrene.

Thus the second-order theory is applicable as long as the moduli vary linearly with pressure. Figures 3 and 4 show the variable shear modulus and bulk modulus for polystyrene and Pyrex glass. In the case of the polystyrene, the moduli remain linear throughout the entire pressure range. The Pyrex moduli may depart from linearity at the upper end of the pressure range, although this departure is on the borderline of experimental accuracy. The results of the measurements of the Armco iron are not presented here, but the moduli were linear within experimental error.

These experiments on three very different elastic solids imply two general conclusions. First, the second-order theory is adequate in describing the behavior of elastic solids under large hydrostatic pressures and under anisotropic stress up to the elastic limit, even if moduli are measured directly rather than computed from static measurements. Second, there seems to be no physical reason for assuming particular values of the Murnaghan constants as has been done in some cases. It is evident that in many practical problems they are not important, simply because the strains are small. In static measurements of extreme precision, problems of wave propagation in which the moduli are measured

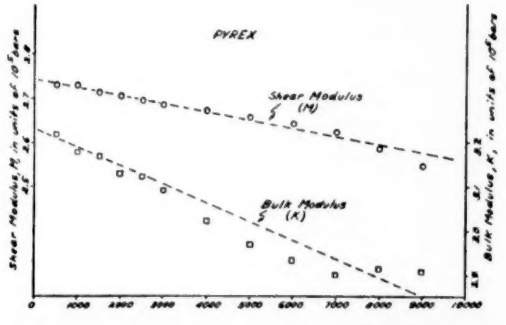

FIG. 4. Shear modulus M and bulk modulus K as a function of pressure for Pyrex.

directly, and determination of density at extremely high pressure these constants are important.

Lazarus[11] studied the variation of the moduli of several cubic crystals under hydrostatic pressures up to 1000 bars. Hearmon[13] has used his data to compute three relations between the third-order constants of the cubic crystals. The methods of measurement under anisotropic stress described here in addition to measurements under hydrostatic stress would in principle make possible the evaluation of all the third-order constants of cubic crystals of both classes.

Several authors[4,9,14] have considered the effect of stress upon elastic wave velocities. Brillouin[4] in the first approximation concluded that pressure decreased the velocity of both dilational and rotational waves. This was obtained by neglecting the third-order terms in the energy. When these terms are included, however, [Eqs. 76, 77 of reference 4] results agreeing exactly with the first two equations of set (12) of the present paper are obtained. It is necessary in Brillouin's equation to set the initial pressure equal to zero since our equations are referred to zero strain as the initial state.

As was forecast by Brillouin,[5] the third-order constants appear to be in general negative and an order of magnitude larger than the second-order constants λ and μ. Our present data are not conclusive on this point, but reference to Eq. (12) shows that this is true for any material if the elastic velocities increase with applied hydrostatic pressure. This is the case for every material that has been studied except glasses.

[13] R. F. S. Hearmon, Acta. Cryst. **6**, 331 (1953).
[14] F. Birch, J. Appl. Phys. **9**, 279 (1938).

PHYSICAL REVIEW VOLUME 92, NUMBER 5 DECEMBER 1, 1953

Search for the Hall Effect in a Superconductor. I. Experiment

H. W. LEWIS
Bell Telephone Laboratories, Murray Hill, New Jersey
(Received August 24, 1953)

A search has been made for a Hall effect in superconducting vanadium, using a new method that avoids some of the difficulties previously encountered. The result is negative, with an upper limit of 150×10^{-6} emu, which can be compared with the value of 800×10^{-6} emu for normal vanadium. The theoretical implications will be discussed in a separate paper.

I. INTRODUCTION

SINCE the early work of Kamerlingh Onnes and Hof,[1] it has been generally supposed that there is no Hall effect in a superconductor. Kamerlingh Onnes and Hof searched for the effect in tin and lead samples, and showed that, within the sensitivity of their method, the Hall voltage disappeared when the magnetic field was below the critical field for the sample. Since, however, they were working as pioneers in the study of superconductivity, they were unaware of some of the properties of the superconducting state that we now understand, in particular, the existence of the intermediate state. We wish to point out that their samples were almost certainly in the intermediate state, and that this alone would probably have been sufficient to lead to their negative result. Consequently, the experimental question must still be considered open, and, in view of the significance attached to the Hall coefficient in the study of any phenomenon of electrical conduction,[2] it has seemed worth while to repeat the experiment, using a method that avoids this difficulty. In Sec. II we will discuss the early experiment more carefully, and the simpler aspects of the question of whether or not there ought to be a Hall effect.

II. DISCUSSION OF THE KAMERLINGH ONNES-HOF EXPERIMENT, AND CURRENT MOBILITY

The arrangement used by Kamerlingh Onnes and Hof was the one ordinarily used for Hall effect measurements; a thin flat plate was oriented perpendicularly to the magnetic field, and pairs of current electrodes and Hall probes were in contact with the edge of the sample. We now know that such a flat plate cannot, except in very small fields, exclude the magnetic field in a real Meissner effect—this would lead to extremely high fields near the edges, which would destroy the superconductivity, and allow the magnetic field to penetrate

[1] H. Kamerlingh Onnes and K. Hof, Leiden Comm. No. 142b (1914); see comments by D. Schoenberg, *Superconductivity* (Cambridge University Press, London, 1952).

[2] In the cases in which current carriers of only one sign are involved, it is well known that the Hall coefficient measures (inversely) the number of current carriers per unit volume. This is, from the theoretical standpoint, an especially important number to know for a superconductor. If current carriers of both signs are present, their contributions to the Hall effect tend to cancel, leading to small Hall coefficients. For example, tin and lead have Hall coefficients about five times smaller than that of copper, and this can be attributed to this effect of their complex band structure. In these cases, one might expect the Hall coefficient in the superconducting state, if it existed, to tell us whether all bands go superconducting at once, or whether only one band actually superconducts. In the latter case, the Hall coefficient should jump as we go into the superconducting state. Unfortunately, the superconducting Hall effect seems not to exist.

the sample. The actual thickness of the sample was $\lesssim 1$ mm, and its lateral dimensions ~ 1 cm, so that even if it were in the optimum shape of an oblate spheroid, an applied field of 300 gauss would lead to fields at the edge of about 2000 gauss. In fact the sample was not an oblate spheroid, so that the fields must have been even higher, and we can be sure that the sample was in the intermediate state. What then has this to do with the Hall effect?

To see this, consider first a simple picture of the origin of the Hall effect, in the case of carriers of only one sign. Suppose we have a long rod of rectangular cross section aligned parallel to the z axis, with its faces determining the x and y axes. Suppose further that a current of density j is flowing in the z direction and a magnetic field H is applied in the y direction. Before the field is applied the charge density in the rod will be uniform according to the theorems of electrostatics. When the field is applied the charges will be accelerated and deflected in the x direction, thus producing a nonuniform charge distribution across the rod.[3] This will continue until the nonuniform charge distribution produces a transverse electric field E, sufficient to counteract the deflection forces of the magnetic field. This is the Hall field. This state of equilibrium is well known to occur when $E=vH$, where v is the drift velocity of the charges and everything is measured in electromagnetic units. In fact, this gives us a simple derivation of the value of the Hall coefficient R, which is defined by

$$R=E/jH, \tag{1}$$

since $j=nev$, where n is the number of carriers per unit volume, and e is their charge. Thus, from (1) we obtain

$$R=v/j=1/ne, \tag{2}$$

which is the usual expression for the simple situation here described. In fact, here lies the importance of the Hall coefficient—it measures directly the number of carriers per unit volume. It cannot be too strongly emphasized, however, that this description is valid only in the simplest cases.

Why, now, this digression? It shows that if for any reason the curreuts filaments were not mobile in the metallic lattice, perpendicularly to their direction of motion, the electric field would not be set up to counterbalance the effects of the magnetic forces, and we would have no Hall effect. But this is the situation in the intermediate state, according to Kamerlingh Onnes and Tuyn,[4] so that we can easily believe that there ought not to be a Hall effect in the intermediate state.[5] This argument does not, however, apply to the superconducting state, as has been shown by several experiments,[6] so that the question of the existence of the Hall effect in the superconducting state must still, from this point of view, be considered open.

III. METHOD AND RESULTS

The method used will be described in greater detail in a separate publication, since it is generally applicable to high-conductivity substances for which measurements of the Hall coefficient are normally most difficult. Consequently, we will be satisfied here with a description of its application to the superconductor used.

The sample was a prolate spheroid of pure, ductile, polycrystalline vanadium, originally from the Electro-Metallurgical Corp.,[7] and its claimed purity was 99.7 percent. Runs were made with the surface machined and then cleaned by soaking in hydrochloric acid, and then after electropolishing, all with the same results.

The spheroid was mounted in a Helmholtz coil, which was also immersed in the helium, and so arranged as to provide a longitudinal magnetic field. Contacts were made to the sample by pressure (provided by phosphor bronze springs) at two points on the equator of the sample, and at one pole.

An audiofrequency current (frequencies of 80 cycles and 800 cycles were used) was then passed through the coil, providing an alternating longitudinal magnetic field. Special precautions were taken to insure that the field wave form was pure. This field then induced the diamagnetic currents in the sample that were necessary to exclude it from the interior of the sample, and we will now be concerned only with the situation in the penetration region of some 500A, since it is only there that we have the magnetic field and current required to produce a Hall effect.

Call the penetration depth λ, the current density j, the magnetic field H, and the Hall electric field E. Then

$$\mathbf{E}=-R(\mathbf{J}\times\mathbf{H}) \tag{3}$$

where R is the Hall constant. This is the more precise form of Eq. (1). Now, in the skin,

$$\mathrm{curl}\mathbf{H}=4\pi\mathbf{J}, \tag{4}$$

since we can certainly neglect the displacement current, so that

$$\mathbf{E}=\frac{R}{4\pi}(\mathbf{H}\times\mathrm{curl}\mathbf{H}). \tag{5}$$

However, there is a vector identity to the effect that

$$\tfrac{1}{2}\nabla(H^2)=\mathbf{H}\times\mathrm{curl}\mathbf{H}+(\mathbf{H}\cdot\nabla)\mathbf{H}, \tag{6}$$

[3] In this particular geometry, the nonuniform charge distribution will consist of surface charge distributions on the faces determined by the y-z plane.

[4] H. Kamerlingh Onnes and W. Tuyn, Proc. Acad. Sci. Amsterdam **25**, 443 (1923).

[5] Another way of expressing this is to say that if in their transverse displacement the superconducting currents meet restraining forces *which do not also affect normal electrons*, equilibrium may be set up without a Hall field. If, on the other hand, they meet mainly forces that act on all electrons alike, whether electrical or not, we will observe a Hall effect.

[6] E. U. Condon and E. Maxwell, Phys. Rev. **76**, 578 (1949); W. V. Houston and N. Muench, Phys. Rev. **79**, 967 (1950).

[7] I am indebted to Mr. D. H. Wenny of these Laboratories for supplying the vanadium, and to Mr. R. A. Ehrhardt, also of these Laboratories, for electropolishing it.

in which the last term on the right-hand side is of order λ/a with respect to the first, where a is a dimension of the sample. This follows from the fact that the magnetic field at the surface of the sample is almost exactly parallel to the surface, and changes appreciably in a distance λ going into the material, as compared with a distance of order a along the surface.

Consequently,

$$\mathbf{E}=\frac{R}{8\pi}\nabla(H^2), \tag{7}$$

and the Hall potential e between the surface of the sample and its interior, obtained by integrating (7), is

$$e=RH_0^2/8\pi, \tag{8}$$

where H_0 is the value of the magnetic field at that point on the surface of the sample with which contact is being made.

It should be noted that (8) is an instantaneous, or dc equation in the case of a superconductor. If, now, H_0 is varying sinusoidally with time, we notice that e will have a dc and a second harmonic component, but no fundamental. This makes it possible to use tuned amplifiers for detection, and in this way to eliminate all difficulties with pickup and therefore neutralization of the fundamental signal.

If we confine ourselves to rms values, and only to the second harmonic part e_2 of the Hall signal, (8) reads

$$e_{2(\text{rms})}=RH_{0(\text{rms})}^2/16\pi\sqrt{2}, \tag{8'}$$

which is the practical form to use. If, for example, R has a typical value of 700×10^{-6} emu, and H_0 is 1000 gauss, then e_2 will be 10 emu, or 0.1 μv, which, in view of the low output impedance of the Hall signal, can be easily and accurately measured. If one were not concerned about staying under the critical field of the specimen, the fact that the signal goes up quadratically with field could be exploited to give really large signals.

The detection system used in this experiment began with a step-up transformer with a gain of 140, to take advantage of the low impedance mentioned above. This was followed by a low-noise amplifier with a gain of 100, and finally by a General Radio type 736-A Wave Analyzer, which is a tuned vacuum-tube voltmeter, with a 4-cycle bandwidth. The combination provided a full scale sensitivity of about 0.02 μv, with a 4-cycle bandwidth.

The procedure was to search for a signal between one of the equatorial electrodes and the polar electrode, and to monitor by looking at the two equatorial electrodes between which there ought not to be a Hall signal. This was done at various magnetic fields up to the critical field as peak, and at temperatures from 1.5°K to 4.2°K. The transition temperature in zero field for vanadium is about 5.1°K.

No observable Hall signal was found, and an upper limit on R of 150×10^{-6} emu can be set. This upper limit is to be compared with the normal value for vanadium at room temperature of 800×10^{-6} emu.[8]

In a separate theoretical paper, we will try to get some insight into this result, and to make more precise its implications for the molecular and phenomenological theories of superconductivity.

In conclusion, I would like to thank Dr. B. T. Matthias for the use of his cryostat for this experiment.

[8] Recently measured by Dr. S. Foner, to whom I am indebted for communicating his result prior to publication.

Energy Loss of Moving Electrons to Dipolar Relaxation

H. FRÖHLICH* AND R. L. PLATZMAN
Department of Physics, Purdue University, Lafayette, Indiana
(Received August 19, 1953)

The relation between energy loss of a moving charged particle and dielectric loss in an insulator is analyzed, and a formula giving the rate of energy loss to dielectric relaxation of an electron traversing a dipolar medium is deduced. For an electron having kinetic energy lower than the lowest electronic excitation potential, this interaction makes a substantial contribution to the total energy loss, one often comparable to the loss to molecular or lattice oscillations. Possible applications in physics and in radiobiology are mentioned.

A PURPOSE of this note is to point to a close relationship between the energy loss of a moving charged particle and dielectric loss in an insulator. This implies in particular that dielectric absorption stemming from dipolar relaxation, which in dipolar substances such as water is very important, should also give rise to a substantial energy loss of a moving charged particle—a fact which appears to have been overlooked, or at least rarely appreciated, heretofore. An understanding of this process is of considerable importance for many theoretical and practical problems in the study of the electrical behavior of solids and liquids, and in the study of chemical and biological effects of ionizing radiations.

For an electron of kinetic energy sufficiently high to excite the electronic system of a molecule, atom, or ion of the medium, that interaction always dominates, and is well understood.[1] If the kinetic energy is lower than the lowest electronic excitation potential, further dissipation of the kinetic energy proceeds by excitation of oscillational modes of the lattice or of individual molecules; the rate of energy loss by this interaction is also rather well understood.[2] It will be shown here that the aforementioned interaction of the electron with the permanent electric dipole moments of molecules in a dipolar medium may contribute significantly to the energy loss in this second energy region. An approximate expression for this contribution to the rate of energy loss will now be deduced.

We shall use a method whereby the moving particle is considered as a moving point charge, and in calculating the rate of transfer of energy to the medium shall neglect in first order the reaction on the particle, which will thus be considered to be moving along a straight path. The rate of transfer of energy can be obtained with the use of the empirically determined complex dielectric constant by developing the field of the point charge into its Fourier components. This method is similar to (and, in first approximation, gives a result identical with) that of the equivalent radiation field first developed by Fermi[3] (see also Williams[4]). It should be noted that, in the problem under consideration, all magnetic effects can properly be neglected.[4] The method is limited, of course, to sufficiently fast particles, and to small energy transfer per "collision."

The electric displacement vector $\mathbf{D}(p, t)$ at a point P due to a point charge e moving with velocity v in a path having shortest distance from P (impact parameter) equal to p has components

$$D_1(p, t)=ep(p^2+v^2t^2)^{-\frac{1}{2}}, \quad D_2(p, t)=evt(p^2+v^2t^2)^{-\frac{1}{2}}, \quad (1)$$

perpendicular and parallel to the direction of motion, respectively (with appropriate choice of the zero of time t). Let

$$\mathbf{D}(p, t)=\int_{-\infty}^{\infty}\mathbf{D}_\omega(p)e^{-i\omega t}d\omega, \qquad \mathbf{E}(p, t)=\int_{-\infty}^{\infty}\mathbf{E}_\omega(p)e^{-i\omega t}d\omega, \quad (2)$$

whence

$$\mathbf{D}_\omega(p)=(2\pi)^{-1}\int_{-\infty}^{\infty}\mathbf{D}(p, t)e^{i\omega t}dt, \qquad \mathbf{E}_\omega(p)=(2\pi)^{-1}\int_{-\infty}^{\infty}\mathbf{E}(p, t)e^{i\omega t}dt. \quad (3)$$

Here $\mathbf{E}(p, t)$ is the electric field strength, and reality of $\mathbf{D}(p, t)$ and $\mathbf{E}(p, t)$ requires that

$$\mathbf{D}_\omega=\mathbf{D}_{-\omega}^*, \quad \mathbf{E}_\omega=\mathbf{E}_{-\omega}^*. \quad (4)$$

Hence,[5] if

$$\epsilon_\omega=\epsilon_1(\omega)+i\epsilon_2(\omega), \quad \epsilon_\omega=\epsilon_{-\omega}^* \quad (5)$$

is the complex dielectric constant (ϵ_1 and ϵ_2 are real), $\omega/2\pi$ being the frequency, then

$$\mathbf{D}_\omega=\epsilon_\omega\mathbf{E}_\omega, \quad \text{or} \quad \mathbf{E}_\omega=\epsilon_\omega^*\mathbf{D}_\omega/\epsilon_\omega\epsilon_\omega^*. \quad (6)$$

The energy transfer from the particle to unit volume at P, due to the complete path of a single particle, is given (ignoring quantum effects) by[6]

$$L(p)=(4\pi)^{-1}\int_{-\infty}^{\infty}\mathbf{E}(p, t)\cdot\frac{\partial\mathbf{D}(p, t)}{\partial t}dt.$$

* Regular address: Department of Theoretical Physics, University of Liverpool, Liverpool, England.

[1] N. Bohr, Kgl. Danske Videnskab. Selskab, Math.-fys. Medd. **18**, No. 8 (1948).
[2] H. Fröhlich, Proc. Roy. Soc. (London) **A160**, 230 (1937).
[3] E. Fermi, Z. Physik **29**, 315 (1924).
[4] E. J. Williams, Kgl. Danske Videnskab. Selskab, Math.-fys. Medd. **13**, No. 4 (1935).
[5] H. Fröhlich, *Theory of Dielectrics* (Oxford University Press, Oxford, 1949).

By use of Eqs. (2) and (4) to (6) we find

$$L(p)=-i(4\pi)^{-1}\int_{-\infty}^{\infty}dt\int_{\infty}^{\infty}d\omega\int_{-\infty}^{\infty}d\mu(\mathbf{D}_\omega\cdot\mathbf{E}_\mu)\omega e^{-i(\omega+\mu)t}$$

$$=\int_0^\infty\frac{\epsilon_2(\omega)}{\epsilon_1^2(\omega)+\epsilon_2^2(\omega)}\mathbf{D}_\omega\cdot\mathbf{D}_\omega^*\omega d\omega. \quad (7)$$

Now from Eqs. (1) and (3),

$$\mathbf{D}_\omega(p)\cdot\mathbf{D}_\omega^*(p)=|D_{1\omega}(p)|^2+|D_{2\omega}(p)|^2$$
$$=(e^2\alpha^2/\pi^2p^2v^2)[K_0^2(\alpha)+K_1^2(\alpha)], \quad (8)$$

where we have introduced a new parameter

$$\alpha=\omega p/v \quad (9)$$

and K_0 and K_1 are the modified Bessel functions of the second kind, of order 0 and 1, respectively. If W is the kinetic energy of the particle, its average rate of loss of energy then follows, with application of Eqs. (7) to (9):

$$-\frac{dW}{dt}=v\int_{p_{\min}}^{\infty}L(p)2\pi pdp$$
$$=\frac{2e^2}{\pi v}\int_0^\infty d\omega\left\{\frac{\omega\epsilon_2(\omega)}{\epsilon_1^2(\omega)+\epsilon_2^2(\omega)}\times\int_x^\infty[K_0^2(\alpha)+K_1^2(\alpha)]\alpha d\alpha\right\}$$
$$=\frac{2e^2}{\pi v}\int_0^\infty\frac{\omega\epsilon_2(\omega)}{\epsilon_1^2(\omega)+\epsilon_2^2(\omega)}xK_0(x)K_1(x)d\omega, \quad (10)$$

where x is defined by

$$x=\omega p_{\min}/v,$$

$p_{\min}$ being the minimum value of p. This value will be taken to be of the order of magnitude of the intermolecular distance d. If the de Broglie wavelength λ of the particle were greater than d, then $p_{\min}=\lambda$ should be chosen, but in this case it will be shown that the results become inaccurate for another reason, and we therefore restrict our treatment to velocities which satisfy

$$v>\hbar/md, \quad (11)$$

where m is the mass of the particle.

It has already been mentioned that a condition for the validity of the method used here requires that, in general, the transfer of energy in a single "collision" be small compared to W. The individual energy-transfer events can in this context be assumed to occur in quanta of energy $\hbar\omega$. Hence the final integral (10) may not be extended beyond

$$\omega_{\max}=W/\hbar,$$

and the main contributions to the integral should arise from frequencies small compared to $\omega_{\max}$. If this is the case, then the value of the integral will be altered only insignificantly if it is extended to infinity instead of to $\omega_{\max}$. Now the maximum effective frequency in the Fourier development occurs at about $\omega\sim v/p_{\min}$. The aforementioned condition thus requires that

$$\omega_{\max}=W/\hbar\gg v/d, \quad \text{or,} \quad x_{\max}=\omega_{\max}d/v\gg1. \quad (12)$$

Since $W=mv^2/2$, this condition is essentially the same as condition (11).

Evaluation of the final integral (10) requires knowledge of $\epsilon_1(\omega)$ and $\epsilon_2(\omega)$. In general $\epsilon_2(\omega)$ has contributions due to the various absorption mechanisms of the medium. [Empirical values of $\epsilon_1(\omega)$ and $\epsilon_2(\omega)$ could, in principle, be used in (10).] For dipolar substances which, like water, show Debye absorption (single relaxation time),[5]

$$\epsilon_1(\omega)=\epsilon'(\omega)+\frac{\epsilon_s-\epsilon_{ir}}{1+\omega^2\tau^2} \quad (13)$$

and

$$\epsilon_2(\omega)=\epsilon''(\omega)+\frac{(\epsilon_s-\epsilon_{ir})\omega\tau}{1+\omega^2\tau^2}, \quad (14)$$

where τ is the relaxation time, $\epsilon_s=\epsilon_0=\epsilon_1(0)$ the static dielectric constant, and ϵ_{ir} the dielectric constant at frequencies sufficiently lower than the lowest main infrared absorption frequency ω_{ir}. The quantity $\epsilon''(\omega)$ describes the absorption due to ionic oscillations in the infrared, and in the regions of still greater frequency; $\epsilon'(\omega)$ describes the corresponding dispersion. In particular,

$$\epsilon'(\omega)\approx\epsilon_{ir} \quad \text{if} \quad \omega<\omega_{ir}, \quad \epsilon'(\omega)\approx n^2 \quad \text{if} \quad \omega>\omega_{ir}, \quad (15)$$

where n is a suitable average of the optical refractive index.

To find the contribution to dW/dt due to Debye absorption alone, we substitute, in the final integral (10), $[\epsilon_2(\omega)-\epsilon''(\omega)]$ for $\epsilon_2(\omega)$. It will be seen from (14) that the quantity $\omega[\epsilon_2(\omega)-\epsilon''(\omega)]$ increases proportionally to ω^2 for small ω, but becomes $(\epsilon_s-\epsilon_{ir})/\tau$, independent of ω, if $\omega\gg1/\tau$. Now Eq. (15) shows that the denominator $(\epsilon_1^2+\epsilon_2^2)$ is smallest for $\omega>\omega_{ir}$, where it is $\epsilon_1^2+\epsilon_2^2\approx n^4$. Thus

$$\frac{\omega[\epsilon_2(\omega)-\epsilon''(\omega)]}{\epsilon_1^2(\omega)+\epsilon_2^2(\omega)}\approx\frac{\epsilon_s-\epsilon_{ir}}{\tau n^4} \quad \text{if} \quad \omega>\omega_{ir}. \quad (16)$$

For $\omega<\omega_{ir}$, the left-hand expression has a considerably smaller value. Therefore the ω integration in (10) can, with sufficient accuracy for our purposes, be restricted to values $\omega>\omega_{ir}$, provided that

$$x_{ir}=\omega_{ir}d/v\ll1, \quad (17)$$

because relatively little energy is then transferred in the region $\omega<\omega_{ir}$, owing to the effective "screening" manifested as a relatively great value of $(\epsilon_1^2+\epsilon_2^2)$. In water, for example,

$$\omega_{ir}\approx3\times10^{13}\ \text{sec}^{-1}, \quad d\approx3\times10^{-8}\ \text{cm},$$

so that, in view of (11), condition (17) is always fulfilled for electrons. (This value of ω_{ir} is obtained from an examination of the available data on the frequency-

dependent refractive index of water,[6] and is that value of ω above which n has essentially the optical magnitude.)

The average rate of energy loss is now found by inserting (16) in (10), and restricting the integration as indicated in the preceding paragraphs:

$$-\frac{dW}{dt}\approx\frac{2e^2}{\pi d}\frac{\epsilon_s-\epsilon_{ir}}{\tau n^4}\int_{x_{ir}}^{x_{\max}}xK_0(x)K_1(x)dx. \quad (18)$$

In view of (17) and (12), the limits of integration can with adequate accuracy now be extended from 0 to infinity. The integral is then equal to $\pi^2/8$. Thus, finally,

$$-\frac{dW}{dt}\approx\frac{\pi e^2}{4d}\frac{\epsilon_s-\epsilon_{ir}}{\tau n^4}. \quad (19)$$

It should be noted that $-(dW/dt)/v$ gives the energy loss per unit of actual path length, but that, because (chiefly) of elastic scattering, there is frequent angular deflection, and the actual path is usually tortuous. Therefore Eq. (19) cannot be used to ascertain a measurable range.

A further limitation of Eq. (19) must be mentioned. According to Sack,[7] the Debye equations (13), (14) become inapplicable at frequencies greater than

$$\omega_c\sim kT\tau/I, \quad (20)$$

where I is an average moment of inertia of the dipolar molecule. Thus expression (19) is not valid when the maximum effective frequency v/d is of order of magnitude greater than ω_c. Together with condition (12), this would limit the applicability of Eq. (19) to particle energies W within the limits given by

$$2\hbar^2/md^2<W<md^2\omega_c^2/2. \quad (21)$$

For water ($I\approx10^{-40}$ g cm^2), $\omega_c\sim5\times10^{15}$ sec^{-1}, and Eq. (19) therefore applies in this case to electrons having kinetic energies in the range between about 1 ev and 10 ev. This restriction does not imply, of course, that energy loss to dipolar relaxation does not occur without the specified range, but rather that Eq. (19) there requires modification. However, the upper limit to W given by (21) does not appreciably diminish the usefulness of (19), because it is usually as high as or higher than the lowest electronic excitation potential, and loss by electronic excitation or ionization,[1] when it is energetically possible, is always very great compared to the dipolar relaxation loss. In this connection it may be noted that dipolar relaxation loss could not possibly account for the allegedly anomalously great stopping power of liquid water for alpha particles,[8] for (19) will always yield too *great* a value of $-dW/dt$ when $v/d>\omega_c$, and even so it gives, for high-energy charged particles, a contribution negligible compared to the electronic loss.

To judge the magnitude of the rate of energy loss, we consider first the case of electrons penetrating liquid water. Here, recent data[9] give, at 20°C, $\epsilon_s=80.4$, $\epsilon_{ir}=4.9$, $\tau=1.01\times10^{-11}$ sec; furthermore, $n\approx1.3$. Then

$$-dW/dt\approx10^{13}\text{ ev/sec}\quad(H_2O_{\text{liquid}},\ 20°C).$$

Equation (19) shows that this rate of energy loss is independent of the electron energy, in the range from 1 ev to 10 ev. Its magnitude is indeed comparable to that of the energy loss[10] by transfer of vibrational quanta (for example, for electrons with an energy of several electron volts, emission of a quantum of 0.1 ev every 10^{-14} second). Moreover, it is temperature dependent, chiefly because of the temperature dependence of τ: in water at 75°C it is about four times[9] as great as at 0°C.

For the case of ice slightly below the melting point, we note that[10] at −0.1°C only $\tau(2\times10^{-5}$ sec) is markedly different from the corresponding quantity for the liquid. Thus

$$-dW/dt\approx10^{7}\text{ ev/sec}\quad(H_2O_{\text{solid}},\ -0.1°C).$$

This result should be valid for all electrons with kinetic energy greater than about 1 ev (the great value of the relaxation time effectively removes the restriction imposed by $v/d<\omega_c$). This will usually be an insignificant magnitude; indeed, the striking difference between liquid and solid water near the melting point could provide the basis for an experimental measurement of the dipolar-relaxation energy loss. As the temperature drops, the reciprocal relaxation time, and therefore the energy loss, declines extremely rapidly.[11]

Our results show that in problems dealing with the motion of electrons of low velocity (below the lowest electronic excitation potential) in dipolar solids or liquids, neglect of the dipolar relaxation excited by the moving charge must introduce an error which may be a great one. This conclusion has an obvious bearing on experiments, with dipolar materials, involving such phenomena as photoconductivity, dielectric breakdown, etc., and in interpretations in radiation chemistry of aqueous systems and radiobiology. In the latter, especially, consideration of the interaction of the many secondary, tertiary (etc.) electrons produced by ionizing radiation, with the medium, which is almost always aqueous in nature, must be essential for a realistic appraisal of fundamental mechanisms. The general role of the dielectric dispersion in radiobiology has already been emphasized.[12]

[6] N. E. Dorsey, *Properties of Ordinary Water-Substance* (Rheinhold Publishing Corporation, New York, 1940), p. 285.

[7] R. A. Sack (private communication, to be published).

[8] R. L. Platzman, in *Symposium on Radiobiology* (John Wiley and Sons, Inc., New York, 1952), Chap. 9.

[9] Collie, Hasted, and Ritson, Proc. Phys. Soc. (London) **60**, 145 (1948); J. A. Lane and J. A. Saxton, Proc. Roy. Soc. (London) **A213**, 400 (1952).

[10] The energy loss due to other types of absorption can, of course, be calculated from the general expression (10), provided that the appropriate dielectric constants and dielectric loss are known as a function of frequency.

[11] R. P. Auty and R. H. Cole, J. Chem. Phys. **20**, 1309 (1952).

[12] J. Franck and R. Platzman, *Radiation Biology* (McGraw-Hill Book Company, Inc., New York, 1954), Vol. 1, Chap. 3.

Absolute Value of Avogadro's Number and the Soundness of Crystals

M. E. STRAUMANIS
Department of Metallurgy, School of Mines and Metallurgy, University of Missouri, Rolla, Missouri
(Received March 30, 1953; revised manuscript received September 8, 1953)

The experimental determination of Avogadro's number by the x-ray-density method is uncertain because of imperfections in crystals. It is proposed to regard the lattice of purest calcite as a reference lattice because of its proximity to a sound lattice, and to accept the value $N_0=6.02567\times10^{23}$ g mole^{-1} (phys.) which is equivalent to 6.02403×10^{23} g mole^{-1} (chem.) for Avogadro's number as derived from measurements on pure calcite. The perfection of the lattices of all other crystalline substances then would be determined in comparison with the calcite as either sound (equal in perfection to that of calcite) within the error limits or as defective (vacancies, interstitial atoms), using the number above for the calculations.

THE most precise value for Avogadro's number is obtained, as already pointed out by other authors,[1] by means of lattice parameter and density measurements in applying the equation

$$N=nM/dv, \tag{1}$$

n being the number of atoms or molecules per unit cell; M the atomic or molecular weight of the substance under investigation; d the density (in g/cm^3); and v the volume of the unit cell (in cm^3). While d and v can be determined to a high degree of accuracy by steadily improving experimental methods, the value of n is somewhat uncertain. Because of imperfections in crystals,[2] n, as the average of a great number of unit cells, might not be an integer but instead a quantity very close to an integer. If the real n is slightly larger than the closest integer (interstitial atoms in the crystal) which is substituted for n, a smaller value for N will be obtained. The reverse relationship holds in the case where there are vacancies in the crystal. N determinations by Eq. (1), using a larger number of different substances, may also not solve the problem, for vacancies are more frequent than interstitial atoms in crystal lattices.

Therefore, in order to obtain the correct Avogadro's number, it is necessary to know the number of imperfections per g atom or per g mole of the crystalline substance. Such a determination, of course, should not be made by the x-ray method, but by an independent method, for instance by conductivity measurements.[3] Unfortunately, such estimations are very uncertain. Consequently, it seems there is no way for the precise determination of the absolute number N_0 to be made, unless a method is found, other than the x-ray, for the exact determination of the extent of lattice defects in crystals.

However, there is still a possibility of solving the problem by agreement. If it is found that a certain substance has a lattice which in its perfection may be very near to a sound lattice (a sound lattice being defined as one with no vacancies and no interstitial atoms), the absolute Avogadro's number N_0 can be calculated by careful density and lattice parameter measurements. Since we now have the absolute Avogadro's number, the x-ray molecular weight M_x of other crystalline substances can be determined, using the same Eq. (1). If one compares these weights with the chemical weights M, one can estimate the number of defects D per g mole of the respective substance[4]

$$D=N_0(M_x-M)/M \text{ (chem. scale)}.$$

With D positive there are interstitial atoms in the lattice; with D negative vacant sites are predominant. If, within the error limits, $M_x-M=0$, then the lattice of the substance is as perfect as that of the reference or normal substance used for the determination of N_0: the lattice is sound. In case there happen to be submicroscopic regions with vacancies and interstitial atoms in equal amounts within the same crystal, then the crystal would appear sound if we apply the above method. However, such a distribution of imperfections is unlikely, especially after heat treatment of the crystals.

The imperfection I of a crystalline substance, that is the ratio of the numbers of imperfect sites to all sites, can also be determined simply by

$$I=(M_x-M)/M, \text{ or } (N_0-N)/N, \text{ or } (d-d_x)/d_x,$$

if one prefers to calculate from x-ray data the value of N for the substance, or the density d_x, instead of M_x.

Thus, for the determination of the soundness of crystals a definite N_0 is needed, which in turn can be found using a substance with a *sound lattice* to make the necessary measurements. It is herewith proposed to regard *purest calcite crystals* as being such a substance, because of the following reasons:

(1) The growth of calcite occured only very slowly during long periods and its lattice should be perfect.

(2) Siegbahn obtained the sharpest x-ray spectral lines only with calcite crystals; this serves as an indication of the perfection of the lattice for the best calcite samples.

[1] R. T. Birge, Phys. Rev. **62**, 301 (1942); U. Stille, Z. Physik **121**, 142 (1943); **125**, 174 (1948).
[2] See, for instance, F. Seith, *Imperfections in Nearly Perfect Crystals* (John Wiley and Sons, Inc., New York, 1952), pp. 3–76.
[3] H. W. Etzel and R. J. Maurer, J. Chem. Phys. **18**, 1003 (1950); F. Seitz, Revs. Modern Phys. **23**, 328 (1951).
[4] M. E. Straumanis, Acta Cryst. **2**, 83 (1949).

TABLE I. The absolute value of Avogadro's constant (physical scale).

	N_0
Du Mond and Cohen (1948)[a]	6.02514×10^{23}
The author (1949)[b, c]	6.02567
Bearden and Watts (1951)[d]	6.02566
Du Mond and Cohen (1952)[e]	6.02544
Stille (1952)[f]	6.02533

[a] See reference 15.
[b] See reference 4.
[c] See reference 13.
[d] See reference 16.
[e] See reference 14.
[f] See reference 17.

(3) Siegbahn's Avogadro constant (N_s) is related to all x-ray wavelength measurements,[5] which in turn, if multiplied by the conversion factor $\lambda_g/\lambda_c=1.00202$, agree perfectly with wavelength measurements made by means of gratings.[6]

(4) $N_{\text{universal}}$ (see Table I, DuMond and Cohen) agrees within the experimental error with N_0 determined from calcite, as shown below.

There also are disadvantages, since even the purest calcite samples contain some impurities in solid solution with the parent crystal,[7] and this changes the molecular weight of the substance.[8] Nevertheless, accurate determinations of N_0 are possible, if thorough analysis of the calcite (for the calculation of M) and precision determinations of lattice parameters and of density are made with the same samples.

However, it is also possible to calculate N_0 using the data already available. Siegbahn's Avogadro number ($N_s=6.0594\times10^{23}$ mole^{-1}),[5] obtained with the molecular weight of $CaCO_3=100.075$, can be easily corrected using the molecular weight for purest calcite (a mixed crystal), and the absolute wavelength in A.

N_0 calculated by means of Eq. (1) is

$$N_0=nM(\text{calcite})/dv, \tag{2}$$

where the volume of the unit cell v is expressed in $A^3/10^{24}$. N_s was obtained, and can be checked, by expressing the volume of the unit cell in $kX^3/10^{24}$ (1 kX is 1000X units), and using the above-mentioned molecular weight for $CaCO_3$:[5]

$$N_s=nM(CaCO_3)/dv'. \tag{3}$$

Assuming that the lattice of calcite is sound (in the sense mentioned above) and that the densities of purest calcite agree within the error limits with that used by Siegbahn, it is easily obtained from (2) and (3) that

$$N_0=\frac{M(\text{calcite})}{M(CaCO_3)}\frac{v'}{v}N_s=\frac{kN_s}{(1.00202)^3}, \tag{4}$$

because $v'/v=1/(1.00202)^3$. The latter is the conversion factor obtained by comparing the x-ray wavelengths, as measured by means of a grating and by the calcite crystal.[9]

The factor $k=100.095/100.075=1.00020\pm0.00003$ was previously determined by the author in 1944, and its necessity emphasized for determinations of x-ray molecular weight and Avogadro's number.[8,10] However, the respective papers, because of the war, did not appear in print until 1949, although they were accepted for printing in October, 1944. A paper by Birge, suggesting the same correction for Avogadro's number because of solid solution formation, appeared in 1945.[11]

If one considers only the change in the atomic weights of Ca and C since the time of Siegbahn's measurements, a value of $100.090/100.075=1.000149$ could be obtained. On the basis of the analysis of purest calcite samples,[12] a molecular weight of 100.095 was calculated for calcite, and the factor k then became 1.0002. Substituted for k in Eq. (4) the absolute Avogadro's number is[4,13]

$$N_0=(6.02403\pm0.00025)\times10^{23}\text{ g mole}^{-1}\text{ (chem.)},$$
$$N_0=(6.02567\pm0.00026)\times10^{23}\text{ g mole}^{-1}\text{ (phys.)}.$$

The relative error was computed assuming that $\Delta k=3\times10^{-5}\ k$, $\Delta(\lambda_g/\lambda_c)=1.1\times10^{-5}(\lambda_g/\lambda_c)$,[14] and $\Delta r=0.5\times10^{-5}\ r$, Δr being the error for the Smythe factor.[14] The systematic error, which is caused by the imperfections which still may be present in the crystals, is of course not known.

The reciprocal value of N_0 is 1.66002×10^{-24} (chem. scale) and not 1.66035×10^{-24} as derived from the old $N=6.02282\times10^{23}$. Calculated densities d_x then are given by the relation

$$d_x=1.66002\ nM_{\text{chem}}/v,$$

with v in A^3. Thus, the density value of purest calcite appears as a reference value.

Table I shows the agreement of N_0 (in the physical scale) with the evaluation of Avogadro's number by some other investigators.[4,13–17] These figures show that the value of N_0, derived from measurements made with purest calcite, is in excellent agreement with other evaluations, especially with those made by Bearden and Watts. It agrees also with the universal constant as calculated by the method of DuMond and Cohen, confirming the assumption of the soundness of the calcite lattice.

The proposition of regarding calcite as a reference substance with a lattice nearest to a sound one is therefore justified, and the perfection of lattices of other crystalline substances can now be compared with that

[5] M. Siegbahn, *Spektroskopie der Röntgenstrahlen* (J. Springer, Berlin, 1931), second edition, p. 43.
[6] K. Lonsdale, Acta Cryst. **3**, 400 (1950); W. L. Bragg, J. Sci. Instr. **24**, 27 (1947).
[7] A. Ieviņš and M. Straumanis, Z. Physik **116**, 194 (1940); see also K. W. Andrews, Mineralog. Mag. **29**, 85 (1950).
[8] M. Straumanis, Z. Physik **126**, 49, 60 (1949).
[9] J. A. Bearden, J. Appl. Phys. **12**, 395 (1941).
[10] M. Straumanis, Z. Physik **126**, 65 (1949).
[11] R. T. Birge, Am. J. Phys. **13**, 67 (1945).
[12] M. Straumanis and A. Dravnieks, Z. anal. Chem. **120**, 168 (1940).
[13] M. E. Straumanis, J. Appl. Phys. **20**, 726, 733 (1949).
[14] J. W. M. DuMond and E. R. Cohen, Am. Scientist **40**, 447, 450, 458 (1952).
[15] J. W. M. DuMond and E. R. Cohen, Revs. Modern Phys. **20**, 82 (1948).
[16] J. A. Bearden and H. M. Watts, Phys. Rev. **81**, 73 (1951).
[17] U. Stille, Physik. Bl. **8**, 397, 403 (1952).

one of calcite, using the value for N_0 as derived in the foregoing.

Note added in proof:—The new value for λ_g/λ_c recently calculated by DuMond and Cohen[18] is 1.002063. Substituting this value for 1.00202 in Eq. (4), $N_0=6.02489\times10^{23}$ (physical scale) is obtained, which is even in a better agreement with 6.02472×10^{23}, the newest $N_{\text{universal}}$ of the two authors,[18] than those of Table I. But if one uses the newest N_0, the respective λ_g/λ_c also must be used.

[18] J. W. M. DuMond and E. Cohen, Revs. Modern Phys. **25**, 691, 706 (1953).

PHYSICAL REVIEW VOLUME 92, NUMBER 5 DECEMBER 1, 1953

The Binary Rearrangement Collision*

SAUL ALTSHULER
Department of Physics, Iowa State College, Ames, Iowa

(Received July 3, 1953)

The theory of the general binary collision is discussed, and it is demonstrated that the rearrangement scattered amplitude can be derived from the integral equation which is convenient for determining the direct (no rearrangement of particles) scattered amplitudes. As a consequence, it is shown that no ambiguity in matrix element for the rearrangement amplitude in Born approximation exists.

THE binary rearrangement collision is a process in which a system A in state n collides with a system B in the state m, and systems C in state s and D in state t emerge. We shall consider events in which no photons are involved and that no particles appear or disappear. In previous treatments[1,2] of the general two-body collision different unperturbed Hamiltonians are employed for developing the stationary state integral equations. If no rearrangement of particles occurs in the collision, the relevant unperturbed Hamiltonian is that describing the relative motion of the two noninteracting systems A and B. If a rearrangement of particles occurs so that systems C and D appear, then it is convenient to select as unperturbed Hamiltonian that pertaining to the relative motion of C and D as noninteracting systems. However, with the latter procedure it is not clear from the derived integral equation in what way the boundary conditions are met since the incident wave, which is an eigenfunction of the alternative unperturbed Hamiltonian referring to systems A and B, is manifestly not present. Indeed, it is not apparent that the corresponding integral equations resulting from the separate imposition of the outgoing boundary condition describe the same wave function. Clearly, a single integral equation satisfying the boundary conditions should provide the amplitudes pertinent to any event, rearrangement or otherwise. It is the purpose of this note to demonstrate that this is indeed the case, and incidently to remove the serious ambiguity in matrix element arising in the Born approximation for rearrangement amplitudes. This ambiguity stems from the fact that either of the interaction energy operators between systems A and B, or C and D, yield the same matrix element[2] when exact wave functions for the unperturbed systems are presumed. However, such wave functions do not exist except in the very special three-body collision of electrons with hydrogen atoms, so that, in general, a difference in matrix element necessarily arises. For rearrangement (exchange) scattering of electrons from atoms this ambiguity has been referred to as "prior-post discrepancy,"[3,4] and has been clarified by an analysis[5] which will now be extended to the general binary collision.

We wish to solve the wave equation

$$(H-E)\Psi=0, \tag{1}$$

where the Hamiltonian can be written in either of two ways,

$$H=H_{AB}+V_{AB}=H_{CD}+V_{CD}. \tag{2}$$

Since the entire calculation is performed in the center-of-mass system, the unperturbed Hamiltonians for the initial and final systems may be written as

$$H_{AB}=H_A(\mathbf{r}_a)+H_A(\mathbf{r}_b)-\frac{\hbar^2}{2\mu_{AB}}\nabla_{r_{ab}}{}^2,$$

$$H_{CD}=H_C(\mathbf{r}_c)+H_D(\mathbf{r}_d)-\frac{\hbar^2}{2\mu_{CD}}\nabla_{r_{cd}}{}^2.$$

Here $\mathbf{r}_a$, $\mathbf{r}_b$, $\mathbf{r}_c$, and $\mathbf{r}_d$ are the internal coordinates of the respective systems, while $\mathbf{r}_{ab}$ and $\mathbf{r}_{cd}$ denote the vectors that connect the centers of mass of the systems A, B and C, D respectively. For the internal motion we

* The research reported in this paper has been sponsored by the Geophysical Research Directorate of the Air Force Cambridge Research Center, Air Research and Development Command.

[1] N. F. Mott and H. S. W. Massey, *Theory of Atomic Collisions* (Oxford University Press, New York, 1949), second edition.

[2] L. I. Schiff, *Quantum Mechanics* (McGraw-Hill Book Company, Inc., New York, 1949), p. 230.

[3] Bates, Fundaminsky, and Massey, Trans. Roy. Soc. (London) **243**, 93 (1950).

[4] Corinaldesi, Trainor, and Wu, Nuovo cimento **9**, 436 (1952).

[5] S. Altshuler, Phys. Rev. **91**, 1167 (1953).

introduce the sets of eigenfunctions and eigenvalues $u_n^A(\mathbf{r}_a)$, $u_n^B(\mathbf{r}_b)$, $u_n^C(\mathbf{r}_c)$, $u_n^D(\mathbf{r}_d)$ and ϵ_n^A, ϵ_n^B, ϵ_n^C, ϵ_n^D, corresponding to the internal energy operators $H_A(\mathbf{r}_a)$, $H_B(\mathbf{r}_b)$, $H_C(\mathbf{r}_c)$ and $H_D(\mathbf{r}_d)$.

In order to deduce the appropriate integral equation for the problem, we introduce the outgoing Green's function which is defined by

$$(E-H_{AB}(\mathbf{r}_{ab},\mathbf{r}_a,\mathbf{r}_b))(\mathbf{r}_{ab},\mathbf{r}_a,\mathbf{r}_b|G_{AB}|\mathbf{r}_{ab}',\mathbf{r}_a',\mathbf{r}_b')=\delta(\mathbf{r}_{ab}-\mathbf{r}_{ab}')\delta(\mathbf{r}_a-\mathbf{r}_a')\delta(\mathbf{r}_b-\mathbf{r}_b'), \quad (3)$$

where

$$(\mathbf{r}_{ab},\mathbf{r}_a,\mathbf{r}_b|G_{AB}|\mathbf{r}_{ab}',\mathbf{r}_a',\mathbf{r}_b')=\frac{-\mu_{AB}}{2\pi\hbar^2}\sum_{\alpha,\beta}\frac{\exp[ik_{\alpha\beta}|\mathbf{r}_{ab}-\mathbf{r}_{ab}'|]u_\alpha^A(\mathbf{r}_a)u_\beta^B(\mathbf{r}_b)u_\alpha^{A*}(\mathbf{r}_a')u_\beta^{B*}(\mathbf{r}_b')}{|\mathbf{r}_{ab}-\mathbf{r}_{ab}'|}. \quad (4)$$

Here the sums include integration over continuum states, $k_{rs}^2\equiv(2\mu_{AB}/\hbar^2)(E-\epsilon_r^A-\epsilon_s^B)$, and μ_{AB} denotes the reduced mass associated with the motion of systems A and B. We are now prepared to write the integral equation for the motion in the usual form of an incident plus scattered wave,

$$\Psi(\mathbf{r}_{ab},\mathbf{r}_a,\mathbf{r}_b)=\exp[i\mathbf{k}_{nm}\cdot\mathbf{r}_{ab}]u_n^A(\mathbf{r}_a)u_m^B(\mathbf{r}_b)+\Phi(\mathbf{r}_{ab},\mathbf{r}_a,\mathbf{r}_b), \quad (5)$$

where

$$\Phi(\mathbf{r}_{ab},\mathbf{r}_a,\mathbf{r}_b)=\int\int\int(\mathbf{r}_{ab},\mathbf{r}_a,\mathbf{r}_b|G_{AB}|\mathbf{r}_{ab}',\mathbf{r}_a',\mathbf{r}_b')\times V_{AB}(\mathbf{r}_{ab}',\mathbf{r}_a',\mathbf{r}_b')\Psi(\mathbf{r}_{ab}',\mathbf{r}_a',\mathbf{r}_b')d\tau_{ab}'d\tau_a'd\tau_b' \quad (6)$$

and

$$\operatorname*{Lim}_{r_{ab}\to\infty}\Phi=\sum_{\alpha,\beta}\frac{\exp[ik_{\alpha\beta}r_{ab}]}{r_{ab}}F_{\alpha\beta}u_\alpha^A(\mathbf{r}_a)u_\beta^B(\mathbf{r}_b).$$

It is the scattered part of the total wave function which provides the amplitudes for any prescribed process. Consequently, we proceed to deduce the amplitude for finding system D in state t while system C is in the state s. To do so, we shall demonstrate that

$$\operatorname*{Lim}_{r_{cd}\to\infty}\Phi=\sum_{\alpha,\beta}\frac{\exp[iK_{\alpha\beta}r_{cd}]}{r_{cd}}G_{\alpha\beta}u_\alpha^C(\mathbf{r}_c)u_\beta^D(\mathbf{r}_d), \quad (7)$$

which then identifies the required rearrangement amplitude as G_{st}. The F_{ij} are the direct scattered amplitudes (no rearrangement of particles).

We begin with the observation that the Jacobian of the transformation between the two sets of coordinates $\mathbf{r}_{ab}$, $\mathbf{r}_a$, $\mathbf{r}_b$ and $\mathbf{r}_{cd}$, $\mathbf{r}_c$, $\mathbf{r}_d$ is unity. The proof is elementary and will be omitted. Therefore, the element of integration can be represented either as $d\tau_{ab}d\tau_ad\tau_b$ or $d\tau_{cd}d\tau_cd\tau_d$ and is abbreviated in what follows as $d\tau$. Furthermore,

$$\delta(\mathbf{r}_{ab}-\mathbf{r}_{ab}')\delta(\mathbf{r}_a-\mathbf{r}_a')\delta(\mathbf{r}_b-\mathbf{r}_b')=\delta(\mathbf{r}_{cd}-\mathbf{r}_{cd}')\delta(\mathbf{r}_c-\mathbf{r}_c')\delta(\mathbf{r}_d-\mathbf{r}_d').$$

With this result, we now define the Green's function for the operator $(E-H_{CD})$,

$$(E-H_{CD}(\mathbf{r}_{cd},\mathbf{r}_c,\mathbf{r}_d))(\mathbf{r}_{cd},\mathbf{r}_c,\mathbf{r}_d|G_{CD}|\mathbf{r}_{cd}',\mathbf{r}_c',\mathbf{r}_d')=\delta(\mathbf{r}_{cd}-\mathbf{r}_{cd}')\delta(\mathbf{r}_c-\mathbf{r}_c')\delta(\mathbf{r}_d-\mathbf{r}_d'), \quad (8)$$

or

$$(E-H_{CD}(\mathbf{r}_{cd}',\mathbf{r}_c',\mathbf{r}_d'))(\mathbf{r}_{cd},\mathbf{r}_c,\mathbf{r}_d|G_{CD}|\mathbf{r}_{cd}',\mathbf{r}_c',\mathbf{r}_d')=\delta(\mathbf{r}_{cd}-\mathbf{r}_{cd}')\delta(\mathbf{r}_c-\mathbf{r}_c')\delta(\mathbf{r}_d-\mathbf{r}_d'), \quad (9)$$

because of the symmetry character of the Green's function for Hermitian operators. This alternative Green's function is explicitly given by

$$(\mathbf{r}_{cd},\mathbf{r}_c,\mathbf{r}_d|G_{CD}|\mathbf{r}_{cd}',\mathbf{r}_c',\mathbf{r}_d')=\frac{-\mu_{CD}}{2\pi\hbar^2}\sum_{\gamma,\mu}\frac{\exp[iK_{\gamma\mu}|\mathbf{r}_{cd}-\mathbf{r}_{cd}'|]u_\gamma^C(\mathbf{r}_c)u_\mu^D(\mathbf{r}_d)u_\gamma^{C*}(\mathbf{r}_c')u_\mu^{D*}(\mathbf{r}_d')}{|\mathbf{r}_{cd}-\mathbf{r}_{cd}'|}, \quad (10)$$

with $K_{\gamma\mu}^2\equiv(2\mu_{CD}/\hbar^2)(E-\epsilon_\gamma^C-\epsilon_\mu^D)$. Proceeding with the analysis, we rewrite (6) as follows:

$$\begin{aligned}\Phi(\mathbf{r}_{ab},\mathbf{r}_a,\mathbf{r}_b)&=\int\int\int\int\int\int\delta(\mathbf{r}_{ab}-\mathbf{r}_{ab}')\delta(\mathbf{r}_a-\mathbf{r}_a')\\&\times\delta(\mathbf{r}_b-\mathbf{r}_b')(\mathbf{r}_{ab}',\mathbf{r}_a',\mathbf{r}_b'|G_{AB}|\mathbf{r}_{ab}'',\mathbf{r}_a'',\mathbf{r}_b'')\\&\times V_{AB}(\mathbf{r}_{ab}'',\mathbf{r}_a'',\mathbf{r}_b'')\Psi(\mathbf{r}_{ab}'',\mathbf{r}_a'',\mathbf{r}_b'')d\tau'd\tau''\\&=\int\int\int\int\int\int\delta(\mathbf{r}_{cd}-\mathbf{r}_{cd}')\delta(\mathbf{r}_c-\mathbf{r}_c')\\&\times\delta(\mathbf{r}_d-\mathbf{r}_d')(\mathbf{r}_{ab}',\mathbf{r}_a',\mathbf{r}_b'|G_{AB}|\mathbf{r}_{ab}'',\mathbf{r}_a'',\mathbf{r}_b'')\\&\times V_{AB}(\mathbf{r}_{ab}'',\mathbf{r}_a'',\mathbf{r}_b'')\Psi(\mathbf{r}_{ab}'',\mathbf{r}_a'',\mathbf{r}_b'')d\tau'd\tau'' \quad (11)\end{aligned}$$

after transformation to the set of coordinates $(\mathbf{r}_{cd},\mathbf{r}_c,\mathbf{r}_d)$. That is, the sets $(\mathbf{r}_{ab},\mathbf{r}_a,\mathbf{r}_b)$ and $(\mathbf{r}_{ab}',\mathbf{r}_a',\mathbf{r}_b')$ are now regarded as functions of $(\mathbf{r}_{cd},\mathbf{r}_c,\mathbf{r}_d)$ and $(\mathbf{r}_{cd}',\mathbf{r}_c',\mathbf{r}_d')$, respectively. Upon substituting (9) into (11) and utilizing the Hermitian[5-7] property of H_{CD}, we are led to

$$\begin{aligned}\Phi=\int\int\int\int\int\int&(\mathbf{r}_{cd},\mathbf{r}_c,\mathbf{r}_d|G_{CD}|\mathbf{r}_{cd}',\mathbf{r}_c',\mathbf{r}_d')\\&\times[(E-H_{CD}(\mathbf{r}_{cd}',\mathbf{r}_c',\mathbf{r}_d'))\\&\times(\mathbf{r}_{ab}',\mathbf{r}_a',\mathbf{r}_b'|G_{AB}|\mathbf{r}_{ab}'',\mathbf{r}_a'',\mathbf{r}_b'')]\\&\times V_{AB}(\mathbf{r}_{ab}'',\mathbf{r}_a'',\mathbf{r}_b'')\Psi(\mathbf{r}_{ab}'',\mathbf{r}_a'',\mathbf{r}_b'')d\tau d\tau''. \quad (12)\end{aligned}$$

[6] The Hermitian behavior of H_{CD} with respect to G_{AB} and G_{CD} is established by applying Green's theorem and proving that the resulting surface integrals vanish. The proof is analogous to that carried out in detail in reference 5 for the special case of electron exchange impact with hydrogen atoms. A less elaborate, albeit formal, approach is to treat the modified problem in the usual way through the use of a large but finite space for the scattering process with periodic boundary conditions (reference 7).

[7] Reference 2, p. 102.

By making use of the identity given in (2), (12) may be rewritten as

$$\Phi=\int\int\int\int\int\int(\mathbf{r}_{cd},\mathbf{r}_c,\mathbf{r}_d|G_{CD}|\mathbf{r}_{cd}',\mathbf{r}_e',\mathbf{r}_d')\times[\{E-H_{AB}(\mathbf{r}_{ab}',\mathbf{r}_a',\mathbf{r}_b')+V_{CD}(\mathbf{r}_{cd}',\mathbf{r}_e',\mathbf{r}_d')-V_{AB}(\mathbf{r}_{ab}',\mathbf{r}_a',\mathbf{r}_b')\}\times(\mathbf{r}_{ab}',\mathbf{r}_a',\mathbf{r}_b'|G_{AB}|\mathbf{r}_{ab}'',\mathbf{r}_a'',\mathbf{r}_b'')]\times V_{AB}(\mathbf{r}_{ab}'',\mathbf{r}_a'',\mathbf{r}_b'')\Psi(\mathbf{r}_{ab}'',\mathbf{r}_a'',\mathbf{r}_b'')d\tau'd\tau''; \quad (13)$$

and, finally, upon employing (3) and (6) the scattered part of the wave function becomes

$$\Phi=\int\int\int(\mathbf{r}_{cd},\mathbf{r}_c,\mathbf{r}_d|G_{CD}|\mathbf{r}_{cd}',\mathbf{r}_c',\mathbf{r}_d')\times V_{AB}(\mathbf{r}_{ab}',\mathbf{r}_a',\mathbf{r}_b')\Psi(\mathbf{r}_{ab}',\mathbf{r}_a',\mathbf{r}_b')d\tau'+\int\int\int(\mathbf{r}_{cd},\mathbf{r}_c,\mathbf{r}_d|G_{CD}|\mathbf{r}_{cd}',\mathbf{r}_c',\mathbf{r}_d')\times\{V_{CD}(\mathbf{r}_{cd}',\mathbf{r}_c',\mathbf{r}_d')-V_{AB}(\mathbf{r}_{ab}',\mathbf{r}_a',\mathbf{r}_b')\}\times\Phi(\mathbf{r}_{ab}',\mathbf{r}_a',\mathbf{r}_b')d\tau'. \quad (14)$$

In the Born approximation the scattered part of the wave function in (5) is set equal to zero under the integral, with the result that

$$\Phi_{(\mathrm{Born})}=\int\int\int(\mathbf{r}_{cd},\mathbf{r}_c,\mathbf{r}_d|G_{CD}|\mathbf{r}_{cd}',\mathbf{r}_c',\mathbf{r}_d')\times V_{AB}(\mathbf{r}_{ab}',\mathbf{r}_a',\mathbf{r}_b')\exp[i\mathbf{k}_{nm}\cdot\mathbf{r}_{ab}']\times u_n^A(\mathbf{r}_a')u_m^B(\mathbf{r}_b')d\tau'. \quad (15)$$

Consequently,

$$\lim_{r_{cd}\to\infty}\Phi_{(\mathrm{Born})}=\frac{-\mu_{CD}}{2\pi\hbar^2}\sum_{\alpha,\beta}\frac{\exp[iK_{\alpha\beta}r_{cd}]}{r_{cd}}u_\alpha^C(\mathbf{r}_c)u_\beta^D(\mathbf{r}_d)\times\int\int\int\exp[-i\mathbf{K}_{\alpha\beta}\cdot\mathbf{r}_{cd}]u_\alpha^{C*}(\mathbf{r}_c)u_\beta^{D*}(\mathbf{r}_d)\times V_{AB}(\mathbf{r}_{ab},\mathbf{r}_a,\mathbf{r}_b)\exp[i\mathbf{k}_{nm}\cdot\mathbf{r}_{ab}]\times u_n^A(\mathbf{r}_a)u_m^B(\mathbf{r}_b)d\tau, \quad (16)$$

and the Born rearrangement amplitude for finding systems C in state s and D in the state t after A in state n collides with B in state m is given by

$$G_{st}^{(\mathrm{Born})}=\frac{-\mu_{CD}}{2\pi\hbar^2}\int\int\int\exp[-i\mathbf{K}_{st}\cdot\mathbf{r}_{cd}]\times u_s^{C*}(\mathbf{r}_c)u_t^{D*}(\mathbf{r}_a)V_{AB}(\mathbf{r}_{ab},\mathbf{r}_a,\mathbf{r}_b)\times\exp[i\mathbf{k}_{nm}\cdot\mathbf{r}_{ab}]u_n^A(\mathbf{r}_a)u_m^B(\mathbf{r}_b)d\tau. \quad (17)$$

In a similar manner (14) will provide the exact functional for the rearrangement amplitude.

In conclusion, it is evident from (17) that V_{AB}, and not V_{CD}, is the correct interaction energy so that, in principle, no ambiguity in matrix element exists. It should be pointed out that we have treated all the particles as if they were distinguishable. This produces no loss in generality, since linear combinations of the exchange degenerate wave functions can be conveniently formed in the end so that the proper symmetry in each group of identical particles is assured.

A Precision Measurement at 24 500 Volts of the Conversion Constant λ_A*

GAELEN L. FELT,† JOHN N. HARRIS,‡ AND JESSE W. M. DUMOND
Norman Bridge Laboratory of Physics, California Institute of Technology, Pasadena, California

(Received July 21, 1953)

A precision determination of the wavelength in x-units (Siegbahn scale) at the quantum limit of the continuous spectrum from a tungsten target sealed-off x-ray tube operating under an accurately stabilized and measured applied voltage, $V_H = 24\,498.7 \pm 1.1$ absolute volts (emu) is described. This experiment, often loosely described as a measurement of h/e, is, in the present state of our knowledge of the general physical constants, more properly to be referred to as a determination of the conversion constant $V_A\lambda_s$ between x-ray wavelengths and quantum energy in electron volts. If $V_A = V_H + V_w$ is the sum of the absolute applied voltage V_H and the work function V_w of the tungsten cathode emitter and if λ_s is the quantum limit wavelength on the Siegbahn scale expressed in kilo x-units (kx-units), then $V_A\lambda_s = (h/e)c^2(\lambda_g/\lambda_s)^{-1}\,10^8$, wherein h is Planck's constant in erg sec, e is the electronic charge in absolute cgs electrostatic units, c is the velocity of light in cm sec^{-1}, and λ_g/λ_s is the conversion factor from wavelengths measured on the Siegbahn nominal scale in x-units to absolute wavelengths in milliangstrom units (10^{-11} cm). Using the method of isochromats, the value obtained in this experiment, with the 2-meter focusing curved quartz crystal spectrometer for the monochromator was $V_A\lambda_s = 12\,370.02 \pm 0.63$ emu·kx-units, the error ± 0.63, a relative error of 51 parts per million, being our estimated standard deviation. A comparison with other determinations of this type is given. This value has been used as one of some thirteen precision data of eight different types in DuMond and Cohen's recent least-squares adjustment (November, 1952) to determine the "best" values of five fundamental constants: α, the fine structure constant; c, the velocity of light; e, the electronic charge; N, Avogadro's number; and $\lambda = (\lambda_g/\lambda_s)$, the above mentioned wavelength conversion factor; and to obtain from these a large number of other useful constants.

I. INTRODUCTION

MANY precision determinations[1–10] of the wavelength at the quantum limit of the continuous x-ray spectrum from x-ray tubes operating under precisely measured stable dc operating voltages have been made since the first discovery of the inverse photoelectric effect in (1915). This experiment has been variously described as a measurement of Planck's constant h or as a measurement of the ratio h/e, where e is the electronic charge. In the present state of our knowledge of the atomic and other physical constants, the precision with which the electronic charge, e, the velocity of light c, and the conversion factor, (λ_g/λ_s), relating wavelengths expressed on the Siegbahn scale of x-units[11] to absolute wavelengths in milliangstroms are known, is comparable to the precision attainable in the present experiment. It is therefore better to describe this experiment more strictly as a measurement of the conversion constant from quantum energy in electron volts to wavelengths in x-units.

The measurement consists in exciting an x-ray tube with an extremely stable and very accurately measured dc voltage, V_H, and determining with a spectrometer of highest possible resolution the wavelength at the foot of the continuous x-ray spectrum emitted by the tube. Let this quantum limit wavelength, expressed in kx-units (Siegbahn scale), be λ_s. It has been shown,[12] both by theoretical reasoning and by experimental evidence internal to this experiment (coming from determinations made at different voltages), that the quantum energy of the short wavelength limit of the continuous x-ray spectrum corresponds to the energy acquired by the cathode electrons in falling through a voltage $V_A = V_H$

* Supported by funds from the U. S. Office of Naval Research and the U. S. Atomic Energy Commission.

† Now at Los Alamos Scientific Laboratory. This work was the subject of the thesis of G. L. Felt for the doctorate.

‡ Now at the Massachusetts Institute of Technology, Cambridge, Massachusetts.

[1] Duane, Palmer, and Yeh, J. Opt. Soc. Am. **5**, 376 (1921).
[2] H. Feder, Ann. Physik [5] **1**, 497 (1929).
[3] P. Kirkpatrick and P. A. Ross, Phys. Rev. **45**, 454 (1934).
[4] G. Schaitberger, Ann. Physik **24**, 84 (1935).
[5] J. W. M. DuMond and V. L. Bollman, Phys. Rev. **51**, 400 (1937).
[6] P. Ohlin, Inaugural Dissertation, Uppsala University, 1941 (unpublished); Arkiv Mat. Astron. Fysik **A27**, No. 10; **A29**, No. 3; **B29**, No. 4; **A31**, No. 9; **A33**, No. 23.
[7] J. A. Bearden and G. Schwarz, Phys. Rev. **59**, 934 (1941).
[8] Panofsky, Green, and DuMond, Phys. Rev. **62**, 214 (1942).
[9] J. A. Bearden and G. Schwarz, Phys. Rev. **79**, 674 (1950).
[10] Bearden, Johnson, and Watts, Phys. Rev. **81**, 70 (1951).
[11] The wavelengths of a great number of x-ray lines on the Siegbahn nominal scale of wavelengths, in which the unit is now designated as one x-unit (approximately but not exactly 10^{-11} cm), are known by crystal diffraction measurements *relative to each other* with very high accuracy, in many cases one part in 10^5 or better. The constant λ_g/λ_s for converting these wavelengths to the absolute scale in milliangstroms has been determined by a number of workers by ruled grating diffraction at grazing incidence, an outstanding example is the work of J. A. Bearden. (λ_g/λ_s) is probably uncertain to about 3 or 4 parts in 10^5. The abbreviation kx-unit will be used here to denote a unit 1000 times as large as 1 x-unit, hence, approximately but not exactly one angstrom.
[12] The cathode work function correction was first shown to be required in a paper by one of us (see reference 5, also references 8–10). Its validity has been questioned by Ohlin from evidence internal to his experiment but without any theoretical justification of the objection. Later work (references 9 and 10 and the present results) are in accord with the need for this correction. The electron energy converted into x-rays comes in part (chiefly, of course) from the high tension supply which maintains the voltage difference V_H between cathode and anode. A small part of this energy comes also, however, from the cathode filament heating supply which communicates to the thermally emitted electrons enough energy to surmount the cathode work-function barrier V_w. The cooling of the cathode under a heavy demand for such thermally emitted electrons is a well-known phenomenon.

$+V_w$, where V_H is the measured voltage difference between cathode and target, and V_w is the work function of the cathode. The equation,

$$e'V_A=(e/c)V_A=h\nu=hc\lambda_g^{-1}\,10^8 \\ =hc\lambda_s^{-1}(\lambda_g/\lambda_s)^{-1}\,10^8, \quad (1)$$

expresses the conservation of energy for the case of complete conversion (of electron energy to photon energy) in the transition of a free electron[13] from the region of potential just outside the cathode surface to a potential corresponding to the lowest unfilled conduction level in the target. In Eq. (1), e' is expressed in absolute electromagnetic cgs units, e in absolute electrostatic cgs units, V_A and V_w in absolute electromagnetic cgs units, c in centimeters per second, h in erg seconds, λ_s in kx-units (Siegbahn), and λ_g in angstrom units (10^{-8} cm).

Equation (1) then leads to the following expression for the conversion constant $V_A\lambda_s$, the quantity for which the measurements to be described here are designed to yield a numerical value:

$$V_A\lambda_s=(h/e)c^2(\lambda_g/\lambda_s)^{-1}\,10^8. \quad (2)$$

The right-hand member of Eq. (2) gives then the function of the fundamental constants h, e, c, and (λ_g/λ_s) which this experiment really measures. The datum obtained in the present experiment has been introduced in this manner as one of thirteen experimentally obtained numerics belonging to eight different types in a least squares adjustment[14] to obtain the best values (as of November 1952) of five fundamental constants, namely, $\alpha=2\pi e^2h^{-1}c^{-1}$, the fine structure constant; N, Avogadro's number; and the constants, c, e, and (λ_0/λ_s) already defined. From these a large number of other useful constants are obtained.

The chief experimental difficulties result from the necessity for (1) extreme stability and very accurate measurement of the applied voltage, and (2) sufficient luminosity and energy resolution in the x-ray spectrometer to give a very accurate delineation of the profile at the foot of the continuous x-ray spectrum. Since the resolution of crystal diffraction spectrometers is such as to give an approximately constant wavelength uncertainty $|\Delta\lambda|$ nearly independent of wavelength, λ the relative energy uncertainty, equal to $|\Delta\nu|/\nu$ or $|\Delta\lambda|/\lambda$, diminishes with increasing quantum energy in inverse proportion. This places a limit on the highest voltage at which it is profitable to do this experiment; said voltage being higher, the higher the resolving power of the spectrometer. The difficulties in making a high-precision measurement as well as the expense for the precision high-voltage high-resistance potential divider also increase rapidly with increasing voltage at which the experiment is done.

There are, on the other hand, certain reasons why it is desirable to do this experiment at several radically different voltages, some of which shall be as high as possible consistent with the high precision now required for a datum to be used in a least-squares adjustment for the atomic constants. These reasons are related to certain sources of both systematic and random error or uncertainty in the experiment which are of the nature of small unknown or ill-defined additive increments to the measured voltage. They are: (1) impurity films of low atomic number atoms which, if present even in very thin layers on the surface of the target, can retard the incident electrons by many volts before they hit the heavy nuclei of the target proper. Such films, because of their low atomic number, do not themselves yield sufficient continuous spectral intensity to detect the "true" short-wavelength limit from unretarded electron encounters with the light atoms. Other energy uncertainties come from: (2) cathode work function correction, (3) thermal emission velocities of the electrons from the cathode, (4) Thomson effect corrections or thermal electromotive forces, (5) potential differences due to the heating current over the emitting surface of the cathode (unless precautions are taken to insure a constant potential cathode), and (6) sources of voltage ripple in the supply. Correction (2) can easily be by far the largest (4.52 volts, for example, in the case of a tungsten cathode). The value obtained for the constant $V_A\lambda_s$ or h/e will be too high if cause (1) is present and uncorrected. Causes (2) and (3), if uncorrected, make these values too low. Causes (4) and (5) may produce shifts in either direction, and causes (5) and (6) may blur the sharpness of definition of the quantum limit of the spectrum in much the same way as does the limited resolving power of the spectrometer. The reasons, then, why it is desirable to perform the experiment at as high a voltage as possible are: (1) that, by so doing, the relative importance of the above mentioned sources of error is diminished, and (2) that, by comparing results of a high-voltage experiment with those from a lower voltage experiment, internal evidence for the validity of correction (2) can be obtained.

A comparison of the results obtained in this experiment over the last three decades shows a more or less steady increase in the measured values of $V_A\lambda_s$ (or of h/e if one recalculates the results using the same value of c and λ_g/λ_s throughout). This is chiefly due to the fact that as better and better spectral resolving power was used, more and more new structural details at the foot of the continuous x-ray spectrum were progressively revealed which had in previous work been ignored. At each stage the practice of extrapolating the slope of the spectral profile at its lowest observed point with a straight tangent to an intercept with the background tended to give a higher limiting frequency (or a shorter

[13] At the voltage of the present experiment the thermokinetic energy of the electrons just outside the cathode is completely negligible.

[14] J. W. M. DuMond and E. R. Cohen, Revs. Modern Phys. **25**, 693 (1953).

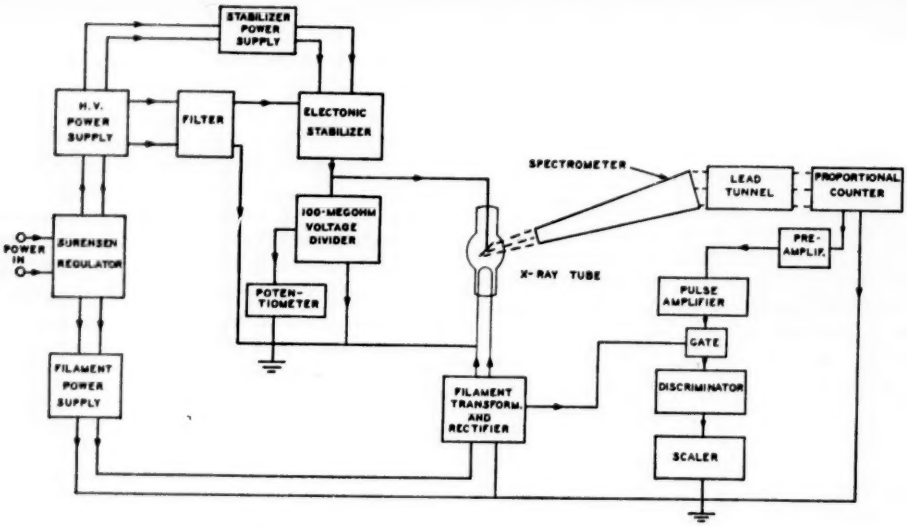

FIG. 1. Block diagram of complete equipment for measuring the conversion constant between quantum energy in electron volts and wavelengths in x-units.

limiting wavelength) than the true quantum limit[15] because the true spectral profile actually fell off to the background more abruptly than did the extrapolated tangent.

On the other hand, the possibility of electron retardation by low atomic number films on the target surface makes it unsafe to regard a *higher* value of $V_A\lambda_s$ (or of h/e) as necessarily a *more reliable* value. All of the later and spectroscopically better resolved experiments[6–10] of this type performed within the last fifteen years have been done with continuously pumped x-ray tubes using organic vapor pumps. It is notoriously difficult to avoid the accumulation of hydrocarbon and other low atomic number deposits in such cases. For this reason we have felt that, in spite of the impressive number of careful recent determinations, there would be a real value in performing one more at as high a voltage as possible consistent with adequate resolution and *made with a completely sealed-off x-ray tube* to remove the last vestige of suspicion regarding accumulation of organic films on the target. It was especially attractive to attempt this because of the availability at this laboratory of the two-meter curved crystal-focusing spectrometer with its exceptionally high luminosity and resolving power.

This work here described has been reported in greater technical detail in the doctorate thesis[16] of one of us, available for private distribution on request, which should be consulted for a more detailed description of the experiment.

II. APPARATUS

The main elements of the apparatus are the x-ray tube, the power supply, the voltage measuring equipment, the monochromator, and the detection and counting equipment. A block diagram of the complete system is shown in Fig. 1.

A. The X-Ray Tube

A "shock-proof" type x-ray tube manufactured by the Eureka X-Ray Tube Corporation of Chicago intended primarily for industrial radiography with a voltage rating of 150 kvp was used. In such a tube the glass vacuum envelope is completely enclosed in an oil-filled metal housing at ground potential which also serves as an x-ray shield. Coaxial high-tension cables enter the housing through large well insulated bushings. The oil not only serves to insulate the high-voltage terminals from the grounded jacket but also cools the x-ray tube target, the heat being removed from the oil by a water jacket on the metal housing. The grounded housing permitted mounting the tube conveniently close to the grounded metal structure of the 2-meter spectrometer[17] without fear of breakdown. It was supported on the upper arm of the spectrometer immediately behind the spherical lead container which usually contains the radioactive gamma-ray source. In place

[15] This statement is worded to fit the case where the voltage is held constant and the x-ray spectrum is explored to find the quantum limit. If, as in the present case, the more usual method of "isochromats" is used, in which the x-ray monochromator is left at a fixed wavelength and the x-ray intensity is plotted as a function of varying applied tube voltage, exactly the same sort of error is introduced.

[16] Doctoral thesis of Gaelen L. Felt, California Institute of Technology, 1951 (unpublished).

[17] For adequate descriptions of the two-meter curved quartz crystal focusing spectrometer, see J. W. M. DuMond, Rev. Sci. Instr. **18**, 626 (1947); also Muller, Hoyt, Klein, and DuMond, Phys. Rev. **88**, 775 (1952).

of this source a special slit was provided exactly on the focal circle, the tube being aligned so that radiation from the target shining through this slit would illuminate the entire aperture of the curved crystal.

B. The Stabilized Power Supply

The elements composing the stabilized high voltage power supply were: (1) the primary voltage regulator (a 2-kva 220-volt Sorenson type, Model 2000-2S, which regulates its output to 0.1 percent against large fluctuations in both line voltage and load); (2) the main high tension transformer and diode rectifiers which were components of a Philips "Search Ray" outfit built for industrial radiography; (3) the high tension ripple filter; (4) the electronic voltage stabilizer which deamplifies fluctuations of the high voltage (both ripple and secular or accidental fluctuations) by absorbing them on the plate of a vacuum tube (Eimac 3C24); and (5) the x-ray tube filament power supply. We describe some of these elements briefly below. For a more detailed description, the thesis[16] should be consulted.

The H.T. transformer with its oil immersed diode rectifiers contained in the same oil tank was altered by a change in the internal connections so as to convert the output from the original 180-kvp half-wave rectified operation to 75-kvp full-wave operation. An x-ray tube filament heating transformer, already built into this unit to supply power insulated from ground for 90 kvp, was adapted to an entirely different use as a source of power for the electronic stabilizer. The latter was entirely at high tension. The x-ray tube filament ran at essentially ground potential, and its power supply was insulated from ground by an insulation transformer merely to permit the insertion of the milliameter for measuring the tube emission current. Further alterations in the Philips set were made by the addition of an extra step-down transformer and Variac (V_1) in the primary winding to furnish a finer control of the high voltage.

A ripple filter was inserted between the high-voltage output from the diode rectifiers and the electronic stabilizer. This filter consisted essentially of three 0.25μf condensers separated by two large 1000-henry oil-immersed chokes on insulated stands especially designed with air-gap cores to avoid saturation of the iron under dc operation. The high-voltage power supply and filter circuits are shown in Fig. 2.

An electronic stabilizer inside a well shielded case at high potential on an insulating stand was placed between the 50 000-ohm protective series resistor (Fig. 2) at the output end of the high-voltage filter and the "load." The load consisted of the 100-megohm working voltage divider in parallel with either (1) the precision megohm calibrating divider, or (2) the x-ray tube depending on whether the object was to check the 100-megohm ratio or to measure the continuous x-ray spectrum quantum limit.

The stabilizer, whose schematic is shown in Fig. 3, is a three-stage direct-current negative feedback amplifier whose output stage is in series with the load. The control signal is developed across 100 000 ohms, (R_s) at the high end of the 100-megohm divider (R_0 and r_0). The signal is amplified primarily in the first two stages and then applied to the grid of the series control tube (V_5). The main power supply (about 20 watts) for the stabilizer, which must be insulated above ground to

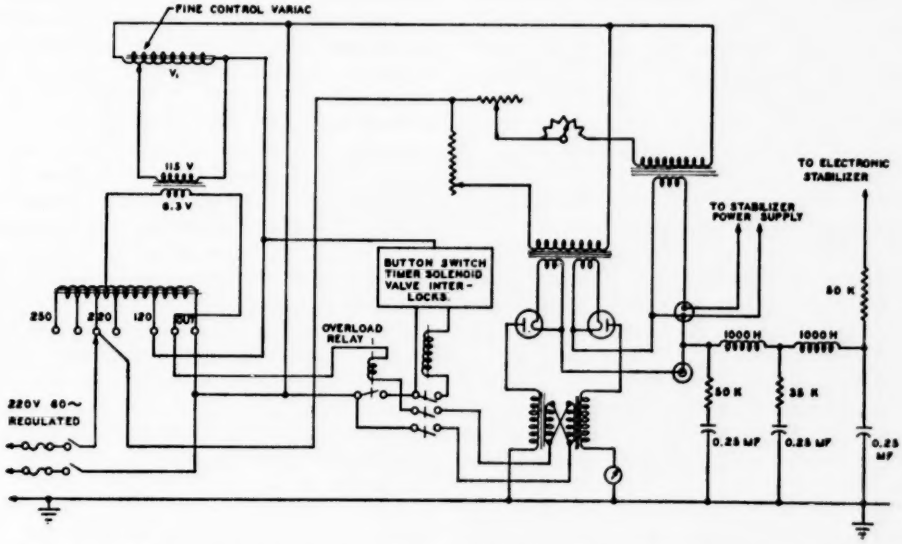

FIG. 2. Two-wave rectified high-voltage power supply and ripple filter. The Sorenson regulator which supplies the regulated 220-volt power is not shown.

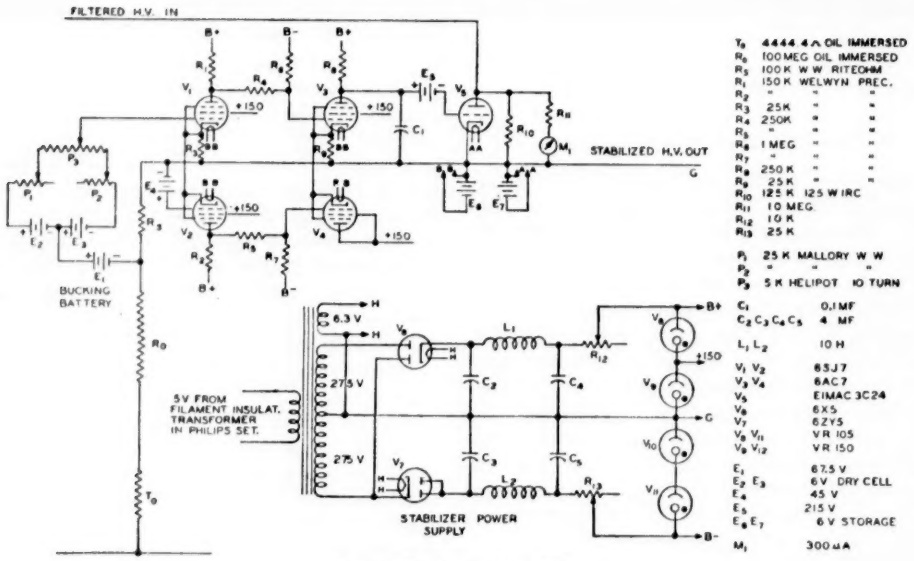

FIG. 3. The electronic stabilizer.

withstand about 30 kv, was derived as stated, from the unused filament transformer in the Philips set, one end of whose five-volt secondary winding was already tied to the high voltage at the input end of the filter. The pentode heaters and the triode filament were supplied by two storage batteries (E_6 and E_7) of approximately 200-ampere-hour capacity.

At some sacrifice of frequency band width in the stabilizer response (as regards the higher frequencies), a much improved stable operation was obtained by placing a 0.1-μf condenser (C_1) from the plate of the second amplifier tube (V_3) to the stabilizer "ground." The high-frequency response thus sacrificed proved unnecessary after visual examination of the stabilizer output on an oscilloscope trace. The secular stability of the stabilizer comes from the 67.5-volt bucking battery (E_1). No current flowed in this battery under operating conditions. A very delicate setting of the bias of the input grid of V_1 over a twelve volt range was permitted by the combination of two banks of four 1.5-volt flashlight batteries, (E_2) and (E_3), with the two 25 000-ohm Mallory controls, (P_1) and (P_2), ganged so as to give, with the 5000-ohm ten-turn Helipot (P_3), a constant resistance of 30 000 ohms across the 12 volt battery.

Once the various elements of the experimental apparatus had reached thermal equilibrium, the electronic stabilizer could maintain a preset voltage, for several minutes at a time, within limits of 5 parts per million and even under rather poor conditions could hold to a part in 10^6.

The exploration of the isochromat over the entire interesting range in the vicinity of the quantum limit could be made by turning the Helipot (P_3) control rod alone. The high-voltage vernier variac (V_1, Fig. 2) did not need to be reset during the runs except after the bridge measurements for checking the 100-megohm divider ratio.

A very stable and finely controllable power supply for the x-ray tube filament was obtained by a combination of three transformers and two variacs. This circuit is shown in Fig. 4. The selector switch was provided with silver contacts and in series with it was a vernier or fine control given by the output of two variacs stepped down, one through a 12.5-, the other through a 2.5-volt filament transformer.

Across the secondary of the x-ray tube filament transformer were connected the x-ray tube filament and a Selenium rectifier in series. The voltage supplied to the filament was about 9 volts peak and was half-wave rectified so that the filament was heated only during a half-cycle. During the other half-cycle the filament, though still emitting electrons because of its slow thermal response, was electrically essentially at ground potential over its entire length. The potential drop of 0.03 volt through the meter, ($M.A$), under the operating load current of 10 milliamperes was completely negligible. A signal through the lead marked "gate" in Fig. 4 went to the counting equipment which was gated to record counts only during the interval of each cycle while the tube filament was not being supplied with power.

Convenient switching facilities were provided in the high voltage power supply so that the x-ray tube could be disconnected and replaced by the precision megohm divider (to permit checking of the ratio of the working 100-megohm divider) and *vice versa*. A movable copper link on an insulating handle with the ends of the link dipping in mercury cups was used for this.

Under working conditions a residual ripple of about 2 volts remained in the 24 500 volts applied to the x-ray tube. This residue, which the electronic stabilizer, was unable further to reduce, appeared as a result of the transients from the half-wave rectified heating supply for the x-ray tube filament reacting back through the main power supply. Ripple does not, of course, affect the mean value of the high voltage (the quantity we measure) but it does reduce the sharpness of the quantum threshold in a manner similar to the limited resolving power of the monochromator. The dc measurement of the high voltage (by means of resistance divider, potentiometer, and galvanometer) measures the *mean value* of the voltage averaged over a time of the order of the galvanometer period.

The high-voltage power supply and precision high-voltage measuring equipment were in one room, the x-ray tube, monochromator, and counting equipment in another. This arrangement, originally occasioned by space requirements, proved of great value since it reduced many problems of both x-ray shielding and electrical interference and most important of all made possible much better constancy of ambient temperatures.

C. The H.T. dc Voltage Measuring Equipment

The elements of the equipment for the high precision measurement of the high dc voltage applied to the x-ray tube were the 100-megohm working voltage divider (operating continuously in parallel with the x-ray tube), the precision manganin megohm divider (for calibrating the ratio of the 100-megohm working divider), the potentiometer, and the galvanometer.

The working divider, by means of which the voltage applied to the x-ray tube could be continuously observed, consisted of 100 Shallcross 1-megohm Nichrome[18] wire-wound resistors (rated current 1 ma) connected in series with a 100 000-ohm Riteohm wire-wound resistor at the high voltage end (R_0 in Fig. 3), which provided the control signal for the electronic stabilizer, and with a specially wound Manganin low resistance (r_0 in Fig. 3) across which the voltage applied to the potentiometer was developed at the low end of the divider.

The 100 Shallcross resistors were mounted in six Lucite tubes each $1\frac{1}{2}$ inches in inside diameter and 52 inches long and with $\frac{1}{4}$-inch walls. These tubes were held in a horizontal position, one above the other, on bakelite supporting brackets which supported each tube at points 10 inches from either end. The oil-tight metal caps closing both ends of each tube were connected alternately in pairs at either end by $\frac{3}{8}$-inch copper tubing to form a sort of switchback array through which oil was continuously pumped. The resistors were centered in the Lucite tubes by means of Lucite spacers $1\frac{1}{2}$ inches in diameter and $\frac{1}{2}$ inch thick through each of which five holes were drilled. The center hole held a short piece of brass tubing threaded to engage the studs on the ends of the individual Shallcross resistors. The remaining four holes permitted the oil to flow through the tubes.

The practice in using this working resistance divider was to adjust its dividing ratio, by a bridge measurement, so as to coincide with a standard ratio set up with the precision manganin megohm divider. To make the working divider ratio adjustable a 100 000-ohm decade box (not shown in Fig. 3) was inserted between the bottom Shallcross resistor and the 4444.4-ohm low-resistance member r_0 of the divider. Both the 100 000-ohm signal resistor at the high end for the stabilizer and the 100 000-ohm decade box trimmer at the low end were thus included in the nominal 100 megohms of the high-resistance segment of the working divider.

The oil was pumped through the Lucite resistor tubes and through a water-cooled (or heated) heat exchanger by a small motor-driven gear pump backed by a reservoir with a 6-foot head, the entire oil system being carefully shielded from contact with atmospheric water vapor to insure maintenance of a high leakage resistance for the shunt electrical path, offered by the oil, around the Shallcross megohms. The oil flowed into the resistor tubes at the low-voltage end and returned from the high-voltage end to the pump through a long Lucite fall pipe. Owing to the relatively large temperature coefficient of the Nichrome wire the oil temperature was carefully regulated by controlling the water tem-

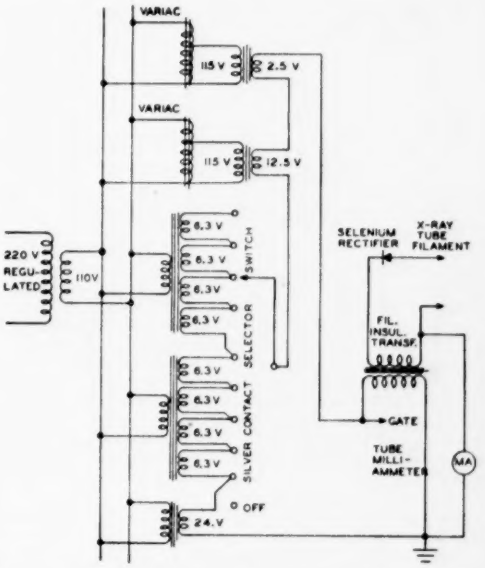

FIG. 4. The filament power supply for the x-ray tube cathode.

[18] Manganin wire, whose much lower temperature coefficient of resistance would have made it far more suitable for the working divider, would have been prohibitively expensive in sufficient resistance not to overload the power supply with the x-ray tube also operating in parallel.

perature in the heat exchanger to within 0.1°C at 31° by means of a mercury thermal regulator and an electrical heater. The 4444.4-ohm low-resistance manganin segment of the divider was oil-immersed (at room temperature) and was very insensitive to temperature changes compared to the 100-megohm Nichrome segment. Any variations in the divider ratio could therefore be attributed with negligible error to the 100-megohm segment alone.

The 1-megohm manganin precision divider[19] was entirely designed and built at this Institute to serve as a means of establishing very large resistance ratios to extremely high precision by an ingenious series-parallel method discussed by Wenner[20] and attributed to Lord Rayleigh. It consist of one hundred coils of 10 000 ohms and twelve other coils of low resistance: five 80-ohm, four 100-ohm, and three $133\frac{1}{3}$-ohm coils. The 10 000-ohm coils were wound with No. 36 manganin wire and the low resistance coils with No. 30 manganin. All the coils were wound on enameled brass tubing 1 inch in diameter and 21 gauge. Each 10 000-ohm coil occupies seven inches on each coil form. Great care and attention was paid to the enameling, insulation, winding, baking, and thermal normalizing of these coils to give maximum stability of resistance and freedom from electrical leakage.

The coils were mounted with the bottom ends of the tubes in holes in the false bottom of a spacious oil-tight Lucite box. A Lucite well opening through the false bottom and containing a thermoregulator, a heater, and an impeller shaft was placed in the center of the box with the impeller itself below the level of the false bottom on which the coils were mounted. The entire box was filled with high-resistance oil. The rows of coils were separated by Lucite baffles in such a way that oil from beneath the false bottom was forced up inside each coil form to its top and was then drawn down the outside of the coils before returning to the impeller through the central well.

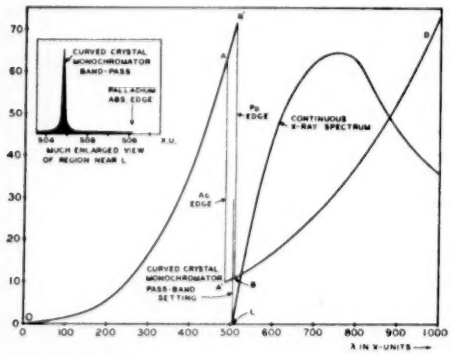

FIG. 5. To illustrate the operation of the filtering technique. Curves $OAA'BD$ and $OAB'BD$ give, for the silver and palladium filters respectively, as a function of wavelength in x-units the product of the mass absorption coefficient into the effective surface density of each filter. The surface densities of the filters are "balanced" to make the curves coincide in the regions OA and BD. The insert shows how the wing or tail of the monochromator pass-band, which would otherwise transmit appreciable intensity when integrated over the intense regions of the continuous spectrum, is clipped by applying the Ross balanced filter technique. One can also see why the silver filter alone, curve $A'BD$, is very effective.

The entire unit was thermostated to maintain the oil at the optimum working temperature for the manganin wire. In ± 2°C variation from the operating temperature the divider changes by as little as 3 parts per million. The divider was intended to be operated at 10 kv but the design was so generous that operation at 25 kv for limited periods proved entirely feasible. This fortunate circumstance permitted a determination of the 100-megohm divider ratio directly at the working voltage and thereby eliminated the necessity for making an extrapolation by means of the 100-megohm load coefficient.

The potentiometer used to measure the voltage across the low-resistance segment of the working divider was a Rubicon High Precision Type B designed with compensating slide-wire contacts which serve to reduce thermal emf's developed by the usual single slider to a very low value indeed. Since the bulk of the voltage developed across the low segment of the working divider was bucked out by a standard cell, the potentiometer could be used in its 0 to 160-millivolt range with a limit of error of 10 microvolts.

A Leeds and Northrup 2430-D galvanometer was used with the potentiometer for the voltage measurement (but not for calibration of the dividers). With a sensitivity of 0.0004 microampere per mm, one-mm deflection on this instrument represented a deviation of 2 parts per million in the applied high voltage.

D. The X-Ray Monochromator

In the present experiment, monochromatization was effected in two stages, firstly and roughly through the use of filters to suppress the strong integrated effect of the continuous spectrum at wavelengths longer than the immediate quantum limit value and secondly, with high resolving power by means of the 2-meter curved crystal focusing spectrometer. Figure 5 illustrates the operation of the filtering technique and shows to scale the location of the spectrometer band-pass setting between the K-absorption edges of the two filters used.

A Ross "balanced filter" arrangement[21] using balanced

[19] This precision divider or ratio box, on which considerable care and expense was lavished to make it the last word of reliability and accuracy, has been described in much more detail in a separate article by John N. Harris, Rev. Sci. Instr. **23**, 409 (1952).

[20] F. Wenner, J. Research Natl. Bur. Standards **25**, 229 (1940).

[21] In the P. A. Ross method of balanced filters, two filtering foils of materials having adjacent atomic numbers are alternately introduced in the x-ray beam. In a preliminary experiment, by varying the obliquity of the foils in the beam, the absorptions of the x-rays by each foil are carefully balanced to equality for wavelengths longer than the K-absorption edge of the foil of lower atomic number and shorter than the K edge of the foil of higher atomic number. These are the regions OA and BD in Fig. 5. Thus

foils of silver ($Z=47$) and palladium ($Z=46$) of optimum thickness was tried but isochromats obtained with the silver foil alone filtering the x-ray beam were found to be as good or perhaps better (because of the limited counting statistics of the present experiment) than those obtained by taking the difference between readings with each filter. A substantial loss in statistical accuracy is suffered with the 2-filter method because the uncertainty in the difference of the readings for the two filters is the square root of the sum of the squares of the separate uncertainties of each reading whereas only the statistical uncertainty of one reading is involved in the single filter method. In the present instance, circumstances beyond our control placed unfortunate time limits and deadlines on the performance of this experiment which limited the accumulation of counting statistics to just about such a degree that the data collected with the two-filter method lost by poor statistics about the same amount or perhaps a little more than they gained by the sharpening of the fillet at the foot of the isochromat. With better statistics the Ross balanced filter method would in all probability have proved superior.

The effectiveness of the single filter of silver is clearly due on the one hand to the low absorption coefficient it offers to radiation of the wavelength for which the crystal monochromator is set, (a wavelength purposely chosen just slightly shorter than the critical wavelength of the K edge of the palladium filter and only some four percent longer than the K edge of silver) and on the other hand to the rapidly increasing absorption coefficient it offers, (because that coefficient is proportional to λ^3) to the longer wavelengths where the continuous spectrum is intense.

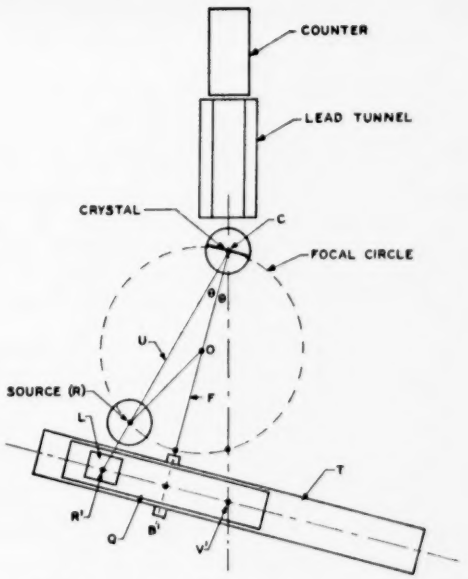

FIG. 6. Schematic lay-out of 2-meter curved crystal spectrometer used as the monochromator. For convenience in identifying the parts the same letters have been used as those in a perspective drawing given in reference 18.

The optimum thicknesses calculated for the foils were

$$X_{Pd}=0.00109 \text{ inch}, \quad X_{Ag}=0.00113 \text{ inch},$$

and these were realized with sufficient accuracy for a good balance, first by rolling and then properly adjusting the foil obliquity in the beam.

The two-meter curved crystal spectrometer was used with a curved quartz monocrystalline slab 2 inches square and 2 mm thick mounted in a stainless steel crystal clamp whose convex jaw was precision profiled to a two-meter circular cylindrical shape. The (310) atomic planes of the crystal, for which $d=1177.637 \pm 0.020$ x-unit (Siegbahn scale) at 18°C,[22] are the ones used for the selective reflection and these stood normal to the large faces of the slab and parallel to the generators and to the axis of the cylinder of curvature imposed by the clamp.

Figure 6 shows schematically the general layout of the spectrometer in plan view in sufficient detail to illustrate and clarify the present discussion.

The defining slit is placed at the point labelled "source," R, in Fig. 6, and the x-ray tube mounted close behind the slit on the upper arm, U, furnishes a diverging beam of radiation through this slit which nearly fills the entire curved crystal aperture (about 20 cm²) at two meters distance. The great advantage of the focusing spectrometer of this type, for x-ray as well as for gamma-ray spectroscopy, lies in the large solid

the *difference* in the two observed intensities when the two foils are successively introduced into a heterogeneous beam of x-rays measures only the spectral intensity in the region between the two K edges. This isolation of a part of the spectrum, it should be noted, is obtained by an arithmetical not a physical subtraction. Ross and others have discussed the calculation of the optimum filter thicknesses. Because of the large value of the K-absorption jump ratio, it is usually possible to make the smaller of the two subtracted readings only a quarter as large as the larger reading, and for lower atomic number filters even more favorable results are obtainable. No more readings are required than without the foils since the method without filters should properly include a "background reading" with a lead shutter blocking the beam for every regular reading with shutter open.

In conjunction with a high resolution crystal monochromator, the use of the balanced filter method for preliminary rough monochromatization to suppress the integrated effect of leakage of the intense continuous spectrum through the long wavelength wing of the crystal monochromator pass-band was first proposed by one of us to improve this type of experiment, and its advantages were more fully illustrated and discussed in the paper by Panofsky, Green and DuMond (see reference 8). At large distances from its peak the crystal diffraction pass-band curve decays with an inverse square law, while the more or less linear rise of the continuous spectral profile upward from the quantum limit gives an integrated leakage effect through the wing of the pass-band to which radiation spectrally quite remote from the limit can contribute materially.

For a treatment of the Ross balanced filter technique, see P. A. Ross, Rev. Sci. Instr. **16**, 433 (1928); P. Kirkpatrick, Rev. Sci. Instr. **10**, 186 (1939).

[22] Watson, West, Lind, and DuMond, Phys. Rev. **75**, 505 (1949).

angle from which monochromatic radiation is collected with excellent resolving power. It was this feature of high luminosity which permitted us to do this experiment with the intrinsically low power delivered by the sealed off x-ray tube in a very limited time.

The instrument was designed primarily to study much shorter wavelengths, of course. At the wavelength of this experiment the need for the "collimator" (a carefully constructed fan-shaped array of lead partitions) disappears, and since this component entails a sacrifice of more than half the radiation, it was removed and replaced by the lead tunnel shown in Fig. 6.

The upper precision drive-screw in the long carriage, Q, is equipped with a carefully divided drum and vernier which enables one to set the screw to 0.001 of a revolution, corresponding quite closely to 0.001 of an x-unit. Since the kinematics of the instrument are such that displacements of the small carriage, L relative to Q, effected by means of this screw, measure the sine of $\frac{1}{4}$ the Bragg angle, the screw revolutions provide a linear wavelength

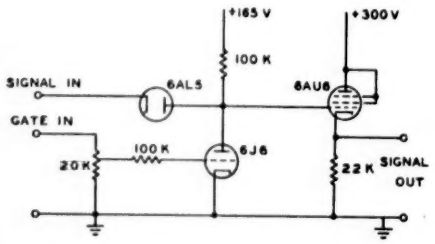

FIG. 7. External discriminator gate. This gate was so phased that counting of x-ray intensity was only recorded during each half-cycle of the rectified filement power supply when no filament current was flowing.

scale of about one x-unit per revolution (save for very small corrections). Since the spectrometer was to be used as a monochromator in one, and only one, fixed position during the running of the isochromats, the elaborate provisions for exploring a spectrum with this instrument were only of use in establishing the calibration of the fixed monochromator setting. This was done by exploring the profiles of four very accurately known calibration lines lying close to that setting, as will be explained. It turns out that the accuracy of the wavelength calibration of the spectrometer, therefore, scarcely plays any role in the wavelength accuracy involved in the present experiment.

A slit width of 0.004 inch was used corresponding to a spectral spread of about 0.1 x-unit. This together with the small aberrations of focus of the crystal and the intrinsic selective diffraction curve of the quartz lattice gave a monochromator band-pass or "window" half-width at half-maximum intensity of somewhat less than 0.12 x-unit equivalent to an energy difference of somewhat less than six volts.

E. The Detection and Counting Equipment

The intensity of the radiation selected by the monochromator was measured by means of a xenon-filled proportional counter, a preamplifier and linear pulse amplifier, two discriminator channels, and two double decade scalers.

The counter case consisted of a copper plated rectangular arc-welded steel box 8 inches long and with an inside cross section 3 inches square. One of the square ends was fitted with a plate in which the pumping line and four Kovar seals were set. The other end was covered by an aluminum window 0.006 inch thick. Because of the large area of the window, required for admitting the diverging beam of radiation from the entire curved quartz crystal aperture, three thin spring-steel ribs were mounted inside the counter to support the window. Two $\frac{1}{8}$-inch glass rods were mounted $\frac{1}{2}$ inch back from the window, parallel to and in the shadows of the two outer ribs. Four tungsten collecting wires of 0.001-inch diameter were stretched between these glass rods and the four Kovar seals at the back of the counter. These four wires were parallel to each other and each was $\frac{3}{4}$ inch from its nearest side walls. Since the inside walls of the counter were slightly rough, a 0.016-inch polished copper liner was inserted in the case. Great care in the construction to observe cleanliness, especially as regards radioactive contamination, was found necessary to maintain a low background counting rate.

This counter was operated with 14 cm of xenon and 1 cm of CO_2 and it proved to be very stable and reliable. For the 500 x-unit radiation used, its length was sufficient to absorb about 25 percent of the beam.

The counter was shielded from local radiation and soft cosmic ray components by heavy removable lead shields providing four inches of lead on all sides save for the opening for the x-ray beam from the lead tunnel.

The electronic circuits were entirely similar to circuits used at the Los Alamos Scientific Laboratory described by Elmore and Sands[23] and they will not be described in great detail here. The pulse amplifier, a modified version of the Los Alamos Model 100 had a gain of 10^4. Both an integral and a differential discriminator were included in one chassis. The integral discriminator puts out a shaped pulse to a scalar for all input pulses larger than an adjustable predetermined amplitude while the differential discriminator puts out a pulse for each input pulse of amplitude lying between two adjustable limits. A fixed pulse-height window width up to 15 volts was used.

Figure 7 shows the gating arrangement inserted between the pulse amplifier and the discriminator input. This gate prevented counting through both discriminators during the part of each x-ray tube filament heating cycle while current was flowing to heat the filament. The phasing of the gate with the filament heating

[23] W. C. Elmore and M. L. Sands, *Electronics: Experimental Techniques* (McGraw-Hill Book Company, Inc., New York, 1949).

current was checked with an oscilloscope, the gate being closed for slightly more than a half-cycle. Thus the x-ray cathode was essentially a unipotential one while the counts were being observed.

Each discriminator was followed by a scale-of-one-hundred scaler consisting of two Berkeley decades in tandem each provided with a Mercury mechanical register.

III. CALIBRATION

A. Voltage Calibration

The primary reference voltage consisted of a bank of six standard cells of the saturated type calibrated and certified by the National Bureau of Standards in September, 1947, and guarded with care in the Calibration Laboratory of this Institute. The bank was kept in a well-insulated box whose temperature was controlled within 0.01° at 30.09°C, and periodic intercomparisons of the six cells have shown a maximum deviation of only 3 microvolts for one of the six from the mean of the group.[24]

A second group of four cells of the unsaturated type was also used. One of these was used as the potentiometer current standardizing cell. The remaining three were available for use as bucking cells in the voltage measurement. These unsaturated cells were also kept at constant temperature in an insulated box. They were recalibrated frequently during the course of the experiment using the saturated cell bank as a primary standard. The electromotive force of the bucking cell used in all final runs in opposition to the voltage developed across the low-resistance segment of the 100-megohm working divider (so that the potentiometer measured the difference of these two) was

$$\text{emf S.C. "B"} = 1.019161 \text{ absolute volts}, \qquad (3)$$

with a conservative limit of error of 5 microvolts.

The determination of the dividing ratio of the 1-megohm precision divider under working load conditions (24.5 kv) requires a knowledge of the "cold" ratio (essentially at no load) and of the load coefficient. The reader is referred to the thesis[16] for the complete details of how these were determined. The paper[19] on the megohm divider also describes these procedures briefly. The precision megohm divider was purposely designed such that the Rayleigh method described by Wenner[20] could be applied to its calibration. The idea essentially depends upon reconnecting the several closely equal units of which both the high and low resistance divider segments consist, the high from series to parallel, the low from parallel to series, in such a way that the two segments which normally have very different resistances, after reconnection have very closely the same resistance so that their ratio, close to unity, can be measured with extremely high accuracy. The high ratio, when the two divider segments are reconnected in the normal working manner, can then be calculated from this measured ratio with high accuracy. It is easy to show that small deviations from the mean of the individual resistor units in each segment only affect the calculation to the second order.

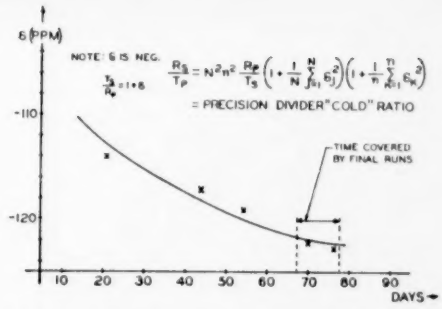

FIG. 8. Slow variation of precision manganin divider "cold" ratio.

The method followed for determining the load coefficient of the precision manganin megohm divider was one described by Curtis.[25] By this method not only the load coefficient of the divider but a slow variation of this coefficient with time after first application of the load were determined. By these means the value of the precision manganin divider ratio at the end of five minutes load under working voltage was determined to be

$$\text{p.d.r.} = 22\,503.52 \pm 0.10 \text{(L.E.)}, \qquad (4)$$

where the uncertainty is a very conservative limit of error. Figures 8 and 9 show the slow variations of the precision divider cold ratio over a period of some

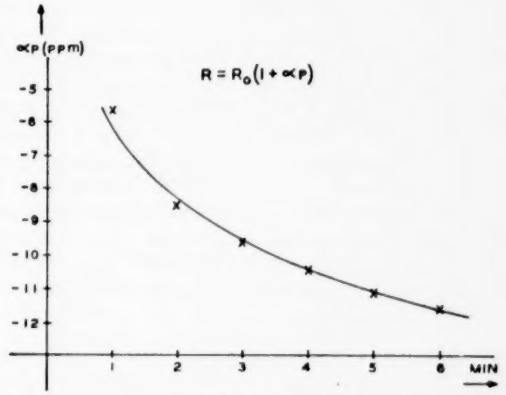

FIG. 9. Time dependence of precision divider load coefficient.

[24] One may therefore safely assume that the mean of the group has not drifted appreciably from the original mean determined at the time of calibration, three years prior to use in this experiment. This conclusion was based on a letter of December 12, 1949, from G. W. Vinal of the NBS to J. N. Harris discussing such possible drifts of the mean. See also F. B. Silsbee, National Bureau of Standards Circular 475 (1949), pp. 9–11.

[25] H. L. Curtis, *Electrical Measurements* (McGraw-Hill Book Company, Inc., New York, 1937); see also reference 19 for a description of this method.

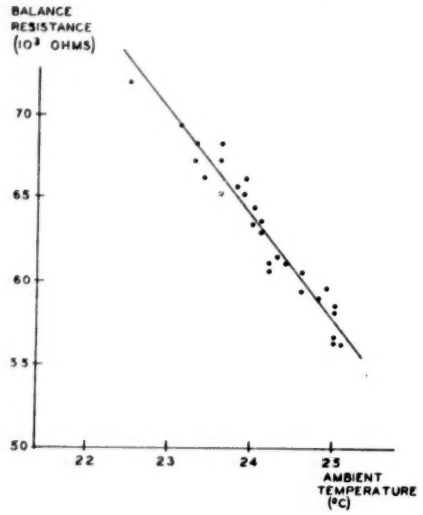

FIG. 10. Dependence of 100-megohm nichrome working divider on ambient temperature.

months and the time dependence of the load coefficient over five minutes. The latter is seen to indicate a change of about one part per million per minute after five minutes loading.

The procedure in the "calibration" of the 100-megohm working divider should in the strict sense be described as an *adjustment* rather than a calibration. Before and after every run of the isochromat the x-ray tube was disconnected from the high-tension supply and the 1-megohm precision divider was put in its place in parallel with the 100-megohm working divider. A Leeds and Northrup 2284-X galvanometer with a sensitivity of 0.25 microvolt per mm at 1 meter and with a circuit resistance of 1100 ohms was used in all of the divider calibration measurements. With this instrument connected across the intermediate terminals between high and low segments of each divider, the 100 000-ohm decade box trimming resistance at the low-voltage end of the 100-megohm segment of the working divider was adjusted to balance this bridge arrangement so that the working divider ratio was made just equal to the precision megohm divider ratio (5-minute loading ratio). In this adjustment a 1.5-mm deflection corresponded to 1 part per million variation in the working divider ratio. After each run on the isochromat was completed (usually $3\frac{1}{2}$ to $4\frac{1}{2}$ hours was required for a run) the working divider ratio was again checked against the manganin precision divider. Except in one or two runs this final bridge balance differed from the initial by less than 5000 ohms (5 parts in 10^5). Corrections were made to the working divider ratio for intermediate potentiometer settings based on a knowledge of the ambient room temperature measured every half hour during each run. Figure 10 shows the measured dependence of the 100-megohm working divider ratio on ambient room temperature. The ordinates give the amount of compensation required in the 100 000-ohm decade balancing resistance as a function of ambient room temperature. The drift of about 5000 ohms per ambient degree corresponds to about 50 parts per million and by using this curve and the recorded room temperatures a correction to each setting of the potentiometer during the isochromat run could be made which in the worst cases, for runs in which temperature variations were greatest, gave an accuracy of the voltage measurement within limits of 2 parts in 10^5.

The load coefficient of the 100-megohm working divider was also measured to ascertain how accurately the high voltage had to be adjusted during the bridge measurements for calibrating the working divider before and after each run. These studies showed that a voltage setting within 250 volts of the working value (24 500 volts), i.e., to one percent amounted to a limit of error of only 5 parts per million from this cause.

TABLE I. Wavelengths of calibration lines on the Siegbahn scale (x-units).

Ag $K\beta_3$	496.65±0.005
Ag $K\beta_1$	496.01±0.005
Sn $K\alpha_2$	494.02±0.005
Sn $K\alpha_1$	489.57±0.005

B. Wavelength Calibration

The wavelength of the pass-band at which the monochromator was set for running the isochromats was, as already stated, selected so as to fall between the K edges of the Ag and Pd filters just to the short-wavelength side of the Pd K edge. The mean value determined for the setting was

$$\bar{\lambda}_{SWL}{}^{(S)} = 504.833 \pm 0.008 \text{ x-units (Siegbahn) at } 24°\text{C}. \quad (5)$$

This wavelength was determined by using four already known and carefully measured[26] x-ray lines as local reference points on the spectrometer wavelength screw. These lines and their wavelengths are listed in Table I.

These four lines were produced by fluorescent excitation using back illumination in foils of silver and tin placed behind the spectrometer resolving slit and in front of the x-ray tube. They were excited by the continuous radiation from the same tungsten target x-ray tube as was used for the isochromat runs. The tube was slightly displaced for this purpose so that direct primary radiation transmitted through the foil and slit would not hit the curved crystal. The tube was mounted on a small transversely displaceable carriage supported on the upper beam of the spectrometer and provided with

[26] Y. Cauchois and H. Hulubei, *Longuerers d'Onde des Emissions X et des Discontinuites d'Absorption X* (Hermann et Cie, Paris, 1947). The silver wavelengths in question were measured by Kellström and the tin wavelengths of Stenman. G. Kellström, Z. Physik **41**, 516 (1927); John Stenman, Z. Physik **48**, 349 (1928).

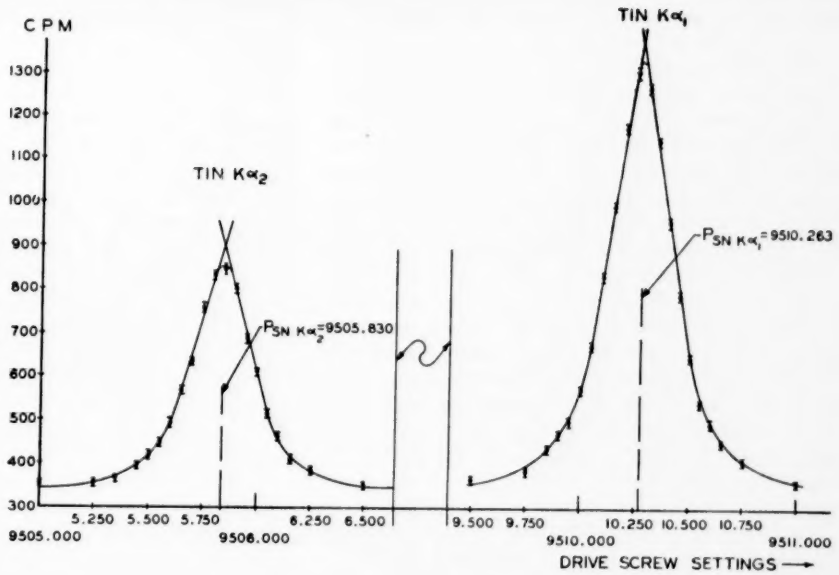

FIG. 11. Fluorescent tin $K\alpha_{1,2}$ doublet used in precision calibration of spectrometer for the monochromator setting. One unit on the scale of the wavelength screw settings corresponds to one x-unit. The $K\alpha_1$ line is seen to have a half-width at half maximum of 0.18 x-unit. The instrumental contribution is about 0.12 x-unit or the equivalent of 6 volts.

a micrometer screw to facilitate this transverse displacement. Most of the weight of the tube was supported by a counterbalancing sling to minimize any possible deflection of the spectrometer slit setting which might be occasioned by this slight shift in the weight of the tube on the spectrometer beam. The fluorescence line profiles were spectrally explored with the tube displaced both to left and to right and no shift in the lines was detected as a result of this process.

Optimum thicknesses for the fluorescer foils were computed using the approximate formula:[27]

$$t_{opt} = (\mu_1 - \mu_2)^{-1} \ln(\mu_1/\mu_2), \qquad (6)$$

wherein μ_1 is the mean linear absorption coefficient in the foil for a wavelength just short of its K edge and μ_2 is the linear absorption coefficient of the fluorescer for its own characteristic K line, the line to be used.

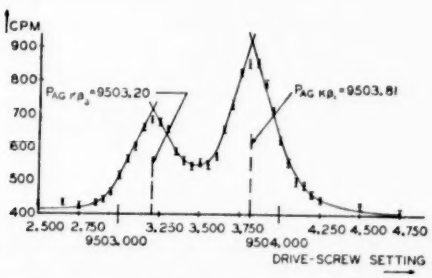

FIG. 12. Fluorescent silver $K\beta_{1,3}$ doublet used in precision calibration of monochromator setting. One unit on the scale of drive screw-settings corresponds to one x-unit.

[27] The approximation is based on the assumption that only that part of the primary continuous spectrum harder than and very close to the K edge is effective in exciting the foil.

Essentially μ_1/μ_2 is the K-jump ratio. This leads to thicknesses of 0.0015 and 0.003 inch, respectively, for silver and tin.

Examples of the profiles obtained for these fluorescence lines with the primary tube operated at 35 kv and 10 ma are shown in Figs. 11 and 12. Several such runs were taken and the mean values of the spectrometer screw settings (for the intersections of straight lines tangent to each side of a line profile) yielded the results shown in Table II. A change of one unit (one turn) in the screw reading corresponds quite closely to a change of wavelength of one x-unit.

The mean screw calibration factor used was

$$\text{S.F.} = 1.00029 \text{ turns/x-unit}, \qquad (7)$$

as obtained in other recent calibration work on the spectrometer.

The estimated probable error in the location of the lines as given above is based on examination of the

TABLE II. Nominal spectrometer screw readings at calibration lines.

Line	Mean reading of wavelength screw[a]
Ag $K\beta_3$	9503.20 ±0.020
Ag $K\beta_1$	9503.81 ±0.015
Sn $K\alpha_2$	9505.830±0.010
Sn $K\alpha_1$	9510.263±0.005

[a] Turns of the screw are read with a Veeder-Root counter coupled to the shaft. The position at which this counter reads "zero" is quite closely, but not absolutely exactly, at the zero wavelength setting of the instrument. For reflections on one side of the crystal planes, save for the small additive zero corrections, turns of the screw indicate nominal x-units directly (before corrections for screw constant and for periodic and secular errors). For reflections on the other side of the crystal planes the reading of the Veeder-Root counter must be subtracted from 10 000 (its maximum and therefore also its zero reading) to obtain the corresponding nominal reading in x-units.

measurements themselves and on the discrepancies arising from the determination of the line location (1) by means of intersecting tangents and (2) by finding the position of the midpoint of the full width at half-maximum intensity. The Sn-$K\alpha_1$ line was much the sharpest and was, therefore, given more weight in determining the wavelength of the monochromator setting for the isochromats. That setting was at a screw reading of 9495.000; i.e., slightly more than 8 x-units from the nearest reference line (Ag $K\beta_3$) and a little over 15 x-units from Sn $K\alpha_1$. In order to locate to 1 part in 10^5 an extrapolated position 15 x-units from a reference point in the region of 500 x-units, one need know the screw calibration factor to only one part in 3000. Thus our knowledge of the decimal digits in the above screw correction factor is only just marginally needed at all. Within the precision with which they could be located, the positions of all four fluorescent lines were entirely consistent with their above listed wavelengths and with the screw calibration factor.

Small changes in room temperature leave the angular geometry of the two-meter spectrometer practically unchanged, so long as no serious local differences in temperature exist, because the entire metal structure has everywhere a quite uniform thermal expansion coefficient. The chief effect of ambient temperature changes on the monochromator pass-band setting come therefore from thermal expansion of the curved quartz crystal lattice. For the (310) planes used this introduces a deviation of 1 part in 10^5 per degree centigrade. For this reason the temperature of the quartz crystal was recorded during isochromat runs and also fluorescent calibration line runs, and all data were referred to 24°C.

IV. OBSERVATIONS AND RESULTS OF THE EXPERIMENT

A. Procedures

Procedures were carefully worked out for the various phases of this precision experiment after considerable preliminary experimentation. These cannot be treated in detail here.[28] Each isochromat run consisted of a preheating stage to stabilize the x-ray tube, the electronic stabilizer and the 100-megohm working divider. To shorten the time for this the practice was adopted of keeping these three components including the oil circulation systems warmed up almost continuously. The stabilizer, for example, when not in operation at 25 kv, was kept switched to an auxiliary power supply. The warming up of the x-ray tube before each run then remained the most time-consuming factor. After about 30 minutes to warm up the electronic counting equipment to stability and while the x-ray tube was still being warmed up, a check of the counting, by comparing the results of the two discriminators, would be made. The setting of the "window" in the differential discriminator relative to the pulse height distribution curve would be checked for any possible shifting and remedied if required. In the course of a run such a shift, which occurred very rarely after sufficient warming, could be recognized and remedied. The integral discriminator which passed all pulses of amplitude greater than 20 volts was virtually insensitive to the small changes which could introduce erratic results in the differential channel and it served, therefore, as a valuable monitor, particularly so when scanning the pulse-distribution curve with the differential discriminator during the x-ray tube warm-up period. The x-ray warm-up period was also used as a good time for zeroing the galvanometers and standardizing the potentiometer current. Such economies of time were valuable in order to complete an isochromat run properly in a day's work.

Counting periods were divided into 5-minute intervals. At a minimum counting rate in the integral discriminator channel of about 200 to 225 counts per minute, a fairly satisfactory sample could be obtained in 5 minutes and a neighboring point could be reached before any large change in conditions could take place.

The sequence of counting through the two filters and changing the voltage by increments followed one of two patterns. In all cases the potentiometer settings were the same, but in some of the runs double readings through the silver filter were taken at points lying within about 15 volts on either side of the quantum limit. In this way, though the background readings through the palladium filter were more widely separated in time, much more information could be obtained in this highly important region near the limit. Furthermore, since readings through the palladium filter were intended (and proved to serve) primarily as background readings and were not themselves strongly involved in locating the limit, these readings were taken only at alternate voltage settings except in the case of the first six runs.

The data were collected in the course of 16 "final" runs across the continuous spectrum quantum limit. In addition to the counting data the following information was recorded for each and every run: (1) balance resistance required in the 100-megohm working divider, (2) x-ray tube current, (3) xenon counter voltage, (4) discriminator bias settings, (5) electromotive force of the bucking standard cell, (6) ambient temperature in the power supply room, (7) temperature of the quartz crystal. The temperatures were read every half-hour during the run.

B. Reduction of the Data

The data taken on the 16 isochromats were combined to give a single composite isochromat with better statistics. Although the same potentiometer settings were used in all 16 runs the actual voltage applied to the tube corresponding to these settings in a few cases differed by as much as 4 or even 5 parts in 10^5 by reason of the various corrections required. Such extreme cases were

[28] For an adequate description, see reference 16.

infrequent but these departures though usually small constituted the chief reason for adopting the following adjustment procedure. A preliminary rough isochromat was plotted by combining all the counting data at the same potentiometer setting ignoring the necessity for the small corrections to the potentiometer settings needed to obtain applied tube voltages precisely. The slope of this rough preliminary composite isochromat then furnished the necessary information to correct the number of counts observed on each of the 16 isochromats to what would have been obtained if the desired voltage for that setting had been applied to the tube instead of the actual voltage that was applied. None of the voltage deviations calling for this correction were as large as 3 parts in 10^5 in the critical region of the isochromat. An additional correction of this same type was made because of temperature variations of the quartz crystal from run to run. (The crystal temperature was usually quite constant during a run). A voltage rather than a wavelength correction was applied to meet this situation. The wavelength selectively diffracted by the crystal at the fixed angular setting of the spectrometer will change by 1 part in 10^5 per degree centigrade, and clearly one may consider this equivalent to a change of the voltage in the same proportion. The total variation in crystal temperature over all runs combined was about 2.5°C and the variation during a run was rarely as great as 1°C so that this was a very unimportant correction. All such voltage corrections proved to be completely "swamped" by the error (chiefly due to restricted statistics) in locating the limit from the plotted isochromats.

No data were discarded on the grounds of large statistical deviations alone, since we consider this practice, which tends to reduce the variance of the data artificially, a very dangerous one bordering on dishonesty. Only good and sufficient *a priori* reasons such as a known fluctuation in applied counter voltage or a shifting of the peak of the differential discriminator pulse-height distribution curve would justify discarding of data. It was finally decided not to discard any data taken through the integral channel of the discriminator on any of the 16 runs.

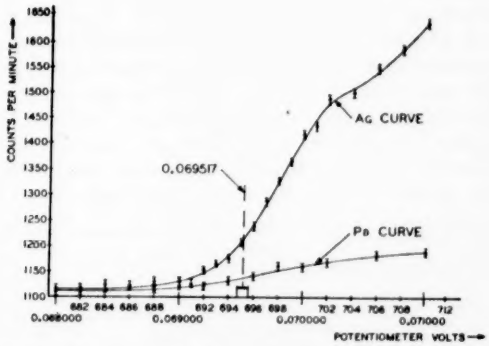

FIG. 13. Averaged isochromats obtained through silver and palladium filters. The point at a potentiometer voltage 0.069517 is the point of maximum bending of the "best" smoothed curve through the silver filter and the spread on either side of this point, indicated by the arrows, is the estimated uncertainty based on the deviations from this position obtained when the points of maximum bending were determined for intentionally poorly smoothed curves through the same filter. To the abscissa readings here shown must be added the potential of the bucking standard cell to obtain the total potential across the low-resistance segment of the working divider.

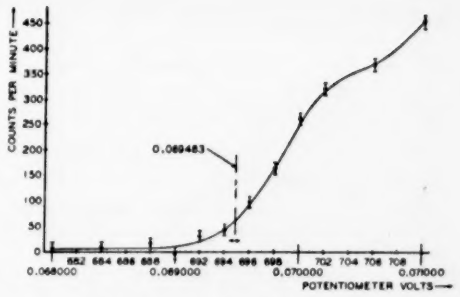

FIG. 14. The difference isochromat. This is the difference between the Ag and Pd curves of Fig. 13. The abscissa point at a potentiometer voltage of 0.069483 is the point of maximum bending of the "best" smoothed curve plotted through these difference observations and the spread indicated by the arrows is the estimated uncertainty based on points of maximum bending determined for intentionally poorly smoothed curves through the same points. Here as in Fig. 13, the bucking standard cell voltage must be added to the potentiometer readings given as abscissas.

C. The Isochromats

Figures 13 and 14 show all the data adjusted to the same abscissae for each run and plotted against potentiometer microvolts as abscissas. Each ordinate plotted gives the mean number of counts observed in 5 minutes averaged for from 16 to 22 separate measurements. The indicated spread about the mean value for any ordinate is given by the square root of the total number of counts at that setting divided by the number of separate 5-minute observations made at that point (16 or, for silver points in the middle of the curve, 22). Figure 13 gives the two composite isochromats obtained through the silver and the palladium filters separately, while Fig. 14 gives the difference of these two curves.

The data were plotted to large scale and smooth curves were drawn through these points with a spline. The smoothed ordinates were then read off numerically and the third derivative of this curve was computed by a method of numerical differentiation based on the calculus of finite differences given by Whittaker and Robinson.[29] The method consists essentially in the fitting of a high degree polynomial to an array of adjacent points read from the graph at equal abscissas intervals and a simultaneous differentiation of the

[29] E. T. Whittaker and G. Robinson, *Calculus of Observations* (Blackie and Sons, Ltd., London, 1924), p. 65.

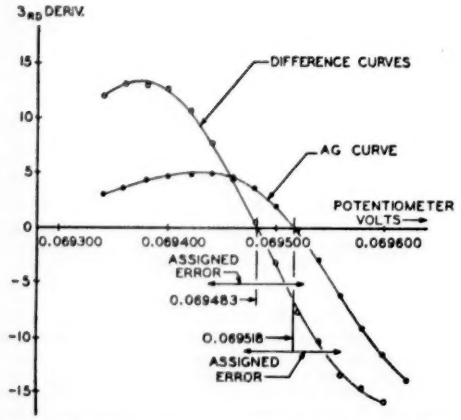

FIG. 15. Third derivatives of the "best" smoothed isochromats for the silver curve of Fig. 13 and for the difference curve of Fig. 14, obtained by a numerical differentiation process based on the theory of finite differences. The "zero" of each curve gives the point of maximum bending of the isochromat. By differentiating intentionally poorly smoothed isochromats in this same way the deviations of the zero points of these gave the spread from which the assigned error, indicated by the arrows, was obtained.

resulting polynomial. The curves of Fig. 15 are the third derivatives of the isochromats of Figs. 13 and 14. The point where the third derivative vanishes corresponds to the point of maximum bending of the isochromat, and this has been shown by one of us[30] to be a reliable criterion for finding the true threshold position at the quantum limit.

The virtue of the above described method of numerical differentiation is that by selecting abscissas rather widely spaced (30 or 40 microvolts on our graphs) one can include a large region of the curve in the calculation of the third derivative at the center of this region. Our calculations were based on regions 500 microvolts wide. On the other hand, this method of locating the limit gives a deceptive appearance of precision because it is in reality no more precise than the smoothing of the curve is reliable.

As always, the "best" smooth curve which can be drawn through points subject to statistical uncertainty, when little is known of the nature of the curve, must be somewhat a matter of opinion. For this reason, several curves were drawn through the measured points and differentiated before the final curve was selected. We found that the location of the limit varied by about 3 parts in 10^5 among the several "good" curves. In order to form a satisfactory estimate of probable error, we drew in addition several curves which were intentionally not good in that they ignored some of the data while remaining close to the statistically determined ranges of the rest. The third derivatives of these exhibited shifts in the limit point of as much as 7 parts in 10^5. (It should not be forgotten that the emf of the bucking cell, 1.019161 absolute volts, must be added to the potentiometer readings plotted as abscissas in Figs. 13 and 14 to obtain the total figure proportional to the applied high voltage.)

The limit points (shown in Fig. 15) which we consider the "best" for each of the two isochromats, (1) the silver isochromat and (2) the silver-palladium difference isochromat, are seen to differ by only about 35 parts per million.

The striking features of the true spectrum, the peaks and valleys slightly above the quantum limit found at lower voltages by Ohlin,[6] by Bearden and Schwarz,[9] and by Bearden, Johnson, and Watts[10] are clearly evident in these curves though they are less accentuated than in the longer wavelength isochromats.

D. Calculation of Final Results and Estimation of Errors

The data described above in Sec. III B, yield the results shown in Table III on which the calculation of the monochromator window wavelength and its uncertainty are based. Columns 2 and 3 list the separation in screw turns, ΔS, and in x-units, $\Delta\lambda$,[31] between each fluorescence line and the monochromator setting, 3 being calculated from 2 using the screw factor S.F. $=1.00029\pm0.0003$ turns per x.u.[31] Column 4 gives the accepted wavelengths of the lines and 5 is the monochromator window wavelength computed by adding $\Delta\lambda$ and λ, columns 3 and 4. The estimated probable errors in column 3 are computed in the usual quadratic way from the relative error in location and the relative error in screw factor and those of column 5 are computed from the quadratically compounded absolute errors of 3 and 4. The determination of the error of the above weighted mean value of the monochromator window wavelength differs insignificantly whether calculated by internal or by external consistency.

A weighted average of the potentiometer readings corresponding to the points of maximum bending of the two "best" curves, $v_{Ag}=0.069517$ abs. volts and $v_{dif}=0.069483$ abs. volts (for the "silver" and the "difference" isochromats respectively) was taken with respective weights 1.4 and 1.0. These were chosen because the statistical counting rate uncertainties near the

TABLE III. Calculation of mean value of monochromator window wavelength.

1	2	3	4	5
Line	ΔS in screw turns	$\Delta\lambda$ in x-units	λ of line in x-units	Monoch. window wavelength in x-units
Sn $K\alpha_1$	15.263 ± 0.005	15.259 ± 0.0067	489.57 ± 0.005	504.829 ± 0.0083
Sn $K\alpha_2$	10.830 ± 0.010	10.827 ± 0.0105	494.02 ± 0.005	504.847 ± 0.0116
Ag $K\beta_1$	$8.81\ \pm0.015$	8.807 ± 0.015	496.01 ± 0.005	504.817 ± 0.016
Ag $K\beta_3$	$8.20\ \pm0.02$	8.198 ± 0.02	496.65 ± 0.005	504.848 ± 0.021

Weighted mean value of $\bar{\lambda}_{SWL^{(S)}}$ in x-units $=\lambda_S=504.833\pm0.008$

[30] First discussed in reference 5. A better proof by Panofsky is given in reference 8.

[31] The error ±0.0003 in S.F. represents a very liberal increase above the value determined for the shorter wavelength regions near the center of the screw. Its effect on the calibration is negligible however because the increments ΔS are relatively so small.

limit were very nearly such as to call for this ratio. The potentiometer reading adopted was, therefore,

$$v_p = 0.069503 \pm 0.000045. \quad (8)$$

The estimated probable error is based on our finding that the "poor" curves could shift the low voltage (standard bucking cell voltage added to v_p above) by as much as 70 parts per million. We regard ± 0.000045 volts which is plotted on Figs. 13, 14, and 15 as a generous estimate for the probable error in determining the point of maximum bending. It is admittedly little more than an educated guess.

Adding to v_p above the bucking standard cell voltage, $v_{sc} = 1.019161 \pm 0.000005$ (L.E.) abs. volts, one obtains for the voltage across the low resistance arm of the working divider

$$v_L = 1.088664 \pm 0.000046 \text{ abs. volts}, \quad (9)$$

in which the contribution to the probable error from the limits of error of the bucking standard cell and the potentiometer measurement play a completely negligible role even if they are treated as probable errors instead of limiting errors.

The conversion from low to high voltage is accomplished by means of the precision divider ratio used to set the 100-megohm divider

$$\text{p.d.r.} = 22\,503.52 \pm 0.10 \text{ (L.E.)}. \quad (10)$$

The error limit in this ratio is generous but it still contributes insignificantly to the error of the nominal high voltage, V_N, obtained from the product of (9) and (10).

$$V_N = 24\,498.7 \pm 1.0 \text{ abs. volts}.$$

The effects of ripple, uncertainty in the 100-megohm divider (1 part in 10^6) and uncertainty from possible errors in the electronic stabilizer (also estimated at 1 part in 10^6) raise the latter error estimate to ± 1.1 absolute volts and give the following value for V_H, the high voltage applied to the tube:

$$V_H = 24\,498.7 \pm 1.1 \text{ abs. volts}. \quad (12)$$

To this must be added the cathode work function, taken as

$$V_w = 4.52 \text{ abs. volts}, \quad (13)$$

to obtain the voltage V_A corresponding to the maximum electron energy available to be converted into photon energy. Clearly any error in tungsten work function at the voltage of this experiment would have to be of the unlikely order of 20 percent before the final error would be appreciably altered. One obtains then for the final voltage,

$$V_A = 24\,503.2 \pm 1.1 \text{ abs. volts}. \quad (14)$$

From this, one computes immediately the value of

$$V_A\lambda_S = (h/e)c^2(\lambda_g/\lambda_s)^{-1}\,10^8 = 12\,370.02 \pm 0.63 \text{ emu}\cdot\text{kx-units}. \quad (15)$$

This last value, the conversion constant between electron volts and wavelengths in kx-units (Siegbahn), is the numerical result which should strictly be regarded as the output value of the present experiment. To avoid confusion in the literature we shall resist the temptation of combining it with other measured values (c^2 and λ_g/λ_s) to calculate h/e for instance. We confine ourselves to comparing in Table IV our value of the voltage—wavelength conversion constant with values obtained in two other recent sets of experiments.

TABLE IV. Comparison of three independent measurements of $V_A\lambda_s$.

(Felt, Harris, and DuMond)	$V_A\lambda_s = (h/e)c^2(\lambda_g/\lambda_s)^{-1}\,10^8 = 12\,370.02 \pm 0.63$ emu·kx-units
Bearden, Johnson, and Watts)[a]	$V_A\lambda_s = (h/e)c^2(\lambda_g/\lambda_s)^{-1}\,10^8 = 12\,371.03 \pm 0.48$ emu·kx-units
(Bearden and Schwarz)[b]	$V_A\lambda_s = (h/e)c^2(\lambda_g/\lambda_s)^{-1}\,10^8 = 12\,370.77 \pm 1.03$ emu·kx-units

[a] See reference 10.
[b] See reference 9.

It is a pleasure to acknowledge our indebtedness to Dr. David A. Lind for his generous assistance and advice throughout this experiment; to Henry N. Beets and John C. Scott (North American Philips and Eureka Company representatives) for donating the x-ray tube used in all of the final work and for their prompt and much needed cooperation when an unsuspected minute water leak into the oil jacket of the first (newly purchased) "shockproof" tube housing caused a most disconcerting, expensive, and time-consuming series of tube failures at a critical time in the experiment; and to Martin Walt and Gerald Jacobs for their diligent and able assistance, both in the construction of the 100-megohm precision manganin divider and, in the case of Mr. Walt, also during the performance of the experiment. Some of the expensive components used in this experiment, such as the 0.25-μf H.T. condensers, the 1000-henry chokes, and the 100-megohm units of the nichrome wire-wound working resistance divider were purchased at an earlier date with funds donated by Dr. Leon L. Watters of New York City, known as the Frances Hayes Watters Memorial Research Fund, and it is a pleasure to express our gratitude to this donor as well as to our sponsors, the U. S. Office of Naval Research.

Nuclear Surface Oscillations*†

A. K. KERMAN
Department of Physics and Laboratory of Nuclear Science, Massachusetts Institute of Technology, Cambridge, Massachusetts
(Received August 6, 1953)

The extreme shell model of the nucleus is extended by allowing the last odd nucleon to interact with collective modes of motion of the even-even nuclear core. The interaction between a nucleon and the surface oscillations of the core was given by Bohr and is employed here with a Fock space representation for the core excitation. Because of the interaction neither the nucleon nor the core conserve their angular momentum, but the total angular momentum is conserved. The problem is treated by the Tamm-Dancoff method. In terms of the Tamm-Dancoff wave function, formulas are derived for the magnetic moment and the quadrupole moment of an odd nucleus. The energy of excitation of the core is taken empirically from the first excited state of the corresponding even-even nucleus. With this procedure all the parameters of the theory are fixed. The magnetic moment deviations calculated in this manner agree with experiment for nuclei in which the total angular momentum is one half, but the agreement does not exist for higher angular momenta. It is also possible to obtain a qualitative fit for the large quadrupole moments of nuclei with odd numbers of nucleons between fifty and eighty-two. The problem of two equivalent nucleons outside a closed shell is treated in the same manner, and it is shown that the first and second excited states have spins 2 and 4 as usually observed. In addition there is a pairing energy binding effect in the ground state which is larger when the individual angular momenta of the two nucleons is larger. This is the pairing energy rule usually employed in shell model calculations.

INTRODUCTION

IT is well known that the success of the spin-orbit coupling shell model of the nucleus[1-4] begins to break down on close examination of some of the specific properties of nuclei such as magnetic moments,[5] quadrupole moments,[6] and excited states.[7] It has become clear that the rigorous single-particle picture must be augmented by taking into account in some way the interaction of the single particle with the nuclear core. Attempts to do this have fallen into several categories.

At first sight the simplest hypothesis is the one which assumes that the intrinsic properties of the nucleon (charge, mass, spin g factor) are different inside nuclear matter from what they are in free space.[8,9] This may be interpreted as the result of the nucleon-core interaction and has been called the "quenching" effect.

Quenching may have its origin in the exchange nature of nuclear two body forces[10] or in the nonlinearity of the meson fields underlying nuclear forces.[11] Russek and Spruch[12] have shown that it is possible to explain the trend of the magnetic moments of odd nuclei by a very general treatment of the exchange effects. However they do not relate their parameters to any of the usual parameters of the two-body force. Calculations which make this correlation[13] have shown that the effect is too small by an order of magnitude. In addition, it is not clear how this kind of mechanism could give rise to some of the large observed quadrupole moments.

One can improve on the single-particle results by taking into account the interactions of some or all of the particles in the incomplete shell containing the last odd nucleon.[14-16] In this procedure one assumes a short-range interaction among the nucleons in question. It is then possible to explain such facts as large quadrupole moments and the order of the first few excited states of even-even nuclei.

In this paper we consider the model of nucleon-core interaction which arises as an extension of the shell model when the nuclear core is considered to be deformable[17] and capable of collective oscillations.[18] This has been severally called the spheroidal core nuclear model[19] and the collective model.[20,21]

In the collective model the nucleons are assumed to move in the static potential of a deformed core, and the total energy is computed as a function of the deformation. This is essentially a classical treatment of the core, and neglects the possible transfer of angular momentum.

The strong-coupling approximation as used by Bohr[18] and Ford[21] assumes that the nucleon-core interaction is such that the nucleon angular momentum is a good quantum number. As was pointed out by Davidson and Feenberg,[19] the exact interaction proposed by Bohr

* This work was assisted in part by the joint program of the U. S. Office of Naval Research and the U. S. Atomic Energy Commission.

† Part of a doctoral thesis submitted to the Physics Department at the Massachusetts Institute of Technology.

[1] E. Feenberg and K. C. Hammack, Phys. Rev. **75**, 1877 (1949); **81**, 285 (1951).
[2] M. G. Mayer, Phys. Rev. **75**, 1894 (1949); **78**, 16 (1950).
[3] L. Nordheim, Phys. Rev. **75**, 1969 (1949).
[4] Haxel, Jensen, and Suess, Phys. Rev. **75**, 1766 (1949).
[5] P. F. A. Klinkenberg, Revs. Modern Phys. **24**, 63 (1952).
[6] Townes, Foley, and Low, Phys. Rev. **76**, 1415 (1947).
[7] G. Scharff-Goldhaber, Phys. Rev. **90**, 587 (1953).
[8] F. Bloch, Phys. Rev. **83**, 839 (1951).
[9] A. de-Shalit, Helv. Phys. Acta **24**, 296 (1951).
[10] H. Miyazawa, Prog. Theor. Phys. **6**, 801 (1951).
[11] L. I. Schiff, Phys. Rev. **84**, 1 (1951).
[12] A. Russek and L. Spruch, Phys. Rev. **87**, 1111 (1952).
[13] Villars, Weisskopf, and Kerman (unpublished).
[14] D. Kurath, Phys. Rev. **87**, 218 (1952).
[15] B. H. Flowers, Phys. Rev. **86**, 254 (1952); Proc. Roy. Soc. (London) **215**, 398 (1952).
[16] A. de-Shalit and M. Goldhaber, this issue [Phys. Rev. **92**, 1211 (1953)].
[17] J. Rainwater, Phys. Rev. **79**, 432 (1950).
[18] A. Bohr, Phys. Rev. **81**, 134 (1951); Kgl. Danske Videnskab. Selskab, Mat.-fys. Medd. **26**, No. 14 (1952); Phys. Rev. **89**, 316 (1953).
[19] J. P. Davidson and E. Feenberg, Phys. Rev. **89**, 856 (1953).
[20] D. L. Hill and J. A. Wheeler, Phys. Rev. **89**, 1102 (1953).
[21] K. W. Ford, Phys. Rev. **90**, 29 (1953).

does not have this property. Some of the matrix elements which are nondiagonal in the nucleon angular momentum are quite large. They come to the conclusion that a perturbation treatment employing the occupation numbers of the surface oscillation states as diagonal variables might be more appropriate. Such a treatment had previously been reported by Foldy and Milford[22] who showed that some of the deviations from the single-particle values for the magnetic moments could be accounted for.

Preliminary calculations by the present author have shown that a simple perturbation treatment is inadequate. This is so because the matrix elements of the interaction, which are diagonal in the nucleon quantum numbers, are not small compared to the lowest excitation energy of the surface vibrations. This means that the first-order term in the perturbation expansion of the total wave function is close to unity. As an alternative the method of Tamm and Dancoff[23] has been employed. Essentially this is a variational treatment, and it may be hoped that results obtained in this manner represent the exact ones to a fair degree of accuracy. This could be checked by using better trial wave functions.

The principal results obtained here are the following.

(1) For odd nuclei it is possible to calculate deviations from the single-particle magnetic moments. These deviations arise because the nucleon is not always in its zero-order state. When the surface is excited the nucleon can "recoil" to other states consistent with the conservation of parity and *total* angular momentum. Thus, the resultant g factor for the system is some combination of the core g factor and the different nucleon g factors. It is found that the calculated deviations for nuclei with angular momentum one-half agree quite well with experiment, although the agreement becomes progressively worse for higher angular momenta. As is the case with all other mechanisms, this model gives a very small deviation for Bi^{209} compared to the large experimental deviation.

(2) Quadrupole moments are calculated for the odd nuclei with odd number of nucleons between the magic numbers fifty and eighty-two. In this region the core is easily deformable (corresponding to the fact that first excited states in this region are very low-lying). The last odd nucleon acts to deform the core in such a way as to magnify the quadrupole moment. This is because the core assumes a shape similar to the wave function of the odd nucleon, and since it has charge Ze, it gives a larger contribution to the quadrupole moment.[17] It is found that the calculated quadrupole moments fit the general experimental trend, although they are too large by almost a factor of two.

(3) The interaction of two nucleons via the surface gives the familiar pairing energy rule used in shell model calculations. That is, the depression of the energy of a pair of equivalent[24] nucleons increases with their mutual angular momentum (j). It is also found that the first and second excited states of two equivalent nucleons outside a core have spin two and spin four as experiment requires,[7] and that the ground state has spin zero. This can be qualitatively explained by the usual sort of overlap argument.[25] A pair of nucleons with total angular momentum zero have wave functions with the maximum possible overlap. Thus, they aid one another in deforming the core, giving rise to a lower energy than when the angular momentum is not zero.

SURFON MODEL OF NUCLEON-CORE INTERACTION

Following the notation of Bohr,[18] the Hamiltonian for the core considered as a liquid drop is

$$H=\sum_{k\mu}\{\tfrac{1}{2}B_k|\dot{\alpha}_{k\mu}|^2+\tfrac{1}{2}C_k|\alpha_{k\mu}|^2\}, \tag{1.1}$$

with

$$B_k=3MAR_0^2/4\pi k; \quad R_0=r_0A^{\frac{1}{3}}; \tag{1.2}$$

$$C_k=(k-1)\{(k+2)-[(10\gamma)/(2k+1)]\} \times(u_s/4\pi)A^{\frac{1}{3}}; \tag{1.3}$$

$$\gamma=(3/5)[e^2/(r_0u_s)](Z^2/A); \; r_0\cong 1.5\times 10^{-13}\text{ cm}; \tag{1.4}$$

$$E_s=\text{surface energy}=u_sA^{\frac{2}{3}}; \quad u_s\simeq 13\text{ Mev}. \tag{1.5}$$

The frequency of the collective oscillations of order k is

$$\omega_k=(C_k/B_k)^{\frac{1}{2}}. \tag{1.6}$$

We notice that the only undetermined parameter here is the surface energy. An average value for this quantity may be obtained from nuclear binding energies.[25] However, it is generally conceded that individual nuclei may be far from this average.

The quantization of this system of harmonic oscillators is done in the usual way by setting

$$\alpha_{k\mu}=e_k\{b_{k\mu}+(-1)^\mu b_{k,-\mu}^*\};$$

$$e_k=\{(\hbar^2/B_k)/(2\hbar\omega_k)\}^{\frac{1}{4}}; \tag{1.7}$$

$$\pi_{k\mu}=(i\hbar/e_k)\{b_{k\mu}^*-(-1)^\mu b_{k,-\mu}\}=B_k\dot{\alpha}_{k\mu}; \tag{1.8}$$

$$[b_{k\mu}, b_{k'\mu'}^*]=\delta_{kk'}\delta_{\mu\mu'}; \tag{1.9}$$

$$b_{k\mu}^*b_{k\mu}=n_{k\mu}, \tag{1.10}$$

where $n_{k\mu}$ is the number of quanta in the mode $(k\mu)$. For purposes of convenience we shall call these deformation quanta *surfons* because in a certain sense they are quanta of nuclear surface oscillation. Bohr[18] shows that the z component of the angular momentum

[22] L. Foldy and F. J. Milford, Phys. Rev. **80**, 751 (1950).

[23] I. Tamm, J. Phys. (U.S.S.R.) **9**, 449 (1945); S. M. Dancoff, Phys. Rev. **78**, 382 (1950).

[24] Equivalent nucleons are protons or neutrons with the same shell model assignment for their individual angular momentum states, e.g., $d_{5/2}^2$ for two protons.

[25] J. M. Blatt and V. F. Weisskopf, *Theoretical Nuclear Physics* (John Wiley and Sons, Inc., New York, 1952), pp. 286, 302.

of the excited drop is

$$C_z=\hbar\sum_{k\mu}\mu n_{k\mu}. \tag{1.11}$$

This gives an interpretation of the surfons as Bose-Einstein particles of spin k ($k=2, 3, \cdots$), with z component $\mu(\mu=-k, \cdots, 0, \cdots, k)$. Then the first excited state of an even-even nucleus considered in this way has spin two and energy $\hbar\omega_2$. Since $\hbar\omega_2$ depends upon the surface energy, it is possible only to give an average over many nuclei. In order to treat individual nuclei, we shall consider $\hbar\omega_2$ to be a parameter which is determined from the energy of the first excited state. Thus, all our results will be correlated in some way with the energy of the first excited state of the core considered as an even-even nucleus.

The form of the nucleon-surfon interaction can be easily derived.[18,19] Assume that the odd nucleon sees a potential only when inside the boundary of the nucleus (a well defined boundary is supposed to exist). For a spherical core the potential has the form $V(r/R_0)$. When the core is deformed so that

$$R=R_0(1+\delta);\quad \delta=\sum_{k\mu}(-1)^{\mu}\alpha_{k,-\mu}Y_{k\mu}(\theta,\varphi)\ll 1, \tag{1.12}$$

the potential is

$$V(r/R_0)=V(r/R_0)-(r/R_0)V'(r/R_0)\sum_{k\mu}(-1)^{\mu}\alpha_{k,-\mu}Y_{k\mu}$$
$$+\text{higher order terms.}$$

The second- and higher-order terms in this potential contain both the nucleon coordinates and the coordinates of the deformation. Therefore, they constitute a nucleon-surfon interaction:

$$H^{i}=-R_0V_0\delta(r-R_0)\sum_{k\mu}e_k\{(-1)^{\mu}b_{k,-\mu}Y_{k\mu}$$
$$+\text{Hermitian conjugate}\}, \tag{1.13}$$

where we have taken only the second term, and used a square well of depth V_0 and radius R_0. It is clear from the form of this interaction that only the total angular momentum is a good quantum number. We shall employ a set of zero-order wave functions which exhibit this explicitly.

For this purpose we introduce surfon eigenvectors which are denoted by $\chi_{00}{}^{(0)}$ for the ground state of the core, and by $\chi_{k\mu}{}^{(1)}$ for the state containing one spin k surfon with z component μ. The angular and spin part of the nucleon wave function will be written in the spin-orbit coupling scheme as

$$\mathcal{Y}_{l\frac{1}{2}jm}=\sum_{m_l m_s}Y_{lm_l}(\theta,\varphi)\eta_{\frac{1}{2}m_s}(lm_l\tfrac{1}{2}m_s|l\tfrac{1}{2}jm). \tag{1.17}$$

We can then write the composite zero-order wave functions as

$$\varphi_{l'\frac{1}{2}j'kjm}{}^{(1)}=\sum_{m'\mu}\mathcal{Y}_{l'\frac{1}{2}j'm'}\chi_{k\mu}{}^{(1)}(j'm'k\mu|j'kjm) \tag{1.18}$$

when there is one surfon, and

$$\varphi_{l\frac{1}{2}j0jm}{}^{(0)}=\mathcal{Y}_{l\frac{1}{2}jm}\chi_{00}{}^{(0)} \tag{1.19}$$

when there are no surfons. The quantities $(j'm'k\mu|j'kjm)$ are the usual Clebsch-Gordon coefficients for the composition of angular momenta. These wave functions can easily be generalized to the case of two or more surfons. The interaction (1.13) will mix (1.18) and (1.19) because it contains creation and destruction operators for one surfon. Then the most general normalized wave function of the composite system which takes into account one surfon, has the form

$$\Psi_{ljm}=p(r)\varphi_{l\frac{1}{2}j0jm}{}^{(0)}+\sum_{l'j'k}q_{l'j'k}(r)\varphi_{l'\frac{1}{2}j'kjm}{}^{(1)}, \tag{1.20}$$

where

$$\int r^2dr\{|p(r)|^2+\sum_{l'j'k}|q_{l'j'k}(r)|^2\}=1, \tag{1.21}$$

and $p(r)$, $q_{l'j'}(r)$ are radial functions for the odd nucleon.[26] By the laws of conservation of parity and angular momentum it is clear that

$$\begin{aligned} &l'=|l-2|, l, (l+2);\\ &j'=l'\pm\tfrac{1}{2}=|l-5/2|, \cdots, (l+5/2). \end{aligned} \tag{1.22}$$

Using the perturbation wave function as a model, one can write the trial wave function as

$$\Psi_{nljm}=\alpha(\Re_{nlj}(r)\varphi_{l\frac{1}{2}j0jm}{}^{(0)}$$
$$+\sum_{n'l'j'k}\beta_{n'l'j'k}(\Re_{n'l'j'}(r)\varphi_{l'\frac{1}{2}j'kjm}{}^{(1)}, \tag{1.24}$$

$$\alpha^2+\sum_{n'l'j'k}(\beta_{n'l'j'k})^2=1, \tag{1.25}$$

where α and $\beta_{n'l'j'k}$ are essentially variational parameters. Inserting (1.24) into the Schrödinger equation, and taking matrix elements with respect to

$$\Re_{nlj}(r)\varphi_{l\frac{1}{2}j0jm}{}^{(0)} \quad\text{and}\quad \Re_{n'l'j'}(r)\varphi_{l'\frac{1}{2}j'kjm}{}^{(1)},$$

one obtains a set of homogeneous linear equations for α and $\beta_{nlj}{}^{k}$:

$$\alpha(E_{nlj}-E)+\sum_{n'l'j'k}\beta_{n'l'j'k}$$
$$\times(nl\tfrac{1}{2}j0jm|H^{i}|n'l'\tfrac{1}{2}j'kjm)=0,$$

$$\alpha(n'l'\tfrac{1}{2}j'kjm|H^{i}|nl\tfrac{1}{2}j0jm)$$
$$+\beta_{n'l'j'}{}^{k}(E_{n'l'j'}+\hbar\omega_k-E)=0. \tag{1.26}$$

The secular equation of this set determines the energy of the system. It has the form

$$(E_{nlj}-E)-\sum_{n'l'j'k}\frac{|(nl\tfrac{1}{2}j0jm|H^{i}|n'l'\tfrac{1}{2}j'kjm)|^2}{(E_{n'l'j'}+\hbar\omega_k-E)}=0, \tag{1.27}$$

[26] If we applied perturbation theory, $p(r)$ would be the normalized shell model radial wave function $\Re_{nlj}(r)$ and

$$q_{l'j'}(r)=\Sigma_{n'}\frac{(n'l'\tfrac{1}{2}j'kjm|H^{i}|nl\tfrac{1}{2}j0jm)}{(E_{nlj}-\hbar\omega_k-E_{n'l'j'})}\Re_{n'l'j'}(r). \tag{1.23}$$

Were the perturbation theory applicable here, this would give a total wave function (1.20) normalized to first order. But the matrix element $(nl\tfrac{1}{2}j2jm|H^{i}|nl\tfrac{1}{2}j0jm)$ is as large as $\hbar\omega_2$ and this invalidates perturbation methods.

where we have dropped the zero-point energy of the core because it is just an additive constant in the Hamiltonian.

A similar procedure can be carried out taking into account the possibility of two or more surfons. In this case the secular equation becomes quite formidable and it is necessary to use very drastic approximations. (See Appendix II.) Even Eq. (1.27) cannot be solved exactly because it contains an infinite number of terms. As a first approximation one neglects all terms in the sum except $(n'l'j')=(nlj)$. This is an adiabatic approximation in the sense that the nucleon does not "recoil" in the intermediate state. If in addition we neglect the effect of surfons with spin greater than two, the secular equation becomes a simple quadratic, and the solution for minimum energy is

$$E=E_{nlj}+(\hbar\omega_2/2)-\{(\hbar\omega_2/2)^2+|(nl\tfrac{1}{2}j0jm|H^i|nl\tfrac{1}{2}j2jm)|^2\}^{\frac{1}{2}}. \quad (1.28)$$

The quantities $E_{n'l'j'}$ are the usual shell model energy levels as given by Klinkenberg.[5] On examining the level structure, it is seen that in many cases two levels are quite close together. If the zero-order level in question is one of these pairs, it is clear that the adiabatic approximation is not a good one. As a better approximation we assume that the pair is degenerate. In this event the solution to (1.27) is

$$E=E_{nlj}+(\hbar\omega_2/2)-\{(\hbar\omega_2/2)^2+\sum'_{n'l'j'}|(n'l'\tfrac{1}{2}j'2jm|H^i|nl\tfrac{1}{2}j0jm)|^2\}^{\frac{1}{2}}, \quad (1.29)$$

where the prime indicates summation on levels which are close enough to (n, l, j) to be considered approximately degenerate. With this solution for the energy and the definitions

$$h_{nlj}^{n'l'j'}=(2/\hbar\omega_2)(n'l'\tfrac{1}{2}j'2jm|H^i|nl\tfrac{1}{2}j0jm),\qquad h^2=\sum'_{n'l'j'}|h_{nlj}^{n'l'j'}|^2,\ f=\{1+(1+h^2)^{\frac{1}{2}}\}^{-1}, \quad (1.30)$$

one obtains the relations

$$|\alpha|^2=\{1+f^2h^2\}^{-1}, \quad (1.31)$$

$$\alpha\beta_{nlj}{}^{(2)}=-fh_{nlj}{}^{nlj}\{1+f^2h^2\}^{-1}, \quad (1.32)$$

$$|\beta_{n'l'j'}{}^{(2)}|^2=f^2|h_{nlj}{}^{n'l'j'}|^2\{1+f^2h^2\}^{-1}, \quad (1.33)$$

$$\Delta E\equiv(E-E_{nlj})=-(\hbar\omega_2/2)\{(1+h^2)^{\frac{1}{2}}-1\}, \quad (1.34)$$

by making use of (1.25) and (1.26). This completes what we shall call the semi-adiabatic one surfon approximation. All physical quantities are functions of α and $\beta_{n'l'j'}{}^{(2)}$ as determined above. Our next task is to determine the quadrupole moment and the dipole moment as functions of these quantities. Before going on to this, we discuss the range of validity and the shortcomings of the above approximation. There are several points to be considered:

(1) We have approximated the exact wave function by ignoring the contribution of more than one surfon. From energetic considerations it seems reasonable to assume that the excitation of two surfons in the intermediate state would be less probable. This can be checked in the adiabatic approximation (see Appendix II). However, this does not prove that the contribution of two surfons is negligible because of the many non-adiabatic terms.

(2) In order to obtain a simple solution, we have restricted ourselves to the semi-adiabatic approximation. This result could be improved upon by taking more terms and solving the secular equation numerically. An alternative procedure has been developed (Appendix III) which effectively does the sum in Eq. (1.27). This method involves choosing a special form for the spin-orbit coupling and solving a transcendental equation for the energy levels. Preliminary calculations with this procedure indicate that the results obtained above are not radically altered.

QUADRUPOLE MOMENTS

The quadrupole moment of the composite system consists of independent contributions of the core and the odd nucleon,

$$Q=Q_c+Q_N. \quad (2.1)$$

It is well known that the quadrupole moment operator for the nucleon is given by

$$Q_N{}^{op}=(16\pi/5)^{\frac{1}{2}}r^2Y_{20}(\theta,\varphi), \quad (2.2)$$

and that this term is in some cases too small by an order of magnitude.[6] We shall therefore omit it in the following.

The quadrupole moment operator for the core may be obtained in terms of the classical quadrupole moment of a deformed spherical charge distribution. If the deformation is given by

$$R=R_0\{1+\textstyle\sum_{k\mu}(-1)^\mu\alpha_{k,-\mu}Y_{k\mu}(\theta,\varphi)\}, \quad (2.3)$$

and the charge is assumed to be uniformly distributed over the deformed core, then

$$Q_c=3Z(5\pi)^{-\frac{1}{2}}R_0{}^2\alpha_{20}, \quad (2.4)$$

to first order in the small quantity α_{20}. Then in the quantized theory the core quadrupole moment operator is

$$Q_c{}^{op}=3Z(5\pi)^{-\frac{1}{2}}e_2\{b_{20}+b_{20}{}^*\}, \quad (2.5)$$

$$e_2=(\hbar^2/2B_2\hbar\omega_2)^{\frac{1}{2}}. \quad (2.6)$$

Taking the matrix element of this operator in the one-surfon wave function (1.24) with $m=j$, one obtains

$$Q_c=6Z(5\pi)^{-\frac{1}{2}}R_0{}^2e_2\left\{\frac{2j(2j-1)}{(2j+3)(2j+2)}\right\}^{\frac{1}{2}}\alpha\beta_{nlj}{}^{(2)}, \quad (2.7)$$

$$(Q_c/R_0{}^2)=-\frac{6Z}{(5\pi)^{\frac{1}{2}}}e_2\left\{\frac{2j(2j-1)}{(2j+3)(2j+2)}\right\}^{\frac{1}{2}}\times fh_{nlj}{}^{nlj}\{1+f^2h^2\}^{-1}, \quad (2.8)$$

where we have used (1.32) and (1.30) in the adiabatic approximation. Thus,

$$h_{nlj}{}^{n'l'j'}=\frac{2}{\hbar\omega_2}[R_0{}^3V_0|\mathcal{R}_{nlj}(R_0)|^2]\times e_2\left\{\frac{5}{16\pi}\frac{(2j+3)(2j-1)}{2j(2j+2)}\right\}^{\frac{1}{2}}, \quad (2.9)$$

$$h^2=|h_{nlj}{}^{n'l'j'}|^2. \quad (2.10)$$

Then the quadrupole moment is completely determined in terms of the energy of the first excited state $\hbar\omega_2$ and the quantity

$$\langle T\rangle=\tfrac{1}{2}R_0{}^3V_0|\mathcal{R}_{nlj}(R_0)|^2. \quad (2.11)$$

This quantity is somewhat uncertain because the exact radial functions $\mathcal{R}_{nlj}(r)$ are not very well known. In the work of Ford[21] and of Davidson and Feenberg[19] $\langle T\rangle$ has been taken to be a constant equal to 20 Mev. We shall do the same here. Extensive calculations by Feenberg and Hammack[1] indicate that this is a reasonable approximation.

Table I has been compiled using this estimate for $\langle T\rangle$ and taking the energy of the first excited state of the corresponding even-even nucleus from a recent compilation by Scharff-Goldhaber.[7] It is seen that the calculated quadrupole moments are all somewhat larger than those observed (in most cases by a factor of two), but the variation with odd nucleon number has essentially the experimental shape.

The fact that this theory gives larger quadrupole moments is perhaps not surprising. The deformability of the core was determined from the first excited state of the corresponding even-even nucleus. Very probably this excitation is in the main provided by the motion of the nucleons in the unfilled shells only. Hence, we overestimate the deformability of the total core, which consists of the completed shells plus the unfilled ones.

All these large quadrupole moments are positive. This can be traced to the "accident" that the odd nucleon in each case is a "hole" in an unfilled shell.[27] Since the core quadrupole moment has the same sign as that for a single nucleon, and since "holes" always give positive quadrupole moments, the result follows.

TABLE I. Quadrupole moments of some odd nuclei.

	Z	N	A	j	$\hbar\omega$[a]	$(Q/R_0{}^2)_{\text{exp}}$	$(Q/R_0{}^2)_{\text{calc}}$
Eu	63	88	151	5/2	0.34	2	5
Eu	63	90	153	5/2	0.12	4	8
Lu	71	104	175	7/2	0.09	8.5	12
Ta	73	108	181	7/2	0.09	8.5	12
Re	75	110	185	5/2	0.14	4	8.8
Re	75	112	187	5/2	0.15	3.6	8.6

[a] The value of $\hbar\omega$ is taken from the first excited state of the corresponding even-even nucleus. [G. Scharff-Goldhaber, Phys. Rev. **90**, 587 (1953)].

[27] See tables in reference 5.

MAGNETIC MOMENTS

The magnetic moment operator for the composite system is given in the usual way by

$$\mu^{op}=g_l l_z+g_s s_z+g_c c_z, \quad (3.1)$$

where all symbols have their usual meaning.

c_z is the z component of the surfon angular momentum; g_c depends on the specific charge of the nuclear matter participating in the collective motion. A reasonable figure would be

$$g_c\simeq Z/A. \quad (3.2)$$

Then the magnetic moment of the system is given by the matrix element of μ^{op} in the wave function (1.24) with $m=j$. Thus,

$$\mu=g^{lj}j+\sum'_{n'l'j'}|\beta_{n'l'j'}{}^{(2)}|^2\{P_{l'j'}{}^{lj}+g_cQ_{j'}{}^j\}j+\sum_n{}'_{l'j'j''\neq j}\beta_{n'l'j'}{}^{(2)}\beta_{n'l'j''}{}^{(2)}(g_s-g_l)R_{l'}{}^jj, \quad (3.3)$$

where we have neglected the effect of surfons of spin greater than two, and g^{lj} is the usual single-particle g factor (Schmidt values),

$$Q_{j'}{}^j=\left\{\frac{j(j+1)-j'(j'+1)+6}{2j(j+1)}\right\}, \quad (3.4)$$

$$P_{l'j'}{}^{lj}=g^{l'j'}(1-Q_{j'}{}^j)-g^{lj}, \quad (3.5)$$

$$R_{l'}{}^j=\{2(2l'+1)j(j+1)\}^{-1}\{(l'+j+7/2)\times(l'+j-3/2)(5/2+l'-j)(5/2-l'+j)\}^{\frac{1}{2}}. \quad (3.6)$$

We note that in all of the cases calculated below there is never a cross term $\beta_{n'l'j'}{}^{(2)}\beta_{n'l'j''}{}^{(2)}$ because the corresponding shell model states are separated by the spin-orbit splitting. Thus, they do not both appear in the semi-adiabatic approximation. For such cases then, the deviation from the single-particle g factor is

$$\Delta g=\sum'_{n'l'j'}|\beta_{n'l'j'}{}^{(2)}|^2\{P_{l'j'}{}^{lj}+g_cQ_{j'}{}^j\}, \quad (3.7)$$

and $|\beta_{n'l'j'}{}^{(2)}|^2$ is given by (1.33). Again fixing the parameters as was done for the quadrupole moment, it is possible to determine Δg. The cases calculated are given in Table II. We note that this theory agrees well with experiment only for those nuclei whose shell model assignment is $s_{\frac{1}{2}}$. The apparent reason why the agreement is good in this case is that there is always a close lying $d_{\frac{3}{2}}$ state into which the nucleon recoils on "emitting" the spin 2 surfon. This was pointed out as a possibility by Davidson and Feenberg.[20] Thus it is seen that a strong spin-orbit coupling is necessary in this model in order to obtain agreement for $s_{\frac{1}{2}}$ states. Actually, there does not seem to be any other simple mechanism which gives the large deviation in this case.[28]

[28] It has been pointed out by Davidson and Feenberg that Bohr's strong-coupling model gives no deviation. A possibility which has not been quantitatively checked is that the large $s_{\frac{1}{2}}$ deviations arise from three or more nucleons in intermediate coupling (mixture of LS and jj) [A. de-Shalit (private communication)].

TABLE II. Magnetic moments of some odd nuclei.

	Z	N	A	l	j	$\hbar\omega^{a}$	l'	j'	$\lvert\beta_{Lj'}^{(3)}\rvert^2$	Δg_{exp}	Δg_{calc}
						Odd neutron					
Cd	48	63	111	0	$\frac{1}{2}$	0.656	2	3/2	0.452	2.64	1.77
Cd	48	65	113	0	$\frac{1}{2}$	0.600	2	3/2	0.461	2.59	1.80
Sn	50	65	115	0	$\frac{1}{2}$	1.3	2	3/2	0.370	1.99	1.45
Sn	50	67	117	0	$\frac{1}{2}$	1.3	2	3/2	0.369	1.83	1.44
Sn	50	69	119	0	$\frac{1}{2}$	1.3	2	3/2	0.369	1.74	1.44
Te	52	71	123	0	$\frac{1}{2}$	0.568	2	3/2	0.461	2.36	1.81
Te	52	73	125	0	$\frac{1}{2}$	0.607	2	3/2	0.457	2.06	1.78
Xe	54	75	129	0	$\frac{1}{2}$	0.428	2	3/2	0.473	2.28	1.84
Yb	70	103	173	3	5/2	0.08	1	3/2	0.100	−0.71	−0.09
Zn	30	37	67	3	5/2	1.0	1	$\frac{1}{2}$	0.208	−0.19	−0.02
Nd	60	83	143	3	7/2	1.6	5	9/2	0.022	0.26	0.06
Sr	38	49	87	4	9/2	1.1	...	...	...	0.18	0.04
						Odd proton					
Tl	81	122	203	0	$\frac{1}{2}$	0.427	2	3/2	0.457	−2.36	−2.23
Tl	81	124	205	0	$\frac{1}{2}$	0.5	2	3/2	0.449	−2.32	−2.19
P	15	16	31	0	$\frac{1}{2}$	2.3	2	3/2	0.396	−2.96	−1.86
Bi	83	126	209	5	9/2	1.0	3	7/2	0.02	0.34	0.01

[a] The value of $\hbar\omega$ is taken from the first excited state of the corresponding even-even nucleus. [G. Scharff-Goldhaber, Phys. Rev. **90**, 587 (1953).]

It is possible that inclusion of two spin-2 surfons and one spin-3 surfon in a more accurate treatment would improve these results. However, on the basis of the preliminary adiabatic two-surfon calculation this does not seem probable (see Appendix).

TWO EQUIVALENT NUCLEONS

We are here treating the problem of two equivalent nucleons outside a closed shell. The total system is an even-even nucleus and as such must have spin zero in the ground state. In addition we expect that the spin of the first excited state will be two and that of the second usually four because this is the general experimental situation.[7]

In the preceding sections we have always assumed that any even-even nucleus can support surface oscillations in the form of surfons. The question arises: how shall we treat an even-even nucleus which consists of a highly bound magic core plus two equivalent nucleons. If we assume that the total system (core plus two nucleons) is capable of supporting surface oscillations, then the ground state and excited states will have the usual spins, (0–2–4).

But if we consider it explicitly as a core plus two equivalent nucleons, it is not immediately obvious for example that the first excited state will have spin two. To show that our treatment is at least self-consistent, we shall prove that this is indeed the case.

The interaction Hamiltonian is the sum of the separate nucleon core interactions:

$$H^{i}=-R_0V_0e_2\sum_{\mu}(-1)^{\mu}b_{2,-\mu}\{\delta(r_1-R_0)Y_{2\mu}(\theta_1\varphi_1)+\delta(r_2-R_0)Y_{2\mu}(\theta_2\varphi_2)\}+\text{Hermitian conjugate}. \quad (4.1)$$

We use the coupling scheme

$$(l_1\tfrac{1}{2}j_1;\, l_2\tfrac{1}{2}j_2;\, L'cLM), \quad (4.2)$$

where subscripts 1 and 2 refer to the two nucleons, c is the core angular momentum, L is the total angular momentum, and L' is the vector sum of the two nucleon angular momenta. When the nucleons have the same quantum numbers, L' must be an even integer in order to satisfy the antisymmetry condition on the two-nucleon wave function.

Although it is quantitatively incorrect, we shall employ perturbation theory. This is expected at least to give the order of the energy levels. (Using the Tamm-Dancoff method, it is seen that the same quantity determines the order of the energy levels in the one-surfon approximation.) The second-order shift in energy arising from the interaction with the surface is

$$\Delta E_L=\sum_{\substack{n_1l_1j_1L'\\ n_2l_2j_2}}\times\frac{|(nl\tfrac{1}{2}j;\, nl\tfrac{1}{2}j;\, L0LM|H^{i}|n_1l_1\tfrac{1}{2}j_1;\, n_2l_2\tfrac{1}{2}j_2;\, L'2LM)|^2}{(2E_{nlj}-\hbar\omega_2-E_{n_1l_1j_1}-E_{n_2l_2j_2})}, \quad (4.3)$$

where we have assumed the total angular momentum of the system is L. On computing the matrix elements, it is seen that only the adiabatic terms depend on L. Thus, the part of the energy which depends on L is

$$\Delta E_L\sim-\langle T\rangle^2\left\{\frac{(2j+3)(2j-1)}{2j(2j+2)}\right\}\frac{e_2^2}{\hbar\omega_2}\frac{5}{16\pi}\times\{1-(2j+1)W(jjjj;2L)\}, \quad (4.4)$$

where $W(jjjj;2L)$ is one of the well-known Racah coefficients. The quantity in curly brackets is given in Table III and it is evident that the order of the levels of the composite system is 0–2–4 as expected.

The ground state ($L=0$) energy depends on the common state of the two nucleons through j.

$$\Delta E_0\sim-\langle T\rangle^2\frac{(2j+3)(2j-1)}{2j(2j+2)}\frac{e_2^2}{\hbar\omega_2}\frac{5}{16\pi}. \quad (4.5)$$

TABLE III. Values of $\frac{1}{2}\{1-(2j+1)W(jjjj;L2)\}$.

j \ L	0	2	4	6	8
$\frac{1}{2}$	1				
3/2	1	0.1			
5/2	1	0.55	0.25		
7/2	1	0.73	0.33	0.33	
9/2	1	0.83	0.50	0.28	0.41

Thus, we see that two equivalent nucleons in the ground state have a surfon interaction which makes those of higher j more tightly bound. This is the pairing energy rule often used in shell model calculations. It is not certain that this rule will follow from a more exact treatment of the problem. Further investigation is necessary.

ACKNOWLEDGMENTS

Acknowledgments are due to Professor V. F. Weisskopf who originally suggested this problem to me and whose help is greatly appreciated, and also to Professor F. Villars and Dr. A. de-Shalit for many helfpul discussions.

APPENDIX

I. Matrix Elements

We use the theorems on tensor operators and the properties of the Clebsch-Gordon and Racah coefficients which are summarized by Biedenharn.[29] For example,

$$(nl\tfrac{1}{2}j0jm|H^i|n'l'\tfrac{1}{2}j'2jm) = -R_0^3V_0\Re_{nlj}(R_0)\Re_{n'l'j'}(R_0)e_2W(j0j'2;j2) \times(l\tfrac{1}{2}j\|Y^{(2)}\|l'\tfrac{1}{2}j')(0\|b^{(2)}\|2), \quad \text{(A1.1)}$$

where

$$(l\tfrac{1}{2}j\|Y^{(2)}\|l'\tfrac{1}{2}j') = (-1)^{\frac{1}{2}-l'-j}\{(2j'+1)(2j+1)\}^{\frac{1}{2}} \times W(ljl'j';\tfrac{1}{2}2)(l\|Y^{(2)}\|l'), \quad \text{(A1.2)}$$

$$(l\|Y^{(2)}\|l') = \{5(2l+1)/4\pi\}^{\frac{1}{2}}(l2l'0|l020), \quad \text{(A1.3)}$$

$$(0\|b^{(2)}\|2) = \sqrt{5}. \quad \text{(A1.4)}$$

The quadrupole moment matrix element is

$$(l\tfrac{1}{2}j0jm|b_{20}|l\tfrac{1}{2}j2jm)_{m=j} = (2j+1)^{-\frac{1}{2}}(j2jj|jj20)(l\tfrac{1}{2}j0j\|b^{(2)}\|l\tfrac{1}{2}j2j) = \left\{\frac{2j(2j-1)}{(2j+3)(2j+2)}\right\}^{\frac{1}{2}}. \quad \text{(A1.5)}$$

II. Adiabatic Two-Surfon Problem

The state of the core with two spin-2 surfons is given by

$$\chi_{c\nu}^{(2)} = \sum_{\mu\sigma}\chi_{2\mu}^{(1)}\chi_{2\sigma}^{(1)}(2\mu2\sigma|22c\nu). \quad \text{(A2.1)}$$

Since the surfons are Bose-Einstein particles, this wave function must be symmetric and this requires that c be an even integer;

$$c=0,\ 2,\ 4. \quad \text{(A2.2)}$$

Then the zero-order two-surfon state is

$$\varphi_{l'\frac{1}{2}j'cjm}^{(2)} = \sum_{m'\nu}\mathcal{Y}_{l'\frac{1}{2}j'm'}\chi_{c\nu}^{(2)}(j'm'c\nu|j'cjm), \quad \text{(A2.3)}$$

and the adiabatic wave function for the composite system becomes

$$\Psi_{nljm} = \alpha\Re_{nlj}(r)\varphi_{l\frac{1}{2}j0jm}^{(0)} + \beta\Re_{nlj}(r)\varphi_{l\frac{1}{2}j2jm}^{(1)} + \sum_c\gamma^c\Re_{nlj}(r)\varphi_{l\frac{1}{2}jcjm}^{(2)}. \quad \text{(A2.4)}$$

In terms of the definitions

$$\epsilon = (E_{nlj}-E)/\hbar\omega_2, \quad \text{(A2.5)}$$

$$h(01) = (2/\hbar\omega_2)(nl\tfrac{1}{2}j0jm|H^i|nl\tfrac{1}{2}j2jm), \quad \text{(A2.6)}$$

$$h^c(12) = (2/\hbar\omega_2)(nl\tfrac{1}{2}j2jm|H^i|nl\tfrac{1}{2}jcjm) = \{(2c+1)(2j+1)\}^{\frac{1}{2}}W(j2jc;j2)h(01), \quad \text{(A2.7)}$$

the secular equation takes the form

$$\epsilon(\epsilon+1)(\epsilon+2) - \tfrac{1}{4}|h(01)|^2(\epsilon+2) - \tfrac{1}{4}\sum_c|h^c(12)|^2\epsilon = 0, \quad \text{(A2.8)}$$

and

$$\sum_c\left|\frac{\gamma_c}{\alpha}\right|^2 = \left(\frac{\epsilon}{\epsilon+2}\right)^2\tfrac{1}{2}\{1-(2j+1)W(jjjj;22)\}. \quad \text{(A2.9)}$$

A solution to (A2.8) is

$$\epsilon\sim\tfrac{1}{2} \quad \text{for} \quad \tfrac{1}{4}|h(01)|^2\sim\tfrac{4}{5}. \quad \text{(A2.10)}$$

Thus,

$$\sum_c|\gamma^c/\alpha|^2\lesssim 1/25,$$

which indicates that in this approximation two spin-2 surfons will not be very important.

III. Green's Function Treatment

Inserting (1.20) into the Schrödinger equation, and taking matrix elements with respect to

$$\varphi_{l\frac{1}{2}j0jm}^{(0)} \quad \text{and} \quad \varphi_{l'\frac{1}{2}j'2jm}^{(1)},$$

we arrive at a set of coupled equations for

$$p(r) \quad \text{and} \quad q_{l'j'}(r).$$

In terms of the definitions

$$x = r/R_0, \quad \text{(A3.1)}$$

$$\sigma^2(E) = 2MR_0^2|E|/\hbar^2, \quad \text{(A3.2)}$$

$$U_{l'j',lj} = (l\tfrac{1}{2}j0jm|e_2\textstyle\sum_\mu(-1)^\mu b_{2,-\mu}Y_{2\mu}|l'\tfrac{1}{2}j'2jm), \quad \text{(A3.3)}$$

[29] L. C. Biedenharn, Oak Ridge National Laboratory Report ORNL-1098, 1952 (unpublished); E. U. Condon and G. H. Shortley, *Theory of Atomic Spectra* (Cambridge University Press, London, 1935); G. Racah, Phys. Rev. **62**, 438 (1942); **63**, 367 (1943); J. Schwinger, Atomic Energy Commission Report NYO-3071, 1952 (unpublished).

these equations are

$$\left\{\frac{1}{x^2}\frac{d}{dx}x^2\frac{d}{dx}-\frac{l(l+1)}{x^2}+\sigma^2[V(x)-|E|]\right\}p(x)$$
$$=\delta(x-1)\{-\sigma^2(V_0)\textstyle\sum_{lj'}U_{lj'}{}^{lj}q_{lj'}(1)\},$$
$$\left\{\frac{1}{x^2}\frac{d}{dx}x^2\frac{d}{dx}-\frac{l'(l'+1)}{x^2}+\sigma^2[V(x)-|E|-\hbar\omega_2]\right\}g_{lj'}(x)$$
$$=\delta(x-1)\{-\sigma^2(V_0)U_{lj'}{}^{lj}p(1)\}. \quad \text{(A3.4)}$$

If the Green's functions for these equations are formally denoted by

$$\mathcal{G}_E{}^l(x,x') \quad \text{and} \quad \mathcal{G}_{E\omega}{}^{l'}(x,x'), \quad \text{(A3.5)}$$

the final solutions will take the form

$$p(x)=-\sigma^2(V_0)\mathcal{G}_E{}^l(x,1)\textstyle\sum_{lj'}U_{lj'}{}^{lj}q_{lj'}(1), \quad \text{(A3.6)}$$

$$q_{lj'}(x)=-\sigma^2(V_0)\mathcal{G}_{E\omega}{}^{l'}(x,1)U_{lj'}{}^{lj}p(1). \quad \text{(A3.7)}$$

The condition of compatibility between these equations gives us an eigenvalue condition for the energy

$$\mathcal{G}_E{}^l(1,1)\sigma^4(V_0)\textstyle\sum_{lj'}(U_{lj'}{}^{lj})^2\mathcal{G}_{E\omega}{}^{l'}(1,1)=1. \quad \text{(A3.8)}$$

The set of energies E_{nlj} which satisfy this condition will be the new energy levels of our one surfon model. The quantum number n corresponds to the usual principal quantum number of the shell model.

When the eigenvalue condition is satisfied

$$p(x)=p(1)\mathcal{G}_{E_n}{}^l(x,1)/\mathcal{G}_{E_n}{}^l(1,1), \quad \text{(A3.9)}$$

$$q_{lj'}(x)=q_{lj'}(1)\mathcal{G}_{E_n\omega}{}^{l'}(x,1)/\mathcal{G}_{E_n\omega}{}^{l'}(1,1), \quad \text{(A3.10)}$$

$$q_{lj'}(1)=-\sigma^2(V_0)U_{lj'}{}^{lj}\mathcal{G}_{E_n\omega}{}^{l'}(1,1)p(1). \quad \text{(A3.11)}$$

Applying the boundary conditions that they be finite at the origin and tend to zero at infinity, the Green's functions have the form

$$\mathcal{G}_E{}^l(1,1)=\left\{\alpha\frac{j_l'(\alpha)}{j_l(\alpha)}-i\beta\frac{h_l^{(1)\prime}(i\beta)}{h_l^{(1)}(i\beta)}\right\}^{-1}, \quad \text{(A3.12)}$$

where

$$\alpha\equiv\sigma(V_0-|E|), \quad \beta\equiv\sigma(|E|), \quad \text{(A3.13)}$$

and j_l, $h_l^{(1)}$ are the usual spherical Bessel and Hankel functions.[30]

We note that the usual energy eigenvalue condition for the shell model with a spherical well is

$$\{\mathcal{G}_E{}^l(1,1)\}^{-1}=0. \quad \text{(A3.14)}$$

It is not very difficult to extend this procedure to include spin-orbit coupling terms of the form

$$D(\mathbf{l}\cdot\mathbf{s}) \quad \text{or} \quad D\delta(\mathbf{r}-R_0)(\mathbf{l}\cdot\mathbf{s}). \quad \text{(A3.15)}$$

The use of this method is an entirely numerical procedure. For a given nucleus one must choose the parameters V_0, R_0, D, and $\hbar\omega_2$, and assign the l, j, and n quantum numbers. Then it is necessary to plot the eigenvalue condition as a function of energy and to determine the energy corresponding to the particular principal quantum number in question. One must choose the parameters, if possible, so that the binding energy of the last particle is what it should be and so that the energy levels have the right order. Once this is done it is a simple matter to determine $p(x)$, $q_{lj'}(x)$, and all the necessary integrals of these functions.

Numerical computations have been carried out for ${}_{83}\mathrm{Bi}^{126}(l=5, j=9/2)$ and ${}_{81}\mathrm{Tl}^{124}(l=0, j=\frac{1}{2})$. The parameters used were

$$\begin{aligned}\hbar\omega_2&=1\ \text{Mev},\\ V_0&=30\ \text{Mev},\\ r_0&=1.45\times10^{-13}\ \text{cm}.\end{aligned} \quad \text{(A3.16)}$$

In both cases it was found that

$$\int p^2(x)x^2dx\sim0.2. \quad \text{(A3.17)}$$

Now this integral corresponds to the parameter α^2 of the adiabatic procedure. For the adiabatic procedure it can be shown that

$$1>\alpha^2>\tfrac{1}{2}, \quad \text{(A3.18)}$$

so that the adiabatic procedure overestimates α^2 and consequently underestimates

$$\beta^2=\textstyle\sum_{lj'}\int q_{lj'}{}^2(x)x^2dx. \quad \text{(A3.19)}$$

Thus we may say that the Schmidt value deviations calculated in Sec. 3 are probably a little underestimated.

[30] L. I. Schiff, *Quantum Mechanics* (McGraw-Hill Book Company, Inc., New York, 1949), p. 77.

Angular and Energy Distributions of Photoprotons from Aluminum and Tantalum*†

M. M. HOFFMAN‡ AND A. G. W. CAMERON
Department of Physics and Institute for Atomic Research, Iowa State College, Ames, Iowa
(Received June 29, 1953)

Foils of aluminum and tantalum were irradiated at energies from 25 to 65 Mev in the x-ray beam of the Iowa State College synchrotron. Photoprotons produced at various angles were recorded in nuclear emulsions. Those emitted with low energies appear isotropically distributed and have energy distributions characteristic of statistical evaporation processes. The higher-energy protons from aluminum have an angular distribution of the form $(\sin\theta + p\sin\theta\cos\theta)^2$ with $p \approx 0.7$, whereas those from tantalum have a nearly pure $\sin^2\theta$ distribution. Their energy distributions can be represented in the form E_p^{-n}, where E_p is the proton energy. For aluminum, sharp increases in the exponent n occur at a value of E_p slightly greater than half the maximum photon energy of the irradiation. The increases are considerably less in the case of tantalum. The aluminum results are qualitatively consistent with Levinger's quasi-deuteron model of the nucleus. None of the proposed photon interaction models gives a good explanation of the tantalum results.

I. INTRODUCTION

SOME investigations of the angular distributions of photoprotons have recently been carried out using bremsstrahlung energies in the neighborhoods of 25 and 300 Mev. Earlier irradiations[1] with 22-Mev bremsstrahlung had indicated a slight excess of photoprotons emitted from rhodium and silver at 90° to the beam direction as compared to the numbers in the forward and backward directions. In recent more accurate measurements with 25-Mev bremsstrahlung, it has been found[2] that the lighter elements tend to give photoproton distributions peaked near 60°. This was taken as evidence for an interference between electric dipole and electric quadrupole photon absorption processes according to a quasi-deuteron model of the nucleus developed by Levinger.[3]

Investigations[4] with bremsstrahlung energies in the neighborhood of 300 Mev have indicated that very high-energy photoprotons prefer to be emitted nearly into the forward direction. This behavior is also qualitatively but not quantitatively consistent with Levinger's model. The energy distributions of these high-energy photoprotons can be roughly represented in the form $I(E) = \text{const} E^{-n}$, where n is of the order of 2 for proton energies lower than half the maximum photon energy, and n is of the order of 4 for the more energetic protons.

In the present investigation aluminum and tantalum have been irradiated in the x-ray beam of the Iowa State College synchrotron at bremsstrahlung energies of 25, approximately 40, and 65 Mev. The energy and angular distributions of the ejected photoprotons have been studied. In the irradiations at 40 and 65 Mev, attention was concentrated on those photoprotons with energies greater than one would expect to obtain from statistical evaporation processes.[5] However, their energies were not sufficiently large to require corrections to convert angular distributions from the center-of-mass system to that of the laboratory. It was hoped that the results would exhibit a behavior characteristic of the direct interaction of photons with nuclei.

II. EXPERIMENTAL PROCEDURE

The photoprotons were detected in Ilford *C*2 nuclear research emulsions of 500 microns thickness. The emulsions were exposed in an evacuated camera (Fig. 1) provided with a thin window in each end through which passed the x-ray beam. The camera was divided into two parts, each containing a thin target of the material under investigation. In the forward half the target was set at an angle of 45° to the beam direction, and protons were recorded at angles of 25°, 60°, and 90°. The backward half of the camera was a mirror image of this arrangement: the target was set at an angle of 135° to the beam direction and protons were recorded at angles of 90°, 120°, and 155°. Thus the observed protons left the targets at angles making not more than 45° with the normal to the planes of the targets, and the corrections for proton energy losses in the targets were small. Since each half of the camera contained an emulsion recording protons ejected at 90° to the beam direction, it was possible to check to be sure that there were no differences in proton yields attributable to differing geometry of the two halves of the camera.

Approximately 40 cm of lead was placed between the

* Contribution No. 268 from the Institute for Atomic Research and Department of Physics, Iowa State College, Ames, Iowa. Work was performed in the Ames Laboratory of the U. S. Atomic Energy Commission.

† This paper is based on a thesis submitted by M. M. Hoffman in partial fulfillment of the requirements for the Ph.D. degree at Iowa State College.

‡ Now at Los Alamos Scientific Laboratory, Box 1663, Los Alamos, New Mexico.

[1] Curtis, Hornbostel, Lee, and Salant, Phys. Rev. **77**, 290 (1950); B. C. Diven and G. M. Almy, Phys. Rev. **80**, 407 (1950).

[2] Halpern, Mann, and Rothman, Phys. Rev. **87**, 146, 164 (1952).

[3] J. S. Levinger, Phys. Rev. **84**, 43 (1951).

[4] D. Walker, Phys. Rev. **81**, 634 (1951); C. Levinthal and A. Silverman, Phys. Rev. **82**, 822 (1951); J. C. Keck, Phys. Rev. **85**, 410 (1952); J. W. Rosengren and J. M. Dudley, Phys. Rev. **89**, 603 (1953); Wattenberg, Feld, and Godbole, Phys. Rev. **90**, 380 (1953); J. W. Weil and B. D. McDaniel, Phys. Rev. **90**, 380 (1953).

[5] J. M. Blatt and V. F. Weisskopf, *Theoretical Nuclear Physics* (John Wiley and Sons, Inc., New York, 1952), Chap. VIII.

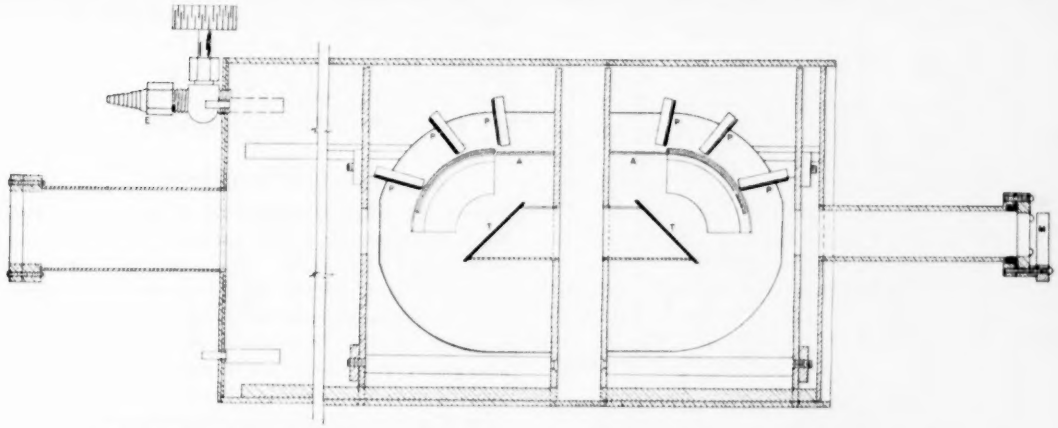

FIG. 1. Sectional view of the nuclear emulsion camera. P = nuclear emulsions; T = target foil; A = absorber; E = exhaust valve; M = monitor holder.

camera and the synchrotron to shield against scattered radiation. The x-ray beam passed through two circular apertures in the lead and had a diameter of 1.12 cm at the position of the targets. A magnetic field of about 4000 gauss immediately preceding the camera served to deflect electrons away from the emulsions.

Photoprotons ejected from the illuminated area of the targets entered the emulsion surfaces at an angle near grazing incidence. Under these conditions protons with energies up to 20 Mev would have been stopped before traversing the thickness of the emulsions. Copper absorbers were placed between the targets and the emulsions in order to reduce the energies of the incident protons by suitable amounts.

In all exposures the irradiation time was adjusted in an attempt to obtain the best possible track density without excessive electronic blackening of the emulsions. The plates were processed by the low-temperature method[6] with 22-percent extra amidol in the developer. For the scanning and measurements a Cooke binocular microscope with 21× objective was used. Tracks were measured only if they satisfied a set of selection criteria which insured that the protons came from the direction of the illuminated areas of the target foils.

It was assumed that all tracks satisfying these criteria were produced by protons. However, it is possible that an appreciable number of the tracks were produced by deuterons.[2,7] Grain counts were made on selected groups of short- and long-range tracks in some of the 25-Mev plates, but no significant differences were observed which might be attributed to deuterons. It is possible that the developing conditions might minimize such differences; hence it is not possible to set any limits on the numbers of deuterons present.

[6] Stiller, Shapiro, and O'Dell, Phys. Rev. **85**, 712 (1952).
[7] P. R. Byerly and W. E. Stephens, Phys. Rev. **83**, 54 (1951); W. H. Smith and L. J. Laslett, Phys. Rev. **86**, 523 (1952).

Details of the various exposures are given in Table I. At the time of the exposures the synchrotron energies were uncertain by about 2 Mev. Measurements were made on a total of over 2500 tracks in the various plates.

The minimum proton energies observable with any given absorber thickness were calculated using the range-energy-loss relationship of Lindhard and Scharff.[8] This relation was also used to calculate the energy loss in targets and absorbers for protons with varying residual ranges in the emulsions. The energy distributions of such protons were further corrected for the energy interval distortion introduced by the absorption process.

Unfortunately, the plates exposed in the backward half of the camera to aluminum targets in the 25- and 40-Mev irradiations were spoiled. Also, in all the irradiations with tantalum targets, the 25° emulsions were found to be too darkened for measurement. Fortunately the nature of the results appears to minimize the importance of the lost information.

III. RESULTS

A. Angular Distributions

The relative numbers of protons observed at various angles from the aluminum and tantalum foils irradiated at the various bremsstrahlung energies are plotted

TABLE I. Data for the exposures.

Target Material	Target Thickness (mg/cm²)	Synchrotron energy (Mev)	Proton energies observed (Mev)	Absorber thickness (mg/cm² of Cu)
Al	29	25	0 to 17	none
Al	76	40	16 to 28.5	520
Al	150	65	27 to 43	1253
Ta	264	25	0 to 19	none
Ta	420	38	18.6 to 28	670
Ta	840	65	27 to 40	1253

[8] J. Lindhard and M. Scharff, Phys. Rev. **85**, 1058 (1952).

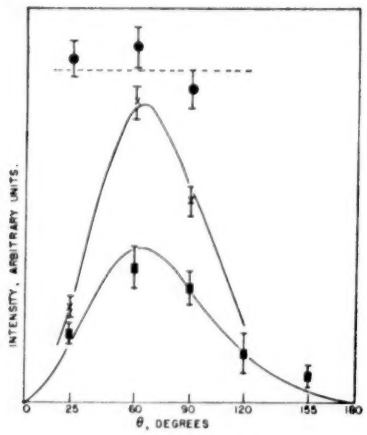

FIG. 2. Angular distributions of the photoprotons from aluminum. The separate irradiations are indicated as follows: ● 25 Mev, × 40 Mev, ■ 65 Mev. These data have been arbitrarily normalized so that the errors on the points do not overlap. The two lower curves are fitted by Eq. (1).

in Figs. 2 and 3. The numbers of tracks in the different plates have been normalized to equal solid angles and to equal minimum proton energies.

Figure 2 gives the results for aluminum irradiated at the various energies. The angular distribution of the photoprotons from the 25-Mev irradiation appears isotropic within statistical errors. Such a distribution is consistent with a statistical evaporation of the protons at the low energies observed here. A rough calculation based on the optical model[9] of the nucleus indicates that if the incoming photon transfers its energy to a proton in the nucleus, that proton will share such energy with the rest of the nucleus (through collisions) in more than 90 percent of the cases for the energies involved in this irradiation. Such compound nuclei may be expected to decay according to the theory given by Blatt and Weisskopf.[5]

In the case of aluminum irradiated at 40 Mev, there is a definite asymmetry with the greatest number of protons being emitted at approximately 60° to the direction of the x-ray beam. This asymmetry cannot arise from the decay of a compound nucleus (which would have to give reaction products emitted symmetrically about 90°),[10] but evidently indicates the effects of some direct interaction between the photons and the nucleus. The energies of these protons vary from 16 to 28.5 Mev, so that in any case not many of them are likely to arise from statistical evaporation.

The quasi-deuteron model of the nucleus proposed by Levinger[3] predicts an asymmetry of the type observed. In this model the photon is absorbed by a pair of nucleons, considered to constitute a quasi-deuteron, and a neutron and a proton are excited each with approximately half of the photon energy. Levinger has adapted the theories of the photodisintegration of the deuteron of Schiff[11] and of Marshall and Guth[12] to this situation. This leads to an interference between electric dipole and electric quadrupole absorption of photons, with an angular asymmetry produced approximately in the form

$$I(\theta)=(\sin\theta+p\sin\theta\cos\theta)^2, \tag{1}$$

where θ is the angle between the x-ray beam and the direction of emission of the proton $p=(5\sigma_q/\sigma_d)^{\frac{1}{2}}$, and σ_q and σ_d are, respectively, the cross sections for electric quadrupole and electric dipole absorption. Levinger expected this model to be valid only for photon energies greater than about 200 Mev; hence it would be surprising to find it valid for the low energies which are involved here.

For this experiment p may be considered as a parameter to be adjusted. If the Levinger model with the existence of deuteron sub-units should be quantitatively valid, then one would expect σ_q to be of the order of 5 percent of σ_d, leading to $p\approx 0.5$. This is indeed the order of magnitude for p found by Halpern *et al.*,[2] for the angular distribution of the non-isotropic fraction of the photoprotons emitted from the lighter elements irradiated with 25-Mev bremsstrahlung.

Since it was expected that the angular distribution of these protons might be partly isotropic, resulting from the presence of evaporation protons and of non-evaporation protons which had made nuclear collisions before escaping, it was at first attempted to fit the points by the equation

$$I(\theta)=a+b(\sin\theta+p\sin\theta\cos\theta)^2, \tag{2}$$

where a and b are constants to be adjusted. However it

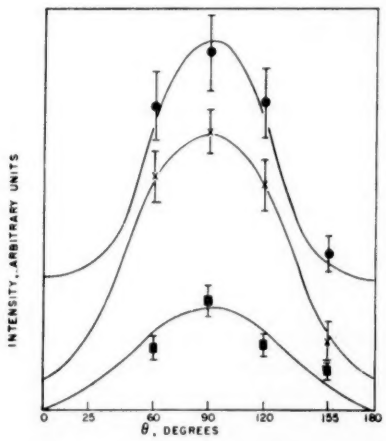

FIG. 3. Angular distributions of the photoprotons from tantalum. The separate irradiations are indicated as follows: ● 25 Mev, × 38 Mev, ■ 65 Mev. These data have been arbitrarily normalized so that the errors on the points do not overlap. The curves are fitted by Eq. (3).

[9] D. C. Peaslee, Phys. Rev. **86**, 269 (1952).
[10] Reference 5, Chap. X.
[11] L. I. Schiff, Phys. Rev. **78**, 733 (1950).
[12] J. F. Marshall and E. Guth, Phys. Rev. **78**, 738 (1950).

was found that $a/b \leq 0.1 (E_p > 18.5$ Mev), indicating that the isotropic component must be small compared to the "interference" component. The curve in the middle of Fig. 2 is therefore that of equation (1), with the constant found to be $p = 0.7 \pm 0.1$. Hence $\sigma_q/\sigma_d = 0.10 \pm 0.03$, if this interpretation of the theory can be trusted.

There is a similar situation in the results for aluminum irradiated at 65 Mev, also shown in Fig. 2. Again an attempted fit with Eq. (2) indicates that the fraction of the distribution which is isotropic is negligibly small. The points are therefore fitted with Eq. (1) with the constant found to be $p = 0.6 \pm 0.2$. This would give $\sigma_q/\sigma_d = 0.07 \pm 0.05$. These errors have been determined by finding the values of p for which the curve fell outside the root-mean-square deviations of more than one of the experimental points.

The angular distributions of the photoprotons from tantalum are shown in Fig. 3. In the case of the protons from the 25-Mev irradiation, there is a pronounced asymmetry at 90°, and there appears to be no appreciable excess of tracks at 60° over the number at 120°. The angular distribution formula used for aluminum thus appears inapplicable for tantalum, unless $p \approx 0$. A combination of an isotropic component and a $\sin^2\theta$ component appears sufficient to fit the uppermost points of Fig. 3. Such a $\sin^2\theta$ component would be characteristic of electric dipole absorption of photons. We may therefore write

$$I(\theta) = A + B \sin^2\theta, \tag{3}$$

where A and B are constants to be adjusted. The points are fitted by Eq. (3) with $B/A = 1.7$.

The two lower sets of points in Fig. 3 show the angular distributions of the higher-energy photoprotons emitted by tantalum irradiated, respectively, by 38- and 65-Mev bremsstrahlung. Again there is no indication in these figures of an excess of protons at 60° as compared with the numbers at 120°. The points in each figure have been fitted by Eq. (3). The best values of B/A were found to be 8 for the 38-Mev irradiation and infinity (i.e., $A = 0$) for the 65-Mev irradiation. The isotropic part of these distributions is therefore insignificant compared to the $\sin^2\theta$ part.

The angular distribution of Eq. (3) was predicted by Courant[13] for "directly ejected" protons. His calculations were based on a single-particle model. The ratio B/A is expected to depend on the orbital angular momenta of the protons which can be excited by the incoming photons. However, the large values of B/A observed for the high-energy photoprotons from tantalum would only be compatible with Courant's calculations if the great majority of the observed protons possessed zero orbital angular momentum in the nucleus before excitation, which seems unlikely. It would be difficult to understand why the photon excitation process should be so selective.

[13] E. D. Courant, Phys. Rev. **82**, 703 (1951).

Courant remarks that a pure $\sin^2\theta$ distribution would be obtained if similar calculations were carried out for an alpha-particle model with the alpha particles at rest. However, the internal motion of the alpha particles would introduce an isotropic component. Thus in principle this would appear not to be a good alternative model. However, quantitative calculations with it have not been carried out, and it might turn out that the isotropic component would be sufficiently small to be compatible with the results found here for tantalum.

Since the observed isotropic component occurs principally for the low-energy protons, it may be that this component chiefly represents statistically evaporated protons, with the directly ejected protons having chiefly the $\sin^2\theta$ distribution.

B. Energy Distributions

The higher-energy protons observed in this experiment may be expected to have been produced for the most part directly in the photon interaction process. The observed protons are those which have managed to avoid losing appreciable amounts of energy in collisions with other nucleons before escaping from the nucleus. The probability of successful escapes can be calculated roughly using an optical model[9] of the nucleus. Such calculations indicate that if 20 to 40 Mev is transferred to a proton in an average nucleus, the entire energy of this proton will go into the formation of a compound nucleus in about 70 percent of the cases. The proton should escape only after suffering some energy loss in a good fraction of the remaining cases. Thus most excitations in the energy range involved here should lead to the formation of a compound nucleus, and high-energy photoprotons should be produced in only a rather small fraction of the excitations. Any other photon interaction mechanism which does not excite a nuclear proton should in part also lead to the formation of a compound nucleus.

Some of these compound nuclei will decay by the emission of a proton of relatively small energy. The energy distribution is expected[5] to be given by

$$I(E_p) = \text{const} E_p \sigma_c(E_p) \omega_R(\hbar\omega - E_p - Q), \tag{4}$$

where E_p is the proton energy, $\sigma_c(E_p)$ is the capture cross section by the residual nucleus for protons of energy E_p, and $\omega_R(\hbar\omega - E_p - Q)$ is the energy level density of the residual nucleus, Q being the binding energy of the proton. The densities of energy levels may be approximately represented by

$$\omega_R(\epsilon) = \text{const} \exp[2(a\epsilon)^{\frac{1}{2}}]. \tag{5}$$

Equation (4) gives the proton energy distribution to be expected for a single photon energy $\hbar\omega$, on the assumption that all of the photon energy goes into the formation of the compound nucleus. To find the distribution to be expected for a continuous bremsstrahlung spectrum, it is necessary to multiply this expres-

sion by the (γ,p) cross section and by the number of photons of energy $\hbar\omega$ in the beam, and then to integrate the resulting expression over all photon energies present. The shape of the bremsstrahlung spectrum was assumed to be that calculated by Schiff.[14]

In order to compare the above distribution with that observed experimentally, it was necessary to make corrections for target thickness. This was particularly important for the case of the tantalum targets in the 25-Mev irradiation, where the target thickness was an appreciable fraction of the observed mean proton energy. In that case the target was considered to consist of six equal laminations, at the centers of which were sources emitting the above proton spectrum. With the help of the range-energy-loss relationship of Lindhard and Scharff,[8] calculations were made to obtain the spectral shapes to be expected after transmission through the laminations between the sources and detectors. The contributions from the various laminar sources were then summed.

The energy distribution of the photoprotons from aluminum irradiated with 25-Mev bremsstrahlung is shown in Fig. 4. The theoretical curve was calculated from Eq. (4), using the values of Heidmann and Bethe[15] for $\sigma_c(E_p)$ and $\omega_R(\hbar\omega-E_p-Q)$, and the results of Halpern and Mann[16] for the $Al^{27}(\gamma,p)Mg^{26}$ cross-section curve. There appears to be good agreement between the theoretical spectrum shape and the experimental points, and we therefore conclude that the majority of protons observed in this irradiation originated in a statistical evaporation process.

In Fig. 5 the energy spectra of the photoprotons from the 40- and 65-Mev irradiations of aluminum are presented in a log-log plot against the proton energy. The straight lines drawn through the points indicate that it is reasonable to represent the data over limited energy regions by the formula

$$I(E_p)=\text{const}E_p^{-n}. \tag{6}$$

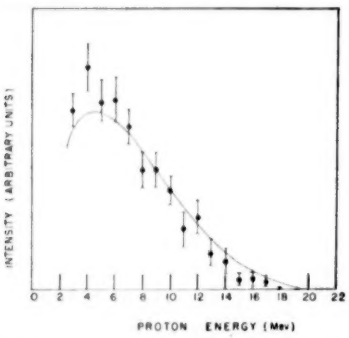

FIG. 4. Energy distribution of photoprotons from aluminum irradiated at 25 Mev. The theoretical curve is calculated from Eq. (4) for a statistical evaporation process and normalized to enclose the same area as the experimental points.

[14] L. I. Schiff, Phys. Rev. **83**, 252 (1951).
[15] J. Heidmann and H. A. Bethe, Phys. Rev. **84**, 274 (1951).
[16] J. Halpern and A. K. Mann, Phys. Rev. **83**, 370 (1951).

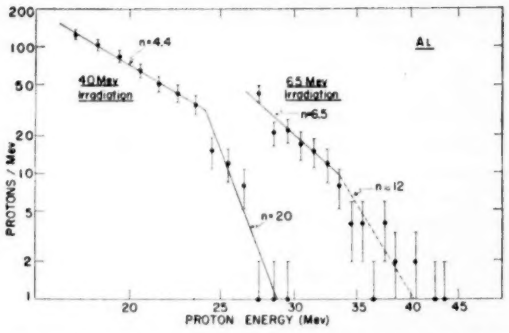

FIG. 5. Energy distributions of photoprotons from aluminum irradiated at 40 and 65 Mev. The data have been fitted as well as possible by straight lines according to Eq. (6).

It may be observed that each curve appears to have a break, with an increase in the value of n, at a proton energy which is a little more than half of the maximum energy available at the upper limit of the bremsstrahlung spectrum. Similar breaks are obtained in experiments at higher energies,[4] but the values of n obtained here are considerably larger than the values of approximately 2 and 4 obtained with 300-Mev bremsstrahlung.

The breaks obtained in higher-energy experiments have been interpreted as giving qualitative support to the Levinger quasi-deuteron model.[3] It has been argued that the two components of the quasi-deuteron will usually receive nearly equal shares of the incoming photon energy, but that occasionally the proton component will have a large momentum inside the nucleus and hence will receive considerably more than half of the photon energy. The results obtained here do not give quantitative support to this argument. On the foregoing picture one would expect the break to occur approximately at a proton energy equal to half of the bremsstrahlung energy, minus the proton binding energy in aluminum. Thus for the 40-Mev irradiation the break is expected to be at about $E_p=12$ Mev, whereas the observed break is at $E_p=24$ Mev. For the 65-Mev irradiation one would expect the break at $E_p=25$ Mev as compared to the observed position at $E_p=33$ Mev. However, the present data are not sufficient to be considered in definite disagreement with the Levinger model, since no protons were observed at energies where the breaks were predicted. Thus one cannot be sure that the observed breaks are not secondary phenomena.

In Fig. 6 is plotted the photoproton energy distribution obtained from tantalum in the 25-Mev irradiation. The theoretical distribution was calculated from Eq. (4) using values of $\sigma_c(E_p)$ interpolated for a nuclear radius of $1.3\times10^{-13}A^{\frac{1}{3}}$ cm in tables given by Blatt and Weisskopf.[5] Similar calculations made with a nuclear radius of $1.5\times10^{-13}A^{\frac{1}{3}}$ cm gave nearly identical results. The level densities for the residual hafnium nucleus were assumed to be given by Eq. (5) with $a=11$. The

cross-section curve for the (γ,p) reaction in tantalum is not known, nor is it known for any element in the immediate neighborhood of tantalum. It therefore was assumed that the (γ,p) cross-section curve measured for lead[17] would not be greatly different from that for tantalum, and hence that it might be used to weigh the energy distributions computed for different photon energies. This was checked by observing that the distributions expected to be produced by 20- and 30-Mev photons differed in energy at the peak by only 1 Mev and were very similar in relative shape. It is therefore believed that the errors introduced by this assumption are of a minor nature.

The theoretical curve, after corrections had been made, was normalized to enclose an area equal to that under the histogram of the experimental points of Fig. 6. It may be seen that this curve does not agree with the experimental points. There are fewer protons with low energies and more with high energies than are expected to result from a statistical evaporation process. This is the form that the disagreement would take if there was a substantial proportion of directly ejected protons present, which would tend to come off with more than normal evaporation energies.

Accordingly, the theoretical curve was normalized to the observed number of protons at 5 Mev (lower curve of Fig. 6). This energy is lower than is likely to arise in direct ejection. Although the point of normalization is highly uncertain, it is apparent that, if the lower curve of Fig. 6 correctly represents the numbers of evaporated protons, there are approximately equal numbers of evaporated and directly ejected protons. This is in qualitative agreement with the corresponding angular distribution in Fig. 3 if the evaporated protons have the isotropic distribution and the directly ejected protons have the $\sin^2\theta$ distribution.

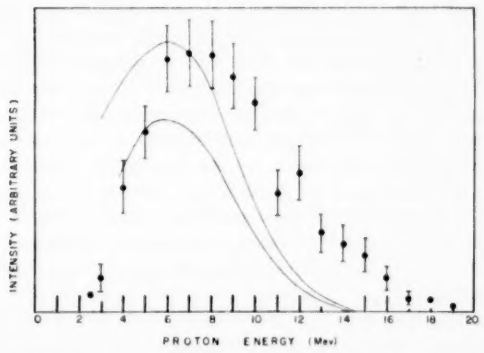

FIG. 6. Energy distribution of photoprotons from tantalum irradiated at 25 Mev. A theoretical curve has been calculated from Eq. (4) for a statistical evaporation process. The upper curve is this expression normalized to enclose the same area as the experimental points. The lower curve is this expression normalized to the experimental data at 5 Mev.

[17] Cameron, Harms, and Katz, Phys. Rev. **83**, 1264 (1951). Curve (a) of Fig. 1 of this reference was used.

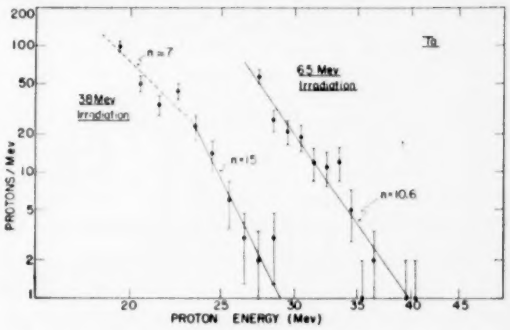

FIG. 7. Energy distributions of photoprotons from tantalum irradiated at 38 and 65 Mev. The data have been fitted as well as possible by straight lines according to Eq. (6).

In Fig. 7 the energy spectra of the photoprotons from the 38- and 65-Mev irradiations of tantalum are presented. The data appear to be reasonably well fitted by Eq. (6). The 38-Mev data appears to contain a break in slope at the same proton energy as did the 40-Mev aluminum data, but the change in slope is much less than in the aluminum case. However, there appears to be either no break at all in the 65-Mev data, or else one which involves too small a change of slope to be determined by the experimental points. If the Levinger quasi-deuteron model[3] were valid for tantalum, then according to the argument given previously one would expect that the 38- and 65-Mev data would have breaks at approximately 13 and 27 Mev, respectively. Since these proton energies were not observed, nothing definite can be said about the applicability of this model from the energy distribution data. However, the much smaller changes in slope of the tantalum data may well be related to the differing angular distributions of the high energy photoprotons from tantalum and aluminum.

The values of the slopes and break energies obtained in Figs. 5 and 7 are summarized in Table II. In the cases of both aluminum and tantalum, there is some qualitative evidence that the energy distributions of the high-energy photoprotons are a little steeper (larger n) in the forward and backwards directions than at 90°. The individual statistics are not sufficient to permit a quantitative estimation of this effect.

C. Photoproton Yields

During the synchrotron runs the x-ray dose received by the targets was monitored by tantalum foils, in which an 8-hour activity was produced by the $Ta^{181}(\gamma,n)Ta^{180}$ reaction. These foils were calibrated against the $Cu^{63}(\gamma,n)Cu^{62}$ activity, which in turn was determined absolutely in terms of the dose measured at 22 Mev by a Victoreen ionization chamber placed at the center of an 8-cm block of Lucite.[18] From the

[18] Johns, Katz, Douglas, and Haslam, Phys. Rev. **80**, 1062 (1950).

TABLE II. The slopes n of Eq. (6) and the break energies for the higher-energy photoprotons.

Target material	Synchrotron energy (Mev)	Break energy (Mev)	Slope Below break	Slope Above break
Al	40	24	4.4	20
Al	65	33	6.5	12
Ta	38	24	7	15
Ta	65	?	?	10.6

$Cu^{63}(\gamma,n)Cu^{62}$ and $Ta^{181}(\gamma,n)Ta^{180}$ cross-section curves[19] and the Schiff bremsstrahlung spectra it was possible to compare the number of protons observed per mole of target to the number of neutrons which would have been produced per mole of Cu^{63} had the target been composed of that substance. Since the (γ,n) yields had to be extrapolated to higher bremsstrahlung energies, the photoproton yields may not be very accurate, but they are probably correct to within a factor two. They are given in Table III, together with other results obtained in this experiment.

These yields allow estimates to be made of the (γ,p) cross sections, as distinct from the (γ,pn) cross sections, in aluminum and tantalum. These estimates are of interest because they are obtained here for energies in the "tail" of the (γ,p) cross-section curves, a region which cannot be determined accurately by ordinary yield curve analysis.[19]

A lower limit to the (γ,p) cross section is obtained by counting the number of protons in the range

$$E_0-Q(\gamma,p)-x\leq E_p\leq E_0-Q(\gamma,p),$$

and an upper limit is obtained by counting the number of protons in the range

$$E_0-Q(\gamma,pn)-x\leq E_p\leq E_0-Q(\gamma,p).$$

Here E_0 is the upper limit of the bremsstrahlung spectrum, $Q(\gamma,p)$ and $Q(\gamma,pn)$ are the binding energies, respectively, of a proton and of a proton and neutron, and x is an energy interval varied here from 4 to 10 Mev. In these criteria it is assumed that if a nucleus, following the emission of a proton, is left sufficiently excited to emit a further particle, such emission will take place (thus removing the event from classification as a (γ,p) reaction).

It was found that the upper and lower cross-section limits which were obtained by this procedure did not depend very strongly on the value of the energy interval x. Rough average estimates of these limits are given in Table IV. They may be compared to the peak cross section of the $Al^{27}(\gamma,p)Mg^{26}$ reaction of 22 millibarns at 21 Mev, and to that of the (γ,p) reaction in lead of 5 millibarns in the neighborhood of 26 Mev. It appears from the large differences obtained between the upper and lower cross section limits that the (γ,pn) cross sections are considerably larger than the (γ,p) cross sections at these energies.

TABLE III. Angular distributions and partial yields of the photoprotons.

Target material	Synchrotron energy (Mev)	Proton energies (Mev)	Angular distribution	Partial yield[a]
Al	25	0 to 17	isotropic	0.3
Al	40	16 to 28.5	$p=0.7$	0.03
Al	65	27 to 43	$p=0.6$	0.008
Ta	25	0 to 19	$B/A=1.7$	0.06
Ta	38	18.6 to 28	$B/A=8$	0.006
Ta	65	27 to 40	$B/A=\infty$	0.004

[a] Yield of protons in observed energy range per mole of target compared to yield of neutrons per mole of Cu^{63} had the target been composed of the latter substance.

[19] L. Katz and A. G. W. Cameron, Can. J. Phys. **29**, 518 (1951).

IV. DISCUSSION

From the foregoing results it may be seen that the photoprotons emitted by each element can be attributed to two sources. The lower-energy protons appear to be isotropically distributed and are presumed to have evaporated from a compound nucleus. The higher-energy protons fall off very rapidly with increasing energy, are nonisotropically distributed, and presumably result directly from the interaction between photons and nuclear matter.

TABLE IV. Estimates of the upper and lower limits of the (γ,p) cross sections.

Target material	Effective photon energy (Mev)	Cross-section limit (millibarns) minimum	maximum
Al	~35	0.05	10
Al	~60	0	0.05
Ta	~35	0.08	2.4
Ta	~60	0	0.02

The angular distribution of the protons directly ejected from aluminum may be well represented by Eq. (1), whereas those from tantalum can be fitted very well with Eq. (3). The first remarkable feature of this situation is the apparent lack of an isotropic component at higher energies. One might expect that a good fraction of the protons directly excited in the nucleus would make one or two "glancing" collisions with other nucleons before escaping, sufficient to change the angle of emission by a considerable amount but not sufficient to reduce the energy very much. This would have the effect of broadening the nonisotropic distribution; with only a few angular points available for analysis the result would probably look like a small isotropic component. The irradiations at 40 and 38 Mev reveal small isotropic components, but these are of a reasonable size to represent the high-energy tail of the statistical evaporation process. Neither of the irradiations at 65 Mev reveals any trace of an isotropic component.

The second remarkable feature of the situation is the difference in form of the nonisotropic distributions for

aluminum and tantalum. In the case of aluminum the angular distribution supports Levinger's quasi-deuteron model, and the energy distribution is not definitely in disagreement with it. This happens in an energy region where the model was not intended to be applied. If this theory is interpreted in a literal fashion, the magnitude of the asymmetric peaking at 60° indicates that electric quadrupole absorption is about nine percent as strong as electric dipole absorption of photons. This is of the order of magnitude to be expected from sum-rule considerations.[20]

It is then rather strange to find that this theory seems not to apply to tantalum. In this substance the directly ejected protons appear to obey a pure $\sin^2\theta$ law. This is characteristic of electric dipole absorption but it tells little about the nature of the absorption mechanism. The independent-particle model calculations of Courant appear to be excluded by the result, and similar calculations based on an alpha-particle model may well be similarly excluded. The quasi-deuteron model can explain the results only if $p \approx 0$, which, if the literal interpretation of the theory is correct, implies that the electric quadrupole absorption in tantalum is much less than one would expect.

It therefore appears that none of the postulated photon interaction mechanisms gives suitable predictions applicable to any element in the "intermediate" energy range.

[20] J. S. Levinger and H. A. Bethe, Phys. Rev. **78**, 115 (1950).

ACKNOWLEDGMENT

The authors are greatly indebted to Dr. L. J. Laslett and Dr. D. J. Zaffarano for their interest and assistance in this experiment.

PHYSICAL REVIEW VOLUME 92, NUMBER 5 DECEMBER 1, 1953

Beta-Gamma Polarization Correlations*

DONALD R. HAMILTON, *Palmer Physical Laboratory, Princeton University and Institute for Advanced Study, Princeton, New Jersey*

AND

AARON LEMONICK AND FRANCIS M. PIPKIN,† *Princeton University, Princeton, New Jersey*

(Received August 3, 1953)

The polarization of the gamma ray emitted at an angle of 90 degrees to the preceding beta particle has been measured for certain beta-gamma cascades in potassium-42, arsenic-76, rubidium-86, antimony-124, and cesium-134, as selected by beta absorbers when necessary. The polarimeter was checked by observing the polarization of the gamma rays of cesium-137 and cobalt-60 when Compton-scattered through 90 degrees. Of the gammas investigated, those of potassium-42 and cesium-134 have no observable polarization. For the other three elements, the sign of the polarization correlation, taken in combination with the sign of the angular correlation reported by other observers, uniquely determines that no parity change occurs in the gamma emission, corresponding to electric quadrupole radiation in decay of the excited state.

INTRODUCTION

THE gamma-gamma and beta-gamma angular correlations[1,2] have become recognized tools of nuclear spectroscopy and of the search for the fundamental beta interaction; concerning the gamma rays involved, these angular correlations usually tell the angular momenta of the levels involved and the multipole order of the gammas. If the gamma detector is in addition polarization-sensitive, then one may expect to learn whether the given multipole is electric or magnetic (that is, the parity change in the transition), for the fields of the electric and magnetic type of given order multipole differ by interchange of E and H and hence by a 90 degree rotation of polarization, and differ in parity.

Information concerning multipole order and parity change may also be obtained from internal conversion data. This procedure involves elaborate calculations using relativistic electron wave functions and is, in principle, perhaps not quite so direct as a measurement of gamma angular distribution and polarization; but with the exact calculations now available, the interpretation of experiments seems just as satisfactory. The principal difference between the two methods lies, therefore, in convenience of use; and one relevant factor here is the energy dependence of the two effects. Internal conversion coefficients become small for high energies and low Z; for example, for an electric quadrupole gamma the coefficient α_k has values[3] 2×10^{-6} and 0.11 for 2.5 Mev, $Z=10$ and 0.25 Mev, $Z=96$, respec-

* This work was supported in part by the U. S. Atomic Energy Commission and the Higgins Scientific Trust Fund. A preliminary report on this work was given at the New York-in-Cambridge meeting of the American Physical Society, January, 1953.

† Class of 1860 Fellow, 1951–1952.

[1] H. Frauenfelder, Ann. Rev. Nuc. Sci. **2**, p. 129 (1953).

[2] M. Deutsch, Repts. Progr. Phys. **14**, 196 (1951).

[3] Rose, Goertzel, Spinrad, Harr, and Strong, Phys. Rev. **83**, 79 (1951).

tively. The Compton scattering process upon which the polarization depends is less energy-sensitive; in going from 0.25 to 2.5 Mev, the cross section for 90° scattering is reduced by a factor 0.28 and the effect produced in a polarization measuring experiment like the present one (more specifically, the ratio C/B, as defined later, for ideal geometry) is reduced by a factor 0.23. Polarization correlation is thus well suited to cases where internal conversion coefficients are small.

The present experiment investigates the polarization of the gamma ray emitted at 90° to the beta ray which leaves in its first excited state the daughter nucleus (all of which happen to be of even-even type); the parent nuclei involved were Sb^{124}, K^{42}, Rb^{86}, and As^{76}. Beta-gamma directional anisotropy has been previously observed for each of these[1] and polarization-correlation

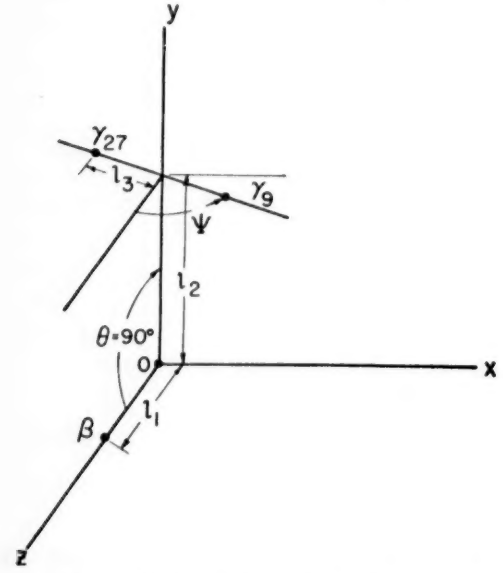

FIG. 1. Schematic diagram of geometry of detectors. $l_1=3.8$ cm; $l_2=7.0$ cm; $l_3=2.2$ cm; diameter of beta crystal, 4.0 cm.

measurements on Sb^{124}, similar to ours, have been reported by Stump,[4] and by Kloepper *et al.*[5] In addition, as a check, measurements were made on Cs^{134}, which has been observed to have no anisotropy.[1]

The gamma-ray polarimeter utilizes the polarization sensitivity of Compton scattering and is similar in design to those developed by Metzger and Deutsch[6] and used by Kraushaar and Goldhaber[7] and others,[4,5] except that its use solely for $\beta\gamma$ correlation reduces the number of scintillation crystals from three to two.

[4] R. Stump, Phys. Rev. **86**, 249 (1952).
[5] Kloepper, Lennox, and Wiedenbeck, Phys. Rev. **88**, 695 (1952).
[6] F. R. Metzger and M. Deutsch, Phys. Rev. **78**, 551 (1950).
[7] J. J. Kraushaar and M. Goldhaber, Phys. Rev. **89**, 1081 (1953).

THEORY

The theory of direction-polarization correlation has been investigated with particular reference to gamma-gamma correlation,[8,9] but the results necessary to the present case may be taken over *in toto*. These results take a particularly simple form when the gammas are dipole or quadrupole, which will be assumed in what follows.

If a gamma ray is observed to be emitted with an angular distribution

$$W(\theta)=1+\alpha_2\cos^2\theta+\alpha_4\cos^4\theta, \tag{1}$$

and, if we define

$$A=[W(180)-W(90)]/W(90), \tag{2}$$

then $A=\alpha_2+\alpha_4$. If now, at $\theta=90°$, we observe the intensities J_θ and J_ϕ of radiation for which the E vector lies in the usual θ and ϕ directions, then we know the following information from Eq. (8) of reference (8):

$$J_\phi/J_\theta=(1+A)/(1-A) \quad (E1, M2) \quad \text{(Yes)},$$
$$J_\phi/J_\theta=(1-A)/(1+A) \quad (E2, M1) \quad \text{(No)}.$$

Here the multipoles to which each alternative applies are indicated; and "yes" "no" refers to the parity change involved in the gamma transition. Thus (for dipoles and quadrupoles) the value of J_ϕ/J_θ at $\theta=90°$ depends not upon multipole order, but only upon parity change and A. If we define

$$B=(J_\phi/J_\theta)-1, \tag{3}$$

then observation of the signs of both A and B determines the parity change uniquely; for we have

$$\begin{aligned} A&=B/(B+2) \quad \text{(Yes)},\\ A&=B/(B-2) \quad \text{(No)}, \end{aligned} \tag{4}$$

and $B<2$ always. Applying the results of Zinnes,[9] this conclusion is not valid for octupole radiation; but octupole radiations have a long enough lifetime[10] ($>10^{-3}$ sec) to make them unlikely in beta-gamma correlation.

The polarization correlation measurement may, of course, be taken for $\theta\neq90°$, and for any quadrupole transitions with $\alpha_4\neq0$. Such measurements could establish the quadrupole, as against dipole, nature of the gamma; but this would already have been established by the fact $\alpha_4\neq0$. But many quadrupole gammas will have $\alpha_4=0$, and in fact $\alpha_4=0$ for any gamma multipole order in beta-gamma correlation unless the order of forbiddenness of the beta is second or higher.[11] If $\alpha_4=0$, then J_θ/J_ϕ has its maximum deviation from unity at $\theta=90°$. All told, there seems little point to measurements at $\theta\neq90°$.

[8] D. R. Hamilton, Phys. Rev. **74**, 782 (1948).
[9] I. Zinnes, Phys. Rev. **80**, 386 (1950).
[10] M. Goldhaber and A. W. Sunyar, Phys. Rev. **83**, 906 (1951).
[11] D. L. Falkoff and G. E. Uhlenbeck, Phys. Rev. **79**, 334 (1950).

APPARATUS

The apparatus used to measure the polarization of the gamma emitted at 90° to the beta in a beta-gamma cascade is indicated in Figs. 1 and 2. The beta and two gamma counters are composed of trans-stilbene crystals and mu-metal magnetically shielded photomultipliers. The beta crystal is 1.6 inches in diameter, 0.020 inch thick, while the gamma crystals are sections of cones 1.0 inch high and 0.7 inch mean diameter. The locations of the centers of mass of the crystals (omitting minor asymmetries) are shown in Fig. 1. The gamma crystals and associated photomultipliers and preamplifiers rotate about the Oy axis as indicated in Fig. 1.

A true triple coincidence between the counters β, $\gamma 9$, and $\gamma 27$ requires that the gamma undergo Compton scattering from one gamma counter to the other; if the gamma is polarized, say, parallel to Oz, then as discussed below the triple rate will be greater for $\psi = 90°$, 270° than for 0°, 180°. The pair of gamma crystals thus act as a polarization analyzer; and the basic datum of the experiment is the variation of the true triple coincidence counting rate with ψ, the angle of rotation of the analyzer. Because of the symmetry between $\gamma 9$ and $\gamma 27$, either gamma counter may serve as initial scatterer for the gammas. Geometry is nonideal because $l_3 > 0$ as well as because of nonzero crystal dimensions.

Below the gamma counters and above the source and beta counter is a plate ($\frac{1}{8}$-in. aluminum, $\frac{1}{8}$-in. Lucite below) which prevents betas from reaching the gamma counters. Surrounding the whole apparatus but not shown in either figure (the supporting ridges on the top and bottom plates appear in Fig. 2) is a thin ($\frac{1}{32}$-in.) aluminum can which serves as a light shield and also serves to contain helium at atmospheric pressure; the helium atmosphere serves to reduce by the factor $Z(\text{He})/Z(\text{air}) \approx \frac{1}{4}$ the electron energy at which a given degree of electron scattering in the gas occurs.

The net result of light construction, magnetic shielding, etc., is that there is no observable dependence of single channel gamma-counting rates on ψ except those which are attributable to asymmetry of source location.

ELECTRONICS

A block diagram of the electronics used is shown in Fig. 3. The three scintillation crystals work into 5819 photomultiplier tubes operated at 900 volts and followed by a cathode follower preamplifier, giving output pulses of order 0.1 volt. These pulses are amplified by 35-Mc amplifiers with two separated outputs. Two stages before the output the pulses are passed through a crystal diode limiting circuit which makes the gamma pulses quite uniform in height and makes the betas more so than they would otherwise be; the pulses out of the amplifiers are of the order of 7 volts. These pulses are then clipped with a 0.75-meter, RG7U, clipping cable before going into the coincidence circuit. The latter is a modified Garwin-type circuit with high

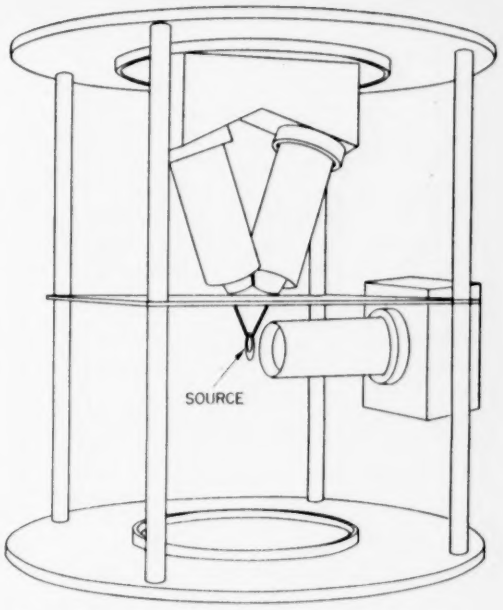

FIG. 2. Schematic drawing of apparatus with helium-and-light shield removed.

stability and high discrimination against doubles (or singles) when counting triples (or doubles); the circuit and its performance characteristics have been described elsewhere.[12] The coincidence circuit output is amplified to the order of 50 volts and then fed to a conventional scaler-discriminator combination.

The resolving time of the coincidence circuit under the above conditions was found to be approximately 2×10^{-8} second, as measured either by use of a delay line in one channel or by observing chance rates. Upward variations of this resolving time, as determined by final discriminator setting, and as made possible by good voltage regulation, were used when an increase in chance/total ratio seemed desirable.

ACCESSORY CALCULATIONS AND EXPERIMENTS

Expected Polarization Effects

As discussed under "Theory," this experiment provides its basic information about the gamma ray in the

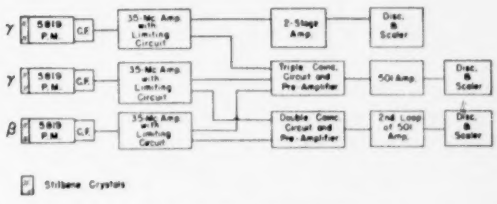

FIG. 3. Block diagram of electronics.

[12] Pipkin, Daubin, Lemonick, and Hamilton, Phys. Rev. **90**, 353 (1953).

$\beta\gamma$ cascade by comparing the signs of the angular correlation coefficient A and of the polarization coefficient B [Eqs. (2) and (3)]. In the geometry of Fig. 1, J_ϕ and J_θ are, respectively, J_x and J_z, J_x and J_z being the intensities of gammas traveling along Oy and with polarization $\mathbf{i}$ and $\mathbf{k}$, respectively. From the preference of the Compton scattered photon to have polarization parallel to that of the incident photon, it is obvious that if $J_x > J_z$ (i.e., $B>0$), the triple coincidence rate will be greatest at $\psi = 0, \pi$. Thus, if the relative experimentally observed triple coincidence rate is given by

$$N(\psi) = 1 + C\cos^2\psi, \tag{5}$$

the signs of C and B are the same.

However, it is desirable to be able to deduce from the observed value of C not only the sign but also the magnitude of B, for comparison with the value of B deduced from the angular correlation coefficient A and Eq. (4). For relating B and C, following Metzger and Deutsch[6] we define a quantity R, the "asymmetry ratio" of the polarimeter, as the value of $N(0°)/N(90°)$ observed when the radiation incident in the polarimeter is linearly polarized in the x direction in Fig. 1 (i.e., $B=\infty$). This definition makes $R>1$. For incident partially polarized radiation described by B, we then have

$$C = B(R-1)/(1+B+R). \tag{6}$$

The asymmetry ratio R is easily calculated for ideal geometry (that is, point gamma counters) and 90° scattering in the polarimeter; in this case it is given by

$$R = (k_0^2 + 2k_0 + 2)/k_0^2,$$

where k_0 is the incident gamma energy in units of mc^2. However (at least for low energies), this value of R falls off rapidly as the scattering angle departs from the vicinity of 90°; since for counting rate considerations the polarimeter gamma crystals must be large and close together, the value of R for use in Eq. (6) needs to be determined, at least in part, empirically, as follows.

Calibration of the Polarimeters

A Co^{60} or Cs^{137} source (approximately 20 millicuries) was placed at the center of a lead brick (with a great deal of accessory lead brick shielding); an emergent beam of gammas was collimated by a hole in the lead block $\frac{1}{4}$ inch in diameter, three inches long. This beam travels in the positive x direction in Fig. 1, and three inches from where it leaves the lead it is incident upon a 1-cm³ stilbene crystal cube which is located at the origin (the usual location of the $\beta\gamma$ source) in Fig. 1. (The linear dimensions of this crystal and the subsequent $\beta\gamma$ sources are comparable hence give rise to similar geometric effects.) The crystal is connected by a Lucite light pipe to the beta photomultiplier which remains in its usual position.

For the ninety-degree Compton scattered gammas of Cs^{137} and Co^{60} ($k_0 = 0.57$, 0.71, respectively; this same respective order applies throughout this paragraph), the values of $J_z/J_x = 1/(1+B)$, as deduced from the Klein-Nishina formula, are 3.7 and 2.1. The values of the coefficient C as experimentally observed with this polarimeter were -0.49 ± 0.03 and -0.34 ± 0.03. These calculated values of B and observed values of C, with Eq. (6), give for the asymmetry ratios of the polarimeter $R = 3.60\pm0.5$, 3.63 ± 0.7.

The asymmetry ratio will be dependent upon energy, and one now needs to deduce from the Cs^{137} and Co^{60} data the value of R at other energies. Because of the strong dependence of ideal R upon scattering angle in the polarimeter, the nonideal geometry must be taken into account. This point has been thoroughly discussed by Metzger and Deutsch,[6] whose geometry is very similar to ours and whose notation we adopt in what follows. Our scattering angle δ is 110° by pure geometry, and the effective angle should be somewhat less because of the preference for forward scattering; our crystal counter angular spreads, $\Delta\delta$ and $\Delta\phi$ in scattering angle and scattering azimuth, are comparable with each other and are expected to be approximately 50 degrees. We find that the observed values of R for Cs^{137} and Co^{60} are fitted well by values calculated from the ideal geometry R as modified by taking $\delta = 103°$, $\Delta\delta = \Delta\phi = 56° \pm 10°$; we therefore use these values for nonideal geometry to calculate R as a function of energy. For $k_0 = 1, 2, 3$, we find $R = 2.60\pm0.15$, 1.75 ± 0.05, 1.50 ± 0.04, respectively.

The procedure in analyzing the experimentally observed polarization data will then be as follows. The angular correlation coefficient reported by other workers and corrected by them to correspond to ideal geometry, which we call A_0, needs first to be corrected to the value A which would be observed if one of the detectors in the angular correlation experiment had the size of our beta detector; this means $A = 0.82A_0$. Then by use of Eqs. (4) and (6), the values of A, and the above stated values of R, we calculate the predicted value of the polarization correlation coefficient C on each of the two hypotheses concerning gamma parity change; this then is compared with the observed value of C.

Parameters for Angular Dependence of Counting Rates

Discussion so far has been on the basis of only a $\cos^2\psi$ variation of the triple coincidence counting rate $N(\psi)$. Various asymmetries, to be discussed shortly, exist and will give variations with $\cos(\psi-\beta)$, where β is a phase angle not necessarily zero. These asymmetries will also contribute $\cos^2\psi$ terms of arbitrary phase which are always much smaller than the $\cos^2\psi$ terms resulting from polarization effects. Hence finally we analyze all data in terms of the three coefficients α, β, C of the relation,

$$N(\psi) \sim 1 + \alpha\cos(\psi-\beta) + C\cos^2\psi. \tag{7}$$

Readings of $N(\psi)$ for four values of ψ (0°, 90°, 180°, 270°) suffice to determine these coefficients, as given

by the following relations:

$$\tan\beta=[N(90)-N(270)]/[N(0)-N(180)], \quad -(\pi/2)\leqslant\beta\leqslant(\pi/2); \quad (8a)$$

$$\alpha=[N(90)-N(270)]/(2N_0\sin\beta)=[N(0)-N(180)]/(2N_0\cos\beta); \quad (8b)$$

$$C=[N(0)+N(180)-N(90)-N(270)]/[N(90)+N(270)]. \quad (8c)$$

Here N_0 is the average of N over ψ. The fact that the denominator in Eq. (8c) is not simply $2N_0$ arises from the fact that the omitted constant of proportionality in Eq. (7) is $N_0/(1+\frac{1}{2}C)$.

Discussion of Accessory Angular Dependences

The values of α and β are valuable primarily for a check on reproducibility of data and on the anatomy of the experiment. Relevant angular dependences, other than the polarization $\cos^2\psi$ dependence of the triples, will be summarized briefly in the following paragraphs.

Rotation of the apparatus as a whole, which would show effects of external fields or scattering, produces no α or C in single rates greater than statistics (0.002 in this instance).

The single gamma channels for various sources have values of $|\alpha|$ in the range 0.01 to 0.03; the phase β is such ($\beta\approx 0$) that the asymmetry could be caused either by scattering by the beta photomultiplier shield or by the source being displaced from the symmetry axis toward the beta crystal. The former possibility seems ruled out by the fact that when 0.1 inch of aluminum absorber was placed in front of the beta crystal without moving the source (see later discussion of Sb^{124} and As^{76}), changes in $|\alpha|$ of only 0.003 resulted; these aluminum absorbers should have been roughly equivalent (taking into account solid angles and distances) to the photomultiplier shield in ability to scatter gammas into the gamma counters. A source displacement of 0.050 in., caused, for example, by bending of the mica when placing in position, would produce the observed α and β; to this there corresponds $C\approx\alpha^2$ which should be negligible. The observed values of C for single gamma channels averaged 0.005 ± 0.002.

For $\beta\gamma$ doubles the angle β lay in the same range as for gamma singles, but α was increased in magnitude by factors up to two. This is what is expected from the contribution to $\beta\gamma$ doubles by any gamma scattering from the photomultiplier which simultaneously triggers a "beta" count; such scattering could give a negligible contribution to gamma singles, but not necessarily to $\beta\gamma$ coincidences. The relative increases in C and α caused by this phenomenon are known from data taken with 0.1-inch aluminum absorbers in front of the beta counter (see next section); here $|\alpha|$ and C increased to approximately 0.10 and 0.025, respectively. From all this data we calculate an expected contribution to the C for $\beta\gamma$ coincidences of 0.008 ± 0.003 due to scattering from the beta counter. An additional contribution to C is expected from slight residual angular correlation arising from the fact that the separation of the gamma counters makes $\cos^2\theta\approx 0.09\cos^2\psi$ instead of zero. The total C thus calculated is in good agreement with that observed.

As to the $\gamma\gamma$ double coincidences, one would expect here an angular dependence which is a simple average of the two single gammas. It turns out, to the contrary, that in α and β the $\gamma 27$-dependence appears weighted by at least 2 to 1 over the $\gamma 9$ dependence, as if doubles which were initiated in $\gamma 27$ were much preferred to those initiated in $\gamma 9$. This is probably, although not obviously, related with three incidental facts: the existence of a horizontal crack which bisects the $\gamma 9$ scintillation crystal, the apparent lower efficiency of $\gamma 9$, and the fact that α for $\gamma 9$ singles is some 0.7 as large as for $\gamma 27$, as would be the case if only the top half of the $\gamma 9$ crystal were sensitive. The values of C fluctuate, in magnitude and sign, from element to element, and are of the same magnitude as the standard deviations in C, about 0.007. Since C has the same sign ($C>0$) for $\gamma 9$ and $\gamma 27$, as compared to α which reverses sign, we would in any case not expect to see in C any reflection of peculiar weighting of $\gamma 9$ and $\gamma 27$ in $\gamma\gamma$.

The α and β asymmetries just discussed for singles and doubles do not appear in the triples; with standard deviations in α of order 0.01, the sign of α varies from element to element and in three out of four elements $|\alpha|$ is less than the standard deviation.

These angular dependences of the various channels which have just been discussed seem to be minor and understood, with exception of the unexplained α in the $\gamma\gamma$ doubles, which, however, is not reflected in the triples or in the C for $\gamma\gamma$ doubles. We therefore feel that there will be no errors, beyond statistics, in deducing the gamma polarization from values of C for true triples, calculated according to Eq. (8c) and normalized with respect to $\beta\gamma$ doubles as discussed below.

GENERAL PROCEDURE

Source Preparation

Sources were in every instance prepared by vacuum evaporation onto mica, using a source area 3.3 cm^2 in area and mica thickness approximately 2 mg/cm^2. The active deposit faces the β counter in Fig. 2, and the source is supported from above by two thin (1-mm by 2-mm) Lucite fingers.

Since it is important that there be a minimum of beta scattering, the critical voltage for backscattering was kept as low as possible. This critical voltage V_c, defined by the semiempirical relation,[13]

$$V_c(\text{kev})=1700[Z^2t(\text{g/cm}^2)/A]^{\frac{1}{2}}, \quad (9)$$

is the voltage below which, for a given thickness of

[13] D. R. Hamilton and L. Gross, Rev. Sci. Instr. **21**, 912 (1950).

source and backing, deviations from the beta spectrum Kurie plot will appear. It will be noted that the voltage V_c for the 3 cm of helium between source and beta counter is 39 kev, which is well below the values of V_c for specific sources listed later.

Counting Procedure

As will be apparent from Fig. 3, it was possible to count simultaneously triples and one double channel, or triples and two single channels. (To each of these combinations could have been added also one more single channel; this was not done in practice.) Normally readings of one-half hour apiece at $\psi=0°$, 90°, 180°, 270° were interspersed with readings of chance at 0° (delay lines inserted in one or two channels before the 35-Mc amplifiers), the amount of time being spent on chance readings being dependent upon the chance/total ratio.

The variation of the chance rate with ψ, which must be known in subtracting chance from total, was obtained by composition from the angular dependence of the various double and single rates which give the chance triples; since the single and double rates were much higher than the triples, these single and double angular dependences were always determined much better than was necessary for purposes of chance correction, and served as a useful check on proper operation.

Gamma Scattering by Beta Absorber

In two of the elements used (Sb^{124}, As^{76}) there exist other beta-gamma cascades (with a lower end-point beta component) in addition to the one under investigation. In these cases aluminum absorbers were placed in front of the beta crystal to absorb the low-energy beta component. Triples resulting when these absorbers enable a gamma to fire the beta counter are called "spurious" triples; these should initially increase with absorber thickness and then level off. With an absorber thick enough to cut out all betas, the number and angular dependence of the spurious triples were obtained in each case; from this, the spurious triples for any absorber were deduced and subtracted from total triples.

Normalization of Triple Coincidences

As already noted in the discussion of the angular dependence of the $\beta\gamma$ doubles, the latter may show a $\cos^2\psi$ dependence. This will be reflected in the angular dependence of the triples, which must, therefore, be normalized with respect to the $\beta\gamma$ doubles by subtracting C ($\beta\gamma$ doubles) from C (triples). For the true polarization effects on the triples, $|C|$ and $|A|$ are comparable according to Eqs. (4) and (6); C ($\beta\gamma$ doubles) has magnitude of order 0.01. Thus it turned out empirically that the normalization has not much effect on C for the three cases (Rb^{86}, Sb^{124}, As^{76}) for which a definite polarization effect was observed.

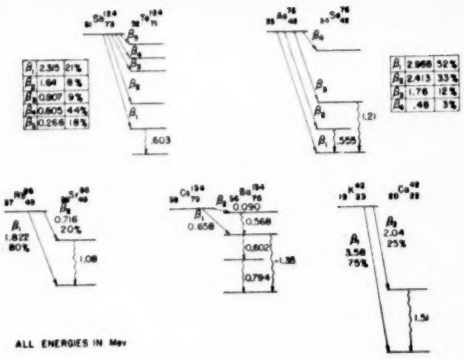

FIG. 4. Decay schemes of nuclides investigated.

RESULTS

The normalized values of C obtained experimentally for each of the five elements under discussion are listed below, with relevant comments. The indicated ranges represent over-all standard deviations; since the chance triples were small compared to true in all cases except arsenic-76, where chance and true were about equal, the standard deviation is approximately that calculated from the total number of true triples. True triple counting rates were several tenths of a count per second in each case. Values of V_c (in kilovolts) are obtained from Eq. (9) using full backing and half source thickness; V_0 is the end point of the beta component in question.

The decay schemes of the five nuclides investigated are summarized in Fig. 4, with data from the NBS compilation[14] as slightly modified by later information;[7] not all the gammas in antimony-124 and arsenic-76 are shown.

All plus-minuses in these results and throughout the paper represent standard deviations.

Cesium-134

Cesium-134 was obtained as an impurity in a Chalk River bombardment of Rb_2CO_3. An evaporated RbCl source (0.9 mg/cm² on 1.09 mg/cm² mica backing; $V_c/V_0=0.33$ for the cesium V_0) was prepared and allowed to decay for a total of five months after bombardment, at which time gamma-ray scintillation spectrometer measurements and observation of rate of decay indicated that (88±3) percent of the $\beta\gamma$ coincidences were due to Cs^{134}. The value of C obtained for this source, without a small correction for rubidium 86, was

$$C=0.009\pm0.013.$$

Antimony 124

Antimony 124 was obtained from Oak Ridge as $SbCl_3$ and $SbCl_5$ and was vacuum evaporated as metal

[14] Way, Fano, Scott, and Thew, *Nuclear Data*, National Bureau of Standards Circular 499 (U. S. Government Printing Office, Washington, D. C., 1950).

to form a source 0.8 mg/cm² thick on 2.2 mg/cm² mica; $V_c/V_0=0.11$.

As is seen from the decay scheme in Fig. 4, the highest-energy beta component is the one which is involved in the most direct correlation with the 607-kev gamma. Data were taken with aluminum beta absorbers of thickness 0.041 and 0.110 inch to remove lower-energy beta components, and with 0.207-in. aluminum to remove all betas and hence to check on spurious triples caused by gamma scattering from beta absorber to gamma counter or by γ-γ correlation.

We estimate that with the 0.110-in. absorber, the relative amounts of the components β_2 and β_3 are 16 and zero percent, respectively; this makes the 0.110-in. absorber sound better than the 0.041-in. But the relative values of the counting rates for these absorbers showed that a large number of the triples observed at 0.110-in. thickness (possibly as many as two-thirds) were spurious. The large size of the spurious-true ratio makes the 0.110-in. data almost meaningless, in spite of the fact that C has the same sign and order of magnitude for true and spurious triples for antimony. (Lest one suspect a common cause here, it is reassuring to observe that for arsenic, C for spurious triples has the same sign as for antimony, but for true triples the opposite sign.) But the same fact (C similar for true and spurious triples) makes the correction of 0.041-in. triples practically independent of how one assumes the spurious triples to depend on absorber thickness. For the 0.041-in. absorber we estimate the spurious triples as 15 percent of true, and obtain finally, for this absorber as corrected for spurious triples,

$$C=+0.147\pm0.012.$$

Potassium-42

Potassium was bombarded at Brookhaven as the carbonate and vacuum evaporated as the chloride. Because of the short life of K^{42}, three sources were used; source thicknesses were 1.1, 4.0, 2.0 mg/cm² on mica backings of 2.2, 2.1, 1.8 mg/cm², giving $V_c/V_0<0.14$ in each case. The half-life of these sources was measured as 12.7±0.5 hours, in agreement with the expected 12.4 hours.

There are no complications here beyond the need for thin sources. The results for the three sources agree within statistics; chance triples are low; the final result is

$$C=-0.003\pm0.015.$$

Arsenic-76

Arsenic was bombarded at Brookhaven as the metal and vacuum evaporated as the metal, 1.5 mg/cm² on 2.3 mg/cm² mica; $V_c/V_0=0.11$. The half-life of the sources was observed to be 25.6±0.4 hours as compared to the expected 26.8 hours.

In the complex decay of arsenic-76, the $\beta\gamma$ correlation under investigation here arises from the beta which goes to the first excited state. Chance rates are high because of the intense beta transition direct to ground, which cannot be absorbed out, and because of the large number of gammas. The correlations were observed with a 0.088-in. aluminum beta absorber, which is calculated to transmit approximately 26 and 6½ percent of β_2 and β_3, respectively; since β_3 is weaker than β_2, as shown in Fig. 4, the β_2 electrons should be about 11 times as abundant as the β_3 after passing through the absorber. Further measurements on angular dependence of triple rate were made with an 0.238-in. absorber which absorbs all betas and gives only the "spurious" triples. Consideration of the range of the Compton electrons in the absorber indicates that the number of spurious triples arising from this source with 0.088 and 0.238 absorbers should be approximately the same; on this basis, the triples from gamma scattering in the 0.088-in. absorber are estimated as 12 percent of the total and corresponding corrections are made.

It should be noted, without going into details, that the process of correcting back to a common time the readings at four different angles for a rapidly decaying source, and then sorting out the various angular dependences, is a complex one when counting rates are comparable for true triples (half-life τ), double-single chance triples (half-life $\tau/2$) and single-single-single chance triples (half-life $\tau/3$). This makes the standard deviation larger than the simple statistics value in the final result,

$$C=-0.114\pm0.035.$$

Rubidium-86

Rubidium was bombarded at Chalk River as the carbonate, vacuum evaporated as the chloride; the active source was 0.9 g/cm² on 2.1 mg/cm² mica, giving $V_c/V_0=0.32$.

The rubidium-86 source was checked with a gamma scintillation spectrometer for the presence of cesium-134, which was found to contribute 16±4 percent of the gammas from the source. With a small correction for the presence of cesium-134, the final value for C obtained was

$$C=-0.060\pm0.019.$$

DISCUSSION

In Table I the observed values of C which have just been listed are summarized. Also listed is A_0, the value

TABLE I. Values of angular correlation coefficient C(obs) and C(pred), as observed in present experiment and as predicted (on basis of parity change "no" for the gamma) from the angular correlation coefficient A_0 reported by other workers for beta-energy discrimination conditions similar to ours.

Nucleus	A_0	C(pred)	C(obs)
Cs^{134}	0.00±0.01	0.00 ±0.003	0.009±0.013
Rb^{86}	0.13±0.01	−0.068±0.005	−0.060±0.025
As^{76}	0.07±0.02	−0.067±0.018	−0.114±0.035
K^{42}	−0.06±0.02	0.022±0.007	−0.007±0.016
Sb^{124}	−0.27±0.04	0.151±0.022	0.142±0.010

of the angular correlation coefficient for ideal geometry, as found by other workers: the values of A_0 are those obtained from integral experiments like ours, or represent averages over that part of the differential spectrum which we used. For cesium-134, A_0 is that of Beyster and Wiedenbeck,[15] and Stump and Frankel.[16] For rubidium-86, A_0 is the integral over the differential spectrum of Stevenson and Deutsch[17] as checked by Ridgway and Pipkin;[18] reference 1 lists a number of other integral results with lower A_0, perhaps caused by source difficulties. For arsenic-76, A_0 is obtained by combining the integral value of Walter, Huber, and Zunti[19] with differential results of reference 18. For potassium-42, we have combined the results of reference 15 and Stevenson and Deutsch.[20] For antimony 124, for which A_0 is sensitive to absorber thickness, we have used the data of reference 15 which is taken for nearly the same absorber thickness as ours.

The values of C predicted from the value of A_0, as discussed under "Accessory Calculations and Experiments" above, and assuming parity change "no" in the gamma transition, are also indicated. If parity change "yes" had been used, the sign of the predicted C would have been reversed and the magnitude slightly altered.

For Cs^{134}, for which no polarization correlation is expected, none is observed. For Rb^{86}, As^{76}, and Sb^{124}, the observed polarization and that predicted on the basis of no parity change in the gamma ray agree very satisfactorily. The comparison of the signs of observed and predicted C is all that is needed to determine the parity change in the gamma transition; the agreement in magnitudes which is apparent in Table I is useful as a check on the experiment and on the details of the radiation and correlation processes.

For K^{42}, an essentially zero polarization is observed; we have no ready explanation for this, although it may be noted that part of the discrepancy corresponds to a discrepancy of 0.006 between the observed and predicted values for C for $\beta\gamma$ doubles, the observed value of the latter having been used in the normalization. If the sign of C (predicted) were reversed, as discussed above, the predicted and observed values would overlap; we do not feel that any significance can be attached to this.

In each of the three cases above with nonzero polarization, i.e., Rb^{86}, As^{76}, and Sb^{124}, $\beta\gamma$ or $\gamma\gamma$ correlation results or both indicate that the first excited level of the daughter nucleus, from which gamma emission occurs, has $I=2$, it being assumed that the ground state has $I=0$ (even-even nucleus). The polarization result, that there is no parity change in the gamma transition, therefore determines that this is an electric quadrupole gamma and that the first excited state has the same parity as the ground state. This is in accord with the systematics of even-even nuclei.[21]

The internal conversion coefficients of the $2-0$ gamma ray have been measured for arsenic-76[22] and antimony-124[23] and agree with our results in describing the gamma as electric quadrupole.

ACKNOWLEDGMENTS

The material for the Rb^{86} and Cs^{134} sources was obtained from Chalk River, for K^{42} and As^{76} from Brookhaven National Laboratory, for Sb^{124} from Oak Ridge National Laboratory.

We are indebted to Lt. Scott C. Daubin, USN, for assistance during the course of this experiment.

The analysis and writing up of the results of this experiment took place while one of us (DRH) was at the Institute for Advanced Study and at Brookhaven National Laboratory, the hospitality of both of which he greatly appreciates.

[15] J. R. Beyster and M. L. Wiedenbeck, Phys. Rev. **79**, 728 (1950).
[16] R. Stump and S. Frankel, Phys. Rev. **79**, 243 (1950).
[17] D. T. Stevenson and M. Deutsch, Phys. Rev. **83**, 1202 (1951).
[18] S. L. Ridgway and F. M. Pipkin, Phys. Rev. **87**, 202 (1952).
[19] Walter, Huber, and Zunti, Helv. Phys. Acta **23**, 697 (1950).
[20] D. T. Stevenson and M. Deutsch, Phys. Rev. **84**, 1071 (1951).
[21] G. Scharff-Goldhaber, Phys. Rev. **90**, 587 (1953).
[22] E. P. Tomlinson and S. L. Ridgway, Phys. Rev. **88**, 170 (1952).
[23] F. R. Metzger, Phys. Rev. **86**, 435 (1952).

Gamma Radiation from the Reaction $C^{13}(p, \gamma)N^{14}$†

H. H. Woodbury,* R. B. Day,‡ and A. V. Tollestrup
Kellogg Radiation Laboratory, California Institute of Technology, Pasadena, California
(Received August 28, 1953)

The capture radiation from $C^{13}(p, \gamma)N^{14}$ has been investigated and found to show cascade transitions which involve bound levels in N^{14} at 2.31, 3.95, 5.09, 5.81, 6.26, and 6.44 Mev in addition to the resonance levels at 8.06, 8.62, 8.70, 8.90, 8.98, 9.17, and 9.49 Mev.

INTRODUCTION

THE thin-target excitation curve for the reaction $C^{13}(p, \gamma)N^{14}$ has previously been investigated in this laboratory for proton bombarding energies up to 2.7 Mev.[1] Five definite resonances were found, corresponding to excited states of N^{14} at 8.06, 8.62, 8.70, 9.17, and 9.49 Mev. It was observed that the gamma-ray spectrum changed considerably from one resonance to another and involved cascades through intermediate levels of N^{14}. In addition, recent work in this laboratory on the elastic scattering of protons on C^{13} has clearly demonstrated the existence of two other resonances corresponding to excited states at 8.90 Mev and 8.98 Mev[2] which were tentatively reported in reference 1.

In order to obtain more information on the energy levels of N^{14} below 9.5 Mev, we have investigated the gamma-ray spectrum in detail at each of the 7 resonances by using a sodium iodide scintillation counter as a gamma-ray spectrometer.

EXPERIMENTAL PROCEDURE

The NaI(Tl) crystals used most frequently in our work were $1\frac{1}{2}$ inches in diameter by $1\frac{1}{2}$ inches long. Originally the crystals were enclosed in mineral oil in a Lucite container which was placed on the photocathode of a selected 5819 photomultiplier tube. Mineral oil was used to provide optical contact between the Lucite and the phototube, while a magnesium oxide reflector was placed around the sides and top of the Lucite container. Later, a more permanent arrangement was employed in which the crystal was cemented to a quartz disk which in turn was cemented to a magnesium oxide coated aluminum can enclosing the crystal. A thin Lucite light pipe and viscous silicone oil were used to provide optical contact between the photomultiplier and the quartz disk. A smaller ($\frac{1}{2}$-inch cube) NaI(Tl) crystal, which was placed directly on the photomultiplier with a small aluminized cup used as a reflector, was occasionally used to give supplementary information on the pulse-height spectra. These three crystal arrangements appeared to have about the same light-gathering efficiency. The resolution obtained with Cs^{137} (0.661 Mev) and the type-5819 photomultiplier tube ranged from 9 to 12 percent depending on the phototube used. In the most recent work, a DuMont type 6292 photomultiplier tube was used with which the instrument has a resolution of 7.5 percent for the Cs^{137} radiation.

The spectrum obtained with the small crystal for gamma rays of about 3.5 to 7 Mev consists primarily of a "pair peak" at an energy 1.02 Mev less than the gamma-ray energy. On the other hand, the larger crystal also gives peaks at E_γ and $E_\gamma - 0.51$ Mev, which are produced by the absorption of the scattered photon as well as the primary Compton electron or by the absorption of one or both annihilation quanta in addition to an electron-positron pair. At higher energies, even with the larger crystal, the resolution of the scintillation counter was not sufficient to permit these three peaks to be well separated and the resulting spectrum showed only an asymmetric peak with two bumps on the high-energy side.

After amplification the pulse-height spectrum was obtained either by a photographic method or by means of a single channel pulse-height analyzer designed by M. Sands. Later, a ten-channel analyzer of Los Alamos design[3] was employed. For the oscilloscope presentation, the pulses were shaped by a 1.5-microsecond delay-line clipper and were applied to the vertical deflection plates of a Tectronix 511D oscilloscope with the horizontal sweep being triggered by the pulse. The face of the oscilloscope was masked except for a vertical strip 2 cm wide, and a sweep speed of 10 cm per microsecond was used. Peaks in the pulse-height distribution then appeared as horizontal lines and a permanent record was obtained by making a time exposure with a Land camera. The range of intensities obtainable with a single exposure was increased by means of a colored cellophane filter placed over 1 cm of the 2-cm wide strip. To correct for non-linearities in the system, which were mainly in the oscilloscope tube and in the optical system of the camera, a series of pulses whose height could be varied in equal voltage increments was fed into the input of the preamplifier and photographed on the oscilloscope. Since five exposures could be made on

† This work was assisted by the joint program of the U. S. Office of Naval Research and the U. S. Atomic Energy Commission.
* Now at General Electric Research Laboratory, Schenectady, New York.
‡ Now at Los Alamos Scientific Laboratory, Los Alamos, New Mexico.
[1] J. D. Seagrave, Phys. Rev. **85**, 197 (1952).
[2] E. A. Milne, Ph.D. thesis, California Institute of Technology, 1953 (unpublished) and private communication.
[3] C. W. Johnstone, Nucleonics **11**, No. 1, 36 (1953).

each film the general practice was to include this linearity calibration with each pulse-height spectrum of interest, in addition to the spectrum of gamma-rays of known energy which were used to establish the energy calibration. For this latter purpose, Na^{22} (0.511 Mev and 1.277 Mev) and ThC″ (2.615 Mev) were most frequently used. This technique proved to be very rapid and convenient, not only for qualitative "surveying" but also for energy measurements accurate to about 2 percent.

The oscilloscope arrangement was also used in obtaining pulse-height spectra in gamma-gamma coincidence measurements. A second counter with a NaI(Tl) crystal $1\frac{1}{2}$ inches in diameter by $1\frac{1}{2}$ inches long was placed on the opposite side of the target from the first (both counters were at 90° to the beam). Their outputs went to a coincidence circuit with a resolving time of 0.1 microsecond which was used to trigger the sweep of the oscilloscope. The output of one of the counters was applied to the vertical deflection plates of the oscilloscope, while a sufficiently high bias on the coincidence input fed by the other prevented false coincidences from back-scattered Compton gamma rays or from annihilation radiation. The counting rates were low enough that accidental coincidences could easily be taken into account.

In using the pulse-height analyzer, the procedure was to alternate the measurement of pulse-height spectra from $C^{13}(p, \gamma)$ with those from artificial radioactive sources (such as Na^{22} or ThC″), which were used to provide the energy calibration. After each spectrum had been obtained, the pulse height corresponding to peaks in the spectrum was measured with a precision pulser which was accurate to a few tenths of a percent. These pulses were fed into the preamplifier in parallel with those from the photomultiplier. It was thus possible to eliminate the effects of any non-linearities in the amplifier or analyzer. Since the alternation of the gamma rays from $C^{13}(p, \gamma)$ with known pulse-height spectra gave one a check on drifts in the photomultiplier gain, one could feel confident that the gamma-ray energy measurements were not being affected by instrumental difficulties.

Since the energies of the transitions to the ground state of N^{14} could be calculated from the Q value of the reaction and the proton bombarding energy, it was possible to check the pulse-height linearity of the scintillation counter up to 9 Mev. It was found that as long as the voltage on the type 5819 photomultiplier was kept less than about 750 volts this linearity was good within the experimental accuracy (1 percent). For lower-energy gamma rays it was possible to raise the photomultiplier voltage above 750 volts before nonlinear effects were encountered. The type 6292 photomultiplier showed considerably more nonlinearity and it was not used where much extrapolation was involved.

The gamma rays were produced by bombarding C^{13} targets with protons from the 3-Mev electrostatic generator. The protons were analyzed by either an electrostatic or a magnetic analyzer set to give an energy resolution of 0.1 to 0.2 percent. At each resonance, before observing the pulse-height spectrum, an excitation curve was run in order to obtain the maximum intensity and also to be sure that the observed radiation was characteristic of the resonance. The two targets used were 7 and 16 kev thick at 1.7 Mev and were composed of carbon, enriched to 60 percent C^{13}, deposited on a tantalum backing. The preparation of these targets is described in detail in reference 1. The background radiation produced by reactions in the C^{12} content of the target or the tantalum backing was investigated independently and found to be much less intense than the radiation from the reaction $C^{13}(p, \gamma)$. It could also be distinguished from the latter by its excitation function, since the resonances in $C^{13}(p, \gamma)$ are well known.[1] In most cases the pulse-height spectra were measured with the scintillation counter placed at 90° to the beam about $\frac{3}{4}$ inch from the target. Several resonances were also investigated at 0° to the beam and these results will be discussed in a later section.

EXPERIMENTAL RESULTS OBSERVED AT 90° TO THE BEAM

Typical pulse-height distributions, which show the various features encountered at three of the resonances in $C^{13}(p, \gamma)$, are illustrated in Figs. 1–3. In Fig. 1 are shown the results obtained at a resonance bombarding energy of 0.55 Mev corresponding to an excited state in N^{14} at 8.06 Mev. In what follows such a state will be referred to as the 8.06(0.55)-Mev resonance level.[4] The peaks at 1.3 and 2.3 Mev in Fig. 1 have the proper shape and separation to be the pair and photopeaks of a 2.3-Mev gamma ray, while the rise just below 2 Mev is the Compton edge for this gamma ray. The peak at 1.6 Mev is the photopeak of a 1.6-Mev gamma ray whose Compton edge is obscured by the 1.3-Mev pair peak. The rise below 1.3 Mev is the tail of the annihilation radiation from the positron decay of N^{13} which is formed in the reaction $C^{12}(p, \gamma)N^{13}$. A similar pulse-height spectrum also occurred at the 8.62(1.16)-Mev resonance, which suggests that the 1.6- and 2.3-Mev gamma rays are part of a cascade through the lower levels of N^{14}. In the region of pulse heights from 3 to 4 Mev in Fig. 1, there occur three peaks characteristic of a 4-Mev gamma ray. The peak at 7 Mev in this figure is produced by an 8-Mev gamma ray. Its structure is caused by contributions from the high-energy end of the Compton distribution in addition to the secondary effects mentioned previously.

In attempting to detect a weak gamma ray in the presence of other radiation, one is limited by statistical fluctuations in the counting rates of the pulse-height

[4] The Q of this reaction is 7.54 Mev as given by C. W. Li *et al.*, Phys. Rev. **83**, 512 (1951). Thus, the excitation energy of N^{14} in Mev is given by $E_X = 7.54 + (13/14)E_p$, where E_p is the proton bombarding energy in Mev.

analyzer channels and also by variations in channel width. The photographic method of pulse-height analysis eliminated the second difficulty, and by stopping down the camera one could record enough pulses for good statistical accuracy without overexposing the film. By this means, a search was made at the 8.06(0.55)-Mev resonance for a gamma ray at 5.8 Mev corresponding to a transition from the resonance level to the known level at 2.31 Mev. However, no radiation was found in the region from 5 to 7 Mev with an intensity greater than 2 percent of the ground state transition.

The radiation from the 8.06(0.55)-Mev resonance level was intense enough to permit a gamma-gamma coincidence experiment to be performed using the photographic technique to record the pulse-height distribution. This experiment showed that the 4-Mev gamma ray plus the 2.3- and 1.6-Mev gamma rays were related in some sort of cascade transition.

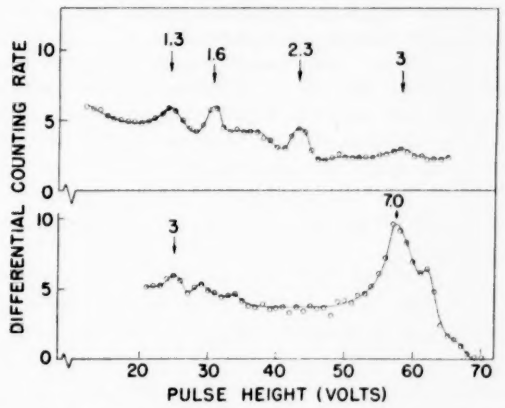

FIG. 1. Differential pulse-height spectrum of the gamma rays from the 8.06(0.55)-Mev resonance level of $C^{13}(p,\gamma)N^{14}$.

The gamma-ray results obtained at this resonance do not agree with previously published results. Fowler and Lauritsen[5] report a 5.8-Mev gamma ray, while Barnes *et al.*[6] found a possible line at 5.81 Mev. It seems likely, as suggested by Barnes *et al.*, that this line is actually due to fluorine contamination. Recently, Hicks *et al.*[7] have published a brief account of their measurements with a scintillation pair spectrometer. They find several gamma rays which we do not detect at this resonance, although the radiation they ascribe to a 5.0-Mev level does show up in our work at the 9.49(2.10)-Mev resonance. Since the details of their work are lacking, it is difficult to account for this discrepancy. Clegg and Wilkinson[8] have also investigated the radiation at the

[5] W. A. Fowler and C. C. Lauritsen, Phys. Rev. **76**, 314 (1949).
[6] Barnes, Carver, Stafford, and Wilkinson, Phys. Rev. **86**, 359 (1952).
[7] Hicks, Husain, Sanders, and Beghian, Phys. Rev. **90**, 163 (1953).
[8] A. B. Clegg and D. H. Wilkinson (private communication).

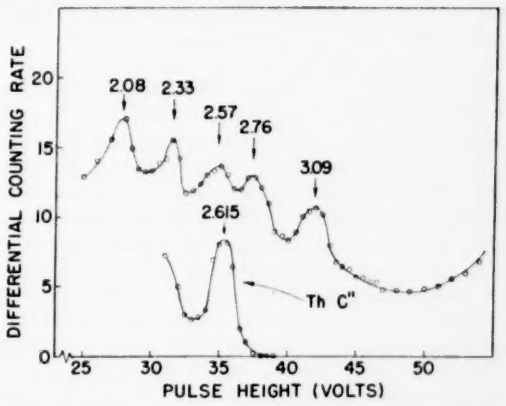

FIG. 2. Differential pulse-height spectrum of the gamma rays from the 8.90(1.47)-Mev resonance level of $C^{13}(p,\gamma)N^{14}$.

8.06(0.55)-Mev resonance and have obtained results in substantial agreement with ours. In particular, they have been able to put an upper limit of 0.7 percent on the intensity of a possible 5.8-Mev line.

At the 8.62(1.16)-Mev resonance, in addition to the 1.6- and 2.3-Mev gamma rays, there appeared in the pulse-height distribution a complicated structure in the 4-Mev region which was resolved into two gamma rays at 3.9 and 4.7 Mev. From energy considerations it is obvious that the 3.9- and 4.7-Mev gamma rays form one cascade while the 1.6-, 2.3-, and 4.7-Mev gamma rays form another. The fact that only one 4.0-Mev gamma ray was found at the 8.06(0.55)-Mev resonance can easily be explained if there is a level at approximately 4.0 Mev in N^{14} since the radiation from the 8.06(0.55)-Mev resonance level to such a level could not be separated from the ground state decay of such a level.

Also at the 8.62(1.16)-Mev resonance, there was found ground state radiation and a 6.3-Mev gamma

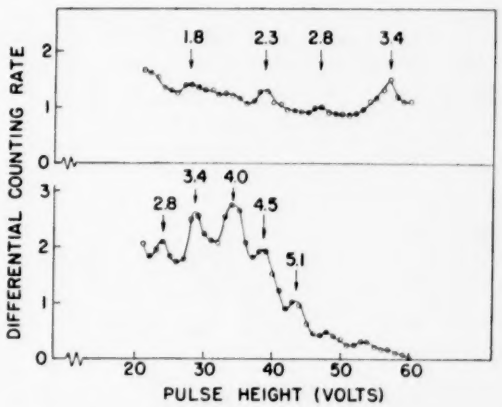

FIG. 3. Differential pulse-height spectrum of the gamma rays from the 9.49(2.10)-Mev resonance level of $C^{13}(p,\gamma)N^{14}$.

ray. At first it was believed that the latter radiation represented a transition to the known 2.31-Mev level, but the interpretation of the elastic scattering of protons by C^{13} indicated that this was improbable since it would require a 0—0 radiative transition (see discussion). Further work then showed the following: First, the 6.3-Mev radiation exhibited the same excitation curve as the other gamma rays at this resonance. Second, the relative intensities confirmed that the 6.3-Mev radiation was in cascade with a single gamma ray with an energy of approximately 2.3 Mev. Although the photopeak from the stronger 2.31-Mev radiation appeared skew on the high energy side, it could be established quantitatively only that the cascade radiation of interest was less than 2.39 Mev. Thus, the higher energy transition must be greater than 6.23 Mev. Finally, the energy of the 6.3-Mev radiation was measured to be 6.25±0.04 Mev by comparing it with the 6.13-Mev $F^{19}(p, \alpha\gamma)O^{16}$ radiation. This is to be compared with the value of 6.31 Mev for a transition directly to the 2.31-Mev level. These results lead us to believe that this radiation corresponds to a cascade through a level in N^{14} which has an energy greater than 6.23 Mev and less than 6.29 Mev (6.26±0.03 Mev).

The 8.70(1.25)-Mev level decayed primarily by radiation to the ground state. This and the fact that the resonance was very weak prohibited a detailed investigation of the cascading with the ten-channel discriminator. However, the photographic method revealed some cascading (10 percent) that may involve a level in N^{14} at 5.69 Mev. This possibility is briefly discussed below.

To measure the energy of a particular gamma ray, one looks at the pulse-height spectrum in detail on an expanded scale and compares it with the spectrum of a standard source as described above. To eliminate systematic errors due to possible differences in channel widths in using the ten channel analyzer, the bias settings are chosen to give overlapping intervals. An example of this is shown in Fig. 2 where the 2.0-Mev to 3.5-Mev region of the spectrum found at the 8.90(1.47)-Mev resonance is shown. This very complicated spectrum is explained as follows. The 2.08-, 2.57-, and 3.09-Mev peaks are the three characteristic peaks of a 3.09-Mev gamma ray. The 2.33- and 2.76-Mev peaks are the photopeaks for two weaker gamma rays of approximately these energies. There is no question that the 2.33-Mev peak is a photopeak, but since the 2.76-Mev peak coincides with the Compton maximum from the 3.09-Mev gamma ray it may be in doubt. However, the pronounced dip between the 2.76-Mev peak and the 2.57-Mev peak and the general rise in counting rate indicate that there is indeed a gamma ray present of approximately this energy. The rather flattened appearance of the ThC″ line (2.615-Mev photopeak) and the 3.09-Mev peak is due to the fact that the channel width used (1 volt) is comparable to the resolution at this particular setting. Besides these gamma rays, three others at 5.7, 5.1, and 0.73 Mev were also found at this resonance. Since the 3.09-Mev gamma ray was the strongest, it most likely is the first in the cascade. If this is correct, then there must be a level at 5.81 Mev (8.90–3.09) in N^{14}. Energy considerations then indicate that the 5.1- and the 0.73-Mev gamma rays result from the decay of this 5.81 level and the 2.3- and 2.8-Mev gamma rays result from an alternative decay of the 5.1 level. This scheme is further confirmed by the spectrum from the 2.1-Mev resonance and from the relative intensities.

The 8.98(1.55)-Mev resonance level decays primarily to the ground state. Because it was so weak and superimposed on the broad 1.25-Mev resonance, any cascade transitions less than 15 percent as intense as the ground state radiation could not have been detected.

The radiation from the 9.17(1.76)-Mev resonance level leads almost wholly to the ground state of N^{14}. There is, however, a weak cascade consisting of a 6.5-Mev and a 2.73-Mev gamma ray. A coincidence meas-

TABLE I. Gamma radiation from $C^{13}(p, \gamma)N^{14}$ (all energies in Mev).

Resonance	8.06(0.55)	8.62(1.16)	8.70(1.25)	8.90(1.47)	8.98(1.55)	9.17(1.76)	9.49(2.10)	Best values
Measured gamma radiation	8.03±0.10	8.6 ±0.1	8.7±0.1		9.0±0.1	9.17±0.10 6.5 ±0.1		6.44 ±0.02
		6.25±0.04						6.26 ±0.03
				5.7 ±0.2				5.81 ±0.02
				5.1 ±0.1			5.09±0.05	5.09 ±0.02
		4.7 ±0.2						4.68 ±0.02
	4.0 ±0.1	3.94±0.06					4.41±0.08	4.36 ±0.02
			(3.9)?					3.95 ±0.02
				3.09 ±0.02				
			(3.4)?					
				2.8 ±0.1			2.78±0.04	2.77 ±0.03
			(3.0)?					
						2.73±0.02		
	2.32±0.02	2.33±0.02	2.3	2.32 ±0.04			2.32±0.02	2.310±0.012
	1.63±0.02	1.64±0.02						1.638±0.008
				0.731±0.007			(0.73)?	0.725±0.004

urement showed that these two were indeed in cascade as can be inferred from the fact that their energies add up to the full energy available.

Gamma rays from the 9.49(2.1)-Mev resonance level (Fig. 3) were found at energies of 2.3, 2.8, 4.4, and 5.1 Mev. The radiation above 5.1 Mev did not show resonance and is believed to be from fluorine contamination in the Ta target backing. Energy considerations indicate that there are two cascades, one consisting of the 4.4- and 5.1-Mev gamma rays and the other consisting of the 2.3-, 2.8-, and 4.4-Mev gamma rays. The relative intensities are consistent with this interpretation.

These data are summarized in Table I while the proposed decay schemes are shown in Fig. 4. In Table I, the best values for the energies of these transitions are listed for comparison with our observed values. They were obtained as follows. The three lowest values and the 3.95 value are from the beta-ray spectrometer analysis of the gamma radiation from $C^{13}(d, n\gamma)N^{14}$.[9] The 6.44 and 5.81 values are obtained by subtracting the energy obtained for the softer cascade gamma ray from the calculated Q values of the corresponding resonance involved. The 5.09 value is obtained by subtracting 0.725[9] from 5.81, and the rest are obtained by taking differences between these energies (see the decay schemes in Fig. 4).

The relative intensities listed for the decay schemes in Fig. 4 were obtained by measuring the area under the pulse-height curve which is produced by each gamma ray. This area is proportional to the gamma-ray yield times the detection efficiency of the counter. The efficiency has been calculated for the particular geometrical arrangement used for a number of gamma-ray energies and has been checked with the known gamma-ray fluxes from the reaction $F^{19}(p, \alpha\gamma)O^{16}$ (6.14-Mev gamma ray) and from a calibrated Na^{22} source (1.28- and 0.511-Mev gamma rays). The agreement between the calculated and measured values was better than 10 percent. In determining the area due to each gamma ray for this counter, it has been found that the pulse-height curve below the pair peak can be extrapolated horizontally back to zero pulse height. This fact has greatly simplified the problem of measuring the gamma-ray yield. At several resonances where two or more gamma rays are within one-half to one Mev of each other, no attempt was made to separate the total areas under each. Thus a complete cross check on the decay scheme was not always possible by this method, although a comparison of the relative size of the photo or pair peaks provided an independent check.

Since the 8.06(0.55)-Mev and 8.70(1.25)-Mev resonance levels are formed by s-wave protons,[1,10] any radiation resulting from their decay will be isotropic

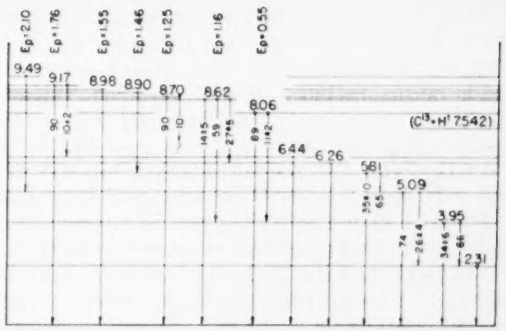

FIG. 4. Gamma-ray decay schemes for seven resonances of $C^{13}(p,\gamma)N^{14}$. The energy levels are designated by the excitation in N^{14} in Mev. The quantities, E_p, represent the proton energies corresponding to the seven resonances investigated. Relative transition probabilities from each level are also given.

and the measured intensity ratios are identical with the ratios obtained by integrating over the whole sphere. Of the other resonance levels, only the relative intensity of the decay of the 9.17(1.76)-Mev resonance level has been corrected for the angular anisotropy of the radiation. However, the expected maximum anisotropy in each of the other cases would not cause more than a 20 percent change in the measured value, and in most cases the difference is probably much less than the experimental error.

RESONANCE CHARACTERISTICS

The resonance characteristics for the seven resonances investigated are listed in Table II. With the exception of the 8.90(1.47)- and 8.98(1.55)-Mev resonance levels and the recalculated reduced widths, the table is essentially Table III in reference 1. The dimensionless reduced width, $\theta^2=\gamma^2(\hbar^2/2Ma)^{-1}$, where γ^2 is the reduced level width of Wigner and Eisenbud,[11] has been calculated employing the Coulomb tables of Bloch *et al.*,[12] with an interaction radius of $1.41(13^{1}+1)10^{-13}$ cm. The quantity $1/\theta^2$ may be interpreted as the number of nuclear traversals of the incident particle in the compound system. In these calculations, the variation of level shift with respect to energy[13] has been taken into account. This correction has little effect on values

TABLE II. Resonance characteristics for $C^{13}(p,\gamma)N^{14}$.

E_R (Mev)	Γ_p (kev)	θ^2 s wave	p wave	d wave	f wave	g wave	σ_R (10^{-3}b)	$\omega\Gamma_\gamma$ (ev)
8.06(0.55)	32.5±1	0.4	13				1.44	8.6
8.62(1.16)	6±2		0.04	0.3	∞		0.56	1.3
8.70(1.25)	500	0.7	4.5				0.062	13
8.90(1.47)	20		0.05	0.5	∞		0.074	0.72
8.98(1.55)	7		0.016	0.1	4		0.037	0.13
9.17(1.76)	2.1±0.2			0.024	0.4	∞	12.0	15
9.49(2.10)	45±3		0.05	0.3	∞		0.20	6.2

[9] R. G. Thomas and T. Lauritsen, Phys. Rev. **88**, 969 (1952).
[10] S. Devons and M. G. N. Hine, Proc. Roy. Soc. (London) **A199**, 56, 73 (1949). See also the section on Resonance Characteristics below.
[11] E. Wigner and L. Eisenbud, Phys. Rev. **72**, 29 (1947).
[12] I. Bloch *et al.*, Revs. Modern Phys. **23**, 147 (1951).
[13] R. G. Thomas, Phys. Rev. **88**, 1109 (1952) and private communication.

of θ^2 less than one but tends to increase those values greater than one. At all but the 8.06(0.55)-Mev and 8.70(1.25)-Mev resonances, a WKB approximation was used in calculating this level shift correction. This resulted in an over correction and hence the infinities in the table. Wigner's criterion places an upper limit on θ^2 of 6.[14] However, both the initial calculations and the level shift corrections are very inaccurate for values of θ^2 greater than 2 or 3. The general interpretation used, however, was to consider values θ^2 greater than 2 or 3 as highly improbable. In the four cases shown in Table II where infinities appear, the uncorrected values were all greater than 6 and thus the corresponding l values for the incident protons can be most certainly ruled out.

From these calculations, it is seen that the 8.06(0.55)- and 8.70(1.25)-Mev resonances are formed by s-wave protons and that all the rest, with the exception of the 9.17(1.76)-Mev resonance and possibly the 8.98(1.55)-Mev resonance, are formed by partial waves with $l \leq 2$.

Table II also gives the total gamma-ray width Γ_γ times the statistical factor ω for each of the seven resonances. In this reaction $\omega = (2J+1)/4$, where $\hbar J$ is the total angular momentum of the compound state.

ANISOTROPY MEASUREMENTS

In an attempt to determine the spins of some of the levels involved in the cascading, the anisotropy ratio, $a = \text{yield}(0°)/\text{yield}(90°) - 1$, was measured for the first gamma ray in the cascades found at the 8.90(1.47)-, 9.17(1.76)-, and the 9.49(2.10)-Mev resonance levels. Also, the anisotropy ratio of the ground state transition from the 8.62(1.16)-Mev resonance level and the angular distribution of the ground state transition from the 9.17(1.76)-Mev resonance level were measured. The latter measurement was in excellent agreement with previous measurements.[15] The anisotropy ratios for these five cases are listed in Table III.

DISCUSSION

The review article of Ajzenberg and Lauritsen[16] gives a summary of the experiments yielding information on the levels involved in this reaction. Two of these will be discussed in more detail in connection with this work. The first of these is the magnetic lens spectrometer analysis of the gamma-radiation from $C^{13}(d, n\gamma)N^{14}$.[9] Although Thomas and Lauritsen do not report a definite ground-state transition from the 3.95-Mev level, further work under improved conditions has confirmed it,[17] in agreement with what was found in this work. Thomas and Lauritsen also report a 3.38-Mev gamma ray which they assign to N^{14} in cascade with the 2.31-Mev gamma ray. Coincidence measurements with two scintillation counters on the $C^{13}(d, n\gamma)N^{14}$ reaction has confirmed this assignment.[18] This, then, places a level at 5.69 Mev in N^{14} which is shown as 5.7 Mev in reference 16. Thomas and Lauritsen also report a 5.69-Mev gamma ray which they believed to be the ground-state transition of this level. It is believed that the weak, low-energy radiation found at the broad 8.70(1.25)-Mev resonance may involve this level. It is noted that this resonance is the *only* resonance of the seven investigated at which there were indications of a 3.38-Mev gamma ray.

As noted before, Thomas and Lauritsen found a strong 0.725-Mev gamma ray which is believed to correspond to the 0.73-Mev gamma ray found at the 1.47-Mev resonance. In the following discussion, these two gamma rays will be assumed to be the same. Coincidence measurements, again on the $C^{13}(d, n\gamma)N^{14}$ reaction, have shown that this 0.725-Mev radiation is in cascade with radiation above 4.5 Mev and below 5.2 Mev, which disproves the suggestion that the 0.725-Mev radiation was the result of a transition between the 4.8-Mev level and the 3.95-Mev level as shown in reference 16. Thus, the possible levels from which the 0.725-Mev gamma ray can originate are a tentative level reported at 5.5 Mev,[19] the level at 5.69 Mev, and the one indicated by these experiments at 5.81 Mev. The first two levels would presumably decay to the 4.8-Mev level, while the latter goes to the 5.08-Mev level. The energy measurements of the cascading gamma rays associated with the 0.725-Mev gamma ray preclude any such level as low as 5.5 Mev. The 5.69-Mev level cannot be associated with the 0.725-Mev radiation since at the resonance at which the 0.725-Mev gamma ray was found there was no indication of the 3.38-Mev gamma ray (see Fig. 2) which results from the decay of the 5.69-Mev level. Thus the 0.725-Mev gamma ray certainly appears to come from the 5.81-Mev level as postulated. However, one would then expect that Thomas and Lauritsen should have found a 5.81-Mev gamma ray one-third as intense as the 0.725-Mev radiation, which they did not. Dr. Thomas has suggested to the authors that the explanation of this discrepancy lies in the reduced sensitivity of the lens spectrometer at higher energies.

TABLE III. Angular anisotropy of four gamma rays from $C^{13}(p, \gamma)N^{14}$.

E_R (Mev)	Transition in N^{14} (Mev)	Anisotropy ratio a
8.62(1.16)	8.62→gnd state	0.00±0.05
8.90(1.47)	8.90→5.81	+0.25±0.10
9.17(1.76)	9.17→gnd state	−0.48±0.03
9.17(1.76)	9.17→6.44	−0.05±0.10
9.49(2.1)	9.49→5.09	+0.48±0.15

[14] T. Teichmann and E. P. Wigner, Phys. Rev. **87**, 123 (1952).
[15] R. B. Day, Ph.D. thesis, California Institute of Technology, 1951 (unpublished).
[16] F. Ajzenberg and T. Lauritsen, Revs. Modern Phys. **24**, 321 (1952).
[17] R. J. Mackin, Jr. (private communication).
[18] The coincidence measurements were made by J. Thirion for the authors.
[19] R. E. Benenson, Phys. Rev. **90**, 420 (1953).

The second experiment to be noted is the recent work of Benenson[19] on the neutron energy spectrum for the reaction $C^{13}(d, n\gamma)N^{14}$. This work has confirmed the existence of the levels at 6.44 and 6.26 Mev.

From the anisotropy measurements and the reduced widths, few unambiguous conclusions can be drawn. However, limits on the angular momentum of some of the levels can be given. Consider first the 9.49(2.10)-Mev resonance level. Since the radiation from this level is not isotropic (Table III) it cannot be formed by s-wave protons nor can it have an angular momentum of 0. Thus, since the reduced width (Table II) indicates that the level can only be formed by partial waves with $l \leq 2$, the angular momentum and parity of the level must be 1^+, 2^+ (p-wave protons) or 2^-, 3^- (d-wave protons). (Here and below the angular momentum will be given in units of $\hbar$.) *If* the radiation resulting from the transition between this level and the 5.09-Mev level is pure dipole (this radiation has an energy of 4.4 Mev and a width $\omega\Gamma_\gamma$ of 6 ev), then the measured anisotropy ratio precludes the possibility of 3^- for the angular momentum. Also, under this assumption of pure dipole radiation, the anisotropy measurements require that the 5.09-Mev level must have the same angular momentum as the 9.49(2.10)-Mev resonance level (1 or 2).

The 9.17(1.76)-Mev resonance level has been given a tentative angular momentum assignment of 2.[15] If this is the case and *if* the transition to the 6.44-Mev level gives pure dipole radiation (this radiation has an energy of 2.7 Mev and a width $\omega\Gamma_\gamma$ of 1.5 ev), then the anisotropy measurements require that the 6.44-Mev level has an angular momentum of 3.

The elastic scattering of protons by C^{13} and the reduced width indicate that the 8.90(1.47)-Mev resonance level in N^{14} is formed by d-wave protons, which means that the level has an angular momentum and parity of 2^- or 3^-. The interpretation of the elastic scattering favors the second value.[2] The transition between this level and the 5.81-Mev level gives 3.1-Mev radiation which has a width $\omega\Gamma_\gamma$ of 0.7 ev. If this radiation is pure dipole, then the anisotropy ratio agrees best with the 2^- assignment and furthermore it requires that the 5.81-Mev level have an angular momentum of 2. Actually, the agreement is not good. Under the most favorable situation with 100 percent channel spin 1, the calculated anisotropy ratio is 0.42, which is to be compared with the experimental value of 0.25 ± 0.10. If, on the other hand, the radiation is pure quadrupole, then the 3^- assignment is permissible only if the 5.81-Mev level has an angular momentum of 5, which value, however, appears improbable from the decay schemes. In the actual situation, as also in the other cases considered above, there may be involved a mixture of dipole and quadrupole radiation, in which case these arguments are invalidated.

The elastic scattering of protons by C^{13} shows that the 8.62(1.16)-Mev resonance level is formed by p-wave protons and that it has a low angular momentum

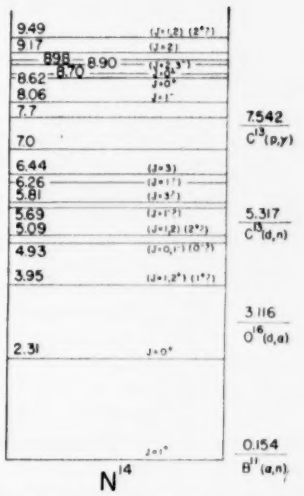

FIG. 5. Energy-level diagram of N^{14} showing established levels below 10 Mev. The energy levels are given in Mev. Values of the total angular momentum (J) and parity which appear to be reasonably well established are indicated on the levels: less certain assignments are enclosed in parentheses while speculative assignment are indicated by question marks.

(0 or 1).[2] The lack of anisotropy at this resonance would appear rather fortuitous if the angular momentum of this level were 1. In particular it would require equal amounts of channel spin 0 and 1, a condition which appears to be definitely ruled out by the elastic scattering experiments.[2] Thus, it seems quite certain that the 8.62(1.16)-Mev resonance level is 0^+. This value of the angular momentum confirms the assignment of the 6.26-Mev radiation to the decay of a 6.26-Mev level. The reason is that a transition directly to the 2.31-Mev level from the 8.62(1.16)-Mev resonance level (the only other alternative) is forbidden since the 2.31-Mev level is known to be a 0^+ level.[16] It has been shown that the 3.95-Mev level has an angular momentum and parity of either 1^+, or 2^+.[19] However, the value of 2^+ seems incompatible with the fact that the transition from the 8.62(1.16)-Mev resonance level to the 3.95-Mev level is favored over the ground state transition of the resonance level. Also, as pointed out by Benenson, the preferential decay of the 3.95-Mev level to the 2.31-Mev level would likewise seem to favor the assignment of 1^+. Similarly, the 6.26-Mev level would certainly seem to require an angular momentum of 1 in order to account for the observed relative intensities.

Besides the 5.69-Mev level, there appears to be only one other well established low lying level in N^{14} that was not involved in the cascading from the seven proton resonances investigated. This is a level with angular momentum and parity of either 0^- or 1^- which has been reported at 4.8 Mev.[19] However, it appears to be responsible for the 4.93-Mev radiation found recently in the reaction $C^{13}(d, n\gamma)N^{14}$ [17] and hence we have assumed that this is the best value for its energy.

The foregoing discussion is summarized in an energy-level diagram of N^{14} (Fig. 5) showing the established levels below 10 Mev. Besides the levels discussed above, there are two additional ones at 7.0 Mev and 7.7 Mev reported in reference 19. Since guesses at the probable types of radiation were made in making some of the angular momentum assignments shown in Fig. 5, one cannot uniquely confirm theoretical estimates of transition probabilities for the different types of radiation. However, further work to determine the complete angular distributions of the many gamma rays found at these several proton resonance levels promises to be a fruitful method for uniquely determining the angular momentum of the levels and the types of radiation involved in N^{14}.

Since this work has extended over a period of two years, it is impossible to list individually all those who aided directly or indirectly in the taking of data or in the interpretation of the results. It is a pleasure, however, to acknowledge the contributions and continued interest of Professor C. C. Lauritsen and the staff of the Kellogg Radiation Laboratory.

PHYSICAL REVIEW VOLUME 92, NUMBER 5 DECEMBER 1, 1953

Formation of the Long-Lived Bi^{210} Isomer*

D. J. HUGHES AND H. PALEVSKY
Brookhaven National Laboratory, Upton, New York
(Received August 20, 1953)

The thermal activation cross section of Bi^{209} is shown to be definitely less than the absorption cross section, 19 ± 2 mb as compared with 33 ± 2 mb. In order to verify the high absorption value, previously obtained by pile reactivity methods, measurements were made with the long wavelength neutrons available with the Brookhaven slow chopper. The absorption cross section is obtained from the chopper measurements by subtraction of thermal inelastic scattering. The latter scattering is determined from the variation of measured scattering with sample temperature. The difference between the absorption and scattering, or 14 ± 3 mb, is ascribed to the formation of the long-lived α-emitting isomeric state of Bi^{210}, leading to a half-life of $(2.6\pm0.8)\times10^6$ years. This long life is in agreement with the expected properties, relative to α and β decay, of a high-spin state of Bi^{210}.

I. INTRODUCTION

THE absorption cross section of bismuth for thermal neutrons is extremely small, constituting only a fraction of a percent of the scattering cross section. Early measurements[1] of the activation cross section, i.e., the cross section for activation of the five-day Bi^{210} (RaE), resulted in a value of about 15 mb. On the other hand, the absorption cross section, which is measured by some phenomenon sensitive to the disappearance of neutrons, gave somewhat higher values, of the order of 30 mb. However interfering effects of the large scattering cross section in the absorption measurements, as well as the possible contribution of impurities, made it seem likely that the true absorption could easily be the same as the activation cross section, i.e., about 15 mb.

It soon became clear that the difference between absorption and activation was not a result of impurities because the preparation of samples of increasing purity, as evidenced by chemical analysis, did not give rise to any decrease in absorption cross sections. The measured values lay in the 30–35-mb range regardless of the sample origin and degree of purification. In 1948, measurements of bismuth absorption were made by Langsdorf[2] with the "pile oscillator," and his value for pure bismuth was again about 30 mb. However, because of the interfering effects of scattering in the pile, it was felt by Langsdorf that some apparent absorption could result from neutron scattering and that the correct absorption of bismuth, after correction for this scattering effect, could be as low as the activation value.

A series of measurements of the absorption and activation cross sections was carried out by Palevsky, Hughes, and Eggler[3] in 1950 to investigate the possibility of a real difference between these cross sections, the experiments being performed in the graphite pile to study the effect of scattering on the absorption cross section. These measurements showed that there was indeed a distinct difference between the cross section for activation of the 5-day RaE and the absorption, indicating the formation of a hitherto undetected activity in bismuth in addition to the well-known five-day period. At about the same time a long-lived α-emitting activity was found in pile-irradiated bismuth by Newman, Howland, and Perlman,[4] and it seemed quite likely that the difference between absorption and activation could be attributed to the formation of the long-lived state. To investigate this possibility, as well

* Work carried out under contract with the U. S. Atomic Energy Commission.
[1] Seren, Friedlander, and Turkel, Phys. Rev. **72**, 888 (1947).
[2] A. S. Langsdorf, Phys. Rev. **74**, 1217 (1948).
[3] Palevsky, Hughes, and Eggler, Phys. Rev. **83**, 234 (1951).
[4] Newman, Howland, and Perlman, Phys. Rev. **77**, 720 (1950).

as to determine the spin-dependent scattering needed in connection with experiments on the neutron-electron interaction,[5] additional work on the thermal cross sections of bismuth has been carried out. This work has included "cold" neutron measurements made with the Brookhaven slow chopper.[6] In the present paper the earlier results will be reviewed briefly, the recent ones given in more detail, and the lifetime of the α-emitting state estimated.

II. THERMAL NEUTRON RESULTS

The activation cross section, while inherently inaccurate to about ten percent, is simple to perform and contains very little chance of gross misinterpretation. As the cross section for the formation of an activity of a particular decay period is measured, there is small possibility of contribution from an impurity. Errors of several percent arise, however, because of the difficulty of flux standardization and disintegration rate measurement of the activated sample.[7] The results that have been obtained for the activation cross section of the five-day period show some variation, but their essential agreement justifies the conclusion that there is no large error in this cross section. The value obtained by Seren[1] was 15 ± 3 mb, that of Palevsky, Hughes, and Eggler[3] was 17 ± 3 mb, and recent measurements at Harwell[8] gave the slightly higher result of 20.5 mb with an error of only 1.1 mb. The "best value" given in the Atomic Energy Commission cross-section compilation[9] is 19 ± 2 mb, which we shall adopt in this work in spite of the larger stated error relative to the Harwell result.

The two common methods of measuring the absorption cross section, usually referred to as the "danger coefficient" and the "pile oscillator" methods, give the neutron absorption in terms of the effect on the reactivity of a pile. In the first method a sample is placed inside the pile, and the reactivity is then determined by adjustment of a control rod; in contrast to this static approach, the sample is oscillated in the second method, and the oscillating component of the pile power is a measure of the neutron absorption. The effect of neutron scattering in causing an apparent absorption in the oscillator method arises because the sample scatters neutrons out of the pile to an extent depending on its position and this removal of neutrons affects the pile reactivity. In the danger-coefficient method, the central position of the absorbing sample means that its scattering has practically no effect. A second scattering effect, thought by Langsdorf[2] to cause a larger apparent absorption in bismuth, consists of a lowering of the neutron energy by inelastic scattering in bismuth so that the neutrons no longer cause fission in U^{238}, resulting in a loss in reactivity that would appear as absorption.

In the measurements made by Palevsky, Hughes, and Eggler[3] in the graphite pile, the possibility of the effect suggested by Langsdorf was checked by variation of the geometrical relationship of the sample to the uranium fuel lumps. The absorption cross section was measured by the standard danger-coefficient method utilizing two arrangements, in one of which all of the uranium fuel lumps were removed from the vicinity of the sample, whereas in the other the fuel lumps were in close proximity to the sample. As these measurements gave no differences in the measured absorption cross section for the two arrangements, it was clear that there was no appreciable effect of inelastic scattering on reactivity. In the danger-coefficient work a number of samples of the highest purity that could be attained were measured, and an extremely small variation in absorption cross section was observed from sample to sample; in fact, most of the samples tested, which had received various degrees of chemical purification, were in the range 30–35 mb. The final value obtained was 33 ± 2 mb, with no correction for absorption by impurities because chemical analysis revealed none that would contribute significant absorption.

The results of these measurements thus seemed to indicate very strongly that the absorption was actually of the order of twice the activation cross section and furthermore that the difference could be attributed to the formation of the long-lived α-emitted state. However, because of the interest in the use of bismuth for the neutron mirror experiment as well as for the definite settlement of the thermal cross section, experiments with the Brookhaven slow chopper were carried out as well.

III. COLD-NEUTRON MEASUREMENTS

In the determination of the absorption cross section of bismuth, a total cross-section measurement made by transmission is of no value when this measurement is made at thermal energies because the scattering is so much larger than the absorption cross section. However for a total cross-section measurement made at long wavelengths (beyond the crystal "cutoff"), the coherent scattering does not appear in a transmission measurement, and the absorption cross section can usually be identified with certainty.[10]

The coherent scattering "disappears" (in actuality it is only forward and hence not observed) at a wavelength equal to twice the longest lattice spacing of the crystal. For longer wavelengths the observed cross section consists only of capture plus elastic incoherent scattering (spin-dependent and isotopic) and inelastic

[5] Hughes, Harvey, Goldberg, and Stafne, Phys. Rev. **90**, 497 (1953).

[6] Seidl, Palevsky, Randall, and Thorne, Phys. Rev. **82**, 345 (1951).

[7] D. J. Hughes, *Pile Neutron Research* (Addison-Wesley Press, Cambridge, 1953), pp. 179–188.

[8] D. J. Littler and E. E. Lockett (private communication).

[9] *Neutron Cross Sections*, Atomic Energy Commission Report AECU-2040-Supplement 2 (Office of Technical Services, Department of Commerce, Washington, D. C., 1952).

[10] See reference 7, pp. 249–254.

lattice-vibration scattering. The elastic incoherent scattering shows no variation with wavelength or sample temperature and the inelastic scattering varies rapidly with temperature and is proportional to wavelength at large wavelength, whereas the capture cross section is usually proportional to wavelength and is always independent of sample temperature. Investigation of the total cross section at wavelengths beyond cutoff as a function of wavelength and sample temperature thus makes it possible to identify the various components of the incoherent scattering.[10]

For certain materials some components of the incoherent scattering are zero, and the analysis is correspondingly simplified; for example, an element of zero nuclear spin (an even-even isotope, such as O^{16}, U^{238}) produces no spin-dependent scattering, and no isotope incoherence results for a monoisotopic element. While it is true that all materials show some inelastic scattering, calculations[11] based on the Debye frequency spectrum of lattice vibrations usually predict the inelastic scattering with reasonable accuracy.

In the case of monoisotopic bismuth no isotopic incoherence will be present, but, as the spin is 9/2, spin-dependent incoherence is possible. The thermal inelastic scattering could be reduced to a negligible value by cooling the sample to a few degrees absolute, and the observed total cross section would then consist only of 1/v capture and spin-dependent incoherence. However, sufficient accuracy can be obtained by cooling the bismuth to only liquid-air temperature (i.e., about 100°K). The absorption and the spin-dependent scattering can be determined by measurements of the total cross section for different sample temperatures and extrapolation to remove the inelastic scattering still present at 100°K. The inelastic scattering itself is of course also measured in the process, but as it is not of direct interest in the absorption discussion, it will not be considered in detail.

The total cross sections for cold neutrons were measured with the Brookhaven slow chopper,[6] which has been used for several years in the long-wavelength region for measurements of inelastic,[12,13] spin-dependent,[14] and absorption cross sections.[15] We shall not describe the techniques used with the chopper for control of fast-neutron background by filters, for background determination and for wavelength standardization; these matters are covered in reference 7, pp. 243–249, and in reference 15. The results for room temperature bismuth are shown in Fig. 1, in which the total cross section is compared with the theoretical inelastic scattering.[11]

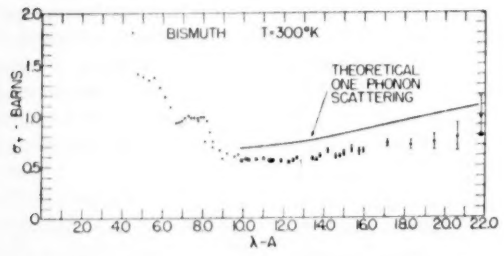

FIG. 1. The measured total cross section of room temperature bismuth compared with the theoretical inelastic scattering in which gain or loss of single phonons alone is considered.

The inelastic scattering in bismuth is unusual in that it exhibits a flat minimum in the region of the cutoff wavelength (about 8A) and then gradually approaches the 1/v or "λ law" region. The room-temperature results exhibit the expected wavelength behavior of the inelastic scattering but cannot be used to obtain a value for the 1/v capture cross section because the observed *total* cross section is less than the theoretical inelastic scattering alone. Because of the failure of the theory to predict the absolute magnitude of the inelastic scattering,[16] it is necessary to investigate the variation of cross section with temperature in order to identify the absorption.

In order to investigate the temperature variation of the inelastic scattering, measurements were made at high sample temperature where the inelastic scattering is the major component of the cross section. In these measurements the bismuth sample was contained in a furnace at a temperature of 500°K, controlled to a few degrees. The results of cross-section measurements at 500°K are shown in Fig. 2, again compared with the theoretical inelastic scattering. At this temperature the inelastic scattering is large, and, as it is the major component of the scattering, it can easily be compared with the theoretical value. Although the experimental points are only about 50 percent of the calculated values (using the danger-coefficient results to correct the former for absorption), the increase at long wavelength

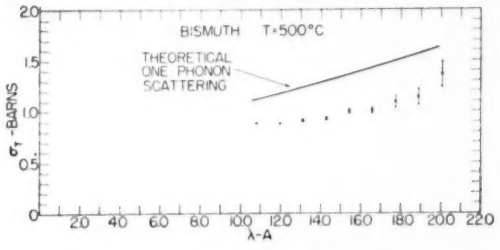

FIG. 2. The measured total cross section of bismuth at 500°K compared with theory.

[11] Carried out for bismuth by D. Kleinman, Phys. Rev. **81**, 326 (1951), and by G. Placzek and L. Van Hove (unpublished).

[12] Palevsky, Hughes, and Smith, Phys. Rev. **87**, 221 (1952).
[13] Johnson, Palevsky, and Hughes, Phys. Rev. **82**, 345 (1951).
[14] H. Palevsky and R. R. Smith, Phys. Rev. **86**, 604 (1952).
[15] Carter, Palevsky, Meyers, and Hughes, Phys. Rev. **92**, 714 (1953).
[16] This "failure" results from an assumption in the theory that waves scattered from different nuclei do not interfere (the "incoherent approximation").

(the λ law) is about as predicted by theory. Fortunately, in the actual extrapolation used to obtain the inelastic scattering at low temperature, only the form of the temperature variation, not the absolute magnitude of the theoretical result, need be used.

For the low-temperature measurements, the sample was placed in a refrigerator in which it could be moved into and out of the beam by remote control and kept at the same temperature (100°K) in both positions. Sturdy construction was necessitated by the large samples; a sample length of 15 in. gave a transmission of 0.7 at the minimum cross section. Careful checks were made to demonstrate that the sample would not affect the open beam intensity when it was out of the beam. The experimental points as well as the theoretical contribution of the inelastic scattering are given in Fig. 3. The flat minimum in the cross section indicates that the inelastic scattering, although small, exhibits the correct wavelength behavior.

In order to obtain the 1/v absorption cross section without use of the calculated absolute value of the inelastic scattering, the measured cross sections can be extrapolated to a temperature where the inelastic contribution is zero. Above 100°K the inelastic scattering is expected[11] to vary almost linearly with temperature, following a line that, *extrapolated*, intersects the temperature axis at 36°K, although the actual cross section below 100°K remains finite. The removal of the inelastic scattering by extrapolation in this manner is exhibited in Fig. 4, in which the observed total cross sections are plotted against temperature for several wavelengths. These long wavelengths were chosen to accentuate the absorption relative to inelastic and spin-dependent scattering. A small theoretical correction (a 7-percent reduction) has been applied to the 100°K points because of a departure from the linear behavior caused by scattering in which the neutrons *gain* energy. The linear extrapolations to 36°K give cross sections consisting primarily of absorption, together with a small spin-dependent contribution. The magnitude of the inelastic scattering present at 100°K, which is removed by extrapolation, is given by comparison of the linear cross-section curve at 36°K and 100°K and is seen to be relatively smaller for long wavelengths.

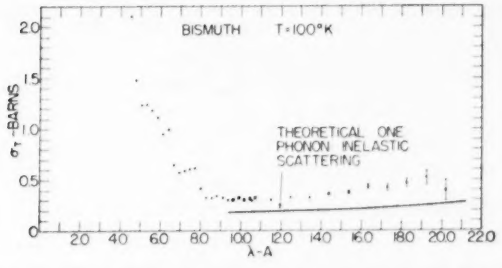

FIG. 3. The total cross section of low temperature (100°K) bismuth and the theoretical inelastic scattering.

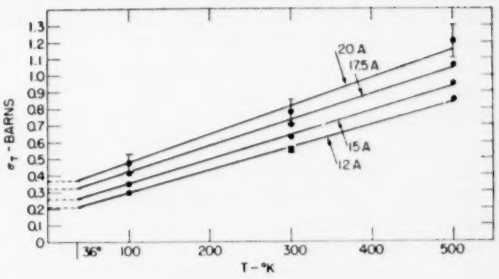

FIG. 4. The observed total cross sections for several wavelengths as functions of temperature. The linear extrapolation to 36°K is used to eliminate the inelastic scattering.

The cross sections determined by extrapolation in Fig. 4 must be corrected for the relatively small (at long wavelength) incoherent scattering before the 1/v absorption can be obtained. The separation of the extrapolated cross sections into these two components is illustrated in Fig. 5, in which are given the results of Fig. 4 as a function of wavelength. The intercept on the cross-section axis in Fig. 5 gives a spin-dependent cross section of 0±20 mb and the slope a 1/v absorption of 33±5 mb at 1.80A (2200 meters/sec).

The spin-dependent scattering obtained in Fig. 5 is extremely small, constituting only 0.2 percent of the scattering cross section at the upper limit of error. As the bismuth nucleus consists of a closed cell plus one proton, it might be expected that the interaction of the neutron, if primarily with the odd proton, would be largely spin-dependent. The extremely small spin-dependence found seems to imply that the interaction takes place with the entire nucleus rather than with the odd proton.

The absorption cross section resulting from the cold-neutron measurements is free from any corrections of the type that affect the pile oscillator and danger-coefficient techniques, although in this case of less accuracy. This constitutes convincing evidence that the absorption cross section is actually 33 mb, definitely higher than the 19-mb absorption cross section. The

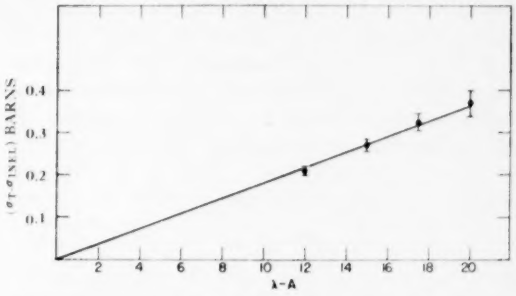

FIG. 5. The extrapolated cross sections of Fig. 4 as a function of wavelength. The slope of the curve gives the 1/v absorption (33±5 mb) and the intercept gives the incoherent elastic (spin-dependent) scattering (0±20 mb).

bismuth used for the cold neutron measurements was carefully checked for impurities by chemical analysis and was also measured relative to other high purity samples by the danger-coefficient technique. No impurities that would contribute significant absorption were detected, and the danger-coefficient results were the same within experimental uncertainty (±2 mb) as for the bismuth of highest purity used in the earlier danger-coefficient work.

IV. CONCLUSIONS

The fact that the cold-neutron measurements give the same absorption for bismuth as the danger-coefficient results shows that the interfering effect of scattering has been successfully eliminated and that the results represent actual neutron absorption. That the absorption is in bismuth itself and not in impurities is indicated by the finding that the cross section as measured by pile reactivity does not decrease with continued chemical purification once the cross section is in the 30–35-mb range. Actual chemical analysis of the various samples used in the danger coefficient as well as in the cold neutron measurements verifies that there is no appreciable absorption contributed by impurities. The impurities in the bismuth samples used by Littler and Lockett[8] constituted about 7-mb absorption, and their absorption result, which is 30.8±2.2 mb after correction for the impurities, is in good agreement with ours (33±2 mb), containing no appreciable impurity contribution. It thus seems certain that the difference between the absorption cross section (33±2 mb) and the activation cross section (19±2 mb), or 14±3 mb, must result in the formation of an activity in Bi^{210} different from the five-day RaE.

The isomeric bismuth activity seems certain to be the long-lived alpha emitter found by Newman, Howland, and Perlman[4] in highly irradiated bismuth. The isomeric activity was shown by Newman *et al.* to have a half-life greater than 25 years, fixed by the failure to decay, and to have a half-life for β or γ emission of greater than 5×10^4 years, determined by the lack of growth of the corresponding daughter activities. The present results allow a calculation of the half-life of the α-activity, a half-life much longer than the lower limit of 25 years. Newman *et al.* observed that their sample had a specific activity of 1.9±0.1 α disintegrations per minute per mg. This specific activity, I, together with the formation cross section of 14 mb, then gives the half-life in terms of the flus nv and irradiation time t,

$$T_{\frac{1}{2}}=0.693nv.N\sigma t/I,$$

where N is the number of Bi nuclei per mg. The quantities nv and irradiation time t were not given by Newman *et al.*, but the product nvt, which is known[17] from the Po^{210} α activity of the sample, gives for the half-life the value,

$$T_{\frac{1}{2}}=(2.6\pm0.8)\times10^6 \text{ years}.$$

The uncertainty in this result arises principally from the quantity nvt and the cross section for formation of the isomeric state. The conclusion is certain, however, that the half-life is extremely long, and much greater than the directly observed lower limit.

There is still some question concerning the location of the α-emitting energy level, although the most recent energy values[18,19] indicate that it is 28±26 kev *below* the 4.85-day state. Should this order of energy levels be correct, the difficulty[20] is removed that was presented by the reverse order, i.e., the long half-life of the α-emitting state toward γ emission. Actually the long half-life obtained in the present work constitutes a solution to the additional problem, discussed by Feather,[20] of the failure of Bi^{210} to fit the Geiger-Nuttall diagram for $Z=83$. Whereas the 100-year half-life used by Feather disagreed seriously with the diagram, the present value gives good agreement. Actually the failure of the α-emitting state to decay by β emission to Po^{210} and the extremely long α half-life both require high spin for this state of Bi^{210}, of the order of 6.

The possibility of levels in Bi^{210}, of widely different spins and small energy separation, has been discussed by Pryce[21] in terms of the single-particle model. He has estimated the energies for different configurations of the neutron and proton moving in the field of the closed shell, taking into account their mutual interaction, and in this way has made plausible the existence of levels of the type needed to explain the properties of the bismuth isomers.

We wish to express our thanks to C. Eggler, of Argonne Laboratory, for his assistance in checking the purity of samples and to D. J. Littler and E. E. Lockett for a prepublication copy of their paper.

[17] I. Perlman (private communication).
[18] H. B. Levy and I. Perlman, Phys. Rev. **85**, 758 (1952).
[19] D. E. Alburger and G. Friedlander, Phys. Rev. **82**, 977 (1951).
[20] N. Feather, Phil. Mag. **42**, 568 (1951).
[21] M. H. L. Pryce, Proc. Phys. Soc. (London) **65**, 773 (1952).

Mixed Configurations in Nuclei*†

A. DE-SHALIT, *Laboratory of Nuclear Science, Massachusetts Institute of Technology, Cambridge, Massachusetts*

AND

M. GOLDHABER, *Brookhaven National Laboratory, Upton, New York*

(Received August 11, 1953)

The role of mixed configurations in nuclear states is discussed and illustrated by various examples; it is discussed in particular for β transitions with anomalous ft values and as a qualitative explanation of the empirically-found smooth variations of the first excited states of even-even nuclei. It is shown by various examples that a nucleon of one kind (neutron or proton) with a given j has a "stabilizing" influence on pairs of the other kind with a given j'. This stabilization effect is calculated on simplified assumptions for different j and j'.

INTRODUCTION

IT is well known that many properties of nuclei can be traced back to the properties of a single nucleon to a surprisingly good approximation.[1] Thus, the clear-cut division of magnetic moments of odd-neutron or odd-proton nuclei into two groups has been nicely correlated with the single-particle Schmidt lines. Also, the assignment of degrees of forbiddenness of the beta decay of odd-even nuclei based on the assumption that the single odd nucleon alone takes part in the transition proves, in general, to be quite successful. Further, in the case of some gamma transitions, matrix elements calculated on the basis of such a single-particle approximation agree with experimental data within an order of magnitude.[2]

Another immediate result of the single-particle approximation which concerns itself with excited states of odd-even nuclei seems to hold in many cases; namely, the similarity of decay schemes of nuclei which differ by two neutrons or two protons. The smooth "movements" of corresponding levels when one goes in such "families" from one nucleus to the other[3] strengthens one's confidence in the interpretation of the similarities.

It seems, however, that a complete neglect of the structure of the "core" of an odd-A nucleus and its consideration only as the "carrier" of the required central force is an oversimplification of the problem, and a natural further step is to see whether effects due to a "core structure" can be established.[4] The configurations of equivalent nucleons and some cases of non-equivalent nucleons have been considered by various authors.[5–8]

THE ROLE OF MIXED CONFIGURATIONS IN NUCLEAR TRANSITIONS

It is well known that the "degree of forbiddenness" of a β spectrum is usually determined experimentally by its ft value, i.e., by the observed energy and half-life, eventually corrected by some factors which can be deduced from the shape of the spectrum. These ft values have been used to determine the spin and parity changes involved in β transitions, assuming that the transition probability depends, apart from a Coulomb correction, on just two parameters of the initial and final states (spin and parity). However, the matrix elements may depend, to a degree which has sometimes not been sufficiently appreciated, on the detailed structure of the wave functions of the initial and final states. An independent assignment of spin and parity to such states by a method which does not depend on the specific nuclear wave functions might, thus, reveal some wrong assignments of degrees of "forbiddenness," or, what often amounts to the same, some "super-fast" or "super-slow" β transitions. The internal conversion coefficients of γ rays depend only on their multipolarity, their energy, and the atomic number, and do not depend on the nuclear wave functions. One should, therefore, consider the spin assignments made on the basis of a measurement of internal conversion coefficients as more reliable than those made on the basis of ft values, and a disagreement between the two methods should be considered as an "irregularity" in the β-decay matrix elements.

One of the most striking examples of such a "disagreement" is the case of mass number 85 studied by Sunyar *et al.*[9] There, a logft value of 9.15 was found for

* Preliminary reports of this work were given at the Amsterdam Conference on Beta and Gamma Radioactivity [M. Goldhaber, Physica **18**, 1091 (1952)] and at the Rochester meeting of the American Physical Society, Phys. Rev. **92**, 843 (T) (1953).

† This work was assisted in part by the U. S. Office of Naval Research and the U. S. Atomic Energy Commission.

[1] For a review of the shell model, see, e.g., B. H. Flowers, Prog. Nuc. Phys. **2**, 235 (1952).

[2] M. Goldhaber and A. W. Sunyar, Phys. Rev. **83**, 906 (1951).

[3] M. Goldhaber and R. D. Hill, Revs. Modern Phys. **24**, 179 (1952).

[4] By "core" here we mean all the nucleons except the odd one and its equivalent nucleons, though sometimes the term is used more loosely to mean all the nucleons except the odd one.

[5] D. Kurath, Phys. Rev. **80**, 98 (1950).

[6] I. Talmi, Helv. Phys. Acta **25**, 185 (1952).

[7] B. H. Flowers, Phys. Rev. **86**, 254 (1952), Proc. Roy. Soc. (London) **215**, 398 (1952) and previous publications.

[8] J. P. Davidson and E. Feenberg, Phys. Rev. **89**, 856 (1953).

[9] Sunyar, Mihelich, Scharff-Goldhaber, Goldhaber, Wall, and Deutsch, Phys. Rev. **86**, 1023 (1952). See also M. Trocheris, J. Phys. **13**, 370 (1952).

a β transition which is definitely "allowed": $g_{9/2} \rightarrow g_{9/2}$. It was suggested[9] that the reason for this behavior might be connected with an extreme lack of overlapping of the initial and final core wave functions which causes this large reduction in the transition probability. It was also noted there that the even-neutron nucleus $_{37}Rb^{85}{}_{48}$ should have different neutron configurations in the ground state ($f_{5/2}$ proton) from that in the excited state ($g_{9/2}$ proton); the effect of the state of the odd particle on the core configuration is discussed below.

An inspection of discrepancies of a similar type in other nuclei (see below) suggests that they can usually be understood in terms of the "purity" of the states involved. This concept of purity of a state can perhaps be most clearly exhibited in the following way:

One knows now that practically without exception the first excited state of an even-even nucleus is a 2+ state.[2,10,11] This is interpreted as evidence for the assumption that this state is an excited state of the ground state configuration,[2,7,12,13] i.e., it is caused by a change of the relative orientation of the j's of the different nucleons, each of them remaining in the same j state which it occupied in the ground state.

It is also known[11,12] that in the regions of the periodic table in which the single-particle model holds it usually requires more energy to excite the 2+ state in an even-even nucleus than that required for the excitation of the first few excited states of a neighboring odd-even nucleus. In those regions where the 0–2 separation in even-even nuclei is large, one finds as a rule that each (low-lying) excited state in an odd-even nucleus is a ground state of a new configuration and that the spacing between ground states of different (odd) configurations is smaller than the spacing of levels in the same configuration. Conspicuous exceptions to this behavior are the occurrence of low-lying 7/2+ states[2] for the configurations $g_{9/2}{}^{3,5,\text{ or }7}$.

For instance, if we consider the two configurations (a) $p_{3/2}{}^2p_{1/2}$ and (b) $p_{3/2}{}^2g_{9/2}$, (a) will have a set of states with total $J_a = 1/2, 3/2, 5/2$, of which $J_a = 1/2$ is the lowest; and (b) will have a set of states with total $J_b = 5/2, 7/2, 9/2, 9/2, 11/2$, and $13/2$, of which $J_b = 9/2$ is the lowest. The experimental data now enable one to conclude that the separation in energy between $J_a = 1/2$ and $J_b = 9/2$ is, as a rule, smaller than the separation between different J_a's or between different J_b's. There will be occasions when we are dealing with different but close lying configurations of equal J, and where we may therefore expect a strong configuration interaction. This configuration interaction arises because of the finer details of the interaction between nucleons which are ignored in the zero-order approximation; deviations from the average central potential can be considered as a perturbation which mixes configurations. One is, therefore, led to believe that it might be a poor approximation to think in terms of pure configurations, and that instead of assigning the ground state of a certain nucleus, say, as $(p_{3/2}{}^4p_{1/2}{}^2g_{9/2}{}^4)_{J=0}$, one should rather consider it as a mixture of the states $(p_{3/2}{}^4g_{9/2}{}^6)_{J=0}$, $(p_{3/2}{}^2p_{1/2}{}^2g_{9/2}{}^6)_{J=0}$, etc. The existing empirical evidence for a strong pairing energy,[1] makes it unlikely that a considerable amount of a configuration in which a pair is broken [say, $(p_{3/2}{}^3p_{1/2}g_{9/2}{}^6)$, which has also a state $J=0$] will be mixed in; but it is most probable that the other combinations (those in which pairs are shifted from one state to another) will be mixed considerably. Clearly such mixtures of configurations in the initial and final states will generally tend to change appreciably any transition probability between these two states, and it is only when the states become "pure"—composed of essentially a single configuration—that the transition probability may approximate closely its "intrinsic" value. Depending on whether in these extreme cases the core does or does not change its state in the transition, we shall find transitions that are either very slow or very fast compared to ordinary ones between "average" impure states. Obviously a state is comparatively pure if for some reason the other states which could have mixed with it require a comparatively high energy for their excitation. This could happen, for instance, if the number of nucleons in the configuration considered (protons or neutrons) approaches a magic number, in which case the configurations available for mixtures are energetically far removed.

One also sees that a fair amount of configuration mixing will destroy the symmetry between particles and holes in a subshell below a magic number. For instance, a $g_{9/2}$ state with 41 protons could be a mixture of $p_{1/2}{}^2g_{9/2}$, $g_{9/2}{}^3$ and perhaps other configurations too; whereas a $g_{9/2}$ state for 49 protons can only be $g_{9/2}{}^{-1}$. Thus, configurations containing one hole in a major shell are expected to be less mixed than those containing one particle beyond a subshell. This, of course is due to the fact that sub-shells are not as tightly closed as the major shells. The absence of symmetry between particles and holes is probably exhibited by the empirically found "movements" of levels,[3] especially the $1h_{11/2}-2d_{3/2}$ separation, and by the spins of odd-odd nuclei in light elements.[14] It seems[3] that even for three holes the configurations are less mixed than for three particles.

OVERLAP STABILIZATION OF ENERGY LEVELS

A possibility deserving investigation is that one group of nucleons (protons or neutrons) influences the other in such a way as to make a particular configuration energetically more favorable. Such an effect might exist in Rb^{85}, where, as has been noted,[9] the predominant core configuration probably depends on the odd-proton

[10] P. Stähelin and P. Preiswerk, Helv. Phys. Acta **24**, 623 (1952).
[11] G. Scharff-Goldhaber, Phys. Rev. **90**, 587 (1953).
[12] de-Shalit, Huber, and Schneider, Helv. Phys. Acta **25**, 279 (1952).
[13] Horie, Umezawa, Yamaguchi, and Yoshida, Prog. Theor. Phys. (Japan) **6**, 254 (1951).
[14] R. W. King and D. C. Peaslee, Phys. Rev. **90**, 1001 (1953).

state. We shall refer to this effect as a stabilization of one configuration by another.

One can obtain a rough idea of the essential features of the stabilization effect by considering the following simple problem: A pair of neutrons in the state $(j_N^2)_{J=0}$ interact with an odd proton in a state j_P. The interaction energy clearly depends on what these two states are. It now turns out, as could be expected, that for a given j_P the first-order interaction is biggest if $j_N \approx j_P$, or more precisely if $l_N \approx l_P$. In fact, it is shown in the Appendix that for a neutron-proton interaction of the type $V(|\mathbf{r}_P - \mathbf{r}_N|)$ the above interaction energy is simply

$$\delta E = \int R^2(n_N l_N) R^2(n_P l_P) V(|\mathbf{r}_P - \mathbf{r}_N|) d(\cos\omega) d\mathbf{r}_P d\mathbf{r}_N,$$

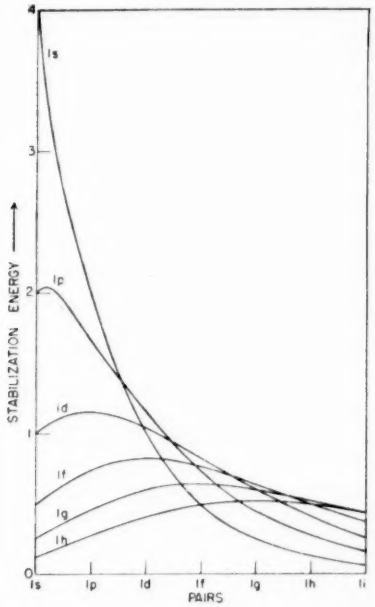

FIG. 1. Stabilization of pairs of nucleons of one kind (neutrons or protons) by a single nucleon of the other kind. The unit of energy is ≈400 kev.

where $\cos\omega = \mathbf{r}_P \cdot \mathbf{r}_N / r_P r_N$ and $R(nl)/r$ is the radial part of the wave function of the nucleon.

For more-or-less reasonable forms of $V(|\mathbf{r}_P - \mathbf{r}_N|)$ this integral would attain its maximum value when $R(n_N l_N)$ and $R(n_P l_P)$ overlap best, i.e., when $l_N \approx l_P$ and $n_N = n_P$. For illustration we show in Fig. 1 a plot of the values of δE for various values of l_N and l_P and $n_N = n_P = 1$. These values were obtained by taking for the wave functions of the nucleons the eigenfunctions of the three-dimensional harmonic oscillator,[6] and assuming a δ interaction, $V(|\mathbf{r}_P - \mathbf{r}_N|) = 4\pi g \delta(\mathbf{r}_P - \mathbf{r}_N)$.

Thus, in the case of Rb^{85}, the $g_{9/2}$ proton in the excited state stabilizes the $g_{9/2}$ neutron pairs so that the neutron configuration of the last pair is predominantly

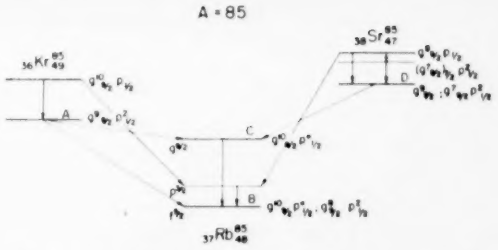

FIG. 2. The main part of the configurations involved in the abnormal β transitions which are important for the present discussion is given in this and the following figures for each level on the right for neutrons and on the left for protons. Whenever two configurations are given, it is meant to imply mixed configurations with comparable amplitudes. For details of the decay schemes, see, e.g., reference 3.

For level C the $g_{9/2}$ proton stabilizes the $g_{9/2}$ pairs of neutrons thus making the neutron configuration mainly $g_{9/2}^{10}$. This makes the transition $A \rightarrow C$ very improbable but does not affect $D \rightarrow C$. The other states of Rb^{85} in which there is no stabilization of $g_{9/2}$ pairs have mixed neutron configurations, as is shown by the "normal" behavior of $A \rightarrow B$.

$(g_{9/2})^2$ rather than $(p_{1/2})^2$; the latter would have yielded a considerably lower ft value than the one observed. The case of mass number 85 and the other β transitions with abnormal ft values mentioned in Table I are illustrated in Figs. 2–8.

EVIDENCE FROM β DECAY

Table I contains some of the "abnormal" ft values together with the spin assignments for both initial and final states when they are known from other sources.[3,15–18] The logft values should be compared with the average ones for normal transitions, namely 4.5–5.5 for allowed and 6.2–7.2 for first forbidden transitions. It is remarkable that most of the examples of abnormal ft values occur close to magic numbers, and mainly

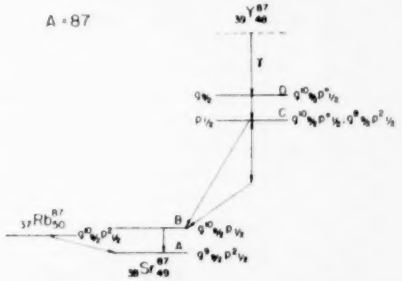

FIG. 3. For level C the $p_{1/2}$ proton stabilizes $p_{1/2}{}^2$ neutrons so that $g_{9/2}{}^8\, p_{1/2}{}^2$ predominates for the neutron configuration, and for level D stabilization by the $g_{9/2}$ proton makes $g_{9/2}{}^{10}$ the predominant neutron configuration. Both transitions $D \rightarrow A$ (unobserved) and $C \rightarrow B$ are thus slowed down.

[15] King Dismuke and Way, Oak Ridge National Laboratory Report ORNL-1450 (unpublished).
[16] L. G. Mann and P. Axel, Phys. Rev. **84**, 221 (1951).
[17] Shore, Bendel, Brown, and Becker (private communication); Phys. Rev. **91**, 1204 (1953).
[18] E. J. Konopinski and L. M. Langer, *Annual Review of Nuclear Science* (Annual Reviews, Inc., Stanford, 1953), Vol. 2, p. 261.

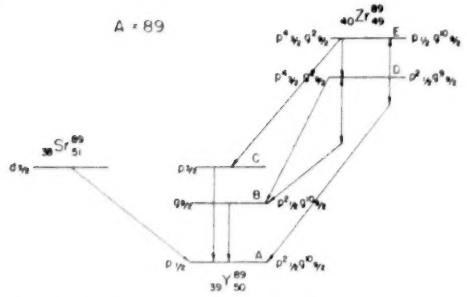

FIG. 4. The big number of $g_{9/2}$'s in the neutron group of Zr stabilize $g_{9/2}^2$ for the proton group, though to a lesser degree in D than in E. Thus $D \rightarrow B$ is only slightly affected, and $E \rightarrow A$ is affected more. $E \rightarrow C$ is normal.

from the lower mass number side (holes); the assumption of "purified" states in these cases, therefore, seems to be quite plausible.

Two more examples which should perhaps be added to this table are the odd-odd isotopes $_{81}Tl^{204}{}_{123}$ and $_{81}Tl^{206}{}_{125}$. The β spectrum of $_{81}Tl^{204}{}_{123}$ to the ground state of $_{82}Pb^{204}{}_{122}$ shows the shape characteristic of a ($\Delta I = 2$, yes) transition. The ground state of Tl^{204} would then be $2-$, consistent with the Nordheim rule ($d_{3/2}$ proton and $p_{1/2}$ neutron). However, the transition to the first excited state in Pb^{204} ($2+$) is not observed,[3] $\log ft > 10$, whereas transitions of this type are usually found to have $\log ft$ values of about 6.2 to 7.2. This behavior might be related to the fact that in Pb^{204} the proton shell is filled, so that the $2+$ state arises from an excitation of the neutrons only. On the other hand, if we assume that the neutrons in Tl^{204} first couple to a $p_{1/2}$ state and, therefore, do not contain a $2+$ state of the neutron core, the absence of a transition to the $2+$ state of Pb^{204} could be understood. The assumption that the $2+$ state in Pb^{204} arises from a neutron configuration gets further support from the slowness of the $E2$ transition to the ground state.[2,19,20]

$_{81}Tl^{206}{}_{125}$ has a very low $\log ft$ (5.18), although the transition is expected to be first forbidden. Even if we assume the most favorable spin and parity compatible with the shell model for the ground state of Tl^{206}, $1-$ ($d_{3/2}$ proton and $p_{1/2}$ neutron), we must conclude that the large size of the matrix element is due to an exceptional purity of the wave function near a magic number. Recently Bleuler *et al.*[21] found a very low ft value for the allowed β transition $_{49}In^{112}{}_{63} \rightarrow {}_{50}Sn^{112}{}_{62}$ ($\log ft = 4.03$). Again we probably are dealing with extremely pure wave functions near a magic number.

We thus see that near closed shells, allowed and first forbidden beta transitions occur with the square of the matrix element either close to unity or smaller than the "average" by a big factor, up to $\sim 10^4$. If we turn to the most completely studied isomeric transitions, we see that for $M4$ transitions,[22,23] and perhaps for some odd proton $E3$ transitions,[24] the matrix elements show a tendency to increase as a closed shell is approached. Very small matrix elements, however, are absent among the $M4$ transitions.

EVEN-EVEN NUCLEI

The idea of configuration interactions seems to be especially useful, at least qualitatively, in even-even nuclei. If we assume, as our zero-order approximation, independent groups of protons and neutrons, then each of them can give rise to the characteristic set of levels $0+$, $2+$, $4+$, etc. If there were no interaction between the protons and the neutrons, we would have observed a lowest state $(0_P 0_N)_0$ where $(J_P, J_N)_J$ represents a state in which the protons are coupled to an angular momentum J_P, the neutrons to J_N and both together give J; the next excited states would have been $(0_P 2_N)_2$, $(2_P 0_N)_2$ and $(2_P 2_N)_{0,1,2,3,4}$, etc. The $(0_P 0_N)_0 - (2_P 0_N)_2$ separation would have been exactly the same as the 0–2 separation for the proton group in the absence of the neutron group. If we now consider the effect of the interaction between the protons and the neutrons, different states with the same total angular momentum will interact, with a resulting "repulsion" of levels.[25] Since this repulsion is inversely proportional to the separation between the unperturbed

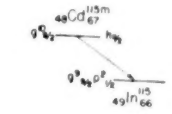

FIG. 5. The $h_{11/2}$ neutron in Cd stabilizes the $g_{9/2}$ protons so that the proton configuration is predominantly $g_{9/2}^{10}$, and β decay becomes slower.

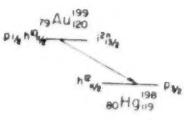

FIG. 6. The $i_{13/2}$ neutrons stabilize $h_{11/2}$ protons both in Au and Hg so that in Au the proton configuration is $p_{1/2}h_{11/2}^{10}$ and in Hg it is $h_{11/2}^{12}$ with a resulting reduction in the transition probability in the β decay.

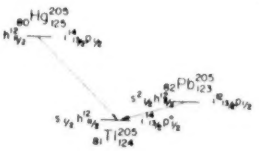

FIG. 7. A similar mutual stabilization of $h_{11/2}$ protons by $i_{13/2}$ neutrons makes the β transitions from Hg^{205} favorable and the electron capture from Pb^{205} unfavorable.

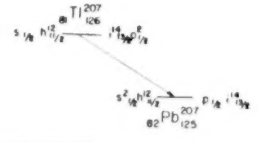

FIG. 8. The configurations are determined uniquely, and it is easy to see that the transition probability should obtain its highest value.

[19] A. Bohr and B. R. Mottelson, Phys. Rev. **89**, 316 (1953).
[20] A. Bohr and B. R. Mottelson, Phys. Rev. **90**, 717 (1953).
[21] Bleuler, Blue, Chowdary, Johnson, and Tendam, Phys. Rev. **90**, 464 (1953).
[22] S. A. Moszkowski, Phys. Rev. **89**, 474 (1953).
[23] K. Gottfried, thesis, McGill University, 1953 (unpublished).
[24] R. D. Hill, Phys. Rev. **88**, 1428 (1952).
[25] E. U. Condon and G. H. Shortley, *The Theory of Atomic Spectra* (Cambridge University Press, London, 1951).

TABLE I. β-Transitions with abnormal ft values.

Nucleus Initial	Nucleus Final	Spin and parity Initial state	Spin and parity Final state	Expected type of transition	Observed log ft	References
$_{36}Kr^{85}{}_{49}$	$_{37}Rb^{85}{}_{48}$	$g_{9/2}$	$g_{9/2}$	allowed	9.03	a
$_{39}Y^{87m}{}_{48}$	$_{38}Sr^{87}{}_{49}$	$g_{9/2}$	$g_{9/2}$	allowed	>8.45	b
$_{39}Y^{87}{}_{48}$	$_{38}Sr^{87}{}_{49}$	$p_{1/2}$	$p_{1/2}$	allowed	7.6	c
$_{40}Zr^{89m}{}_{49}$	$_{39}Y^{89}{}_{50}$	$p_{1/2}$	$p_{1/2}$	allowed	6.85	a
		$p_{1/2}$	$p_{3/2}$	allowed	4.3	d
$_{48}Cd^{115m}{}_{67}$	$_{49}In^{115}{}_{66}$	$h_{11/2}$	$g_{9/2}$	first forbidden	8.8	a
$_{79}Au^{199}{}_{120}$	$_{80}Hg^{199}{}_{119}$	$d_{3/2}$	$p_{1/2}$	first forbidden	7.73	a
$_{80}Hg^{205}{}_{125}$	$_{81}Tl^{205}{}_{124}$	$p_{1/2}$	$s_{1/2}$	first forbidden	5.52	a
$_{82}Pb^{205}{}_{123}$	$_{81}Tl^{205}{}_{124}$	$p_{1/2}$ or $p_{3/2}$	$s_{1/2}$	first forbidden	very big	e
$_{81}Tl^{207}{}_{126}$	$_{82}Pb^{207}{}_{125}$	$s_{1/2}$	$p_{1/2}$	first forbidden	5.16[f]	a
$_{82}Pb^{209}{}_{127}$	$_{83}Bi^{209}{}_{126}$	$i_{11/2}$ or $g_{9/2}$	$h_{9/2}$	first forbidden	5.59	d

[a] See reference 15.
[b] See reference 3.
[c] See reference 16.
[d] See reference 17.
[e] Private communication from C. D. Coryell, based on unpublished results of T. P. Kohman.
[f] The effect of the large Z may be to some extent responsible for the smallness of the ft values of these "first forbidden" transitions (see reference 18), but no general trend with Z is noticeable.

states, one could expect it to be strongest for a pair of $2+$ states $(2_P0_N)_2$ and $(0_P2_N)_2$. This leads to mixing of proton and neutron states, and one of the mixed states would be brought nearer to the ground state, while the other will approach the next higher group of states and eventually pass some of them, provided they are of different total J.[25] If, in the zero-order approximation (no p-n interaction), there were no other $2+$ state between the $(2_P0_N)_2$ and the $(0_P2_N)_2$ states, then the first two $2+$ states of an even-even nucleus would contain only seniority-two components.[7] It would then be difficult to understand the rule found by Kraushaar and Goldhaber[26] for even-even nuclei that for a sequence of states $0+$, $2+$, $2+$ the matrix element for the $E2$ crossover transition $(2+\rightarrow 0+)$ is in many cases considerably smaller than that for the $E2$ fraction in the $2+\rightarrow 2+$ transition. If, however, a $2+$ state with seniority-four components would already exist between $(0_P2_N)_2$ and $(2_P0_N)_2$ in the zero-order approximation, it would remain the second $2+$ state also after considering the p-n interaction, because states of equal J do not cross. If we compare the estimates of the positions of the $2+$ states of seniority two and four[7] with the experimentally found energy of $\sim$1 Mev required to excite a pair of neutrons (protons magic) and the energy of $\sim$1.5 Mev required to excite a pair of protons (neutrons magic),[11] we can expect such a situation to exist when we are fairly close to a magic number in either protons or neutrons. Then the experimentally found rule[26] could be explained in terms of the selection rules for the seniority number v $(\Delta v=\pm 2, 0)$.[27]

The regularities observed for the $0+-2+$ separations in even-even nuclei[10,11] may be described in this way: As one approaches a magic number from either side, the number of different possibilities for states with a total $J=2$ becomes smaller and smaller and this reduces the repulsion of the lowest $2+$ state.[11,28,29] At the magic number of one of the kinds of nucleons (protons or neutrons), this kind can no longer be excited to a $2+$ state. This naturally results in a maximum for the $0+-2+$ separation in that region. The largest number of possibilities of creating a $2+$ state occurs in the middle between closed shells with a corresponding minimum in the $0+-2+$ separation. The states of $J=0$ which may mix and lead to a depression of the ground state are usually higher and fewer in number than those of $J=2$,[7,29] and their effect may thus be expected to be smaller.[30] It is hard to estimate these effects quantitatively since the situation is very complex.[31] The general trend found experimentally is in agreement with what one might qualitatively expect. The strong mixture of configurations is probably responsible for a "smearing out" of most of the sub-shell effects.[11] For the heaviest elements known at present, the $2+$ state is only $\sim$40 kev above the $0+$ ground state. As the middle of either the proton shell or the neutron shell has not yet been reached in this region, the possibility cannot be excluded on these considerations alone that the $2+$ state eventually may cross the $0+$ state to become the ground state.

A somewhat more quantitative idea of the amount of configuration mixing of different states in even-even nuclei may be gained by comparing the rate of β decay from a $1+$ state in an odd-odd nucleus to the ground state $(J=0)$ and the first excited state $(J=2+)$ of the even-even daughter. This ratio, very much like the β^+/K capture ratio, should be independent of the

[26] J. J. Kraushaar and M. Goldhaber, Phys. Rev. **89**, 1081 (1953).
[27] G. Racah, Phys. Rev. **62**, 438 (1942).
[28] P. Preiswerk and P. Stähelin, Physica **18**, 1118 (1953).
[29] H. J. Maehly and P. Stähelin, Helv. Phys. Acta **25**, 624 (1952).
[30] B. J. Hogg and H. E. Duckworth have kindly informed us of their recent mass measurements [Phys. Rev. **91**, 1289 (1953)] which indicate the existence of a broad maximum of the total binding energy in the region in which the $2+-0+$ separation reaches a broad minimum (approximately in the middle of the proton (50–82) and neutron (82–126) shells).
[31] A simplified case has been treated quantitatively by A. Temkin and A. de-Shalit (unpublished).

nuclear matrix elements if both states of the even-even daughter would belong to the same configuration. Its evaluation is then quite straightforward by using Racah's tensor-operator formalism.[27] With Gamow-Teller selection rules one obtains for the transition probability from the state $(j_n j_p J_i)$ to the state $(j_p^2 J_f)$, where j_p and j_n are the angular momenta of the odd proton and the odd neutron, respectively, J_i is the total angular momentum of the initial state in the odd-odd nucleus, and J_f is the total angular momentum of the final state in the even-even nucleus:[32]

$$|M|^2=(2J_f+1)(2j_n+1)\cdot|M_1|^2\cdot|W(j_pJ_fj_nJ_i;\,j_p1)|^2,$$

where $|M_1|^2$ is the transition probability for a single neutron j_n to a proton j_p and W is a Racah coefficient.[27] The ratio in question will then be

$$R=\frac{|M(1\to2)|^2}{|M(1\to0)|^2}=5\cdot\left|\frac{W(j_p2j_n1;\,j_p1)}{W(j_p0j_n1;\,j_p1)}\right|^2=15(2j_p+1)\times W(j_p2j_n1;\,j_p1)|^2.$$

TABLE II. Ratio of ft values for β transitions $1^+\to0^+$ and $1^+\to2^+$.

Parent nucleus	Daughter nucleus	$\log\frac{ft(1\to0)}{ft(1\to2)}$ (exp)	j_n	j_p	$\log R$ (theor)	Remarks
$_5B^{12}{}_7$	$_6C^{12}{}_6$	−0.62	1/2	3/2	+0.40	
$_{15}P^{34}{}_{19}$	$_{16}S^{34}{}_{18}$	+0.41	1/2	3/2	+0.40	spin of excited state not known
$_{29}Cu^{66}{}_{37}$	$_{30}Zn^{66}{}_{66}$	−0.07	3/2	5/2	+0.15	spin of excited state may be 1+ or 2+ (11)
$_{45}Rh^{106}{}_{61}$	$_{46}Pd^{106}{}_{60}$	−0.56	7/2	9/2	−0.26	
$_{47}Ag^{110}{}_{63}$	$_{48}Cd^{110}{}_{62}$	+0.62	7/2	9/2	−0.26	
$_{53}I^{128}{}_{75}$	$_{54}Xe^{128}{}_{74}$	−0.70	3/2	5/2	+0.15	

Table II contains some experimental data on this ratio together with the theoretical predictions for various reasonable spin assignments. The lack of agreement between "theory" and experiment probably arises from the erroneous assumption that the 0+ and the 2+ states are "pure" states of one and the same configuration. It looks as if both states are very well mixed with proper states of other configurations.

SOME SPECIAL EXAMPLES

There are a number of other regularities in nuclear spectroscopy which might possibly be explained along the general lines developed here. Since this paper was meant mainly to suggest a possible direction in which the strict shell model might successfully be modified, we shall say only a few words on some additional applications of present ideas.

It was pointed out[3] that a plot of the $p_{1/2}-g_{9/2}$ separation for odd-proton nuclei as a function of the neutron number has a very pronounced minimum at $N=50$ (see reference 3, Fig. 75). If we assume (as is generally and consistently done) that the last pair of neutrons filling the 50-shell is $p_{1/2}^2$, this minimum is explained by the extra stabilization given to the $p_{1/2}$ proton by this neutron pair. The next pair of neutrons will tend to fill in $g_{7/2}$ states, thus depressing the $g_{9/2}$ proton state again.

Inspecting the $h_{11/2}-d_{3/2}$ separation in, say, $_{52}Te^{129}{}_{77}$, $_{54}Xe^{131}{}_{77}$, $_{56}Ba^{133}{}_{77}$ (reference 3, Fig. 78), one sees that it becomes harder and harder to excite the $h_{11/2}$ state as the number of protons increases. If the $h_{11/2}$ state is interpreted as arising from the breaking of an $h_{11/2}$ pair,[3,12] one might interpret this behavior as due to the increasing stabilization of $h_{11/2}$ pairs as $g_{7/2}$ protons fill in. An alternative interpretation is to say that $d_{5/2}$ protons are filled in this set of nuclei with a corresponding increase in the binding energy of the $d_{3/2}$ neutron states. This last example is typical of many cases in which no unique interpretation is suggested. More information on the nature of the states involved (such as their magnetic and electric moments) and better calculations could perhaps decide the relative importance of each configuration.

A similar effect might be responsible for the different spins of $_{51}Sb^{121}{}_{70}$ and $_{51}Sb^{123}{}_{72}$. These isotopes have a single odd proton outside a closed proton shell. The ground state of Sb^{121} is $d_{5/2}$, whereas that of Sb^{123} is $g_{7/2}$. This could perhaps be explained by the stabilization of the $g_{7/2}$ state due to the two extra neutrons going into $h_{11/2}$ orbits which start not later than for 71 neutrons. On the same argument, one might have expected that the $g_{7/2}$ state is more stable than the $d_{5/2}$ state in $_{53}I^{125}{}_{72}$ and $_{53}I^{127}{}_{74}$. Actually, however, the observed ground state is 5/2+ for these two isotopes, whereas it becomes $g_{7/2}$ for the higher isotopes. On the stabilization principle, we should therefore expect a considerable amount of $(g_{7/2}^3)_{5/2}$ state in I^{125} and I^{127}. The unusually large deviation of the magnetic moment of I^{127} from the Schmidt value for a $d_{5/2}$ proton might be explained in this way. A somewhat smaller deviation might be expected for I^{125}.

One of the properties of nuclei which is sensitively affected by the mixing of different configurations is the g factor. The effect of mixing different configurations in the "odd group" alone is to cause a deviation from the Schmidt lines which is proportional to g_s-g_l, where g_s and g_l are the spin and orbital g-factors of a single nucleon in the odd group.[33] As (g_s-g_l) is 4.6 for protons and −3.8 for neutrons, this would meaa that the distribution of the deviations of odd-P nuclei from the Schmidt lines should be similar to that of the odd-N ones, enlarged by the factor 4.6/3.8. Existing data seem to favor these results and give further support to the hypothesis of mixed configurations. Different types of

[32] H. Brysk, Phys. Rev. **90**, 365 (1953).

[33] A. de-Shalit, Phys. Rev. **90**, 83 (1953).

mixed configurations where the core is excited to a 2+ state have been considered by Davidson and Feenberg.[8]

As magnetic moments of excited states are measured, valuable information on the type of mixing will become available. Thus, for instance, it is easily seen from the Landé formula that all states of a configuration of equivalent nucleons, irrespective of their number, have the same g factor. A measurement for an even-even nucleus of the g factor of a 2+ excited state, and especially of its sign, will thus show how pure these configurations are.

DISCUSSION

Nuclear models have gone from the extreme of the early version of the one-particle model to the other extreme of Bohr's liquid-drop model, then to the revised version of the one-particle strong spin-orbit coupling model, and quite recently several compromises have been considered.[1] In particular, the models, which treat the bulk of nucleons in a nucleus on a collective basis and add the effects of individual particles,[34–36] have many attractive features because calculations carried out on these models have been able to explain several nuclear properties for which the single-particle model failed to account. The approach which we have suggested here as the next approximation to the one-particle model may be more advantageous near closed shells where the relative purity of wave functions plays an important role. In the middle of shells, the existence of large mixtures of configurations may have an averaging effect equivalent to the assumption of a deformable core which is the starting point in the collective model. The relative usefulness of the various models may depend, therefore, very much on the particular nucleus and the phenomenon treated on the one hand, and the ability to overcome the mathematical difficulties of the necessarily complex situations on the other hand.

We should like to thank many of our colleagues who have helped us with valuable discussions, in particular D. R. Hamilton, Gertrude Scharff-Goldhaber, I. Talmi, and J. Weneser.

APPENDIX

To calculate the diagonal matrix elements of the interaction in a state JM between a pair of protons (j_P^2) with total $J_P=0$ and a neutron j_N, we note that $V_{10}+V_{20}$ can be written in the form[27]

$$V=V_{10}+V_{20}=\sum_{k,\kappa}[v_k(\mathbf{r}_1,\mathbf{r}_0)C_\kappa^{(k)}(1)C_\kappa^{(k)}(0)+v_k(\mathbf{r}_2,\mathbf{r}_0)C_\kappa^{(k)*}(2)C_\kappa^{(k)}(0)],$$

where V_{10} is the interaction between the first proton and the neutron, and V_{20} has a similar meaning;

$$C_\kappa^{(k)}(i)=\left(\frac{4\pi}{2k+1}\right)^{\frac{1}{2}}Y_{k,\kappa}(\theta_i,\varphi_i),$$

and

$$v_k(r_i,r_0)=\frac{2k+1}{2}\int V_{i0}P_k(\cos\omega)d(\cos\omega),$$

$$\cos\omega=\mathbf{r}_i\cdot\mathbf{r}_0/r_ir_0.$$

Denoting

$$F^{(k)}\equiv\int R_P^2(n_Pl_P)R_N^2(n_Nl_N)v_k(r_Pr_N)dr_Pdr_N,$$

where R/r is the radial part of the wave function, we find that

$$((j_P^2)J_Pj_NJM\,|\,V\,|\,(j_P^2)J_Pj_NJM)=\sum_{k,\kappa}F^{(k)}(J_Pj_NJM\,|\,C_\kappa^{(k)*}(P)C_\kappa^{(k)}(0)\,|\,J_Pj_NJM)$$

where

$$C_\kappa^{(k)}(P)=C_\kappa^{(k)}(1)+C_\kappa^{(k)}(2).$$

Since $C^{(k)}(P)$ is a tensor of degree k with respect to J_P, we see immediately that for $J_P=0$ only the term with $k=0$ will contribute and since $C^{(0)}(0)=1$ and $C^{(0)}(P)=2$, we finally get

$$\langle|V|\rangle=2F^{(0)}.$$

For the interaction between $2r$ protons coupled to $J_P=0$ and n neutrons, one gets in a similar way

$$\langle|V|\rangle=2r\cdot n\cdot F^{(0)}.$$

For the numerical evaluations of these results we assume an interaction between the protons and the neutrons of the type

$$V_{NP}=4\pi g\delta(\mathbf{r}_N-\mathbf{r}_P)=g\sum_k\frac{\delta(r_N-r_P)}{r_Nr_P}(2k+1)P_k(\cos\omega),$$

and take as the wave function those obtained for a nucleon moving in a harmonic oscillator potential,[37] $[(h\nu)^2/2M]r^2$. $F^{(0)}$ is then obtained in the form:

$$F^{(0)}=g\int_0^\infty R^2(n_Pl_P)R^2(n_Nl_N)\frac{dr}{r^2}.$$

For the special case of $n_P=n_N=1$, one finds

$$F^{(0)}=g\left(\frac{\nu^3}{2\pi}\right)^{\frac{1}{2}}\frac{(2l_P+2l_N+1)!!}{2^{l_P+l_N-1}(2l_P+1)!!(2l_N+1)!!}.$$

The value of $g(\nu^3/2\pi)^{\frac{1}{2}}$ can be determined by comparing the observed 0–2 separation for double-magic-plus-or-

[34] A. Bohr and B. R. Mottelson, Kgl. Danske Videnskab. Selskabs, Mat.-fys. Medd. **27**, No. 16, (1953).
[35] D. L. Hill and J. A. Wheeler, Phys. Rev. **89**, 1102 (1953).
[36] K. W. Ford, Phys. Rev. **90**, 29 (1953).
[37] See, for instance, reference 6.

minus-two even-even nuclei with theoretical predictions. In the δ limit this separation is found to be[38]

$$\tfrac{1}{2}(2j+1)^2[(j\tfrac{1}{2}j-\tfrac{1}{2}|jj00)^2-\tfrac{1}{5}(j\tfrac{1}{2}j-\tfrac{1}{2}|jj20)^2]F^{(0)}$$

for a pair of nucleons in the state (l, j). Comparing this expression with the experimental data[11] on Ca^{42} and Pb^{206}, two nuclei which differ by one nucleon pair from double-magic nuclei, one obtains

$$g(\nu^3/2\pi)^{\frac{1}{3}}\approx 800 \text{ kev}.$$

The same value is obtained by considering the pairing energy.[39]

[38] A. de-Shalit, Phys. Rev. **91**, 1479 (1953).

[39] M. G. Mayer, Phys. Rev. **78**, 22 (1951).

PHYSICAL REVIEW VOLUME 92, NUMBER 5 DECEMBER 1, 1953

Decay of $_{66}Dy^{165m}$ (1.2 min) and $_{66}Dy^{165}$ (2.3 hr)

W. C. Jordan, J. M. Cork, and S. B. Burson
Argonne National Laboratory, Lemont, Illinois and University of Michigan, Ann Arbor, Michigan

(Received August 24, 1953)

The activities induced by neutron capture in Dy^{164} have been studied with 180° photographic internal conversion electron spectrometers and a scintillation coincidence spectrometer. The metastable transition energy is 108.0±0.2 kev. Other gamma rays of approximately 160, 360, and 515 kev are associated with the 1.2-min activity and appear to follow beta decay from the metastable level. Gamma rays of 94.4±0.2, 279.4±0.8, 361.2±1.0, 634±3, 710±20, and 1020±30 kev follow the 2.3-hr beta decay from the ground state. Coincidences are observed between members of the pairs (279)–(710) and (361)–(634). The 94-kev gamma ray is coincident with a beta transition of about 1.2 Mev, while the other gamma radiations are coincident with a softer beta component (~0.3 Mev).

INTRODUCTION

IN 1935, Marsh and Sugden[1] and, independently, Hevesy and Levi[2] reported that a very strong beta activity was produced when Dy was exposed to neutrons from a Ra–Be source. They found the half-life to be about 2.5 hr. A recently reported value is 2.310 ±0.002 hr.[3] Several measurements of the beta energy using cloud chamber and absorption techniques have been made.[2,4–8] The values reported from these investigations range from 1.1 to 1.9 Mev. Two spectrometer measurements have listed the maximum beta energy as 1.18 Mev[9] and 1.24 Mev.[10] In addition to the 1.24-Mev beta ray, Slätis[10] has resolved two lower-energy components of 0.42 and 0.88 Mev. Meitner[6] reported gamma radiation with an average energy of about 0.6 Mev to be associated with this Dy activity. From a study of the internal conversion electron spectrum and the spectrum of electrons from secondary radiators, Slätis[10] concluded that gamma transitions of 0.91, 0.36, and 0.76 Mev were present. With the postulation of one additional unresolved beta component, he was able to propose a reasonable level scheme. Another measurement of the gamma-ray energies has been made by Miller and Curtiss,[11] who report energy values of 0.37 and 1.0 Mev. Clark[9] has set an upper limit of 1.1 Mev for the gamma energy and has also detected beta-gamma and gamma-gamma coincidences.

A short-lived Dy activity with a half-life of 1.25 min was first reported by Flammersfeld.[12] Electrons with an energy of approximately 130 kev were detected. These were interpreted as arising from internal conversion of an isomeric transition in Dy^{163}. Later work by Inghram *et al.*[13] has established that this, as well as the 2.3-hr activity, is associated with Dy^{165}. The cross sections for production of the 1.25-min and 2.3-hr activities were observed to be approximately equal, indicating that only the metastable state is formed directly in the capture process. Since growth of the 2.3-hr activity had not been observed,[12] it was suggested that a small percentage of the decay of the metastable state was by emission of a beta particle. In the present research some additional evidence for the existence of such a transition has been found.

The conversion electron spectrum of this activity has been investigated with spectrometers by Hole[14] and Caldwell.[15] The former noted that conversion was pre-

[1] J. Marsh and S. Sugden, Nature **136**, 102 (1935).
[2] G. Hevesy and H. Levi, Nature **136**, 103 (1935).
[3] Sher, Kouts, and Downes, Phys. Rev. **87**, 523 (1952).
[4] R. Naidu and R. Siday, Proc. Phys. Soc. (London) **48**, 332 (1936).
[5] Gaerttner, Turin, and Crane, Phys. Rev. **49**, 793 (1936).
[6] L. Meitner, Arkiv Mat. Astron. Fysik **A27**, No. 17 (1940).
[7] S. Eklund, Arkiv Mat. Astron. Fysik **A28**, No. 3 (1941).
[8] A. F. Clark, Phys. Rev. **61**, 203, 242 (1942).
[9] B. Dzelepov and A. Konstantino, Compt. rend. acad. sci. (U.R.S.S.) **30**, 701 (1941).
[10] H. Slätis, Arkiv Mat. Astron. Fysik **A33**, No. 17 (1949).
[11] L. Miller and L. Curtiss, Phys. Rev. **70**, 983 (1946).
[12] A. Flammersfeld, Naturwiss. **32**, 68 (1944); Z. Naturforsch. **1**, 190 (1946).
[13] Inghram, Hayden, and Hess, Phys. Rev. **71**, 270 (1947); Inghram, Shaw, Hess, and Hayden, Phys. Rev. **72**, 515 (1947).
[14] N. Hole, Arkiv. Mat. Astron. Fysik **A36**, No. 2 (1948).
[15] R. Caldwell, Phys. Rev. **78**, 407 (1950).

dominantly in the L shell and found the transition energy to be 102 kev. The latter resolved five conversion lines and reported a value of 109.0 kev for the transition energy. By means of a scintillation spectrometer, Kahn[16] found a value of 102 kev. Caldwell also investigated the conversion electron spectrum of the 2.3-hr activity in the region below 300 kev. He observed several electron lines associated with conversion of an 87.8-kev gamma ray, and in addition, a single line at 219 kev. The latter has been interpreted[17] as the K line of a transition which could be fitted into the level scheme proposed by Slätis. As indicated in a preliminary report[18] of the present study, energy values of the transitions involved and the results of coincidence experiments are inconsistent with this interpretation.

An accurate measurement of the low-energy gamma ray has been made by Mihelich and Church.[19] They found the energy to be 95.1 kev and the ratio of conversion in the K and L shells to be 5.9.

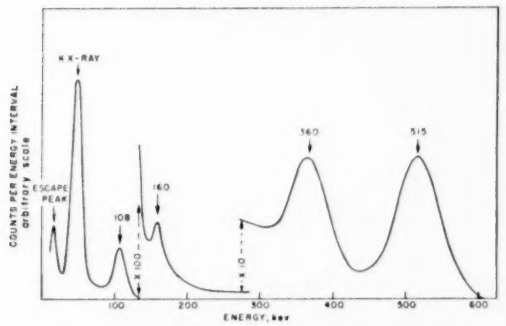

FIG. 1. Gamma-ray pulse-height distribution of $_{66}Dy^{165m}$ (1.2 min).

EXPERIMENTAL PROCEDURE

The apparatus of the present investigation consists of several 180° photographic conversion electron spectrometers[20] and a scintillation coincidence spectrometer.[21]

Sources were normal Dy oxide irradiated in the Argonne heavy water–moderated reactor. Several samples of Dysprosium oxide were used. One was known to be spectrographically pure except for 0.4-percent holmium and 0.1-percent yttrium.

Eastman no-screen x-ray and NTB emulsions were used as detectors in the electron spectrometers. Film backings were used in survey work, but where density and accurate energy measurements were made, a glass plate backing was employed. Photodensitometer measurements of line intensities were practicable in the case of only two of the transitions. These measurements were made with a Leeds and Northrup recording photodensitometer. After the data were replotted on a linear scale and the background due to the beta distribution was subtracted, the area under a line profile was measured. This area, when corrected for variations due to the geometry of the spectrometer and sensitivity of the photographic emulsion, is taken as the relative intensity of the line. The geometry correction consists of simply multiplying each value by the corresponding radius of the electron path in the spectrometer. The emulsion sensitivity factor was determined according to the method described by Rutledge, Cork, and Burson.[20] No corrections are made for differential absorption of the electrons in the source.

TABLE I. Internal conversion electrons associated with the 1.2-min Dy activity.

Electron energy (kev)	Relative intensity	Interpretation	Energy sum (kev)	Transition energy (kev)	K/L
54.2	3	K (Dy)	108.0	108.0±0.2	0.15±0.05
99.4	10	L_2	108.0		
100.3	10	L_3	108.1		
106.3	5	M_2, M_3	108.1		
107.8	1.5	N	108.1		
461		K (Ho)	517	517±3	

RESULTS AND DISCUSSION

1.2 min

Internal conversion electrons associated with the 1.2-min metastable transition are easily detected. Five lines corresponding to a transition of 108.0 kev were observed (Table I). The energy is in fair agreement with the value 109 kev reported by Caldwell. A careful measurement of the separation of the two L-lines was made, and it was found that the energy difference is characteristic of conversion in the L_2 and L_3 sub-shells, as has been proposed by Mihelich.[22] It is interesting to

TABLE II. Internal conversion electrons associated with the 2.3-hr Dy activity.

Electron energy (kev)	Relative intensity	Interpretation	Energy sum (kev)	Transition energy (kev)	K/L
38.8	60	K (Ho)	94.4	94.4±0.2	7.7±2.0
85.0	7.8	L_1	94.4		
92.2	~1.5	M	94.3		
93.9		N	94.3		
223.8		K (Ho)	279.4	279.4±0.8	>5[a]
270.0		L_1	279.4		
305.8		K (Ho)	361.4	361.2±1.0	>5[a]
351.7		L_1	361.1		
578		K (Ho)	634	634±3	
~623		L	~632		

[a] Visual estimate.

[16] J. Kahn, Oak Ridge National Laboratory Report ORNL 1089, 1951 (unpublished).
[17] M. Goldhaber and R. Hill, Revs. Modern Phys. **24**, 179 (1952).
[18] Jordan, Cork, and Burson, Phys. Rev. **91**, 497 (1953).
[19] J. Mihelich and E. Church, Phys. Rev. **85**, 690 (1952).
[20] H. Keller and J. Cork, Phys. Rev. **84**, 1079 (1951); Rutledge, Cork, and Burson, Phys. Rev. **86**, 775 (1952).
[21] S. Burson and W. Jordan, Phys. Rev. **91**, 498 (1953).
[22] J. Mihelich, Phys. Rev. **87**, 646 (1952).

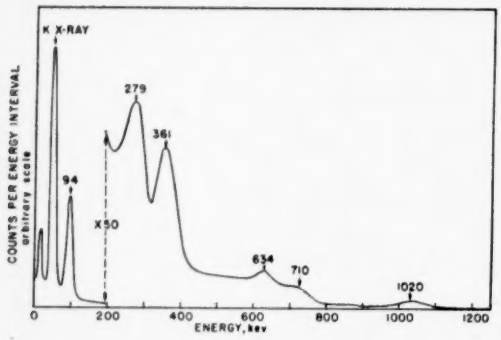

FIG. 2. Gamma-ray pulse-height distribution of $_{66}Dy^{165}$(2.3 hr).

note that the M conversion also appears to be in the M_2 and/or M_3 sub-shell.

The K/L conversion ratio is 0.15 ± 0.05, a somewhat higher value than that obtained by Caldwell, but in good agreement with the Goldhaber and Sunyar[23] empirical relation of Z^2/E *versus* K/L for an electric octopole transition.

An investigation of the 1.2-min activity with the scintillation spectrometer revealed the presence of higher energy gamma radiations. Peaks in the pulse-height distribution corresponding to gamma rays of approximately 160, 360, and 515 kev are present in addition to the K x-ray, its associated escape peak, and the 108-kev peak (Fig. 1). All of these decay with the 1.2-min period. The ratio of the heights of the 360- and 515-kev peaks can be varied by placing lead absorbers between the source and the detector. Therefore, the 360-kev peak is not due entirely to excitation of the crystal by Compton electrons of the 515-kev gamma ray.

Coincidences between the 360- and 515-kev gamma rays were not observed. Pulses in the region of the 360-kev peak were, however, observed to be coincident with those of the 160-kev region. It is probable that the 160- and 360-kev transitions are in cascade and that the 515-kev one is the crossover.

It might be assumed that these gamma transitions follow the 108-kev metastable transition. However, these radiations appear to be coincident with a beta ray and not with the radiations associated with the metastable transition. Beta decay of the metastable state has not been detected previously, although the possibility of its existence has been suggested.[13] Additional evidence of this beta transition was observed with the photographic spectrometers. The background darkening of the emulsion, due to the continuous beta distribution, is markedly different on a plate exposed for short periods immediately after irradiation of the source, as compared with a plate with an equivalent exposure to the 2.3-hr activity after the 1.2-min activity had decayed. An additional weak conversion line was noted which may be associated with the short activity. The energy of the electrons is 461 kev. These are probably K electrons for the ~515-kev transition. If so, a better value for the energy of this transition is 517 kev, assuming the K binding energy of holmium is to be used.

By comparing the heights of the 108-kev and x-ray

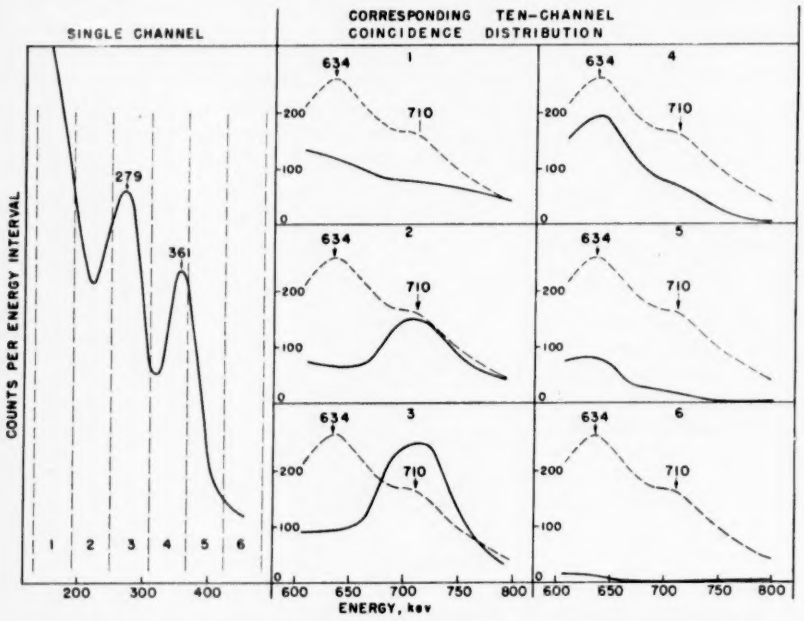

FIG. 3. Coincidence pulse-height distributions of $_{66}Dy^{165}$(2.3 hr). Six coincidence distributions corresponding to six window settings of the single-channel spectrometer are shown. For comparison, the normal spectrum is shown as a dashed curve in each case.

[23] M. Goldhaber and A. Sunyar, Phys. Rev. **83**, 906 (1951).

peaks (Fig. 1), a rough estimate of the K conversion coefficient of the 108-kev transition may be obtained. Neglecting any contribution to the x-ray intensity from conversion of the higher energy gamma rays, this quantity may be estimated to be about four. Since conversion of this transition is only about 10 percent in the K shell, the total conversion coefficient would be about forty.

2.3 hr

Internal conversion electrons associated with the 2.3-hr activity are listed in Table II. The observed conversion lines are interpreted as arising from four transitions of 94.4, 279, 361, and 634 kev. The measured energy of the 94.4-kev transition is in fair agreement with the results of Mihelich and Church. They report the energy to be 95.1 kev and the type of radiation as a mixture of $M1$ and $E2$. The present measurement of the K/L ratio is in good agreement with the value predicted for a pure $M1$ transition; however, the accuracy is too poor to rule out the possibility of the mixture. In the decay scheme of Goldhaber and Hill,[18] this transition is assumed to be in cascade with the 279-kev one, while the 361-kev is the crossover transition. This is not consistent with the present data. The discrepancy in the energy sum is well outside the limits of experimental error.

An investigation of this activity with the scintillation spectrometer showed the presence of peaks in the pulse-height distribution corresponding to the previously mentioned transitions, plus two others of approximately 710 and 1020 kev (Fig. 2). Coincidence studies showed that the 279- and 710-kev gamma rays form one cascade pair and the 361- and 634-kev gamma rays are another. These conclusions are based on the results of two complementary experiments.

In one experiment the ten-channel analyzer was adjusted to cover the region of the 634- and 710-kev peaks, while the single-channel spectrometer was varied in steps across the region of the 279- and 361-kev peaks. The resulting coincidence distributions are shown in Fig. 3. The peak in the coincidence distribution is at the 634-kev position when the single-channel side is accepting pulses from the 361-kev transition, and at the 710-kev position when the single channel is accepting pulses from the 279-kev gamma ray. The complementary experiment, in which the coincidence spectra in the region of the 279- and 361-kev peaks were observed as the single channel was scanned over the 634–710-kev region, yielded results in agreement with these.

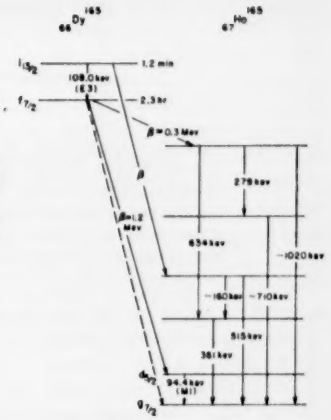

FIG. 4. Proposed decay scheme for $_{66}Dy^{165m}$(1.2 min) and $_{66}Dy^{165}$(2.3 hr). (The order of the 279–710-kev cascade is arbitrarily chosen.)

Coincidences between the other possible pairs of gamma rays were not detected.

The results of beta-gamma coincidence experiments indicate that the 94-kev transition is coincident with a beta ray of maximum energy approximately 1.2 Mev, while the other gamma radiations all appear to be coincident with a lower energy beta component of approximately 0.3 Mev.

The proposed nuclear energy level scheme shown in Fig. 4 is consistent with these data. It should be pointed out that the transition of about 360 kev associated with the 1.2-min activity has been assumed to be the same as the more accurately measured 361-kev transition associated with the 2.3-hr activity. Also, the order of the 279–710-kev cascade as shown in the figure is arbitrarily chosen.

The measured spin of the ground state of Ho^{165} is 7/2.[24] On the basis of shell structure, orbital assignments have been made[18] for the ground and first excited states of both Dy^{165} and Ho^{165}. The results of this investigation are in agreement with these assignments

[24] H. Schüler and T. Schmidt, Naturwiss. **23**, 69 (1935).

Elastic Scattering of Fast Neutrons by He^4†

JOHN D. SEAGRAVE
Los Alamos Scientific Laboratory, University of California, Los Alamos, New Mexico
(Received August 24, 1953)

Angular distributions of neutrons scattered by helium have been measured at five neutron energies between 2.6 and 14 Mev. A large proportional counter filled with helium and krypton was employed, and the distribution in energy of alpha particles recoiling from collimated neutrons observed. All five distributions are similar, and are characterized by strong scattering of the neutrons in the forward direction, a minimum for neutrons scattered near 120° in the center-of-mass system, and a smaller peak for backscattering. The location of the minimum moves forward and the ratio of differential cross sections $\sigma_{back}/\sigma_{min}$ increases smoothly with increasing neutron energy over the range studied. The observed angular distributions are in good agreement with the distributions predicted from analysis of p-He^4 scattering, and support the large splitting of the P states of He^5, and the very broad width of the $P_{\frac{1}{2}}$ state. A summary of n-He^4 phase shifts and recent total cross-section measurements is given.

I. INTRODUCTION

A. Previous Work

THE angular distribution of fast neutrons scattered by He^4 has been studied in the neutron energy region 0.4 to 2.73 Mev by Adair,[1] using a proportional counter, and the region has recently been extended to 4.15 Mev by Huber and Baldinger,[2] using a parallel-plate ionization chamber. Two cloud-chamber investigations at very high neutron energies have been reported,[3,4] but the results are inconclusive for neutron energies less than 40 Mev. Dodder and Gammel[5] have analyzed existing data for p-He^4 elastic scattering up to $E_p=9.5$ Mev in terms of nuclear reaction theory[6–9] and have applied their results for Li^5 to the description of the mirror nucleus He^5 and n-He^4 scattering. Their analysis accounts more successfully for the variation with energy of the n-He^4 total cross section[10] than does that of Adair[1] but leads to phase shifts in disagreement with those derived from the angular distributions observed[2] in the region $E_n=3$ to 4 Mev, particularly with respect to the broad $P_{\frac{1}{2}}$ state of He^5. However, extrapolation of the theoretical analysis to a neutron energy of 14.1 Mev, together with certain assumptions about the d-wave phase shifts, leads to prediction of a total cross section of 1.04 barns, which compares well with the experimental value of 1.03 ± 0.02 barns.[11]

B. Scope and Method of Present Investigation

The work reported below was undertaken initially as part of the program of study of interactions of 14-Mev neutrons with nuclei carried on by this laboratory, with the object of obtaining the angular distribution of n-He^4 scattering at $E_n=14$ Mev and comparing it with theory,[5] in hope of obtaining more information about the d-wave interactions. It was, in addition, possible to make measurements at 2.6, 4.5, 5.5, and 6.5 Mev, where certain of the difficulties encountered in the 14-Mev measurements were less troublesome.

Neutrons scattered elastically from light nuclei lose an appreciable part of their energy to the recoiling nucleus. In the case of 14-Mev neutrons on He^4, the scattered neutrons range in energy from 14 to 5 Mev, and direct observation of the scattered neutrons is impracticable. A much more satisfactory method in such a case is to observe the recoiling charged particles, since the angular distribution of the neutron in the center-of-mass system is directly proportional to the energy distribution of the recoiling target nucleus in the laboratory system.[12] This relation can be put into the form $4\pi\sigma(\cos\theta_n)=\sigma_T E_{max} P(E)$, where $\sigma(\cos\theta_n)=d\sigma/d\Omega$ is the differential elastic-scattering cross section at the cm neutron angle θ_n, σ_T is the total (elastic) cross section, and $P(E)$ is the recoil energy distribution function (number per unit energy interval). This method has been used to study neutron scattering by hydrogen, deuterium, helium, carbon (CS_2), and oxygen[1,2,12–16] for neutron energies up to 4 Mev.

II. EXPERIMENTAL TECHNIQUE

A. Choice of Counter

In their investigation of n-He^4 scattering to $E_n=4.14$ Mev, Huber and Baldinger[2] employed a parallel-plate ionization chamber. Sixteen atmospheres of helium were required to reduce the range of the most energetic recoils to 7 mm. An extension of their technique to $E_n=14$ Mev would require over 100 atmospheres of

† Work performed under the auspices of the U. S. Atomic Energy Commission.

[1] R. K. Adair, Phys. Rev. **86**, 155 (1952).
[2] P. Huber and E. Baldinger, Helv. Phys. Acta **25**, 435 (1952).
[3] C. Schwartz, Phys. Rev. **85**, 73 (1952).
[4] P. Tannenwald, Phys. Rev. **89**, 508 (1953).
[5] D. C. Dodder and J. L. Gammel, Phys. Rev. **88**, 520 (1952).
[6] C. L. Critchfield and D. C. Dodder, Phys. Rev. **76**, 602 (1949).
[7] E. P. Wigner and L. Eisenbud, Phys. Rev. **72**, 29 (1947).
[8] Feshbach, Peaslee, and Weisskopf, Phys. Rev. **71**, 145 (1947).
[9] R. G. Thomas, Phys. Rev. **80**, 136 (1950).
[10] Bashkin, Mooring, and Petree, Phys. Rev. **82**, 562 (1951).
[11] Coon, Graves, and Barschall, Phys. Rev. **88**, 562 (1952); and J. H. Coon (private communication).
[12] H. H. Barschall and M. H. Kanner, Phys. Rev. **58**, 590 (1940).
[13] J. H. Coon and H. H. Barschall, Phys. Rev. **70**, 592 (1946).
[14] T. A. Hall and P. G. Koontz, Phys. Rev. **72**, 196 (1947).
[15] Baldinger, Huber, and Proctor, Phys. Rev. **84**, 1058 (1951).
[16] Huber, Baldinger, and Budde, Helv. Phys. Acta **25**, 444 (1952).

helium to give a similar range of recoil and introduce formidable mechanical and electrical problems. The addition of another "stopping" gas is clearly required for an extension to higher energies.

Adair[1] employed a proportional counter similar to that of Hall and Koontz[14] except for the addition of guard sleeves held at an intermediate potential.[17]

The counter employed in the present investigation was made from 3-in. o.d. by $\frac{1}{16}$-in. wall brass tube, about 14 in. long, with an active length limited to 6 in. by hypodermic needles in a manner described previously.[18,19] The counter wall was lined with platinum and the central wire was 0.005-in. Pt wire. The counter was modified so that an alpha-active deposit of Pu^{239} could be exposed through a hole in the wall, or removed at will. Subsequently, a Pu^{239} deposit was added on the center wire. Operation of the counter could be checked frequently with the aid of these sources, and they provided a reference pulse height (5.16 Mev).

Nearly all materials are disintegrated to some extent by 14-Mev neutrons.[20] However, Pt and Au liners are effective in reducing background pulses from counter walls. Krypton was chosen as the "stopping" gas on the basis of a comparison[21] of A, Kr, and Xe. Kr and Xe give less than $\frac{1}{10}$ as much "gas background" in the region of interest as does A, and moreover the Kr pulse-height spectrum exhibits a minimum near the 9-Mev end point of the He recoil spectrum.

Provision was made for continuous purification of the filling gases by convective circulation over hot calcium metal turnings.[22]

B. Collimators

The strength of the neutron sources available permitted the "luxury" of a collimator of neutrons to localize and render calculable the wall effect. All data were taken with the collimated neutron "beam" transverse to the counter axis and symmetrically located on the sensitive volume. Two collimators made of steel were used: (a) a cylinder 46 cm long, with 1-in. inside diameter and (b) a hollow pyramid 10.5 in. long of angular aperture approximately 9 by 14 degrees. Type (a) was used at $E_n=14.3$ Mev and Type (b) at the lower energies where the mean free path of neutrons in iron is smaller, and the larger solid angle was desired to compensate for the smaller source strengths available.

C. Wall Effects

A correction to the observed pulse-height distributions for recoils which collide with the wall can be made under certain simplifying assumptions: (a) Geiger's formula for alpha-particle ranges $R\sim v^3\sim E^{1.5}$ holds;[23] (b) entrance wall effects can be neglected, due to the effect of collimation and the low-energy limit of usable data (see below); (c) local curvature of the exit wall can be neglected, so that the maximum distance from which a recoil of given energy (or angle) can strike the wall can be averaged over azimuthal angles by taking the projection of its range along the direction of the incident neutron. The "collision distance" so defined can then be expressed as $D(E)=R_0(E/E_0)^2$ by using assumptions (a) and (c) and the relation $E=E_0\cos^2\theta$, where R_0 is the range corresponding to the maximum recoil energy E_0. Calculation of the fraction affected of recoils of energy E can be reduced to calculation of the volume a collision distance $D(E)$ deep from the (curved) wall. The distribution of the degraded pulses can be calculated from the range-energy relation. Errors involved in the above assumptions are small compared to the magnitude of the final correction term. Details will not be given for the calculations of geometrical factors and distribution functions, but the procedure was as follows. Let the recoil energy distribution function be expanded in the form $P(E)=\sum A_nE^n$. The distorted pulse-height distribution function can be developed in the form $p(\xi)=\sum A_nF_n(\xi,\alpha)$, where α is the ratio of maximum recoil range to counter diameter, ξ is the pulse height, and the functions F_n are calculated as outlined above for the geometries in use. Since the coefficients A_n are unknown, they were obtained from the data by an iterative procedure. The observed pulse-height distributions were represented by a power series using the method of least squares. The preliminary coefficients so determined were employed in the above formalism to determine preliminary corrections, which were subtracted from the data. The resulting "corrected" data were re-analyzed and the procedure repeated as a check. However, since the maximum correction applied to any point was 15 percent for some of the data at 14 Mev, and less than 7 percent for the lower-energy data, this procedure converged rapidly, and the second fit was not significantly different from the first.

D. Electronics and Counter Operation

The electronic equipment included a Los Alamos Model 101 amplifier and preamplifier, found to be linear (within 1 percent) for output voltages to 165 volts. This amplifier was usually used with an RC pulse-clipping time of 32 microseconds. A battery box was used for counter voltage and its output monitored. The amplified pulses were displayed on an 18-channel pulse-height analyzer,[24] which greatly facilitated taking data rapidly and reliably.

[17] A. L. Cockroft and S. C. Curran, Rev. Sci. Instr. **22**, 37 (1951).
[18] J. H. Coon and R. A. Nobles, Rev. Sci. Instr. **18**, 44 (1947).
[19] A description of the prototype counter together with its operation at high pressures is given in Los Alamos Report LA-1135, by John Wahl (unpublished).
[20] E. B. Paul and R. L. Clarke, Can. J. Phys. **31**, 267 (1953).
[21] F. L. Ribe, private communication (to be published).
[22] W. Jentschke and S. Prankl, Physik. Z. **40**, 706 (1939).
[23] The relation $R\sim E$ was used for $E_n=2.61$ Mev and the correction carried out as outlined for $R\sim E^{1.5}$.
[24] C. W. Johnstone, Nucleonics **11**, No. 1, 36 (1953).

Although krypton made a fairly satisfactory high-pressure counter filling, counter performance was markedly affected by the presence of helium. Resolution of the Pu^{239} alphas deteriorated steadily with increasing partial pressure of helium, yet the original resolution of about 5 percent was restored when the krypton was condensed in the counter and the helium pumped off. Study of the resolution as a function of purification time of the gas circulating over calcium metal at 300°C showed very little improvement. To explore this effect the counter was provided with a deposit of Pu^{239} on the center wire in addition to the removable wall deposit, so that the behavior of the counter with respect to both central and wall pulses could be studied for a variety of operating conditions. Extensive efforts were made to improve the purity of the gas fillings, and progress was followed by frequent analyses with a mass spectrometer, while the counter operation was followed as outlined above. No consistent improvement resulted. For a given filling, the general behavior of the alpha pulses as a function of gas multiplication was as follows.

At unit gas multiplication, the wall-to-center pulse-height ratio was about 1.3, and the resolution of each group was poor. As multiplication was increased, the ratio decreased and the resolution improved until an optimum resolution was obtained in the vicinity of a multiplication of 8. For higher multiplication, although the wall-to-center ratio approached unity, the resolution deteriorated rapidly. The resolution of the He-recoil end point was also observed for several conditions, and it was found that best resolution of the end point corresponded to the above "optimum" operating conditions. The wall-to-center pulse-height ratio was about 1.1, but the apparent end point of the recoils fell at a point consistent with taking the mean Pu^{239} alpha pulse height as an energy calibration. The operation of the counter was optimized in the manner described for all the data reported below.

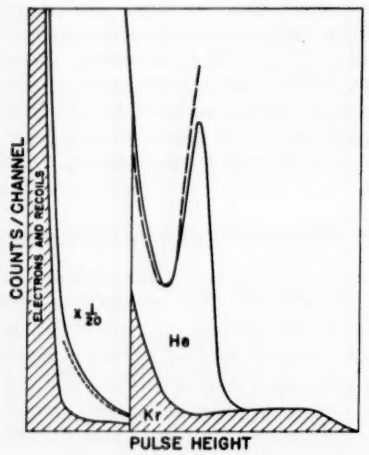

FIG. 1. Composite pulse-height distribution for a typical set of data at $E_n = 14.3$ Mev. Solid curve is observed distribution, shaded region is gas background included, and dotted curve represents the modification of the net helium distribution by the wall-effect correction. Counter filling was 75-psi krypton + 15-psi helium.

E. Background and Limitations of the Method

Krypton was chosen as the stopping gas for its low "gas background" at $E_n = 14$ Mev, but the Kr/He counting ratio was not negligible, being about one-third in the worst case. Better counter operation could be obtained with a larger Kr/He pressure ratio, but at the expense of larger relative background. The addition of CO_2 to the counter filling reduced the pulse rise time, but did not improve the resolution materially, and contributed to the gas background. Use of CO_2 was abandoned. The following procedure was adopted to measure the gas background. After a He+Kr run, one end of the counter was immersed in a bowl of liquid nitrogen to condense the krypton and the helium pumped off until an indicated pressure of 1 mm was reached. The counter was then sealed off and prepared for bombardment. As soon as the counter had warmed to room temperature, the operating conditions were made as nearly as possible like those under which the first run was made. Krypton pressure and collimator geometry being the same in both cases, the principle uncertainty in the "background" spectrum was in the pulse-height energy scale. Fortunately, the krypton reaction spectrum extends to 16 Mev, while the helium recoil spectrum ends at 9 Mev, so the excess could be used as an additional check on the energy scale.

One of the limitations of this method of measuring the angular distribution is that it does not give information (directly) about neutrons scattered through small angles, since the pulses from the corresponding low-energy recoils are masked by pulses due to electrons and recoils from heavier nuclei. Because of the high pressures of krypton required, the gamma or electron end point was about 2 Mev for $E_n = 14$ Mev, which corresponds to a neutron scattering angle of 57°. The krypton recoil end point was only 0.75 Mev. In the results to be presented, the data lying in the electron-masked region are not included because of the large statistical uncertainty of "net" data obtained by subtracting large numbers, although the results are consistent with the indicated extrapolations from the reliable data.

Information about backscattered neutrons is limited by the finite resolution of the counter, since the cusp at the end point of the energy distribution function is smeared out in the corresponding pulse-height distribution. No correction was made for the effect of finite resolution on the basis of the following calculation. The preliminary least-squares fit to the central portion of the data was smeared numerically by a resolution function of the same form as the distribution function observed for the wall-alphas, and only the data which

were substantially unaffected by the operation were retained for correction for the wall-effect.

The nature and extent of these corrections and limitations can be better appreciated by comparison of Figs. 1 and 2, which show a composite of the raw data and the final results, respectively, for $E_n = 14.3$ Mev. Figure 1 is included only to give a general perspective, so the actual data points are not shown, but the relation of observed distributions, the electron "stone wall," and the effects of finite resolution and finite range of the recoils may be seen.

III. EXPERIMENTAL RESULTS

A. $E_n = 14.3 \pm 0.1$ Mev

These measurements were made at the 250-kev Cockcroft-Walton accelerator, using the D-T reaction in a thick Zr-T target. Counter fillings were in the neighborhood of 80-psi krypton and 20-psi helium.

In Fig. 2 are shown the results of three independent measurements of the angular distribution of 14.3-Mev neutrons scattered by He^4. The solid curve is the distribution predicted by the theory of Dodder and Gammel.[5] Since the three runs were consistent with each other and with the theory for the backscattering hemisphere within the statistical uncertainty, no distinction between runs was made in plotting the composite results. However, for the usable portion of the data in the forward hemisphere, the three runs differ significantly and are distinguished by dotted lines. It is believed that these departures represent the effect of inelastic neutrons produced in the target assembly and in the steel collimator. Lower-energy neutrons can be especially troublesome because the n-He^4 cross section is larger (roughly as E^{-1}), and they will produce more pulses per unit energy interval (as E^{-1}). Present information on the cross section and spectrum of 14-Mev neutrons inelastically scattered by iron[25] is consistent with this interpretation, but it was not feasible to calculate a correction for the effect of such neutrons on the pulse-height distribution. If this interpretation is correct, the differing flux of inelastic neutrons reflects small differences in the collimator geometry of the three independent runs. As a test of the theory, however, the shape of the curve for backscattering is much more sensitive to small changes in phase shifts than is the shape in the other hemisphere, and the agreement is quite good, considering the experimental difficulties and the uncertainties in the theory.[26] The data do not warrant analysis for phase shifts. It should be understood that the *absolute* cross section scale was not determined in this experiment; the data were normalized to independent total cross-section measurements.

[25] E. R. Graves and L. Rosen, Phys. Rev. **89**, 343 (1953); Louis Rosen (private communication).

[26] Since this work was completed, an angular distribution over all angles at $E_n = 14.1$ Mev has been obtained by cloud-chamber techniques at the Rice Institute [J. R. Smith (private communication)], and it is also in good agreement with the theory.

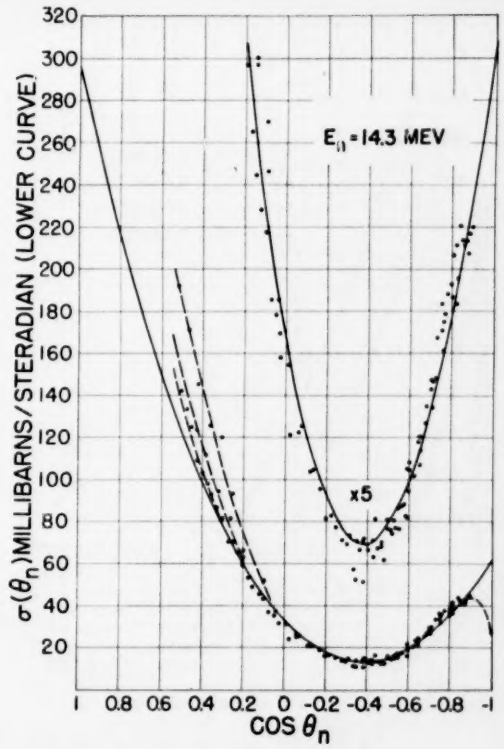

FIG. 2. Comparison of experimental and theoretical results for angular distribution of 14.3-Mev neutrons scattered by helium. θ_n is the angle through which the neutron is scattered in the center-of-mass system. Experimental points for three independent observations are distinguished by dotted curves. The disparities observed are attributed to the effects of energy-degraded neutrons present in the incident flux.

B. $E_n = 4.53 \pm 0.06$, 5.54 ± 0.06, and 6.50 ± 0.06 Mev

These measurements were made at the large Los Alamos Van de Graaff, using the D−D reaction in a gas target, and the short pyramidal collimator. The three lower curves in Fig. 3 show the distributions obtained at these three neutron energies. Although it is possible that at these lower energies, a He−A−CO_2 filling would have given satisfactory results, the measurements were carried out with a He+Kr filling similar to that used at $E_n = 14.3$ Mev, to test whether any systematic error could be attributed to counter operation with this filling or to the wall-effect correction, the latter being less than half as large a correction in this region. No evidence for such effects was found. Performance of the collimator at these energies was checked with a Np^{237} spiral fission chamber and with a stilbene scintillator. The collimator was found to produce about 10 percent scattering-in on the axis, but this increase in flux was due almost exclusively to elastic scattering from iron, which would have no detectable effect on the neutron or recoil spectra.

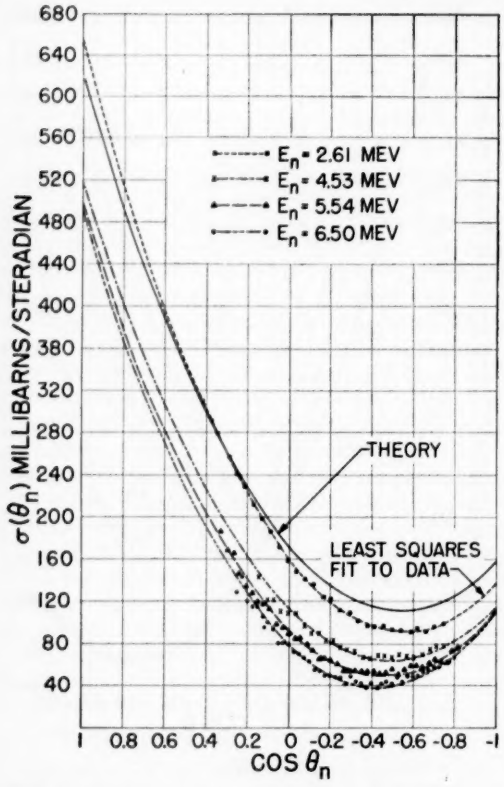

FIG. 3. Comparison of theoretical curves and experimental data for E_n=6.50, 5.54, 4.53, and 2.61 Mev. A separate "experimental" curve is shown only for E_n=2.61 Mev.

Because of the high pressure of krypton, the electron end point was about 1.5 Mev, which prevented obtaining usable data below about 1 Mev for the helium recoils. The available neutron intensity made the data less reliable statistically than those at 14.3 Mev, but the results seem to be in satisfactory agreement with the theoretical prediction. Only theoretical curves are given in Fig. 2 for these three energies, as no separate "experimental" curve seems warranted.

C. $E_n = 2.61 \pm 0.06$ Mev

This measurement was made at the Cockcroft-Walton accelerator, using a collimated neutron "beam" at 75 degrees from the bombarding deuteron beam. In this case neutrons were obtained from the D−D reaction, and the short collimator was used. The counter filling was 15-psi krypton and 15-psi helium. The data are also shown in Fig. 3. The experimental curve appears to depart significantly from the theoretical prediction. A parabola can be fitted to the corrected data with quite small mean square deviation, the fit being better than 2 percent at any point. This curve was used in an attempt to analyze for phase shifts which would be in better agreement with the experiment.

IV. COMPARISON WITH THEORY

A. Phase Shift Analysis

For neutrons scattered elastically by nuclei for which $J=0$, the differential cross section is given by[27]

$$k^2\sigma(\mu)=|\sum\{(l+1)\sin\delta_l^+\exp(i\delta_l^+) +l\sin\delta_l^-\exp(i\delta_l^-)\}P_l(\mu)|^2 +(1-\mu^2)|\sum\{\sin\delta_l^+\exp(i\delta_l^+) -\sin\delta_l^-\exp(i\delta_l^-)\}P_l'(\mu)|^2, \quad (1)$$

where k is the neutron wave number, and $\mu=\cos\theta$. We are concerned with $l\leq 2$, and with $S_{\frac{1}{2}}$, $P_{\frac{1}{2}}$, $P_{\frac{3}{2}}$, $D_{\frac{3}{2}}$, and $D_{\frac{5}{2}}$ phase shifts, designated δ_0, δ_1^-, δ_1^+, δ_2^-, and δ_2^+, respectively. Also,

$$k^2\sigma_T=4\pi\sum\{(l+1)\sin^2\delta_l^+ +l\sin^2\delta_l^-\}. \quad (2)$$

For the graphical interpretation of the shape of elastic scattering resonances,[28] it is convenient to regard $\sin\delta\exp(i\delta)$ as a vector intersecting a unit circle which makes an angle δ with the real axis. In passing through a resonance, the "resonant" vector will trace out its circle, while the others remain nearly constant. For the interpretation of the *angular* variation at fixed energy, it is more convenient to substitute $\sin\delta\exp(i\delta) =\{\exp(2i\delta)-1\}/2i$ in Eq. (1). When a sum of these complex numbers is squared, the factor $|1/2i|^2=\frac{1}{4}$, and we may rewrite Eq. (1) as

$$4k^2\sigma(\mu)=(1-\mu^2)|\mathbf{P}_{\frac{3}{2}}-\mathbf{P}_{\frac{1}{2}}+(\mathbf{D}_{\frac{5}{2}}-\mathbf{D}_{\frac{3}{2}})3\mu|^2 +|\mathbf{S}_{\frac{1}{2}}-\mathbf{1}+(2\mathbf{P}_{\frac{3}{2}}+\mathbf{P}_{\frac{1}{2}}-\mathbf{3})\mu +(3\mathbf{D}_{\frac{5}{2}}+2\mathbf{D}_{\frac{3}{2}}-\mathbf{5})\tfrac{1}{2}(3\mu^2-1)|^2. \quad (3)$$

The bold face symbols are complex vectors *of unit length* which make an angle 2δ with the real axis, where δ is the corresponding phase shift. In a similar manner Eq. (2) may be rewritten

$$k^2\sigma_T=2\pi\{\mathbf{9}-\mathrm{Re}(\mathbf{S}_{\frac{1}{2}}+\mathbf{P}_{\frac{1}{2}}+2\mathbf{P}_{\frac{3}{2}}+3\mathbf{D}_{\frac{5}{2}})\}. \quad (4)$$

A graphical analysis of these relations was carried out for each energy at which a measurement was made, with the result that a "best fit" to the observed distributions did not lead to phase shifts significantly different from those of the theory, except at E_n=2.61 Mev. At this energy the d-wave phase shifts are expected to be nearly zero, so Eqs. (3) and (4) can be simplified by setting $\mathbf{D}_{\frac{3}{2}}=\mathbf{D}_{\frac{5}{2}}=\mathbf{1}$. Since there remain only three phase shifts, they may be determined from three experimental cross sections, which are most conveniently taken to be σ_T, $\sigma(1)$, and $\sigma(-1)$. From Eq. (3),

$$4k^2\sigma(\pm 1)=|\mathbf{S}_{\frac{1}{2}}-\mathbf{1}\pm(2\mathbf{P}_{\frac{3}{2}}+\mathbf{P}_{\frac{1}{2}}-\mathbf{3})|^2, \quad (5)$$

in this case. The total cross section can be determined only to within about 20 percent from the incomplete

[27] F. Bloch, Phys. Rev. **58**, 829 (1940).
[28] R. A. Laubenstein and M. J. W. Laubenstein, Phys. Rev. **84**, 18 (1951).

angular distribution, so the differential cross sections must be normalized by an independent value of the total cross section. Recent measurements at this laboratory[29] of σ_T in the vicinity of 2.61 Mev are 3.16±0.06 barns at 2.49±0.05 Mev and 2.79±0.06 barns at 2.99±0.04 Mev. Taking into account the shape of the σ_T *vs* E_n curve, we may estimate $\sigma_T=3.04\pm0.08$ barns at 2.61 Mev. The resulting uncertainty in normalization dominates the net uncertainty in the angular distributions, or in the values of $\sigma(1)$ and $\sigma(-1)$ calculated from the coefficients of the power-series least-squares fit.

The construction shown in Fig. 4 represents Eqs. (4) and (5). The terminus of the vector sum $\mathbf{S}_{\frac{1}{2}}-\mathbf{1}+(-\mathbf{3}+2\mathbf{P}_{\frac{1}{2}}+\mathbf{P}_{\frac{3}{2}})$ must lie at a distance $2k\sqrt{\sigma(1)}$ from the origin and its real part be $-k^2\sigma_T/2\pi$. These loci, together with the probable error of experimental determination are indicated in the figure and determine an area locus for the vector. Also, according to Eq. (5), the reflection of the **P** vector $-\mathbf{3}+2\mathbf{P}_{\frac{1}{2}}+\mathbf{P}_{\frac{3}{2}}$ through the end point of the **S** vector must fall in the domain determined by $2k\sqrt{\sigma(-1)}$. The locations of the end points $\mathbf{S}\pm\mathbf{P}$ predicted by theory[5] are indicated by solid circles, and it may be seen that they fall slightly outside of the probable error of experimental results. The uncertainty in determination of "experimental" phase shifts and the disagreement with the theory is small (indicated in Fig. 4 by shaded sectors) except for δ_1^-. It can be seen from the diagram how sensitive the "most probable" value of δ_1^- is to the value of the total cross section. For this reason the discrepancy between the present experimental value $\delta_1^-=11\pm6$ degrees and the theoretical estimate $\delta_1^-=20.5$ degree is not very serious. A better determination of the total cross section would be worthwhile, particularly in view of the generally excellent agreement with theory. If the discrepancy is real, it may be interpreted as indicating some curvature in the relation between logarithmic derivative and energy (reference 5, Fig. 1) for the $P_{\frac{1}{2}}$ state (i.e., that the single-level approximation is not quite valid for this broad state).[30]

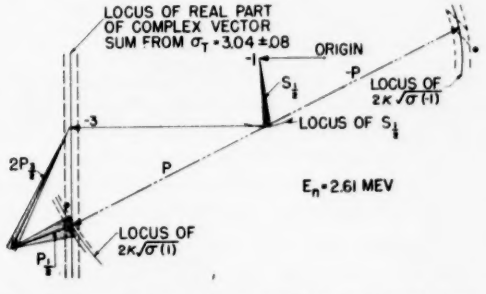

FIG. 4. Complex-vector diagram of phase-shift relations at $E_n=2.61$ Mev. The probable errors of experimental cross sections are indicated by dotted lines, and the corresponding uncertainties in phase shifts are indicated by shaded sectors. The location of the end points of the vectors $\mathbf{S}\pm\mathbf{P}$ predicted by theory are indicated by solid circles (●).

[29] J. H. Coon (private communication).

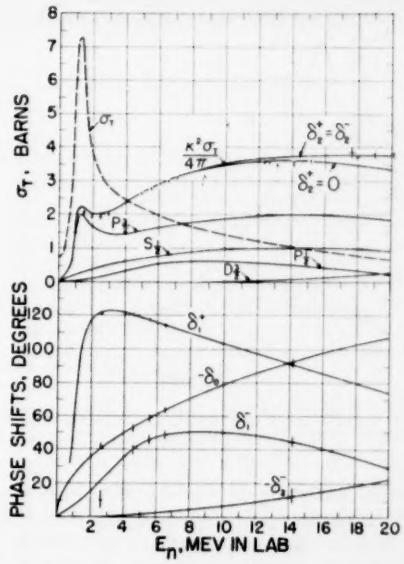

FIG. 5. Summary of phase-shift and cross-section values for the n-He⁴ interaction from $E_n=0$ to 20 Mev. In the lower part of the figure are shown the phase shifts predicted from analysis of the p-He⁴ interaction, together with the values indicated by the present experiment. In the upper part of the figure are shown the total cross section σ_T, the separate terms in the summation of Eq. (2), and their sum $k^2\sigma_T/4\pi$. The results of recent total cross section measurements are plotted in the form $k^2\sigma_T/4\pi$ for two assumptions concerning the $D_{5/2}$ interaction.

B. Graphical Summary

Figure 5 is presented as a summary of present information on n-He⁴ scattering up to 20 Mev. In the lower part are shown the phase shifts derived from analysis[5,6] of p-He⁴ scattering, together with the indicated results of the present experiment. At $E_n=2.61$ Mev, the "most probable" values have been plotted together with their probable errors. At the other points, no "most probable" value is given, and the indicated uncertainties were obtained somewhat arbitrarily from the analyses described above, and should be interpreted as the limits outside of which a discrepancy should have been experimentally detectable.

The corresponding cross sections are shown in the upper part of Fig. 5. The curves designated by spectroscopic symbols are the separate terms in Eq. (2), i.e., $(j+\frac{1}{2})\sin^2\delta_l^j$, and the upper curve their sum $k^2\sigma_T/4\pi$. The $D_{\frac{5}{2}}$ phase shifts are those for scattering by a hard sphere of radius 2.9×10^{-13} cm. The $D_{\frac{5}{2}}$ level in He⁵ occurs at an excitation of 16.64 Mev,[31] and should figure

[30] In reference 5, the cm proton energy scales of Fig. 1 and Fig. 2, and the values of E_λ and $\gamma\lambda^2$ quoted on p. 523 should be multiplied by 1.25. In Eq. (2), the numerator of the first term should read ka/FG.

[31] F. Ajzenberg and T. Lauritsen, Revs. Modern Phys. **24**, 321 (1952). See Fig. 1.

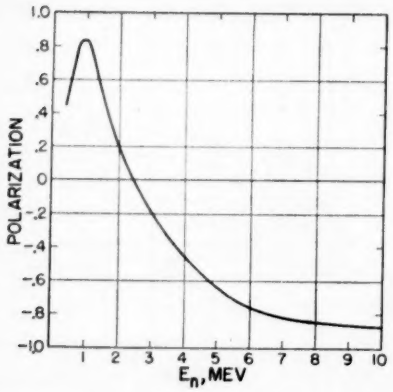

FIG. 6. Polarization of neutrons scattered through 90° in the center-of-mass system.

in neutron scattering at $E_n=22$ Mev, which is well outside the region under consideration. However, very little is known about a possible $D_{\frac{1}{2}}$ level. Were it not for uncertainty concerning this level, the $D_{\frac{1}{2}}$ phase shifts could be set approximately equal to the $D_{\frac{3}{2}}$ phase shifts.

Several measurements of σ_T have been made recently at this laboratory.[30,32,33] For a better comparison with the theory, these data are plotted in Fig. 5 in the form $k^2\sigma_T/4\pi$, together with a curve indicating the contribution of $D_{\frac{1}{2}}$ scattering if $\delta_2{}^+=\delta_2{}^-$. It will be noticed that while the total cross-section values for $E_n\geq 17$ Mev are accounted for by this assumption, the experimental points for E_n between 12 and 14 Mev fall even below the curve for $\delta_2{}^-=0$. Presumably these discrepancies are indicative of the unlocated $D_{\frac{1}{2}}$ resonance. Unfortunately, the angular distribution measurements at $E_n=14.3$ Mev could not be analyzed to give more information about the D interactions than is provided by the theory. Further high-energy total cross-section measurements are planned,[32] and analysis of the implications of p-He^4 scattering measurements at 31.6 Mev[34] is in progress.

[32] R. L. Henkel and J. E. Perry (private communication).
[33] R. B. Day and R. L. Henkel, Phys. Rev. **92**, 358 (1953).
[34] B. Cork, Phys. Rev. **89**, 78 (1953), and private communication to D. C. Dodder.

V. POLARIZATION AND SCATTERED NEUTRONS

Because of the strong spin-orbit forces involved, the n-He^4 interaction results in partial polarization of the scattered neutrons.[1,35–39] For an unpolarized incident beam of neutrons, the polarization of neutrons scattered through an angle θ in the center-of-mass system is directed along the normal to the plane of scattering. Its magnitude is given by[37]

$$P(\theta)=\langle\sigma\rangle/\sigma(\theta)=(AB^*+BA^*)/(AA^*+BB^*), \quad (6)$$

where $\langle\sigma\rangle$ is the expectation value for the spin in the normal direction, $\sigma(\theta)$ is the differential cross section, and A and B are the expressions within the absolute-square signs in Eq. (1), that is, $\sigma(\theta)=AA^*+BB^*$. Using Eq. (6), the polarization may be calculated for any angle and energy from the phase shifts given in Fig. 5. An example of the interesting possibility of using elastic scattering by He^4 as a polarizer or analyzer in experiments involving polarized neutrons has already been reported.[40] As an indication of the large degree of polarization available, $P(90°)$ has been calculated as a function of energy, and the results plotted in Fig. 6. Because of the uncertainties in the d-wave phase shifts, the curve is drawn only to 10 Mev, but the 90° polarization should remain roughly constant from 10 to 20 Mev, except in the vicinity of the $D_{\frac{1}{2}}$ resonance.

VI. CONCLUSION

The present experimental results for n-He^4 scattering are in substantial agreement with the predictions based on analysis of p-He^4 scattering experiments, and support equivalence of the mirror nuclei He^5 and Li^5.

The author wishes to thank Drs. J. H. Coon, E. R. Graves, and F. L. Ribe for their interest and assistance in the experimental details of this investigation, D. C. Dodder and J. L. Gammel for the results of their theoretical analysis, and J. H. Coon, J. E. Perry, R. B. Day, and R. L. Henkel for permission to quote the results of their total cross-section measurements in advance of publication.

[35] J. S. Schwinger, Phys. Rev. **69**, 681 (1946).
[36] L. Wolfenstein, Phys. Rev. **75**, 1664 (1949).
[37] J. V. Lepore, Phys. Rev. **79**, 137 (1950).
[38] R. J. Blin-Stoyle, Proc. Phys. Soc. (London) **A64**, 700 (1951).
[39] A. Simon and T. A. Welton, Phys. Rev. **90**, 1036 (1953).
[40] Bishop, Westhead, Preston, and Halban, Nature (London) **170**, 113 (1953).

Structure of Liquid Nitrogen, Oxygen, and Argon by Neutron Diffraction

D. G. Henshaw, D. G. Hurst, and N. K. Pope*
Division of Physics, Atomic Energy of Canada Limited, Chalk River, Ontario, Canada
(Received August 26, 1953)

The structures of liquid oxygen, nitrogen, and argon have been investigated by measuring the scattering of neutrons of wavelength 1.08A over the angular range 4° to 78°. The scattering curves have been transformed to give the time average of the atomic density as a function of the distance from an atom taken as center. The deviation from the mean density is an oscillating function with an amplitude which decreases more rapidly than the inverse square of the distance from the central atom. In nitrogen a single neighbor is found at a spacing of 1.1A from each atom, corresponding to a diatomic molecule in the liquid. In oxygen 1.5 neighbors are found at approximately 1.25A from each atom, suggesting that the degree of association is greater than diatomic. The results are not inconsistent with the suggested existence of the O_4 molecule. In argon the results are in reasonable agreement with published x-ray determinations.

INTRODUCTION

As part of a program to investigate the scattering of slow neutrons by liquids, the angular distributions of neutrons scattered by liquid nitrogen, liquid oxygen, and liquid argon have been measured. Information about the atomic arrangements of the liquids can be obtained from such distributions. In particular, if a semiclassical model of neutron scattering is assumed[1-3] a transformation, well known in x-ray investigations, may be used to obtain from the measurements the radial variation of density about an atom in the liquid.[4,5] Gingrich[6] has reviewed x-ray investigations of liquid elements including the three discussed here. Previous measurements of the scattering of neutrons by liquids have been made by Chamberlain[7] who investigated sulfur, lead, and bismuth, and by Sharrah and Smith[8] who investigated lead and bismuth. In the interpretation of their measurements these workers assumed that the scattering pattern was the sum of a coherent diffraction pattern, to which the transformation is applicable, and an isotropic incoherent contribution.

The experimental results reported in this paper have been similarly transformed to give the radial density for each of the three liquids. The effects of variations in the treatment of the experimental results on the predicted structure are discussed.

APPARATUS

The angular distribution of scattered neutrons was measured by an automatic spectrometer with the monochromating crystal adjusted to provide neutrons of wavelength 1.08A. Since the earlier description of this instrument[9] some minor modifications have been made; the monoenergetic neutrons were selected by diffraction at a sodium chloride crystal in reflection rather than transmission, the motor drive provided a wider choice of angular steps, and the neutron monitor was improved. The new monitor was a "thin" BF_3 counter interposed in the diffracted beam; this eliminated errors due to changes in the spectrum of neutrons leaving the reactor.

The liquids were held in a cryostat mounted on the specimen table of the spectrometer. A horizontal section, at the level of the neutron beam, is shown in Fig. 1. The cryostat was designed to hold liquid helium[10] which has low scattering power and thus requires a large scattering chamber (12.7-cm diameter with 0.025-cm wall thickness). This chamber was also suitable for argon which has a small scattering cross section. For nitrogen and oxygen, which have larger cross sections, a small cylindrical aluminum cassette (1-cm diameter with 0.01-cm wall thickness) was mounted in the middle of the cryostat.

The scattered neutrons were detected by an enriched BF_3 proportional counter mounted on an arm rotatable about the axis of the cryostat. With nitrogen and oxygen the time to count 3200 neutrons was recorded for each of 44 equally-spaced positions of the arm in the angular

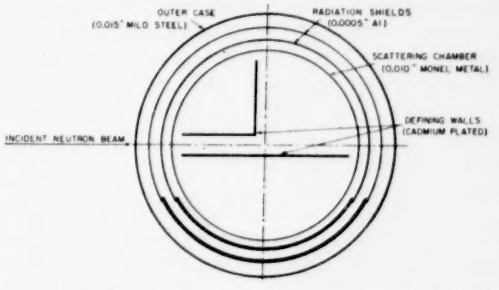

FIG. 1. A horizontal section of the argon scattering chamber at the level of the neutron beam. The cadmium-coated plates define the scattering volume and reduce the error caused by multiply-scattered neutrons. The radiation shields and liquid nitrogen baths to which the shields were connected formed an enclosure at liquid nitrogen temperature for the scattering chamber.

* Now at Physics Department, Canterbury University College, Christchurch, New Zealand.

[1] G. Placzek, Phys. Rev. **86**, 377 (1952).
[2] L. Goldstein, Phys. Rev. **84**, 466 (1951).
[3] N. Z. Alcock and D. G. Hurst, Phys. Rev. **83**, 1100 (1951); N. K. Pope, Can. J. Phys. **30**, 597 (1952).
[4] P. Debye, Ann. Physik **46**, 809 (1915).
[5] F. Zernike and J. Prins, Z. Physik **41**, 184 (1927).
[6] N. S. Gingrich, Revs. Modern Phys. **15**, 90 (1943).
[7] O. Chamberlain, Phys. Rev. **77**, 305 (1950).
[8] P. C. Sharrah and G. P. Smith, J. Chem. Phys. **21**, 228 (1953).
[9] D. G. Hurst and N. Z. Alcock, Can. J. Phys. **29**, 36 (1951).
[10] D. G. Henshaw and D. G. Hurst, Phys. Rev. **91**, 1222 (1953).

range 4° to 77°. With argon the time to count 800 neutrons was recorded. The temperature of each sample was controlled and recorded by means of its vapor pressure using a commercial pressure controller.

EXPERIMENTAL RESULTS

The scattered intensities, normalized by means of the monitor to the same number of neutrons incident on the specimen, were corrected for background, resolution, double scattering, and in the case of argon, for the change in effective scattering volume with angle. The background was measured with the specimen holder empty. At small angles, where the background was large, it was assumed that the background neutrons in excess of those at large angles came predominantly from the region on the source side of the scattering volume. Accordingly this excess was reduced by the transmission loss through the liquid before subtracting from the measurements. For nitrogen and oxygen the background correction at large angles was about 5 percent of the intensity and somewhat greater in the case of argon. The resolution of the instrument was determined by measuring the (200) line of powdered potassium bromide contained in the holder used for nitrogen and oxygen. This (200) line occurs at nearly the same angle as the main peak in nitrogen. The full width at half-height was found to be 1.67 degrees, and was applied as a correction to the measured pattern by a method due to Eckart.[11]

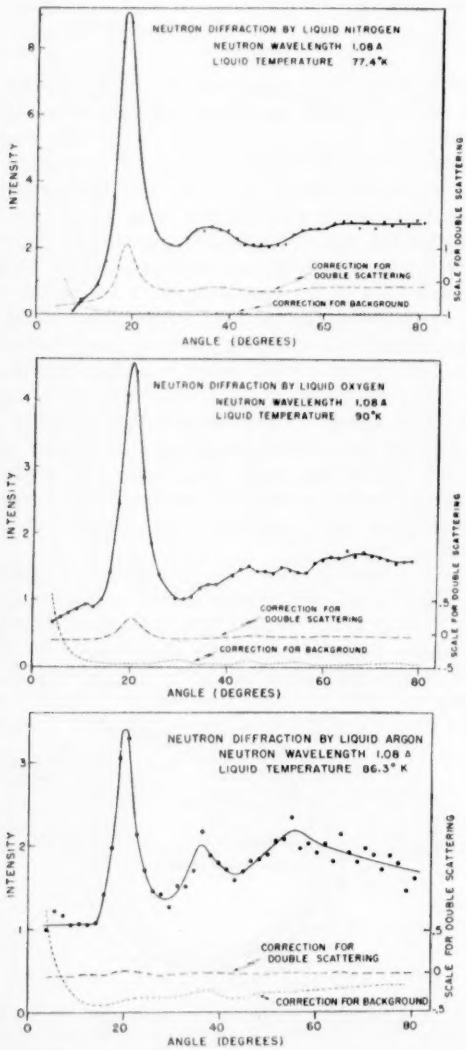

FIG. 2. The corrected intensities (in arbitrary units) for liquid oxygen at 90°K, nitrogen at 77.4°K and argon at 86.3°K as a function of the scattering angle. Also shown are the corrections applied for background and double scattering, while the correction for counter resolution, being small, has been omitted. A neutron wavelength of 1.08A was used.

Corrections for double scattering were made to the results for oxygen and nitrogen with the aid of the theorem that the average path length for particles originating with uniform source strength in a long cylinder of radius a is $(4/3)a$. For argon this same theorem was used for second scattering close to the position of first scattering; the contribution due to second scattering remote from the position of first scattering was calculated by numerical integration over the relevant portions of the scattering chamber. It was assumed, and this assumption was supported by calculations for special cases, that the corrections for multiple scattering could be calculated as if the scattering were isotropic. The attenuation of the neutron beam in its passage through the liquid was taken into account.

The effective scattering volume of argon depended upon the angle of scattering. The scattered intensities were normalized to unit scattering volume neglecting the angular divergences of the incident neutron beam and of the counter acceptance. The corrected results together with the corrections applied for background, counter resolution, and double scattering are plotted in Fig. 2 for nitrogen, oxygen, and argon, respectively.

INTERPRETATION

The formula of Debye[4] and Zernike and Prins[5] connects the coherently scattered intensity with the variation of atomic density measured radially from an atom in the liquid. When applied to neutron scattering without spin and isotope incoherence, it can be written as

$$4\pi r^2[\rho(r)-\rho_0]=(2r/\pi)\int_0^\infty si(s)\sin rs\,ds, \qquad (1)$$

where r = distance from the atom chosen as center, $\rho(r)$ = atomic density at a distance r, ρ_0 = mean atomic density of the liquid, $s=(4\pi/\lambda)\sin(\varphi/2)$, λ = neutron wavelength, φ = angle of scattering, $(is)=[I(s)-I_\infty]/I_\infty$,

[11] C. Eckart, Phys. Rev. **51**, 735 (1937).

$I(s)$ = intensity of coherent scattering (proportional to differential cross section) for the value s of the variable, and I_∞ = value of $I(s)$ for $s=\infty$ (see, however, later discussions).

In the derivation of Eq. (1) the quantity $I(s)$ is assumed to arise from coherent scattering proportional to the density of scattering material. Neutron scattering is considerably more complex than this simple process and it is necessary to inquire into the validity of the formula. The derivation treats the coherent scattering from the liquid as elastic. A rough estimate of the elastic neutron scattering may be obtained by comparing the liquid with an Einstein solid having an appropriate characteristic temperature. The elastic scattering from such a solid[12] is very small beyond the first peak in the angular distribution from the liquid. In practice it is impossible to separate the elastic from the total scattering, and it would not be feasible to restrict $I(s)$ to the elastic component. However, provided the energy transfers between liquid and neutron are small compared to the neutron energy, these transfers may be ignored, and the use of all or nearly all the scattering for $I(s)$ in Eq. (1) may lead to the correct result.[1-3]

Spin and isotope incoherence, which often occur in neutron scattering, are known to be small for the three elements considered in the present paper.

Previous workers[7,8] assumed that the incoherent scattering was isotropic and given by the small-angle scattering. They subtracted from the measured intensity the intensity observed at small angles and assumed that the resultant intensity was the coherent portion to which Eq. (1) applies.

In the present work nitrogen gave very little small-angle scattering but oxygen and argon gave relatively much greater amounts which were larger than those reported for lead, bismuth, and sulfur.[7,8] In view of possible magnetic scattering by oxygen, of the possible existence of other small-angle scattering, and of the large experimental errors at small angle owing to background, it is not certain that the residual scattering should be subtracted. For most of the analysis of the present results $I(s)$ has been taken to be the scattering plotted in Fig. 2. The effect caused by subtracting a constant from the values of $I(s)$ has been studied.

The largest value of s for which measurements were made is 7.4A^{-1}. Unless some form for $i(s)$ is assumed in the range $7.4<s<\infty$ the integration of Eq. (1) can be carried out only to this value of s. The extrapolation of $i(s)$ beyond the experimental limit of s is arbitrary except that $i(s)$ is almost certainly small. In x-ray and electron diffraction $i(s)$ is often assumed to be zero throughout this region,[6] or to approximate to this condition an artificial temperature factor is sometimes introduced.[13] The lack of direct knowledge of $I(s)$ as $s\to\infty$ permits the use of I_∞ as a parameter. For example I_∞ may be chosen to ensure[7] that $\rho(r)\to 0$ as $r\to 0$. This

[12] B. N. Brockhouse and D. G. Hurst, Phys. Rev. **88**, 542 (1952).
[13] C. Degard, Bull. soc. roy. sci. Liége **7**, 115 (1938).

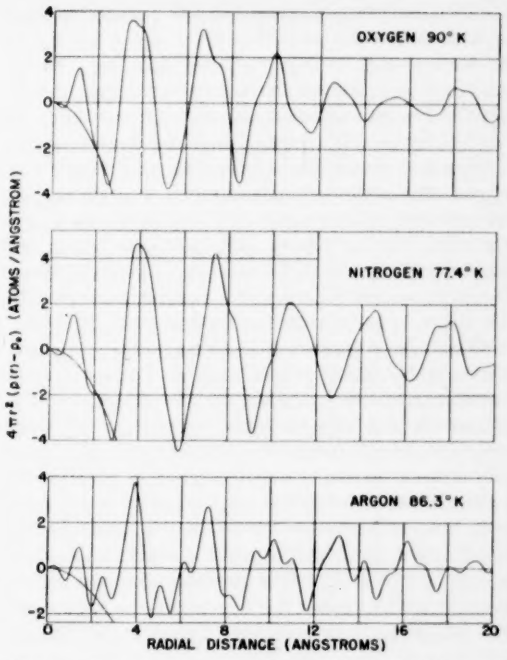

FIG. 3. The transforms $4\pi r^2[\rho(r)-\rho_0]$ for liquid oxygen, nitrogen, and argon calculated from the corresponding intensity curves of Fig. 2. The smooth curve with each transform is $-4\pi r^2\rho_0$, where ρ_0 is the average density. ρ_0 for oxygen $=4.30\times10^{-2}$; for nitrogen $=3.48\times10^{-2}$ and for argon $=2.13\times10^{-2}$ atoms per cubic angstrom.

condition requires that

$$-2\pi^2\rho_0=\int_0^\infty s^2 i(s)ds, \qquad (2)$$

where again the upper limit of integration is experimentally unattainable. Extrapolation of $i(s)$ and the value of I_∞ are of course interrelated.

In the present work, transforms were computed on an I.B.M. Calculating Punch No. 602A at the Chalk River Laboratory and on the Ferranti Electronic Computer (FERUT) at the University of Toronto. Simpson's rule was used for the integrations. Calculations were carried out for several methods of terminating the integration and computing I_∞. In the majority of cases I_∞ was calculated by Eq. (2). An extrapolation $i(s)\propto s^{-4}$ was tried. The effects of these variations were small, being mainly to add ripples with a wavelength [2π/cut-off value of s)] along the r axis; in the case of a sharp density peak these appear as ghosts on either side.[14,15a,15b]

The transform $4\pi r^2[\rho(r)-\rho_0]$ given by Eq. (1) indicates the degree of order in the liquid in that it gives

[14] C. Finbak, Acta Chem. Scand. **3**, 1279 and 1293 (1949).
[15a] T. Sugawara, Sci. Repts. Research Insts. Tôhoku Univ. **A3**, 39 (1951).
[15b] (added in proof) J. Waser and V. Schomacher, Revs. Modern Phys. **25**, 671 (1953).

the deviation from the mean of the number of atoms per unit radial distance. This transform is plotted for the three liquids in Fig. 3. The values for $0<r<3$A merit special attention for it is in this region that information regarding molecular association is obtained. The curves of Fig. 3 show that the transforms for nitrogen and oxygen have peaks at about 1.0A and 1.2A, respectively, while in argon there is a peak at 1.4A. For nitrogen and oxygen the transforms do not go appreciably below $-4\pi r^2\rho_0$ and are equal to it for r in the range $1.8<r<2.3$A. In the case of argon, however, there are regions where the transform goes considerably below $-4\pi r^2\rho_0$ and in fact seems to oscillate about it. Where the transform is less than $-4\pi r^2\rho_0$, negative values of the density are implied. These physically unreal values are probably due to experimental inadequacies. The wide scatter of the experimental points for argon at large values of φ (Fig. 2) permits considerable latitude in the choice of $i(s)$. If a function $i(s)$ is assumed which will yield $\rho(r)=0$ out to $r=3$A, deviations from this function for $s>6.3$A^{-1}, consistent with experimental error, will produce a peak similar to the peak at 1.4A. This peak is probably spurious and the present results cannot be considered as inconsistent with the monatomic nature of liquid argon. It is intended at a later date to repeat the measurements with greater accuracy.

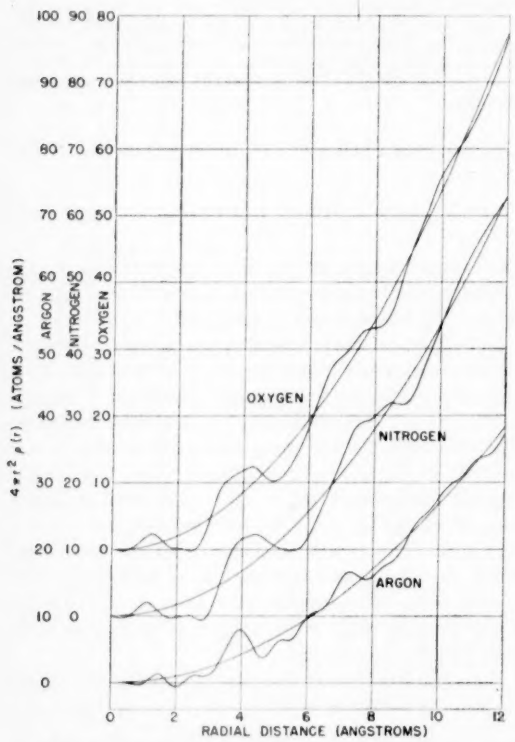

FIG. 4. The radial distribution functions $4\pi r^2\rho(r)$ deduced from the transforms of Fig. 3 for liquid oxygen, nitrogen and argon. In each case $4\pi r^2\rho_0$, the corresponding function for uniform atomic density, is also shown.

The effect of varying the treatment of the experimental results is well illustrated by a comparison of three transforms for argon calculated (a) with the values of $I(s)$ plotted in Fig. 2 and I_∞ chosen to satisfy Eq. (2); (b) I_∞ chosen equal to $I(7.4)$ and (c) with the same values of $I(s)$ reduced by a constant amount equal to 0.62 $I(7.4)$, i.e., by an amount equal to the value of the small angle scattering, and I_∞ satisfying Eq. (2).

The integrations were terminated at $s=7.4$A^{-1}, equivalent to the assumption $i(s)=0$ for $s>7.4$A^{-1}.

In Case (b) the amplitude of the short wavelength ripples was increased. The curve obtained in (c) was very nearly the same form as in (a) but of approximately twice the magnitude. Of the three curves, (a) gave the smallest excursions into the region of negative density and is therefore more physically realistic. Similar behavior was found for oxygen: the subtraction of a constant as in (c) produced negative densities in the region $1.8\text{A}<r<2.3$A where previously the density was nearly zero. It is felt that these results support the decision to use the total scattered intensity in Eq. (1).

The radial distribution function $4\pi r^2\rho(r)$ is such that $4\pi r^2\rho(r)dr$ gives the number of atoms between r and $r+dr$ and is plotted in Fig. 4 for each of the liquids. The radial distribution function is greater than $4\pi r^2\rho_0$ at regions where the density is greater than average. The existence of oscillations in this function indicates a tendency for the atoms to arrange themselves in groups of neighbors. Except for the first neighbors in nitrogen and oxygen, where the density is zero on either side of the peak, the groups are not clearly separated. As r increases the distinct character of the groups is rapidly lost, as can be seen by comparing the magnitude of the oscillations in Fig. 3 with the value of $4\pi r^2\rho_0$. The finite resolution of the experiment contributes to the lack of distinctness.

For small values of r, it is usual to divide atoms into groups associated with the peaks. Some freedom exists in the division of atoms between the peaks. The method used in the present investigation is to write

$$T_n=2(N-T_{n-1}-T_{n-2}\cdots T_1), \qquad (3)$$

where T_n = number of atoms assigned to nth peak, and N = total number of atoms out to the position of the nth peak. N was obtained by integration of the radial distribution function.

Equation (3) insures that the atoms assigned to a peak are evenly divided between the two sides of the peak.

In Table I the positions and the number of atoms per peak have been listed for each of the three liquids. From the number of atoms under the first peak in nitrogen and oxygen the average number of atoms per molecule has been deduced, and this has been used to calculate the number of molecules under each peak.

TABLE I. Positions and magnitudes of atomic concentrations.

Liquid nitrogen 77.4°K			Liquid oxygen 90°K			Liquid argon 86.3°K	
Radius A	Number of atoms	Number of molecules (2 atoms each)	Radius A	Number of atoms	Number of molecular groupings (2.5 atoms each)	Radius A	Number of atoms
1.1	1.0		1.25	1.50		1.45	0.5[a]
4.4	23.6	11.8	4.2	26.0	10.4	2.6	0.6[a]
						3.9	8.2
						5.2	6.4[a]
						6.2	11.0[a]
						7.3	18.6

[a] As discussed in the text, these probably result from the limitation on the experimental range of s and experimental error near this limit.

A study of Table I shows that nitrogen has 1.0 atom centered around a maximum at 1.1A.[16] The existence of this 1 atom supports earlier evidence that nitrogen is diatomic in the liquid state. The second peak occurs at 4.4A and the number of neighbors at this spacing is 23.6 atoms or 11.8 diatomic molecules. Within experimental error this is equal to 12 molecules corresponding to a close packed structure. The spacing of 1.1A is in agreement with the value of 1.09A of the diatomic molecule. X-ray measurements on the liquid give 1.3A. In the x-ray analysis, in addition to the peak at 1.3A, peaks were found at 2.6A, 4.0A and 4.8A. It would appear that the peaks at 4.0A and 4.8A in the x-ray analysis have combined to give a peak at 4.4A in the neutron analysis. In the neutron analysis no peak is found at 2.6A, possibly owing to improved information at the larger values of s.

The results for liquid oxygen show 1.5 atoms centered around $r=1.25$A. The existence of more than one neighbor at $r=1.25$A indicates that oxygen is not solely diatomic in the liquid state. The existence of O_4 has been suggested from the results of both spectroscopic and magnetic measurements on mixtures of liquid oxygen and nitrogen.[17] From the magnetic susceptibilities of such mixtures, Lewis[18] calculated that liquid oxygen at 77.4°K should contain 40 percent by weight of O_4. Assuming that the molecule O_4 is tetrahedral with a spacing between atoms equal to that of the O_2 molecule, a simple calculation on the basis of 1.5 nearest neighbors would indicate the existence of 25 percent by weight of O_4 at 90°K. The agreement between the value of 40 percent by weight as determined from the magnetic measurements for oxygen at 77.4°K and the value of 25 percent by weight determined here for oxygen at 90°K is not unreasonable considering the experimental error which might be expected. The peak found at 4.2A has an area which corresponds to the existence of 26 atoms. On the basis of the 1.5 molecular neighbors, the 26 atoms would correspond to 10.4 molecular neighbors, which is not significantly different from the 12 neighbors required for close packing. X-ray measurements[6] have given peaks at 1.3A, 2.2A, 3.4A, and 4.2A. The appearance in the x-ray analysis of 1.08 atoms at the 1.3A spacing together with the peak at 2.2A has been interpreted as arising from the existence of molecules of O_3. The positions of the peaks at 1.3A and 4.2A correspond well with the neutron determination, but in the neutron determination no peak was found to correspond with the x-ray peak at 2.2A. Sugawara[15] has concluded that this peak is spurious. The 3.4A peak appears to have become part of the broad peak at 4.2A.

The results for liquid argon are more difficult to interpret. An examination of the correlation function (Fig. 3) shows that the curves for liquid oxygen and nitrogen vary smoothly with r, while there appears to be high-frequency oscillations superimposed on the main pattern of argon. As has been pointed out earlier, the validity of the peak at 1.45A is in doubt. From Table I it may be seen that other peaks occur at 2.6A, 3.9A, 5.2A, 6.2A, and 7.3A. The main peaks have been italicized. There is a reasonable agreement between the present results and those obtained from the comprehensive work of Eisenstein and Gingrich with x-rays[19,20] where peaks were found at 3.79A, 5.3A, and 7.3A. The number of atoms under the first main peak at 3.9A was 8.2, if the area under the subsidiary peaks is not included. This is considerably less than the 12 neighbors required for a close packed structure. In solid argon an atom has 12 nearest neighbors. The number of neighbors at the spacing of 3.8A in the liquid has been found by x-rays at three temperatures.[19,20] The results have been plotted in Fig. 5, together with the value 8.2 from the neutron measurement. There appears to be reasonable agreement between the results of the x-ray

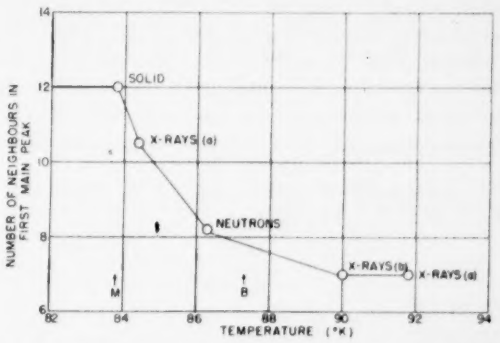

FIG. 5. The number of neighbors in the first main peak at 3.8A for liquid argon as a function of temperature. The x-ray results (a) and (b) were taken from the papers by Eisenstein and Gingrich (see references 19, 20) while the neutron value is from the present investigation. Point M represents the melting point (83.8°K and 512 mm Hg), while B represents the normal boiling point (87.5°K).

[16] The positions of the peaks will now be given at the maxima in the function $4\pi r^2\rho(r)$. The values quoted earlier are the positions of the peaks on the function $4\pi r^2[\rho(r)-\rho_0]$.

[17] M. and B. Reuhmann, *Low Temperature Physics* (Cambridge University Press, London, 1937), p. 228.

[18] G. N. Lewis, J. Am. Chem. Soc. **46**, 2027 (1924).

[19] A. Eisenstein and N. S. Gingrich, Phys. Rev. **58**, 307 (1940).

[20] A. Eisenstein and N. S. Gingrich, Phys. Rev. **62**, 261 (1942).

determinations and the present neutron determination. An examination of the curve (Fig. 5) shows that the number of neighbors under the peak at 3.9A falls rapidly from 12 at 84°K to about 7 at 90°K, beyond which the curve would appear to fall more slowly. This means that the structure of the liquid changes rapidly for temperatures just above the melting point. Since the number of atoms per unit volume is approximately constant, a decrease in the number of atoms at a given spacing requires that these atoms appear elsewhere. It is intended to find the effect of temperature on the positions and heights of the peaks and to check the present results when experimental work can be resumed.

ACKNOWLEDGMENT

The authors wish to thank Dr. H. Gellman of the Theoretical Physics Branch for calculations of the Fourier transforms on the FERUT Computer and Miss B. Sears for assistance in similar calculations. Thanks are also due to Mr. W. McAlpin for the mechanical design of the cryostat, and to Mr. W. Woytowich for technical assistance.

PHYSICAL REVIEW VOLUME 92, NUMBER 5 DECEMBER 1, 1953

Concentration of Uranium and Lead and the Isotopic Composition of Lead in Meteoritic Material

C. PATTERSON AND H. BROWN, *California Institute of Technology, Pasadena, California*
G. TILTON, *Department of Terrestrial Magnetism, Carnegie Institution, Washington, D. C.*

AND

M. INGHRAM, *University of Chicago, Chicago, Illinois and Argonne National Laboratory, Lemont, Illinois*

(Received July 27, 1953)

The cosmic abundance of lead and uranium have been determined by studying the lead and uranium contents of meteoritic materials. Lead is found to be present to 8×10^{-3} atom/10 000 atoms of silicon, and uranium to 1×10^{-4} atom/10 000 atom of silicon. The new value for lead removes the hump in the cosmic abundance curve in the 206–208 mass region. The relative primordial abundances of lead isotopes of mass 204, 206, 207, and 208 are found to be 1:9.4:10.3:29.2, respectively.

THE concentrations of uranium in some stone meteorites and troilite from an iron meteorite were determined by the isotope dilution method.[1,2] The concentrations of lead in a stone and iron meteorite and in troilite from an iron meteorite were determined colorimetrically, using Pb^{210} for yield corrections.[3] The lead samples so isolated were analyzed in a mass spectrometer, using the surface ionization method.[2] The effect of contamination upon the composition of the lead in the sample from the stone meteorite is as yet uncertain and, therefore, only the composition of the troilite and the iron meteorite lead is reported here. The results are given in Table I.

TABLE I. Uranium and lead in meteoritic material.

Sample	U concentration (ppm)	Pb concentration (ppm)	Pb composition (atomic ratios) 206/204	207/204	208/204
Canyon diablo troilite	0.009 ±0.003	18 ±1	9.41	10.27	29.16
Canyon diablo metal phase	—	(0.37 ±0.05)[a]	(9.7)[a]	(10.5)[a]	(29.3)[a]
Modoc (total)	0.011 ±0.002	0.9 ±0.1	—	—	—
Norton county (total)	0.010 ±0.003				

[a] Corrected for terrestrial lead contamination.

Of the uranium concentrations in stone meteorites that have been previously reported,[4–10] only the radon determinations of G. Davis agree with the values reported here. His values are given in Table II. It is believed that the higher values obtained by the early investigators resulted from a failure to exercise proper precautions in excluding moisture from electroscopes during radon measurements. Evans, Kip, and Moberg[11] recognized the critical nature of this phenomenon when they obtained anomalously high values for the radon content of sea water until the most stringent precautions were taken to dry the gases in the electroscope chamber. Other possible sources of error might be contamination

[1] G. Tilton, Atomic Energy Commission Report AECD-3182, 1951 (unpublished).
[2] G. Tilton *et al.*, Bull. Geol. Soc. Amer. (to be published).
[3] C. Patterson, Atomic Energy Commission Report AECD-3180, 1951 (unpublished).
[4] R. J. Strutt, Proc. Roy. Soc. (London) **A77**, 481 (1906).
[5] T. Quirke and L. Finkelstein, Am. J. Sci. **44**, 237 (1917).
[6] G. Halledauer, Wien. Ber. **134** (IIa), 39 (1925).
[7] A. Holmes, Bull. Natl. Research Council **81**, 418 (1931).
[8] F. Paneth and W. Koeck, Z. physik. Chem., Bodenstein-Festband, 145 (1931).
[9] J. R. Horan, Oak Ridge Institute of Nuclear Studies, Oak Ridge, Tennessee reports a uranium concentration greater than 3 ppm in a carbonaceous chondrite from Murray, Callaway County, Kentucky (to be published in a new journal, Meteoritics). Mr. W. Nichiporuk of the California Institute of Technology has checked this meteorite by alpha counting and finds less than about 0.4 ppm of uranium plus thorium (the limit of the method).
[10] G. L. Davis, Am. J. Sci. **248**, 107 (1950).
[11] Evans, Kip, and Moberg, Am. J. Sci. **36**, 241 (1938).

from reagents or glass vessels. Some of the values of uranium concentrations in iron meteorites reported by Paneth[12,13] and by Davis[10] are given in Table II.

The lead concentrations in Table I agree with the spectroscopic value for troilite reported by Goldschmidt and Hormann,[14] but are in disagreement with their values for stone meteorites and the values for stone and iron meteorites and troilite reported by the Noddacks.[15–17] These values are given in Table III.

Studies of meteoritic uranium and lead are of interest because of their relation to problems concerning cosmology and geochemistry. The values given in Tables I and II indicate that the relative cosmic abundance of uranium is 1×10^{-4} atom/10 000 atoms of silicon and that of lead is 8×10^{-3} atom/10 000 atoms of silicon according to the conventions of Brown[18] and Urey,[19]

TABLE II. Previously-reported uranium concentrations on meteoritic material.

Stone meteorite	U concentration (ppm)	Observer
Cumberland	0.010	G. Davis[a]
Shaw	0.048	G. Davis[a]
Iron meteorites		
Average of seven	0.0011	G. Davis[b]
Average of six	0.0025	Arrol, Jacobi, and Paneth[c]

[a] See reference 10.
[b] See reference 10.
[c] See reference 13.

and that (1) a large distinct maximum in the mass 206, mass 208 region of the cosmic-abundance curve, as was evident from previously reported data, does not exist; (2) the previously reported significant decrease between mass 209 and mass 238 is confirmed by our data; (3) the relative primordial abundances of the isotopes of lead are 1:9.4:10.3:29.2 with increasing mass respectively.

[12] F. Paneth, Naturwiss. **19**, 164 (1931).
[13] Arrol, Jacobi, and Paneth, Nature **149**, 235 (1942).
[14] V. M. Goldschmidt, Skrifter Norske Videnskaps-Akad. Oslo. I. Mat.-Natur. Kl. **1937**, No. 4 (1938).
[15] I. Noddack and W. Noddack, Naturwiss. **18**, 757 (1930).
[16] I. Noddack and W. Noddack, Z. physik. Chem. **A154**, 207 (1931).
[17] I. Noddack and W. Noddack, Svenk. kemisk Tidskrift **46**, 173 (1934).
[18] H. Brown, Revs. Modern Phys. **21**, 625 (1949).
[19] H. Urey, Phys. Rev. **88**, 248 (1952).

TABLE III. Previously-reported lead concentrations in meteoritic material.

Pb concentration (ppm)			
Stone meteorites	Iron meteorites	Troilite from iron meteorites	Observer
4	...	20	Goldschmidt and Hormann[a]
5	53	710	I. and W. Noddack[b]
2	60	470	I. and W. Noddack[c]
18	...	...	I. and W. Noddack[d]

[a] See reference 14.
[b] See reference 15.
[c] See reference 16.
[d] See reference 17.

Goldberg, Uchiyama, and Brown[20] have shown by a detailed study of some trace elements in a large number of iron meteorites that extensive, though perhaps systematic, variations in the concentrations of those trace elements occur. For this reason, the values given here might differ somewhat from those chosen as significant after a detailed study of these two elements in meteoritic material has been made. High concentrations in minor phases of heterogeneous occurrence, as indicated by the concentration of lead in troilite, may produce an uncertainty of a factor of about 2 in the concentration of these two elements. The values given here are probably significant to within a factor of about 5 of the meteoritic concentrations, assuming they do not represent extremes of possible variations. Brown has proposed that lead isolated from iron meteorites might be used as a measure of the isotopic composition of lead at the time of formation of the solar system.[21,22] On the basis of these results the concentrations of uranium relative to lead are so small that the isotopic composition of the lead in Canon Diablo troilite could be that present at the time the meteorite was formed. It must be emphasized, however, that in addition to the obscure nature of the relation between meteoritic and other stellar material, the effects of chemical fractionation during the process of meteorite formation upon estimates of the cosmic abundances of uranium and lead are as yet unknown.

[20] E. Goldberg *et al.*, Geochim. et Cosmochim Acta **2**, 1 (1951).
[21] H. Bruwn, Phys. Rev. **72**, 348 (1947).
[22] Initial attempts to study this lead were unsuccessful because of contamination by terrestrial lead. [H. Suess and A. Nier, 1948 (unpublished); Patterson, Brown, and Nier, 1948 (unpublished).]

The Decay Scheme of Ag^{108}†

M. L. Perlman, W. Bernstein, and R. B. Schwartz*
Brookhaven National Laboratory, Upton, New York

(Received August 6, 1953)

The radiations of 2.3-minute Ag^{108} have been examined with scintillation and proportional counter spectrometers and with a coincidence spectrometer. The transitions and their abundances were found to be as follows: β^- 1.77 Mev (97.3 percent); β^- 1.15 Mev accompanied by γ of energy 0.62 Mev (0.8 percent); β^+ (0.14 percent); and K capture to ground and excited states of Pd^{108} (1.6 percent). Gamma rays of energies 0.60 Mev and 0.43 Mev were found to accompany K capture; the abundances of the different capture transitions were measured. Spin and parity assignments were made.

WITH the exception of one study made with coincidence circuitry and counter spectrometry,[1] there has been little reported concerning the radiations of Ag^{108}. Because of the general interest in electron-capture decaying nuclides and because of recent improvements in the techniques of coincidence spectrometry, it was considered reasonable to re-examine the radiations of Ag^{108}.

The Ag^{108} activity was made by the activation in the Brookhaven nuclear reactor of small samples of metallic silver, less than 0.1 mg per cm^2 in thickness, deposited on cellophane by evaporation. For most experiments an irradiation time of two minutes was chosen to give a favorable ratio for the yield of the 2.3-minute Ag^{108} to the yields of 39-second Ag^{109m}, 24-second Ag^{110}, and 44-second Ag^{107m}.[2]

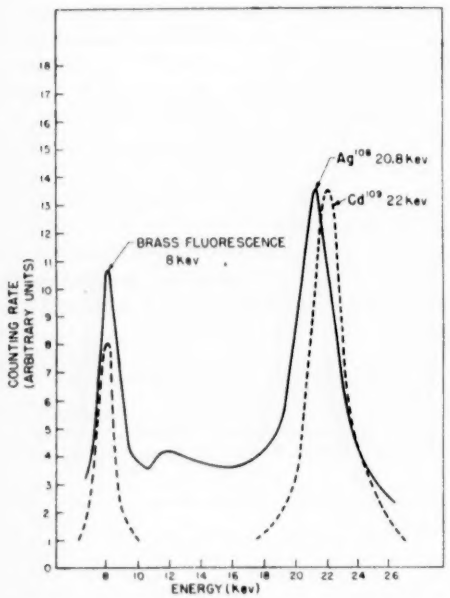

FIG. 1. Spectral distribution of x-radiations from Ag^{108} and Cd^{109}. The peaks at 8 kev represent fluorescence radiation from the brass counter wall.

X-RAY AND BETA-RAY MEASUREMENTS

The x-rays were detected by a brass-walled proportional counter, 12 inches long and 4 inches in diameter; the gas filling consisted of 95 percent argon and 5 percent methane at a pressure of 2 atmospheres. Beryllium absorber, 937 mg per cm^2, was used to prevent β radiations from entering the counter. Amplified counter pulses were examined with a gray-wedge spectrometer[3] and with a single channel analyzer. In Fig. 1 are shown the gray-wedge spectrum of Ag^{108} and, for comparison, that of Cd^{109}, a source of Ag K x-rays. It is seen that the energy of the Ag^{108} radiation, about 4 percent less than that of the Ag K x-ray, corresponds to that of Pd K x-radiation, which would accompany K capture. The x-ray intensity was found to decay with the characteristic period of Ag^{108}. No change in the pulse-height distribution could be observed when a source 10 times as thick as the standard ones was used. It was thus established that the contribution of Ag fluorescence from the beta activity to the x-ray intensity from the thin samples could not have been more than 5 percent. It was assumed that a negligible contribution to the x-ray intensity was made by internal conversion of gamma rays. This assumption will be considered in a following section. The absolute x-ray disintegration rate was determined by measurement of the x-ray pulse-height distribution with the single channel analyzer. Points on the pulse-height distribution curve were corrected for decay occurring during the measurements. From the area under the curve, after the bremsstrahlung contribution had been subtracted, the absolute K electron-capture rate was derived by a method previously described.[4] For Pd K x-rays the transmission of the beryllium absorber and window was 80 percent and the absorption of the counter gas was 21 percent; the fluorescence yield of Pd was taken to be 0.81.[5] Immediately after the x-ray pulse-height distri-

† Work carried out under auspices of the U. S. Atomic Energy Commission.

* Present address: Sloane Physics Laboratory, Yale University, New Haven, Connecticut.

[1] M. Goodrich and E. C. Campbell, Phys. Rev. **85**, 742 (1952).

[2] *Nuclear Data*, National Bureau of Standards Circular 499 (U. S. Government Printing Office, Washington, D. C., 1950).

[3] Bernstein, Chase, and Schardt, Rev. Sci. Instr. **24**, 437 (1953).

[4] Friedlander, Perlman, Alburger, and Sunyar, Phys. Rev. **80**, 30 (1950).

[5] Broyles, Thomas, and Haynes, Phys. Rev. **89**, 715 (1953).

bution had been scanned, the beryllium absorber was removed and the total rate in the proportional counter was measured. This rate, corrected for decay, for backscattering, and for window absorption in accordance with the beta energy determination to be described, was taken to be the product of the beta disintegration rate and the geometry; and it was directly compared with the K-capture rate obtained in the same geometry. The ratio of the K-capture rate to the beta rate was calculated to be 0.016 ± 0.001. The ratio of L capture to K capture is expected to be 0.11.[6]

The beta spectrum was obtained by gray-wedge analysis of the pulse-height distribution from a scintillation counter; the anthracene crystal used was 1.5 cm in thickness. Energy and resolution calibrations were made with the Cs^{137} internal conversion electron line (624 kev). The thickness of the Ag^{108} source was less than 0.1 mg per cm^2; there was no backing other than the 3.5 mg per cm^2 Cellophane. Figure 2 shows the Fermi plot derived from the observed pulse-height distribution corrected for the variation in resolution with pulse height.[7] Within the accuracy of the measurement the spectrum appears to be simple with a maximum energy of 1.77 ± 0.06 Mev. The deviation from the line of points below 0.8 Mev is attributed to scattering of betas out of the crystal.

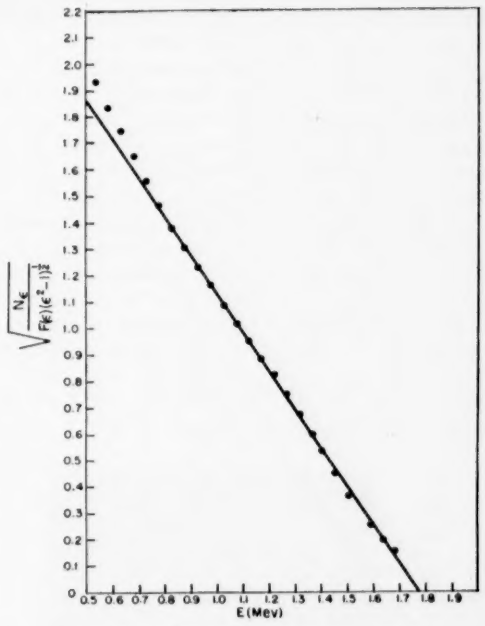

FIG. 2. Fermi plot for the β radiations of Ag^{108}.

GAMMA-RAY MEASUREMENTS

The gamma rays from Ag^{108} were examined with the gray-wedge spectrometer and scintillation detector. A DuMont Type K1186 photomultiplier tube was used together with a NaI(Tl) crystal 3 cm in diameter and 2 cm high; this combination had a resolution of 8 percent for the 662-kev gamma ray of Cs^{137}. The spectrum, as displayed on the instrument, is shown in Fig. 3. Beryllium absorbers served to screen beta rays from the crystal. Gamma rays of energies 616 ± 20 kev, 510 ± 20 kev, and 435 ± 20 kev may be identified. The indication of a peak in the vicinity of 200 kev is probably attributable to backscattering; and the pulse continuum, which increases in intensity at low energies, is produced by bremsstrahlung from beta rays. The character of the spectrum did not change as the sources decayed.

COINCIDENCE MEASUREMENTS

Coincidence measurements were made with pairs of scintillation detectors appropriate to the various radiations and a coincidence gray-wedge spectrometer.[8] With this instrument it is possible to display all events in one detector which occur in time coincidence with events of selected amplitude in a second detector. The effective coincidence time is 10^{-7} sec. Accidental coincidence effects are evaluated by the introduction of a delay line, 5×10^{-7} sec, between the selecting detector and the coincidence circuit. Data were recorded with a Polaroid Land Camera. No information could be obtained earlier than 2 minutes after irradiation because of high accidental rates produced by the 24-second Ag^{110} activity.

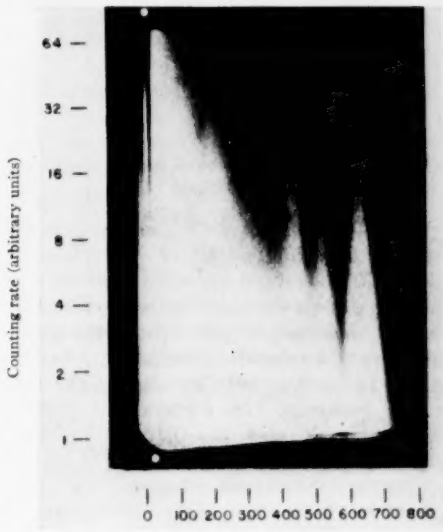

FIG. 3. Gamma-ray spectrum of Ag^{108}.

[6] M. E. Rose and J. L. Jackson, Phys. Rev. **76**, 1540 (1949).
[7] G. E. Owen and H. Primakoff, Phys. Rev. **74**, 1406 (1948).
[8] Chase, Bernstein, and Schardt, Phys. Rev. **90**, 353 (1953); Chase, Bernstein, and Schardt, Brookhaven National Laboratory Report BNL-237 (T37) (unpublished).

Gamma-gamma coincidence measurements were made with two 3-cm×2-cm NaI(Tl) detectors. Sufficient beryllium absorber was interposed between sample and detectors to screen out β rays. In coincidence with the 435-kev gamma ray there was observed only a gamma ray of energy 602 kev, approximately three percent lower in energy than the 616-kev line which appeared in the "singles" gamma spectrum. That the 510-kev gamma line represents a ground-state positron transition is shown by the facts that it was in coincidence only with a 510-kev gamma ray and that these coincidences disappeared when the counter-source-counter geometry was other than 180 degrees. The presence of the annihilation line as an internal reference made possible the definite detection of the small energy shift from the 616-kev line in the "singles" spectrum to the 602-kev line in the coincidence spectrum.

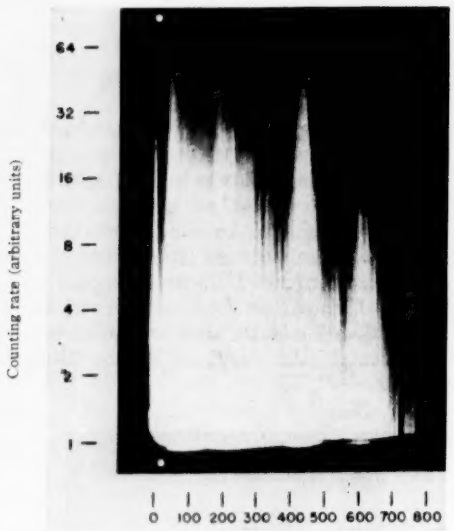

FIG. 4. Spectrum of gamma rays in coincidence with x-rays from Ag^{108}.

For the x-ray–gamma-ray coincidence measurements one of the thick NaI(Tl) detectors was replaced by a 2 mm deep NaI(Tl) crystal in order to provide a more favorable x to gamma sensitivity ratio. Beryllium beta-ray absorbers were used. Figure 4 shows the spectrum of gamma rays in coincidence with the x-rays; the lines at 435 kev and at 602 kev appear. The inverse experiments confirmed the existence of these x-γ coincidences. It is seen in the x-γ coincidence photograph that the 602-kev photopeak is much less intense than the 435-kev peak, whereas in the "singles" photograph the 616-kev line is the more intense. The 616-kev "singles" line is therefore composed of two lines not resolved from each other, only one of which, the 602-kev, is in coincidence with the x-rays. Examination of the "singles" spectrum in the region of 1 Mev gave no evidence for the possible cross-over transition. From the areas under the 435-kev and 602-kev photopeaks, the relative intensities of the two gamma transitions were calculated to be 1.00 and 0.79±0.12, respectively; correction was made for variation of photopeak efficiency in the scintillator[9] with energy. These intensities are interpreted to mean that of the capture events which produce the excited states of Pd^{108}, 79 percent give rise to the 602, 435 cascade and 21 percent give rise only to the 435-kev lower state. The area of the 435-kev photopeak was derived from the coincidence spectrum after subtraction of the Compton contribution from the 602-kev gamma ray and of a small bremsstrahlung contribution.

All coincidence spectra observed with the 180-degree geometry show a broad peak in the vicinity of 200 kev, which disappeared when the displaying detector was so positioned as not to intercept backscattered radiation from the other detector. This 200-kev peak may be what was previously reported to be a 190-kev gamma ray.[1]

The anthracene detector described above was used in combination with one of the thick NaI(Tl) detectors for the β-γ coincidence measurements. A beryllium beta-ray absorber was placed between the gamma detector and the source; and the discriminator bias on the selecting anthracene detector was set so as to cut off the response to the x-rays. The 616-kev line and annihilation radiation were observed. The 616-kev gamma ray is therefore associated with beta decay; however, the 510-kev line arises from the detection in the NaI crystal of annihilation quanta of the positrons whose kinetic energy is expended in the anthracene detector.

In order to determine the fraction of K electron-capture events which lead to excited states of Pd^{108}, the measured ratio of x-γ coincidences to x-rays in Ag^{108} was compared with the ratio measured in the same geometry for 65-day Sr^{85}. The gamma-ray detector was operated so as to be sensitive to essentially all of the pulse-height distribution of the gamma rays involved. The Sr^{85} activity was chosen as a reference because all capture transitions in it have been found to be followed by one gamma ray of energy 513 kev,[10–12] and because this gamma-ray energy is not greatly different from those associated with electron capture in Ag^{108}. Corrections for the variation with energy of the NaI efficiency are therefore relatively small. Corrections for x-ray fluorescence yield, sensitivity, and absorption are unnecessary because they cancel in each ratio. The

[9] P. R. Bell (unpublished data).
[10] M. Ter-Pogossian and F. T. Porter, Phys. Rev. **81**, 1057 (1951).
[11] Sunyar, Mihelich, Scharff-Goldhaber, Goldhaber, Wall, and Deutsch, Phys. Rev. **86**, 1023 (1952).
[12] W. S. Emmerich and J. D. Kurbatov, Phys. Rev. **85**, 149 (1952).

activity was produced by the irradiation in the Brookhaven nuclear reactor of $SrSO_4$ enriched[13] in Sr^{84}. No gamma radiation of energy other than 513 kev was observed at the time when the Sr^{85} measurements were made. The contribution of radiations other than x-rays to the count-rate in the thin NaI detector was determined, for the Sr^{85}, by the interposition of a thin copper absorber between source and detector. In the case of the Ag^{108} the fraction of the measured count-rate attributable to Pd K x-rays in a pulse-height interval which included the Pd K x-rays was evaluated from a gray-wedge photograph; the absorber method could not be used because it would remove some bremsstrahlung in addition to x-rays. The fraction of Pd x-rays was 0.70 ± 0.05. A difficulty associated with the use of Sr^{85} in this experiment is that the 513-kev gamma ray has a half-life of $(0.9\pm0.2)\times10^{-6}$ sec.[11] This means that there is recorded only a fraction of the coincidences, the fraction being a function of the ratio of the coincidence resolution time to the half-life. Because of the uncertainty in the lifetime, measurements on the Sr^{85} were made at two resolution times, 0.12×10^{-6} sec and $(1.5\pm0.2)\times10^{-6}$ sec. The two values for the ratio (x-γ coinc)/x calculated for infinite resolution time agreed within 10 percent; and their average, 0.066 ± 0.006, was used. In the case of the Ag^{108} the ratio (x-γ coinc)/x was 0.0183 ± 0.0015. The individual x, γ, and coincidence count-rates decayed with the characteristic 2.3 to 2.4-minute half-life. The value, corrected for total NaI gamma efficiencies,[9] of the ratio

$$\frac{(\text{x-}\gamma)\ \text{coinc/x Ag}^{108}}{(\text{x-}\gamma)\ \text{coinc/x Sr}^{85}},$$

was calculated to be 0.155 ± 0.021. In the Ag^{108}, therefore, 15 percent of the capture transitions are to excited states of Pd^{108}, and the remaining 85 percent are to the ground state.

From the photopeak areas in the "singles" gamma-ray spectrum, the abundances of the annihilation radiation and of the sum of the 602- and 616-kev transitions were determined relative to the abundance of the 435-kev transition. The appropriate corrections for efficiency and backgrounds were made. Because the abundance of the 602-kev gamma relative to that of the 435-kev gamma was already determined and because the abundance of the 435-kev gamma transition in the scheme was known, the abundances of all radiations of Ag^{108} could be evaluated. The final results are given in the decay scheme shown in Fig. 5. It may be noted that the positron abundance is less than the upper limit established by Barber.[14]

[13] Supplied by the Y-12 plant, Carbide & Carbon Corporation, through the Isotopes Division, U. S. Atomic Energy Commission, Oak Ridge, Tennessee.

[14] W. C. Barber, Phys. Rev. **72**, 1156 (1947).

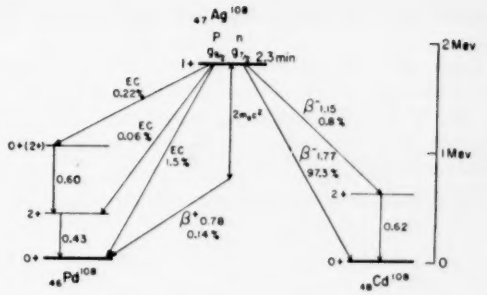

FIG. 5. Decay scheme of Ag^{108}.

DISCUSSION

The assignments, based on the experimental results, of 435 kev and 616 kev as the energies for the first excited states of Pd^{108} and Cd^{108}, respectively, are consistent with expectations based on the observed excited states of neighboring even-even nuclei.[15] The value of logft for the transition to the ground state of Cd^{108} is calculated to be 4.6; for the upper state transition logft is 6.0. The two β^- transitions thus appear to be allowed; and if the Cd^{108} ground and excited state spins and parities are taken to be 0+ and 2+, respectively,[15] the spin-parity assignment for Ag^{108} is restricted to 1+. This assignment is in agreement with the expectation of Nordheim.[16] Because the Pd^{108} ground-state assignment is 0+, the positron and electron-capture ground-state transitions must be allowed; and the K/β^+ ratio calculated from experiment may be used to evaluate the energy of these transitions.[17] The positron energy is thus determined to be 0.78 ± 0.05 Mev. For the transition to the ground state and first and second excited states of Pd^{108} the values of logft are 4.8, 6.0, and 4.8, respectively. The first excited state of Pd^{108} is expected[15] to have spin 2 and even parity, so that the transition to this state should be allowed. If, from its ft value, the transition to the second excited state is taken to be allowed, the choice for spin-parity assignment for this state is limited to either 0+ or 2+. Although 0+ would appear to be the preferred assignment because of the absence of the cross-over transition, the value 2+ cannot be excluded on this basis.[18]

The assignment of spins and parities to the Cd^{108} and Pd^{108} levels makes possible the evaluation of the internal conversion coefficients for the gamma-ray transitions.[19]

[15] G. Scharff-Goldhaber, Phys. Rev. **90**, 587 (1953).

[16] L. W. Nordheim, Revs. Modern Phys. **23**, 322 (1951).

[17] E. Feenberg and G. Trigg, Revs. Modern Phys. **22**, 399 (1950).

[18] J. J. Kraushaar and M. Goldhaber, Phys. Rev. **89**, 1081 (1953); also A. de-Shalit and M. Goldhaber, Phys. Rev. **92**, 1211 (1953).

[19] Rose, Goertzel, Spinrad, Harr, and Strong, Phys. Rev. **83**, 906 (1951).

X-rays from conversion are thus calculated to contribute 1/300 of the x-ray intensity from capture.

From the energies of the ground-state transitions, the mass difference Cd^{108} minus Pd^{108} is estimated to be 30 ± 80 kev. This estimate is believed to be more accurate than that obtainable from the mass measurements now available.[20]

[20] R. E. Halsted, Phys. Rev. **88**, 666 (1952).

ACKNOWLEDGMENT

We would like to thank R. L. Chase, who designed the coincidence spectrometer, and A. W. Schardt for their cooperation. The Sr^{84} was furnished by the courtesy of A. W. Sunyar; the Ag foils were prepared by A. Weinstein. The existence of unexpectedly weak 2+ to 0+ cross-over transitions was pointed out to us by M. Goldhaber.

PHYSICAL REVIEW VOLUME 92, NUMBER 5 DECEMBER 1, 1953

Nuclear Quadrupole Resonance of the Stable Gallium Isotopes*

H. G. DEHMELT
Department of Physics, Duke University, Durham, North Carolina
(Received August 6, 1953)

Eight absorption lines have been observed in a sample of polycrystalline $GaCl_3$. Of these, six are ascribed to the Cl isotopes. The remaining two, which are due to the stable gallium isotopes $Ga^{69,71}$, allow us to determine the ratio of their quadrupole moments. $Q_{Ga^{69}}/Q_{Ga^{71}}=1.5867\pm0.0004$, in agreement with earlier atomic beam measurements.

NUCLEAR quadrupole resonance[1,2] in the spectral region from 9.3 to 36.8 Mc/sec has been investigated in a sample of about 10 g $GaCl_3$. A recording superregenerative spectrometer was used, employing 30-cps Zeeman modulation.[3] All together eight absorption lines were observed whose frequencies are given in Table I. As the spins of the gallium isotopes $Ga^{69,71}$ as well as the chlorine isotopes $Cl^{35,37}$ are $\frac{3}{2}$, only the one transition $m=\pm\frac{1}{2}\leftrightarrow\pm\frac{3}{2}$ is expected for each of the four nuclear species. With the help of the known ratio[4,5] of the chlorine quadrupole moments, $Q_{Cl^{35}}/Q_{Cl^{37}}=1.26878\pm0.00015$, six of the observed lines could be grouped into three pairs corresponding to three different lattice sites for the Cl atoms. The two remaining lines, whose frequency ratio is found to be the same as the ratio of the gallium quadrupole moments, $Q_{Ga^{69}}/Q_{Ga^{71}}=1.5868\pm0.0004$, known from atomic beam experiments,[6] were assigned to the gallium isotopes. These lines were 5 kc/sec wide as compared to a width of 2 kc/sec for the Cl lines; also, in contrast to the Cl lines, they showed signs of partial saturation for the same rf power level. Both aspects can be understood in view of the fact that the magnetic moments of the gallium isotopes are two to three times larger than those of the Cl isotopes.

TABLE I. Absorption frequencies in $GaCl_3$.

Nucleus	Lattice site	T °C	Frequency kc/sec	Frequency ratio of isotopic pairs
Ga^{69}		31.8±0.1	29 060±2	1.5867±0.0002
Ga^{71}			18 315±1	
Cl^{35}	1*a*		20 225±3	1.2692±0.0004
Cl^{37}			15 935±2	
Cl^{35}	1*b*	33.2±0.6	19 084±3	1.2689±0.0004
Cl^{37}			15 040±2	
Cl^{35}	2		14 667±2	1.2686±0.0003
Cl^{37}			11 562±1	

The ratio of the observed gallium frequencies should agree with that of the quadrupole moments at least to the same degree as given by the experimental error of 0.02 percent, since, for molecules which are made up from atoms that heavy, the effects of small isotopic differences in zero-point vibration on the field gradient are proven to be negligible.[5] Therefore, we obtain $Q_{Ga^{69}}/Q_{Ga^{71}}=1.5867\pm0.0004$, in close agreement with the atomic beam value.

Investigations of other gallium compounds are under way.

* Work supported by the U. S. Office of Ordnance Research.
[1] H. G. Dehmelt and H. Krüger, Z. Physik **129**, 401 (1951); H. G. Dehmelt, Am. J. Physics (to be published).
[2] R. V. Pound, Phys. Rev. **79**, 685 (1950).
[3] H. G. Dehmelt, Phys. Rev. **91**, 313 (1953).
[4] R. Livingston, Phys. Rev. **82**, 289 (1951).
[5] Wang, Townes, Schawlow, and Holden, Phys. Rev. **86**, 809 (1952).
[6] G. E. Becker and P. Kusch, Phys. Rev. **73**, 584 (1948).

The Directional Correlation of the Pb^{204} $\gamma-\gamma$ Cascade*

H. FRAUENFELDER, J. S. LAWSON, JR., W. JENTSCHKE, AND G. DEPASQUALI
University of Illinois, Urbana, Illinois

(Received August 3, 1953)

The directional correlation of the Pb^{204} $\gamma-\gamma$ cascade has been measured in chemical compounds and in a liquid Pb–Tl alloy. The values for the anisotropy of the Pb^{204} cascade in the chemical compounds vary between 0.08 ± 0.04 and 0.46 ± 0.04, thus showing a pronounced influence of extranuclear fields. The anisotropy in the liquid Pb–Tl alloy, 0.49 ± 0.05, excludes the assignment 7^- for the second excited state of Pb^{204}. The only decay scheme compatible with all experimental data requires the assignments 2^+ and 6^+ to the first and second state, respectively. The first γ transition in Pb^{204} must be a mixture of approximately 90 percent $E4$ and 10 percent $M5$.

I. INTRODUCTION

RECENT experimental[1–3] and theoretical[4–6] evidence indicates that the influence of extranuclear fields in solids and liquids on the directional correlation of nuclear γ rays is largely (or entirely) due to the interaction of the nuclear quadrupole moment with inhomogeneous electric fields. Most of the experimental work up to now has been done with the $\gamma-\gamma$ cascade of Cd^{111}. However, the fact that this cascade follows K capture in In^{111} introduces some uncertainty in the interpretation of the experiments: the electronic shell, excited after the K capture, may have properties different than those of its ground state. This difficulty does not exist in the case of isomeric transitions. Therefore, we decided to investigate the directional correlation of the $\gamma-\gamma$ cascade in Pb^{204}.

Pb^{204} has been carefully studied by the Brookhaven group.[7] They found that the isomeric transition takes place in two steps (γ_1: $E=0.905$ Mev, $T_{\frac{1}{2}}=65$ min; γ_2: $E=0.374$ Mev, $T_{\frac{1}{2}}=3\times10^{-7}$ sec), and measured the conversion coefficients of the two successive γ rays. Moreover, they determined a value $A=0.22\pm0.05$ for the anisotropy $A\equiv[W(180°)/W(90°)]-1$ of the directional correlation function $W(\theta)$. Comparison of the conversion coefficients and the half-lives of the two γ rays with theory led to the identification of γ_1 as $E5$ and γ_2 as $E2$. The first two excited states of Pb^{204} therefore were given the assignments 2^+ and 7^-.[8] The theoretical anisotropy for the resulting cascade $7(E5)\,2(E2)0$, $A_{\text{theor}}=0.407$, need not be in disagreement with the experimental value 0.22, because extranuclear fields can attenuate the theoretical correlation.

The data of the Brookhaven group show that Pb^{204} has many excellent properties for an investigation of the effect of extranuclear fields on the nuclear directional correlation. The decay scheme is simple, the γ-ray energies are suitable for work with scintillation counters, and the half-life of the intermediate state (3×10^{-7} sec) is long enough to expect strong perturbations. The only experimental difficulty is the short half-life (65 min) of the initial isomeric state. All measurements must be made in a relatively short time, and no involved source preparation is possible.

Despite the fact that no K capture or beta decay complicates the problems, we found that the influence of the extranuclear fields on the correlation of Pb^{204} is not as simple as we expected. The present paper is only a preliminary report and contains no conclusions as to the nature of the interactions between the nucleus and its surroundings. We shall show, however, that the directional correlation in some of the present measurements is really undisturbed, and we provide consistent spin and parity assignments for the Pb^{204} levels. Further investigations of the influence of extranuclear fields can therefore be based on a unique decay scheme and a knowledge of the highest possible anisotropy.

II. APPARATUS AND CORRECTIONS

The isomeric state in Pb^{204} was produced by irradiating metallic thallium with 12-Mev deuterons. Unfortunately, such a bombardment produces simultaneously, and with much greater intensity, the 52-hr Pb^{203}. A counter system for the determination of the directional correlation of Pb^{204} has therefore to be so designed that it discriminates effectively against coincidences from Pb^{203}.

We measured the directional correlation of Pb^{204} with NaI scintillation counters.[9] The desired discrimination against the Pb^{203} radiation was achieved by using suitable front absorbers and discriminator levels, and by inserting a delay in channel I of the circuit. The relevant counter data are given in Table I. All coincidences due to scattered radiation and to Pb^{203} were reduced by a factor of more than 10^3.

* Assisted by the joint program of the U. S. Office of Naval Research and the U. S. Atomic Energy Commission.

[1] Albers-Schönberg, Hänni, Heer, Novey, and Scherrer, Phys. Rev. **90**, 322 (1953).

[2] Albers-Schönberg, Heer, Novey, and Rüetschi, Phys. Rev. **91**, 199 (1953).

[3] R. M. Steffen, Phys. Rev. **90**, 1119 (1953).

[4] A. Abragam and R. V. Pound, Phys. Rev. **89**, 1306 (1953).

[5] R. V. Pound and A. Abragam, Phys. Rev. **90**, 993 (1953).

[6] A. Abragam and R. V. Pound, Phys. Rev. **92**, 943 (1953).

[7] Sunyar, Alburger, Friedlander, Goldhaber, and Scharff-Goldhaber, Phys. Rev. **79**, 181 (1950).

[8] M. Goldhaber and R. D. Hill, Revs. Modern Phys. **24**, 230 (1952).

[9] J. S. Lawson, Jr., and H. Frauenfelder, Phys. Rev. **91**, 649 (1953).

TABLE I. Characteristics of the counting system.[a]

Counter	α_0	Lead shielding lateral	Lead shielding front	Discriminator level	Delay	Resolving time
I	25°	1.5 cm	0.5 cm	0.55 Mev	0.432 μsec	
II	25°	1.5 cm	0.2 cm	0.22 Mev	none	0.310 μsec

[a] α_0 denotes the width of the counter efficiency curve at half maximum.[9]

The measured anisotropy was corrected for finite angular resolution of the counters and for scattering in the source. The first correction was straightforward.[9] The correction for scattering of the γ rays in the source, however, presented a serious difficulty. Sources thin enough to make the scattering correction small have two disadvantages: the activity is extremely low, and possible surface effects (e.g., in solids: oxidation and field gradients at the boundaries; in liquids: adsorption at the wall) are relatively more important.

We therefore measured the anisotropy in sources of different diameters and extrapolated to zero thickness by the following semiempirical method: We calculated for each source the probability w_1w_2 that a genetically related γ-ray pair, $\gamma_1-\gamma_2$, escape from the source without scattering. The measured anisotropy A_m for each source was then plotted against the corresponding value of w_1w_2. A simple calculation shows that for "thin" sources, A_m should vary linearly with w_1w_2. (A "thin" source means that the probability for single scattering of the γ rays is much larger than that for multiple scattering.) Therefore a straight line was fitted to the points and extrapolated to $w_1w_2=1$ to obtain the anisotropy for zero-source thickness.

In order to test the method experimentally, and to find its limits of applicability, we measured the anisotropy of a very small Ni^{60} source (linear dimensions <0.05 cm) surrounded by cylindrical lead absorbers of different thicknesses. These results are shown in the lower part of Fig. 1. In the region $w_1w_2\sim0.4$ to 0.8, the measured values *can* be fitted by a straight line. The extrapolation to $w_1w_2=1$ then gives a result $A=0.175$ which is only slightly higher than the correct value 0.167. An overestimation of the correction is reasonable: the multiple scattering of the γ rays, which increases with decreasing w_1w_2, tends to enhance the "smearing-out" effect, and bends the measured curve towards the w_1w_2-axis. We expect our correction method to work better for cascades with lower γ-ray energies than Ni^{60}, e.g., Pb^{204}: at high γ-ray energies, the scattering occurs predominantly in the forward direction, and the multiple scattering therefore is more important in averaging out the correlation than is the single scattering.

TABLE II. Anisotropy A of Pb^{204} and Cd^{111} in various compounds.

Compound	Solvent	Anisotropy $A=\frac{W(180°)}{W(90°)}-1$ $T=-185$°C	$T=+25$°C	Number of independent measurements
$Pb(NO_3)_2$	HNO_3(1N−16N)	0.08 ±0.04	0.30 ±0.03	5
		0.22 ±0.03	0.42 ±0.03	3
$Pb(CH_3CO_2)_2$	NH_4 Acetate, sat.	0.10 ±0.05	0.38 ±0.03	2
$Pb(HSO_4)_2$	H_2SO_4 36N		0.23 ±0.05	1
			0.44 ±0.03	1
H_2PbCl_6	HCl 12N		0.46 ±0.04	4
$In_2(SO_4)_3$	H_2SO_4 36N	−0.04 ±0.02	−0.10 ±0.01	2
	32N	−0.04 ±0.02	−0.15 ±0.01	1
	18N	−0.03 ±0.01	−0.21 ±0.01	2
	1N	−0.03 ±0.01	−0.20 ±0.01	3
	aqueous	−0.02 ±0.02	−0.20 ±0.01	1
$InCl_3$	HCl 12N	−0.04 ±0.01	−0.21 ±0.01	1
	1N	−0.02 ±0.01	−0.19 ±0.01	1

III. MEASUREMENTS WITH CHEMICAL COMPOUNDS

The object of the first set of measurements was to observe the directional correlation of Pb^{204} in various liquid sources at several temperatures. We hoped to get, in analogy with the case of Cd^{111}, the highest anisotropy in the liquid state.[3,10,11] Furthermore, we expected to find direct evidence for the influence of extranuclear fields by cooling the specimens down to liquid nitrogen temperature and thereby solidifying them. These experiments were carried out with several Pb compounds in various solvents.

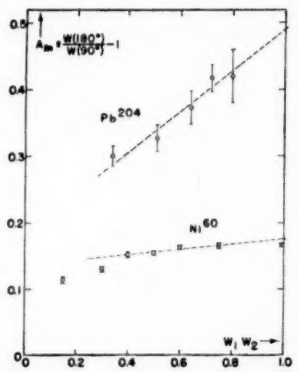

FIG. 1. Measured anisotropy A_m as a function of source thickness (w_1w_2) for Pb^{204} and Ni^{60}.

The Pb^{204} sources were produced by irradiating metallic thallium with deuterons in the cyclotron. The radioactive Pb^{204} and the simultaneously produced 52-hr Pb^{203} were chemically separated from the Tl by extracting the Tl as $TlCl_3$ with ether from a 4N HCl solution. The desired Pb compound was then synthesized and sealed in a thin-walled Pyrex tube. We also investigated Cd^{111}. Typical results are summarized in Table II.

Cd^{111} shows the expected behavior: the solid (frozen) state displays a markedly reduced correlation as compared with that in the liquid state. All measurements at −185°C are consistent with a value $A=-0.031$ ±0.005. The liquid sources yield, in accordance with earlier investigations,[3,10,11] a value of the anisotropy close to the value $A=-0.23$.[1] Only $In_2(SO_4)_3$ in con-

[10] J. C. Kluyver and M. Deutsch, Phys. Rev. **87**, 203 (1952).
[11] R. M. Steffen, Phys. Rev. **89**, 903 (1953).

centrated H_2SO_4 deviates strongly from the maximum value.

Pb^{204} also exhibits a large anisotropy in the liquid state and considerably reduced values in the solid state. However, sources which are expected to give the same results have widely differing anisotropies. This fact is especially visible in the cases of $Pb(NO_3)_2$ and $Pb(HSO_4)_2$. Only H_2PbCl_6, where the Pb is tetravalent, shows consistently high values. This may be due to the fact that the Pb in $(PbCl_6)^{=}$ has coordination number 6, and is octahedrally surrounded by the 6 Cl atoms. In this case the electric field gradient at the side of the Pb nucleus should be small.

In both series of measurements (Pb^{204} and Cd^{111}), heating the liquids to 90° did not increase the anisotropy above its value at 25°C.

IV. MEASUREMENTS WITH A LIQUID LEAD-THALLIUM ALLOY

Table II shows that the behavior of the Pb^{204} correlation function in liquids is rather erratic. We therefore

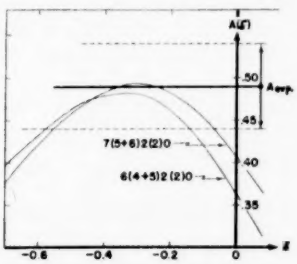

FIG. 2. Theoretical anisotropy $A(\delta)$ as a function of the mixing ratio between competing multipoles, and experimental anisotropy A_{exp}.

sought sources in which the influence of crystalline fields might be controlled, or made vanishingly small.

Lead single crystals (face-centered cubic) or lead melt[12] would constitute a good choice, but experimental difficulties prevent their use: after production in the cyclotron, the Pb^{204} is dispersed in metallic thallium. The chemical separation of the Pb from Tl and the transformation back into its metallic state then invariably yields very weak sources.

Our sources for this experiment therefore were prepared directly from the target material. The irradiated thallium was carefully melted and cleaned in vacuum and sealed into a Pyrex glass tube. Such a source can be regarded as a Pb-Tl mixed crystal[12,13] with vanishingly small Pb content. Because Pb-Tl mixed crystals with high Tl concentration possess, below the melting point, a body-centered cubic phase,[14] we do not expect appreciable electric field gradients at the lattice sites. However, we considered liquid Tl to be even better suited

[12] W. Hückel, *Structural Chemistry of Inorganic Compounds* (Elsevier Publishing Company, Inc., New York, 1950), p. 703.
[13] Y. C. Tang and L. Pauling, Acta Cryst. **5**, 39 (1952).
[14] H. Lipson and A. R. Stokes, Nature **148**, 437 (1941).

TABLE III. Lifetime and conversion data for the γ rays of Pb^{204}.

γ	Assignment	K-shell conversion coefficient exptl[a]	K-shell conversion coefficient theor	γ half-life (sec) exptl[a]	γ half-life (sec) theor[b]
γ_1	$E5$	0.06	0.06	4.3×10^{3}	1×10^{4}
γ_2	$E2$	0.034	0.040	3×10^{-7}	8×10^{-10}

[a] See reference 7.
[b] See reference 16.

for the present work: in the molten state, metals retain their structure in small regions.[15] The Pb^{204} atoms therefore, as in the cubic phase, would experience only small field gradients in most sites. Moreover, the rapid Brownian motion in the melt would probably average out any residual local field gradients, which could arise even in the cubic phase from lattice imperfections and strains.

All measurements were therefore made with the source at 390°C. The final results include only those sources which showed a mirrorlike surface and which did not change in appearance during the experiment. (In two cases, the Pyrex tube leaked during the measurement. The process of oxidation caused a continuous decrease in anisotropy, which was observed over a period of two hours, as well as a visible change in the appearance of the material.)

In order to apply our correction method for scattering of the γ rays in the source, we measured the anisotropy of sources with different diameters. The results are shown in the upper part of Fig. 1. The extrapolated anisotropy for the Pb^{204} $\gamma-\gamma$ cascade is $A=0.49\pm0.05$. This value is in good agreement with the anisotropy $A=0.46\pm0.04$, reported for H_2PbCl_6 in Table II.

V. THE DECAY OF Pb^{204}

As pointed out in the introduction, the first and second excited state of Pb^{204} have been assigned spin and parity 2^+ and 7^-, respectively.[8] These assignments have been made on the basis of lifetime and conversion coefficient considerations for the two transitions $7^-(\gamma_1)2^+$ and $2^+(\gamma_2)0^+$. The relevant experimental[7] and theoretical[16] data are given in Table III. They agree especially well for γ_1.

However, our experimentally determined anisotropy 0.49 ± 0.05 for the directional correlation between γ_1 and γ_2 is higher than the theoretical value 0.407 for the cascade 7(5)2(2)0. We therefore looked for a possible modification in the decay scheme of Pb^{204} which could explain the measured anisotropy.

The assignment 2^+ for the first excited state cannot be altered: the measured conversion coefficient and the K/L conversion ratio of γ_2 (which, as a transition to the ground state 0, must be pure), exclude any transition except $E2$. Moreover, a state 2^+ agrees with the Gold-

[15] Reference 12, p. 851.
[16] J. M. Blatt and V. F. Weisskopf, *Theoretical Nuclear Physics* (John Wiley and Sons, Inc., New York, 1952), p. 627.

TABLE IV. Mixing ratios and conversion coefficients.

Second excited state Spin	Parity	First transition mixture	Mixing ratios δ_{min}	Mixing ratios δ_{max}	K-shell conversion coefficient theoretical for δ_{min}	K-shell conversion coefficient theoretical for δ_{max}	K-shell conversion coefficient exptl
6	+	$E4+M5$	−0.15	−0.58	0.031	0.096	
	−	$M4+E5$			0.17	0.14	0.06
7	+	$M5+E6$	−0.07	−0.55	0.32	0.27	
	−	$E5+M6$			0.06	0.17	

haber-Sunyar rule.[17,18] The fact that the experimental half-life is longer than the theoretical one is also not unexpected for an electric transition.[16]

If we restrict ourselves to pure multipole radiations for the first transition also, then no possible spin assignment for the second excited state yields a large enough anisotropy. This forces us to assume that the first transition γ_1 is mixed.

Even if we admit a mixed transition, the spin of the second excited state is restricted to 6 or 7. A spin value of 5 (or less) is excluded by the fact that the half-life of γ_1 is $\sim 10^7$ times longer than what one expects for a transition with spin change 3.[17] A spin of 8 (or more) would require a transition at least 10^6 times faster than a single proton transition,[16] and a conversion coefficient larger than the experimentally determined value.

We therefore assume a spin of 6 or 7 for the second excited state. The mixed transition to the first excited state 2^+ then can proceed with or without parity change, and we are left with the four possibilities listed in Table IV. In order to decide among these four cascades and to determine the mixing ratio δ of the competing multipoles, we have calculated the anisotropy A as a function of δ.[19] [δ^2 is defined as the intensity ratio of the $(L+1)$-pole radiation to the L-pole radiation.] The resulting curves $A(\delta)$ and the measured anisotropy A_{exp} are plotted in Fig. 2.

We have stated above that the spins 6 and 7 for the second excited state are the only values compatible with lifetime and conversion considerations. Hence, the anisotropy of the Pb^{204} $\gamma-\gamma$ cascade cannot assume values larger than those given by the two theoretical curves in Fig. 2. However, our experimental value of the anisotropy in a Pb-Tl melt lies approximately on the maximum of the theoretical curves. Therefore the directional correlation is not appreciably disturbed by extranuclear fields.

The lower limit of the experimental anisotropy determines the extreme mixing ratios δ_{min} and δ_{max} (see Fig. 2). These mixing ratios and the K conversion coefficients calculated from them are given in Table IV. A comparison of the experimental with the theoretical conversion coefficients rules out the mixtures $M4+E5$ and $M5+E6$.

The decision between the two remaining possibilities has to be made on the basis of lifetime estimates. In Table V we compare the experimental partial half-lives for an intermediate value of δ ($\delta=0.3$) with the corresponding theoretical values for a single proton transition.

These data induce us to abandon the $E5+M6$ cascade for the following reason. Single-particle estimates constitute lower limits for the half-lives. In the case $E5+M6$, however, the observed magnetic transition would be faster than the theoretical estimate by a factor of $\sim 10^7$, whereas the corresponding factor in the first alternative, $E4+M5$, would be only ~ 20. Ratios of the latter order of magnitude have been found for $M4$ transitions[17,20] but no factor of the order of 10^7 has ever been observed. A mixture of $E4$ and $M5$ explains also the measured conversion coefficient. (The excellent agreement in Table III between theoretical and experimental data for the first transition seems to have been only an accident.)

Taking all information together, we conclude that the second excited level in Pb^{204} is a 6^+ state, and the first transition γ_1 is a mixture of approximately 90 percent $E4$ and 10 percent $M5$. (A similar mixture between $E3$ and $M4$ has recently been found by Hill and Mihelich.[20]) The transition probabilities for the $E4$ in the first, and the $E2$ in the second transition are reduced, compared with those for a single proton, by factors of 1×10^{-5} and 2×10^{-3}, respectively. This reduction is very probably due to the fact that the protons in Pb^{204} form a closed shell. It is also interesting to note that Moszkowski's calculation[21] for the transition probability of a single neutron yields values of this order of magnitude.

TABLE V. Experimental and theoretical half-lives for a mixed transition.

Mixture	Exptl partial half-life (sec) E	Exptl partial half-life (sec) M	Theor half-life[a] (sec) E	Theor half-life[a] (sec) M
$E4+M5$	5×10^9	5×10^4	7×10^{-2}	1×10^6
$E5+M6$	5×10^9	5×10^4	1×10^4	4×10^{11}

[a] See reference 16.

VI. ACKNOWLEDGMENTS

We thank Professors J. M. Blatt, F. Coester, M. Gell-Mann, H. S. Gutowsky, F. E. Low, D. Pines, C. P. Slichter, and Dr. R. Norberg for valuable discussions, Mr. D. H. Fraembs for his continuous help during measurements and evaluation, and Mr. W. H. Rosenfeld for help with the calculations.

[17] M. Goldhaber and A. W. Sunyar, Phys. Rev. **83**, 906 (1951).
[18] G. Scharff-Goldhaber, Phys. Rev. **90**, 587 (1953).
[19] L. C. Biedenharn and M. E. Rose, Revs. Modern Phys. **25**, 729 (1953).
[20] R. D. Hill and J. W. Mihelich, Phys. Rev. **89**, 323 (1953).
[21] S. A. Moszkowski, Phys. Rev. **89**, 474 (1953).

The Statistical Theory of Nuclear Reactions

BERNARD L. COHEN
Oak Ridge National Laboratory, Oak Ridge, Tennessee
(Received July 9, 1953)

It is pointed out that the discrepancies between experimental results and the predictions of the statistical theory of nuclear reactions can be traced to peculiarities in the energy distribution of particles emitted in the breakup of the compound nucleus. Experimental energy distributions are analyzed, and it is shown that very strange assumptions—susceptible to experimental check—are necessary to explain them in any way without the introduction of a new selection rule in nuclear transitions. Experiments are suggested to clarify these problems.

IT has by now become quite clear that large discrepancies exist between the predictions of the statistical theory of nuclear reactions and the results of experiments designed to test them. In particular, it appears that nuclear temperatures calculated from experimental-level densities[1] are much higher than those obtained from measurements of energy spectra of emitted particles,[2–5] much lower than those required to explain the cross sections of (n,p), (n,α), (p,pn), and (α,pn)[6–10] reactions, but nevertheless, approximately equal to those found from $(n,2n)$[6–8] and $(\alpha,2n)$[11,12] cross-section measurements. In an effort to clarify this situation, the theory is here developed to a form more suitable for comparison with the experimental results, the experiments are analyzed in this light, and some conclusions about the difficulties with nuclear reaction theory are pointed out.

We begin with a derivation of the equation for the energy spectrum of particles emitted in the breakup of a compound nucleus. Consider the reversible reaction,

$$C(E_0+B) \leftrightarrows A(E_0-E)+a+E, \tag{1}$$

where C, A, and a are the compound nucleus, residual nucleus, and emitted particle, respectively, the quantities in parentheses are their excitation energies (E_0 is maximum possible kinetic energy available, B is binding energy of a to A), and E is the kinetic energy released, practically all of it appearing as the kinetic energy of a. The probability per unit time, $\lambda(\rightarrow)$, of (1) proceeding to the right into energy interval ΔE, is

$$\lambda(\rightarrow)=(2\pi/h)|M|^2\omega_A(E_0-E)\omega_a(E)\Delta E, \tag{2}$$

where $|M|$ is the average matrix element for the transition (averaged over the levels within energy interval ΔE), $\omega_A(E_0-E)$ is the level density of A at excitation E_0-E, and $\omega_a(E)$ is the degeneracy of a (in spin, momentum, and physical space). By the same token, the probability per unit time of (1) proceeding to the left is

$$\lambda(\leftarrow)=2\pi/h|M|^2\omega_C(E_0+B)\Delta E. \tag{3}$$

However, $\lambda(\leftarrow)$ may be expressed in terms of the cross section for (1) proceeding to the left, σ, as

$$\lambda(\leftarrow)=\sigma v/V, \tag{4}$$

where v is the velocity of a and V is the volume in which the system is contained. Using (4) and (3),

$$|M|^2=\frac{h}{2\pi}\frac{\sigma v}{V}\frac{1}{\omega_C(E_0+B)\Delta E}, \tag{5}$$

whence (2) becomes

$$\lambda(\rightarrow)=\frac{\sigma v}{V}\frac{\omega_A(E_0-E)}{\omega_C(E_0+B)}\omega_a(E). \tag{6}$$

The physical space degeneracy of a is proportional to V, the momentum space degeneracy is proportional to $E^{\frac{1}{2}}\Delta E$, and $v\propto E^{\frac{1}{2}}$, so that $I(E)\Delta E$, the dependence of $\lambda(\rightarrow)$ on E, may be expressed as

$$I(E)=\sigma E\omega_A(E_0-E). \tag{7}$$

Formula (7), which was originally due to Weisskopf,[13] was derived here without taking into account angular momentum and parity selection rules. This problem, however, was treated in detail by Wolfenstein,[14] who found that the energy distribution, while similar to (7), also depends on the density of energy levels with respect to spin. With any reasonable assumption about this quantity, (7) is altered only slightly; however, it is important to bear in mind that (7) is not an exact formula.

For purposes of the discussion below, we introduce the "sticking probability," η, by

$$\eta=\sigma/\sigma_0, \tag{8}$$

where σ_0 is the reaction cross section given in reference 1 with all $\eta_l=0$. For neutrons, σ_0 is approximately con-

[1] J. Blatt and V. F. Weisskopf, *Theoretical Nuclear Physics* (John Wiley and Sons, Inc., New York, 1952).
[2] P. C. Gugelot, Phys. Rev. **81**, 51 (1951).
[3] P. C. Gugelot and H. A. Lauter, Phys. Rev. **91**, 486 (1953). (The author is indebted to Dr. Gugelot for permission to use this data in advance of publication.)
[4] P. H. Stelson and C. Goodman, Phys. Rev. **52**, 69 (1951).
[5] E. R. Graves and L. Rosen, Phys. Rev. **89**, 343 (1953).
[6] H. Wäffler, Helv. Phys. Acta **23**, 239 (1950).
[7] B. L. Cohen, Phys. Rev. **81**, 184 (1951).
[8] E. B. Paul and R. L. Clarke, Can. J. Phys. **31**, 267 (1953).
[9] S. N. Ghoshal, Phys. Rev. **80**, 939 (1950).
[10] Newman, Cohen, and Handley, Phys. Rev. **91**, 486 (1953).
[11] J. Bradt and D. J. Tendam, Phys. Rev. **72**, 1118 (1947).
[12] Bleuler, Stebbens, and Tendam, Phys. Rev. **90**, 460 (1953).
[13] V. F. Weisskopf, Phys. Rev. **52**, 295 (1937).
[14] L. Wolfenstein, Phys. Rev. **82**, 690 (1951).

stant ($=\pi r^2$) for energies above about 1 Mev, while for charged particles it is less by the Coulomb barrier-penetration factor. From (8) and (5) we see that η must contain any selection rules that are effective in nuclear transitions.

In the measurement of energy spectra of emitted particles, the quantity determined is the rate of change of $I(E)$ with E. Thus, a quantity very directly obtainable from the measurements is

$$\Sigma=\left[-\frac{\partial \log(I(E)/\sigma_0 E)}{\partial E}\right]^{-1}. \tag{9}$$

From (7) and (8), the measured quantity Σ may be interpreted as

$$\Sigma^{-1}=-\frac{\partial \log\eta}{\partial E}-\frac{\partial \log\omega(E_0-E)}{\partial E}. \tag{10}$$

Using the conventional thermodynamic analogies,

$$S=\log\omega, \quad \partial S/\partial\epsilon=1/T(\epsilon), \tag{11}$$

Equation (10) becomes

$$\frac{1}{\Sigma}=-\frac{\partial \log\eta}{\partial E}+\frac{1}{T(E_0-E)}. \tag{12}$$

Equation (12) may be compared with three types of experimental results. Measurements of energy distributions of particles emitted from nuclear reactions give $I(E)$, and therefore Σ, directly. The total cross section for nuclear reactions in which charged particles are emitted is given by[1]

$$\sigma(a,b)\simeq\sigma_a f_b/\textstyle\sum_i f_i, \tag{13}$$

where σ_a is the cross section for capture of a to form a compound nucleus, f_i is

$$f_i=\frac{2m_i}{\hbar^2}\int_0^\infty I_i(E)dE \tag{14}$$

(m_i is the mass of particle i), and the summation in (13) is over all particles that can be emitted. Thus, cross sections for nuclear reactions are determined by $I(E)$ and, therefore, give information about Σ. Somewhat better information is obtained from $(x, 2n)$ reactions; the cross sections for these are[1]

$$\sigma(x,2n)=\sigma_x\int_0^{\epsilon-B} I_n(E)dE\Big/\int_0^\infty I_n(E)dE, \tag{15}$$

where ϵ is the incident energy of x, and B is the threshold for the $(x, 2n)$ reaction. Experimental excitation functions of $(x, 2n)$ reactions can therefore be differentiated to give relatively direct information on $I(E)$.

In comparing (12) with the experimental results, we first take the point of view of the usual theory, as presented in reference 1. The basic assumption of this theory is that η is identically unity (except for reflections due to sudden change of wavelength which are negligible above about 1 Mev). With this assumption, (12) becomes

$$\Sigma=T(E_0-E). \tag{16}$$

To investigate (16), an analysis was made of published experimental results to determine values of Σ. Figures 1 and 2 show the values of Σ obtained from Gugelot's data[2,3] on energy spectra of inelastically-scattered protons and of neutrons from (p,n) reactions. The most striking feature of these curves is that in every one of the twelve cases, Σ decreases as (E_0-E) increases. This feature was verified by performing similar analyses on every other applicable work; on the inelastic proton scattering energy spectrum of Levinthal *et al.*[15] (see Fig. 3); on the spectra of neutrons emitted from (d,n) reactions at 90°[16,17] (in the latter reference there is good evidence that at angles as large as 90°, compound nucleus interaction is predominant); and on

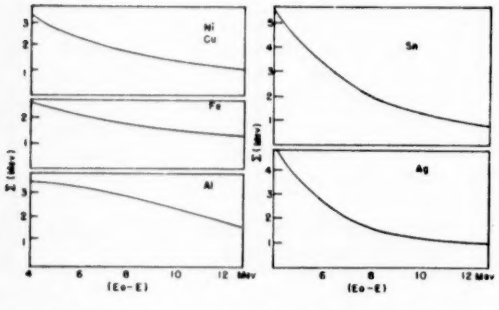

FIG. 1. Σ vs (E_0-E) from inelastic proton scattering. According to the usual theory, the slopes of these curves should be positive rather than negative. Σ was calculated from the lines drawn through the 150° data by the authors of reference 3. We are indebted to them for permission to use their data in advance of publication.

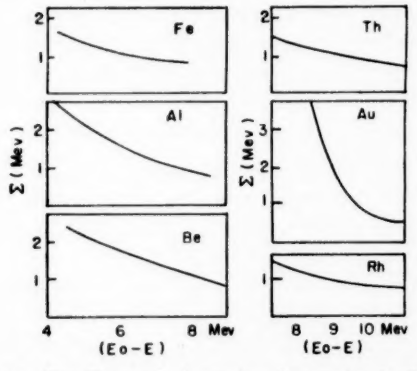

FIG. 2. Σ vs (E_0-E) from (p,n) reactions (see caption for Fig. 1). Σ was calculated from the data of reference 2.

[15] Levinthal, Martinelli, and Silverman, Phys. Rev. **78**, 199 (1950).
[16] C. Grosskreutz, Phys. Rev. **76**, 482 (1949).
[17] B. L. Cohen and C. E. Falk, Phys. Rev. **84**, 173 (1951).

inelastically scattered neutron spectra[4,5] (although the statistics are somewhat poor in this case). In each case, without a single exception, Σ decreases with increasing (E_0-E). In the light of (16), this result is very surprising; it indicates that temperatures decrease as excitation energy increases. This runs contrary to the most basic tenets of the thermodynamic analogy. But even if we are unwilling to assign any thermodynamic properties whatsoever to the nuclear temperature, this result demands that temperatures measured, for example, by Gugelot's method,[2] would increase as the energy of the bombarding particle decreases. Extrapolated to higher energies, it would mean that energy distributions of particles emitted from stars produced by cosmic rays and synchrocyclotrons would have very low temperatures; this is contrary to the findings of many experimenters.

Another requirement for the validity of (16) is that, for a given final nucleus, Σ must be a function of (E_0-E) only. The most directly applicable data on this is the case of Al^{27} which is the final nucleus in inelastic scattering of either protons or neutrons from aluminum. Figure 3 shows the results of three inelastic-scattering experiments in which the incident particles were 30-Mev protons,[15] 18-Mev protons,[2] and 14-Mev neutrons.[5] In each case the values of Σ for a given value of (E_0-E) are very different.

An additional, though less reliable, check of this type is available from the neutron-energy spectra from (d,n) reactions on copper induced by 10-Mev[16] and by 16-Mev[17] deuterons. The values of Σ differ by at least 40 percent for the same values of (E_0-E).

If one is willing to assume that temperatures of nuclei of approximately the same mass are equal, there are several other tests available. Data on (n,p), (n,α), $(n,2n)$, and $(\alpha,2n)$ cross sections, neutron energy spectra, and proton energy spectra (see Figs. 1 and 2) provide several cases where, for the same value of (E_0-E) and approximately the same nuclear mass, experimental values of Σ vary widely. Thus, certainly for nuclei up to mass 30, probably for nuclei up to mass 60, and possibly for nuclei up to mass 100, there is good experimental evidence that Σ is not a function of (E_0-E) alone, as is indicated by (16).

In summary, the validity of (16) is supportable only if one is willing to accept *each* of the following seemingly improbable consequences.

(a) Nuclear temperatures, as defined in (11), do not increase with excitation energy in the energy region investigated here.[18] This demands, for example, that if Gugelot's neutron spectra[2] were measured with 12-Mev incident protons rather than with 16 Mev, the temperatures obtained would be higher.

[18] V. F. Weisskopf (private communication) has pointed out, however, that the nuclear spectrum might change character when going from one energy region to another (independent particle character to statistical character). Then the level density might increase so strongly in that energy region that the nuclear temperature defined by (11) is decreasing with increasing excitation.

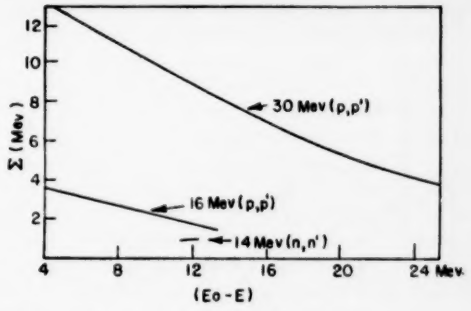

FIG. 3. Σ *vs* (E_0-E) for the final nucleus Al^{27}. These curves were calculated from the data of references 3, 5, and 15.

(b) For some reason, the derivation of Eq. (7) breaks down badly for aluminum and probably for elements at least up to mass 60, causing Σ not to be a function of (E_0-E) only.

To test whether (16) is tenable at all, measurements of neutron energy spectra similar to Gugelot's[2] with ~12-Mev incident protons [for higher proton energies, $(p,2n)$ reactions interfere], and of inelastic proton energy spectra for incident protons of about 14 Mev, 24 Mev, and 30 Mev should be performed. Actually, any one of these experiments would probably settle the matter fairly conclusively, although the neutron energy spectra might not be sufficiently accurate for heavy elements.

If these experiments should indicate that (16) is untenable, two alternatives remain. One is that other interactions besides compound nucleus formation are important in the reactions under consideration. McManus and Sharpe[19] have proposed that they may be due to a direct interaction ("knock-out" process). It would seem that this should influence only the highest energy portion of the spectrum of emitted particles, whereas the difficulties described above are in evidence at all energies. In addition, it would influence the spectrum only at small angles, whereas the data for Fig. 1 were taken at 150°. (Actually, there is some evidence in reference 2 for more high-energy inelastically scattered protons at 60° than at 150°. However, the effect is not large and might be explained, for example, as inelastic scattering by electric interactions). The matter can be settled experimentally, by looking for a forward peak in the angular distributions. Allen *et al.*[20,21] have measured angular distributions of neutrons from (α,n) reactions for several elements, and their data shows no evidence for a forward peak. Similar measurements for (n,p), (n,α), (p,n), and (p,α) reactions would give a conclusive answer to this problem. However, as mentioned above, even if it were proved that direct interactions are important, the difficulties in explaining energy spectra at large angles

[19] H. McManus and W. T. Sharpe, Phys. Rev. **87**, 188 (1952).
[20] Allen, Nechaj, Sun, and Jennings, Phys. Rev. **81**, 526 (1951).
[21] B. L. Cohen, Phys. Rev. **81**, 632 (1951).

would still remain. Also, the experiments of Ghoshal[9] lend strong support to the general validity of the compound nucleus model at these energies.

The only remaining alternative that seems obvious is to retain the compound nucleus model, but abandon (16) in favor of the more general formula (12). If the $\partial \log\eta/\partial E$ term in (12) is to contribute appreciably, it must be of the order of an inverse nuclear temperature; that is, η must decrease by a factor of $e(2.7)$ for a decrease in the emitted particle energies of a few Mev. In view of (5) and (8), this would mean that there are selection rules operating in nuclear transitions such as to make transitions between distant levels more probable than transitions between levels of nearly equal energy.

One objection to this alternative is that the many published measurements of total reaction cross sections for neutrons, protons, alphas, and pi mesons are actually direct measurements of the sticking probability, η; and in every case, they indicate that η is its maximum theoretical value, unity. In these cases, of course, only ground-state nuclei were bombarded whereas the η in (12), which entered through the reciprocity theorem, is the sticking probability when excited nuclei are bombarded. Obviously, there can be no direct experimental measurements of η for such cases.

Another objection to this alternative, pointed out by Weisskopf,[18] is that it requires that sticking probabilities be less for excited than for ground state nuclei, whereas according to current theories of nuclear structure, the opposite should be the case.

On the other hand, Wigner[22] has pointed out independent evidence for the selection rule mentioned above in heavy elements from comparison of known absolute level densities with Gugelot's data.[3]

ACKNOWLEDGMENT

The author is happy to acknowledge the many helpful suggestions, comments, and opinions of J. L. Fowler, V. F. Weisskopf, T. A. Welton, and E. P. Wigner.

[22] E. P. Wigner (private communication).

PHYSICAL REVIEW VOLUME 92, NUMBER 5 DECEMBER 1, 1953

The Radionuclides of Arsenic Produced by Deuteron Bombardment of Germanium*

H. J. WATTERS†‡ AND J. F. FAGAN, JR.‡§
Department of Physics and Radioactivity Center, Laboratory for Nuclear Science, Massachusetts Institute of Technology, Cambridge, Massachusetts

(Received July 13, 1953)

The arsenic produced by a deuteron bombardment of germanium has been studied to determine the nuclides present in the mixture. Identification of the isotopes was made by comparing measured values of half-life and maximum β energy with published values. Counting rates were measured with 4π and coincidence counters, obtaining half-lives which indicated that the nuclidic mixture was made up of As^{71}, As^{72}, As^{73}, As^{74}, and As^{77}. These findings were confirmed by maximum β energy values obtained by absorption measurements and by γ-energy values found using a γ-ray scintillation spectrometer. Measurements indicated that the 40-hr half-life reported for As^{77} is in error by a significant amount, and that no As^{76} was obtained from this bombardment. Thick target yield data were determined for each nuclide from the 4π counter measurements.

AN investigation was made of the radionuclides of arsenic produced by the cyclotron bombardment of a thick germanium target with 15-Mev deuterons. After chemical separation of the arsenic,[1] identification of the isotopes present was made by correlating measured values of γ, β^+, and total β half-lives with maximum β energy and γ-ray energy.

Arsenic activity was measured continuously for a period of 53 days with a 4π proportional counter, a γ-γ coincidence counter, and with a thin end-window Geiger Muller tube using calibrated aluminum absorbers. Gamma-ray energy measurements were made using a thallium-activated sodium iodide scintillation spectrometer. The energy spectrum up to 3 Mev was scanned continuously for the first 72 hours (Fig. 1) and an additional spectrum was obtained 52 days after bombardment.

By application of the method of least squares to 4π and coincidence counter data, the decay curves were analyzed in a total of four periods: 25.8 hours, 48.2 hours, 17.8 days, and 88.9 days. Comparison of total β-decay curves with those due only to positron disintegration yielded an additional period slightly greater

* This work has been supported in part by the joint program of the U. S. Office of Naval Research and the U. S. Atomic Energy Commission, and also in part by the Bureau of Ordnance, U. S. Navy.

† Lieutenant Commander, U. S. Navy.

‡ Now on sea duty, U. S. Navy. Investigation performed while a U. S. naval postgraduate student at Massachusetts Institute of Technology, Cambridge, Massachusetts.

§ Lieutenant, U. S. Navy.

[1] Brownell, Backofen, White, and Irvine, Massachusetts Institute of Technology Progress Report, May 1953 (unpublished).

than 70 hours. These values were verified by analysis of decay curves obtained with the end-window β counter. The four experimental components shown in Fig. 2 were obtained from analysis of total β decay observed with the 4π counter.

The energy of the hardest γ ray detected with the scintillation spectrometer was 0.85 Mev, with a half-life of about 29 hours. An additional γ-ray energy of 0.60 Mev was resolved several weeks after bombardment.

Maximum β energies were found from absorption curves obtained with the end-window β counter. From measurements of maximum range made at various times, the energy of the most energetic β was determined for both the 25.8-hour and the 17.8-day isotopes. In addition mass-absorption coefficients were determined

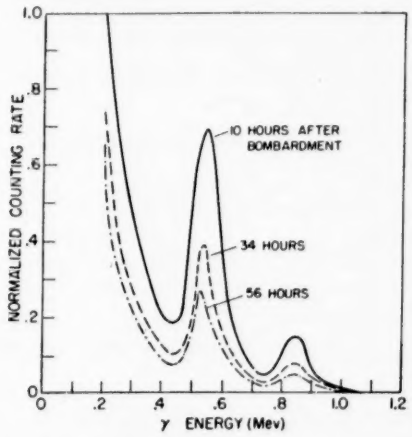

FIG. 1. γ-ray energy spectrum of arsenic produced by 15-Mev deuteron bombardment of germanium.

from semilog plots of counting rate *vs* absorber thickness taken at various times. Using these values, maximum β energies were computed for the 48.2-hour and the 17.8-day isotopes. Close agreement was found for the 17.8-day isotope by both methods.

Correlation of data indicated that the nuclidic mixture consisted of As^{71}, As^{72}, As^{73}, As^{74}, and As^{77}. Because of the absence of γ-ray energies greater than 0.85 Mev it was concluded that As^{76} was not present in the mixture.

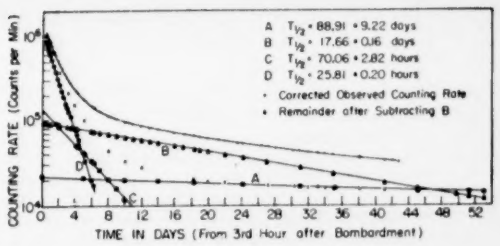

FIG. 2. Data of counting rate *vs* time, taken with 4π counter, showing half-life values determined by method of least squares.

Since the efficiency of the 4π solid-angle β counter constructed for this investigation was shown to be very nearly 100 percent for particles which escape the source, these data were used to determine absolute β activities. These activities were corrected to the time of completion of bombardment and the results specified in terms of yield for each isotope.

A summary of the results of this investigation is given in Table I.

The Master's thesis submitted by these writers to the Massachusetts Institute of Technology contains details of the investigation and a complete treatment of the construction and operating technique of the 4π β counter. This investigation was suggested by Dr. Gordon L. Brownell of the Massachusetts General Hospital and was conducted under the supervision of Professor Robley D. Evans.

TABLE I. Summary of the characteristics of the mixture of radionuclides determined by this investigation.

Isotope	Method of decay	Energy (Mev)	$T_{\frac{1}{2}}$[a]	Thick-target yield[b] (μC/μa-hr)
As^{71}	β^+	0.66	48.2 ±1.2 hr	7.6
As^{72}	β^+	3.25	25.8 ±0.2 hr	64.9
	γ	0.85		
As^{73}	β^-	$0.11 > E_{max} > 0.02$	86.9 ±9.2 days	1.1
As^{74}	β^+	0.99, 1.49	17.82±0.13 days	5.2
	β^-			
As^{76}		Not present in the mixture		
As^{77}	β^-	<0.7	>70 hours	5<yield<15[c]

[a] Half-lives are stated with their respective standard errors.
[b] The thick-target yield values specified apply if the deuteron beam current was exactly 36 μa and if the arsenic separation efficiency was 100 percent. Yield values quoted are based on β counting only and do not include orbital electron capture.
[c] Based on ratios of total β to β^+ counting rates.

Two-Body Scattering at Low Energy

BENJAMIN ROTH
University of Connecticut, Storrs, Connecticut

(Received December 24, 1952; revised manuscript received August 26, 1953)

A series expansion in k is derived for the scattered wave $f(\theta)$ in a short-range field. All angular momentum waves are treated. The "shape-independent approximation" formula is derived from this series, and limits on its validity are given. It is shown that for large scattering lengths one must use the series for $k\cot\delta$; for small scattering lengths, the series for f must be used.

INTRODUCTION

LOW-ENERGY $n-p$ scattering is often described by the "shape-independent approximation."[1,2] The expression $k\cot\delta$, where δ is the phase shift, is given by a power series in energy. An alternative expression is here derived for two-body scattering (to be extended in a future article to collisions of neutrons with more complex nuclei). The scattered wave in all angular momenta is expressed as a power series in ik, from which the series for $k\cot\delta$ can be derived. On the basis of this derivation, an energy limit on the series for $k\cot\delta$ is obtained, for large and for small scattering lengths. It is also shown that the size of the scattering length will determine which of the two expressions is more suitable to use. This knowledge is valuable in the analysis of the scattering of neutrons by complex nuclei.

TWO-BODY SCATTERING

The Schrödinger equation for two-body scattering is

$$(\nabla^2+k^2-U)\psi=0, \tag{1}$$

with $k^2=ME/\hbar^2$ and $U=MV/\hbar^2$. We will take the force to be noncentral, i.e.,

$$V=V(r,\theta,\phi).$$

Due to the short range of nuclear forces, U goes to zero for $r\geqslant R$, and we can follow established procedures in joining the solutions inside and outside the potential field. In the field-free region, ψ is a solution of

$$(\nabla^2+k^2)\psi=0. \tag{2}$$

The boundary condition on ψ is

$$\psi_{r\to\infty}\to f(\theta,\phi)e^{ikr}/r+e^{ikz}=\sum_{l,m}f_{lm}Y_{lm}(\theta,\phi)e^{ikr}/r +\sum_l i^l(2l+1)j_l(kr)P_l(\cos\theta). \tag{3}$$

r is the $n-p$ separation; z is the direction of motion of the incident neutrons; Y is a spherical harmonic; and P is a Legendre polynomial. The solution of Eq. (2) is

$$\psi=\sum_{l,m}\psi_{lm}(r)Y_{lm}(\theta,\phi), \tag{4}$$

where

$$\psi_{lm}=A_{lm}j_l(kr)+B_{lm}n_l(kr).$$

j_l and n_l are the regular and irregular solutions of the radial equation derived from Eq. (2).[3] A_{lm} and B_{lm} are integration constants. The boundary condition Eq. (3) determines the constants thus:

$$\begin{aligned}A_{lm}&=i^{l+1}kf_{lm}+i^l(2l+1)\delta(m,0),\\ B_{lm}&=-i^lkf_{lm}.\end{aligned} \tag{5}$$

For the region within the potential we can write ψ in the form of Eq. (4), and then

$$\nabla^2\psi=\sum_{l,m}Y_{lm}[\nabla^2-l(l+1)/r^2]\psi_{lm}(r),$$

$$U\psi=\sum_{l,m}Y_{lm}\int U\psi Y_{lm}^*d\omega,$$

with $d\omega=\sin\theta d\theta d\phi$. Equation (1) then breaks up into the independent equations for all l and m:

$$\nabla^2\psi_{lm}-\psi_{lm}l(l+1)/r^2+k^2\psi_{lm}-\int U\psi Y_{lm}^*d\omega=0. \tag{6}$$

We integrate each term of this equation over a sphere of radius R and use the divergence theorem. The result is

$$R^2(d/dR)[A_{lm}j_l(kr)+B_{lm}n_l(kr)] =\int_0^R U\psi Y_{lm}^*d\tau+(1/4\pi)\int_0^R l(l+1)\psi_{lm}r^{-2}d\tau -(k^2/4\pi)\int_0^R\psi_{lm}d\tau. \tag{7}$$

This equation, together with Eq. (5), relates the scattered wave functions f_{lm} to integrals over the force region.

It is worth while to investigate the dependence of f_{lm} on k. An expansion in energy will be made for ψ within the potential region. It is interesting to compare this with a method used by Ferretti and Krook.[4] They expand $r\psi$ in powers of r around a point a, the edge of the potential well, and from the series they derive an expression for the logarithmic derivative of $r\psi$ at the

[1] H. A. Bethe, Phys. Rev. **76**, 38 (1949); J. M. Blatt and J. D. Jackson, Phys. Rev. **76**, 18 (1949); G. F. Chew and M. L. Goldberger, Phys. Rev. **75**, 1637 (1949).
[2] G. Breit, Revs. Modern Phys. **23**, 238 (1951).
[3] P. M. Morse, *Vibration and Sound* (McGraw-Hill Book Company, Inc., New York, 1948), second edition, p. 317.
[4] B. Ferretti and M. Krook, Proc. Phys. Soc. (London) **60**, 481 (1948).

point a. Their method depends upon the fact that the logarithmic derivative has a circle of convergence.

For our expansion we will require $kr<1$. The upper limit that this requirement imposes on the neutron energy depends upon the lowest possible R, which in turn depends on the choice of V. If, for example, R can go down to 2.5×10^{-13} cm, then our series expansion will hold up to an energy of 13 Mev. It will later be seen that another restriction can considerably lower this upper limit.

For $kr<1$, it follows from Eqs. (4) and (5) that

$$\psi_{lm}]_{r=R}=\frac{(kR)^l}{L(2l+1)}[i^{l+1}kf_{lm}+i^l(2l+1)\delta(m,0)]\times\left[1-\frac{(kR)^2}{2(2l+3)}\cdots\right]+i^lkf_{lm}\frac{L}{(kR)^{l+1}}\times\left[1+\frac{(kR)^2}{2(2l-1)}\cdots\right], \quad (8)$$

$$L\equiv1\cdot1\cdot3\cdots(2l-1).$$

From Eq. (8) we infer that as $k\to0$, $f_{lm}\to0$ at least as fast as k^l, otherwise ψ_{lm} would become infinite at $k=0$.

It now remains to express the right-hand side of Eq. (7) as a power series in k, and this we accomplish by expanding ψ in such a series. For any point P within the potential region, ψ_{lm} is a solution of Eq. (6), and by Green's Theorem it can be written as

$$\psi_{lm}(P)=\int_0^R\rho^{-1}\left[l(l+1)\psi_{lm}/r^2-k^2\psi_{lm}+\int U\psi Y_{lm}{}^*d\omega'\right]d\tau+\int^R[\rho^{-1}\partial\psi/\partial r+\rho^{-2}\psi\cos(\rho,r)]d\sigma. \quad (9)$$

ρ is the distance from P to an integration point. Let $\psi_{lm}{}^{(0)}(P)$ be the solution for zero energy and with the proper boundary condition at $r=R$, namely, the one given by Eq. (8),

$$\psi_{lm}{}^{(0)}(R)=i^l\frac{Lf_{lm}{}^{(0)}}{R(kR)^l}+\frac{i^l(kR)^l}{L}\delta(m,0). \quad (10)$$

For low energies the term $k^2\psi_{lm}$ in Eq. (9) can be treated as a perturbation, and by a process of iteration a solution can be obtained for any energy for which the series Eq. (11) converges:

$$\psi_{lm}{}'(P)=\psi_{lm}{}^{(0)}(P)+\sum_{r=1}^{\infty}k^{2r}\alpha_{lm}{}^{(r)}(P). \quad (11)$$

The $\alpha_{lm}{}^{(r)}$ are some functions of the point P. $\psi_{lm}{}'(P)$ is not identical with $\psi_{lm}(P)$, since it does not have the required boundary condition, Eq. (3).

The series Eq. (11) will converge for only very low energies if there is a resonance near zero energy, for then ψ_{lm} changes rapidly with small changes in energy. This limitation is reflected in the series for f_0 which is given below; it converges for only low energies if the scattering length is large. The scattering length is large when there is a resonance near zero energy.

The correct solution for $\psi_{lm}(P)$ appearing in Eq. (7) is related to $\psi_{lm}{}'(P)$ in the same way as the boundary values at $r=R$, namely,

$$\psi_{lm}(P)=[\psi_{lm}{}'(P)/\psi_{lm}{}'(R)]\psi_{lm}(R)=\frac{1}{\psi_{lm}{}^{(0)}(R)}[\psi_{lm}{}^{(0)}(P)+\sum_{r=1}^{\infty}\alpha_{lm}{}^{(r)}(P)k^{2r}]\times\left\{1-\frac{\sum k^{2r}\alpha_{lm}{}^{(r)}(R)}{\psi_{lm}{}^{(0)}(R)}+\cdots\right\}\psi_{lm}(R). \quad (12)$$

With the help of Eqs. (5), (8), and (12), Eq. (7) can be written as a series in k in the following way:

$$\sum_r k^{2r}\{\rho_{lm}{}^{(r)}f_{lm}/(ik)^l+\nu_{lm}{}^{(r)}(ik)^l\delta(m,0)+\mu_{lm}{}^{(r)}(ik)^{l+1}f_{lm}\}=\sum_r\sum_{l'}k^{2r}\{\xi_{l'm}{}^{(r)}f_{l'm}/(ik)^{l'}+\eta_{l'm}{}^{(r)}(ik)^{l'}\delta(m,0)+\zeta_{l'm}{}^{(r)}f_{l'm}(ik)^{l'+1}\}. \quad (13)$$

The constants ρ, ν, μ are given by the left side of Eq. (7) together with Eq. (8), and ξ, η, ζ are given by the right side of Eq. (7) together with Eq. (12). For central forces the right-hand side of Eq. (13) gives the one term for $\sum_{l'}$, $l'=l$. Upon setting to zero the factor of each power of k, we arrive at the series expression for f_{lm},

$$f_l=\sum_{r=0}^{l}f_l{}^{(2r)}(ik)^{2l+2r}+\sum_{r=1}^{\infty}f_l{}^{(2l+r)}(ik)^{4l+r} \quad \text{for central forces;} \quad (14)$$

$$f_{lm}=\sum_{r=0}^{\infty}f_{lm}{}^{(r)}(ik)^{l+r} \quad \text{for noncentral forces.} \quad (15)$$

The coefficients $f_l{}^{(r)}$, $f_{lm}{}^{(r)}$ are solved for by Eq. (13) and are expressed in terms of the constants ρ, ν, μ, ξ, η, ζ. For the S wave, for example, the series Eq. (14) is written as $f_0=\sum_r f_0{}^{(r)}(ik)^r$, and the first few terms are given by

$$\begin{aligned}
&f_0{}^{(0)}=-\int U\psi_0{}^{(0)}d\tau/4\pi;\\
&f_0{}^{(1)}=[f_0{}^{(0)}]^2;\\
&f_0{}^{(2)}=f_0{}^{(0)}R^2+[f_0{}^{(0)}]^2R+[f_0{}^{(0)}]^3+R^3/3+\alpha_0{}^{(1)}(R)f_0{}^{(0)}/\psi_0{}^{(0)}(R)+\int_0^R[U\alpha_0{}^{(1)}+\psi_0{}^{(0)}]d\tau/4\pi;\\
&f_0{}^{(3)}=2f_0{}^{(0)}f_0{}^{(2)}-[f_0{}^{(0)}]^4.
\end{aligned} \quad (16)$$

The connection between f_l and the phase shift δ_l is given by[5]

$$f_l = e^{i\delta_l} \sin\delta_l (2l+1)/k. \tag{17}$$

If, in Eqs. (14) and (17), we equate reals and imaginaries, we find

$$\cot\delta_l = i\sum_r f_l^{(2r)} (ik)^{2l+2r} / \sum_r \left[f_l^{(2l+2r+1)} (ik)^{4l+2r+1} \right],$$

or

$$k^{2l+1} \cot\delta_l = \sum_r a_l^{(r)} k^{2r}. \tag{18}$$

This result was arrived at by Teichmann[6] for nuclei in general, on the basis of resonance theory. The results (14) and (15) are more general. The S wave of Eq. (18) is customarily written as

$$k \cot\delta = -1/a + \tfrac{1}{2} r_0 k^2 + \cdots, \tag{19}$$

where a is the scattering length and r_0 is known as the effective range. Through our series for f_0 we arrive at the series for $k\cot\delta$ according to the procedure outlined above:

$$k\cot\delta = \frac{f_0^{(0)} - f_0^{(2)} k^2 + f_0^{(4)} k^4 - \cdots}{f_0^{(1)} (1 - f_0^{(3)} k^2 / f_0^{(1)} + f_0^{(5)} k^4 / f_0^{(1)} - \cdots)}$$

$$= 1/f_0^{(0)} + (k^2/f_0^{(1)}) \times (-f_0^{(2)} + f_0^{(3)} f_0^{(0)} / f_0^{(1)}) + \cdots. \tag{20}$$

If we equate the constants of (19) and (20), we obtain

$$f_0^{(0)} = -a,$$

which is true by definition.[7] We also get, with the help of Eq. (16),

$$\tfrac{1}{2} r_0 = f_0^{(2)} / \left[f_0^{(0)} \right]^2 - f_0^{(0)}.$$

For $l \neq 0$, Eq. (13) leads to

$$f_l^{(0)} = \frac{lR^{2l+1}}{L^2(l+1)} - \frac{R^l}{4\pi i^l L(l+1)} \int \frac{U \psi_l^{(0)} d\tau}{k^l}$$

$[\psi_l^{(0)} \sim i^l k^l$; see Eq. (10)$]$, and

$$f_l^{(2l+1)} = i \left[f_l^{(0)} \right]^2 / (2l+1);$$

so that the constant term in the series (18) is

$$(2l+1)/f_l^{(0)}.$$

The f function (different from my f function) used by Breit and collaborators to describe proton-proton scattering goes into $k\cot\delta$ in the absence of a Coulomb field. Expansions of Breit's f around an energy other than zero and expansions in terms of parameters multiplying the potential, have been given by Breit and Yovits.[8] Expansions of Breit's f for the case $l>0$ have been given by Breit.[2] The form of Eq. (20), in fact, is given for the $p-p$ case by Eq. (7.5) of Breit, Condon, and Present,[9] and more explicitly by Eq. (7) of Breit and Bouricius.[10]

CONCLUSIONS

A solution of Eq. (13) for the S wave of the series given by Eq. (14) shows that it contains powers of $f_0^{(0)}$, the leading term being $k^n \left[f_0^{(0)} \right]^{n+1}$. The series is therefore good only up to $f_0^{(0)} k < 1$. This, in the $n-p$ case, is a more stringent restriction than the one requiring that $kR < 1$. Thus, for the $n-p$ triplet collision, the series is valid up to an energy of 2.9 Mev, and for the singlet case, up to 0.14 Mev. The series for $k\cot\delta$ is a better one to use where $f_0^{(0)} k$ is close to 1, since in it the positive powers of $f_0^{(0)}$ drop out, making the coefficients of k^n smaller than they are in the series for f. On the basis of our derivation of the series for $k\cot\delta$, it would appear that for large scattering lengths the energy limit for it is the same as for our series for f, namely $f_0^{(0)} k < 1$. This would throw doubt on the use of the series beyond this limit.

In the scattering of neutrons by complex nuclei it is possible to get small scattering lengths, and for these cases the expression for $k\cot\delta$ might be invalid even for low energies. The derivation according to Eq. (20) shows that if $f_0^{(3)} k^2 / \left[f_0^{(0)} \right]^2 > 1$, the series for $k\cot\delta$ would be invalid. The series for f, on the other hand, would be very useful in this case, as the requirement $f_0^{(0)} k < 1$ could lead to a high upper limit on the incident neutron energy.

[5] N. F. Mott and H. S. W. Massey, *The Theory of Atomic Collisions* (Oxford University Press, London, 1949), second edition, p. 24.
[6] T. Teichmann, Phys. Rev. **83**, 141 (1951).
[7] J. M. Blatt and V. F. Weisskopf, *Theoretical Nuclear Physics* (John Wiley and Sons, Inc., New York, 1952), Chap. II.
[8] G. Breit and M. C. Yovits, Proc. Natl. Acad. Sci. U. S. **37**, 771 (1951).
[9] Breit, Condon, and Present, Phys. Rev. **50**, 825 (1936).
[10] G. Breit and W. G. Bouricius, Phys. Rev. **75**, 1029 (1949).

Lifetime Measurements for the First Excited States of O^{17} and B^{10} from Recoil Studies*

JACQUES THIRION AND VALENTINE L. TELEGDI†
Kellogg Radiation Laboratory, California Institute of Technology, Pasadena, California
(Received August 24, 1953)

The following lifetimes have been measured: O^{17} 870-kev level, $(2.5\pm1)\times10^{-10}$ sec; B^{10} 720-kev level, $(7\pm2)\times10^{-10}$ sec. These values are compared with theoretical estimates based on the independent-particle model. Core excitation is required to explain the O^{17} lifetime.

THE measurement of the distance traversed by an excited recoil nucleus before de-excitation can be used for determining lifetimes of the order of 10^{-11} sec or longer.[1] We have applied this method to the γ rays emitted by the first excited states of O^{17} (870 kev) and B^{10} (720 kev).[2] These states were excited by deuteron-induced reactions on O^{16} and Be^{9}; a schematic view of the experimental setup is shown in Fig. 1. A collimated deuteron beam ($\frac{1}{8}$-in. diam) strikes a thin target mounted on a Ni backing (0.6 mg/cm^2) and the recoils are ejected into vacuum. The γ rays are detected by means of a NaI(Tl) spectrometer[3] (10 channels) of 8 percent resolution for the 870-kev photopeak. The crystal sees the region accessible to the recoils through a tungsten collimator and subtends a solid angle of 5×10^{-4} steradians. Mechanical displacement of the target with respect to this collimator enables one to vary the distance of flight of the recoils seen by the detector.

$O^{16}(d, p)O^{17*}$. The targets consisted of thin uniform SiO layers on Ni backing foils; the SiO was directly evaporated onto these foils. They were bombarded with 0.5 μa of deuterons of 1.32 Mev. Some preliminary runs with thin mica gave reproducible results, but these were discarded as these targets displayed some change in appearance after long bombardments. The thickness of these SiO targets was determined in a magnetic spectrometer[4] by measuring the energy loss, in the SiO layer, of monoenergetic protons scattered by the Ni foil. The result was 18 kev (for protons of 1230 kev); the uniformity of the targets, checked by the same method, was found to be better than 10 percent.

Figure 2 shows a comparison of the results obtained with theoretical curves calculated for various lifetimes. The magnitude of the effect is seen by comparison with the points obtained (curve B) with targets covered by a Ni foil thick enough to stop all recoils. Curve B represents the transmission of the collimator and should ideally be a step function. Its rounded-off edges determine the resolution of the set-up, which is seen to be of the order of 0.1 mm. The curve obtained without the additional Ni backing intersects curve B at a point which corresponds to the fraction of recoils escaping in the forward direction from the target; in the case illustrated in Fig. 2 this fraction is 0.8.

To calculate theoretical curves such as shown in Fig. 2, the range-velocity relation for the recoils as well as their angular distribution have to be known. For simplicity we assumed that R depends linearly on v, an assumption which finds some support in the available data.[5] The critical parameter is clearly the ratio, $f=t/R_M$, of the thickness, t, of the target to the maximum range, R_M, of the (forward) recoils. While the value of t is determined experimentally as indicated above with fair accuracy, R_M is known to only about

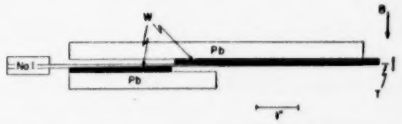

FIG. 1. Experimental set up. T=target, B=beam. Vacuum enclosure of target, mechanical means for moving it in direction of double-headed arrow, and equipment associated with the NaI crystal are not shown.

20 percent. In calculating the probability $W(z,\theta)d\theta$ that a recoil of radiative lifetime τ, emitted with an initial velocity $v_0(\theta)$ at an angle θ with respect to the normal, Z, to the target, radiates after traversing a distance z from the target surface it is convenient to measure the velocity component along Z, $v_0^{(z)}(\theta)$, in units of $v_0(0)$ and z in units of $v_0(0)\tau$, i.e., to introduce the dimensionless variables

$$u=v_0^{(z)}(\theta)/v_0(\theta)=v_0(\theta)\cos\theta/v_0(0), \quad \text{and} \quad x=z/v_0(0)\tau.$$

One finds easily

$$W(x,\theta)=\begin{cases}(u/f)F(x/u)-(1/f)(u-f)F(x/(u-f)) & \text{for } \theta\leqslant\theta_c,\\ (u/f)F(x/u) & \text{for } \theta>\theta_c,\end{cases}$$

* Assisted by the joint program of the U. S. Office of Naval Research and the U. S. Atomic Energy Commission.
† Visiting Research Fellow from the Institute for Nuclear Studies, University of Chicago, Chicago, Illinois.
[1] J. C. Jacobsen, Phil. Mag. **47**, 23 (1924); Devons, Hereward, and Lindsay, Nature **164**, 586 (1949).
[2] R. G. Thomas and T. Lauritsen, Phys. Rev. **88**, 969 (1952).
[3] H. H. Woodbury, thesis, California Institute of Technology, 1953 (unpublished).
[4] We are indebted for these measurements to Prof. W. A. Fowler and his group.
[5] P. M. S. Blackett and D. Lees, Proc. Roy. Soc. (London) **A134**, 658 (1932), and other papers discussed in reference 2.

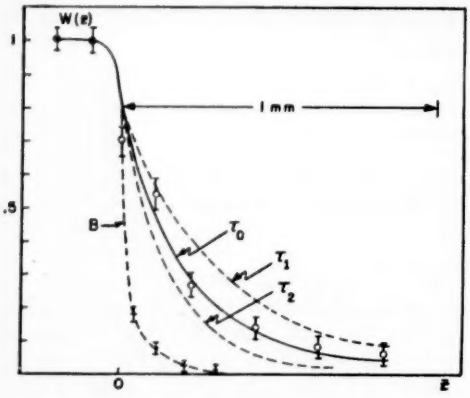

FIG. 2. Normalized intensity $W(z)$ *vs* target position z for 870-kev γ ray from $O^{16}(d, p)O^{17*}$ at 1.32-Mev deuteron energy. SiO target, 0.77-mm air equivalent (f=0.51); B=experimental curve obtained with target covered with Ni foil. The theoretical curves were calculated for the following lifetimes in units of 10^{-10} sec: $\tau_0=2.5$, $\tau_1=3.75$, $\tau_2=1.67$.

where θ_c is that "critical" angle for which the projected range, $t/\cos\theta_c$, is just equal to the range of the recoils, $t/\cos\theta_c \equiv R(v_0(\theta_c))$, while $F(y)\equiv \exp[-y]-y\int_y^\infty \exp[-\eta]d\eta/\eta$. $W(x,\theta)$ has to be weighted with the angular distribution of the recoils and integrated over θ. This was done numerically, using a distribution interpolated from published data;[6] effects of scattering in the target, which are estimated to be small, were not considered at this point. Figure 3 shows the distributions W(x) obtained for various values of f. For the purposes of this experiment, it is practical to use thicknesses such that $0<f<1$; thus 18 kev correspond to f=0.51. One sees that in this range f influences mainly the fraction of recoils stopped in the target, $1-W(0)$. This quantity, which is difficult to determine accurately, becomes thus the principal source of uncertainty in the fitting of theoretical curves to the experimental data and therefore in the determination of the lifetime.

The curves in Fig. 2 represent theoretical distributions corrected for scattering[7] and for the deviation of the transmission of the collimator from an ideal step function. The solid curves through the experimental points were calculated for a lifetime of 2.5×10^{-10} sec, and the dashed ones for lifetimes of 3.75×10^{-10} and 1.7×10^{-10} sec, respectively.

[6] N. P. Heydenburg and D. R. Inglis, Phys. Rev. **73**, 230 (1948).

[7] $\langle\theta^2\rangle$, the mean square angle of multiple scattering, is 0.04 for an O^{17} ion traversing an SiO layer of the thickness of our targets with a *constant* average velocity 10^8 cm/sec and an effective charge $z^*=1$, which is slightly larger than the value predicted by J. K. Knipp and E. Teller, Phys. Rev. **59**, 659 (1941). The value of $\cos\theta$ being reduced by a factor $\exp[-\theta^2/4]$, the effect of multiple scattering appears to be small for such velocities. On the other hand, for slower recoils, say for those leaving the target with velocities of $\sim5\times10^7$ cm/sec, it will be appreciable, leading to quasi-isotropy. In modifying the theoretical curves we assumed complete isotropy for the "slow" recoils as defined above. This procedure, which incidentally tends to overemphasize the effect of scattering, seems justified by the smallness of the correction.

We conclude that the lifetime of the 870-kev state of O^{17} is $(2.5\pm1)\times10^{-10}$ sec. This transition to the ground state is $E2$, $1/2^+\rightarrow5/2^+$, assigned to the extra neutron as $s_{\frac{1}{2}}\rightarrow d_{\frac{5}{2}}$ in the $j-j$ independent particle model (IPM). This description predicts[8] for a *proton* making the same transition a lifetime of 8×10^{-11} sec (using a "radius" of $1.5A^{\frac{1}{3}}\times10^{-13}$ cm), whereas a neutron outside the O^{16} core should yield a lifetime $Z^{-2}A^4$ times longer, i.e., 10^{-7} sec, due entirely to the motion of the core. To fit the observed lifetime on this picture, one has to assume a 2.9 times larger "radius," which does not appear reasonable. The observed lifetime can, however, be explained in terms of small departures from the extreme IPM, as the following somewhat rough argument shows: Write the wave function of O^{17} in its ground state as

$$\Psi(O^{17})=a_0\varphi_{d\frac{5}{2}}(n)\psi_0(O^{16})+a_2\varphi_{s\frac{1}{2}}(n)\psi_{2+}(O^{16})+\cdots,$$

where $\psi_{2+}(O^{16})$ describes a "collectively" excited state of the core and $|a_2|^2/|a_0|^2<1$, and for the excited state as

$$\Psi(O^{17*})=b_0\varphi_{s\frac{1}{2}}(n)\psi_0(O^{16})+b_2\varphi_{d\frac{5}{2}}(n)\psi_{2+}(O^{16})+\cdots.$$

Now, if the transition probability,

$$|\varphi_{s\frac{1}{2}}(n)\psi_{2+}(O^{16})H(E2)\varphi_{s\frac{1}{2}}(n)\psi_0(O^{16})|^2,$$

is assumed to be 20 times larger than the one previously considered for single proton transition, one sees that $|a_2|^2/|a_0|^2$ needs only to be 2/100 to fit the experimental result. This deviation does not necessarily conflict with the small quadrupole moment[9] of O^{17}.

$Be^9(d, n)B^{10*}$. Thin Be foils[10] where bombarded with deuterons at different energies. Best results were obtained at 1.32 Mev with targets of 40 μg/cm^2. The experimental points are shown in Fig. 4. Their interpretation is not quite straightforward, because the

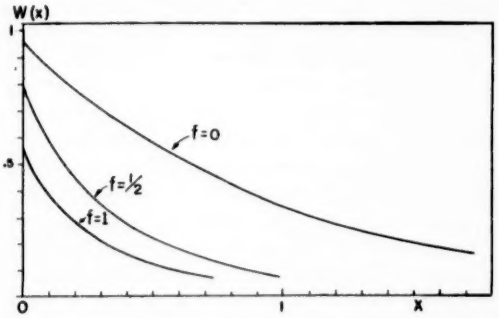

FIG. 3. Theoretical curves $W(x)$ *vs* $x=z/v_0(0)\tau$ for different ratios f of the target thickness t to the maximum range R_M of the recoils.

[8] V. F. Weisskopf, Phys. Rev. **83**, 1073 (1951); S. A. Moszkowski, Phys. Rev. **83**, 1071 (1951).

[9] Geschwind, Gunther-Mohr, and Townes, Phys. Rev. **83**, 209 (1951).

[10] Courtesy of Dr. Hugh Bradner, Radiation Laboratory, University of California, Berkeley, California.

lowest (720-kev) level of B^{10} can be produced both directly and by γ decay from higher states (1.76, 2.15, and 3.6 Mev). To calculate the curve for a given lifetime, one has to know the relative intensities and angular distributions of the neutrons leading to all the states involved. Lacking this information, we made the assumptions contained in Table I, based on available data.[11] Taking the lack of information just mentioned into account, we conclude that the lifetime is $(7\pm2)\times10^{-10}$ sec.

TABLE I. Assumptions on the transitions leading to the 720-kev level of B^{10} in $Be^9(d, n)B^{10}$.

B^{10} level (kev)	Contribution to the 720-kev γ ray (%)	C.m. distribution of neutrons
720	50	$1-\frac{1}{2}\cos^2\theta$
1740	8	1
2150	21	1
3580	21	1

In the IPM picture, the corresponding transition involving a single nucleon would lead a lifetime of 5×10^{-10} sec, which is a lower limit for the actual case in which two unpaired nucleons are coupled. A transition between two terms of a $(p_{\frac{1}{2}})^2$ configuration yields a value of 5×10^{-9} sec. The observed lifetime is thus compatible with the IPM picture.

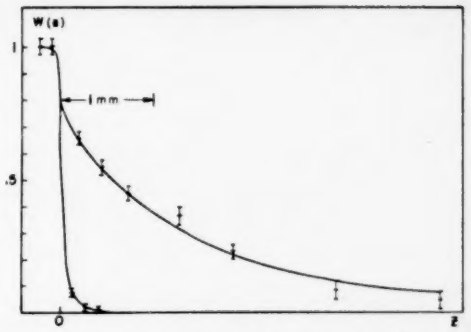

FIG. 4. Normalized intensity $W(z)$ *vs* target position x for 720-kev γ ray from $Be^9(d, n)B^{10*}$. Target 40 $\mu g/cm^2$ Be foil, $E_d=1.32$ Mev. Same notation as in Fig. 2. Theoretical curve calculated for $\tau=7\times10^{-10}$ sec.

It is a pleasure to express our gratitude for the kind hospitality received in this laboratory. We also wish to thank Professors C. C. Lauritsen, W. A. Fowler, and R. F. Christy for much assistance and helpful discussions. This experiment could not have been carried out without the electronic equipment built by Dr. H. H. Woodbury, to whom we are also indebted for much patient assistance.

[11] F. Ajzenberg and T. Lauritsen, Revs. Modern Phys. **24**, 347 (1952).

The Spin of Si^{29} and Mass Ratios of the Stable Si Isotopes*

R. L. WHITE AND C. H. TOWNES
Columbia University, New York, New York

(Received August 25, 1953)

The $J=0\rightarrow1$ microwave transition of $Si^{29}D_3F$ has been examined under high resolution for hyperfine structure due to Si^{29}. No hyperfine structure was found, which sets an upper limit of 1×10^{-28} cm² to the quadrupole moment of Si^{29}. This is good evidence that the Si^{29} spin is 1/2. The measurement also allows an accurate determination of mass difference ratios for the Si isotopes.

CONFLICTING and somewhat inconclusive pieces of evidence on the spin of Si^{29} are already available from microwave and radiofrequency spectroscopy.[1-3] Although a recent angular correlation experiment[4] appears to provide evidence that the spin is 1/2, it seemed desirable to press the microwave measurements somewhat further than has previously been done.

If the spin of Si^{29} were greater than 1/2 and the nuclear quadrupole moment nonzero, the rotational microwave spectra of Si^{29} compounds would be expected to exhibit hyperfine structure arising from the coupling of the nuclear quadrupole moment to the molecular fields. The spectrum of $Si^{29}D_3F$ was examined with a high-resolution spectrometer in this laboratory, and no such hyperfine structure was found.

If the nuclear quadrupole coupling constant, eqQ, were small, an unresolved hyperfine structure appearing as line broadening might be expected. The $J=0\rightarrow1$ transition of $Si^{29}D_3F$ has been measured to have a line width at half-intensity of 64 ± 6 kc/sec at $-78°$C in X-band waveguide at a pressure less than 10^{-3} mm. The same transition in $Si^{28}D_3F$ under identical conditions was observed to have a half-width of 63 ± 3 kc/sec. Si^{28} may be assumed to have spin 0, and hence no hyperfine structure. No evidence of line broadening in $Si^{29}D_3F$ is indicated. A quadrupole coupling constant eqQ of 50 kc/sec would give a line broadening of over 10 kc/sec. Hence if the spin of Si^{29} is not 1/2, its eqQ is less than 50 kc/sec in the compound examined. This is 2000 times smaller than the quadrupole coupling constant of Ge^{73} in the similar chemical compound GeH_3Cl.

One can calculate approximately what the maximum quadrupole moment of the Si^{29} nucleus might be consistent with the upper limit of 50 kc/sec on eqQ. This is accomplished by obtaining an approximate value of q, the gradient of the electric field along the molecular axis, from a knowledge of the bonding structure.[5] In the covalent structure of SiD_3F the three p orbitals are equally populated, hence are spherically symmetric and cannot contribute to q. In the ionic structure one p orbital is 75 percent vacated, assuming tetragonal hybridization. The Si−F bond might be expected to be 70 percent or more ionic on the basis of curves[6] of ionic character *versus* electronegativity differences, as well as from the bond length.[2] Let us assume then that the ionic structure is 80 percent important. Then the q in SiD_3F would be 60 percent of that in SiII. The q of SiII may be calculated by the usual method from the known doublet separation, 287 cm^{-1}, to be $q=8.5\times10^{15}$ esu. Hence, for the partially ionic structure of SiD_3F, $q=5.1\times10^{15}$ esu. This makes the quadrupole moment of Si^{29} a factor of 30 smaller than the smallest value observed for a nucleus (the deuteron) with a spin greater than 1/2, and a factor of several hundred smaller than the moments for neighboring nuclei. The quadrupole moment of Si^{29} would not be expected to be large from what is known of its structure. However, if the Si^{29} spin is not one half, its quadrupole moment should be roughly 100 times larger than the upper limit set by this experiment.

From the above, it may be seen that our failure to observe hyperfine structure in the $Si^{29}D_3F$ spectrum affords strong evidence that the spin of Si^{29} is 1/2.

The isotopic mass ratio for the stable silicon isotopes was also measured. The frequencies of the $J=0\rightarrow1$ transition of the various isotopes were as follows:

$$Si^{30}D_3F=24\ 203.898\pm0.002\ \text{Mc/sec},$$
$$Si^{29}D_3F=24\ 351.160\pm0.003\ \text{Mc/sec},$$
$$Si^{28}D_3F=24\ 506.229\pm0.003\ \text{Mc/sec}.$$

From these frequencies one computes the mass ratio:

$$\frac{M(30)-M(29)}{M(30)-M(28)}=0.49934\pm0.00003.$$

This compares extremely well with the measurement of Duckworth, Preston, and Woodcock,[7] from mass spectrographic data:

$$\frac{M(30)-M(29)}{M(30)-M(28)}=0.49934\pm0.00006.$$

* Work supported by the U. S. Atomic Energy Commission.

[1] Townes, Mays, and Dailey, Phys. Rev. **76**, 700 (1949).
[2] Sharbaugh, Thomas, and Pritchard, Phys. Rev. **78**, 64 (1950).
[3] R. H. Sands and G. E. Pake, Phys. Rev. **89**, 896 (1953).
[4] C. F. Black, Phys. Rev. **90**, 381 (1953).
[5] C. H. Townes and B. P. Dailey, J. Chem. Phys. **17**, 782 (1949).
[6] L. Pauling, *The Nature of the Chemical Bond* (Cornell University Press, Ithaca, 1945); C. H. Townes and B. P. Dailey, Phys. Rev. **78**, 346 (1950); W. Gordy, J. Chem. Phys. **19**, 792 (1951).
[7] Duckworth, Preston, and Woodcock, Phys. Rev. **79**, 188 (1950); H. E. Duckworth and R. S. Preston, Phys. Rev. **79**, 402 (1950).

It also compares well with an earlier microwave determination by Geschwind and Gunther-Mohr.[5]

$$\frac{M(30)-M(29)}{M(30)-M(28)}=0.49941\pm0.00005.$$

ACKNOWLEDGMENT

We are very grateful to Drs. Børge Bak and John Anderson of the University of Copenhagen for furnishing us the SiD_3F used in this investigation.

[5] S. Geschwind and G. R. Gunther-Mohr, Phys. Rev. **81**, 882 (1951).

PHYSICAL REVIEW VOLUME 92, NUMBER 5 DECEMBER 1, 1953

The Isomeric Transition of Pb^{207} as an Energy Standard in Beta Spectroscopy

DAVID E. ALBURGER*
Nobel Institute of Physics, Stockholm, Sweden
(Received August 24, 1953)

The K-conversion line of the 1.06-Mev isomeric transition following the electron-capture decay of Bi^{207} is suggested as a useful energy standard for beta-spectroscopy. While the 50-year half-life and 10 percent conversion coefficient are comparable to Cs^{137}, the 60 percent higher energy, larger percentage K to L momentum separation, and the possibility of making thin and more uniform sources may be advantageous. Precision measurements have been carried out in a double-focusing spectrometer by comparison with the 1.02-Mev electrons of RaC. The Pb^{207} K-line has a momentum of 4657.9 ± 1.0 gauss-cm from which an electron energy of 975.9 ± 0.3 kev and a transition energy of 1063.9 ± 0.3 kev are derived. Measurements have also been made on the K/L and $K/(L+M)$ ratios, which are 3.95 ± 0.25 and 3.00 ± 0.25 respectively. When compared with data on other $M4$ transitions, these results indicate that deviations from the empirical K/L curves take place at high Z. The usefulness of Bi^{207} as a test source for beta-gamma coincidence detectors is discussed.

INTRODUCTION

ABOVE 0.5 Mev the only generally useful internal-conversion reference standards which have been measured[1] up to the present with an accuracy of ~2 parts in 10^4 are the 3381.3 gauss-cm line of Cs^{137} and the 9986.7 gauss-cm line of ThX. Although the 1.33-Mev gamma ray of Co^{60} and two electron lines of RaC at 1.02 and 1.32 Mev have now been determined[2] within this accuracy, the Co conversion electrons are impractical to use because of low-conversion coefficient, small K to L separation, and poor specific activity, while the RaC has the difficulties of a 20-min half-life and a large beta-ray continuum under the lines.

Bi^{207} offers the possibility of partially filling in the wide gap between Cs^{137} and ThX, insofar as electron lines are concerned. This isotope, which decays by electron capture to Pb^{207}, was first reported[3] by Neumann and Perlman. They estimated the half-life as being approximately 50 years, and they found a number of internal-conversion lines which they measured in a shaped magnetic field beta-ray spectrometer at 1.5 percent resolution. By far the strongest line occurs at 975 kev, corresponding to a transition energy of 1063 kev. A 0.9-sec isomeric activity in lead, observed[4] somewhat earlier by Campbell and Goodrich, was interpreted[5] by Goldhaber and Sunyar as belonging to the 1.06-Mev gamma ray of Pb^{207}, which they then assigned as an $M4$ transition. Relative conversion coefficients of the 1.06- and 0.56-Mev gammas, derived by Grace and Prescott[6] and by Wapstra,[7] supported this assignment. Recently Friedlander *et al.* have shown[8] conclusively that the 0.9-sec activity belongs to Pb^{207}.

Although the decay scheme of Bi^{207} is not yet established, it is probable that the isomeric transition occurs in a fairly large percentage of the decays. The theoretical K-shell conversion coefficient of the isomer is 0.103, and one can expect a yield of conversion electrons quite comparable to that from a similar source strength of Cs^{137}. Because there is no electron continuum and the other lines in the Bi^{207} spectrum are relatively low in intensity and widely separated, the K-1064 line can be used with virtually no scattered background effects.

Aside from extending the energy range of electron reference lines by approximately 60 percent above Cs^{137}, the bismuth activity has several advantages over the latter. One of these is the larger percentage momentum separation between K and L lines resulting from the higher atomic number. In the case of cesium the K to L separation amounts to 3.5 percent in momentum. When

* National Science Foundation Fellow on leave from Brookhaven National Laboratory, now returned to latter address.

[1] Lindström, Siegbahn, and Wapstra, Proc. Phys. Soc. (London) **B66**, 54 (1953).

[2] Lindström, Hedgran, and Alburger, Phys. Rev. **89**, 1303 (1953).

[3] H. M. Neumann and I. Perlman, Phys. Rev. **81**, 958 (1951).

[4] C. Campbell and M. Goodrich, Phys. Rev. **78**, 640 (1950).

[5] M. Goldhaber and A. W. Sunyar, Phys. Rev. **83**, 906 (1951).

[6] M. A. Grace and J. R. Prescott, Phys. Rev. **84**, 1059 (1951).

[7] A. H. Wapstra, thesis, Amsterdam, 1953 (unpublished).

[8] Friedlander, Wilson, Ghiorso, and Perlman, Phys. Rev. **91**, 498 (1953).

working at a spectrometer resolution no better than 2.5 percent, it is not possible for calibration purposes to establish the extrapolated high-energy edge of the K line with an accuracy which could be expected if the L-conversion electrons did not interfere. Bi^{207}, on the other hand, has a K to L separation of 5.5 percent in momentum, or 1.6 times that of Cs^{137}. Thus at 3 percent resolution there will still not be any calibration difficulties because of the L electrons.

Another advantage results from the ease with which thin and very uniform sources of Bi^{207} can be prepared by carrier-free chemistry and electroplating techniques. In part of this work measurements have been made at a resolution of 0.23 percent with no perceptible energy-spread of the 976-kev line as a result of source thickness.

Conversion electron intensity ratios of this transition are of interest for comparison with the improved empirical curve of $K/(L+M)$ ratios for $M4$ transitions published[9] by Graves, Langer, and Moffat. Experimental $K/(L+M)$ values of the Pb^{207} isomer have been reported as 4.6 by Neumann and Perlman[3] and 3.4 by Wapstra,[7] These results differ widely from each other, and neither falls as close to the curve of Graves *et al.* as one would like unless the unstated experimental errors are large or there exist deviations at high Z. In Wapstra's measurements the K- and L-lines were barely resolved, and the intensity ratio was obtained by a certain amount of curve analysis.

EXPERIMENTAL PROCEDURE AND RESULTS

The Bi^{207} sources, prepared originally in connection with an investigation of Bi^{206} decay, were made by bombarding lead targets in the large cyclotron with 25-Mev deuterons for 100–200 microampere-hours. After allowing several days for 12-hour Bi^{204} to decay, separations of bismuth were carried out by Dr. W. Forsling and Mr. T. Karlsson according to the chemical procedures described[10] earlier. Final energy measurements were made on the Bi^{207} line with a 2 mm×14 mm sample which had been electroplated on a copper-foil backing at a potential of 3 volts for 30 minutes. Conversion intensities were studied with a larger and somewhat stronger source estimated to contain approximately 1 microcurie of Bi^{207}.

The 1.02-Mev electron line of RaC mentioned earlier is a very convenient reference standard since its momentum, which has been measured[2] absolutely as 4839.8±0.8 gauss-cm, lies only 3.8 percent higher than the Bi^{207} K line. In this energy region the nonlinearity of the spectrometer has proved[2] to be not more than 1 part in 10^4 per 10 percent change of momentum. Thus any effect of nonlinearity in these experiments is expected to be small compared with other errors. Strong sources of RaC were made by electrostatic collection on copper strips using 75–400 mC ampules of radon in a special radon chamber designed by Professor H. Slätis.

Comparisons of Bi^{207} and RaC were carried out in the 50-cm radius double-focusing spectrometer at a resolution of 0.23 percent by determining the extrapolated high-energy edges of the K lines. The sources were attached to a holder which has a 2-mm wide slit and whose position in the spectrometer can be reproduced accurately. In the RaC runs, a monitoring technique corrected for source decay. The average of four comparison measurements which agreed with each other to within 1 part in 10^4 gives the ratio of Bi^{207}: RaC momenta as 0.96241±0.00017. From this figure a momentum of 4657.9±1.0 gauss-cm can be derived for Bi^{207} based on the absolute value of RaC. The corresponding Bi^{207} electron energy is 975.9±0.3 kev and the transition energy, found by adding the 88.0-kev binding energy[11] of lead, is 1063.9±0.3 kev.

In one of the runs a check was made by determining the extrapolated edge of the Cs^{137} line. The spectrometer calibration constant obtained in this measurement differed by 3.7 parts in 10^4 from that derived from RaC. This is just at the limit of the combined probable errors of the two absolute values and cannot be interpreted as establishing a definite nonlinearity of the spectrometer as great as $1:10^4$ per 10 percent momentum change.

A study of the relative conversion intensities of the 1.06-Mev transition was made at a spectrometer resolution of 0.40 percent where the L and M electrons are completely separated. From measurements of the shapes and amplitudes of the lines the following ratios are derived: $K/L=3.95\pm0.25$ and $K/(L+M)=3.00\pm0.25$. The L line has a width and shape closely similar to the K line, and it is easily shown at this resolution that it corresponds in energy to L_{I} and/or L_{II} electrons. There is no suggestion that L_{III} electrons are present. In any case their intensity is not more than 15 percent of the total L conversion.

Recent work[12] of Prescott has indicated that a hitherto undetected or unresolved "prompt" transition of about 1.0-Mev may be present in Bi^{207} decay. A careful search was made over the gamma-energy range 1064 kev±25 percent both at 0.75 and 0.4 percent resolution for the K-conversion electrons associated with such a transition. An upper limit of 1.5 percent intensity relative to K-1064 can be placed on the existence of such a line unless it falls on one of the 1064-kev conversion lines.

DISCUSSION

Counting rates at the peak of the K-1064 line varied from 500 per minute at 0.75-percent resolution down to 40 per minute at 0.23-percent resolution. While these intensities are admittedly very low for use as calibration

[9] Graves, Langer, and Moffat, Phys. Rev. **88**, 344 (1952).
[10] D. E. Alburger and G. Friedlander, Phys. Rev. **81**, 523 (1951).
[11] Hill, Church, and Mihelich, Rev. Sci. Instr. **23**, 523 (1952).
[12] J. R. Prescott, thesis, Oxford, 1953 (unpublished).

standards, it may be pointed out that the chemical separations were made at a time when more than half of the active bismuth atoms consisted of Bi^{205} and Bi^{206} and furthermore no attention was paid to the amount of Bi^{207} in the samples. The experiments described here were performed 6 months after bombardment, by which time the Bi^{207} was essentially the only activity remaining. When the original plating solution was counted, it was found that less than one-third of the total activity had been removed in preparing the samples. From the standpoint of Bi^{207} calibration sources, it would be more favorable to make a long deuteron bombardment of lead, i.e., at least 1000 microampere-hours, and then to allow several months to elapse before doing chemistry on the target. With careful chemistry very high specific activities of Bi^{207} can be expected since, in the carrier-free state, one microcurie of Bi^{207} corresponds to a mass of 3×10^{-5} mg. Sources of 1 to 10 microcurie per mm^2 should be adequate for most purposes, and even if a small amount of bismuth carrier is added during the separation, the source thickness should not be appreciable.

The K-565 conversion line of Bi^{207}, whose intensity according to Neumann and Perlman is lower than K-1064 by a factor of 5, might also make a useful calibration standard. The sources now available here are too weak to carry out precision determinations on this line.

Cross-section functions for the production of various bismuth-isotopes are not known at present. However, it has been observed by study of the conversion electron lines that the ratio of Bi^{207} to Bi^{206} produced by thick lead target bombardment with deuterons at 25 Mev is several times as great as it is at 16 Mev. At the same time the 14-day lines of Bi^{205} are extremely weak in the sources made at the lower energy, which indicates that this isotope is probably formed by the $Pb^{206}(d,3n)Bi^{205}$ reaction whose threshold must be in the neighborhood of 16 Mev. Although the yield of Bi^{207} at 16 Mev is considerably lower than it is at 25 Mev, there is an advantage in that the waiting period which must be allowed for decay of shorter-lived activities depends mainly on 6-day Bi^{206} and not on 14-day Bi^{205}.

The $K/(L+M)$ ratio of 3.00 ± 0.25 obtained in the present work is lower than the value 4.0 from the curve of Graves *et al.* by considerably more than the error. This is not the first time that deviations from the empirical curves at high Z and high energy have been observed. Another case is that of Pb^{206}, whose first excited state at 803 kev results in $E2$ radiation giving[10] a $K/(L+M)$ ratio of 3.7. Later and more accurate measurements[13] on Po^{210} and Bi^{206} have yielded the values 3.8 and 4.0 respectively for this transition. The ratio according to the curve of Goldhaber and Sunyar, extended[14] to lower Z^2/E, should be greater than 6 for electric quadrupole radiation. The results on Bi^{207} presented here give further evidence that deviations from the empirical curves occur for energetic transitions in high-Z elements. Both of the transitions considered above have $K/(L+M)$ ratios which are approximately 30 percent lower than the empirical curves. In such cases the assignments of multipole orders based on conversion ratios should be made with some degree of caution.

Since the 1.06- and 0.565-Mev transitions of Pb^{207} have been shown[6] to be in cascade and to be approximately equal in intensity, Bi^{207} can be expected to be useful for testing the over-all efficiency of beta-gamma coincidence arrangements. Application can be made either to simple counters or to coincidence spectrometers such as a magnetic lens for electrons in conjunction with a gamma scintillation detector. The 10-percent K-conversion coefficient of the 1.06-Mev transition together with the reasonably high efficiency for detecting the gammas in a crystal allows a good yield of coincidences between the conversion electrons and the 565-kev gammas to be observed. Dr. S. Thulin of this laboratory has recently used Bi^{207} samples electroplated on 2.5 mg/cm^2 copper backings for such purposes in the Slätis-Siegbahn intermediate-image spectrometer modified with a NaI gamma detector near the source.

ACKNOWLEDGMENTS

The author is indebted to Dr. A. Hedgran for helpful discussions of precision techniques. Cyclotron bombardments were kindly performed under the direction of Dr. H. Atterling, and chemical separations of the activity were carried out by Dr. W. Forsling and Mr. T. Karlsson. The author would like to thank Professors Manne Siegbahn and Kai Siegbahn for the generous hospitality of the Nobel Institute during 1952–53.

[13] D. E. Alburger (unpublished values).
[14] D. E. Alburger, Phys. Rev. **88**, 339 (1952).

Erbium[163] and Thulium[165]

THOMAS H. HANDLEY AND ELMER L. OLSON
Oak Ridge National Laboratory, Oak Ridge, Tennessee

(Received July 20, 1953; revised manuscript received August 20, 1953)

A 75-minute activity produced by bombarding Ho^{165} with protons is assigned to Er^{163}. A 24.5-hour activity produced by proton bombardment of erbium is assigned to Tm^{165}. Gamma-ray spectra are given for both isotopes.

ERBIUM[163]

HIGHLY purified holmium oxide was bombarded with 24-Mev protons in the ORNL (Oak Ridge National Laboratory) 86-inch cyclotron.[1] Following bombardment, chemical separations were made by ion exchange techniques[2] and an activity of 75-minute half-life was found in the erbium fraction. The excitation function, Fig. 1, shows a threshold of 19 Mev which indicates that the activity was produced by a $(p,3n)$ reaction. This would assign to the 75-minute activity a mass of 163. An initial separation was made immediately following bombardment, then a second separation was made immediately on the erbium fraction from the first separation. An analysis of decay curves from the second separation places a limit of <30 minutes on the half-life of the daughter of Er^{163}, assuming it to be short. In another determination, the decay of the erbium fraction was followed for a sufficient time to place a limit of >1 year on the half-life of the daughter, assuming it to be long. Proton bombardment of dysprosium did not give a 5.2-day activity as previously reported[3] for Ho^{163}. From the yield of the 5.0-hour holmium activity, as determined by counting the electron capture activity on the x-ray peak with a scintillation spectrometer, it was determined that the production of any 5.2-day activity was less by a factor of 10^5 than for the 5.0-hour activity. These activities would have been produced from dysprosium isotopes of approximately equal abundance and, since the cross sections for these reactions are very nearly equal, it may be safely assumed that a 5.2-day activity is not a product of this reaction. Similar measurements were obtained by means of an end-window G. M. tube with the same results, thus eliminating the possibility of a positron emitter. This would eliminate the 5.2-day activity as a product of proton bombardment of dysprosium and also as the daughter of Er^{163}. The problem of holmium activities produced by proton bombardment of dysprosium is being investigated and will be reported at a later date. The 65-hour activity previously assigned[4] to Er^{163} was not observed as a product of proton bombardment of holmium oxide. A gamma spectrum was run with a scintillation spectrometer. In order to resolve the more energetic portion of the spectrum and to prevent jamming of the instrument with the more abundant x-rays, a lead absorber was used with a very strong sample. A much weaker sample was used to resolve the less energetic portion of the spectrum; this accounts for the break in the spectrum curve, Fig. 2. Gamma-ray peaks were found at 0.430 Mev and 1.10 Mev, and an x-ray peak at 0.053 Mev. The 0.51-Mev annihilation peak was not observed; if positrons are present they constitute a very small fraction of the activity.

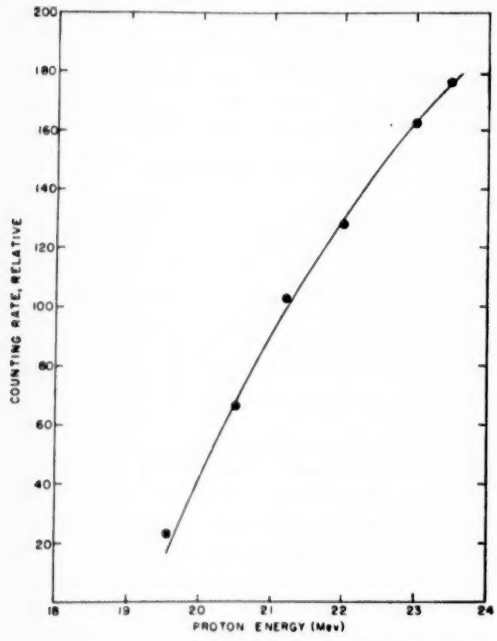

FIG. 1. Excitation function of the reaction $Ho^{165}(p,3n)Er^{163}$.

THULIUM[165]

Highly purified erbium oxide was also bombarded with 24-Mev protons in the ORNL 86-inch cyclotron. In separations made by ion exchange, a 24.5-hour activity was found associated with the thulium fraction. When the energy of the protons was reduced to 12 Mev

[1] R. S. Livingston, Nature **170**, 221 (1952).
[2] B. H. Ketelle and G. E. Boyd, J. Am. Chem. Soc. **69**, 2800 (1947).
[3] G. Wilkinson and H. G. Hicks, Phys. Rev. **79**, 815 (1950).
[4] Folger, Stevenson, and Seaborg, University of California Radiation Laboratory Classified Report UCRL-1195, revised May, 1951 (unpublished).

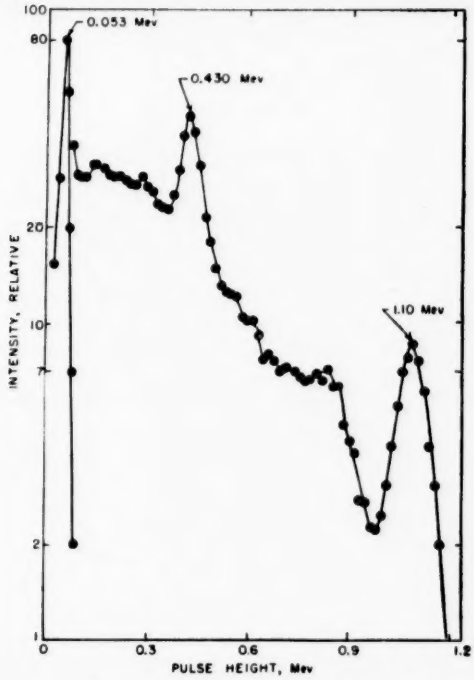

FIG. 2. Gamma-ray spectrum of Er^{163}.

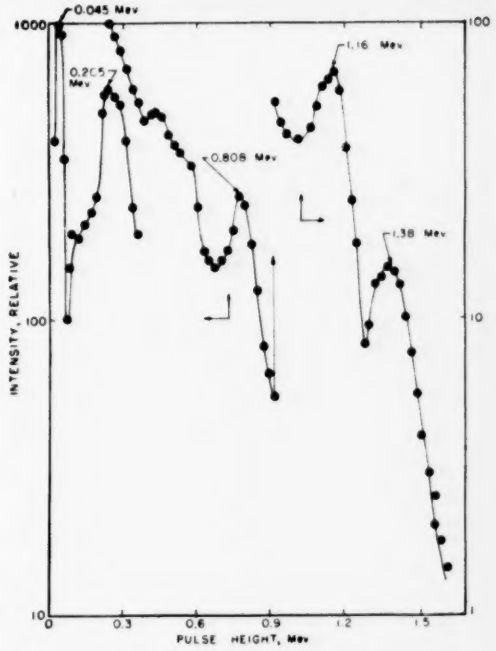

FIG. 3. Gamma-ray spectrum of Tm^{165}.

with aluminum absorbers, no 24.5-hour activity was obtained. This test excludes a (p,n) reaction for the formation of the 24.5-hour activity and therefore excludes all mass assignments higher than 165. In two other experiments, initial separations were made immediately following bombardment and a second separation was made three days later on the thulium fraction from the first separation. The only activity found with the erbium fraction was 10.5-hour Er^{165}. A third separation was made seven days after the second separation and again Er^{165} was found to have grown in. A fourth separation, made twenty days after the bombardment, did not show the presence of Er^{165}. Relative intensities of the 10.7-hour Er^{165} fraction indicated that the parent must have a half-life of the order of 25 hours. These separations also eliminate the possibility of the 7.7-hour or 9.5-day thulium activities as being the parent of Er^{165}, if they had previously been given incorrect mass assignments. Therefore, the 24.5-hour activity is assigned to Tm^{165} and it is the parent of 10.5-hour Er^{165}.

The gamma spectrum was resolved by waiting 80 hours following bombardment to allow the 7.7-hour Tm^{166} to decay before making a separation. The spectrum was run each day for twenty days and decay curves were plotted for each experimental point. These were analyzed for the 24.5-hour component and corrections were made in the low-energy range for the growth of 10-hour Er^{165}; the results are plotted in Fig. 3. The spectrum of the longer-lived background activity was very similar to the corrected spectrum for the 24.5-hour activity. The investigation is being continued in an effort to obtain spectra for Tm^{167} and Tm^{168}.

To prevent jamming of the spectrometer by the low-energy portion of the spectrum, an appropriate lead absorber was used with a very strong sample to resolve the more energetic portion of the spectrum since this constituted a very small fraction of the decay scheme. A much weaker source was used without absorbers to obtain the spectrum of the low-energy fraction. This accounts for the break in the spectrum curve, Fig. 3. It may be noted that gamma peaks were obtained at 1.38 Mev, 1.16 Mev, 0.808 Mev, and 0.205 Mev, with the x-ray peak at 0.045 Mev. The 0.51-Mev annihilation peak was not observed; if positrons are present, they constitute a very small fraction of the decay scheme.

ACKNOWLEDGMENTS

The authors are indebted to B. L. Cohen and B. H. Ketelle of this laboratory for their interest in this work, and their helpful suggestions.

The Spin and Magnetic Moment of Ti^{47} and Ti^{49} and the Magnetic Moment of Ge^{73}

C. D. JEFFRIES
Physics Department, University of California, Berkeley, California
(Received August 3, 1953)

The spin and magnetic moment of Ti^{47} and Ti^{49} have been measured by nuclear induction. The results are: $I(Ti^{47})=5/2$, $I(Ti^{49})=7/2$, $\mu(Ti^{47})=-(0.78706\pm0.0001)$ nm, $\mu(Ti^{49})=-(1.1022\pm0.0002)$ nm. The magnetic moment of Ge^{73} has been measured by nuclear induction with the result: $\mu(Ge^{73})=-(0.87675\pm0.00012)$ nm. These results are compared to the predictions of the shell model of nuclear structure.

I. TITANIUM 47 AND 49

A NUCLEAR induction signal in $TiCl_4$ which showed a structure has been previously reported;[1] this resonance signal was attributed to either Ti^{47} or Ti^{49}. Using a nuclear induction spectrometer similar to those described by Proctor[2] and by Weaver,[3] recent measurements made with separated Ti isotopes have shown that the structure of the line is not due to chemical effects as was previously thought but is actually the superposition of the close lying resonance lines of Ti^{47} and Ti^{49}. Using two different samples of $TiCl_4$, one containing 63-percent Ti^{47} and only 0.7-percent Ti^{49}, the other containing only 1.2-percent Ti^{47} and 77-percent Ti^{49}, we have observed in the same magnetic field the ratio of the nuclear magnetic resonance frequencies of Ti^{47} and of Ti^{49} to that of D^2 in a sample of D_2O containing 1 molar Mn^{++} ions as a paramagnetic catalyst. Our results are

$$\nu(Ti^{47})/\nu(D^2)=0.36721\pm0.00006, \quad (1)$$

$$\nu(Ti^{49})/\nu(D^2)=0.36731\pm0.00006. \quad (2)$$

The polarity of the Ti^{47} and Ti^{49} signals has been observed to be opposite to that of D^2, indicating that their magnetic moments are negative. Using a sample of $TiCl_4$ containing Ti^{47} and Ti^{49} in their natural abundances, we have furthermore clearly resolved the two Ti resonances under conditions of higher resolution than originally used. The frequency ratios are identical to those of (1) and (2) above. We have also observed in the same magnetic field $\nu(Ti^{49})/\nu(Ti^{47})=1.00026\pm0.00002$. Thus the gyromagnetic ratios of Ti^{47} and Ti^{49} are remarkably close; since the spins are different, as will be shown, this is probably a coincidence.

Ti signals have also been observed in H_2TiF_6 at a frequency approximately 0.1 percent lower than in $TiCl_4$. This "chemical shift"[4] has not yet been measured exactly because of the chemical instability of H_2TiF_6, but its existence indicates a possible uncertainty of this order of magnitude in the magnetic moments of Ti^{47} and Ti^{49} reported below in (6) and (7).

According to Bloch's theory[5] of nuclear induction, the spins $I(a)$ and $I(b)$ of two nuclei a and b may be compared, in principle, by observing the heights $H(a)$, $H(b)$ and the widths $W(a)$, $W(b)$ of the nuclear induction signals for the two nuclei. It can be shown[6] that if slow passage conditions prevail and if the radiofrequency field is small compared to its saturation value, then when the radiofrequency is the same for both nuclei,

$$R\equiv\frac{I(a)[I(a)+1]}{I(b)[I(b)+1]}=\left[\frac{N(b)}{N(a)}\right]\left[\frac{H(a)}{H(b)}\right]\left[\frac{W(a)}{W(b)}\right]^2\left[\frac{\gamma(b)}{\gamma(a)}\right]^3, \quad (3)$$

where $N(a)$, $N(b)$ are the relative number of nuclei and $\gamma(a)$, $\gamma(b)$ are the gyromagnetic ratios. Previous spin determinations[6,7] have compared an unknown spin $I(a)$ to a known spin $I(b)$. However Eq. (3) will also uniquely determine both $I(a)$ and $I(b)$ even if both are unknown [except in the case $I(a)=I(b)$], if the additional assumption is made that the spins have quantized values. In the present case the line shape of the Ti resonances is different from that of Cl^{35} in $TiCl_4$ and a comparison of $I(Ti)$ to $I(Cl^{35})$ is not justified. The line shapes of the Ti^{47} and the Ti^{49} resonances, on the other hand, are identical under widely varying conditions and it is believed that application of Eq. (3) is valid. For a series of 13 measurements of the heights and widths of the Ti^{47} and Ti^{49} resonances in natural abundance $TiCl_4$ we find, using Eq. (3),

$$R\equiv\frac{I(Ti^{47})[I(Ti^{47})+1]}{I(Ti^{49})[I(Ti^{49})+1]}=0.568\pm0.037, \quad (4)$$

where we have used the abundance ratio $N(Ti^{49})/N(Ti^{47})=0.743$, which is the average of the reported values.[8] Both these Ti isotopes are odd nuclei and it may be safely assumed that the spins are half odd integers. The above experimental result then establishes

[1] Jeffries, Loeliger, and Staub, Phys. Rev. **85**, 478 (1952).
[2] W. G. Proctor, Phys. Rev. **79**, 35 (1950).
[3] H. E. Weaver, Phys. Rev. **89**, 923 (1953).
[4] W. C. Dickinson, Phys. Rev. **81**, 717 (1951).
[5] F. Bloch, Phys. Rev. **70**, 406 (1950).
[6] C. D. Jeffries, Phys. Rev. **90**, 1130 (1953).
[7] W. G. Proctor, Phys. Rev. **79**, 35 (1950); F. Alder and F. C. Yu, Phys. Rev. **81**, 1067 (1951).
[8] A. O. Nier, Phys. Rev. **53**, 282 (1938); R. F. Hibbs, Oak Ridge National Laboratory Report *Y*-508, 1949 (unpublished); H. C. Mattraw and C. F. Pachucki, U. S. Atomic Energy Commission Report AECU-1903 (unpublished).

that

$$I(\mathrm{Ti}^{47})=5/2, \quad \text{and} \quad I(\mathrm{Ti}^{49})=7/2, \tag{5}$$

for which the ratio $R=0.555$; the nearest other possible R values are excluded: $R=0.636$ for $I(\mathrm{Ti}^{47})=7/2$, $I(\mathrm{Ti}^{49})=9/2$ and $R=0.440$ for $I(\mathrm{Ti}^{47})=7/2$, $I(\mathrm{Ti}^{49})=11/2$.

Using the results (1), (2) and (5) we find for the magnetic moments, without diamagnetic correction,

$$\mu(\mathrm{Ti}^{47})=-(0.78706\pm0.0001)\ \text{nm}, \tag{6}$$

$$\mu(\mathrm{Ti}^{49})=-(1.1022\ \pm0.0002)\ \text{nm}, \tag{7}$$

where we have used in this calculation the ratio $\mu(\mathrm{D}^2)/\mu(\mathrm{H})=0.307015$ as given by Mack[9] and $\mu(\mathrm{H})=2.7925$ as determined by Bloch and Jeffries.[10]

This experiment assigns an $f_{7/2}$ orbit to the odd neutron in Ti^{49}, as anticipated by the nuclear shell model of Mayer[11] and of Jensen, Haxel, and Suess.[12] For Ti^{47}, with $I=5/2$, the situation is more complicated: the single-particle model would predict an $f_{5/2}$ orbit for the odd neutron, whereas this experiment would assign a $d_{5/2}$ orbit. This "discrepancy" is quite analogous to that for the odd-proton nuclei Na^{23} and Mn^{55} as discussed by Mayer,[11] where the empirical ground level can be understood by taking into account all the protons outside the closed shells instead of just the single odd proton. A theoretical explanation has been given by Kurath[13] and by Talmi.[14] It is supposed that Mn^{55} with 25 protons has a $D_{5/2}$ ground state obtained by the jj coupling of the five protons in the incomplete $f_{7/2}$ subshell. This experiment shows that Ti^{47}, with 25 neutrons, behaves similarly, as anticipated by Rosenfeld[15] and others. The five neutrons in the incomplete $f_{7/2}$ subshell can couple to a $D_{5/2}$ state; a simple jj coupling calculation of the resultant magnetic moment yields $\mu=-1.36$ nm, which is nearer to the experimentally observed value than either of the Schmidt limits.

The magnetic moments of Ti^{47} and Ti^{49} as predicted by the scheme of Schawlow and Townes[16] agree well with our measured values (6) and (7).

II. GERMANIUM 73

Using the nuclear induction spectrometer we have observed a nuclear magnetic resonance in pure $GeCl_4$ at a frequency of 1.48 Mc/sec in a field of 10 000 gauss. We ascribe this resonance to Ge^{73}, the only stable odd isotope of germanium. The observed signal-to-noise ratio agrees approximately with that calculated for Ge^{73} using the spin value of 9/2 as measured by Townes, Mays, and Dailey.[17] We have been unable to observe the Cl^{35} or Cl^{37} resonance signals in $GeCl_4$, presumably because of excessive electric quadrupolar broadening of the line. However by comparing the Ge^{73} signal to the Cl^{35} signal in $TiCl_4$ we observe the magnetic moment of Ge^{73} to be negative. This is in agreement with the prediction of the Mayer-Jensen nuclear shell model, which assigns a $g_{9/2}$ orbit to the odd neutron in Ge^{73}. In the same magnetic field the ratio of the nuclear resonance frequency of Ge^{73} in $GeCl_4$ to that of Cl^{35} in $TiCl_4$ is observed to be

$$\nu(\mathrm{Ge}^{73})/\nu(\mathrm{Cl}^{35})=0.35572\pm0.00004.$$

We have observed a slight "chemical shift"[14] between the Cl^{35} resonance frequency in $TiCl_4$ and in an aqueous solution of RbCl. The ratio of the resonance frequencies is found to be 1.00088 ± 0.000025 in these two compounds, respectively. Using this correction and the ratio $\nu(\mathrm{Cl}^{35})/\nu(\mathrm{D}^2)$ in $RbCl+D_2O$ as measured by Walchli, Leyshon, and Scheitlin[18] we find

$$\nu(\mathrm{Ge}^{73})/\nu(\mathrm{D}^2)=0.22725\pm0.00003. \tag{8}$$

From this we find for the nuclear magnetic moment of Ge^{73}, without diamagnetic correction,

$$\mu(\mathrm{Ge}^{73})=-(0.87675\pm0.00012)\ \text{nm}, \tag{9}$$

where we have used in this calculation the ratio $\mu(\mathrm{D}^2)/\mu(\mathrm{H})$ and $\mu(\mathrm{H})$ as given above, and the value 9/2 for the spin of Ge^{73} as measured by Townes *et al.*[17] Our measured value of $\mu(Ge^{73})$ is considerably less than the predicted values.[19] We have also searched for the Ge^{73} resonance in the powdered element without success. It should be pointed out that possible "chemical shifts"[14] can make the result (9) uncertain, to about 0.1 percent.

The loan of the enriched Ti isotopes by the Stable Isotope Division of the Atomic Energy Commission is gratefully acknowledged. Thanks are due to Mr. Charles Cook for the chemical preparation of the enriched samples, and to Mr. P. B. Sogo for assistance with the measurements.

[9] J. E. Mack, Revs. Modern Phys. **22**, 64 (1950).
[10] F. Bloch and C. D. Jeffries, Phys. Rev. **80**, 305 (1950).
[11] M. G. Mayer, Phys. Rev. **78**, 16 (1950).
[12] Haxel, Jensen, and Suess, Z. Physik **128**, 295 (1950).
[13] D. Kurath, Phys. Rev. **80**, 98 (1950).
[14] I. Talmi, Phys. Rev. **82**, 101 (1950).
[15] L. Rosenfeld, Physica **17**, 461 (1951).
[16] A. L. Schawlow and C. H. Townes, Phys. Rev. **82**, 268 (1951). The calculated value for $\mu(Ti^{47})$ is in error and should be -0.80 (private communication).
[17] Townes, Mays, and Dailey, Phys. Rev. **76**, 700 (1949).
[18] Walchli, Leyshon, and Scheitlin, Phys. Rev. **85**, 922 (1952).
[19] A. L. Schawlow and C. H. Townes, Phys. Rev. **82**, 268 (1951); J. P. Davidson, Phys. Rev. **85**, 432 (1952); G. J. Bene, J. phys. et radium **13**, 161 (1952).

Degradation of Gamma Rays in Water*

M. M. Weiss and W. Bernstein
Brookhaven National Laboratory, Upton, New York
(Received August 26, 1953)

The spectra of degraded gamma rays from Co^{60} and Hg^{203} have been examined with a scintillation spectrometer, as a function of distance from the source, in an infinite water medium. The energy region below 0.150 Mev corresponding to multiple scattering was studied in greatest detail. Both the attenuation and the spectrum shape showed good agreement with the theoretical predictions of Spencer and Fano.

SPENCER and Fano[1] have calculated the attenuation of Co^{60} gamma rays in an infinite water medium and the changes in the shape of the spectrum as a function of distance. Their calculations have been verified experimentally by White[2] using integrated-dose measuring devices and Geiger counters, and by Hayward[3] using a scintillation spectrometer. The first experiment gave relatively little information regarding changes in the spectrum shape; the latter covered only the region above 0.1 Mev and lacked the resolution necessary to show the distortion in the primary energy region.

We have investigated in detail the spectrum below 0.1 Mev and above 1 Mev as a function of distance, using scintillation spectrometers. Measurements were taken in a water tank, 6 ft×15 ft×10 ft, with both the source and detector located at least three feet from a boundary. Several sources were used to cover the desired intensity range, and were normalized at overlapping points. Both single-channel and gray-wedge[4] pulse-height analyzers were used to obtain the spectra.

Figure 1 is a drawing of the scintillation counter employed for the low-energy measurements. In this energy region the photoelectric effect in NaI is predominant, and the pulse-height distribution is proportional to the gamma-ray energy distribution. A thin (1.6-mm thick) NaI(Tl) crystal is used to reduce the sensitivity to high-energy events. The crystal is shielded on three sides by the tin cap and quartz light piper from low-energy photons and gives approximately a 2π geometry. Since high-energy events often appear as low-energy events, especially in small crystals, measurements were taken with and without an absorber which completely removes the low-energy quanta and attenuates the higher energies to only a small extent. The difference represents the low-energy radiation entering the unshielded face of the crystal. A tin absorber with 10 percent transmission at 0.150 Mev was used because its fluorescence radiation is below the region of interest, and it is relatively transparent to higher energies. The escape of the iodine K x-ray following a photoelectric process also distorts the spectrum toward lower energies.

A large (3-cm×2-cm) NaI(Tl) crystal with a resolution of 8 percent at 0.662 Mev was used for the region

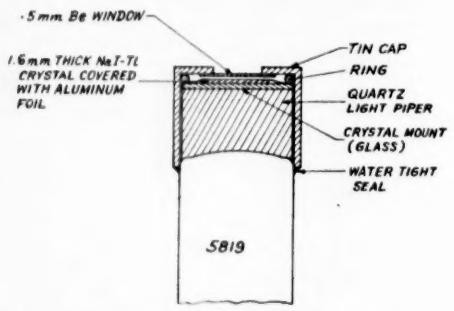

FIG. 1. Drawing of the low-energy scintillation counter.

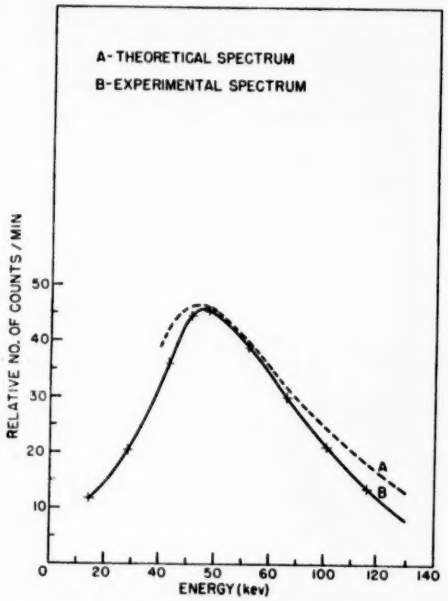

FIG. 2. Comparison of the experimental low-energy spectrum of Co^{60} with the theoretical curve.

* This work was done under the auspices of the U. S. Atomic Energy Commission and was supported in part by the Department of Defense.

[1] L. V. Spencer and U. Fano, J. Research Natl. Bur. Standards **46**, 446–456 (1951).
[2] G. R. White, Phys. Rev. **80**, 154 (1950).
[3] E. Hayward, Phys. Rev. **86**, 493 (1952).
[4] Bernstein, Chase, and Schardt, Rev. Sci. Instr. **24**, 437 (1953).

above 1 Mev and for some measurements using 0.275-Mev gamma rays from Hg^{203}.

Low-energy spectra were obtained for distances of 70 cm to 190 cm from the Co^{60} source in 10-cm steps. Neither the shape nor peak energy showed any change for distances greater than 30 cm from the source. The spectrum is gradually broadened and the peak position shifted toward higher energies for distances less than 30 cm from the source. Figure 2 is a linear plot of a representative curve obtained at 160 cm from the source normalized in intensity to a calculated curve.[5]

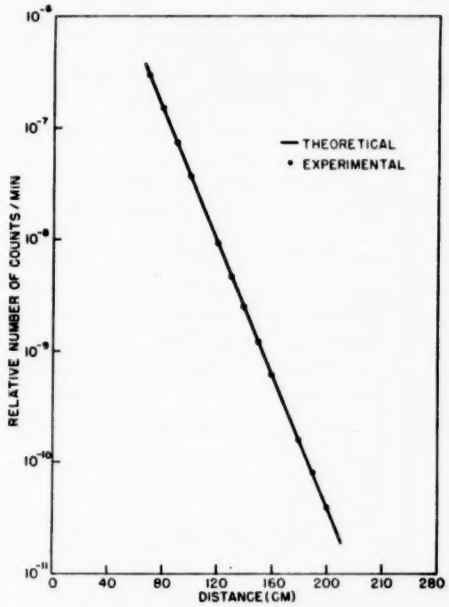

FIG. 3. Attenuation of the low-energy spectrum of Co^{60} with distance. The theoretical and experimental curves are normalized to equal intensity at 70 cm.

The latter is corrected for the crystal efficiency[6,7] and resolution. The shape of the curve below 0.030 Mev is doubtful because of the tin fluorescence, and some distortion toward lower energies caused by the escape radiation.

The attenuation with distance of the low-energy spectrum is shown in Fig. 3. Since the shapes of both the theoretical and experimental curves do not change with distance beyond 30 cm, peak intensities rather than total counting rates were plotted.

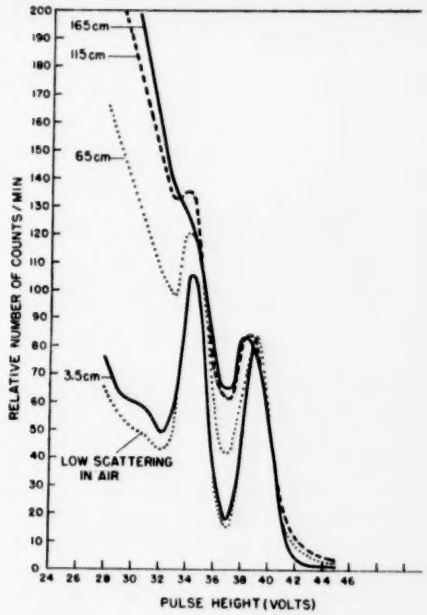

FIG. 4. High-energy spectra of Co^{60} obtained at several distances from the source. The curves are normalized to equal intensity of the 1.33-Mev gamma ray.

Very similar curves were obtained for the 0.275-Mev Hg^{203} gamma rays. The shape of the low-energy region is independent of the incident gamma-ray energy; however the attenuation is related to the incident energy. All the measurements were taken at sufficiently large distances so that the Tl K x-ray contribution was unimportant.

Figure 4 is a plot of the primary Co^{60} spectrum and shows a gradual loss in resolution, peak-to-trough ratio, and an increase in lower-energy events with increasing distance. A curve for a Co^{60} source in air is also included to show the optimum resolution of the instrument under conditions when scattering is small.

ACKNOWLEDGMENT

We are indebted to Drs. U. Fano, A. W. Schardt, and M. Widgoff for many helpful discussions, and to Mr. B. Manowitz for the use of his water tank. We also wish to thank E. Crouse and D. Clareus for their assistance in the experimental work.

[5] H. Goldstein and P. Mittelman (private communication).
[6] The absorption coefficients for NaI were obtained from the G. R. White, National Bureau of Standards Report No. 1003, May 15, 1952 (unpublished).
[7] W. Rubinson and W. Bernstein, Phys. Rev. **86**, 545 (1952).

Scattering of 9.5-Mev Protons by Carbon and Oxygen

W. E. BURCHAM, *University of Birmingham, Birmingham, England*
W. M. GIBSON* AND A. HOSSAIN, *University of Bristol, Bristol, England*

AND

J. ROTBLAT, *University of London, London, England*

(Received August 10, 1953)

The elastic and inelastic scattering of 9.5-Mev protons by C^{12} and O^{16} nuclei has been studied by means of photographic plates. The 4.43-Mev state of C^{12}, as well as the 6.05-, 6.13-, 6.9-, and 7.1-Mev states of O^{16} have been observed. The angular distribution of the protons elastically scattered by C^{12} and O^{16} has been determined and compared with Rutherford scattering. In the case of the protons inelastically scattered by C^{12}, the angular distribution shows symmetry around 90°.

EXPERIMENTS have been carried out using a beam of molecular hydrogen accelerated in the 60-inch Birmingham cyclotron; when passing through the aluminium window into the scattering camera the hydrogen molecules split and give rise to a beam of protons of an energy of 9.5-Mev. The scattering camera was the same as that described by Burrows, Powell, and Rotblat;[1] some minor modifications were made, mainly to make possible the absolute measurement of the beam intensity. Gaseous targets of hydrogen, helium, carbon, nitrogen, oxygen, fluorine, neon, and argon were used, and the scattered particles were recorded in photographic emulsions.

For the experiments on carbon the scattering chamber was filled with acetylene at pressures of 15–20 cm. The range distribution of the scattered particles showed (a) the group of elastically scattered protons, (b) the inelastically scattered protons corresponding to the 4.43-Mev state[2] of C^{12}, and (c) at angles less than 90°, the group of protons scattered by hydrogen. The differential cross section of p-p scattering was found to vary with angle in the same way as that described recently by Allred *et al.*,[3] but our values of the absolute differential cross sections are about 20 percent lower than theirs. A survey of values of the proton-proton scattering cross section at 90°, at various proton energies, published by a number of authors in recent

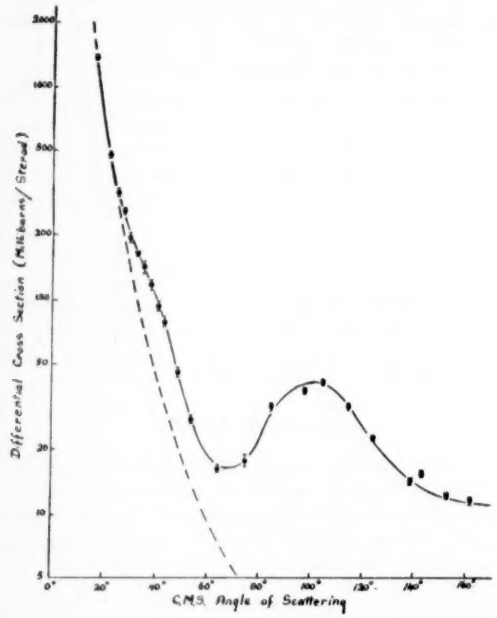

FIG. 1. Angular distribution in the center-of-mass system of protons elastically scattered by carbon. $\sigma(\phi)$ = c.m. differential cross section in millibarns per steradian.

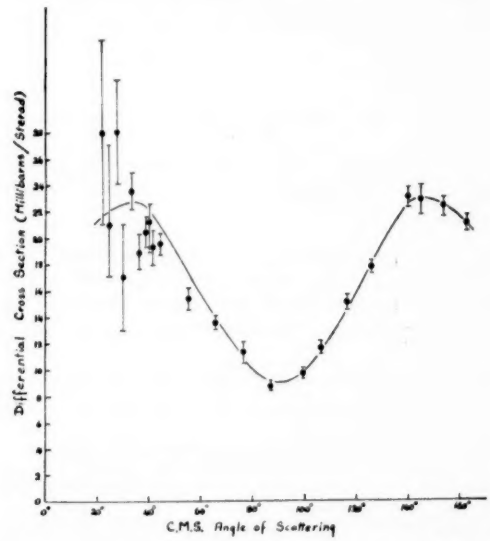

FIG. 2. Angular distribution in the center-of-mass system of protons inelastically scattered from carbon, leading to the 4.43-Mev state of C^{12}. $\sigma(\phi)$ is given in millibarns per steradian.

* Now at Queen's University, Belfast, Northern Ireland.

[1] Burrows, Powell, and Rotblat, Proc. Roy. Soc. (London) **209**, 461 (1951).

[2] F. Ajzenberg and T. Lauritsen, Revs. Modern Phys. **24**, 321 (1952).

[3] Allred, Armstrong, Bondelid, and Rosen, Phys. Rev. **88**, 433 (1952).

years, indicates that our values are probably too low, while Allred's values are probabiy too high. Possible sources of error in our beam integrating system are being investigated; for the time being we have to assume an uncertainty of the order of 8 percent in our absolute cross-section measurements; the relative error is much smaller, only of the order of 2 or 3 percent. Figure 1 shows the observed angular distribution of protons elastically scattered by C^{12}; the broken line gives the Rutherford scattering. Figure 2 shows the distribution observed for the protons inelastically scattered from carbon, with formation of the 4.43-Mev state of C^{12}. Unlike the findings of Gove and Stoddart,[4] who at 7.3-Mev observed an asymmetrical distribution, our curve seems to be symmetrical around 90°. Below 40° the measurements are difficult but the more reliable

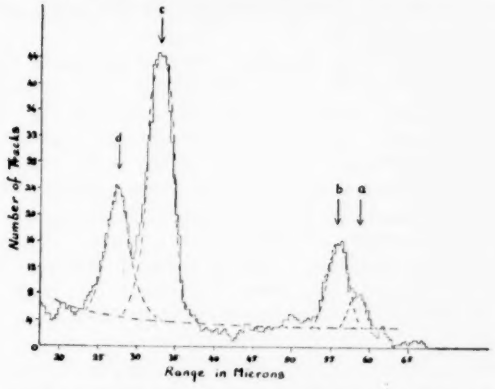

FIG. 3. Histogram of ranges of 9.5-Mev protons inelastically scattered from O^{16}, emitted at an angle of 85°; the four groups correspond to the excited states of O^{16} at (a) 6.05, (b) 6.13, (c) 6.9, and (d) 7.1-Mev.

results for angles greater than 40° show no sign of asymmetry.

In the experiments with oxygen the camera was filled with pure oxygen at pressures of 5–10 cm. In addition to the elastically scattered protons, we observed inelastically scattered protons leading to the four excited states of O^{16} at 6.05, 6.13, 6.9, and 7.1-Mev.[2] Figure 3 shows a histogram of tracks of the short-range

[4] H. E. Gove and H. F. Stoddart, Phys. Rev. **86**, 572 (1952).

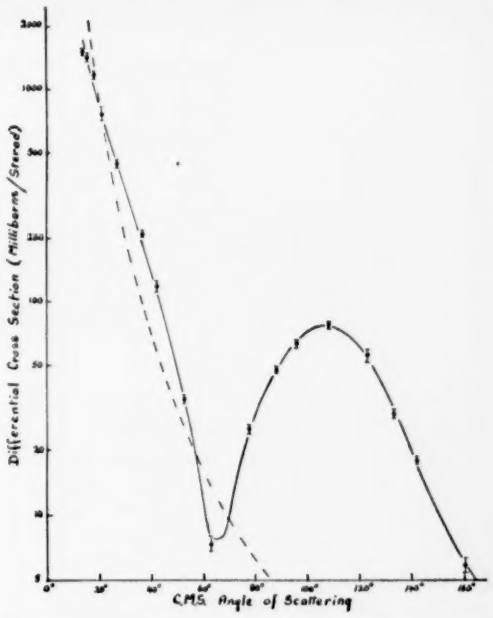

FIG. 4. Angular distribution in the center-of-mass system of protons elastically scattered by O^{16}. $\sigma(\phi)$ is given in millibarns per steradian.

protons observed at an angle of 85°. The tracks were measured to an accuracy of 0.4 micron and the distributions were smoothed out by averaging the tracks in five consecutive intervals of 0.4 micron each. Although the two lowest states, 6.05 and 6.13-Mev, are not completely resolved, their analysis into two groups can be easily carried out as indicated on the graph. Figure 4 gives the observed angular distribution of the protons elastically scattered by O^{16}, together with the Rutherford scattering curve. The observed angular distribution has a shape similar to that found in C^{12}, showing a minimum at around 65° and a maximum at about 110°, but the minimum is much more pronounced in O^{16} than in C^{12}.

Results obtained on the scattering of protons by the other elements, and the interpretation of these distributions, will be published later.

Interaction of 19-Mev Deuterons with Oxygen

R. G. FREEMANTLE, *University of Birmingham, Birmingham, England*
W. M. GIBSON* AND D. J. PROWSE, *University of Bristol, Bristol, England*

AND

J. ROTBLAT, *University of London, London, England*

(Received August 10, 1953)

The charged particles emitted when oxygen is bombarded with 19-Mev deuterons have been studied by a photographic plate method. The angular distributions of the two groups of protons from the reaction $O^{16}(d,p)O^{17}$, O^{17} being formed in the ground and 0.88-Mev states, have been found to be in qualitative agreement with the predictions of the stripping theory. Similar measurements have been made for the elastically scattered deuterons and for the α particles from the reaction $O^{16}(d,\alpha)N^{14}$; the curve for the latter shows peaks at about 40°, 90°, and 140°, and is nearly symmetrical about 90°.

A STUDY has been made of the charged products of bombarding various light elements with 19-Mev deuterons from the Birmingham cyclotron. The particles were recorded in photographic plates, in the scattering camera described by Burrows, Powell, and Rotblat.[1] The camera has been modified by the introduction of improved shielding and stop systems to minimize neutron background, by the use of thicker emulsions which the particles enter slightly more steeply, so that tracks are less likely to leave the emulsion at either surface, and by the use of a Faraday cup which gives absolute values of the integrated beam current.

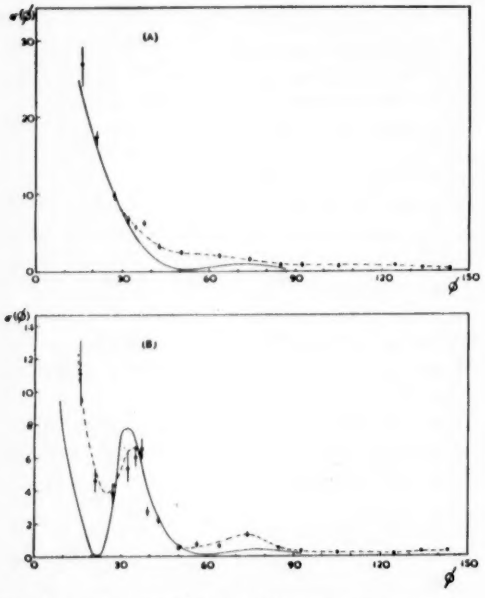

FIG. 1. Angular distributions in the center-of-mass system of protons from reaction $O^{16}(d,p)O^{17}$; (A) O^{17} formed in the ground state ($l=2$, $Q=1.92$ Mev); (B) O^{17} formed in the 0.88-Mev excited state ($l=0$, $Q=1.04$ Mev). $\sigma(\phi)$ is given in millibarns per steradian. The dashed lines are the experimental curves. The theoretical curves (solid lines) are obtained from Butler's theory, with $r_0=4.77\times10^{-13}$ cm.

The angular distributions of protons emitted in the reaction $O^{16}(d,p)O^{17}$, O^{17} being formed in the ground and 0.88-Mev excited states, are shown in Fig. 1, together with curves based on Butler's stripping theory.[2] According to this theory the angular distribution of protons from a (d,p) reaction depends characteristically on the angular momentum, l, transferred by the neutron to the nucleus which it enters. For the two groups observed, l must be 2 and 0 since the O^{17} levels have spin and parity $5/2+$ and $\frac{1}{2}+$, respectively.[3,4] It will be seen that there is qualitative agreement between the curves expected for these values of l and the experimental points; the agreement is not close, being in fact slightly worse than that observed at 8 Mev,[2,4] but indicates that the theory is correct in principle if not in detail at an energy of 19 Mev. The theory successfully predicts the observed differences in angle of corresponding peaks at 8 Mev and 19 Mev. We are much indebted to Mr. W. M. Fairbairn for calculating the theoretical curves.

The total cross sections for the formation of the ground and 0.88-Mev levels of O^{17} have been calculated from the angular distributions; the contributions from very small and very large angles, at which measurements were impossible, were estimated with the aid of the theoretical curves. The values obtained are 35.5 ± 3.5 and 22.7 ± 3.5 millibarns respectively, while those obtained at 8 Mev[4] were 125 ± 9 and 112 ± 11 millibarns.

Figure 2 shows the angular distribution of deuterons elastically scattered by oxygen, with the Rutherford scattering curve for comparison. Although we cannot be sure of our absolute cross sections to within less than about 8 percent[5] there is no doubt that the cross

* Now at Queen's University, Belfast, Northern Ireland.

[1] Burrows, Powell, and Rotblat, Proc. Roy. Soc. (London) **209**, 461 (1951).

[2] S. T. Butler, Proc. Roy. Soc. (London) **208**, 559 (1951).

[3] Geschwind, Gunther-Mohr, and Silvey, Phys. Rev. **85**, 474 (1952).

[4] Burrows, Gibson, and Rotblat, Proc. Roy. Soc. (London) **209**, 489 (1951).

[5] Burcham, Gibson, Hossain, and Rotblat, preceding paper [Phys. Rev. **92**, 1266 (1953)].

section at 30° is at least 5 times less than the Rutherford value. The results may be compared with those obtained at 8 Mev.[4]

Groups of protons and deuterons are usually identified by their range, but α-particle tracks may be recognized at sight by their high grain density and low multiple scattering. Separate range distributions have been obtained for the α particles from the reaction $O^{16}(d,\alpha)N^{14}$; groups from the formation of N^{14} in its ground state and in the excited state at 3.9 Mev, as well as several incompletely resolved levels above 5 Mev, have been found.

In common with other workers, we find no sign of the 2.31-Mev level; this level is thought to have

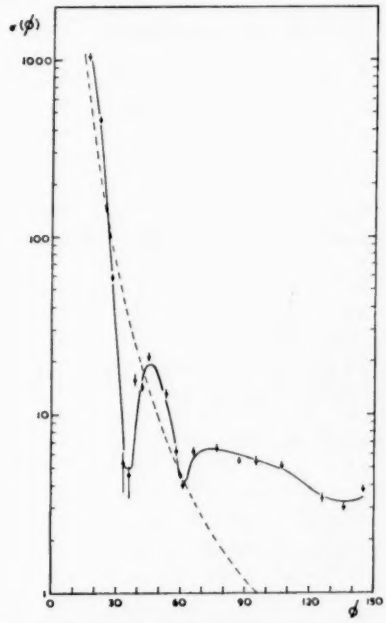

FIG. 2. Angular distribution in the center-of-mass system of deuterons elastically scattered from oxygen. $\sigma(\phi)$ is given in millibarns per steradian. The solid line is the experimental curve. The dashed line is the Rutherford scattering curve.

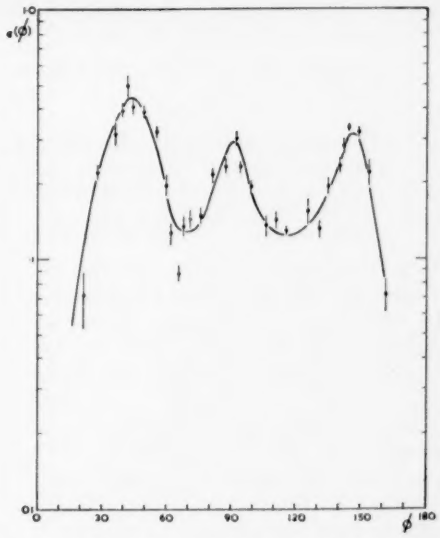

FIG. 3. Angular distribution in the center-of-mass system of α particles from reaction $O^{16}(d,\alpha)N^{14}$, N^{14} being formed in the ground state. $\sigma(\phi)$ is given in millibarns per steradian.

isotopic spin $T=1$, forming a triplet with the ground states of C^{14} and O^{14}; it would not then be formed by the interaction of a deuteron and an oxygen nucleus with emission of an α particle, since these three all have zero isotopic spin. Our measurements allow us to set an upper limit of 0.1 millibarn to the total cross section for the formation of this level, while the total cross section for the ground state is 2.6 ± 0.3 millibarns. In view of the fact that at 19 Mev the emitted α particles are not affected by the potential barrier, these figures support the view that the 2.31-Mev level is predominantly $T=1$.

The angular distribution of the ground state α particles is shown in Fig. 3. The curve is not unlike that obtained for the reaction $N^{14}(d,\alpha)C^{12}$ at 8 Mev,[6] but it is much more nearly symmetrical about 90°.

[6] W. M. Gibson and E. E. Thomas, Proc. Roy. Soc. (London) **210**, 543 (1951).

A Vector Addition Coefficient Identity

R. L. GUERNSEY AND G. B. ARFKEN
Miami University, Oxford, Ohio
(Received July 22, 1953)

The identical results of different theoretical approaches to the angular correlation of mixed multipole gamma rays imply the existence of a vector addition coefficient identity. This is found to be a special case of a more general identity, the proof of which is outlined.

THE investigations of Ling and Falkoff[1] on one hand, and of Lloyd[2] and of Biedenharn and Rose[3] on the other, imply the existence of a certain identity among the Clebsch-Gordan or vector addition coefficients. Ling and Falkoff, starting with electromagnetic theory, obtained an expression for the interference contribution to the angular distribution function for a mixture of 2^L and 2^{L+1} pole radiation, in terms of squares of spherical harmonics. Transforming to a series of spherical harmonics, their distribution function contains terms of the form

$$(L+M+1)^{\frac{1}{2}}(L-M+1)^{\frac{1}{2}}[2M(LLM\ -M\,|\,\nu 0) - (L-M)(LL\ M+1\ -M-1\,|\,\nu 0) + (L+M)(LL\ M-1\ -M+1\,|\,\nu 0)]Y_\nu^0, \quad (1)$$

using the Condon and Shortley[4] phase convention. Lloyd, and Biedenharn and Rose, employing a group theoretical analysis, found terms of the form

$$(L+1\ LM\ -M\,|\,\nu 0)Y_\nu^0. \quad (2)$$

The identical numerical results following from expressions (1) and (2) suggest that they are equal to within a multiplicative factor independent of the magnetic quantum number M. This was first recognized by Rose, Biedenharn, and Arfken in the course of an earlier investigation.[5] Since the identical numerical results give only an indirect proof of the identity and do not supply the expression for the multiplicative factor, it was felt that a direct proof was in order. The desired relation was found to be a special case of a slightly more general identity the proof of which is outlined below.

We may write the vector addition coefficient,

$$(L+1\ L'M\ -M\,|\,\nu 0) = A(L+1, L', M, -M)S(L+1, L', M, -M), \quad (3)$$

where the function S denotes the summation terms in Racah's expression,[6] the function A giving the other factors. After repeated application of the binomial coefficient addition formula,[7] the function S in Eq. (3) may be written

$$S(L+1, L', M, -M) = (\nu+1)(L+L'-\nu+1)^{-1} \times (L-L'+\nu+1)^{-1}[S(L, L', M-1, -M) - S(L, L', M+1, -M)]. \quad (4)$$

Substituting in Eq. (3), one obtains

$$(L+1\ L'M\ -M\,|\,\nu 0) = [\nu(\nu+1)/(L'-L+\nu) \times (L-L'+\nu+1)(L+L'-\nu+1)(L+L'+\nu+2)]^{\frac{1}{2}} \times\{[(L+M)(L+M+1)]^{\frac{1}{2}}(LL'\ M-1\ -M\,|\,\nu\ -1) -[(L-M)(L-M+1)]^{\frac{1}{2}}(LL'\ M+1\ -M\,|\,\nu 1)\}. \quad (5)$$

Upon applying Eqs. (3) and (5) of reference 6, Eq. (5) above is transformed into the desired identity:

$$\lambda(L, L', \nu)[(L+M+1)(L-M+1)]^{-\frac{1}{2}} \times(L+1\ L'M\ -M\,|\,\nu 0) = 2M(LL'M\ -M\,|\,\nu 0) -[(L-M)(L'-M)(L'+M+1)/(L+M+1)]^{\frac{1}{2}} \times(LL'\ M+1\ -M-1\,|\,\nu 0) +[(L+M)(L'+M)(L'-M+1)/(L-M+1)]^{\frac{1}{2}} \times(LL'\ M-1\ -M+1\,|\,\nu 0) \quad (6)$$

with

$$\lambda(L, L', \nu) \equiv [(L'-L+\nu)(L-L'+\nu+1) \times (L+L'-\nu+1)(L+L'+\nu+2)]^{\frac{1}{2}}. \quad (7)$$

When L' is set equal to L, Eq. (6) reduces to the simpler form suggested by the angular correlation results. This explains why the two strikingly different approaches to the angular correlation of mixed multipole gamma rays yielded identical results.

It was thought at one time that Eq. (6) might be useful in the calculation of explicit forms of the vector addition coefficients $(LL'M\ -M\,|\,\nu 0)$ for given values of M. However, the well-known relation,

$$[(L+M)(L'+M)(L-M+1)(L'-M+1)]^{\frac{1}{2}} \times(LL'\ M-1\ -M+1\,|\,\nu 0) +[(L-M)(L+M+1)+(L'+M)(L'-M+1) -\nu(\nu+1)](LL'\ M\ -M\,|\,\nu 0) +[(L-M)(L'-M)(L+M+1)(L'+M+1)]^{\frac{1}{2}} \times(LL'\ M+1\ -M-1\,|\,\nu 0)=0, \quad (8)$$

appears better adapted for this purpose.

[1] D. S. Ling, Jr. and D. L. Falkoff, Phys. Rev. **76**, 1639 (1949).
[2] S. P. Lloyd, Phys. Rev. **85**, 904, (1952).
[3] L. C. Biedenharn and M. E. Rose, Revs. Modern Phys. **25**, 729 (1953).
[4] E. U. Condon and G. H. Shortley, *Theory of Atomic Spectra* (Cambridge University Press, Cambridge, 1951).
[5] Rose, Biedenharn, and Arfken, Phys. Rev. **85**, 5 (1952).
[6] G. Racah, Phys. Rev. **62**, 438 (1942), Eq. (16).
[7] H. Margenau and G. M. Murphy, *The Mathematics of Physics and Chemistry* (D. Van Nostrand Company, Inc., New York, 1943), Chap. 12.

The Nuclear Spin and Quadrupole Moment of I^{131}†

RALPH LIVINGSTON AND BEN M. BENJAMIN, *Oak Ridge National Laboratory, Oak Ridge, Tennessee*

AND

J. T. COX AND WALTER GORDY, *Department of Physics, Duke University, Durham, North Carolina*

(Received July 27, 1953)

Measurements on the $J=2\rightarrow3$ rotational transition of CH_3I^{131} have been made in the 6.75-mm wavelength region. The nuclear spin of I^{131} was found to be 7/2 and the quadrupole coupling, -973 ± 9 Mc/sec. This coupling gives -0.412×10^{-24} cm² for the quadrupole moment of I^{131}.

THE nuclear spin and quadrupole moment of radioactive, 8-day half-life I^{131} has been determined from measurements on the $J=2\rightarrow3$ rotational transition of CH_3I^{131} which occurs in the 6.75-mm wavelength region. I^{131} has a nuclear spin of 7/2 as evidenced by the closeness of the fit of the lines in Fig. 1. Calculated spectra for spin cases of 3/2, 5/2, and 9/2 could not be fit. Only the stronger lines were observed because of the small sample size, estimated to be approximately 2μg of I^{131} as CH_3I.

The quadrupole coupling was computed to be -973 ± 9 Mc/sec. Table I shows the closeness of the fit of the observed to calculated line frequencies using this coupling value. The value of D_{JK} for CH_3I^{127} was used in the calculations since it should be essentially unchanged for CH_3I^{131}. Second-order corrections were not calculated, but these are expected to be much smaller than for I^{127} or I^{129} in view of the smaller coupling. These corrections may, in part, account for the small differences between the observed and calculated frequencies of Table I.

The stronger lines of CH_3I^{129} present in the sample were also observed, and these were easily identified from previous accurate measurements. One pair of I^{129} lines did appear, however, at about the same frequency as I^{131} lines as indicated in Table I. The computed center of the CH_3I^{131} spectrum was shifted the expected amount from the center for CH_3I^{129}.

The above coupling and the coupling value of −1934 Mc/sec[1] for CH_3I^{127} gives a quadrupole moment ratio of

TABLE I. Observed and calculated hyperfine structure for CH_3I^{131} relative to hypothetical $J=2\rightarrow3$ transition. $I=7/2$, $eqQ=-973$ Mc/sec, $D_{JK}=0.0994$ Mc/sec.

$K, F\rightarrow F'$	Calculated Mc/sec	Observed Mc/sec	|Calc| − |Obs| Mc/sec
2,9/2→11/2 2,9/2→9/2 2,9/2→7/2	−96.71	−96.65	+0.06
1,7/2→9/2	−32.13	−32.40	−0.27
0,7/2→9/2	−15.56	−16.01	−0.45
1,9/2→11/2	−5.56	−5.76	−0.20
0,11/2→13/2	11.58	[a]11.58	0.00
2,5/2→5/2 2,5/2→7/2 2,5/2→3/2	22.43	[b]23.01	+0.58
0,9/2→11/2 0,3/2→1/2	24.82	[b]25.11	−0.29
1,11/2→13/2	25.46		+0.35
2,11/2→11/2 2,11/2→13/2 2,11/2→9/2	67.11	67.55	−0.44

[a] Normalized to match at this frequency.
[b] CH_3I^{129} lines were unresolved from these lines.

$Q(I^{131})/Q(I^{127})=0.5031$. With $Q(I^{129})/Q(I^{127})=0.701213$[2] it is apparent that the magnitude of the quadrupole moment in the sequence I^{127}:I^{129}:I^{131} varies as 1.0000:0.7012:0.5031. The magnitude of the moment appears to approach a minimum as I^{135} (full neutron shell) is approached.[3] Using Jaccarino, King, and Stroke's[4] recent atomic-beam value $Q(I^{127})=-0.819\times10^{-24}$ cm² the quadrupole moment of I^{131} is -0.412×10^{-24} cm². The spin of 7/2 is consistent with recent β-decay studies.[5]

All of the chemical operations[6] for synthesizing CH_3I were carried out by remote control, and observations

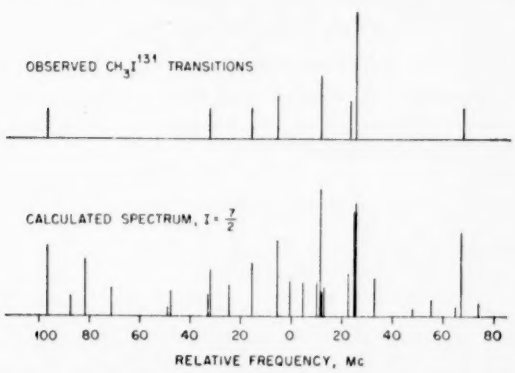

FIG. 1. Observed and calculated hyperfine structure for the $J=2\rightarrow3$ transition of CH_3I^{131}. Several of the weaker, calculated lines are off the ends of the figure.

† The work by Oak Ridge National Laboratory was performed for the U. S. Atomic Energy Commission. The work by Duke University was supported by the United States Air Force under a contract monitored by the Office of Scientific Research, Air Research and Development Command.

[1] Gordy, Simmons, and Smith, Phys. Rev. **74**, 243 (1948).
[2] R. Livingston and H. Zeldes, Phys. Rev. **90**, 609 (1953).
[3] W. Gordy, Phys. Rev. **76**, 139 (1949).
[4] Jaccarino, King, and Stroke (to be published).
[5] R. E. Bell and R. L. Graham, Phys. Rev. **86**, 212 (1952).
[6] Details will be published elsewhere.

were made on the oscilloscope of a video type microwave spectrometer. Relative line frequencies were measured with frequency markers derived from a stabilized microwave oscillator. We plan to measure the magnetic moment of I^{131}. In view of the decreased magnitude of Q and the same spin as I^{129} it will be interesting to see if the magnetic moment decreases.[3]

The I^{131} was obtained from the isotope production division at Oak Ridge National Laboratory. We wish to acknowledge the help of O. R. Gilliam in the early phases of the work.

Note added in proof:—In later work the $K=1$, $F=9/2\rightarrow 9/2$ and the $K=2$, $F=7/2\rightarrow 7/2$, $7/2\rightarrow 5/2$, $7/2\rightarrow 9/2$ lines were seen at frequencies in good agreement with those calculated from the parameters of Table I.

PHYSICAL REVIEW VOLUME 92, NUMBER 5 DECEMBER 1, 1953

Photoproduction of π-Meson Pairs*

R. D. LAWSON
Stanford University, Stanford, California
(Received August 25, 1953)

A perturbation study of the photoproduction of π-meson pairs by gamma rays incident on protons is made for both pseudoscalar and pseudovector coupling. Expressions are derived for the possible cross sections assuming the nucleon is infinitely heavy. The effect of first-order nucleon recoil on the (π^+, π^-) cross section, assuming pseudoscalar coupling, is considered. Curves illustrating the results are given. The possibility of obtaining information on the type of interaction operative between mesons and nucleons from a study of the pair production cross sections is discussed.

INTRODUCTION

ALTHOUGH the pseudoscalar nature of the π meson has been more or less definitely established,[1] the question of the coupling between the meson and nucleon fields remains unanswered. It is well known[2] that the pseudoscalar and pseudovector interactions give identical results to lowest order in the coupling constant provided $f=(2M/\mu)g$; where f and g are the pseudoscalar and pseudovector coupling constants respectively, and M and μ are the nucleon and meson masses. Assuming weak coupling theory to be approximately valid we must, therefore, study processes which do not proceed in lowest order of the coupling constant in order to gain insight into the type of interaction operative between mesons and nucleons.

Kaplon[3] has investigated the cross section for the production of π mesons in nucleon-nucleon collisions. His calculations indicate that the differential cross sections for the production process differ when the two types of coupling are used. However, aside from the assumption of weak coupling theory, the interaction between the two final state nucleons is neglected and consequently one cannot draw quantitative conclusions from the calculation.

This latter difficulty is partly obviated when we consider the photoproduction of π-meson pairs by gamma rays incident on protons.[4] It has been shown[5] that in the low-energy region the (π^+, π^-) and (π^0, π^0) cross sections for pseudoscalar coupling are considerably larger than those for the pseudovector interaction. On the other hand, the (π^+, π^0) cross section has approximately the same magnitude when either type of coupling is used. In this paper we shall investigate the possibility of obtaining information on the meson-nucleon interaction from a study of the photoproduction of meson pairs.

(π^+, π^-) PAIR PRODUCTION

A. Pseudoscalar Coupling

Assuming pseudoscalar coupling, the interaction energy between the meson, nucleon, and electromagnetic field is written as[6]

$$H=\int H_1 d\mathbf{r}+\int H_2 d\mathbf{r}+\int H_3 d\mathbf{r},$$

where

$$H_1=if\bar{\psi}\gamma_5\tau_\alpha\phi_\alpha\psi,$$

$$H_2=-eA_\nu\left(\phi_1\frac{\partial\phi_2}{\partial x_\nu}-\phi_2\frac{\partial\phi_1}{\partial x_\nu}\right), \tag{1}$$

$$H_3=-ie\bar{\psi}\gamma_\nu A_\nu\tau_3\psi,$$

* Assisted by the joint program of the U. S. Office of Naval Research and the U. S. Atomic Energy Commission, and by the Office of Scientific Research, Air Research and Development Command.

[1] R. E. Marshak, *Meson Physics* (McGraw-Hill Book Company, Inc., New York, 1952), pp. 1–201.

[2] F. J. Dyson, Phys. Rev. **73**, 929 (1948); L. L. Foldy, Phys. Rev. **84**, 168 (1951); G. Wentzel, Phys. Rev. **86**, 802 (1952); S. D. Drell and E. M. Henley, Phys. Rev. **88**, 1053 (1952).

[3] M. F. Kaplon, Ph.D. thesis, University of Rochester, 1951 (unpublished). Details of the calculation are given by R. E. Marshak, reference 1, p. 47.

[4] The possibility of a strong attractive interaction between the emerging π mesons has been pointed out by K. A. Brueckner and K. M. Watson, Phys. Rev. **87**, 621 (1952).

[5] R. D. Lawson and S. D. Drell, Phys. Rev. **90**, 326 (1953).

[6] Throughout this work the system of units in which $\hbar=c=1$ will be used. The fine structure constant in our notation is $e^2/4\pi$ and the meson-nucleon coupling constant is $f^2/4\pi$.

and ψ is the nucleon field strength; $\bar{\psi}=\psi^*\gamma_4$; ϕ_α is the meson field strength, $\alpha=3$ describing neutral mesons; τ_α is the isotopic spin operator with $\tau_p=\frac{1}{2}(1-\tau_3)$; A_ν ($\nu=1-4$) refers to the electromagnetic field; and the gammas are the usual Dirac matrices with $\gamma_5=\gamma_1\gamma_2\gamma_3\gamma_4$.

The Feynman diagrams to order ef^2 for the process $\gamma+p\rightarrow p'+\pi^++\pi^-$ are shown in Fig. 1. The effective S matrix for the process is calculated by the usual methods[7] and yields

$$S=\frac{-ief^2\epsilon_\nu\delta(p_1+K-p_2-k_+-k_-)}{[(2\pi)^7 2E_\gamma\omega(k_+)\omega(k_-)]^{\frac{1}{2}}}\left\{\frac{k_{+\nu}k_{-\lambda}\bar{u}_f\gamma_\lambda u_i}{(k_+K)(k_-^2+2p_2k_-)}\right.$$
$$+\frac{k_{-\nu}k_{+\lambda}\bar{u}_f\gamma_\lambda u_i}{(k_-K)(k_+^2-2p_1k_+)}-\frac{k_{-\lambda}\bar{u}_f\gamma_\lambda(2p_{1\nu}+\gamma_\alpha\gamma_\nu K_\alpha)u_i}{2(p_1K)(k_-^2+2p_2k_-)}$$
$$\left.-\frac{k_{+\lambda}\bar{u}_f(2p_{2\nu}-\gamma_\nu\gamma_\alpha K_\alpha)\gamma_\lambda u_i}{2(p_2K)(k_+^2-2p_1k_+)}\right\}, \quad (2)$$

where k_+, k_-, and K refer to the energy-momentum four vectors of the π^+, π^- and gamma ray respectively; u_i and u_f are the Dirac spinors for the initial and final nucleons whose energy-momentum four-vectors are p_1 and p_2; $\bar{u}_f=u_f^*\gamma_4$; $\boldsymbol{\epsilon}$ is a unit vector in the direction of polarization of the gamma ray; and all products are understood to be four-vector products. The order of the terms in Eq. (2) is the same as the order of the Feynman diagrams in Fig. 1.

In the extreme nonrelativistic limit for the nucleon, $M\rightarrow\infty$, only the first two Feynman diagrams are important. In this approximation the differential cross section as a function of $\omega(k_-)$ is

$$\frac{d\sigma}{d\omega(k_-)}=\frac{8}{137}\left(\frac{g^2}{4\pi}\right)^2\left(\frac{2M}{\mu}\right)^2\frac{k_-k_+}{\mu^2E_\gamma^3}\{A+B\}, \quad (3)$$

where

$$A=\frac{\omega(k_+)}{k_+}\left(\ln\frac{\omega(k_+)+k_+}{\omega(k_+)-k_+}\right)-2,$$
$$B=\frac{\omega(k_-)}{k_-}\left(\ln\frac{\omega(k_-)+k_-}{\omega(k_-)-k_-}\right)-2; \quad (4)$$

and for convenience we have set

$$f=(2M/\mu)g, \quad (5)$$

where g is the coupling constant in the derivative coupling theory.

To find the total cross section we need only integrate Eq. (3) over the energy range of $\omega(k_-)$. For 400-Mev incident gamma rays in the laboratory coordinate system, the energy E_γ in the center-of-mass coordinate system is 294 Mev. Thus on the basis of a strict no recoil approximation the energy range of the emitted mesons is from 140 Mev (their rest energy) to an upper limit of 154 Mev. Carrying out the integration of Eq. (3) numerically we find

$$\sigma=2.3\times10^{-2}\left(\frac{g^2}{4\pi}\right)^2 \text{ millibarns.}$$

In view of the small energy spread it is necessary to look more closely into the kinematics of the process since any kinetic energy carried by the nucleon could easily affect this energy interval by an order of magnitude and hence materially change the cross section.[8] The kinetic energy of the initial proton in the center-of-mass coordinate system is easily found to be $\sim$46 Mev. To calculate the energy carried off by the recoil nucleon at the upper end of the spectrum we use the laws of conservation of energy and momentum,

$$E_\gamma+p_1^2/2M=\omega(k_+)+\omega(k_-)+(\mathbf{k}_-+\mathbf{k}_+)^2/2M, \quad (6)$$

and assume that the upper end of the π^- spectrum is defined by setting $\omega(k_+)=\mu$ in Eq. (6). Under this assumption the kinetic energy of the recoil nucleon is 9 Mev. Thus, according to this reasoning, the energy spread of the emitted mesons would be from $\omega(k_-)=140$ Mev to $\omega(k_-)=154+46-9=191$ Mev. One would certainly expect the numerical value of the cross section to be closer to that observed if in some way the energy range of the emitted mesons were made close to the experimentally observed range. For this reason, in the no-recoil formula, Eq. (3), let us set $\omega(k_-)+\omega(k_+)=294+46-9=331$ Mev. In this case the energy limits are at least almost correct.[9] The total cross section is then

$$\sigma_{ps}(\pi^+,\pi^-)=1.15(g^2/4\pi)^2 \text{ millibarns.} \quad (7)$$

One might doubt the validity of Eq. (7) because of our method of treating energy conservation. We there-

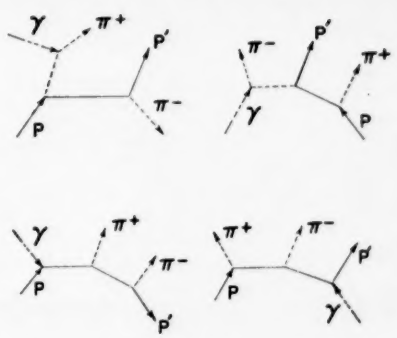

FIG. 1. Feynman diagrams for the process $\gamma+p\rightarrow p'+\pi^++\pi^-$ assuming pseudoscalar coupling.

[7] F. J. Dyson, Phys. Rev. **75**, 486 (1949); R. P. Feynman, Phys. Rev. **76**, 749, 769 (1949); G. C. Wick, Phys. Rev. **80**, 268 (1950).

[8] Since we are producing meson pairs, the volume element in phase space is extremely sensitive to the available energy.

[9] In Using Eq. (6) to calculate the recoil energy of the proton, if the angle between the momentum vectors of the π^+ and π^- mesons is taken to be 180°, one finds that at the upper end of the differential cross section $\omega(k_+)$ is slightly greater than μ. However, our original assumption gives results valid to about three percent.

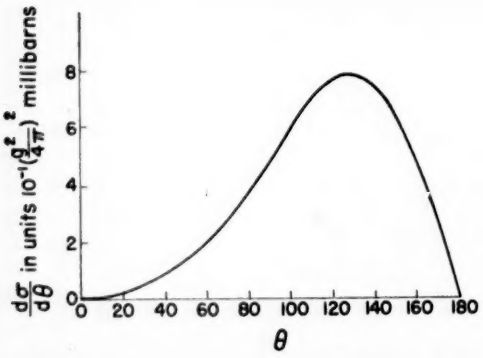

FIG. 2. Differential cross section for the photoproduction of (π^+, π^-) pairs as a function of θ, the angle between the two mesons in the center-of-mass coordinate system. The curve is plotted for 400-Mev incident gamma rays in the laboratory coordinate system. Pseudoscalar coupling is assumed. First-order nucleon recoil effects are considered.

fore calculate the cross section taking into account first-order nucleon recoil effects. To do this it is necessary to evaluate S^*S to order M^{-1}. This result should then be combined with the approximate expression for the density of final states obtained by making a binomial expansion of the denominator of the expression

$$\rho = \frac{k_- k_+ \omega(k_-)\omega(k_+) d\Omega_- d\Omega_+}{1+[\omega(k_+)/Mk_+](k_+ + k_- \cos\theta)}; \tag{8}$$

where ρ is the density of final states, k_- and k_+ refer to the magnitude of $\mathbf{k}_-$ and $\mathbf{k}_+$ respectively, $d\Omega_-$ and $d\Omega_+$ are the elements of solid angle in k_- and k_+ phase space, and θ is the angle between $\mathbf{k}_-$ and $\mathbf{k}_+$ in the center-of-mass coordinate system.

However, the binomial expansion of Eq. (8) does not converge near the upper end of the π^- spectrum since there $k_+ \to 0$. On the other hand, no terms of the form $1/k_+$ occur in the expansion of S^*S. Consequently, if we convert S^*S to a cross section by using the exact nonrelativistic expression for the density of final states, Eq. (8), the results will be valid to order $(\mu/M)^2$. The results for 400-Mev gamma rays are shown in Figs. 2 and 3.

The total cross section obtained in this way is

$$\sigma_{ps}(\pi^+, \pi^-) = 1.16(g^2/4\pi)^2 \text{ millibarns}, \tag{9}$$

which certainly compares favorably with our "pseudo no-recoil" result. One might argue that this agreement is fortuitous. However, if the first order recoil calculation for 600-Mev incident gamma rays in the laboratory coordinate system is carried out one obtains a cross section, $\sigma = 16.1(g^2/4\pi)^2$ millibarns, whereas a calculation similar to that used in deriving Eq. (7) yields $\sigma = 15.9\ (g^2/4\pi)^2$ millibarns. From these results it follows that for incident gamma-ray energies up to 600 Mev an excellent approximation to the total cross section is obtained by using Eq. (3), providing we set $\omega(k_+)+\omega(k_-)$ equal to the actual energy available to the two mesons when recoil is considered.

One may understand the shift of the differential cross section to higher values of θ (see Fig. 2) by noting that as θ increases, the recoil energy of the proton decreases. Thus the volume element in phase space is not symmetric about $\theta = 90°$, but tends to have a maximum value for $\theta > 90°$.

The plot of the cross section as a function of the energy of the emitted meson, Fig. 3, shows that when recoil is considered the π^- tends to come out with higher energy than the π^+. It appears difficult to attach much physical significance to this result. The origin of part of the shift is evident from the form of the energy denominators in the S matrix, Eq. (2). In the low energy limit, the denominator of the term corresponding to the emission of the π^+ in a P state (the k_{+v} term) is larger than the denominator for the term in which the π^- is emitted in a P state. Thus the matrix elements favor the π^- coming off in a P state. Since it is more probable for mesons with $l \neq 0$ to be emitted with greater energy, it follows that these two terms shift the differential cross section to higher π^- energies. The remainder of the shift comes from the interference of the first and second terms of Eq. (2) with the third and fourth.

A useful expression which gives the form of the differential cross section as a function of the energy of one of the emitted mesons, without recourse to tedious numerical integrations, is obtained by evaluating S^*S to order M^{-1} and combining this with the zero order density of final states [i.e., $M \to \infty$ in Eq. (8)]. The differential cross section in the center-of-mass coordinate system as a function of the energy of the π^- meson is

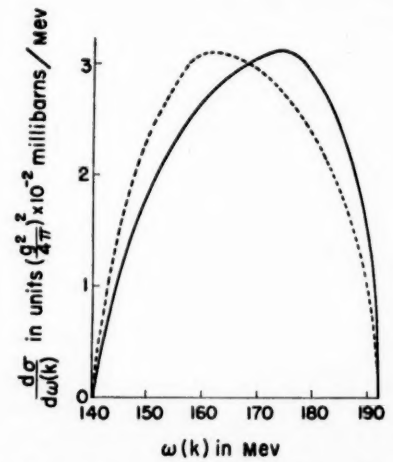

FIG. 3. Differential cross section in the center-of-mass coordinate system for the photoproduction of (π^+, π^-) pairs as a function of energy of one of the mesons. The curves are plotted for 400-Mev gamma rays in the laboratory coordinate system. Pseudoscalar coupling is assumed and first-order nucleon recoil effects are considered. The dotted (solid) curve refers to the cross section as a function of the energy of the $\pi^+(\pi^-)$ meson.

then given by

$$\frac{d\sigma}{d\omega(k_-)}=\frac{8}{137}\left(\frac{2M}{\mu}\right)^2\left(\frac{g^2}{4\pi}\right)^2\frac{k_-k_+}{\mu^2E_\gamma^3}\left\{\left(1-\frac{\omega(k_-)}{M}\right)A+\left(1+\frac{\omega(k_+)}{M}\right)B-\frac{k_-[E_\gamma-2\omega(k_-)]}{2M\omega(k_-)}C+\frac{k_+[E_\gamma-2\omega(k_+)]}{2M\omega(k_+)}D+\frac{k_-k_+[\omega(k_+)-\omega(k_-)]}{8M\omega(k_+)\omega(k_-)}CD\right\},\quad(10)$$

where

$$C=\left(1-\frac{\omega^2(k_-)}{k_-^2}\right)\ln\frac{\omega(k_-)+k_-}{\omega(k_-)-k_-}+2\frac{\omega(k_-)}{k_-},$$
$$D=\left(1-\frac{\omega^2(k_+)}{k_+^2}\right)\ln\frac{\omega(k_+)+k_+}{\omega(k_+)-k_+}+2\frac{\omega(k_+)}{k_+}.\quad(11)$$

In Eq. (10) the terms in the brackets proportional to $1/M$ are antisymmetric in the $+$ and $-$ indices. Therefore, although these terms do not contribute to the total cross section they materially affect the form of the differential cross section. This gives us further insight into why the two values for the cross section, Eqs. (7) and (9), are in such good agreement.

FIG. 4. Additional Feynman diagrams for the process $\gamma+p\rightarrow p'+\pi^++\pi^-$ for pseudovector coupling.

B. Pseudovector Coupling

The interaction energy for pseudovector coupling is given by

$$H=\int H_1d\mathbf{r}+\int H_2d\mathbf{r}+\int H_3d\mathbf{r}+\int H_4d\mathbf{r},$$

where

$$H_1=\frac{ig}{\mu}\bar{\psi}\gamma_5\gamma_\lambda\tau_a\frac{\partial\phi_a}{\partial x_\lambda}\psi,$$
$$H_4=\frac{ieg}{\mu}\bar{\psi}\gamma_5\gamma_\nu A_\nu(\tau_1\phi_2-\tau_2\phi_1)\psi,\quad(12)$$

and H_2 and H_3 are given by Eq. (1).

In addition to the Feynman diagrams for pseudoscalar coupling there are two diagrams arising from the combinations of H_1 and H_4. These are shown in Fig. 4.

The effective S matrix to order eg^2 is

$$S=\frac{eg^2\epsilon_\nu\delta(p_1+K-p_2-k_+-k_-)}{\mu^2[(2\pi)^7 2E_\gamma\omega(k_+)\omega(k_-)]^{\frac{1}{2}}}\left\{\frac{k_{+\alpha}\bar{u}_f\gamma_\nu(2M\gamma_\alpha+2ip_{1\alpha}-ik_{+\alpha})u_i}{(k_+^2-2p_1k_+)}-\frac{k_{-\alpha}\bar{u}_f(2M\gamma_\alpha+2ip_{2\alpha}+ik_{-\alpha})\gamma_\nu u_i}{(k_-^2+2p_2k_-)}\right.$$
$$-\frac{k_{+\nu}k_{-\lambda}(k_+-K)_\alpha\bar{u}_f(2ip_{2\lambda}+ik_{-\lambda}+2M\gamma_\lambda)\gamma_\alpha u_i}{(k_+K)(k_-^2+2p_2k_-)}+\frac{k_{-\nu}k_{+\alpha}(k_--K)_\lambda\bar{u}_f(2ip_{2\lambda}+i(k_--K)_\lambda+2M\gamma_\lambda)\gamma_\alpha u_i}{(k_-K)(k_-^2+2p_2k_--2p_2K-2k_-K)}$$
$$\left.+\frac{k_{+\alpha}k_{-\lambda}\bar{u}_f(\gamma_\nu\gamma_\beta K_\beta-2p_{2\nu})\gamma_\lambda(2ip_{1\alpha}+2M\gamma_\alpha-ik_{+\alpha})u_i}{2(p_2K)(k_+^2-2p_1k_+)}+\frac{k_{+\alpha}k_{-\lambda}\bar{u}_f(2M\gamma_\lambda+2ip_{2\lambda}+ik_{-\lambda})\gamma_\alpha(2p_{1\nu}+\gamma_\beta\gamma_\nu K_\beta)u_i}{2(p_1K)(k_-^2+2p_2k_-)}\right\}.\quad(13)$$

In the extreme nonrelativistic limit for the nucleon the last two terms in Eq. (13) become unimportant. The differential cross section as a function of the energy of the π^- meson is, in this case,

$$\frac{d\sigma}{d\omega(k_-)}=\frac{2}{137}\left(\frac{g^2}{4\pi}\right)^2\frac{k_-k_+}{\mu^4E_\gamma}\left\{8\left(\frac{k_-^2}{\omega^2(k_-)}+\frac{k_+^2}{\omega^2(k_+)}\right)-\frac{k_-k_+}{\omega(k_-)\omega(k_+)}CD-\frac{4k_-^2(2E_\gamma\omega(k_+)-k_+^2-E_\gamma^2)}{\omega^2(k_-)E_\gamma^2}A\right.$$
$$\left.-\frac{4k_+^2(2E_\gamma\omega(k_-)-k_-^2-E_\gamma^2)}{\omega^2(k_+)E_\gamma^2}B\right\},\quad(14)$$

where A, B, C, and D are defined by Eqs. (4) and (11).

The differential cross section is completely symmetric between the $+$ and $-$ indexes and is similar in shape to that obtained for pseudoscalar coupling (shown in Fig. 1 of reference 5). If energy conservation is treated in the same way as discussed in deriving Eq. (7), the total cross section for 400-Mev gamma rays in the center-of-mass coordinate system is

$$\sigma_{pv}(\pi^+,\pi^-)=0.064(g^2/4\pi)^2\text{ millibarns}.\quad(15)$$

Comparing this to the result obtained for pseuoscalar coupling we see that

$$\sigma_{ps}(\pi^+,\pi^-)/\sigma_{pv}(\pi^+,\pi^-)=18\text{ for 400-Mev gamma rays}.$$

Thus as stated in the introduction, the cross section derived using pseudoscalar coupling is considerably larger than that obtained from the pseudovector interaction.

Near threshold the differential cross section, Eq. (14), may be integrated exactly in terms of elementary

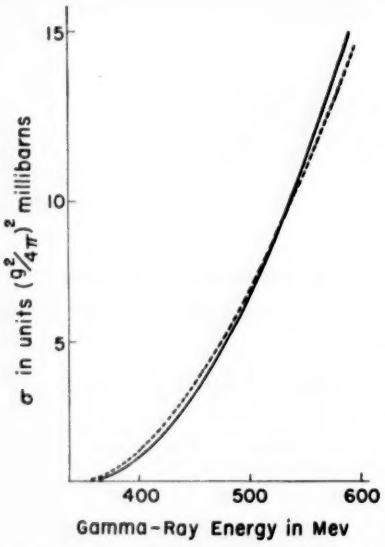

FIG. 5. Total cross section for the photoproduction of (π^+, π^-) pairs as a function of incident gamma-ray energy in the laboratory coordinate system. The dotted curve refers to pseudoscalar coupling and the solid curve to pseudovector. The pseudovector cross section has been multiplied by 15.

functions. Carrying out the calculation, one obtains[10]

$$\sigma \simeq \frac{8\pi}{137}\left(\frac{g^2}{4\pi}\right)^2 \frac{1}{\mu E_\gamma}\left(\frac{E}{\mu}-2\right)^3, \tag{16}$$

where E is the energy available to the meson pair (in a strict no recoil calculation $E \rightarrow E_\gamma$). Comparing this to the total cross section for pseudoscalar coupling [given by Eq. (4) of reference 5] we find

$$\frac{\sigma_{ps}(\pi^+, \pi^-)}{\sigma_{pv}(\pi^+, \pi^-)} \simeq \frac{1}{3}\left(\frac{2M}{\mu}\right)^2\left(\frac{\mu}{E_\gamma}\right)^2.$$

For $E_\gamma \simeq 2\mu$ this ratio becomes $\simeq 15$.

To find the recoil corrections to Eq. (14) is tedious, and in view of the non-renormalizability of the pseudovector interaction it is felt that the calculation is not warranted.

The total cross section for the production of (π^+, π^-) pairs as a function of gamma-ray energy is shown in Fig. 5 for both pseudoscalar and pseudovector coupling.

(π^+, π^0) PAIR PRODUCTION

In this section we shall calculate the cross section for the reaction $\gamma + p \rightarrow n + \pi^+ + \pi^0$, assuming the nucleon to be infinitely heavy. Consequently all Feynman diagrams in which the gamma ray interacts with the proton will be neglected. As we shall see, it is convenient to calculate first the cross section for pseudovector coupling.

A. Pseudovector Coupling

The Feynman diagrams to order eg^2 for the process are shown in Fig. 6. The effective S matrix is

$$S = \frac{eg^2\epsilon_\nu\delta(p_1+K-p_2-k_+-k_0)}{2\mu^2[(2\pi)^7 E_\gamma\omega(k_+)\omega(k_0)]^{\frac{1}{2}}}\left\{\frac{k_{0\alpha}\bar{u}_f\gamma_\nu(2ip_{1\alpha}-ik_{0\alpha}+2M\gamma_\alpha)u_i}{(k_0^2-2p_1k_0)} - \frac{k_{0\alpha}\bar{u}_f(2ip_{2\alpha}+ik_{0\alpha}+2M\gamma_\alpha)\gamma_\nu u_i}{(k_0^2+2p_2k_0)}\right.$$
$$\left. + \frac{k_{+\nu}k_{0\lambda}(k_+-K)_\alpha\bar{u}_f\gamma_\alpha(2ip_{1\lambda}-ik_{0\lambda}+2M\gamma_\lambda)u_i}{(k_+K)(k_0^2-2p_1k_0)} - \frac{k_{+\nu}k_{0\lambda}(k_+-K)_\alpha\bar{u}_f(2ip_{2\lambda}+ik_{0\lambda}+2M\gamma_\lambda)\gamma_\alpha u_i}{(k_+K)(k_0^2+2p_2k_0)}\right\}. \tag{17}$$

Converting Eq. (17) to a cross section, we obtain

$$\frac{d\sigma}{d\omega(k_+)} = \frac{16}{137}\left(\frac{g^2}{4\pi}\right)^2 \frac{k_+k_0}{3E_\gamma\omega^2(k_0)\mu^4} \times\left\{2k_0^2+\frac{k_0^2(k_+^2+E_\gamma^2-2\omega(k_+)E_\gamma)}{E_\gamma^2}A\right\}, \tag{18}$$

where A is given by Eq. (4).

The differential cross section is shown in Fig. 7 for 400-Mev incident gamma rays in the laboratory coordinate system. If energy conservation is treated in the same way as discussed in deriving Eq. (7), we find

$$\sigma_{pv}(\pi^+, \pi^0) = 2.22\times10^{-2}(g^2/4\pi)^2 \text{ millibarns}.$$

Comparing this to the result for (π^+, π^-) pair production at the same energy and with the same coupling we see that

$$\sigma_{pv}(\pi^+, \pi^-)/\sigma_{pv}(\pi^+, \pi^0) = 2.9.$$

One may qualitatively understand the shift of the differential cross section to lower π^+ energies as follows:

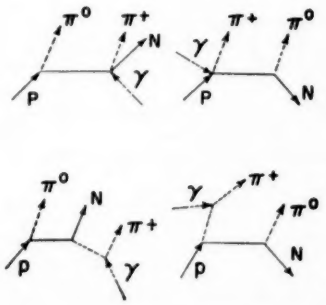

FIG. 6. Feynman diagrams for the process $\gamma + p \rightarrow n + \pi^+ + \pi^0$ assuming pseudovector coupling.

[10] Equation (16) has the same form as the result given by K. A. Brueckner and K. M. Watson, reference 4.

the eg term in the meson-nucleon coupling tends to emit the π^+ meson in an S state. On the other hand, the gradient coupling emits the mesons in a P state. Since the π^0 is emitted through the derivative coupling, it always has angular momentum >0. The π^+, however, is produced sometimes in an S state by the eg term in the interaction and sometimes in a P state due to its direct interaction with the gamma ray. Since it is more difficult to emit low-energy mesons in angular momentum states with $l\neq 0$, it follows that the differential cross section should be shifted to higher π^0 energies (lower π^+ energies).

Another interesting feature of the differential cross section is the fact that near the upper end of the π^+ spectrum the cross section goes to zero with zero slope. This may be understood by noting that the gradient coupling brings down an extra factor k_0 which when combined with the k_0 arising from the density of final states leads to a zero slope of the differential cross section for $k_0\rightarrow 0$.

B. Pseudoscalar Coupling

It is well known that the pseudoscalar interaction may be transformed by the Dyson transformation into one large term which is bilinear in the meson field,[11]

$$2M\left(\frac{g^2}{\mu^2}\right)\int\bar{\psi}\psi\phi_a{}^2 d\mathbf{r}, \tag{19}$$

plus other terms, one of which is the usual pseudovector interaction. It is obvious that the core term, Eq. (19), cannot contribute to the (π^+, π^0) cross section since it contains no mechanism for changing the nucleon charge. Consequently, to calculate the (π^+, π^0) cross section for pseudoscalar coupling we must consider nucleon recoil. This follows from the fact that to leading order there is a cancellation of the S matrices associated with the two Feynman diagrams in which the gamma ray interacts with the charged meson. However, if we use the transformed pseudoscalar coupling,[11] we may calculate the cross section without considering recoil since the zero contribution from the core term has already been separated out.

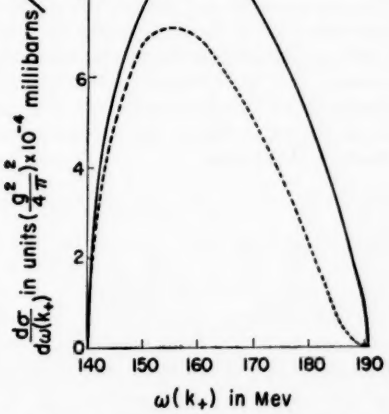

FIG. 7. Differential cross section in the center-of-mass system for the photoproduction of (π^+, π^0) meson pairs as a function of the energy of the emitted π^+ meson. The curve is plotted for 400-Mev gamma rays in the laboratory coordinate system. The nucleon is treated as being infinitely heavy. The dotted curve refers to pseudovector coupling; the solid curve to pseudoscalar.

[11] See for example S. D. Drell and E. M. Henley, reference 3.

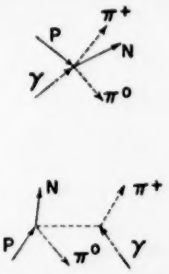

FIG. 8. Additional Feynman diagrams for the process $\gamma+p\rightarrow n+\pi^++\pi^0$ for pseudoscalar coupling.

In the transformed pseudoscalar interaction, aside from the usual derivative coupling, the term

$$H'=\frac{ieg^2}{\mu^2}\int\bar{\psi}\gamma_\nu A_\nu\phi_3(\tau_1\phi_1+\tau_2\phi_2)\psi d\mathbf{r}$$
$$-\frac{g^2}{2\mu^2}\int\phi_{a'}\frac{\partial\phi_a}{\partial x_\lambda}\bar{\psi}\gamma_\lambda[\tau_a, \tau_{a'}]\psi d\mathbf{r} \tag{20}$$

may contribute to the process. The additional Feynman diagrams arising from these terms are shown in Fig. 8.

The S matrix associated with these two diagrams is

$$S=\frac{ieg^2\epsilon_\nu\delta(p_1+K-p_2-k_+-k_0)}{2\mu^2[(2\pi)^7E_\gamma\omega(k_+)\omega(k_0)]^{\frac{1}{2}}}$$
$$\times\left\{\bar{u}_f\gamma_\nu u_i-\frac{2k_{+\nu}k_{0\alpha}\bar{u}_f\gamma_\alpha u_i}{(k_+K)}\right\}. \tag{21}$$

Combining Eqs. (17) and (21) we obtain the total effective S matrix to order eg^2 for pseudoscalar coupling. Converting this to a cross section we find

$$\left(\frac{d\sigma}{d\omega(k_+)}\right)_{ps}=\left(\frac{d\sigma}{d\omega(k_+)}\right)_{ps}$$
$$+\frac{16}{137}\left(\frac{g^2}{4\pi}\right)^2\frac{k_+k_0\omega^2(k_0)}{\mu^4E_\gamma{}^3}A, \tag{22}$$

where $[d\sigma/d\omega(k_+)]_{ps}$ is given by Eq. (18) and A is defined by Eq. (4).

The differential cross section for 400-Mev gamma rays is illustrated in Fig. 7. The total cross section has the value

$$\sigma=3.12\times10^{-2}(g^2/4\pi)^2 \text{ millibarns}.$$

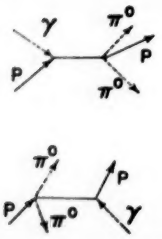

FIG. 9. Feynman diagrams for the process $\gamma+p\rightarrow p'+\pi^0+\pi^{0\prime}$ assuming pseudoscalar coupling.

From this we see that the ratio of the pseudoscalar to pseudovector cross section is 1.41 for 400-Mev gamma rays. The ratio of the (π^+, π^-) to (π^+, π^0) cross section for pseudoscalar coupling and the above energy is

$$\sigma_{ps}(\pi^+, \pi^-)/\sigma_{ps}(\pi^+, \pi^0)=37.$$

It is interesting to note that the most pronounced difference between pseudoscalar and pseuovector coupling in the production of a (π^+, π^0) meson pair is that the slope of the differential cross section at the upper end of the π^+ spectrum is zero for pseudovector coupling and infinite for pseudoscalar coupling. If Eq. (8) is used for the density of final states the slope of the differential cross section at the upper end of the π^+ spectrum becomes finite (but not zero) for pseuodscalar coupling but remains zero for the pseudovector interaction.

(π^0, π^0) PAIR PRODUCTION

For completeness we mention briefly the cross section for the photoproduction of a (π^0, π^0) meson pair assuming pseudoscalar coupling. From the discussion given in reference 5 we see that in the low energy limit the entire contribution to this cross section comes from the core term, Eq. (19). The Feynman diagrams for the process are shown in Fig. 9.

The effective S matrix is given by

$$S=\frac{Meg^2\epsilon_\nu\delta(p_1+K-p_2-k_0-k_0')}{\mu^2[(2\pi)^7 2E_\gamma\omega(k_0)\omega(k_0')]^{\frac{1}{2}}} \times\left\{\frac{\bar{u}_f(2p_{1\nu}+\gamma_\lambda\gamma_\nu K_\lambda)u_i}{(p_1K)}-\frac{\bar{u}_f(2p_{2\nu}-\gamma_\nu\gamma_\lambda K_\lambda)u_i}{(p_2K)}\right\}. \quad (23)$$

Converting Eq. (23) to a cross section, we obtain

$$\frac{d\sigma}{d\omega(k_0)}=\frac{64}{137}\left(\frac{g^2}{4\pi}\right)^2\frac{k_0k_0'}{3\mu^4E_\gamma^3}(k_0^2+k_0'^2). \quad (24)$$

The total cross section for 400-Mev incident gamma rays in the laboratory coordinate system is

$$\sigma_{ps}(\pi^0, \pi^0)=0.059(g^2/4\pi)^2 \text{ millibarns}.$$

Comparing this to the other possible pair production cross sections at the same energy and with the same coupling, we see that

$$\sigma_{ps}(\pi^+, \pi^-)/\sigma_{ps}(\pi^0, \pi^0)=19.5,$$
$$\sigma_{ps}(\pi^+, \pi^0)/\sigma_{ps}(\pi^0, \pi^0)=0.53.$$

Since the core term does not appear in the pseudovector interaction, it follows from Eq. (5) that

$$\sigma_{pv}(\pi^0, \pi^0)\sim(\mu/M)^2\sigma_{ps}(\pi^0, \pi^0).$$

The explicit evaluation of the pseuodovector (π^0, π^0) cross section is laborious and will not be given here.

DISCUSSION OF RESULTS

From the preceding work we see that information on the meson-nucleon interaction may be obtained by studying the photoproduction of meson pairs when a gamma-ray bombards a hydrogen target. We shall briefly discuss possible experiments which may help in determining the type of coupling.

A. Absolute Value of the (π^+, π^-) Cross Section

To obtain a theoretical value for the pair-production cross section, we shall assume that the meson-nucleon coupling constant in the derivative coupling theory has a value[12] $g^2/4\pi=1/15$. Under this assumption the total pair-production cross section for 400-Mev gamma rays is

$$\sigma_{ps}(\pi^+, \pi^-)=5.1\times10^{-30} \text{ cm}^2,$$
$$\sigma_{pv}(\pi^+, \pi^-)=2.8\times10^{-31} \text{ cm}^2.$$

For this choice of coupling constant and gamma-ray energy the ratio of the single meson photoproduction cross section[13] to the pair cross section is

$$\sigma_{ps}(\pi^+)/\sigma_{ps}(\pi^+, \pi^-)\simeq35, \quad \sigma_{pv}(\pi^+)/\sigma_{pv}(\pi^+, \pi^-)\simeq650.$$

For 500-Mev gamma rays the above ratios become approximately 7 and 100, respectively.

The major contribution to the (π^+, π^-) cross section for pseudoscalar coupling comes from the important pair term, Eq. (19). However, the effective value of this term may be smaller, as indicated by scattering experiments.[14] In this case the pair-production cross section for the pseudoscalar interaction would be decreased. Further, it is obvious that given an experimental value for the cross section, a coupling constant may be found which makes either form of the interaction fit the results. Thus with this type of test we can at best surmise the the answer to our problem.

B. Ratio of the (π^+, π^-) to (π^+, π^0) Cross Section

A sensitive test, dependent only on the assumption that the meson-nucleon coupling constant is small, is provided by a measurement of the ratio of the (π^+, π^-) to (π^+, π^0) cross sections. According to our results, in the low energy limit this ratio should be $\sim(M/\mu)^2$ if pseudoscalar coupling is operative and should be ~1

[12] M. M. Lévy, Phys. Rev. **86**, 806 (1952); **88**, 72 (1952). Lévy's analysis gives a value for the pseudoscalar coupling constant. Converting this by Eq. (5), one finds that the value of the interaction constant in the derivative coupling theory is $g^2/4\pi=1/18$. A Klein [Phys. Rev. **89**, 1158 (1953)] and Drell, Huang, and Weisskopf [Phys. Rev. **91**, 460 (1953)] have indicated that an error exists in this work.

[13] L. L. Foldy, Phys. Rev. **76**, 372 (1949).

[14] See for example S. D. Drell and E. M. Henley, reference 3.

if the pseudovector interaction is involved. However, this difference is a direct consequence of our perturbation approach with weak coupling theory. If an intermediate or strong coupling calculation were made, the important core term which provides the entire contribution to the low energy (π^+, π^-) cross section in the pseudoscalar theory might be damped out[15] and the two coupling schemes would give approximately the same ratio for these cross sections.

C. Measurement of the Differential (π^+, π^0) Cross Section

Detailed experimental data on the shape of the (π^+, π^0) cross section near the upper end of the π^+ spectrum should indicate the type of interaction between mesons and nucleons.

D. Other Possibilities

It is quite possible that a measurement of the differential (π^+, π^-) cross section either as a function of the angle between the emitted mesons or as a function of the energy of the π^- meson may give information on the type of interaction operative.

The author would like to express his sincere appreciation to Dr. S. D. Drell who originally suggested this investigation and who was a constant source of encouragement and stimulation during the couse of the work. Thanks are also due Prof. L. I. Schiff for many helpful suggestions. During the latter stages of this work the writer benefited greatly from many interesting discussions with Dr. D. R. Yennie.

[15] The damping of the pair term arising from one particular class of Feynman diagrams has been shown by Brueckner, Gell-Mann, and Goldberger, Phys. Rev. **90**, 476 (1953).

PHYSICAL REVIEW VOLUME 92, NUMBER 5 DECEMBER 1, 1953

A Hypothesis Concerning the Relations among the "New Unstable Particles"*

M. GOLDHABER
Brookhaven National Laboratory, Upton, New York

(Received August 17, 1953)

An attempt is made to systematize the present knowledge of phenomena concerned with the production, absorption, and decay of the "new unstable particles" in terms of only one "new" particle and its "compounds" with nucleons and π mesons.

THE great variety of new particles which cosmic-ray experiments have revealed in the last few years invites attempts to search for some unifying principle. We should like to put forward here a hypothesis which we are not able to work out in its complete form, but which we have found useful in correlating many phenomena. We shall start from some of the general ideas of Nambu, Oneda, Pais, and others[1] on pair production of V particles and make a number of tentative but specific assumptions. We find in this way that the fairly well-established experimental data are consistent with the following scheme which is designed to unify our knowledge of the "new unstable particles" in terms of only one "new" particle.

ASSUMPTIONS

(1) We shall assume that besides the π mesons there exists one other particle, fundamental in nucleon-nucleon interactions, which we shall call here the η meson. We shall assume that this is the particle which has sometimes been called phenomenologically V_2^0 or V_4^0, and which decays into two π mesons:[2]

$$\eta \rightarrow \pi^+ + \pi^- + 210 \text{ Mev}.$$

Thus, its mass is $m_\eta = 962 m_e$. If we take this decay scheme for granted, the η meson is a boson.[3] It further follows that the spin and parity of η are either both even $(0+, 2+, \cdots)$, or both odd $(1-, 3-, \cdots)$.

(2) Following previous considerations,[1] we shall assume that η mesons are created in pairs either through nucleon-nucleon or pion-nucleon collisions. (This assumption seems necessary to reconcile their comparatively long lifetime, of $\sim 10^{-10}$ sec, with their comparatively copious production.)

(3) We shall assume that η is a particle of isotopic spin $T=0$. (Reasons for this assumption are given below in 4b.)

(4) We shall assume that η can form "compounds" with either a nucleon or a pion.

(a) We shall assume that the compound of η and a neutron is a V_1^0:

$$V_1^0 = n + \eta - W_1^0,$$

and that the compound of η and a proton is a V_1^+:

$$V_1^+ = p + \eta - W_1^+,$$

where the binding energy $W_1^0 \approx W_1^+ \approx 310$ Mev is calculated from the energy release found in the decay of the V_1^0 (and V_1^+). The fundamental decay of a

* Under the auspices of the U. S. Atomic Energy Commission.

[1] For references, see A. Pais, Phys. Rev. **86**, 663 (1952).

[2] C. C. Butler in *Progress in Cosmic Ray Physics*, edited by J. G. Wilson (Interscience Publishers, Inc., New York, 1952), Chap. 2, pp. 65–123; Thompson, Buskirk, Etter, Karzmark, and Rediker, Phys. Rev. **90**, 329 (1953).

[3] R. W. Thompson *et al.* (see reference 2) emphasize that the present experimental evidence does not exclude the possibility of a decay $V_4^0 \rightarrow \pi + \mu$.

$V_1^{0,+}$ consists of the decay of

$$\eta \rightarrow \pi^+ + \pi^-,$$

with the absorption of one of the π mesons by the nucleon and emission of the other:

$$V_1^0 \rightarrow p + \pi^- + Q_1, \quad \text{where} \quad Q_1 = 37 \text{ Mev.}^4$$

Similarly, the decay $V_1^+ \rightarrow n + \pi^+ + \sim Q_1$ should be expected, but the only decay reported is $V_1^+ \rightarrow p + \pi^0 + \sim Q_1$.[5a] (See also the discussion below.)

(b) We shall assume that the compound of η and a $\pi^{\pm}$ is a $\tau^{\pm}$ meson:

$$\tau^{\pm} = \eta + \pi^{\pm} - W_2^{\pm},$$

where the measured mass $m_\tau = 975 m_e$ leads to a binding energy $W_2^{\pm} = 130$ Mev. The fundamental decay here again is the decay of the $\eta \rightarrow \pi^+ + \pi^-$, leaving a third $\pi^{\pm}$:

$$\tau^{\pm} \rightarrow \pi^{\pm} + \pi^+ + \pi^-.$$

If η were assumed to be a $T=1$ particle, in particular if it were the neutral member of the τ family, doubly charged compounds of nucleons might have been expected on our hypothesis—$T=\frac{3}{2}$ as well as $T=\frac{1}{2}$ "particles." For these there is at present no evidence.

CONCLUSIONS AND DISCUSSION

(I) Some Consequences of T Selection Rules

If we assume the validity of T selection rules, we can draw conclusions about various relative decay rates. The T selection rules have been very successfully employed in describing processes involving strong interactions. While there is no evidence for them in weak interactions such as must be involved in a slow decay process, it still may be of interest to consider their consequences.[5b]

From the assumption that η is a $T=0$ particle and the fact that π mesons are $T=1$ particles of spin 0, it would follow that the hitherto unobserved alternative decay mode,

$$\text{(A)} \quad \eta \rightarrow \pi^0 + \pi^0,$$

should exist with approximately one-half the rate of the observed decay mode,

$$\text{(B)} \quad \eta \rightarrow \pi^+ + \pi^-,$$

if η has an even spin.[6] A decay into two identical bosons would be forbidden for an odd spin. It would further follow that V_1^0 should also have an alternative decay mode $V_1^0 \rightarrow n + \pi^0$. (The decay $V_1^+ \rightarrow p + \pi^0$ has been mentioned under 4a).[7] The corresponding τ decay would be $\tau^{\pm} \rightarrow \pi^{\pm} + \pi^0 + \pi^0$, also hitherto unobserved.[8]

(II) Identity of κ, χ, and τ Mesons

Recent results reported at the Cosmic Ray Congress at Bagnères, France,[9] make it appear possible that $\kappa \equiv \chi \equiv \tau$, and that the observed κ, χ, and τ decays are alternative modes of decay of a single type of particle. Of course, a definite identification is difficult, and all that one can say at present is that no distinction has been made between κ, χ, and τ either on the basis of mass, or mode of production, or lifetime. Some of the alternative modes of decay[9] which would have to be postulated to account for the experimental data are:

$$\kappa \text{ mode} \quad \tau^{\pm} \rightarrow \mu^{\pm} + \nu + \gamma,$$

$$\chi \text{ mode} \quad \tau^{\pm} \rightarrow \pi^{\pm} + \begin{cases} \gamma \\ \pi^0 \end{cases}.$$

These decay processes would be compatible with the hypothesis presented here, though their relative decay rates cannot be calculated without further specifications. The χ mode can only be an alternative to the 3π mode of decay if the τ meson (and, therefore, on our hypothesis probably also the η meson) has a spin ≥ 1.

(III) Stars Produced by τ^--Mesons

The study of τ^- produced stars may show up some of the following possibilities: a proton in a nucleus may absorb a τ^-, the fundamental reaction being

$$p + \tau^- \rightarrow n + \eta + Q,$$

where $Q \sim 5.5$ Mev.[10] Such a reaction, if it occurred, would lead to a rather inconspicuous "star." Other possibilities are given by the fundamental reactions:

$$\text{(a)} \quad p + \tau^- \rightarrow V_1^0 + \pi^0 + 180\text{-Mev energy},$$

or

$$\text{(b)} \quad p + \tau^- \rightarrow V_1^+ + \pi^- + \sim 175\text{-Mev energy}.$$

Some of the available energy may be dissipated in the nucleus, particularly if the $\pi^{0,-}$ is absorbed. The typical appearance of a τ^--produced star will depend on the relative probability of the processes leading to $V_1^0 + \pi^0$ or $V_1^{0,+} + \pi^-$ and the kinetic energy carried away by them. The star will therefore not necessarily be more conspicuous than a π^--produced star. The $V_1^{0,+}$ may also stay bound in the residual nucleus, giving a

[4] Leighton, Wanlass, and Anderson, Phys. Rev. **89**, 148 (1953); Fretter, May, and Nakada, Phys. Rev. **89**, 168 (1953); Bridge, Peyrou, Rossi, and Safford, Phys. Rev. **91**, 362 (1953); Fowler, Shutt, Thorndike, and Whittemore, Phys. Rev. **90**, 1126 (1953).

[5a] York, Leighton, and Bjornerud, Phys. Rev. **90**, 167 (1953). This Q value may be a lower limit (see note added in proof, at end of paper).

[5b] *Note added in proof.*—A very general discussion of selection rules for elementary particle decay has been recently given by L. Michel (private communication).

[6] The ratio 1:2 for the decay rates $A:B$ arises from the fact that when two $T=1$ states are combined to form a $T=0$ state the states $(T_z=1)(T_z=-1)$, $(T_z=-1)(T_z=+1)$, $(T_z=0)(T_z=0)$ occur with equal weights. If η were a $T=1$ particle the decay into two π^0's would be forbidden, since in the resolution of the wave function of a $T=1$ particle into $T=1$ states, the state $(T_z=0) \times (T_z=0)$ appears with zero weight. [See also A. Pais and R. Jost, Phys. Rev. **81**, 871 (1952).]

[7] If a $V_1^{0,+}$ is regarded as a $T=\frac{1}{2}$ particle it would be expected to show the value 2:1 for the ratio of $\pi^{-,+}$ decay: π^0 decay, if T selection rules are applicable.

[8] See forthcoming papers by R. H. Dalitz [private communication (to be published)].

[9] Private communication from R. W. Thompson and M. Schein. A report of the Bagnères Congress is due to be published.

[10] It is well to keep in mind how poorly the small mass difference, $\tau - \eta$, on which the Q value of this reaction depends, is known at present. Also, the available energy must be reduced by the K binding energy of a τ^- if the nuclear capture takes place from a K orbit. This reaction may therefore only play a role for fast τ mesons.

"delayed star,"[11] or be emitted in a fragment, giving the recently discovered[12] "connected stars."

If τ^--produced stars were absent, because τ^- mesons were actually not absorbed by nuclei but rather decayed "at rest," i.e., in a K orbit, the co-planarity of the 3 emitted π mesons would, as a rule, be destroyed.

(IV) Thresholds for Production of V_1 Particles and Heavy Mesons

Any of the particles $V_1^{0,+}$, η, and $\tau^\pm$ can be produced in pairs, the threshold being lowest for production of $V_1^{0,+}+V_1^{0,+}$. The next energetically possible pairs with approximately equal thresholds would be $V_1^{0,+}+\eta$ and $V_1^{0,+}+\tau^\pm$, and at still higher energies one would obtain 2η, $\eta+\tau^\pm$, or $2\tau^\pm$. The approximate threshold energies in the center-of-mass system of two colliding nucleons are:

$$V_1^{0,+}+V_1^{0,+}\colon \sim 355 \text{ Mev}, \qquad 2\eta\colon \sim 980 \text{ Mev},$$
$$V_1^{0,+}+\eta\colon \sim 668 \text{ Mev}, \qquad \eta+\tau^\pm\colon \sim 990 \text{ Mev},$$
$$V_1^{0,+}+\tau^\pm\colon \sim 675 \text{ Mev}, \qquad 2\tau^\pm\colon \sim 1000 \text{ Mev}.$$

A π meson colliding with a free nucleon can produce $V_1^{0,+}+\eta$,[13] 2η, $\eta+\tau^\pm$, or $2\tau^\pm$, but not $V_1^{0,+}+V_1^{0,+}$. The energies necessary in the rest system are here lower by $m_\pi=140$ Mev compared with nucleon-nucleon collisions, as the π-meson mass can be "used up." On the compound idea presented here, some of the above reactions are of the nature of "pick-up" processes, and may show pronounced angular correlations.

(V) Further Particles

Some of the other "particles," for which only a few examples are known in each case, and where the exact nature of the events observed is still under discussion, do not fit, into the scheme discussed here. Among these are:[14]

$$\zeta^\pm \rightarrow \pi^\pm+\pi^0+\sim 1\text{–}2 \text{ Mev}, \qquad V_3^0 \rightarrow \tau^\pm+\pi^\mp+\sim 60 \text{ Mev},$$

and others, especially a charged V particle, with a Q value higher than that which we have assumed here for a V_1^+. A further difficulty for the scheme presented here is the apparent rarity of $V_1^{0,+}$ pairs as well as the apparently small value observed for the occurrence of V_1^+ relative to V_1^0. It is too early to say to what extent this may be ascribed to experimental difficulties.

(VI) Indirect Evidence for Pair Production of V_1^0 Particles

The existence of nuclear fragments[15] containing a $V_1^{0,+}$ appears to be a strong point in favor of the assumption of $V_1^{0,+}$ production in pairs; if they were produced singly, e.g., with an angular momentum sufficiently high to explain their lifetime in the free state, it would seem difficult to understand their survival inside nuclear matter for times $\gtrsim 10^{-12}$ sec.

A further point in favor of the assumption that $V_1^{0,+}$ production takes place in pairs is the observation by Schein and collaborators[14] of what appear to be slow V_1^0 particles, with energies up to ~ 5 Mev, emitted from carbon bombarded by π^- mesons of 227 ± 15 Mev. The cross section found was $\sim 2\times 10^{-30}$ per nucleon. At their upper limit, the energy of the mesons used is sufficient to produce one free V_1^0 of a few Mev, with the other member of the pair probably remaining bound with a "typical" nuclear binding energy (~ 10 Mev). Here the interaction of the π^- mesons must have taken place with at least two nucleons. If the V_1^0 particles observed had been produced singly, their energies would have ranged up to ~ 180 Mev.

A tendency for one $V_1^{0,+}$ to stay behind in the residual nucleus might explain in part why V_1^0 pairs have been so rarely reported. The decay of the bound $V_1^{0,+}$ may lead to emission of a slow π meson from a star from which a V_1^0 has been emitted. Such a process might account for the observation of the simultaneous production of a slow V_1^0 and a slow π^+ meson in a cosmic ray interaction reported by Althaus and Sard.[16]

Without specifying further some of the interactions which we have assumed to exist, quantitative predictions remain necessarily limited. We nevertheless publish the hypothesis in its present rudimentary form in the hope that it may be of some heuristic value.

My thanks for several valuable discussions are due to G. F. Chew, M. L. Goldberger, N. M. Kroll, and J. Weneser.

Note added in proof:—In a report on the Cosmic Ray Congress at Bagnères-de-Bigorre given by C. F. Powell [Nature **172**, 477 (1953)], evidence for a charged particle heavier than a proton and decaying with a $Q\sim 130$ Mev is quoted. Should this particle turn out to be the charged counterpart of the V_1^0 particle, such a surprisingly large "charge dependence" of the Q value might help explain the apparent asymmetry in the relative production rate of V_1^+ and V_1^0.—At the Cosmic Ray Congress the symbol θ^0 was suggested for the particle which we have here called η.

[11] Such a star may, under favorable circumstances, show a "double center," the first center corresponding to the location of the nucleus before absorbing the τ^- meson, the second center corresponding to the location of the recoil nucleus after it has come to rest, at which point the $V_1^{0,+}$ decay takes place. The $V_1^{0,+}$ decay may give rise to comparatively slow mesons (see reference 12). It is of interest that of the four stars induced by particles with a mass $\sim 1000m_e$ which Lal, Pal, and Peters [private communication; Phys. Rev. **92**, 438 (1953)] have recently observed, two show mesons of an energy of ~ 25 Mev, which it is not unreasonable to expect from the decay of a V_1^0 bound with "nucleonic" forces.—Stars with a double center might also be produced by fast nucleons or mesons which can produce $V_1^{0,+}$ pairs, with one $V_1^{0,+}$ staying in the nucleus.

[12] M. Danysz and J. Pniewski, Phil. Mag. **44**, 348 (1953); Tidman, Davis, Herz, and Tennent, Phil. Mag. **44**, 350 (1953); J. Crussard and D. Morellet, Compt. rend. **236**, 64 (1953).

[13] Evidence which can tentatively be interpreted in this manner has been found by Fowler, Shutt, Thorndike, and Whittemore, Phys. Rev. **91**, 1287 (1953).

[14] See Report of Third Rochester Conference on High Energy Nuclear Physics, 1952 (Interscience Publishers, New York, 1953) and Discussions at Bagnères Congress (to be published).

[15] If the existence of connected stars were explained by the presence inside a nucleus, of some particle other than a V_1^0 (or V_1^+), it would be surprising if that particle were not also found bound to single nucleons, thus giving rise to other kinds of $V^{0,+}$ particles decaying into nucleons, for which there is at present no definite evidence.

[16] E. J. Althaus and R. D. Sard, Phys. Rev. **91**, 373 (1953).

Semiclassical Methods in Meson Processes*

JOSEPH A. THIE
Argonne National Laboratory, Lemont, Illinois
(Received July 29, 1953)

Simple calculations analogous to the electrodynamical Weizsäcker-Williams method have been carried out for pseudoscalar mesons with pseudoscalar coupling. By integrating a fast nucleon's virtual meson spectrum with the appropriate meson scattering cross section, a nucleon-nucleon cross section is obtained. Results are given for neutron-proton bremsstrahlung and nucleon-nucleon meson production. When comparison is possible, results obtained by this method agree approximately with more exact calculations.

THE analogue to the Weizsäcker-Williams[1] method in meson theory was introduced by Heitler and Peng[2] and by Wang.[3] These authors calculated nucleon-nucleon meson production by scattering the fast nucleon's beam of virtual mesons on the other nucleon. From field theory they find that the number of charged virtual pseudoscalar mesons within an energy interval, $d\omega$, accompanying a moving nucleon of energy, γM, is ($c=\hbar=\mu=1$)

$$N(\omega)d\omega=\frac{g^2\omega z^2}{4\pi\gamma^2M^2}\left\{\frac{K_1^2-K_0^2}{1+\gamma^2\omega^{-2}}+K_0^2-K_1^2+2\frac{K_0K_1}{z}\right\}d\omega. \quad (1)$$

Here the argument of the K's[4] is $z=(1+\omega^2\gamma^{-2})^{\frac{1}{2}}/M$ and g is the *PSPS* coupling constant (not in Heaviside units). In (1) it is assumed that (a) $\gamma\gg1$, (b) corrections resulting from nonclassical effects will not give rise to appreciably different final results, and (c) weak-coupling theory may be used. Integration of (1) with the appropriate meson-induced reaction cross section, $\sigma_m(\omega)$,

$$\sigma=\int_{\omega_{\min}}^{\omega_{\max}}N(\omega)\sigma_m(\omega)d\omega, \quad (2)$$

gives the nucleon's total cross section.

To calculate $n-p$ bremsstrahlung the *PSPS* radiative capture cross section is needed. By Feynman-Dyson techniques one finds for $p(\pi^-,\gamma)n$ and $n(\pi^+,\gamma)p$, respectively[5]

$$\frac{d\sigma_-}{d\omega'}=\frac{\pi g^2e^2}{M(\omega^2-1)}\left\{\frac{2M\omega+1}{2M\omega'}+\frac{1}{2\omega'^2}+\frac{2}{[2M(\omega-\omega')+1]^2}-\frac{2\omega}{\omega'[2M(\omega-\omega')+1]}\right\}, \quad (3)$$

$$\frac{d\sigma_+}{d\omega'}=\frac{2\pi g^2e^2}{(\omega^2-1)(2M\omega+1)^2}\left\{\omega'(2M\omega+1)+M+\frac{4M\omega'^2}{[2M(\omega-\omega')+1]^2}-\frac{4M\omega\omega'}{2M(\omega-\omega')+1}\right\}, \quad (4)$$

where ω and ω' are the meson and γ-ray energies. The limits in the integration over ω, Eq. (2), are determined by $\cos\theta=\pm1$ in the Compton law for radiative capture, although $\omega_{\max}=\gamma M/2$ is used when it is a stronger limit.[2] Using $M=20/3$, (1) may be approximated as

$$N(\omega)=\frac{9g^2}{1600\pi\omega}\times\frac{3\omega^2}{\gamma^2} \quad \text{for } \omega\leqslant\gamma, \quad (5a)$$

$$N(\omega)=\frac{9g^2}{1600\pi\omega}\left\{21.5-0.6\left(6.6-\frac{\omega}{\gamma}\right)^2\right\} \quad \text{for } \omega>\gamma. \quad (5b)$$

After integrating (3) and (4) with (5) over ω and then over ω', one adds the results to obtain the total cross section for $n-p$ bremsstrahlung resulting from π^+ and π^- exchange,[6]

$$\sigma_++\sigma_-=0.0054e^2g^4\gamma^{-1}[\ln(0.57\gamma)-0.53\gamma^{-1}\ln(13\gamma)], \quad (6)$$

where $1/\gamma^2$ terms are neglected. Presumably a relativistic third-order field theoretic calculation of the charge exchange contribution would have a leading term of the same order as (6).

Although nucleon-nucleon meson production by the

* This work was performed while the author held a U. S. Atomic Energy Commission Postdoctoral Fellowship at Cornell University.

[1] C. F. v. Weizsäcker, Z. Physik **88**, 612 (1934); E. J. Williams, Phys. Rev. **45**, 729 (1934).

[2] W. Heitler and H. W. Peng, Proc. Roy. Irish Acad. **A49**, 101 (1943); see also W. Heitler and P. Walsh, Revs. Modern Phys. **17**, 252 (1945).

[3] F. S. Wang, Z. Physik **115**, 431 (1940).

[4] G. N. Watson, *A Treatise on the Theory of Bessel Functions* (Macmillan Company, New York, 1948), p. 78.

[5] Nonrelativistic calculations have been published by Aidzu, Fujimoto, Fukuda, Hayakawa, Takayanagi, Takeda, and Yamaguchi, Progr. Theoret. Phys. (Japan) **5**, 931 (1950); S. Ogawa and E. Yamada, Progr. Theoret. Phys. (Japan) **5**, 977 (1950); R. E. Marshak and A. S. Wightman, Phys. Rev. **76**, 114 (1949). It is somewhat disturbing that these three calculations, while retaining terms of order μ/M, disagree among themselves regarding these terms.

[6] J. Ashkin and R. E. Marshak, Phys. Rev. **76**, 58 (1949), find that charge exchange gives the major contribution at low energies.

method of virtual quanta has been treated[2] using various meson theories, it is of interest to calculate the *PSPS* result. Using the meson-scattering cross sections of Ashkin *et al.*[7] and proceeding exactly as above, one obtains for charged mesons from $n-p$ collisions:

$$\sigma=0.0034g^6\gamma^{-1}(1-0.94\gamma^{-1}), \tag{7}$$

and for π^+ from $p-p$ (or π^- from $n-n$) collisions:

$$\sigma=0.0068g^6\gamma^{-1}[\ln(0.31\gamma)+4.3\gamma^{-1}]. \tag{8}$$

Comparison with the third-order field-theoretic calculation of Morette[8] shows substantial agreement in the leading term. Similar agreement between virtual quanta methods and rigorous calculations in the scalar theory has been found by Strick and ter Haar.[9]

[7] Ashkin, Simon, and Marshak, Progr. Theoret. Phys. (Japan) **5**, 634 (1950).
[8] C. Morette, Phys. Rev. **76**, 1432 (1949).
[9] E. Strick and D. ter Haar, Phys. Rev. **76**, 304 (1949).

Because of the assumptions entailed in (1), the above results are of theoretical interest only. In practice one should integrate perhaps a phenomenological $N(\omega)$ with experimental meson-scattering cross sections. This might enable one to correlate meson-induced with nucleon-induced reactions, in a manner similar to Guth and Mullin's[10] correlation of experiments on the disintegration of Be^9 by γ rays and by electrons. A comparison of a high energy $n-p$ bremsstrahlung calculation using nuclear force phenomenology[11] with the method of virtual quanta might enable one to express $N(\omega)$ in terms of nuclear force parameters. Finally it might be pointed out that the method of virtual quanta would lend itself more readily to heavier particles with weaker coupling.

[10] E. Guth and C. J. Mullin, Phys. Rev. **76**, 234 (1949).
[11] J. Ashkin and R. E. Marshak, Phys. Rev. **76**, 58 (1949) and T. Muto, Phys. Rev. **59**, 837 (1941) have done low-energy $n-p$ bremsstrahlung calculations in which the nucleon-nucleon interaction is handled by nuclear force phenomenology rather than by weak-coupling meson theory.

PHYSICAL REVIEW VOLUME 92, NUMBER 5 DECEMBER 1, 1953

The Theory of Quantized Fields. IV

JULIAN SCHWINGER
Harvard University, Cambridge, Massachusetts
(Received August 6, 1953)

The principal development in this paper is the extension of the eigenvalue-eigenvector concept to complete sets of anticommuting operators. With the aid of this formalism we construct a transformation function for the Dirac field, as perturbed by an external source. This transformation function is enlarged to describe phase transformations and, when applied to the isolated Dirac field, yields the charge and energy-momentum eigenvalues and eigenfunctions. The transformation function describing the system in the presence of the source is then used as a generating function to construct the matrices of all ordered products of the field operators, for the isolated Dirac field. The matrices in the occupation number representation are exhibited with a classification that effectively employs a time-reversed description for negative frequency modes. The last section supplements III by constructing the matrices of all ordered products of the potential vector, for the isolated electromagnetic field.

INTRODUCTION

THIS paper and its sequel are continuations of III[1] in their concern with a single externally perturbed field. We shall discuss the Dirac field as perturbed by a second prescribed Dirac field, which appears as an external source, or by a prescribed Bose-Einstein field, as exemplified by a given electromagnetic field. The Lagrange function of this system is

$$\begin{aligned}\mathfrak{L}=&-\tfrac{1}{4}[\bar\psi,\gamma_\mu(-i\partial_\mu-eA_\mu)\psi+m\psi]\\&-\tfrac{1}{4}[(i\partial_\mu-eA_\mu)\bar\psi\gamma_\mu+m\bar\psi,\psi]\\&+\tfrac{1}{2}[\bar\psi,\eta]+\tfrac{1}{2}[\bar\eta,\psi].\end{aligned} \tag{1}$$

The resulting field equations are

$$\begin{aligned}\gamma_\mu(-i\partial_\mu-eA_\mu)\psi+m\psi=\eta,\\(i\partial_\mu-eA_\mu)\bar\psi\gamma_\mu+m\bar\psi=\bar\eta,\end{aligned} \tag{2}$$

and the generators of infinitesimal changes in ψ or $\bar\psi$ on a surface σ are given by

$$G(\psi)=i\int d\sigma_\mu\bar\psi\gamma_\mu\delta\psi=i\int d\sigma\bar\psi\gamma_{(0)}\delta\psi \tag{3}$$

and

$$G(\bar\psi)=-i\int d\sigma_\mu\delta\bar\psi\gamma_\mu\psi=-i\int d\sigma\delta\bar\psi\gamma_{(0)}\psi. \tag{4}$$

It was shown in III that the vacuum state of a closed system, Ψ_0 can be characterized as the right eigenvector, with zero eigenvalues, of the positive frequency parts of the field components, and that $\Psi_0^\dagger$ is the left eigenvector, with zero eigenvalues, of the negative frequency parts of the field components. The inference that the totality of eigenvectors of these types would be of particular utility led us, in discussing a Bose-Einstein system, to introduce eigenvectors and eigenvalues for complete sets

[1] J. Schwinger, Phys. Rev. **91**, 728 (1953).

of commuting non-Hermitian operators. We shall now find it desirable to extend the eigenvalue-eigenvector concept to complete sets of *anticommuting*, non-Hermitian operators.

THE TRANSFORMATION FUNCTION

The discussion in this paper will be limited to the situation of zero electromagnetic field, as described with the elementary gauge, $A_\mu=0$. Relative to a coordinate system based on a given surface, the field equations in the absence of the sources can be written as the equations of motion,

$$\begin{aligned} i\partial_0\psi &= -i\gamma_0\gamma_k\partial_k\psi + m\gamma_0\psi = H\psi, \\ -i\partial_0\bar{\psi} &= i\partial_k\bar{\psi}\gamma_k\gamma_0 + m\bar{\psi}\gamma_0 = \bar{\psi}\gamma_0 H\gamma_0. \end{aligned} \tag{5}$$

We define two Hermitian coordinate operators,

$$P^{(\pm)} = \tfrac{1}{2}(1 \pm (H/E)), \tag{6}$$

where E is the positive-definite quantity

$$E = (H^2)^{\frac{1}{2}}. \tag{7}$$

These operators have the projection properties

$$P^{(+)} + P^{(-)} = 1, \quad P^{(+)}P^{(-)} = P^{(-)}P^{(+)} = 0 \tag{8}$$

and

$$P^{(\pm)}H = \pm EP^{(\pm)}. \tag{9}$$

Hence the representation of ψ and $\bar{\psi}$ as

$$\psi = \psi^{(+)} + \psi^{(-)}, \quad \bar{\psi} = \bar{\psi}^{(+)} + \bar{\psi}^{(-)}, \tag{10}$$

where

$$\psi^{(\pm)} = P^{(\pm)}\psi, \quad \bar{\psi}^{(\pm)} = \bar{\psi}\gamma_0 P^{(\mp)}\gamma_0 \tag{11}$$

is a decomposition into positive and negative frequency parts, according to the resulting form of the equations of motion,

$$i\partial_0\psi^{(\pm)} = \pm E\psi^{(\pm)}, \quad i\partial_0\bar{\psi}^{(\pm)} = \pm E\bar{\psi}^{(\pm)}. \tag{12}$$

It should also be noted that

$$\bar{\psi}^{(\pm)} = \overline{\psi^{(\mp)}}. \tag{13}$$

In view of the orthogonality properties expressed by

$$\int d\sigma\bar{\psi}^{(+)}\gamma_0\psi^{(+)} = \int d\sigma\bar{\psi}\gamma_0 P^{(-)}P^{(+)}\psi = 0, \tag{14}$$

and

$$\int d\sigma\bar{\psi}^{(-)}\gamma_0\psi^{(-)} = \int d\sigma\bar{\psi}\gamma_0 P^{(+)}P^{(-)}\psi = 0, \tag{15}$$

the generator $G(\psi)$ appears as

$$G(\psi) = i\int d\sigma\bar{\psi}^{(-)}\gamma_0\delta\psi^{(+)} + i\int d\sigma\bar{\psi}^{(+)}\gamma_0\delta\psi^{(-)}. \tag{16}$$

By the addition of suitable variations to this generator, we deduce the generators of infinitesimal changes in the positive frequency, or in the negative frequency parts of ψ and $\bar{\psi}$,

$$G_+ = i\int d\sigma\bar{\psi}^{(-)}\gamma_0\delta\psi^{(+)} - i\int d\sigma\delta\bar{\psi}^{(+)}\gamma_0\psi^{(-)}, \tag{17}$$

$$G_- = i\int d\sigma\bar{\psi}^{(+)}\gamma_0\delta\psi^{(-)} - i\int d\sigma\delta\bar{\psi}^{(-)}\gamma_0\psi^{(+)}. \tag{18}$$

The orthogonality properties contained in (14) and (15) also enable us to write these generators as

$$G_+ = i\int d\sigma\bar{\psi}\gamma_0\delta\psi^{(+)} - i\int d\sigma\delta\bar{\psi}^{(+)}\gamma_0\psi \tag{19}$$

and

$$G_- = i\int d\sigma\bar{\psi}\gamma_0\delta\psi^{(-)} - i\int d\sigma\delta\bar{\psi}^{(-)}\gamma_0\psi, \tag{20}$$

or, alternatively, as

$$G_+ = i\int d\sigma\bar{\psi}^{(-)}\gamma_0\delta\psi - i\int d\sigma\delta\bar{\psi}\gamma_0\psi^{(-)} \tag{21}$$

and

$$G_- = i\int d\sigma\bar{\psi}^{(+)}\gamma_0\delta\psi - i\int d\sigma\delta\bar{\psi}\gamma_0\psi^{(+)}. \tag{22}$$

The latter forms facilitate the derivation of commutation properties on σ for the field components $\psi^{(\pm)}$, $\bar{\psi}^{(\pm)}$. These are expressed by the vanishing of all anticommutators save

$$\{\psi^{(+)}(x), \bar{\psi}^{(-)}(x')\} = P^{(+)}\gamma_0\delta_\sigma(x-x') \tag{23}$$

and

$$\{\psi^{(-)}(x), \bar{\psi}^{(+)}(x')\} = P^{(-)}\gamma_0\delta_\sigma(x-x'). \tag{24}$$

In particular, all positive frequency components are anticommutative, as are all negative frequency components.

Complete sets of anticommuting operators on σ are thus provided by $\chi^{(+)}(x)=\psi^{(+)}(x)$, $\bar{\psi}^{(+)}(x)$, and by $\chi^{(-)}(x)=\psi^{(-)}(x)$, $\bar{\psi}^{(-)}(x)$. The existence of right and left eigenvectors, respectively, with null eigenvalues, follows from the equivalence of these states with the vacuum state. Let us now extend the number system by introducing quantities $\chi^{(+)'}(x)=\psi^{(+)'}(x)$, $\bar{\psi}^{(+)'}(x)$ and $\chi^{(-)'}(x)=\psi^{(-)'}(x)$, $\bar{\psi}^{(-)'}(x)$, which anticommute among themselves and with all Dirac field operators. Then the operators

$$'\chi^{(\pm)} = \chi^{(\pm)} - \chi^{(\pm)'}$$

have the same commutation properties as the $\chi^{(\pm)}$, so that there exists a right eigenvector of the complete set $'\chi^{(+)}$ with zero eigenvalues,

$$(\chi^{(+)}(x) - \chi^{(+)'}(x))\Psi(\chi^{(+)'}\sigma) = 0,$$

and a left eigenvector of the complete set $'\chi^{(-)}$ with zero eigenvalues,

$$\Phi(\chi^{(-)'}\sigma)(\chi^{(-)}(x) - \chi^{(-)'}(x)) = 0.$$

As the notation indicates, we thereby obtain a right eigenvector of the complete set $\chi^{(+)}$ with the "eigenvalues" $\chi^{(+)\prime}$, and a left eigenvector of the set $\chi^{(-)}$ with the "eigenvalues" $\chi^{(-)\prime}$. In view of the relation (13), the eigenvectors and eigenvalues are connected by

$$\Phi(\chi^{(-)\prime}\sigma)=\Psi(\chi^{(+)\prime}\sigma)^{\dagger}, \tag{25}$$

$$\bar{\psi}^{(\pm)\prime}=\overline{\psi^{(\mp)\prime}}. \tag{26}$$

The interpretation of the infinitesimal transformation equations

$$\delta\Psi(\chi^{(+)\prime}\sigma)=-iG_{+}\Psi(\chi^{(+)\prime}\sigma) \tag{27}$$

and

$$\delta\Phi(\chi^{(-)\prime}\sigma)=i\Phi(\chi^{(-)\prime}\sigma)G_{-}, \tag{28}$$

employs the identical operator properties of the field variations and of the eigenvalues. Thus $\Psi(\chi^{(+)\prime}\sigma)+\delta\Psi(\chi^{(+)\prime}\sigma)$ is the eigenvector of the $\chi^{(+)}-\delta\chi^{(+)}$ with the eigenvalues $\chi^{(+)\prime}$. But this is also the eigenvector of the $\chi^{(+)}$ with the eigenvalues $\chi^{(+)\prime}+\delta\chi^{(+)}$. Hence the alteration given by (27) is that associated with the change of the eigenvalues by $\delta\chi^{(+)}$. A similar statement applies to (28).

We shall now discuss the Dirac field under the influence of the external sources η, $\bar{\eta}$ in terms of the transformation function

$$(\chi^{(-)\prime}\sigma_1|\chi^{(+)\prime}\sigma_2)=(\Phi(\chi^{(-)\prime}\sigma_1)\Psi(\chi^{(+)\prime}\sigma_2)).$$

The dependence of this transformation function upon the eigenvalues is expressed by

$$\delta_{\chi'}(\chi^{(-)\prime}\sigma_1|\chi^{(+)\prime}\sigma_2)=i(\chi^{(-)\prime}\sigma_1|(G_{-}(\sigma_1)-G_{+}(\sigma_2))|\chi^{(+)\prime}\sigma_2), \tag{29}$$

where

$$\begin{aligned}G_{-}(\sigma_1)-G_{+}(\sigma_2)&=-i\int_{\sigma_1}d\sigma_\mu\delta\bar{\psi}^{(-)\prime}\gamma_\mu\psi+i\int d\sigma_\mu\bar{\psi}\gamma_\mu\delta\psi^{(-)\prime}\\&\quad+i\int_{\sigma_2}d\sigma_\mu\delta\bar{\psi}^{(+)\prime}\gamma_\mu\psi-i\int_{\sigma_2}d\sigma_\mu\bar{\psi}\gamma_\mu\delta\psi^{(+)\prime}\\&=-i\oint d\sigma_\mu\delta\bar{\psi}'\gamma_\mu\psi+i\oint d\sigma_\mu\bar{\psi}\gamma_\mu\delta\psi'.\end{aligned} \tag{30}$$

In the latter form, it is understood that negative frequency eigenvalues are employed on σ_1, and positive frequency eigenvalues on σ_2.

An infinitesimal change of the external source produces the alteration

$$\delta(\chi^{(-)\prime}\sigma_1|\chi^{(+)\prime}\sigma_2)=i\left(\chi^{(-)\prime}\sigma_1\left|\int_{\sigma_2}^{\sigma_1}(dx)(\delta\bar{\eta}\psi+\bar{\psi}\delta\eta)\right|\chi^{(+)\prime}\sigma_2\right). \tag{31}$$

Accordingly, an infinitesimal change in the eigenvalues can be simulated by the surface distributed source variation

$$\begin{aligned}\delta\bar{\eta}(x)&=-i\delta\bar{\psi}^{(-)\prime}(x)\gamma_\mu\delta_\mu(x,\sigma_1)+i\delta\bar{\psi}^{(+)\prime}(x)\gamma_\mu\delta_\mu(x,\sigma_2),\\\delta\eta(x)&=i\delta_\mu(x,\sigma_1)\gamma_\mu\delta\psi^{(-)\prime}(x)-i\delta_\mu(x,\sigma_2)\gamma_\mu\delta\psi^{(+)\prime}(x),\end{aligned} \tag{32}$$

where $\delta_\mu(x,\sigma)$ is defined by

$$\int(dx)\delta_\mu(x,\sigma)f_\mu(x)=\int_\sigma d\sigma_\mu f_\mu(x).$$

We conclude that the general transformation function is obtained from the one referring to zero eigenvalues on making the followlng substitution in the latter,

$$\begin{aligned}\bar{\eta}(x)&\rightarrow\bar{\eta}(x)-i\bar{\psi}^{(-)\prime}(x)\gamma_\mu\delta_\mu(x,\sigma_1)+i\bar{\psi}^{(+)\prime}(x)\gamma_\mu\delta_\mu(x,\sigma_2),\\\eta(x)&\rightarrow\eta(x)+i\delta_\mu(x,\sigma_1)\gamma_\mu\psi^{(-)\prime}(x)-i\delta_\mu(x,\sigma_2)\gamma_\mu\psi^{(+)\prime}(x).\end{aligned} \tag{33}$$

With the notation

$$(0\sigma_1|0\sigma_2)=\exp(i\mathfrak{W}_0) \tag{34}$$

and

$$(0\sigma_1|F|0\sigma_2)/(0\sigma_1|0\sigma_2)=\langle F\rangle, \tag{35}$$

the dependence of the null eigenvalue transformation function upon the source is expressed by

$$\begin{aligned}\delta_l\mathfrak{W}_0/\delta\bar{\eta}(x)&=\langle\psi(x)\rangle,\\\delta_r\mathfrak{W}_0/\delta\eta(x)&=\langle\bar{\psi}(x)\rangle,\end{aligned} \tag{36}$$

or

$$\delta\mathfrak{W}_0=\int_{-\infty}^{\infty}(dx)[\delta\bar{\eta}\langle\psi\rangle+\langle\bar{\psi}\rangle\delta\eta], \tag{37}$$

in which it is supposed that the source vanishes externally to the volume bounded by σ_1 and σ_2. According to the field equations (2), we have

$$-i\gamma_\mu\partial_\mu\langle\psi(x)\rangle+m\langle\psi(x)\rangle=\eta(x), \tag{38}$$

and

$$i\partial_\mu\langle\bar{\psi}(x)\rangle\gamma_\mu+m\langle\bar{\psi}(x)\rangle=\bar{\eta}(x), \tag{39}$$

which are to be solved subject to the boundary conditions

$$\langle\psi^{(-)}\rangle=\langle\bar{\psi}^{(-)}\rangle=0,\quad\text{on }\sigma_1, \tag{40}$$

and

$$\langle\psi^{(+)}\rangle=\langle\bar{\psi}^{(+)}\rangle=0,\quad\text{on }\sigma_2, \tag{41}$$

that follow from the nature of the null eigenvalue states on σ_1 and σ_2. We can express these as boundary conditions in the extended domain through the requirement that the fields shall contain only positive frequencies in the region constituting the future of σ_1, and only negative frequencies in the region prior to σ_2.

The solutions meeting these conditions are

$$\langle\psi(x)\rangle=\int_{-\infty}^{\infty}(dx')G_{+}(x,x')\eta(x') \tag{42}$$

and

$$\langle\bar{\psi}(x')\rangle=\int_{-\infty}^{\infty}(dx)\bar{\eta}(x)G_+(x,x'),\tag{43}$$

where $G_+(x,x')$ is the Green's function defined by the differential equations

$$\begin{aligned}-i\gamma_\mu\partial_\mu G_+(x,x')+mG_+(x,x')&\\ =i\partial_\mu'G_+(x,x')\gamma_\mu+mG_+(x,x')&\\ =\delta(x-x'),&\end{aligned}\tag{44}$$

and the boundary condition that G_+, as a function of x, shall contain only positive frequencies for $x_0>x_0'$, and only negative frequencies for $x_0<x_0'$. Since G_+ is only dependent upon $x-x'$, the same statement applies with x and x' interchanged. That the identical Green's function is encountered in (42) and (43) follows from the integrability condition deduced from (36),

$$(\delta_r/\delta\eta(x'))\langle\psi(x)\rangle=(\delta_l/\delta\bar{\eta}(x))\langle\bar{\psi}(x')\rangle=G_+(x,x').$$

We thus construct $\mathcal{W}_0$ as

$$\mathcal{W}_0=\int_{-\infty}^{\infty}(dx)(dx')\bar{\eta}(x)G_+(x,x')\eta(x'),\tag{45}$$

with a constant of integration that has the value zero since, in the absence of sources, the null eigenvalue states have the significance of the σ-independent vacuum state

$$\eta=\bar{\eta}=0:\quad(0\sigma_1|0\sigma_2)=1,\quad\mathcal{W}_0=0.$$

On performing the substitution (33), the general transformation function is obtained as

$$(\chi^{(-)'}\sigma_1|\chi^{(+)'}\sigma_2)=\exp(i\mathcal{W}),\tag{46}$$

where

$$\begin{aligned}\mathcal{W}=&\int(dx)(dx')\bar{\eta}(x)G_+(x,x')\eta(x')\\ &-i\oint d\sigma_\mu\int(dx')\bar{\psi}'(x)\gamma_\mu G_+(x,x')\eta(x')\\ &+i\int(dx)\oint d\sigma_\nu'\bar{\eta}(x)G_+(x,x')\gamma_\nu\psi'(x')\\ &+\oint d\sigma_\mu\oint d\sigma_\nu'\bar{\psi}'(x)\gamma_\mu G_+(x,x')\gamma_\nu\psi'(x').\end{aligned}\tag{47}$$

In particular,

$$\begin{aligned}\eta=\bar{\eta}=0:\quad&(\chi^{(-)'}\sigma_1|\chi^{(+)'}\sigma_2)\\ =\exp&\left[i\oint d\sigma_\mu\oint d\sigma_\nu'\bar{\psi}'(x)\gamma_\mu G_+(x,x')\gamma_\nu\psi'(x')\right].\end{aligned}\tag{48}$$

The Green's function $G_+(x,x')$ can be exhibited in the three-dimensional symbolic form

$$\begin{aligned}G_+(x,x')&=iP^{(+)}\exp[-iE(x_0-x_0')]\gamma_0\delta(\mathbf{x}-\mathbf{x}'),\\ &\qquad\qquad x_0>x_0'\\ &=-iP^{(-)}\exp[-iE(x_0'-x_0)]\gamma_0\delta(\mathbf{x}-\mathbf{x}'),\\ &\qquad\qquad x_0<x_0',\end{aligned}\tag{49}$$

or, combining both situations,

$$\begin{aligned}G_+(x,x')=&(i\partial_0+H)\tfrac{1}{2}iE^{-1}\\ &\times\exp(-iE|x_0-x_0'|)\gamma_0\delta(\mathbf{x}-\mathbf{x}').\end{aligned}\tag{50}$$

The function of E in the latter equation has the integral representation

$$\begin{aligned}\tfrac{1}{2}iE^{-1}&\exp(-iE|x_0-x_0'|)\\ &=\frac{1}{2\pi}\int_{-\infty}^{\infty}dp_0\frac{e^{-ip_0(x_0-x_0')}}{E^2-p_0^2-i\epsilon},\quad\epsilon\to+0.\end{aligned}\tag{51}$$

The Fourier integral expression of the three-dimensional delta function in (50), combined with (51), leads to the four-dimensional integral

$$\begin{aligned}G_+(x,x')&=\frac{1}{(2\pi)^4}\int(dp)\frac{m-\gamma p}{p^2+m^2-i\epsilon}e^{ip(x-x')}\\ &=\frac{1}{(2\pi)^4}\int(dp)\frac{1}{\gamma p+m-i\epsilon}e^{ip(x-x')},\\ &\qquad\qquad\epsilon\to+0,\end{aligned}\tag{52}$$

which shows that the mass m must be supplemented with an infinitesimal negative imaginary constant in constructing the Green's function as the reciprocal of the differential operator in (44).

The three-dimensional Fourier integrals derived from (49) are advantageously presented as

$$\begin{aligned}G_+(x,x')=\tfrac{1}{2}i\int\frac{(d\mathbf{p})}{(2\pi)^3}\frac{1}{p_0}&\\ \times\begin{cases}(m-\gamma p)e^{ip(x-x')}, & x_0>x_0'\\ (m+\gamma p)e^{-ip(x-x')}, & x_0<x_0',\end{cases}&\end{aligned}\tag{53}$$

where p_0 is a *posilive* frequency

$$p_0=(\mathbf{p}^2+m^2)^{\frac{1}{2}}.$$

The four-rowed square matrix $-\gamma p$ has two distinct eigenvalues, $\pm m$,

$$(-\gamma p)^2=-p^2=m^2,$$

each of which is twofold degenerate. We shall designate the eigenvectors by $u_{\lambda p}$ where $\lambda=1,2$ refers to the eigenvalue $+m$, and $\lambda=-1,-2$ indicates the eigenvalue m. Thus

$$-\gamma pu_{\lambda p}=\epsilon(\lambda)mu_{\lambda p},\tag{54}$$

and

$$-\bar{u}_{\lambda p}\gamma p = \bar{u}_{\lambda p}\epsilon(\lambda)m,$$

where

$$\epsilon(\lambda) = \lambda/|\lambda|.$$

In view of the indefinite character of the quantities

$$(\bar{u}_{\lambda p}u_{\lambda p}) = (u_{\lambda p}{}^{*}\gamma_0 u_{\lambda p}),$$

the orthonormality and completeness properties of these eigenvectors appear as

$$(\bar{u}_{\lambda p}u_{\lambda' p}) = \delta_{\lambda\lambda'}\epsilon(\lambda),$$

and

$$\sum_\lambda \epsilon(\lambda)u_{\lambda p}\bar{u}_{\lambda p} = 1.$$

The positive definite quantities

$$(\bar{u}_{\lambda p}\gamma_0 u_{\lambda p}) = (u_{\lambda p}{}^{*}u_{\lambda p})$$

are then given by

$$(\bar{u}_{\lambda p}\gamma_0 u_{\lambda' p}) = \delta_{\lambda\lambda'}(p_0/m).$$

The latter result is deduced from

$$\begin{aligned}-(\bar{u}_{\lambda p}\{\gamma_0, \gamma p\}u_{\lambda' p}) &= 2p_0(\bar{u}_{\lambda p}u_{\lambda' p}) \\ &= m(\epsilon(\lambda)+\epsilon(\lambda'))(\bar{u}_{\lambda p}\gamma_0 u_{\lambda' p}),\end{aligned}$$

which shows that $(\bar{u}_{\lambda p}u_{\lambda p})$ is indeed negative for $\lambda<0$.

When the eigenvalue equation (54), in the form

$$(1/2m)(m-\gamma p)u_{\lambda p} = \tfrac{1}{2}(1+\epsilon(\lambda))u_{\lambda p},$$

is multiplied by $\epsilon(\lambda)\bar{u}_{\lambda p}$ and summed over all λ with the aid of the completeness relation, there results

$$(1/2m)(m-\gamma p) = \sum_{+} u_{\lambda p}\bar{u}_{\lambda p},$$

where $+$ signifies the eigenvectors with $\lambda>0$. Similarly,

$$(1/2m)(m+\gamma p) = -\sum_{-} u_{\lambda p}\bar{u}_{\lambda p}.$$

We employ these projection operator representations in (53), and replace the integral by a summation over cells of volume $(d\mathbf{p})$. This yields

$$\begin{aligned}G_+(x, x') &= i\sum_{+,p}\psi_{\lambda p}(x)\bar{\psi}_{\lambda p}(x'), \qquad x_0>x_0' \\ &= -i\sum_{-,p}\psi_{\lambda p}(x)\bar{\psi}_{\lambda p}(x'), \quad x_0<x_0',\end{aligned} \tag{55}$$

in which

$$\psi_{\lambda p}(x) = \left(\frac{(d\mathbf{p})}{(2\pi)^3}\frac{m}{p_0}\right)^{\frac{1}{2}} u_{\lambda p}e^{i\epsilon(\lambda)px}.$$

The completeness of these functions on a given surface is implied by the discontinuity of the Green's function at $x_0=x_0'$, as derived from (44),

$$\sum_{\lambda p}\psi_{\lambda p}(x)\bar{\psi}_{\lambda p}(x') = \gamma_0\delta_\sigma(x-x'), \tag{56}$$

The associated *ortho*-normality statement is

$$\int d\sigma\bar{\psi}_{\lambda p}\gamma_0\psi_{\lambda' p'} = \delta_{\lambda p,\lambda' p'}. \tag{57}$$

EIGENVALUES AND EIGENFUNCTIONS

We begin our applications of (46) with the isolated Dirac field, as described by (48). The eigenvalues and eigenfunctions of the energy-momentum vector P_μ are obtained from the transformation function that connects representations associated with parallel surfaces. The effect of infinitesimal translations of σ_1 and σ_2 is given by

$$\begin{aligned}\delta_x\Phi(\chi^{(-)'}\sigma_1) &= i\Phi(\chi^{(-)'}\sigma_1)P_\mu\delta x_{1\mu}, \\ \delta_x\Psi(\chi^{(+)'}\sigma_2) &= -iP_\mu\delta x_{2\mu}\Psi(\chi^{(+)'}\sigma_2).\end{aligned}$$

Accordingly, if x_1 and x_2 are the finite translations that produce σ_1 and σ_2 from a standard surface, we have

$$\begin{aligned}\Phi(\chi^{(-)'}\sigma_1) &= \Phi(\chi^{(-)'})\exp(iP_\mu x_{1\mu}), \\ \Psi(\chi^{(+)'}\sigma_2) &= \exp(-iP_\mu x_{2\mu})\Psi(\chi^{(+)'}),\end{aligned}$$

and

$$\begin{aligned}(\chi^{(-)'}\sigma_1|\chi^{(+)'}\sigma_2) &= (\chi^{(-)'}|\exp(iP_\mu X_\mu)|\chi^{(+)'}) \\ &= \sum_{\gamma'}(\chi^{(-)'}|\gamma')\exp(iP_\mu' X_\mu)(\gamma'|\chi^{(+)'}),\end{aligned}$$

where

$$X = x_1 - x_2,$$

and the γ are a complete set of constants of the motion.

Before employing the transformation function (48) in this manner, we shall extend it to serve also as a generating function for the eigenvalues and eigenfunctions of the charge operator Q. An infinitesimal phase transformation on σ,

$$\begin{aligned}\delta\psi(x) &= -ie\delta\alpha\psi(x), \\ \delta\bar{\psi}(x) &= ie\delta\alpha\bar{\psi}(x),\end{aligned} \tag{58}$$

induces the eigenvector transformations generated by

$$G_\sigma = Q\delta\alpha.$$

According to the orthogonality properties (14) and (15), the charge operator can be written

$$\begin{aligned}Q &= e\tfrac{1}{2}\int d\sigma([\bar{\psi}^{(-)}, \gamma_0\psi^{(+)}]+[\bar{\psi}^{(+)}, \gamma_0\psi^{(-)}]) \\ &= e\int d\sigma(\bar{\psi}^{(-)}\gamma_0\psi^{(+)}-\psi^{(-)}(\bar{\psi}^{(+)}\gamma_0)).\end{aligned} \tag{59}$$

In arriving at the latter form with the aid of the commutation relations (23) and (24), we have assigned the value zero to the quantity

$$\mathrm{Tr}(P^{(+)}-P^{(-)}) = \mathrm{Tr}(H/E), \tag{60}$$

where the trace is applied to spatial coordinates and spinor indices. This evaluation is based upon the time reflection invariance of the theory, which indicates that a one to one correspondence can be established between positive and negative frequency modes. Thus complete cancellation occurs in summing the eigenvalues of H/E, which are ± 1.

The infinitesimal eigenvector-transformation equations are

$$\delta_a\Phi(\chi^{(-)'}\sigma\alpha)=i\Phi(\chi^{(-)'}\sigma\alpha)e\delta\alpha \times\int d\sigma(\bar\psi^{(-)'}\gamma_0\psi^{(+)}+\bar\psi^{(+)}\gamma_0\psi^{(-)'})$$

and

$$\delta_a\Psi(\chi^{(+)'}\sigma\alpha)=-ie\delta\alpha \times\int d\sigma(\bar\psi^{(-)}\gamma_0\psi^{(+)'}+\bar\psi^{(+)'}\gamma_0\psi^{(-)})\Psi(\chi^{(+)'}\sigma\alpha).$$

A comparison with (17) and (18) shows that the eigenvector transformations are just those produced by the eigenvalue changes

$$\delta\psi^{(\pm)'}=-ie\delta\alpha\psi^{(\pm)'},$$
$$\delta\bar\psi^{(\pm)'}=ie\delta\alpha\bar\psi^{(\pm)'},$$

as we could anticipate from (58). Finite phase transformations

$$\Phi(\chi^{(-)'}\sigma\alpha)=\Phi(\chi^{(-)'}\sigma)\exp(iQ\alpha),$$
$$\Psi(\chi^{(+)'}\sigma\alpha)=\exp(-iQ\alpha)\Psi(\chi^{(+)'}\sigma),$$

are thus described by

$$\Phi(\psi^{(-)'}\bar\psi^{(-)'}\sigma\alpha)=\Phi(e^{-ie\alpha}\psi^{(-)'},e^{ie\alpha}\bar\psi^{(-)'},\sigma) \quad (61)$$

and

$$\Psi(\psi^{(+)'}\bar\psi^{(+)'}\sigma\alpha)=\Psi(e^{-ie\alpha}\psi^{(+)'},e^{ie\alpha}\bar\psi^{(+)'},\sigma). \quad (62)$$

If different phase transformations are performed on σ_1 and σ_2, we have

$$(\chi^{(-)'}\sigma_1\alpha_1|\chi^{(+)'}\sigma_2\alpha_2)=(\chi^{(-)'}\sigma_1|\exp(iQ\alpha)|\chi^{(+)'}\sigma_2), \quad (63)$$

where

$$\alpha=\alpha_1-\alpha_2.$$

Hence

$$(\chi^{(-)'}\sigma_1\alpha_1|\chi^{(+)'}\sigma_2\alpha_2)=(\chi^{(-)'}|\exp(iP_\mu X_\mu+iQ\alpha)|\chi^{(+)'})=\sum_{\gamma'}(\chi^{(-)'}|\gamma')\exp(iP_\mu'X_\mu+iQ'\alpha)(\gamma'|\chi^{(+)'}) \quad (64)$$

is the generating function of the simultaneous eigenfunctions and eigenvalues of the commuting operators P_μ and Q, and this transformation function is obtained from (48) by applying the substitutions indicated in (61) and (62).

It should be noted that (48) does not contain terms in which both integrals refer to a common surface. Consider, for example,

$$\int_{\sigma_1}d\sigma\int_{\sigma_1}d\sigma'\bar\psi^{(-)'}(x)\gamma_0G_+(x,x')\gamma_0\psi^{(-)'}(x') =\int_{\sigma_1}d\sigma\int_{\sigma_1}d\sigma'\bar\psi'\gamma_0P^{(+)}G_+\gamma_0P^{(-)}\psi'. \quad (65)$$

Now $G_+\gamma_0$ becomes $iP^{(+)}$ or $-iP^{(-)}$ as $x_0-x_0'\to\pm0$. Either limit results in a null value for (65) ($P^{(+)}P^{(-)}=0$). Hence,

$$(\chi^{(-)'}\sigma_1\alpha_1|\chi^{(+)'}\sigma_2\alpha_2) =\exp\Big[-i\int_{\sigma_1}d\sigma_\mu\int_{\sigma_2}d\sigma_\nu'\bar\psi^{(-)'}(x)\gamma_\mu e^{ie\alpha} \times G_+(x,x')\gamma_\nu\psi^{(+)'}(x')-i\int_{\sigma_2}d\sigma_\mu \times\int_{\sigma_1}d\sigma_\nu'\bar\psi^{(+)'}(x)\gamma_\mu G_+(x,x')e^{-ie\alpha}\gamma_\nu\psi^{(-)'}(x')\Big] \quad (66)$$

and we need not have indicated the positive or negative frequency parts of the field eigenvalues since these are automatically selected by the structure of the Green's function.

We insert the expressions (55) for the Green's function and introduce the following linear combinations of eigenvalues, which are not explicit functions of the surface,

$$\chi_{\lambda p}^{(-)'}=\int_{\sigma_1}d\sigma_\mu\bar\psi^{(-)'}(x)\gamma_\mu\psi_{\lambda p}(x)e^{-ipx_1}$$

$\lambda>0$:

$$\chi_{\lambda p}^{(+)'}=\int_{\sigma_2}d\sigma_\mu\bar\psi_{\lambda p}(x)e^{ipx_2}\gamma_\mu\psi^{(+)'}(x),$$

$$\chi_{\lambda p}^{(-)'}=\int_{\sigma_1}d\sigma_\mu\bar\psi_{\lambda p}(x)e^{-ipx_1}\gamma_\mu\psi^{(-)'}(x)$$

$\lambda<0$:

$$\chi_{\lambda p}^{(+)'}=\int_{\sigma_2}d\sigma_\mu\bar\psi^{(+)'}(x)\gamma_\mu\psi_{\lambda p}(x)e^{ipx_2}.$$

With these definitions, the transformation function (64) becomes[2]

$$(\chi^{(-)'}\sigma_1\alpha_1|\chi^{(+)'}\sigma_2\alpha_2) =\exp[\sum_{\lambda p}\chi_{\lambda p}^{(-)'}\exp(ipX+ie\epsilon(\lambda)\alpha)\chi_{\lambda p}^{(+)'}] =\prod_{\lambda p}\exp[\chi_{\lambda p}^{(-)'}\exp(ipX+ie\epsilon(\lambda)\alpha)\chi_{\lambda p}^{(+)'}] =\prod_{\lambda p}\sum_{n_{\lambda p}}\frac{1}{n!}(\chi_{\lambda p}^{(-)'}\chi_{\lambda p}^{(+)'})^n \times\exp[in(pX+e\epsilon(\lambda)\alpha)]. \quad (67)$$

In view of the anticommutative nature of the eigenvalues, the square of any $\chi_{\lambda p}^{(\pm)'}$ is zero, whence the expansion of the exponential terminates after the first two terms, $n_{\lambda p}=0,1$. It will be observed that the distinction between B.E. and F.D. systems is embodied primarily in the nature of the eigenvalues rather than in the formula containing those eigenvalues.

[2] A basic statement in all manipulations with eigenvalues is that the product of two eigenvalues, as a unit, behaves like an ordinary number.

On comparison with (64) we see that

$$P_\mu' = P_\mu(n) = \sum_{\lambda p} n_{\lambda p} p_\mu, \quad n_{\lambda p} = 0, 1,$$

where

$$P_0' = \sum_{\lambda p} n_{\lambda p} p_0 \geq 0,$$

and that

$$Q' = \sum_{\lambda p} n_{\lambda p} e\epsilon(\lambda).$$

The occupation numbers $n_{\lambda p}$ thus form the complete set of constants of the motion. The associated eigenfunctions are

$$(n|\chi^{(+)'}) = \prod_{\lambda p} (\chi_{\lambda p}{}^{(+)'})^{n_{\lambda p}} = (\chi_1{}^{(+)'})^{n_1} (\chi_2{}^{(+)'})^{n_2} \cdots,$$

and

$$(\chi^{(-)'}|n) = {}'\prod_{\lambda p} (\chi_{\lambda p}{}^{(-)'})^{n_{\lambda p}} = \cdots (\chi_2{}^{(-)'})^{n_2} (\chi_1{}^{(-)'})^{n_1},$$

in which we have introduced an arbitrary standard order of the field modes. That order, when read from left to right, is symbolized by $\prod$, and in the reverse sense by ${}'\prod$. Thus, if only modes 1 and 2 are occupied, we have in (67)

$$\chi_1{}^{(-)'}\chi_1{}^{(+)'}\chi_2{}^{(-)'}\chi_2{}^{(+)'} = (\chi_2{}^{(-)'}\chi_1{}^{(-)'})(\chi_1{}^{(+)'}\chi_2{}^{(+)'}) = {}'\prod_{\lambda p} (\chi_{\lambda p}{}^{(-)'})^{n_{\lambda p}} \prod_{\lambda p} (\chi_{\lambda p}{}^{(+)'})^{n_{\lambda p}}.$$

With the eigenvalues $\chi^{(\pm)'}(x)$ at corresponding points in the relation (26), we have

$$\chi_{\lambda p}{}^{(-)'} = \chi_{\lambda p}{}^{(+)'\dagger},$$

and therefore

$$(\chi^{(-)'}|n) = (n|\chi^{(+)'})^\dagger,$$

as demanded by the eigenvector connection (25).

The eigenfunction of the vacuum state, referring to an arbitrary surface, is

$$(\chi^{(-)'}\sigma|0) = 1,$$

and therefore

$$(\chi^{(-)'}\sigma|n\sigma) = (\chi^{(-)'}\sigma|0)\,{}'\prod_{\lambda p} (\chi_{\lambda p}{}^{(-)'})^{n_{\lambda p}} = (\chi^{(-)'}\sigma|\,{}'\prod_{\lambda p} (\chi_{\lambda p}{}^{(-)})^{n_{\lambda p}}|0),$$

in which we have introduced the operators on σ possessing the $\chi_{\lambda p}{}^{(-)'}$ as eigenvalues. Accordingly, the eigenvectors of the state with particle occupation numbers $n_{\lambda p}$ are

$$\Psi(n\sigma) = [\,{}'\prod_{\lambda p} (\chi_{\lambda p}{}^{(-)})^{n_{\lambda p}}]\Psi_0,$$

and

$$\Psi(n\sigma)^\dagger = \Psi_0{}^\dagger[\prod_{\lambda p} (\chi_{\lambda p}{}^{(+)})^{n_{\lambda p}}].$$

THE MATRICES OF FIELD OPERATORS

We shall now use the transformation function (46) to obtain the matrix elements, for the isolated Dirac field, of all products of the field operators $\psi(x)$ and $\bar\psi(x)$. For this purpose, we remark that the transformation function describing the system, with sources present, is the matrix of a certain time-ordered operator for the isolated system. Indeed,

$$(\chi^{(-)'}\sigma_1|\chi^{(+)'}\sigma_2) = \left(\chi^{(-)'}\sigma_1\middle|\left(\exp\left[i\int (dx)(\bar\eta(x)\psi(x) + \bar\psi(x)\eta(x))\right]\right)_+\middle|\chi^{(+)'}\sigma_2\right)\Big]_0, \quad (68)$$

where $]_0$ indicates that the operators and states correspond to $\eta = \bar\eta = 0$. To prove this, let us replace η and $\bar\eta$ with $\lambda\eta$ and $\lambda\bar\eta$, where λ is a numerical parameter. The effect of an infinitesimal change of the latter is expressed by

$$(\partial/\partial\lambda)(\chi^{(-)'}\sigma_1|\chi^{(+)'}\sigma_2) = \left(\chi^{(-)'}\sigma_1\middle|\int (dx) l(x)\middle|\chi^{(+)'}\sigma_2\right),$$

in which we have temporarily written

$$l(x) = i(\bar\eta(x)\psi(x) + \bar\psi(x)\eta(x)).$$

On differentiating again, we find[3]

$$(\partial^2/\partial\lambda^2)(\chi^{(-)'}\sigma_1|\chi^{(+)'}\sigma_2) = \left(\chi^{(-)'}\sigma_1\middle|\int (dx_1)(dx_2)(l(x_1)l(x_2))_+\middle|\chi^{(+)'}\sigma_2\right),$$

and, in general,

$$(\partial/\partial\lambda)^n(\chi^{(-)'}\sigma_1|\chi^{(+)'}\sigma_2) = \left(\chi^{(-)'}\sigma_1\middle|\int (dx_1)\cdots(dx_n)(l(x_1)\cdots l(x_n))_+\middle|\chi^{(+)'}\sigma_2\right).$$

If we now construct the transformation function describing the system in the presence of sources ($\lambda = 1$) in terms of that for zero sources ($\lambda = 0$), as a Taylor series expansion, we obtain an infinite series which is compactly represented by (68).

The transformation function (46) can be expressed as

$$(\chi^{(-)'}\sigma_1|\chi^{(+)'}\sigma_2) = (\chi^{(-)'}\sigma_1|\chi^{(+)'}\sigma_2)\Big]_0 \times \exp\left[i\int (dx)(dx')\bar\eta(x)G_+(x,x')\eta(x') + i\int (dx)(\bar\eta(x)\psi'(x) + \bar\psi'(x)\eta(x))\right], \quad (69)$$

in which we have used the symbols $\psi'(x)$, $\bar\psi'(x)$, at points in the interior of the region bounded by σ_1 and σ_2,

[3] J. Schwinger, Phys. Rev. **82**, 914 (1951), Eq. (2.133).

to mean

$$\psi'(x)=i\oint d\sigma_\mu' G_+(x,x')\gamma_\mu\psi'(x')$$

$$=i\int_{\sigma_1} d\sigma_\mu' G_+(x,x')\gamma_\mu\psi^{(-)'}(x')$$

$$-i\int_{\sigma_2} d\sigma_\mu' G_+(x,x')\gamma_\mu\psi^{(+)'}(x'),$$

and

$$\bar\psi'(x)=-i\oint d\sigma_\mu'\bar\psi'(x')\gamma_\mu G_+(x',x)$$

$$=-i\int_{\sigma_1} d\sigma_\mu'\bar\psi^{(-)'}(x')\gamma_\mu G_+(x',x)$$

$$+i\int_{\sigma_2} d\sigma_\mu'\bar\psi^{(+)'}(x')\gamma_\mu G_+(x',x).$$

We see that

$$\psi'(x)=\sum_{+,p}\psi_{\lambda p}(x)e^{-ipx_2}\chi_{\lambda p}{}^{(+)'}+\sum_{-,p}\psi_{\lambda p}(x)e^{ipx_1}\chi_{\lambda p}{}^{(-)'}$$

is the solution of the Dirac equation with the prescribed positive frequency part $\psi^{(+)'}(x)$, on σ_2, and the prescribed negative frequency part $\psi^{(-)'}(x)$, on σ_1. Similarly,

$$\bar\psi'(x)=\sum_{-,p}\bar\psi_{\lambda p}(x)e^{-ipx_2}\chi_{\lambda p}{}^{(+)'}+\sum_{+,p}\bar\psi_{\lambda p}(x)e^{ipx_1}\chi_{\lambda p}{}^{(-)'}$$

is the solution of the adjoint Dirac equation which has the positive and negative frequency parts, $\bar\psi^{(+)'}(x)$ and $\bar\psi^{(-)'}(x)$, on σ_2 and σ_1, respectively. Note, however, that $\bar\psi'(x)$ is not the adjoint of $\psi'(x)$. Indeed,

$$\psi'(x)^\dagger\gamma_0=-i\oint d\sigma_\mu'\bar\psi'(x')\gamma_\mu G_-(x',x),$$

where

$$G_-(x,x')=\gamma_0 G_+(x',x)^\dagger\gamma_0 \tag{70}$$

satisfies the same differential equations as $G_+(x,x')$, but obeys ingoing rather than outgoing wave temporal boundary conditions,

$$G_-(x,x')=i\sum_{-,p}\psi_{\lambda p}(x)\bar\psi_{\lambda p}(x'),\qquad x_0>x_0'$$

$$=-i\sum_{+,p}\psi_{\lambda p}(x)\bar\psi_{\lambda p}(x'),\quad x_0<x_0'. \tag{71}$$

In terms of the notation [not to be confused with (35)]

$$(\chi^{(-)'}\sigma_1|F|\chi^{(+)'}\sigma_2)/(\chi^{(-)'}\sigma_1|\chi^{(+)'}\sigma_2)]_0=\langle F\rangle, \tag{72}$$

we express (68) and (69) as

$$\left\langle\left(\exp\left[i\int(dx)(\bar\eta\psi+\bar\psi\eta)\right]\right)_+\right\rangle$$

$$=\exp\left[i\int(dx)(dx')\bar\eta G_+\eta+i\int(dx)(\bar\eta\psi'+\bar\psi'\eta)\right], \tag{73}$$

or, more simply,

$$\left\langle\left(\exp\left[i\int(dx)(\bar\eta'\psi+'\bar\psi\eta)\right]\right)_+\right\rangle$$

$$=\exp\left[i\int(dx)(dx')\bar\eta(x)G_+(x,x')\eta(x')\right], \tag{74}$$

in which we have introduced the operators

$$'\psi(x)=\psi(x)-\psi'(x),$$

$$'\bar\psi(x)=\bar\psi(x)-\bar\psi'(x).$$

An expansion of both sides in powers of η and $\bar\eta$ will yield the matrix elements of ordered operator products of the ψ and $\bar\psi$.

From the absence of terms that are linear in η and $\bar\eta$, on the right of (74), we see that

$$\langle'\psi(x)\rangle=\langle'\bar\psi(x)\rangle=0,$$

or that

$$\langle\psi(x)\rangle=\psi'(x), \tag{75}$$

$$\langle\bar\psi(x)\rangle=\bar\psi'(x). \tag{76}$$

The term on the left of (74) that in bilinear in η and $\bar\eta$ is

$$-\left\langle\int(dx)(dx')(\bar\eta(x)'\psi(x)'\bar\psi(x')\eta(x'))_+\right\rangle$$

$$=-\int(dx)(dx')\bar\eta(x)\langle('\psi(x)'\bar\psi(x'))_+\rangle\epsilon(x,x')\eta(x'),$$

where

$$\epsilon(x,x')=\begin{cases}+1, & x_0>x_0'\\ -1, & x_0<x_0'.\end{cases}$$

Hence

$$\langle('\psi(x)'\bar\psi(x'))_+\rangle\epsilon(x,x')=-iG_+(x,x'),$$

or

$$\langle(\psi(x)\bar\psi(x'))_+\rangle\epsilon(x,x')=\psi'(x)\bar\psi'(x')-iG_+(x,x'). \tag{77}$$

The complete expansion of the left side in (74) is

$$\sum_{k,l}\frac{i^{k+l}}{k!l!}\int(dx_1)\cdots(dx_k)(dx_1')\cdots(dx_l')\bar\eta(x_k)\cdots$$

$$\times\bar\eta(x_1)\langle('\psi(x_1)\cdots'\psi(x_k)'\bar\psi(x_l')\cdots'\bar\psi(x_1'))_+\rangle\epsilon_{k,l}$$

$$\times\eta(x_1')\cdots\eta(x_l'), \tag{78}$$

where $\epsilon_{k,l}$ is the alternating symbol expressed by

$$\epsilon_{k,l}=(\prod_{i<j}\epsilon(x_i,x_j))(\prod_{i,j}\epsilon(x_i,x_j'))(\prod_{i>j}\epsilon(x_i',x_j')). \tag{79}$$

This is to be compared with

$$\sum_k\frac{i^k}{k!}\int(dx_1)\cdots(dx_k)(dx_1')\cdots(dx_k')\bar\eta(x_k)\cdots$$

$$\times\bar\eta(x_1)G_+(x_1,x_1')\cdots G_+(x_k,x_k')\eta(x_1')\cdots\eta(x_k')$$

$$=\sum_k\frac{i^k}{(k!)^2}\int(dx_1)\cdots(dx_k')\bar\eta(x_k)\cdots\bar\eta(x_1)$$

$$\times[\det{}_{(k)}G_+(x_i,x_j')]\eta(x_1')\cdots\eta(x_k'),$$

where the k-dimensional determinant constructed from the elements $G_+(x_i, x_j')$ has been introduced by subjecting the variables $x_1'\cdots x_k'$ to the set of $k!$ permutations. The anticommutativity of the η provides the algebraic signs to form the alternating combination of terms which constitutes the determinant. Therefore

$$\langle('\psi(x_1)\cdots'\psi(x_k)'\bar\psi(x_l')\cdots'\bar\psi(x_1'))_+\rangle\epsilon_{k,l} = \delta_{k,l}(-i)^k \det{}_{(k)}G_+(x_i, x_j'), \quad (80)$$

in which both sides are completely antisymmetrical in the variables x_i, and in the variables x_j'.

Straightforward algebraic rearrangement would yield the matrix elements for successive products of the operators ψ and $\bar\psi$, as illustrated by (75) and (77). However, one can obtain an explicit formula from (73). We first consider operator products with $k=l$, and remark that such terms are isolated in (73) by substituting $\bar\eta\to t\bar\eta$, $\eta\to t^{-1}\eta$, and evaluating the integral

$$\frac{1}{2\pi i}\oint\frac{dt}{t}\left\langle\left(\exp\left[i\int(dx)(t\bar\eta\psi+t^{-1}\bar\psi\eta)\right]\right)_+\right\rangle = \frac{1}{2\pi i}\oint\frac{dt}{t}\exp\left[i\int(dx)(dx')\bar\eta G_+\eta + i\int(dx)(t\bar\eta\psi'+t^{-1}\bar\psi'\eta)\right]. \quad (81)$$

The further substitution performed on the right, $it\int(dx)\bar\eta\psi'\to t$, yields

$$\frac{1}{2\pi i}\oint\frac{dt}{t}e^t\exp\left[i\int(dx)(dx')\bar\eta(x)(G_+(x,x') + it^{-1}\psi'(x)\bar\psi'(x'))\eta(x')\right].$$

The known result of expanding the right side of (74), as expressed in (80), now shows that

$$\langle(\psi(x_1)\cdots\psi(x_k)\bar\psi(x_k')\cdots\bar\psi(x_1'))_+\rangle\epsilon_{k,k} = \frac{1}{2\pi i}\oint\frac{dt}{t}e^t\det{}_{(k)}[-iG_+(x_i,x_j')+t^{-1}\psi(x_i)\bar\psi(x_j')] = \psi'(x_1)\cdots\psi'(x_k)\bar\psi'(x_k')\cdots\bar\psi'(x_1')+\cdots + (-i)^k\det{}_{(k)}G_+(x_i,x_j'),$$

in which the various terms will be given by the development of the determinant, combined with the theorem

$$\frac{1}{2\pi i}\oint\frac{dt}{t^{n+1}}e^t=\frac{1}{n!}.$$

The effect of the t integration is to compensate the numerical factors that appear on expanding the determinant. An example is

$$\langle(\psi(x_1)\psi(x_2)\bar\psi(x_2')\bar\psi(x_1'))_+\rangle\epsilon_{2,2} = \frac{1}{2\pi i}\oint\frac{dt}{t}e^t\begin{vmatrix}-iG_+(x_1,x_1')+t^{-1}\psi'(x_1)\bar\psi'(x_1'), & -iG_+(x_1,x_2')+t^{-1}\psi'(x_1)\bar\psi'(x_2')\\ -iG_+(x_2,x_1')+t^{-1}\psi'(x_2)\bar\psi'(x_1'), & -iG_+(x_2,x_2')+t^{-1}\psi'(x_2)\bar\psi'(x_2')\end{vmatrix}$$
$$= \psi'(x_1)\psi'(x_2)\bar\psi'(x_2')\bar\psi'(x_1') - i\psi'(x_1)\bar\psi'(x_1')G_+(x_2,x_2') - i\psi'(x_2)\bar\psi'(x_2')G_+(x_1,x_1') + i\psi'(x_1)\bar\psi'(x_2')G_+(x_2,x_1') + i\psi'(x_2)\bar\psi'(x_1')G_+(x_1,x_2') - G_+(x_1,x_1')G_+(x_2,x_2') + G_+(x_1,x_2')G_+(x_2,x_1').$$

Operator products with $k-l>0$ are isolated by the integral

$$\frac{1}{2\pi i}\oint\frac{dt}{t^{k-l+1}}\left\langle\left(\exp\left[i\int(dx)(t\bar\eta\psi+t^{-1}\bar\psi\eta)\right]\right)_+\right\rangle = \frac{1}{2\pi i}\oint\frac{dt}{t}e^t\left(it^{-1}\int(dx)\bar\eta\psi'\right)^{k-l}\times\exp\left[i\int(dx)(dx')\bar\eta(G_+ + it^{-1}\psi'\bar\psi')\eta\right].$$

On expanding the right side, it is seen that

$$\langle(\psi(x_1)\cdots\psi(x_k)\bar\psi(x_l')\cdots\bar\psi(x_1'))_+\rangle\epsilon_{k,l} = \frac{1}{2\pi i}\oint\frac{dt}{t}e^t\det{}_{(k)}[t^{-1}\psi'(x_i)^{(k-l)}, -iG_+(x_i,x_j')+t^{-1}\psi'(x_i)\bar\psi'(x_j')],$$

in which the determinant is constructed with $t^{-1}\psi'(x_i)$, $i=1\cdots k$, occupying the first $k-l$ columns, and the rectangular matrix $-iG_+(x_i, x_j')+t^{-1}\psi'(x_i)\bar\psi'(x_j')$, $i=1\cdots k$, $j=1\cdots l$, completing the k-dimensional square array. It is understood that the determinant is defined by alternating permutations of the *row* indices, applied to the product of the diagonal elements written suc-

cessively from left to right. This is illustrated by

$$\langle(\psi(x_1)\psi(x_2)\psi(x_3)\bar\psi(x_1'))_+\rangle\epsilon_{3,1}=\frac{1}{2\pi i}\oint\frac{dt}{t}e^t\begin{vmatrix} t^{-1}\psi'(x_1), & t^{-1}\psi'(x_1), & -iG_+(x_1,x_1')+t^{-1}\psi'(x_1)\bar\psi'(x_1')\\ t^{-1}\psi'(x_2), & t^{-1}\psi'(x_2), & -iG_+(x_2,x_1')+t^{-1}\psi'(x_2)\bar\psi'(x_1')\\ t^{-1}\psi'(x_3), & t^{-1}\psi'(x_3), & -iG_+(x_3,x_1')+t^{-1}\psi'(x_3)\bar\psi'(x_1')\end{vmatrix}$$

$$=\psi'(x_1)\psi'(x_2)\psi'(x_3)\bar\psi'(x_1')-i\psi'(x_1)\psi'(x_2)G_+(x_3,x_1')$$
$$-i\psi'(x_2)\psi'(x_3)G_+(x_1,x_1')-i\psi'(x_3)\psi'(x_1)G_+(x_2,x_1').$$

A similar treatment for $l-k>0$ yields

$$\langle(\psi(x_1)\cdots\psi(x_k)\bar\psi(x_l')\cdots\bar\psi(x_1'))_+\rangle\epsilon_{k,l}$$
$$=\frac{1}{2\pi i}\oint\frac{dt}{t}e^t\det{}_{(l)}[-iG_+(x_i,x_j')$$
$$+t^{-1}\psi'(x_i)\bar\psi'(x_j'),\ t^{-1}\bar\psi'(x_j')^{(l-k)}],$$

where this determinant contains $t^{-1}\bar\psi'(x_j')$, $j=1\cdots l$ in the first $l-k$ rows, and the l-dimensional array is filled out with the rectangular matrix, $-iG_+(x_i,x_j')+t^{-1}\psi'(x_i)\bar\psi'(x_j')$, $i=1\cdots k$, $j=1\cdots l$. Here the determinant is defined by alternating permutations of the *column* indices applied to the product of the diagonal elements, written successively from right to left. Thus, for the example $k=0$, we have

$$\langle(\bar\psi(x_l')\cdots\bar\psi(x_1'))_+\rangle\epsilon_{0l}=\langle\bar\psi(x_l')\cdots\bar\psi(x_1')\rangle$$
$$=\bar\psi'(x_l')\cdots\bar\psi'(x_1').$$

The Occupation Number Representation

Matrices in the occupation number description can be derived from these results. The simplest examples are the diagonal matrix elements referring to the vacuum state—the vacuum expectation values. Indeed, on placing all eigenvalues equal to zero in (80), we obtain

$$(0|\,(\psi(x_1)\cdots\psi(x_k)\bar\psi(x_l')\cdots\bar\psi(x_1'))_+|\,0)\epsilon_{k,l}$$
$$=\delta_{k,l}(-i)^k\det{}_{(k)}G_+(x_i,x_j'),\quad(82)$$

and, in particular,

$$(0|\,(\psi(x)\bar\psi(x'))_+|\,0)\epsilon(x,x')=-iG_+(x,x').\quad(83)$$

To obtain the occupation number matrices of $\psi(x)$ and $\bar\psi(x)$, we observe that (75), for example, can be written

$$(\chi^{(-)'}\sigma_1|\psi(x)|\chi^{(+)'}\sigma_2)=\psi'(x)(\chi^{(-)'}\sigma_1|\chi^{(+)'}\sigma_2),$$

or

$$\sum_{n,n'}(\chi^{(-)'}|n)(n\sigma_1|\psi(x)|n'\sigma_2)(n'|\chi^{(+)'})$$
$$=[\sum_{+,p}\psi_{\lambda p}(x)e^{-ipx_2}\chi_{\lambda p}{}^{(+)'}+\sum_{-,p}\psi_{\lambda p}(x)e^{ipx_1}\chi_{\lambda p}{}^{(-)'}]$$
$$\times\sum_n(\chi^{(-)'}|n)\exp[iP(n)(x_1-x_2)](n|\chi^{(+)'}),\quad(84)$$

which exhibits it as a generating function for $(n\sigma_1|\psi(x)|n'\sigma_2)$. We shall prefer to construct

$$(n|\psi(x)|n')=\exp(-iP(n)x_1)$$
$$\times(n\sigma_1|\psi(x)|n'\sigma_2)\exp(iP(n')x_2),$$

which is independent of σ_1 and σ_2, and refers to the standard surface. On incorporating e^{-ipx_2} into $\chi_{\lambda p}{}^{(+)'}$ and e^{ipx_1} into $\chi_{\lambda p}{}^{(-)'}$, (84) becomes

$$\sum_{n,n'}(\chi^{(-)'}|n)(n|\psi(x)|n')(n'|\chi^{(+)'})$$
$$=[\sum_{+,p}\psi_{\lambda p}(x)\chi_{\lambda p}{}^{(+)'}+\sum_{-,p}\psi_{\lambda p}\chi_{\lambda p}{}^{(-)'}]$$
$$\times\sum_n(\chi^{(-)'}|n)(n|\chi^{(+)'}).$$

Now

$$\chi_{\lambda p}{}^{(-)'}(\chi_{\lambda p}{}^{(-)'}|n)=\chi_{\lambda p}{}^{(-)'}\prod(\chi^{(-)'})^n$$
$$=0,\quad n_{\lambda p}=1$$
$$=(-1)^{n_{>\lambda p}}(\chi^{(-)'}|n+1_{\lambda p}),\quad n_{\lambda p}=0,$$

where $n_{>\lambda p}$ is the number of occupied states that follow λp in the standard order. Similarly,

$$(n|\chi^{(+)'})\chi_{\lambda p}{}^{(+)'}=\prod(\chi^{(+)'})^n\chi_{\lambda p}{}^{(+)'}$$
$$=0,\quad n_{\lambda p}=1$$
$$=(-1)^{n_{>\lambda p}}(n+1_{\lambda p}|\chi^{(+)'}),\quad n_{\lambda p}=0.$$

We see that the nonvanishing matrix elements of $\psi(x)$ are of the form

$$(n|\psi(x)|n+1_{\lambda p})=(-1)^{n_{>\lambda p}}\psi_{\lambda p}(x),\quad\lambda>0,\quad(85)$$
$$(n+1_{\lambda p}|\psi(x)|n)=(-1)^{n_{>\lambda p}}\psi_{\lambda p}(x),\quad\lambda<0,\quad(86)$$

where $n_{\lambda p}=0$ in both statements. These exhibit $\psi(x)$ as a unit charge annihilator.

In an analogous way,

$$(\chi^{(-)'}\sigma_1|\bar\psi(x)|\chi^{(+)'}\sigma_2)=\bar\psi'(x)(\chi^{(-)'}\sigma_1|\chi^{(+)'}\sigma_2)$$

yields

$$\sum_{n,n'}(\chi^{(-)'}|n)(n|\bar\psi(x)|n')(n'|\chi^{(+)'})$$
$$=[\sum_{-,p}\bar\psi_{\lambda p}(x)\chi_{\lambda p}{}^{(+)'}+\sum_{+,p}\bar\psi_{\lambda p}(x)\chi_{\lambda p}{}^{(-)'}]$$
$$\times\sum_n(\chi^{(-)'}|n)(n|\chi^{(+)'}),$$

from which we obtain the nonvanishing matrix elements

$$(n+1_{\lambda p}|\bar{\psi}(x)|n)=(-1)^{n>\lambda p}\bar{\psi}_{\lambda p}(x), \quad \lambda>0,$$
$$(n|\bar{\psi}(x)|n+1_{\lambda p})=(-1)^{n>\lambda p}\bar{\psi}_{\lambda p}(x), \quad \lambda<0,$$

with $n_{\lambda p}=0$, which display $\bar{\psi}(x)$ as a unit charge creator.

The matrices of ψ and $\bar{\psi}$ suggest the utility of a classification of matrix elements that would unify a given change in occupation number for positive frequency modes with that in the reverse sense for negative frequency modes. This is accomplished by transposing the matrices with respect to the occupation numbers of modes with $\lambda<0$, which effectively introduces a time-reversed description for the negative frequency modes.

The generating function for the matrices of all ordered products is (73), written as

$$\sum_{n,n'}(\chi^{(-)'}|n)\left(n\left|\left(\exp\left[i\int(dx)(\bar{\eta}\psi+\bar{\psi}\eta)\right]\right)_+\right|n'\right)$$
$$\times(n'|\chi^{(+)'})=(\chi^{(-)'}|\chi^{(+)'})$$
$$\times\exp\left[i\int(dx)(dx')\bar{\eta}G_+\eta+i\int(dx)(\bar{\eta}\psi'+\bar{\psi}'\eta)\right], \quad (87)$$

in which all states refer to the standard surface. The sources $\bar{\eta}$ and η are understood to be placed on the extreme left and right, respectively, as we have done in (78). We now indicate the positive and negative frequency modes separately, placing the negative frequency modes first in the standard order,

$$(\chi^{(-)'}|n)=(\chi_+{}^{(-)'}|n_+)(\chi_-{}^{(-)'}|n_-),$$
$$(n'|\chi^{(+)'})=(n_-'|\chi_-{}^{(+)'})(n_+'|\chi_+{}^{(+)'}),$$

and define the mixed eigenfunctions

$$\begin{aligned}[\bar{\psi}'|N]&=(\chi_+{}^{(-)'}|n_+)(n_-'|\chi_-{}^{(+)'})(-1)^{\frac{1}{2}n_-'(n_-'-1)},\\ [N'|\psi']&=(-1)^{\frac{1}{2}n_-(n_--1)}(\chi_-{}^{(-)'}|n_-)(n_+'|\chi_+{}^{(+)'}).\end{aligned} \quad (88)$$

Here the integers n_- and n_-' indicate the respective number of occupied negative frequency modes, while N and N' symbolize the sets of occupation numbers $\{n_+, n_-'\}$ and $\{n_+', n_-\}$, respectively. We shall also write $N_-=n_-'$, $N_-'=n_-$. The notation $[\bar{\psi}'|N]$ refers to the fact that the $\chi_+{}^{(-)'}$ and $\chi_-{}^{(+)'}$ together comprise the quantities

$$\bar{\psi}_{\lambda p}'=\int d\sigma_\mu\bar{\psi}'(x)\gamma_\mu\psi_{\lambda p}(x) \quad (89)$$

for positive and negative λ. Thus

$$[\bar{\psi}'|N]=\prod_{\lambda p}{}'(\bar{\psi}_{\lambda p}')^{N_{\lambda p}}, \quad (90)$$

and this product is in standard order, from right to left, in virtue of the factor $(-1)^{\frac{1}{2}n-'(n-'-1)}$, which effectively reverses the sense of multiplication for the n_-' anticommuting eigenvalues in $(n_-'|\chi_-{}^{(+)'})$. Similarly, $\chi_+{}^{(+)'}$ and $\chi_-{}^{(-)'}$ are comprised in

$$\psi_{\lambda p}'=\int d\sigma_\mu\bar{\psi}_{\lambda p}(x)\gamma_\mu\psi(x)', \quad (91)$$

and

$$[N'|\psi']=\prod_{\lambda p}(\psi_{\lambda p}')^{N_{\lambda p}'}. \quad (92)$$

To carry out the transposition, we must take

$$\sum_{n,n'}(\chi_+{}^{(-)'}|n_+)(\chi_-{}^{(-)'}|n_-)(n_+n_-|F|n_+'n_-')$$
$$\times(n_-'|\chi_-{}^{(+)'})(n_+'|\chi_+{}^{(+)'}), \quad (93)$$

where F is any product of the operators ψ, $\bar{\psi}$, and reverse the positions of the two negative frequency eigenfunctions. This introduces the factor $(-1)^{n_-n_-'}$, so that (93) becomes

$$\sum_{N,N'}(\pm)[\bar{\psi}'|N][N|F|N'][N'|\psi'], \quad (94)$$

in which we have written

$$[N|F|N']=(n|F|n'),$$

and

$$\begin{aligned}(\pm)&=(-1)^{N_-}(-1)^{\frac{1}{2}(N_--N_-')(N_-+1-N_-')}\\ &=(-1)^{N_-'}(-1)^{\frac{1}{2}(N_--N_-')(N_-'+1-N_-)}.\end{aligned} \quad (95)$$

Thus, if F is the unit operator, we have

$$(\chi^{(-)'}|\chi^{(+)'})=\sum_N[\bar{\psi}'|N](-1)^{N_-}[N|\psi']$$
$$=\exp[\sum_{\lambda p}\bar{\psi}_{\lambda p}'\epsilon(\lambda)\psi_{\lambda p}']. \quad (96)$$

To complete the re-expression of the generating function (87), we remark that

$$\psi'(x)=\sum_{\lambda p}\psi_{\lambda p}(x)\psi_{\lambda p}', \quad (97)$$

and

$$\bar{\psi}'(x)=\sum_{\lambda p}\bar{\psi}_{\lambda p}(x)\bar{\psi}_{\lambda p}'. \quad (98)$$

Hence,

$$\sum_{N,N'}(\pm)[\bar{\psi}'|N]$$
$$\times\left[N\left|\left(\exp\left[i\int(dx)(\bar{\eta}\psi+\bar{\psi}\eta)\right]\right)_+\right|N'\right][N'|\psi']$$
$$=\exp\left[i\int(dx)(dx')\bar{\eta}G_+\eta\right]$$
$$\times\exp[\sum_{\lambda p}\bar{\psi}_{\lambda p}'\epsilon(\lambda)\psi_{\lambda p}'+i\bar{\eta}_{\lambda p}\psi_{\lambda p}'+i\bar{\psi}_{\lambda p}'\eta_{\lambda p}], \quad (99)$$

in which we have employed the notation,

$$\bar{\eta}_{\lambda p}=\int(dx)\bar{\eta}(x)\psi_{\lambda p}(x), \quad \eta_{\lambda p}=\int(dx)\bar{\psi}_{\lambda p}(x)\eta(x).$$

It should be emphasized again that the sources $\bar{\eta}$ and η are written to the left and to the right, respectively, rather than as indicated in the left-hand member of Eq. (99), since the sign factor expressed by (95) is valid only if the matrix element in (93) is a number, rather than a quantity possessing anticommutative properties.

The second exponential factor in (99) can be written

$$\prod_{\lambda p}\exp[\bar{\psi}_{\lambda p}'\epsilon(\lambda)\psi_{\lambda p}'+i\bar{\eta}_{\lambda p}\psi_{\lambda p}'+i\bar{\psi}_{\lambda p}'\eta_{\lambda p}]$$
$$=\prod_{\lambda p}\sum_{N,N'}(\bar{\psi}_{\lambda p}')^{N}[\delta_{N,N'}\epsilon^{N}(1+N\epsilon\bar{\eta}\eta)$$
$$+i\bar{\eta}N'(1-N)+i\eta N(1-N')](\psi_{\lambda p}')^{N'}, \quad (100)$$

where the expansion of the exponential referring to a given mode yields only five nonvanishing terms, as represented on the right of (100). We shall first extract the diagonal matrix elements, which constitute the following terms of (100),

$$\prod_{\lambda p}\sum_{N_{\lambda p}}(\bar{\psi}_{\lambda p}')^{N_{\lambda p}}[\epsilon(\lambda)]^{N_{\lambda p}}[1+N_{\lambda p}\epsilon(\lambda)\bar{\eta}_{\lambda p}\eta_{\lambda p}](\psi_{\lambda p}')^{N_{\lambda p}}$$
$$=\sum_{N}\exp[\sum_{\lambda p}N_{\lambda p}\epsilon(\lambda)\bar{\eta}_{\lambda p}\eta_{\lambda p}]$$
$$\times[\bar{\psi}'|N](-1)^{N}[N|\psi'], \quad (101)$$

The exponential so obtained combines with the first factor on the right of (99) to form

$$\exp\Big[i\int(dx)(dx')\bar{\eta}(x)\big(G_{+}(x,x')$$
$$-i\sum_{\lambda p}N_{\lambda p}\epsilon(\lambda)\psi_{\lambda p}(x)\bar{\psi}_{\lambda p}(x')\big)\eta(x')\Big].$$

No minus signs are introduced on moving the η to the right of the eigenfunctions in (101). On comparison with (74) and (80), we see that $(N_{\lambda p}=n_{\lambda p})$:

$$(n|\,(\psi(x_1)\cdots\psi(x_k)\bar{\psi}(x_l')\cdots\bar{\psi}(x_1'))_{+}|\,n)\epsilon_{k,l}$$
$$=\delta_{k,l}\det{}_{(k)}[-iG_{+}(x_i,x_j')$$
$$-\textstyle\sum_{\lambda p}n_{\lambda p}\epsilon(\lambda)\psi_{\lambda p}(x_i)\bar{\psi}_{\lambda p}(x_j')], \quad (102)$$

of which the simplest example is

$$(n|\,(\psi(x)\bar{\psi}(x'))_{+}|\,n)\epsilon(x,x')$$
$$=-iG_{+}(x,x')-\textstyle\sum_{\lambda p}n_{\lambda p}\epsilon(\lambda)\psi_{\lambda p}(x)\bar{\psi}_{\lambda p}(x'). \quad (103)$$

The modes that occur in the general matrix element can be divided into three classes: class a, those for which $N_{\lambda p}=0$, $N_{\lambda p}'=1$; class b, modes with $N_{\lambda p}=N_{\lambda p}'$; class c, those with $N_{\lambda p}=1$, $N_{\lambda p}'=0$. A typical term in the expansion of the product (100) can then be written

$$\prod_{a}(i\bar{\eta}\psi')\prod_{b}[(\bar{\psi}')^{N}\epsilon^{N}(1+N\epsilon\bar{\eta}\eta)(\psi')^{N}]\prod_{c}(i\bar{\psi}'\eta). \quad (104)$$

The b mode product can be re-arranged as in the discussion of the diagonal matrix elements, which yields

$$\exp[\sum_{b}N_{\lambda p}\epsilon(\lambda)\bar{\eta}_{\lambda p}\eta_{\lambda p}](-1)^{N-b}{}'\prod_{b}(\bar{\psi}_{\lambda p}')^{N}\prod_{b}(\psi_{\lambda p}')^{N}.$$

If we now bring the eigenvalues $\psi_{\lambda p}'$ of the a modes and $\bar{\psi}_{\lambda p}'$ of the c modes into standard order, (100) becomes

$$'\prod_{a}(i\bar{\eta}(-1)^{N_{>}})\exp[\sum_{b}N\epsilon\bar{\eta}\eta](-1)^{N-b}(-1)^{N_aN_c}$$
$$\times[\bar{\psi}'|N][N'|\psi']\prod_{c}(i\eta(-1)^{N_{>}}),$$

in which $N_{>\lambda p}$ represents the number of occupied b modes that follow λp in the standard order, while N_a and N_c are the total number of modes in the a and c classes.

The right side of (99) is thus expressed as

$$\sum_{N,N'}{}'\prod_{a}(i\bar{\eta}(-1)^{N_{>}})\exp[\ ](-1)^{N-b+N_aN_c}$$
$$\times[\bar{\psi}'|N][N'|\psi']\prod_{c}(i\eta(-1)^{N_{>}})$$

where

$$\exp[\ ]=\exp\Big[i\int(dx)(dx')\bar{\eta}(x)$$
$$\times\big(G_{+}(x,x')-i\sum_{b}N_{\lambda p}\epsilon(\lambda)\psi_{\lambda p}(x)\bar{\psi}_{\lambda p}(x')\big)\eta(x')\Big].$$

We must obey the injunction that all $\bar{\eta}$ appear on the left, and all η on the right. The effect of moving an η in the above exponential past the product of the eigenfunctions is to introduce a factor of $(-1)^{N-N'}$, where N and N' represent the total number of occupied modes in the respective eigenfunctions. Accordingly,

$$(\pm)\Big[N\Big|\Big(\exp\Big[i\int(dx)(\bar{\eta}\psi+\bar{\psi}\eta)\Big]\Big)_{+}\Big|N'\Big]$$
$$=(-1)^{N-b+N_aN_c}{}'\prod_{a}(i\bar{\eta}(-1)^{N_{>}})\exp\Big[i(-1)^{N-N'}$$
$$\times\int(dx)(dx')\bar{\eta}(G_{+}-i\sum_{b}N\epsilon\psi\bar{\psi})\eta\Big]\prod_{c}(i\eta(-1)^{N_{>}}).$$

On expansion, we obtain the followlng result for the general nonvanishing matrix element,

$$[N|\,(\psi(x_1)\cdots\psi(x_k)\bar{\psi}(x_l')\cdots\bar{\psi}(x_1'))_{+}|\,N']\epsilon_{k,l}$$
$$=(-1)^{\frac{1}{2}(N-a-N-c)^2-\frac{1}{2}(N-a+N-c)}\det{}_{(k+l-r)}\begin{bmatrix}0, & (-1)^{N_{>}}\bar{\psi}_c(x_j')\\ (-1)^{N_{>}}\psi_a(x_i), & -iG_{+}(x_i,x_j')-\sum_{b}N_{\lambda p}\epsilon(\lambda)\psi_{\lambda p}(x_i)\bar{\psi}_{\lambda p}(x_j')\end{bmatrix} \quad (105)$$

in which

$$k-N_a=l-N_c=r \tag{106}$$

must be a non-negative integer. Also,

$$N_a=N'-N_b, \quad N_c=N-N_b.$$

In this determinant, 0 stands for the null matrix of N_c rows and N_a columns, and $(-1)^{N>}\psi_a(x_i)$ represents a matrix of k rows and N_a columns in which the eigenfunctions of the various a modes are standardly arrayed in the successive columns. The matrix $(-1)^{N>}\bar{\psi}_c(x_j')$ is one of N_c rows and l columns, with the various c mode adjoint eigenfunctions, in standard order, occupying the successive rows. Finally, we have the matrix $-iG_+(x_i,x_j')$ $-\sum_b N_{\lambda p}\epsilon(\lambda)\psi_{\lambda p}(x_i)\bar{\psi}_{\lambda p}(x_j')$ of k rows and l columns. Thus the dimension of this determinant is

$$k+N_c=l+N_a=k+l-r.$$

Since this can also be written as N_a+N_c+r, we see that the integer r is also the maximum number of Green's function factors that appear in the development of the determinant.

For the elementary example $k=1$, $l=0$, we have $N_a=1$, $N_c=r=0$, and the nonvanishing matrix element

$$[N|\psi(x)|N+1_{\lambda p}]=(-1)^{N>\lambda p}\psi_{\lambda p}(x)$$

which unifies (85) and (86) as intended. Similarly,

$$[N+1_{\lambda p}|\bar{\psi}(x)|N]=(-1)^{N>\lambda p}\bar{\psi}_{\lambda p}(x).$$

With this classification, $\psi(x)$ and $\bar{\psi}(x)$ appear as single "particle" annihilators and creators, respectively. The selection rules (106) for the general matrix element can then be described as follows. The operator contains k annihilators and l creators. If r of these operators combine in pairs to produce a null net effect, the remaining $k-r$ annihilators and $l-r$ creators will empty $N_a=k-r$ occupied modes, and fill $N_c=l-r$ occupied modes. Of course $N=N'+l-k$.

The diagonal matrix elements (102) represent the extreme situation in which

$$r=k=l, \quad N_a=N_c=0.$$

At the opposite limit is

$$r=0, \quad N_a=k, \quad N_c=l,$$

where the matrix element (105) becomes

$$\pm\det_{(k)}[(-1)^{N>}\psi_a(x_i)]\det_{(l)}[(-1)^{N>}\bar{\psi}_c(x_j')]$$

and

$$\pm=(-1)^{\frac{1}{2}N-a(N-a-1)}(-1)^{\frac{1}{2}N-c(N-c-1)}(-1)^{N_aN_c-N-aN-c}.$$

MAXWELL FIELD MATRIX ELEMENTS

This section is a supplement to paper III, in which the transformation function describing the Maxwell field with an external current is used to construct the matrices of all products of the potential vector for the isolated electromagnetic field. The transformation function (III, 20) can be expressed as

$$(F^{(-)'}\sigma_1|F^{(+)'}\sigma_2)=(F^{(-)'}\sigma_1|F^{(+)'}\sigma_2)]_0$$
$$\times\exp\left[i\mathfrak{W}_0+i\int(dx)J_\nu(x)A_\nu'(x)\right], \tag{107}$$

where $]_0$ indicates zero external current, and

$$A_\nu'(x')=2\int_{\sigma_1}d\sigma_\mu F_{\mu\nu}{}^{(-)'}(x)D_+(x-x')$$
$$-2\int_{\sigma_2}d\sigma_\mu F_{\mu\nu}{}^{(+)'}(x)D_+(x-x')$$
$$=2\oint d\sigma_\mu F_{\mu\nu}{}'(x)D_+(x-x'). \tag{108}$$

We also recall that

$$\mathfrak{W}_0=\tfrac{1}{2}\int(dx)(dx')J_\mu(x)D_+(x-x')J_\mu(x')$$
$$=\tfrac{1}{2}\int(dx)(dx')[J_k(x)(\delta_{kl}D_+(x-x'))^{(T)}J_l(x')$$
$$-J_0(x)\mathfrak{D}(x-x')J_0(x')],$$

where the latter form is appropriate to the radiation gauge.

The dependence of the transformation function upon the external current is expressed by

$$\delta_J(F^{(-)'}\sigma_1|F^{(+)'}\sigma_2)$$
$$=i\left(F^{(-)'}\sigma_1\left|\int(dx)\delta J_\mu(x)A_\mu(x)\right|F^{(+)'}\sigma_2\right). \tag{109}$$

In the radiation gauge, $A_0(x)$ is the numerical quantity

$$A_0(x)=\int(dx')\mathfrak{D}(x-x')J_0(x').$$

Hence

$$\delta_{J_0}(F^{(-)'}\sigma_1|F^{(+)'}\sigma_2)$$
$$=-i\int(dx)(dx')\delta J_0(x)\mathfrak{D}(x-x')J_0(x')(F^{(-)'}\sigma_1|F^{(+)'}\sigma_2),$$

and

$$(F^{(-)'}\sigma_1|F^{(+)'}\sigma_2)=(F^{(-)'}\sigma_1|F^{(+)'}\sigma_2)]_{J_0=0}$$
$$\times\exp\left[-i\tfrac{1}{2}\int(dx)(dx')J_0(x)\mathfrak{D}(x-x')J_0(x')\right],$$

which gives the simple dependence of the transformation function upon J_0, in the radiation gauge. This factor is evident in the radiation gauge version of $\exp(i\mathfrak{W}_0)$. Accordingly, we restrict ourselves to transverse currents, for which $J_0=0$.

On introducing the scale factor λ, $J_k \rightarrow \lambda J_k$ we infer from (109) that

$$(\partial/\partial\lambda)(F^{(-)\prime}\sigma_1|F^{(+)\prime}\sigma_2)$$
$$= i\left(F^{(-)\prime}\sigma_1\left|\int (dx)J_k(x)A_k(x)\right|F^{(+)\prime}\sigma_2\right).$$

Repeated differentiation yields

$$(\partial/\partial\lambda)^n(F^{(-)\prime}\sigma_1|F^{(+)\prime}\sigma_2)$$
$$= i^n\left(F^{(-)\prime}\sigma_1\left|\int (dx_1)\cdots(dx_n)J_{k_1}(x_1)\cdots J_{k_n}(x_n)\right.\right.$$
$$\left.\left.\times(A_{k_1}(x_1)\cdots A_{k_n}(x_n))_+\right|F^{(+)\prime}\sigma_2\right),$$

and the transformation function appropriate to the external current ($\lambda=1$), is obtained from that of the isolated electromagnetic field ($\lambda=0$) as

$$(F^{(-)\prime}\sigma_1|F^{(+)\prime}\sigma_2)$$
$$= \left(F^{(-)\prime}\sigma_1\left|\left(\exp\left[i\int (dx)J_k(x)A_k(x)\right]\right)_+\right|F^{(+)\prime}\sigma_2\right)\Big]_0.$$

If we employ the notation

$$(F^{(-)\prime}\sigma_1|\ \ |F^{(+)\prime}\sigma_2)/(F^{(-)\prime}\sigma_1|F^{(+)\prime}\sigma_2)\Big]_0 = \langle\ \rangle,$$

the transformation function (107) can be expressed by

$$\left\langle\left(\exp\left[i\int (dx)J_k(x)A_k(x)\right]\right)_+\right\rangle$$
$$= \exp\left[i\tfrac{1}{2}\int (dx)(dx')J_k(x)(\delta_{kl}D_+(x-x'))^{(T)}\right.$$
$$\left.\times J_l(x')+i\int (dx)J_k(x)A_k'(x)\right]. \quad (110)$$

It will be advantageous to suppress the vector indices. Accordingly, we rewrite (110) as

$$\left\langle\left(\exp\left[i\int (dx)J(x)A(x)\right]\right)_+\right\rangle$$
$$= \exp\left[i\tfrac{1}{2}\int (dx)(dx')J(x)D_+(x-x')J(x')\right.$$
$$\left.+i\int (dx)J(x)A'(x)\right]. \quad (111)$$

An alternative version is

$$\left\langle\left(\exp\left[i\int (dx)J(x)'A(x)\right]\right)_+\right\rangle$$
$$= \exp\left[i\tfrac{1}{2}\int (dx)(dx')J(x)D_+(x-x')J(x')\right], \quad (112)$$

where

$$'A(x) = A(x)-A'(x).$$

An expansion of both sides in (111) or (112) will supply the matrix elements of ordered A products.

The right side of (112) is an even function of J. Accordingly,

$$\langle('A(x_1)\cdots'A(x_{2n-1}))_+\rangle = 0.$$

In particular,

$$\langle'A(x)\rangle = 0,$$

or

$$\langle A(x)\rangle = A'(x). \quad (113)$$

The general even term in the expansion of the left side in (112) is

$$\frac{i^{2n}}{(2n)!}\int (dx_1)\cdots(dx_{2n})J(x_1)\cdots J(x_{2n})$$
$$\times\langle('A(x_1)\cdots'A(x_{2n}))_+\rangle.$$

This is to be compared with

$$\frac{i^n}{2^n n!}\int (dx_1)\cdots(dx_{2n})J(x_1)\cdots J(x_{2n})$$
$$\times D_+(x_1-x_2)\cdots D_+(x_{2n-1}-x_{2n})$$
$$= \frac{i^n}{(2n)!}\int (dx_1)\cdots(dx_{2n})J(x_1)\cdots J(x_{2n})$$
$$\times \mathrm{sym}_{(n)}D_+(x_i-x_j),$$

in which has been introduced what we shall call the nth symmetrant of D_+. This is defined by

$$\mathrm{sym}_{(n)}D_+(x_i-x_j)$$
$$= \sum_{\mathrm{perm}} D_+(x_{i_1}-x_{i_2})\cdots D_+(x_{i_{2n-1}}-x_{i_{2n}}),$$

and the summation is extended over all distinct permutations of the indices $i_1\cdots i_{2n}$, which are some rearrangement of the integers $1\cdots 2n$. Since D_+ is an even function of its argument, and the order of the n factors is irrelevant, the number of such permutations is $(2n)!/2^n n! = (2n-1)(2n-3)\cdots$.

The matrix of an even product of the $'A$ is thus expressed by

$$\langle('A(x_1)\cdots'A(x_{2n}))_+\rangle = (-i)^n\,\mathrm{sym}_{(n)}D_+(x_i-x_j). \quad (114)$$

The first two such products are

$$\langle('A(x)'A(x'))_+\rangle = -iD_+(x-x'),$$

or

$$\langle(A(x)A(x'))_+\rangle = A'(x)A'(x')-iD_+(x-x') \quad (115)$$

and

$$\langle('A(x_1)'A(x_2)'A(x_3)'A(x_4))_+\rangle$$
$$= -[D_+(x_1-x_2)D_+(x_3-x_4)+D_+(x_1-x_3)D_+(x_2-x_4)$$
$$+D_+(x_2-x_3)D_+(x_1-x_4)].$$

To obtain corresponding results for products of the operators A, as in the simple examples (113) and (115), we first consider the even terms of (111). The even function, $\cos x$, can be obtained from an exponential function of x^2 by a suitable operation

$$\cos x = C_t[\exp(-\tfrac{1}{2}tx^2)],$$

where

$$C_t(t^n) = 2^n n!/(2n)!$$

effectively defines the operator C_t, although an explicit integral representation can also be exhibited, as in (81). Hence the even part of (111) is

$$\left\langle\left(\cos\left[\int (dx)J(x)A(x)\right]\right)_+\right\rangle$$
$$= C_t \exp\left[-\tfrac{1}{2}\int (dx)(dx')J(x) \times(-iD_+(x-x')+tA'(x)A'(x'))J(x')\right],$$

which, in view of (112) and (114), yields

$$\begin{aligned}\langle(A(x_1)\cdots A(x_{2n}))_+\rangle &= C_t\,\mathrm{sym}_{(n)}[-iD_+(x_i-x_j)+tA'(x_i)A'(x_j)] \\ &= A'(x_1)\cdots A'(x_{2n})+\cdots \\ &\quad +(-i)^n\,\mathrm{sym}_{(n)}D_+(x_i-x_j). \quad (116)\end{aligned}$$

As the initial term of the developed version indicates, the effect of the C_t operation is to reinstate the unique counting of each distinct permutation in the expansion of the symmetrant (116).

For the construction of matrices describing odd products of the A, we remark that

$$(\delta/\delta A'(x))\left\langle\left(\exp\left[i\int (dx)JA\right]\right)_+\right\rangle = iJ(x)\left\langle\left(\exp\left[i\int (dx)JA\right]\right)_+\right\rangle.$$

On expanding both sides, we obtain

$$\begin{aligned}(\delta/\delta A'(x))\langle(A(x_1)\cdots A(x_m))_+\rangle &= \delta(x-x_1)\langle(A(x_2)\cdots A(x_m))_+\rangle+\cdots \\ &\quad +\delta(x-x_m)\langle(A(x_1)\cdots A(x_{m-1}))_+\rangle,\end{aligned}$$

which can also be expressed by

$$(\partial/\partial A'(x_m))\langle(A(x_1)\cdots A(x_m))_+\rangle = \langle(A(x_1)\cdots A(x_{m-1}))_+\rangle.$$

Hence the matrices of odd products can be obtained by differentiation from those of even products,

$$\begin{aligned}&\langle(A(x_1)\cdots A(x_{2n-1}))_+\rangle \\ &\quad = (\partial/\partial A'(x_{2n}))\langle(A(x_1)\cdots A(x_{2n}))_+\rangle \\ &\quad = (\partial/\partial A'(x_{2n}))C_t\,\mathrm{sym}_{(n)}[-iD_+(x_i-x_j) \\ &\qquad +tA'(x_i)A'(x_j)],\end{aligned}$$

or

$$\begin{aligned}&\langle(A(x_1)\cdots A(x_{2n-1}))_+\rangle \\ &\quad = C_t\,\mathrm{sym}_{(n)}[-iD_+(x_i-x_j)+tA'(x_i)A'(x_j),\ \ tA'(x_k)],\end{aligned}$$

which is intended to indicate a symmetrant that is obtained from (116) by replacing the elements containing the variables x_k, x_{2n} with $tA'(x_k)$.

The Occupation Number Representation

The diagonal matrix elements referring to the vacuum state are obtained by placing all eigenvalues equal to zero,

$$\begin{aligned}&(0|(A(x_1)\cdots A(x_{2n-1}))_+|0)=0, \\ &(0|(A(x_1)\cdots A(x_{2n}))_+|0) \\ &\qquad = (-i)^n\,\mathrm{sym}_{(n)}D_+(x_i-x_j),\end{aligned} \quad (117)$$

and, in particular,

$$(0|(A(x)A(x'))_+|0) = -iD_+(x-x'). \quad (118)$$

We introduce the mode functions

$$\begin{aligned}A_{\lambda k}(x)_\mu &= \left(\frac{(d\mathbf{k})}{(2\pi)^3}\frac{1}{2k_0}\right)^{\frac{1}{2}} e_\mu(\lambda k)e^{ikx}, \\ \bar{A}_{\lambda k}(x)_\mu &= \left(\frac{(d\mathbf{k})}{(2\pi)^3}\frac{1}{2k_0}\right)^{\frac{1}{2}} e_\mu(\lambda k)e^{-ikx},\end{aligned} \quad (119)$$

in terms of which the tensor Green's function (III, 23) appears as

$$\begin{aligned}\delta_{\mu\nu}D_+(x-x') &= i\textstyle\sum_{\lambda k} A_{\lambda k}(x)_\mu \bar{A}_{\lambda k}(x')_\nu, \quad x_0>x_0' \\ &= i\textstyle\sum_{\lambda k} \bar{A}_{\lambda k}(x)_\mu A_{\lambda k}(x')_\nu, \quad x_0<x_0'.\end{aligned} \quad (120)$$

Accordingly,

$$A_\nu'(x') = 2\oint d\sigma_\alpha F_{\alpha\mu}'(x)\delta_{\mu\nu}D_+(x-x')$$

becomes (suppressing the vector indices)

$$A'(x) = \textstyle\sum_{\lambda k}(A_{\lambda k}(x)e^{-ikx_2}A_{\lambda k}{}^{(+)\prime}+\bar{A}_{\lambda k}(x)e^{ikx_1}A_{\lambda k}{}^{(-)\prime}),$$

where

$$A_{\lambda k}{}^{(-)\prime} = 2i\int_{\sigma_1} d\sigma_\mu F_{\mu\nu}{}^{(-)\prime}(x)A_{\lambda k}(x)_\nu e^{-ikx_1},$$

and

$$A_{\lambda k}{}^{(+)'} = -2i\int_{\sigma 2} d\sigma_\mu F_{\mu\nu}{}^{(+)'}(x)\bar{A}_{\lambda k}(x)_\nu e^{ikx_2}.$$

The latter quantities are the negatives of $a_{\lambda k}{}^{(\pm)'}$ (III, 27, 28). Since these minus signs would be somewhat unfortunate for our present purposes, we notice that the opposite choice of sign in (III, 27, 28) produces relatively trivial changes in the work of III. Thus, in Eq. (III, 34) and its consequences, the signs of the terms contalnlng $J_{\lambda k}$ and $J_{\lambda k}{}^*$ are to be reversed. We now write the eigenfunctions of the isolated electromagnetic field as

$$(F^{(-)'}|n) = \prod_{\lambda k}(n!)^{-\frac{1}{2}}(A_{\lambda k}{}^{(-)'})^n,$$

$$(n|F^{(+)'}) = \prod_{\lambda k}(n!)^{-\frac{1}{2}}(A_{\lambda k}{}^{(+)'})^n,$$

while the transformation function is

$$(F^{(-)'}\sigma_1|F^{(+)'}\sigma_2) = \exp[\textstyle\sum_{\lambda k} A_{\lambda k}{}^{(-)'}e^{ikx_1}e^{-ikx_2}A_{\lambda k}{}^{(+)'}] = \textstyle\sum_n (F^{(-)'}|n)\exp[iP(n)(x_1-x_2)](n|F^{(+)'}).$$

The occupation number matrix of A is derived from (113), written as

$$(F^{(-)'}\sigma_1|A(x)|F^{(+)'}\sigma_2) = \sum_{n,n'}(F^{(-)'}|n)(n\sigma_1|A(x)|n'\sigma_2)(n'|F^{(+)'}) = A'(x)(F^{(-)'}\sigma_1|F^{(+)'}\sigma_2).$$

The substitutions $e^{-ikx_2}A_{\lambda k}{}^{(+)'}\rightarrow A_{\lambda k}{}^{(+)'}$, $e^{ikx_1}A_{\lambda k}{}^{(-)'}\rightarrow A_{\lambda k}{}^{(-)'}$ convert this into a generating function for the matrix referring to a standard surface,

$$(n|A(x)|n') = \exp(-iP(n)x_1)\times(n\sigma_1|A(x)|n'\sigma_2)\exp(iP(n')x_2),$$

namely,

$$\sum_{n,n'}(F^{(-)'}|n)(n|A(x)|n')(n'|F^{(+)'}) = \sum_{\lambda k}(A_{\lambda k}(x)A_{\lambda k}{}^{(+)'}+\bar{A}_{\lambda k}(x)A_{\lambda k}{}^{(-)'})\times\sum_n(F^{(-)'}|n)(n|F^{(+)'}).$$

Now

$$A_{\lambda k}{}^{(-)'}(F^{(-)'}|n-1_{\lambda k}) = (F^{(-)'}|n)n_{\lambda k}{}^{\frac{1}{2}}$$

and

$$(n-1_{\lambda k}|F^{(+)'})A_{\lambda k}{}^{(+)'} = n_{\lambda k}{}^{\frac{1}{2}}(n|F^{(+)'}),$$

so that the nonvanishing matrix elements of $A(x)$ are

$$(n-1_{\lambda k}|A(x)|n) = n_{\lambda k}{}^{\frac{1}{2}}A_{\lambda k}(x)$$

and

$$(n|A(x)|n-1_{\lambda k}) = n_{\lambda k}{}^{\frac{1}{2}}\bar{A}_{\lambda k}(x).$$

The generating function for the matrices of all ordered products, referred to the standard surface, is

$$\sum_{n,n'}(F^{(-)'}|n)\times\left(n\left|\left(\exp\left[i\int(dx)J(x)A(x)\right]\right)_+\right|n'\right)(n'|F^{(+)'})$$

$$= (F^{(-)'}|F^{(+)'})\exp\left[i\tfrac{1}{2}\int(dx)(dx')J(x)\times D_+(x-x')J(x')+i\int(dx)J(x)A'(x)\right]$$

$$= \exp\left[i\tfrac{1}{2}\int(dx)(dx')JD_+J\right]\times\prod_{\lambda k}\exp\left[A_{\lambda k}{}^{(-)'}A_{\lambda k}{}^{(+)'}+iA_{\lambda k}{}^{(-)'}\times\int(dx)J(x)\bar{A}_{\lambda k}(x)+iA_{\lambda k}{}^{(+)'}\times\int(dx)J(x)A_{\lambda k}(x)\right]. \quad (121)$$

The expansion into eigenfunctions is greatly simplified by exploiting the infinitesimal nature of $(d\mathbf{k})$. Thus the second exponential factor of (121) becomes

$$\prod_{\lambda k}\sum_{n,n'}\frac{(A^{(-)'})^n}{(n!)^{\frac{1}{2}}}\left[\delta_{n,n'}\left(1-n\int(dx)JA\int(dx)J\bar{A}\right)+\delta_{n,n'+1}n^{\frac{1}{2}}i\int(dx)J\bar{A}+\delta_{n',n+1}n'^{\frac{1}{2}}i\times\int(dx)JA\right]\frac{(A^{(+)'})^n}{(n'!)^{\frac{1}{2}}}. \quad (122)$$

A change in the occupation number of a given mode by two, for example, would lead to a matrix element proportional to $(d\mathbf{k})$, and thus to a transition probability proportional to $(d\mathbf{k})^2$.

We first consider diagonal matrix elements, which are contained in the following terms of (122),

$$\prod_{\lambda k}\sum_n\frac{(A^{(-)'})^n}{(n!)^{\frac{1}{2}}}\left[1-n\int(dx)JA\int(dx)J\bar{A}\right]\frac{(A^{(+)'})^n}{(n!)^{\frac{1}{2}}} = \sum_n(F^{(-)'}|n)\exp\left[-\int(dx)(dx')J(x)\times\left(\sum_{\lambda k}n_{\lambda k}A_{\lambda k}(x)\bar{A}_{\lambda k}(x')\right)J(x')\right](n|F^{(+)'}).$$

Thus

$$\left(n\left|\left(\exp\left[i\int(dx)J(x)A(x)\right]\right)_+\right|n\right)$$
$$=\exp\Big[-\tfrac{1}{2}\int(dx)(dx')J(x)(-iD_+(x-x')+\sum_{\lambda k}2n_{\lambda k}A_{\lambda k}(x)\bar{A}_{\lambda k}(x'))J(x')\Big],$$

which asserts that

$$(n|(A(x_1)\cdots A(x_{2l-1}))_+|n)=0,$$

and that

$$(n|(A(x_1)\cdots A(x_{2l}))_+|n)$$
$$=\mathrm{sym}_{(l)}[-iD_+(x_i-x_j)+\textstyle\sum_{\lambda k}n_{\lambda k}\times(A_{\lambda k}(x_i)\bar{A}_{\lambda k}(x_j)+\bar{A}_{\lambda k}(x_i)A_{\lambda k}(x_j))]. \quad (123)$$

The elementary example of the latter result is

$$(n|(A(x)A(x'))_+|n)=-iD_+(x-x')+\textstyle\sum_{\lambda k}n_{\lambda k}(A_{\lambda k}(x)\bar{A}_{\lambda k}(x')+\bar{A}_{\lambda k}(x)A_{\lambda k}(x')). \quad (124)$$

We introduce a classification of modes in the general matrix element: class a, those for which $n_{\lambda k}=n_{\lambda k}'-1$; class b, modes with $n_{\lambda k}=n_{\lambda k}'$; class c, those with $n_{\lambda k}=n_{\lambda k}'+1$. A typical term in the expansion of the product (122) can then be written

$$(F^{(-)'}|n)\prod_a\left[n'^{\frac{1}{2}}i\int(dx)JA\right]\times\prod_b\left[1-n\int(dx)JA\int(dx)J\bar{A}\right]\times\prod_c\left[n^{\frac{1}{2}}i\int(dx)J\bar{A}\right](n'|F^{(+)'}).$$

Accordingly,

$$\left(n\left|\left(\exp\left[i\int(dx)J(x)A(x)\right]\right)_+\right|n'\right)$$
$$=\exp\left[i\tfrac{1}{2}\int(dx)(dx')J(x)D_+^{(n)}(x,x')J(x')\right]\times\prod_a\left[n'^{\frac{1}{2}}i\int(dx)JA_{\lambda k}\right]\prod_c\left[n^{\frac{1}{2}}i\int(dx)J\bar{A}_{\lambda k}\right], \quad (125)$$

in which we have introduced the symbol

$$D_+^{(n)}(x,x')=D_+(x-x')+i\sum_b n_{\lambda k}\times[A_{\lambda k}(x)\bar{A}_{\lambda k}(x')+\bar{A}_{\lambda k}(x)A_{\lambda k}(x')].$$

We shall use $A_\alpha(x)$ to denote collectively the a mode functions, $A_{\lambda k}(x)$, and the c mode functions $\bar{A}_{\lambda k}(x)$ (a complete unification would be achieved by transposing the matrices with respect to the occupation numbers of the c modes, which would introduce a time-reversed description for emission processes). With this notation, (125) appears as

$$\left(n\left|\left(\exp\left[i\int(dx)J(x)A(x)\right]\right)_+\right|n'\right)$$
$$=\prod_a(n'^{\frac{1}{2}})\prod_c(n^{\frac{1}{2}})\prod_\alpha\left[i\int(dx)J(x)A_\alpha(x)\right]\times\exp\left[i\tfrac{1}{2}\int(dx)(dx')JD_+^{(n)}J\right].$$

The expansion of this generating function leads to the following formula for the general nonvanishing matrix element,

$$(n|(A(x_1)\cdots A(x_m))_+|n')=\prod_a(n'^{\frac{1}{2}})\prod_c(n^{\frac{1}{2}})(-i)^r\,\mathrm{sym}_{(N,r)}\times[A_\alpha(x_i);D_+^{(n)}(x_j,x_k)], \quad (126)$$

where N is the number of $\alpha=a+c$ modes, and r is a nonnegative integer such that

$$m=N+2r.$$

We have introduced an extension of the symmetrant which is constructed from N different functions of a single variable, $A_\alpha(x_i)$, and a symmetrical function of two variables, $D_+^{(n)}(x_j,x_k)$, taken r times,

$$\mathrm{sym}_{(N,r)}[A_\alpha(x_i);D_+^{(n)}(x_j,x_k)]=\sum_{\text{perm}}A_{\alpha_1}(x_{i_1})\cdots A_{\alpha_N}(x_{i_N})\times D_+^{(n)}(x_{i_{N+1}},x_{i_{N+2}})\cdots D_+^{(n)}(x_{i_{m-1}},x_{i_m}),$$

where the summation is extended over the $(N+2r)!/2^r r!$ distinct permutations of the indexes $i_1\cdots i_m$, which are some rearrangement of the integers $1\cdots m$.

The diagonal matrix elements correspond to the situation where $N=0$, $m=2r$. At the opposite extreme is $r=0$, $N=m$, where the symmetrant reduces to

$$\mathrm{sym}_{(m,0)}[A_\alpha(x_i)]=\sum_{\text{perm}}A_{\alpha_1}(x_{i_1})\cdots A_{\alpha_m}(x_{i_m}).$$

This sum of $m!$ permutations is obtained from the corresponding determinant by omitting the alternating sign factor.

Relativistic Particle Dynamics. II*

B. BAKAMJIAN AND L. H. THOMAS†
Columbia University, New York, New York
(Received June 19, 1953)

The relativistic dynamics for a system of non-interacting particles in Hamiltonian form is separated by a contact transformation into motion of their center of mass and internal motion. Interaction at a distance between them is then introduced into the expression for the rest-mass in terms of the internal variables. This gives a dynamics for which invariance over space displacements and rotations is trivial and which is rigorously invariant over Lorentz transformations. Earlier approximate treatments may be reduced by contact transformations to special cases of the general treatment.

1. INTRODUCTION

IN this paper we adopt the point of view of an earlier paper[1] and describe a system in terms of dynamical variables whose mutual Poisson brackets are given. We shall specify each particle i by three pairs of canonically conjugate dynamical variables forming vector coordinates $\mathbf{q}_i$ and momenta $\mathbf{p}_i$, three variables forming its vector intrinsic spin $\boldsymbol{\omega}_i$, and its rest mass m_i.

We shall take these to transform trivially for simultaneous rotation or displacement of the frame of reference in space, leading to an "instant" form of dynamics,[2,3] (as opposed to a "point" form in which transformation over the homogeneous Lorentz group is trivial, such as the form considered in I[1]).

The dynamics will then be specified by a Hamiltonian function H leading to the changes of the dynamical variables with time, and a vector $\mathbf{V}$, of which the components U, V, and W, give in the same way the infinitesimal transformations for change to relatively moving coordinate systems. In addition we introduce the vectors $\mathbf{R}$, components X, Y, and Z, the total linear momentum, and $\boldsymbol{\Omega}$, components L, M, and N, the total angular momentum of the system, which give in a similar way the here trivial, infinitesimal transformations for space displacement and rotation. These ten functions of the basic dynamical variables $\mathbf{q}_i$, $\mathbf{p}_i$, $\boldsymbol{\omega}_i$ (and m_i) must satisfy the conditions for all the transformations to give the inhomogeneous Lorentz group.[4]

It is, however, not implied, nor is it true, that, even in non-quantum mechanics, there exist world lines $\mathbf{r}_i=\mathbf{q}_i(t)$, for the particles, that are the same loci in space-time when transformed by the corresponding Lorentz transformations, unless there is no interaction and the particles are without spin.[5]

2. DYNAMICS FOR A SINGLE PARTICLE

For a free spinless point particle we have three coordinates q_x, q_y, q_z and canonically conjugate components of momentum p_x, p_y, p_z with Poisson brackets $(q_x, p_x)=1$, $(q_y, p_y)=1$, $(q_z, p_z)=1$, the remaining Poisson brackets vanishing. We may take the usual components of momentum, angular momentum, and energy,

$$X=p_x, \quad L=q_yp_z-q_zp_y,$$
$$Y=p_y, \quad M=q_zp_x-q_xp_z, \quad H=(m^2c^4+p_x^2+p_y^2+p_z^2)^{\frac{1}{2}},$$
$$Z=p_z, \quad N=q_xp_y-q_yp_x,$$

where m is the rest mass and c the speed of light, and then, if we take

$$U=q_xH/c^2, \quad V=q_yH/c^2, \quad W=q_zH/c^2,$$

all the conditions are satisfied,

$$[\text{e.g., } (U, X)=(q_x, p_x)H/c^2=H/c^2].$$

U, V, and W do not have as immediate a physical interpretation as X, Y, Z, L, M, N, and H, because they do not commute with H and are not constants of the motion of the system. They may be called velocity operators.

If we replace q_x, q_y, q_z, by operators

$$\frac{h}{2\pi i}\frac{\partial}{\partial p_x}, \quad \frac{h}{2\pi i}\frac{\partial}{\partial p_y}, \quad \frac{h}{2\pi i}\frac{\partial}{\partial p_z},$$

and write

$$U=\frac{1}{2c^2}(q_zH+Hq_z), \quad V=\frac{1}{2c^2}(q_yH+Hq_y),$$
$$W=\frac{1}{2c^2}(q_zH+Hq_z),$$

we obtain operators giving a relativistic quantum dynamics.

In vector notation,

$$\mathbf{R}=\mathbf{p}, \qquad H=[m^2c^4+\mathbf{p}^2c^2]^{\frac{1}{2}},$$
$$\boldsymbol{\Omega}=[\mathbf{q}\times\mathbf{p}], \quad \mathbf{V}=(1/2c^2)(\mathbf{q}H+H\mathbf{q}). \tag{1.2}$$

* Presented by B. Bakamjian in partial fulfillment of the requirements for the degree of Doctor of Philosophy in the faculty of Pure Science, Columbia University.

† Watson Scientific Computing Laboratory, Columbia University.

[1] L. H. Thomas, Phys. Rev. **85**, 868 (1952); referred to below as I.

[2] See I, Eqs. (4.2) and (4.3).

[3] P. M. Dirac, Revs. Modern Phys. **21**, 392 (1944).

[4] See I, Sec. III.

[5] M. H. L. Pryce, Proc. Roy. Soc. (London) **A195**, 621 (1948).

For a particle with spin, we may write in like fashion:

$$\mathbf{R}=\mathbf{p},\quad H=[m^2c^4+\mathbf{p}^2c^2]^{\frac{1}{2}},$$
$$\boldsymbol{\Omega}=[\mathbf{q}\times\mathbf{p}]+\boldsymbol{\omega}, \tag{2.21}$$

where $(\omega_x,\omega_y)=\omega_z$, $(\omega_y,\omega_z)=\omega_x$, $(\omega_z,\omega_x)=\omega_y$, and ω_x, ω_y, and ω_z have zero Poisson brackets with the rest of the basic dynamical variables. We now find that we must take

$$\mathbf{V}=\frac{1}{2c^2}(\mathbf{q}H+H\mathbf{q})-\frac{[\boldsymbol{\omega}\times\mathbf{p}]}{mc^2+H}. \tag{2.22}$$

Further, the Dirac electron can be obtained from this by introducing negative energy states, putting $\boldsymbol{\omega}=(h/4\pi)\boldsymbol{\sigma}$, and making the unitary transformation given by the matrix

$$[mc^2+E-ic\rho_2(\boldsymbol{\sigma}\cdot\mathbf{p})]/[2E(mc^2+E)]^{\frac{1}{2}},$$

where $E=|H|$ and $H=-\rho_3E$, and σ_x, σ_y, and σ_z, and ρ_1, ρ_2, and ρ_3, are two independent sets of Pauli matrices.

3. DYNAMICS FOR A SYSTEM OF PARTICLES WITHOUT SPIN

In building up a dynamics for more than one particle, it is convenient to start with two non-interacting particles. We write $c=1$ for brevity and take the sums of functions of the form (2.1) for each particle,

$$\mathbf{R}=\mathbf{p}_1+\mathbf{p}_2,\quad \boldsymbol{\Omega}=[\mathbf{q}_1\times\mathbf{p}_1]+[\mathbf{q}_2\times\mathbf{p}_2],$$
$$H=[m_1^2+\mathbf{p}_1^2]^{\frac{1}{2}}+[m_2^2+\mathbf{p}_2^2]^{\frac{1}{2}}, \tag{3.1}$$
$$\mathbf{V}=\mathbf{q}_1[m_1^2+\mathbf{p}_1^2]^{\frac{1}{2}}+\mathbf{q}_2[m_2^2+\mathbf{p}_2^2]^{\frac{1}{2}}.$$

This defines ten functions trivially satisfying the forty-five Poisson bracket relations[4] required for invariance.

The expression

$$m=(H^2-\mathbf{R}^2)^{\frac{1}{2}} \tag{3.2}$$

can be regarded as the effective rest mass of the system viewed as a single entity and has the important property that it commutes, or has zero Poisson bracket, with each of Eqs. (3.1).

We expect, for an instant form of dynamics, that interaction terms will enter only in H and $\mathbf{V}$ and not in $\mathbf{R}$ and $\boldsymbol{\Omega}$, and that they will depend in some sense only on relative or internal variables of the system, affecting the motion of the system as a whole only through m.

Suppose that we make a transformation from $\mathbf{p}_1$, $\mathbf{q}_1$, $\mathbf{p}_2$, $\mathbf{q}_2$ to variables $\mathbf{R}$, $\mathbf{r}$, total momentum and coordinates of the "center of mass," and $\mathbf{P}$, $\boldsymbol{\varrho}$, relative momentum and relative coordinates, twelve variables having similar Poisson bracket relations to $\mathbf{p}_1$, $\mathbf{q}_1$, $\mathbf{p}_2$, and $\mathbf{q}_2$, in such a way that (i) $\boldsymbol{\Omega}=[\mathbf{r}\times\mathbf{R}]+[\boldsymbol{\varrho}\times\mathbf{P}]$, (so that $\boldsymbol{\varrho}$ and $\mathbf{P}$ transform like vectors in a space rotation), (ii) m depends on $\mathbf{P}$ only, and (iii) $\mathbf{V}$ can be expressed in terms of m, $\mathbf{r}$, $\mathbf{R}$, and $\boldsymbol{\Omega}$ only. Then in the expression for H,

$$H=(m^2+\mathbf{R}^2)^{\frac{1}{2}},$$

and in the expression for $\mathbf{V}$ in terms of m, $\mathbf{r}$, $\mathbf{R}$, and $\boldsymbol{\Omega}$, we may introduce an interaction by replacing m by any other function of $\boldsymbol{\varrho}$ and $\mathbf{P}$ which is a scalar for space rotations. Relativistic invariance will be preserved because m still commutes with $\mathbf{r}$, $\mathbf{R}$, and $\boldsymbol{\Omega}$, and the commutation relations of these with each other and with H and $\mathbf{V}$ are not disturbed. (The transformation between $\mathbf{p}_1$, $\mathbf{q}_1$, $\mathbf{p}_2$, $\mathbf{q}_2$ and $\mathbf{R}$, $\mathbf{r}$, $\mathbf{P}$, $\boldsymbol{\varrho}$ must not be altered.)

We now obtain a transformation for many particles as similar to that to center of mass and relative coordinates in Newtonian mechanics as is consistent with the above requirements. We start with non-interacting particles having momenta $\mathbf{R}_u$ and coordinates $\mathbf{r}_u$ relative to an arbitrary observer, and write $H_u=(m_u^2+\mathbf{R}_u^2)^{\frac{1}{2}}$, $\boldsymbol{\Omega}_u=[\mathbf{r}_u\times\mathbf{R}_u]$, $\mathbf{V}_u=\frac{1}{2}(\mathbf{r}_uH_u+H_u\mathbf{r}_u)$, so that we can take

$$\mathbf{R}=\textstyle\sum_u\mathbf{R}_u,\quad \boldsymbol{\Omega}=\sum_u\boldsymbol{\Omega}_u,$$
$$H=\textstyle\sum_u H_u,\quad \mathbf{V}=\sum_u\mathbf{V}_u, \tag{3.3}$$

and the requirements for relativistic invariance will be met.

Next, we make a transformation to a frame in which the total momentum of the system is zero. In this new frame the particles have momenta $\mathbf{S}_u$ and energies K_u such that $\sum_u\mathbf{S}_u=0$ and $\sum_u K_u=m$.

Writing as before $H^2=m^2+\mathbf{R}^2$, and further $R^2=\mathbf{R}^2$, $R=m\sinh v$, $H=m\cosh v$, $R_u=(\mathbf{R}_u\cdot\mathbf{R})/R$, we obtain for this Lorentz transformation in the direction of R,

$$S_u=R_u\cosh v-H_u\sinh v,$$
$$K_u=-R_u\sinh v+H_u\cosh v,$$

or, returning to vectors,

$$\mathbf{S}_u=\mathbf{R}_u-R_u\mathbf{R}/R+S_u\mathbf{R}_u/R$$
$$=\mathbf{R}_u-\left\{\frac{(m+H)H_u-(\mathbf{R}\cdot\mathbf{R}_u)}{m(m+H)}\right\}\mathbf{R}, \tag{3.4}$$
$$K_u=-(\mathbf{R}\cdot\mathbf{R}_u)/m+HH_u/m;$$

while reversely,

$$\mathbf{R}_u=\mathbf{S}_u+\left\{\frac{(m+H)K_u+(\mathbf{R}_u\cdot\mathbf{S}_u)}{m(m+H)}\right\}\mathbf{R}, \tag{3.5}$$
$$H_u=(\mathbf{R}\cdot\mathbf{S}_u)/m+HK_u/m.$$

We verify that

(*a*) $\sum_u\mathbf{S}_u=0$, (*b*) $\sum_u K_u=m$; (*c*) $K_u^2=m_u^2+\mathbf{S}_u^2$,

while also

$$\mathbf{R}_u=\mathbf{S}_u+\frac{K_u+H_u}{m+H}\mathbf{R}. \tag{3.6}$$

The equation (3.4) now defines a "point transformation" in momentum space from the momenta $\mathbf{R}_u$ to the momenta $\mathbf{R}$ and $\mathbf{S}_u$, subject to the condition $\sum_u\mathbf{S}_u=0$, which satisfies the requirement (ii) above in that m

depends only on the relative momenta $\mathbf{S}_u$ in scalar fashion.

We can now find a corresponding transformation for the "coordinates" $\mathbf{r}_u$ of the particles by writing down the condition for a contact transformation which in this case is an "extended point transformation" in momentum space.

$$\sum_u(\mathbf{r}_u\cdot d\mathbf{R}_u)=(\mathbf{r}\cdot d\mathbf{R})+\sum_u(\mathbf{s}_u\cdot d\mathbf{S}_u), \qquad (3.7)$$

subject to $\sum_u \mathbf{S}_u=0$. The requirement (i) above follows now necessarily from the vector form of our equations as

$$\boldsymbol{\Omega}=\sum_u[\mathbf{r}_u\times\mathbf{R}_u]=[\mathbf{r}\times\mathbf{R}]+\sum_u[\mathbf{s}_u\times\mathbf{S}_u].$$

Here, $\mathbf{r}$ may be chosen to be any arbitrary linear combination of the $\mathbf{r}_u$ with coefficients functions of the $\mathbf{R}_u$, and in particular to satisfy requirement (iii). We may take the Eqs. (2.21) and (2.22) in the form

$$\boldsymbol{\Omega}=[\mathbf{r}\times\mathbf{R}]+\boldsymbol{\omega}, \quad \mathbf{V}=\tfrac{1}{2}(\mathbf{r}H+H\mathbf{r})-[\boldsymbol{\omega}\times\mathbf{R}]/(m+H),$$

and solve these to give

$$\mathbf{r}=\frac{1}{m}V+\frac{1}{m(m+H)}[\boldsymbol{\Omega}\times\mathbf{R}]-\frac{\mathbf{R}(\mathbf{V}\cdot\mathbf{R})}{mH(m+H)}, \qquad (3.8)$$

which is of the necessary form and determines the transformation. The detailed calculations are given in Appendix I, the important results being Eqs. (1)–(5). When there are just two particles we may write

$$\mathbf{P}=\mathbf{S}_1=-\mathbf{S}_2, \quad \boldsymbol{\varrho}=\mathbf{s}_1-\mathbf{s}_2,$$

and (3.8) becomes

$$(\mathbf{r}_1\cdot d\mathbf{R}_1)+(\mathbf{r}_2\cdot d\mathbf{R}_2)=(\mathbf{r}\cdot d\mathbf{R})+(\boldsymbol{\varrho}\cdot d\mathbf{P}), \qquad (3.9)$$

where $\boldsymbol{\varrho}$ and its canonically conjugate momentum $\mathbf{P}$ may be interpreted as the relative coordinate and relative momentum of the two particles. Thus, we have performed a contact transformation from the original pairs of conjugate variables describing the separate particles, $(\mathbf{r}_1, \mathbf{R}_1)$, $(\mathbf{r}_2, \mathbf{R}_2)$, to two other pairs $(\mathbf{r}, \mathbf{R})$, giving the state of the system as a whole, and $(\boldsymbol{\varrho}, \mathbf{P})$ giving its internal state.

Now any scalar combinations, $\boldsymbol{\varrho}^2$, $(\boldsymbol{\varrho}\cdot\mathbf{P})$, $\mathbf{P}^2$, and functions of these, of the internal variables commute with the ten fundamental quantities, so an interaction can be introduced consistently by making m any function of these scalar combinations. An explicit expression for $\boldsymbol{\varrho}$ is found from Eq. (2) of Appendix I.

$$\begin{aligned}\boldsymbol{\varrho}&=\mathbf{s}_1-\mathbf{s}_2\\ &=\mathbf{r}_1-\mathbf{r}_2+\frac{(\mathbf{r}_1-\mathbf{r}_2\cdot\mathbf{R})}{m(m+H)}\Big\{\mathbf{R}+\frac{1}{H}\Big(\frac{H_1}{s+m_1^2}-\frac{H_2}{s+m_2^2}\Big)\\ &\quad\times([H_2(m+H)-(\mathbf{R}_1\cdot\mathbf{R}_2)]\mathbf{R}_1\\ &\quad-[H_1(m+H)-(\mathbf{R}_1\cdot\mathbf{R}_2)]\mathbf{R}_2)\Big\}, \qquad (3.10)\end{aligned}$$

where $s=\frac{1}{2}(m^2-m_1^2-m_2^2)$. Likewise

$$\begin{aligned}\mathbf{r}=&\frac{1}{m}(\mathbf{r}_1H_1+\mathbf{r}_2H_2)+\frac{1}{m+H}\Big\{[\mathbf{r}_1\times\mathbf{R}_1]\times\mathbf{R}]\\ &+[[\mathbf{r}_2\times\mathbf{R}_2]\times\mathbf{R}]-\frac{H_1}{H}(\mathbf{r}_1\cdot\mathbf{R})\mathbf{R}-\frac{H_2}{H}(\mathbf{r}_2\cdot\mathbf{R})\mathbf{R}\Big\}. \qquad (3.11)\end{aligned}$$

These equations, with $H_1^2=m_1^2+\mathbf{R}_1^2$, $H_2^2=m_2^2+\mathbf{R}_2^2$, $\mathbf{R}=\mathbf{R}_1+\mathbf{R}_2$, $H=H_1+H_2$, $m^2=H^2-\mathbf{R}^2$, and

$$\mathbf{P}=\mathbf{R}_1-\Big\{\frac{(m+H)H_1-(\mathbf{R}\cdot\mathbf{R}_1)}{m(m+H)}\Big\}\mathbf{R},$$

give the transformation explicitly, while the fundamental quantities giving the dynamics are

$$\begin{aligned}&\mathbf{R}=\mathbf{R}, \quad H=(M^2+R^2)^{\frac{1}{2}},\\ &\boldsymbol{\Omega}=[\mathbf{r}\times R]+[\boldsymbol{\varrho}\times\mathbf{P}],\\ &\mathbf{V}=\tfrac{1}{2}(\mathbf{r}H+H\mathbf{r})-\frac{[[\boldsymbol{\varrho}\times\mathbf{P}]\times\mathbf{R}]}{M+H},\end{aligned} \qquad (3.12)$$

where M may be any function of $\boldsymbol{\varrho}^2$, $(\boldsymbol{\varrho}\cdot\mathbf{P})$, and $\mathbf{P}^2$.

Since $\mathbf{r}$ and $\boldsymbol{\varrho}$ are linear in $\mathbf{r}_1$ and $\mathbf{r}_2$, the extension to quantum mechanics is always possible.

4. SPIN

We may introduce spin into our equations as follows: (*a*) We define the intrinsic spin $\boldsymbol{\omega}$ of a particle relative to an observer O as a four-vector which is space-like in a frame P in which the particle is at rest. Further, we assume that the components ω_x, ω_y, ω_z of $\boldsymbol{\omega}$ satisfy the Poisson bracket relations:

$$(\omega_x, \omega_y)=\omega_z; \quad (\omega_y, \omega_z)=\omega_x; \quad (\omega_z, \omega_x)=\omega_y. \qquad (4.1)$$

(*b*) Viewed from any other frame of reference, the intrinsic spin defined in this manner will be given in general by a different four vector which is also space-like in the frame P. In particular, the intrinsic spin relative to the frame C in which the system has zero linear momentum will be denoted by a vector $\mathbf{n}$. Three successive Lorentz transformations from P to O, O to C, and from C back to P will now give us the relationship between $\boldsymbol{\omega}$ and $\mathbf{n}$:

$$\begin{aligned}\mathbf{n}_u=&\boldsymbol{\omega}_u+(\boldsymbol{\omega}_u\cdot\mathbf{R})\frac{\mathbf{S}_u}{m(m_u+K_u)}+\frac{(\boldsymbol{\omega}_u\cdot\mathbf{R})\mathbf{R}}{m(m+H)}\\ &+\frac{(\boldsymbol{\omega}_u\cdot\mathbf{R}_u)\mathbf{S}_u(m-H)}{m(m_u+K_u)(m_u+H_u)}-\frac{(\boldsymbol{\omega}_u\cdot\mathbf{R}_u)\mathbf{R}}{m(m_u+H_u)},\end{aligned}$$

or

$$\begin{aligned}\boldsymbol{\omega}_u=&\mathbf{n}_u-(\mathbf{n}_u\cdot\mathbf{R})\frac{\mathbf{R}_u}{m(m_u+K_u)}+(\mathbf{n}_u\cdot\mathbf{R})\frac{\mathbf{R}}{m(m+H)}\\ &+\frac{(\mathbf{n}_u\cdot\mathbf{S}_u)\mathbf{R}_u(m-H)}{m(m_u+K_u)(m_u+H_u)}+\frac{(\mathbf{n}_u\cdot\mathbf{S}_u)\mathbf{R}}{m(m_u+K_u)}.\end{aligned} \qquad (4.2)$$

These relations then define the transformation properties of *intrinsic* spin under a Lorentz transformation from the frame O to the frame C. We may further conclude from the properties of successive Lorentz transformations that $\mathbf{n}$ and $\boldsymbol{\omega}$ will have the same magnitude but will differ in orientation. Two successive Lorentz transformations are not equivalent to a single Lorentz transformation, but rather to a Lorentz transformation plus a suitable rotation. In other words, Lorentz transformations do not have the group property. They have the group property if each Lorentz transformation is coupled with a rotation. Thus we associate with the Lorentz transformations $O-C, O-P$, and $C-P$, rotations of the coordinate axes defined by Eulerian angles φ, θ, ψ; α, β, γ; and ξ, η, ζ, respectively. (*c*) Since the components of $\boldsymbol{\omega}$ do not have the Poisson bracket relations of true momenta, we cannot introduce them in our contact transformation (3.7) directly. The angles α, β, γ and ξ, η, ζ, however, represent true coordinates and therefore have canonically conjugate true momenta A, B, C and Ξ, H, Z associated with them. If now we consider an infinitesimal rotation given by a vector $d\boldsymbol{\pi}$ with components defined in the frame O as

$$(d\pi_x)_0=\cos\alpha d\beta+\sin\beta\sin\alpha d\gamma,$$
$$(d\pi_y)_0=\sin\alpha d\beta-\sin\beta\cos\alpha d\gamma,$$
$$(d\pi_z)_0=d\alpha+\cos\beta d\gamma;$$

and we set

$$(\boldsymbol{\omega}\cdot d\boldsymbol{\pi})_0=Ad\alpha+Bd\beta+Cd\gamma, \tag{4.3}$$

then

$$\begin{aligned}(\omega_x)_0&=-\cot\beta\sin\alpha A+\cos\alpha B+\csc\beta\sin\alpha C,\\ (\omega_y)_0&=\cot\beta\cos\alpha A+\sin\alpha B-\csc\beta\cos\alpha C,\\ (\omega_z)_0&=A.\end{aligned} \tag{4.4}$$

$\omega_x, \omega_y, \omega_z$ now form a function group in terms of canonical variables A, α; B, β; C, γ such that the relations (Sec. 2) are satisfied.

Similarly, we may consider an infinitesimal rotation given by a vector $d\boldsymbol{\theta}$ with components $(d\vartheta_x)_c=\cos\xi d\eta+\sin\eta\sin\xi d\zeta$, $(d\vartheta_y)_c=\sin\xi d\eta-\sin\eta\cos\xi d\zeta$, and $(d\vartheta_z)_c=d\xi+\cos\eta d\zeta$. We can write relations similar to (4.3), (4.4) that give the components $(\eta_x)_c$, $(\eta_y)_c$, $(\eta_z)_c$ of $\mathbf{n}$ in terms of canonical variables Ξ, ξ; H, η; Z, ζ.

Now if we write

$$\sum_u \mathbf{r}_u\cdot d\mathbf{R}_u+\sum_u \boldsymbol{\omega}_u\cdot d\boldsymbol{\pi}_u =\mathbf{r}\cdot d\mathbf{R}+\sum_u \mathbf{s}_u\cdot d\mathbf{S}_u+\sum_u \mathbf{n}_u\cdot d\boldsymbol{\theta}_u, \tag{4.5}$$

where the spin terms represent their equivalent expressions in terms of true variables, this represents a contact transformation between true coordinates and momenta. Since $\mathbf{n}_u$ is related to the new variables in the same way that $\boldsymbol{\omega}_u$ is to the old, we can conclude that the components of $\mathbf{n}_u$ will have the correct Poisson bracket relations among themselves.

Further, we can show that we do not need to know either α, β, γ or ξ, η, ζ to find the transformation of $(\omega_x, \omega_y, \omega_z)$ to (η_x, η_y, η_z) or to obtain that from $\mathbf{r}_u$ to $\mathbf{s}_u$. Thus, if we consider an infinitesimal rotation $d\boldsymbol{\sigma}$ related to the Eulerian angles φ, θ, ψ in the same manner that the vectors $d\boldsymbol{\pi}$ and $d\boldsymbol{\theta}$ are related to α, β, and γ and ξ, η, ζ, we can write

$$d\boldsymbol{\pi}=d\boldsymbol{\theta}+d\boldsymbol{\sigma},$$

when all are given in the same coordinate system. Equation (4.5) can now be written as

$$\sum_u \mathbf{r}_u\cdot d\mathbf{R}_u+(\textstyle\sum_u \boldsymbol{\omega}_u\cdot d\boldsymbol{\pi}_u)_0 =\mathbf{r}\cdot d\mathbf{R}+\sum_u \mathbf{s}_u\cdot d\mathbf{S}_u-(\sum_u \mathbf{n}_u\cdot d\boldsymbol{\sigma}_u)_c+(\sum_u \mathbf{n}_u\cdot d\boldsymbol{\pi}_u)_c.$$

Identifying coefficients,

$$(\mathbf{n}_u)_c=(\boldsymbol{\omega}_u)_0 \tag{4.6}$$

and

$$\sum_u \mathbf{r}_u\cdot d\mathbf{R}_u=\mathbf{r}\cdot d\mathbf{R}+\sum_u \mathbf{s}_u\cdot d\mathbf{S}_u-(\sum_u \mathbf{n}_u\cdot d\sigma_u)_c. \tag{4.7}$$

Equation (4.6) means that $\mathbf{n}_u$ can be obtained from $\boldsymbol{\omega}_u$ by a rotation through the Eulerian angles φ, θ, ψ. And Eq. (4.7) means that a knowledge of $d\boldsymbol{\sigma}$ alone is sufficient to give the transformation from the $\mathbf{r}_u$ to $\mathbf{r}$ and $\mathbf{s}_u$. The expression for $d\boldsymbol{\sigma}$ can be found if we observe that

$$d\mathbf{n}=d\boldsymbol{\omega}+[d\boldsymbol{\sigma}\times\boldsymbol{\omega}], \tag{4.8}$$

if $d\mathbf{n}$ and $d\boldsymbol{\omega}$ are evaluated in system C and O and the equation is in either system. The detailed calculations are given in Appendix II.

5. CONCLUSION

In discussing the many-body problem in Newtonian mechanics, one may make a contact transformation from the coordinates and momenta of the various bodies to the coordinates of the center of mass and the total momentum, and to internal coordinates and momenta. We have carried through a similar transformation in relativity mechanics, at the cost of giving up the assumption of invariant world lines.

Spin variables are treated as quasi-momenta, referred, in classical mechanics, to true coordinates like Eulerian angles. Their commutation relations are sufficient, however, to justify the transformations without this reference.

The introduction of interaction by replacing m by the function M of the internal variables in Eqs. (2.21) and (2.22), with $\boldsymbol{\omega}=\sum_u\{[\mathbf{s}_u\times\mathbf{S}_u]+\mathbf{n}_u\}$, gives a dynamics which may be modified by any further contact transformation of the variables.

Darwin's Hamiltonian[6] can be derived from our formalism if we set

$$M=m_1+m_2+\tfrac{1}{2}\mathbf{P}^2\left(\frac{1}{m_1}\times\frac{1}{m_2}\right)-\frac{1}{8}\mathbf{P}^4\left(\frac{1}{m_1^3}+\frac{1}{m_2^3}\right)$$
$$+\frac{q_1q_2}{\rho}+\frac{q_1q_2}{\rho}\frac{1}{2m_1m_2}\mathbf{P}^2+\frac{q_1q_2}{\rho^3}\frac{1}{2m_1m_2}(\boldsymbol{\rho}\cdot\mathbf{P})^2,$$

[6] C. G. Darwin, Phil. Mag. **39**, 537–551 (1920).

and perform a contact transformation generated by the function

$$W=\epsilon[(\boldsymbol{\rho}\cdot\mathbf{P})(\mathbf{R}\cdot\mathbf{P})-(\boldsymbol{\rho}\cdot\mathbf{R})\mathbf{P}^2],$$

where

$$\epsilon=\frac{q_1q_2}{2}\frac{m_2-m_1}{m_1m_2(m_1+m_2)}.$$

Similarly, two Hamiltonians[7] derived by Breit will be equivalent to our Hamiltonians if we take

$$M=2m+\frac{\rho^2}{m}-\frac{\rho^4}{4m^3}-J(\rho)-\frac{3\hbar}{4m^2}(\boldsymbol{\rho}\times\mathbf{P})\cdot(\boldsymbol{\sigma}_1+\boldsymbol{\sigma}_2)$$
$$-\frac{J}{m^2\rho}\rho^2+\frac{\boldsymbol{\rho}}{2m^2}(\boldsymbol{\rho}\cdot\mathbf{P})+\frac{3\hbar f}{2im^2}(\boldsymbol{\rho}\cdot\mathbf{P})$$
$$+\frac{\hbar}{2im^2}\rho\frac{df}{d\rho}(\boldsymbol{\rho}\cdot\mathbf{P})-\frac{\hbar^2f}{8m^2}(15+4\boldsymbol{\sigma}_1\cdot\boldsymbol{\sigma}_2)$$
$$-\frac{\hbar^2}{4m^2}\frac{df}{\rho d\rho}[5\rho^2+\rho^2(\boldsymbol{\sigma}_1\cdot\boldsymbol{\sigma}_2)-(\boldsymbol{\rho}\cdot\boldsymbol{\sigma}_1)(\boldsymbol{\rho}\cdot\sigma_2)]$$
$$-\frac{\hbar^2\rho^3}{8m^2}\frac{d}{d\rho}\left(\frac{df}{\rho d\rho}\right)$$

in one case, and

$$M=2m+\frac{\mathrm{P}^2}{m}-\frac{\mathrm{P}^4}{4m^3}-J(\rho)+\frac{3\mathrm{P}^2}{2m^2}J+\frac{\hbar f}{4m^2}(\boldsymbol{\rho}\times\mathbf{P}\cdot\boldsymbol{\sigma}_1+\boldsymbol{\sigma}_2)$$
$$+\frac{f}{2m}(\boldsymbol{\rho}\cdot\mathbf{P})^2-\frac{\hbar}{2im^2}\left(5f+\rho\frac{df}{d\rho}\right)(\boldsymbol{\rho}\cdot\mathbf{P})$$
$$-\frac{\hbar^2}{8m^2}\left[15f+10\rho\frac{df}{d\rho}+\rho^3\frac{d}{d\rho}\left(\frac{df}{\rho d\rho}\right)\right]$$

in the other case. Here $m_1=m_2=m$ and no further contact transformation is necessary. For two particles with unequal mass Breit derives another classical Hamiltonian[8] which can be derived from our equations if we set

$$M=m_1+m_2+\frac{1}{2}\mathrm{P}^2\left(\frac{1}{m_1}+\frac{1}{m_2}\right)-\frac{1}{8}\mathrm{P}^4\left(\frac{1}{m_1^3}+\frac{1}{m_2^3}\right)$$
$$-J(\rho)+\frac{1}{2m_1m_2}\frac{1}{\rho}\frac{dJ}{d\rho}(\boldsymbol{\rho}\cdot\mathbf{P})^2-\frac{J(\rho)}{2m_1m_2}\mathrm{P}^2,$$

and perform a contact transformation generated by the function

$$W=\epsilon(\boldsymbol{\rho}\cdot\mathbf{R})J(\rho),\quad\text{with}\quad\epsilon=\tfrac{1}{2}(m_2-m_1)/(m_1+m_2)^2.$$

APPENDIX I

For a system of particles defined by coordinates $\mathbf{r}_u$, canonically conjugate momenta $\mathbf{R}_u$, mass m_u, and zero spin we try to find a transformation to a new set of variables describing the system which distinguish between external and internal variables.

We are to have $\mathbf{R}$ and $n-1$ functions of the $\mathbf{S}_u$ subject to $\sum\mathbf{S}_u=0$ as variables and wish to find a set of variables canonically conjugate to these, including

$$\mathbf{r}=\frac{1}{m}\sum_u\mathbf{r}_uH_u+\frac{1}{m+H}\sum_u\left\{[[\mathbf{r}_u\times\mathbf{R}_u]\times\mathbf{R}]-\frac{H_u}{H}(\mathbf{r}_u\cdot\mathbf{R})\mathbf{R}\right\}$$

and $n-1$, other sets of three variables. Differentiating Eq. (3.5) in the text we can write:

$$d\mathbf{R}_u=d\mathbf{S}_u+\left(\frac{(\mathbf{R}\cdot\mathbf{S}_u)}{m(m+H)}+\frac{K_u}{m}\right)d\mathbf{R}$$
$$+\mathbf{R}\left\{\frac{(\mathbf{R}\cdot d\mathbf{S}_u)}{m(m+H)}+\frac{(\mathbf{S}_u\cdot d\mathbf{R})}{m(m+H)}+\frac{(\mathbf{S}_u\cdot d\mathbf{S}_u)}{mK_u}\right.$$
$$-\frac{(\mathbf{R}\cdot\mathbf{S}_u)}{m(m+H)^2}\frac{(\mathbf{R}\cdot d\mathbf{R})}{H}-\sum_v\frac{(\mathbf{S}_v\cdot d\mathbf{S}_v)}{K_v}$$
$$\left.\times\left[\frac{K_u}{m^2}+(\mathbf{R}\cdot\mathbf{S}_u)\left(\frac{1}{m^2(m+H)}+\frac{1+m/H}{m(m+H)^2}\right)\right]\right\},$$

$$\sum_u(\mathbf{r}_u\cdot d\mathbf{R}_u)=\sum_u\left(d\mathbf{S}_u\cdot\mathbf{r}_u+\frac{(\mathbf{r}_u\cdot\mathbf{R})}{m(m+H)}\mathbf{R}+\frac{(\mathbf{r}_u\cdot\mathbf{R})}{mK_u}\mathbf{S}_u\right.$$
$$-\sum_v(\mathbf{r}_v\cdot\mathbf{R})\left\{\frac{K_v}{m^2}+\frac{(\mathbf{R}\cdot\mathbf{S}_v)}{m^2H}\right\}\frac{\mathbf{S}_u}{K_u}\Big)$$
$$+\left[d\mathbf{R}\cdot\sum_u\left(\mathbf{r}_u\left\{\frac{(\mathbf{R}_u\cdot\mathbf{S}_u)}{m(m+H)}+\frac{K_u}{m}\right\}\right.\right.$$
$$\left.\left.+\frac{(\mathbf{r}_u\cdot\mathbf{R})}{m(m+H)}\mathbf{S}_u-\mathbf{R}\frac{(\mathbf{r}_u\cdot\mathbf{R})(\mathbf{R}\cdot\mathbf{S}_u)}{mH(m+H)^2}\right)\right].$$

Comparing this with

$$\textstyle\sum_u(\mathbf{r}_u\cdot d\mathbf{R}_u)\equiv\sum_u(\mathbf{s}_u\cdot d\mathbf{S}_u)+(\mathbf{r}\cdot d\mathbf{R}),\quad\sum_u d\mathbf{S}_u\equiv0,$$

we get:

$$\mathbf{r}=\sum_u\left\{\left(\frac{(\mathbf{R}\cdot\mathbf{S}_u)}{m(m+H)}+\frac{K_u}{m}\right)\mathbf{r}_u+\frac{1}{m(m+H)}\right.$$
$$\left.\times\left[(\mathbf{r}_u\cdot\mathbf{R})\mathbf{S}_u-\frac{(\mathbf{r}_u\cdot\mathbf{R})(\mathbf{R}\cdot\mathbf{S}_u)}{H(m+H)}\mathbf{R}\right]\right\},$$
$$\mathbf{r}=\sum_u\left\{\left(\frac{K_u+H_u}{m+H}\right)\mathbf{r}_u+\frac{(\mathbf{r}_u\cdot\mathbf{R})}{m(m+H)}\right.$$
$$\left.\times\left[\mathbf{S}_u+\frac{HK_u-mH_u}{H(m+H)}\mathbf{R}\right]\right\},\tag{1}$$

[7] G. Breit, Phys. Rev. **51**, 248 (1937), especially p. 259, Eq. (17.6), and p. 260, Eq. (18.2).
[8] G. Breit, reference 7, p. 253, Eq. (13.1).

$$=\sum_u\left\{\left(\frac{H_u}{m}-\frac{(\mathbf{R}\cdot\mathbf{R}_u)}{m(m+H)}\right)\mathbf{r}_u + \frac{(\mathbf{r}_u\cdot\mathbf{R})}{m(m+H)H}[H\mathbf{R}_u-\mathbf{R}H_u]\right\},$$

and, introducing a Lagrange multipler $\boldsymbol{\lambda}$:

$$\mathbf{s}_u+\boldsymbol{\lambda}=\mathbf{r}_u+(\mathbf{r}_u\cdot\mathbf{R})\left\{\frac{\mathbf{S}_u(m+H)+\mathbf{R}K_u}{m(m+H)K_u}\right\} -\sum_v(\mathbf{r}_v\cdot\mathbf{R})\frac{K_vH+(\mathbf{R}\cdot\mathbf{S}_v)}{m^2HK_v}\mathbf{S}_u$$

$$=\mathbf{r}_u+(\mathbf{r}_u\cdot R)\left\{\frac{\mathbf{R}_u(m+H)-\mathbf{R}H_u}{m(m+H)K_u}\right\} -\{\sum_v H_v(\mathbf{r}_v\cdot\mathbf{R})\} \times\left\{\frac{\mathbf{R}_u(m+H)-\mathbf{R}H_u}{mH(m+H)K_u}-\frac{\mathbf{R}}{mH(m+H)}\right\}; \quad (2)$$

$$(\mathbf{s}_u+\boldsymbol{\lambda}\cdot\mathbf{R})=\frac{H_u}{K_u}(\mathbf{r}_u\cdot\mathbf{R})-\left(\frac{H_u}{HK_u}-\frac{1}{m}\right) \times\{\textstyle\sum_v H_v(\mathbf{r}_v\cdot\mathbf{R})\},$$

$$\textstyle\sum_u K_u(\mathbf{s}_u+\boldsymbol{\lambda}\cdot\mathbf{R})=\sum_v H_v(\mathbf{r}_v\cdot\mathbf{R}),$$

$$(\mathbf{r}_u\cdot\mathbf{R})=\frac{K_u}{H_u}(\mathbf{s}_u+\boldsymbol{\lambda}\cdot\mathbf{R})-\left(\frac{K}{m+H}-\frac{1}{H}\right) \times\{\textstyle\sum_v K_v(\mathbf{s}_v+\boldsymbol{\lambda}\cdot\mathbf{R})\},$$

$$\mathbf{r}_u=\mathbf{s}_u+\boldsymbol{\lambda}-(\mathbf{s}_u+\boldsymbol{\lambda}\cdot\mathbf{R})\left\{\frac{\mathbf{S}_u(m+H)+\mathbf{R}K_u}{m(m+H)H_u}\right\} +\{\textstyle\sum_v K_u(\mathbf{s}_v+\boldsymbol{\lambda}\cdot\mathbf{R})\} \times\left\{\frac{\mathbf{S}_u(m+H)+\mathbf{R}K_u}{m^2(m+H)H_u}-\frac{\mathbf{R}}{mH(m+H)}\right\},$$

$$\mathbf{r}=\sum_u\left(\frac{K_u+H_u}{m+H}\right)(\mathbf{s}_u+\boldsymbol{\lambda})-\sum_u\frac{(\mathbf{s}_u+\boldsymbol{\lambda}\cdot\mathbf{R})\mathbf{S}_u}{m(m+H)} -\sum_u\frac{K_u(\mathbf{s}_u+\boldsymbol{\lambda}\cdot\mathbf{R})\mathbf{R}}{m(m+H)}$$

$$=\boldsymbol{\lambda}-\frac{(\boldsymbol{\lambda}\cdot\mathbf{R})\mathbf{R}}{H(m+H)}+\sum_v\left(\frac{K_v+H_v}{m+H}\right)\mathbf{s}_u -\sum_v\frac{(\mathbf{s}_u\cdot\mathbf{R})\mathbf{S}_u}{m(m+H)}-\sum_u\frac{K_u(\mathbf{s}_u\cdot\mathbf{R})\mathbf{R}}{mH(m+H)},$$

$$\mathbf{r}_u=\mathbf{r}+\mathbf{s}_u-\sum_v\frac{K_v+H_v}{m+H}\mathbf{s}_v+\sum_v\frac{(\mathbf{s}_v\cdot\mathbf{R})\mathbf{S}_v}{m(m+H)} -(\mathbf{s}_u\cdot\mathbf{R})\left\{\frac{\mathbf{S}_u(m+H)+\mathbf{R}K_u}{m(m+H)H_u}\right\} +\{\textstyle\sum_v K_v(\mathbf{s}_v\cdot\mathbf{R})\}\left\{\frac{\mathbf{S}_u(m+H)+\mathbf{R}K_u}{m^2(m+H)H_u}\right\}, \quad (3)$$

while

$$\textstyle\sum_u[\mathbf{r}_u\times\mathbf{R}_u]=[\mathbf{r}\times\mathbf{R}]+\sum_u[\mathbf{s}_u\times\mathbf{S}_u], \quad (4)$$

$$\textstyle\sum\mathbf{r}_uH_u=\mathbf{r}H-\frac{[\sum_u[\mathbf{s}_u\times\mathbf{S}_u]\times\mathbf{R}]}{m+H}. \quad (5)$$

APPENDIX II

In this Appendix we take the differential of the expression for $\mathbf{n}_u$ as given in Eq. (4.2) of the text and try to put it in the form of Eq. (4.8). Rewriting Eq. (4.2),

$$\mathbf{n}_0=\boldsymbol{\omega}_0+(\boldsymbol{\omega}_0\cdot\mathbf{R})\frac{\mathbf{S}_0}{m(m_0+K_0)}+\frac{(\boldsymbol{\omega}_0\cdot\mathbf{R})}{m(m+H)}\mathbf{R}+\frac{(\boldsymbol{\omega}_0\cdot\mathbf{R}_0)\mathbf{S}_0(m-H)}{m(m_0+K_0)(m_0+H_0)}-\frac{(\boldsymbol{\omega}_0\cdot\mathbf{R}_0)}{m(m_0+H_0)}\mathbf{R}.$$

We notice that it contains $\boldsymbol{\omega}_0$, $\mathbf{R}$, $\mathbf{S}_0$, m, H, R_0, H_0, K_0 as variables. But we can express the differentials of all these variables in terms of the differentials of the first four variables only. From (3.4), (3.5), (3.6) in the text

$$dH=(m/H)dm+(\mathbf{R}\cdot d\mathbf{R})/H,$$

$$d\mathbf{R}_0=-\frac{H_0}{mH}dm\mathbf{R}+\frac{K_0+H_0}{m+H}d\mathbf{R}+\frac{\mathbf{R}(\mathbf{S}_0\cdot d\mathbf{R})}{m(m+H)}-\frac{\mathbf{R}(mH_0-HK_0)}{mH(m+H)^2}(\mathbf{R}\cdot d\mathbf{R})+d\mathbf{S}_0+\mathbf{R}\left\{\frac{(\mathbf{S}_0\cdot d\mathbf{S}_0}{mK_0}+\frac{\mathbf{R}\cdot d\mathbf{S}_0}{m(m+H)}\right\},$$

$$dH_0=-\frac{dm}{mH}(HH_0-mK_0)+\frac{(\mathbf{S}_0\cdot d\mathbf{R})}{m}+\frac{K_0(\mathbf{R}\cdot d\mathbf{R})}{mH}+\frac{(\mathbf{R}\cdot d\mathbf{S}_0)}{m}+\frac{H(\mathbf{S}_0\cdot d\mathbf{S}_0)}{mK_0},$$

with

$$dm=\textstyle\sum_v dK_v=\sum_v(\mathbf{S}_v\cdot d\mathbf{S}_v)/K_v.$$

Using these relationships we can now get $d\mathbf{n}_0$ as the sum of four expressions: (*a*) one containing terms in $d\boldsymbol{\omega}_0$; (*b*) one containing terms in $d\mathbf{R}$; (*c*) one containing terms in $d\mathbf{S}_0$; (*d*) and one containing terms in dm. For (*a*) we have

$$d\mathbf{n}_0=d\boldsymbol{\omega}_0+(d\boldsymbol{\omega}_0\cdot\mathbf{R})\frac{\mathbf{S}_0}{m(m_0+K_0)}+\frac{(d\boldsymbol{\omega}_0\cdot\mathbf{R})}{m(m+H)}\mathbf{R}+\frac{(d\boldsymbol{\omega}_0\cdot\mathbf{R}_0)\mathbf{S}_0(m-H)}{m(m_0+K_0)(m_0+H_0)}-\frac{(d\boldsymbol{\omega}_0\cdot\mathbf{R}_0)}{m(m_0+H_0)}\mathbf{R}.$$

For (*d*) we have

$$dH=(m/H)dm;\quad d\mathbf{R}_0=-(H_0/mH)dm\mathbf{R};\quad dH_0=-(dm/mH)(HH_0-mK_0),$$

and

$$d\mathbf{n}_0=\left\{\frac{(\boldsymbol{\omega}_0\cdot\mathbf{R})\mathbf{S}_0}{m(m_0+K_0)}+\frac{(\boldsymbol{\omega}_0\cdot\mathbf{R})\mathbf{R}}{m(m+H)}+\frac{(\boldsymbol{\omega}_0\cdot\mathbf{R}_0)\mathbf{S}_0(m-H)}{m(m_0+K_0)(m_0+H_0)}-\frac{(\boldsymbol{\omega}_0\cdot\mathbf{R}_0)\mathbf{R}}{m(m_0+H_0)}\right\}\left(-\frac{dm}{m}\right)+\left\{\frac{(\boldsymbol{\omega}_0\cdot\mathbf{R})\mathbf{S}_0(m-H)}{m(m_0+K_0)(m_0+H_0)}\right.$$

$$\left.-\frac{(\boldsymbol{\omega}_0\cdot\mathbf{R})\mathbf{R}}{m(m_0+H_0)}\right\}\left(-\frac{H_0dm}{mH}\right)-\frac{(\boldsymbol{\omega}_0\cdot\mathbf{R})\mathbf{R}}{mH(m+H)}dm+\frac{(\boldsymbol{\omega}_0\cdot\mathbf{R}_0)\mathbf{S}_0\left(\frac{H-m}{m}\right)dm}{m(m_0+K_0)(m_0+H_0)}$$

$$+\left\{\frac{(\boldsymbol{\omega}_0\cdot\mathbf{R}_0)\mathbf{S}_0(m-H)}{m(m_0+K_0)(m_0+H_0)}-\frac{(\boldsymbol{\omega}_0\cdot\mathbf{R}_0)}{m(m_0+H_0)}\right\}\frac{dm(HH_0-mK_0)}{mH(m_0+H_0)},$$

$$d\mathbf{n}_0\equiv\frac{dm}{m}\frac{1}{H(m_0+H_0)}[\mathbf{n}_0\times[\mathbf{R}\times\mathbf{S}_0]].$$

For (*c*) we have:

$$d\mathbf{R}_0=d\mathbf{S}_0+\mathbf{R}\left\{\frac{(\mathbf{S}_0\cdot d\mathbf{S}_0)}{mK_0}+\frac{(\mathbf{R}\cdot d\mathbf{S}_0}{m(m+H)}\right\},\quad dH_0=\frac{(\mathbf{R}\cdot d\mathbf{S}_0)}{m}+\frac{H(\mathbf{S}_0\cdot d\mathbf{S}_0)}{mK_0},$$

and

$$d\mathbf{n}_0=\frac{(\boldsymbol{\omega}_0\cdot\mathbf{R})d\mathbf{S}_0}{m(m_0+K_0)}-\frac{(\boldsymbol{\omega}_0\cdot\mathbf{R})\mathbf{S}_0(\mathbf{S}_0\cdot d\mathbf{S}_0)}{m(m_0+K_0)^2K_0}+\frac{(\boldsymbol{\omega}_0\cdot\mathbf{R})d\mathbf{S}_0(m-H)}{m(m_0+K_0)(m_0+H_0)}-\frac{(\boldsymbol{\omega}_0\cdot\mathbf{R}_0)\mathbf{S}_0(\mathbf{S}_0\cdot d\mathbf{S}_0)(m-H)}{m(m_0+K_0)^2K_0(m_0+H_0)}$$

$$+\left\{\frac{\mathbf{S}_0(m-H)}{m(m_0+K_0)}-\frac{\mathbf{R}}{m}\right\}\left\{\frac{(\boldsymbol{\omega}_0\cdot d\mathbf{S}_0)+(\boldsymbol{\omega}_0\cdot\mathbf{R})\left[\frac{(\mathbf{S}_0\cdot d\mathbf{S}_0)}{mK_0}+\frac{(\mathbf{R}\cdot d\mathbf{S}_0)}{m(m+H)}\right]}{(m_0+H_0)}-\frac{(\boldsymbol{\omega}_0\cdot\mathbf{R}_0)}{(m_0+H_0)^2}\left[\frac{(\mathbf{R}\cdot d\mathbf{S}_0)}{m}+\frac{H(\mathbf{S}_0\cdot d\mathbf{S}_0)}{mK_0}\right]\right\},$$

$$=\frac{d\mathbf{S}_0}{m(m_0+K_0)}\left\{\frac{(H-m)}{(m_0+H_0)}(\mathbf{n}_0\cdot\mathbf{S}_0)+\frac{(m_0+K_0)}{(m_0+H_0)}(\mathbf{n}_0\cdot\mathbf{R})\right\}+\left\{\frac{\mathbf{S}_0(m-H)}{m(m_0+K_0)}-\frac{\mathbf{R}}{m_0}\right\}\left\{\frac{(\mathbf{n}_0\cdot d\mathbf{S}_0)}{(m_0+H_0)}+\frac{(\boldsymbol{\omega}_0\cdot\mathbf{R})(\mathbf{S}_0\cdot d\mathbf{S}_0)m_0}{mK_0(m_0+H_0)(m_0+K_0)}\right.$$

$$\left.-\frac{(\boldsymbol{\omega}_0\cdot\mathbf{R}_0)(\mathbf{S}_0\cdot d\mathbf{S}_0)(Hm_0+mK_0)}{m(m_0+K_0)K_0(m_0+H_0)^2}\right\}-\frac{(\boldsymbol{\omega}_0\cdot\mathbf{R})\mathbf{S}_0(\mathbf{S}_0\cdot d\mathbf{S}_0)}{m(m_0+K_0)^2K_0}-\frac{(\boldsymbol{\omega}_0\cdot\mathbf{R}_0)(\mathbf{S}_0\cdot d\mathbf{S}_0)}{m(m_0+K_0)^2K_0(m_0+H_0)},$$

$$=\frac{d\mathbf{S}_0}{m(m_0+K_0)}\left\{\frac{(H-m)}{(m_0+H_0)}(\mathbf{n}_0\cdot\mathbf{S}_0)+\left(\frac{m_0+K_0}{m_0+H_0}\right)(\mathbf{n}_0\cdot\mathbf{R})\right\}+\left\{\frac{\mathbf{S}_0(m-H)}{m(m_0+K_0)}-\frac{\mathbf{R}}{m}\right\}\left\{\frac{(\mathbf{n}_0\cdot d\mathbf{S}_0)}{(m_0+H_0)}-\frac{(\mathbf{n}_0\cdot\mathbf{S}_0)(\mathbf{S}_0\cdot d\mathbf{S}_0)}{K_0(m_0+H_0)(m_0+K_0)}\right\}$$

$$-\frac{\mathbf{S}_0(\mathbf{S}_0\cdot d\mathbf{S}_0)}{mK_0(m_0+K_0)^2}\left\{\frac{(H-m)}{(m_0+H_0)}(\mathbf{n}_0\cdot\mathbf{S}_0)+\frac{(m_0+K_0)}{(m_0+H_0)}(\mathbf{n}_0\cdot\mathbf{R})\right\},$$

and

$$d\mathbf{n}_0=[\mathbf{n}_0\times[d\mathbf{S}_0\times\mathbf{R}]]\frac{1}{m(m_0+H_0)}+[\mathbf{n}_0\times[d\mathbf{S}_0\times\mathbf{S}_0]]\frac{(H-m)}{m(m_0+K_0)(m_0+H_0)}+[\mathbf{n}_0\times[\mathbf{R}\times\mathbf{S}_0]]\frac{(\mathbf{S}_0\cdot d\mathbf{S}_0)}{mK_0(m_0+H_0)(m_0+K_0)}.$$

Finally for (*b*) we have:

$$dH=\frac{(\mathbf{R}\cdot d\mathbf{R})}{H},\quad dH_0=\frac{(\mathbf{S}_0\cdot d\mathbf{R})}{m}+\frac{K_0(\mathbf{R}\cdot d\mathbf{R})}{mH},\quad d\mathbf{R}_0=\frac{K_0+H_0}{m+H}d\mathbf{R}+\frac{\mathbf{R}(\mathbf{S}_0\cdot d\mathbf{R})}{m(m+H)}-\frac{\mathbf{R}(mH_0-HK_0)}{mH(m+H)^2}(\mathbf{R}\cdot d\mathbf{R}),$$

and

$$d\mathbf{n}_0=\frac{(\boldsymbol{\omega}_0\cdot d\mathbf{R})\mathbf{S}_0}{m(m_0+K_0)}+\frac{(\boldsymbol{\omega}_0\cdot d\mathbf{R})\mathbf{R}}{m(m+H)}+\frac{(\boldsymbol{\omega}_0\cdot\mathbf{R})d\mathbf{R}}{m(m+H)}-\frac{(\boldsymbol{\omega}_0\cdot\mathbf{R})\mathbf{R}}{m(m+H)^2}\frac{(\mathbf{R}\cdot d\mathbf{R})}{H}+\frac{(\boldsymbol{\omega}_0\cdot d\mathbf{R})\mathbf{S}_0(m-H)(K_0+H_0)}{m(m_0+K_0)(m_0+H_0)(m+H)}$$

$$+\frac{(\boldsymbol{\omega}_0\cdot\mathbf{R})(\mathbf{S}_0\cdot d\mathbf{R})(m-H)\mathbf{S}_0}{m^2(m_0+K_0)(m_0+H_0)(m+H)}-\frac{(\boldsymbol{\omega}_0\cdot\mathbf{R})(\mathbf{R}\cdot d\mathbf{R})(mH_0-HK_0)\mathbf{S}_0(m-H)}{m^2H(m+H)^2(m_0+K_0)(m_0+H_0)}-\frac{(\boldsymbol{\omega}_0\cdot d\mathbf{R})(\mathbf{R})(K_0+H_0)}{m(m_0+H_0)(m+H)}$$

$$-\frac{(\boldsymbol{\omega}_0\cdot\mathbf{R})(\mathbf{S}_0\cdot d\mathbf{R})\mathbf{R}}{m^2(m_0+H_0)(m+H)}+\frac{(\boldsymbol{\omega}_0\cdot\mathbf{R})(mH_0-HK_0)(\mathbf{R}\cdot d\mathbf{R})\mathbf{R}}{m^2H(m+H)^2(m_0+H_0)}-\frac{(\boldsymbol{\omega}_0\cdot\mathbf{R}_0)\mathbf{S}_0(\mathbf{R}\cdot d\mathbf{R})}{m(m_0+K_0)(m_0+H_0)H}-\frac{(\boldsymbol{\omega}_0\cdot\mathbf{R}_0)\mathbf{S}_0(m-H)}{m(m_0+K_0)(m_0+H_0)^2}$$

$$\times\left\{\frac{(\mathbf{S}_0\cdot d\mathbf{R})}{m}+\frac{K_0(\mathbf{R}\cdot d\mathbf{R})}{mH}\right\}-\frac{(\boldsymbol{\omega}_0\cdot\mathbf{R}_0)d\mathbf{R}}{m(m_0+H_0)}+\frac{(\boldsymbol{\omega}_0\cdot\mathbf{R}_0)\mathbf{R}}{m(m_0+H_0)^2}\left\{\frac{(\mathbf{S}_0\cdot d\mathbf{R})}{m}+\frac{K_0(\mathbf{R}\cdot d\mathbf{R})}{mH}\right\}.$$

In this expression we recognize terms in $\mathbf{S}_0$(i), terms in $d\mathbf{R}$(ii), and terms in $\mathbf{R}$(iii). For (i) we have

$$\frac{(\boldsymbol{\omega}_0\cdot d\mathbf{R})}{m(m_0+K_0)}+\frac{(\boldsymbol{\omega}_0\cdot d\mathbf{R})(m-H)(K_0+H_0)}{m(m_0+K_0)(m_0+H_0)(m+H)}+\frac{(\boldsymbol{\omega}_0\cdot\mathbf{R})(\mathbf{S}_0\cdot d\mathbf{R})(m-H)}{m^2(m_0+K_0)(m_0+H_0)(m+H)}-\frac{(\boldsymbol{\omega}_0\cdot\mathbf{R})(\mathbf{R}\cdot d\mathbf{R})(mH_0-HK_0)(m-H)}{m^2H(m+H)^2(m_0+K_0)(m_0+H_0)}$$

$$-\frac{(\boldsymbol{\omega}_0\cdot\mathbf{R}_0)(\mathbf{R}\cdot d\mathbf{R})}{m(m_0+K_0)(m_0+H_0)H}-\frac{(\boldsymbol{\omega}_0\cdot\mathbf{R}_0)(m-H)}{m(m_0+K_0)(m_0+H_0)^2}\frac{(\mathbf{S}_0\cdot d\mathbf{R})}{m}-\frac{(\boldsymbol{\omega}_0\cdot\mathbf{R}_0)(m-H)K_0(\mathbf{R}\cdot d\mathbf{R})}{m(m_0+K_0)(m_0+H_0)^2mH}$$

$$=\frac{(\boldsymbol{\omega}_0\cdot d\mathbf{R})(mm_0+2mH_0+m_0H+mK_0-HK_0)}{m(m+H)(m_0+K_0)(m_0+H_0)}+(\mathbf{S}_0\cdot d\mathbf{R})\left\{\frac{(\boldsymbol{\omega}_0\cdot\mathbf{R})(m-H)}{m^2(m_0+K_0)(m_0+H_0)(m+H)}-\frac{(\boldsymbol{\omega}_0\cdot\mathbf{R}_0)(m-H)}{m^2(m_0+K_0)(m_0+H_0)^2}\right\}$$

$$-(\mathbf{R}\cdot d\mathbf{R})\left\{\frac{(\boldsymbol{\omega}_0\cdot\mathbf{R})(mH_0-HK_0)(m-H)}{m^2H(m+H)^2(m_0+K_0)(m_0+H_0)}+\frac{(\boldsymbol{\omega}_0\cdot\mathbf{R}_0)(mm_0+mH_0+mK_0-HK_0)}{m^2(m_0+K_0)(m_0+H_0)^2H}\right\}$$

$$\equiv\frac{(\mathbf{n}_0\cdot d\mathbf{R})}{m(m_0+H_0)}-\frac{(\mathbf{n}_0\cdot\mathbf{R})(\mathbf{R}\cdot d\mathbf{R})}{mH(m+H)(m_0+H_0)}+\frac{2(\mathbf{n}_0\cdot d\mathbf{R})(mH_0-HK_0)}{m(m+H)(m_0+K_0)(m_0+H_0)}-\frac{2(\mathbf{n}_0\cdot\mathbf{R})(\mathbf{S}_0\cdot d\mathbf{R})}{m(m+H)(m_0+K_0)(m_0+H_0)}.$$

For (ii) we have

$$\frac{(\boldsymbol{\omega}_0\cdot\mathbf{R})}{m(m+H)}-\frac{(\boldsymbol{\omega}_0\cdot\mathbf{R}_0)}{m(m_0+H_0)}\equiv-\frac{(\mathbf{n}_0\cdot\mathbf{R}_0)}{m(m_0+H_0)}+\frac{(\mathbf{n}_0\cdot\mathbf{R})}{m(m+H)}-\frac{2(\mathbf{n}_0\cdot\mathbf{S}_0)(mH_0-HK_0)}{m(m+H)(m_0+K_0)(m_0+H_0)}+\frac{2(\mathbf{n}_0\cdot\mathbf{R})(K_0-m_0)}{m(m+H)(m_0+H_0)}.$$

For (iii) we have

$$\frac{(\boldsymbol{\omega}_0\cdot d\mathbf{R})}{m(m+H)}-\frac{(\boldsymbol{\omega}_0\cdot d\mathbf{R})(K_0+H_0)}{m(m_0+H_0)(m+H)}-\frac{(\boldsymbol{\omega}_0\cdot\mathbf{R})(\mathbf{R}\cdot d\mathbf{R})}{mH(m+H)^2}-\frac{(\boldsymbol{\omega}_0\cdot\mathbf{R})(\mathbf{S}_0\cdot d\mathbf{R})}{m^2(m_0+H_0)(m+H)}+\frac{(\boldsymbol{\omega}_0\cdot\mathbf{R})(mH_0-HK_0)(\mathbf{R}\cdot d\mathbf{R})}{m^2H(m+H)^2(m_0+H_0)}$$

$$+\frac{(\boldsymbol{\omega}_0\cdot R_0)}{m(m_0+H_0)^2}\left\{\frac{(\mathbf{S}_0\cdot d\mathbf{R})}{m}+\frac{K_0(\mathbf{R}\cdot d\mathbf{R})}{mH}\right\}$$

$$\equiv\frac{(\mathbf{n}_0\cdot d\mathbf{R})(K_0+H_0)}{m(m_0+H_0)(m+H)}-\frac{(\mathbf{n}_0\cdot d\mathbf{R})}{m(m+H)}-\frac{(\mathbf{n}_0\cdot\mathbf{R})(\mathbf{R}\cdot d\mathbf{R})(K_0+H_0)}{mH(m+H)^2(m_0+H_0)}+\frac{(\mathbf{n}_0\cdot\mathbf{R}_0)(\mathbf{R}\cdot d\mathbf{R})}{mH(m+H)(m_0+H_0)}-\frac{2(\mathbf{n}_0\cdot d\mathbf{R})(K_0-m_0)}{m(m+H)(m_0+H_0)}$$

$$-\frac{2(\mathbf{n}_0\cdot\mathbf{R})(K_0+H_0)(\mathbf{S}_0\cdot d\mathbf{R})}{m(m+H)^2(m_0+K_0)(m_0+H_0)}+\frac{2(\mathbf{n}_0\cdot\mathbf{R}_0)(\mathbf{S}_0\cdot d\mathbf{R})}{m(m+H)(m_0+K_0)(m_0+H_0)}.$$

Gathering all these expressions, we get

$$d\mathbf{n}_0=-\frac{(\mathbf{n}_0\cdot\mathbf{R}_0)d\mathbf{R}}{m(m_0+H_0)}+\frac{(\mathbf{n}_0\cdot d\mathbf{R})\mathbf{R}_0}{m(m_0+H_0)}-\frac{(\mathbf{n}_0\cdot d\mathbf{R})\mathbf{R}}{m(m+H)}+\frac{(\mathbf{n}_0\cdot\mathbf{R})d\mathbf{R}}{m(m+H)}-\frac{(\mathbf{n}_0\cdot\mathbf{R})(\mathbf{R}\cdot d\mathbf{R})\mathbf{R}_0}{mH(m+H)(m_0+H_0)}+\frac{(\mathbf{n}_0\cdot\mathbf{R}_0)(\mathbf{R}\cdot d\mathbf{R})\mathbf{R}}{mH(m+H)(m_0+H_0)}$$
$$-\frac{2(\mathbf{n}_0\cdot\mathbf{S}_0)(mH_0-HK_0)d\mathbf{R}}{m(m+H)(m_0+K_0)(m_0+H_0)}+\frac{2(\mathbf{n}_0\cdot d\mathbf{R})\mathbf{S}_0(mH_0-HK_0)}{m(m+H)(m_0+K_0)(m_0+H_0)}-\frac{2(\mathbf{n}_0\cdot d\mathbf{R})\mathbf{R}(K_0-m_0)}{m(m+H)(m_0+H_0)}$$
$$+\frac{2(\mathbf{n}_0\cdot\mathbf{R})d\mathbf{R}(K_0-m_0)}{m(m+H)(m_0+H_0)}-\frac{2(\mathbf{n}_0\cdot\mathbf{R})\mathbf{R}_0(\mathbf{S}_0\cdot d\mathbf{R})}{m(m+H)(m_0+K_0)(m_0+H_0)}+\frac{2(\mathbf{n}_0\cdot\mathbf{R}_0)\mathbf{R}(\mathbf{S}_0\cdot d\mathbf{R})}{m(m+H)(m_0+K_0)(m_0+H_0)}.$$

Now combining the terms two by two, we can write this last expression as:

$$d\mathbf{n}_0=\frac{[\mathbf{n}_0\times[\mathbf{R}_0\times d\mathbf{R}]]}{m(m_0+H_0)}-\frac{[\mathbf{n}_0\times[\mathbf{R}\times d\mathbf{R}]]}{m(m+H)}-\frac{[\mathbf{n}_0\times[\mathbf{R}_0\times\mathbf{R}]](\mathbf{R}\cdot d\mathbf{R})}{mH(m+H)(m_0+H_0)}-\frac{2[\mathbf{n}_0\times[d\mathbf{R}\times\mathbf{S}_0]](mH_0-HK_0)}{m(m+H)(m_0+K_0)(m_0+H_0)}$$
$$-\frac{2[\mathbf{n}_0\times[\mathbf{R}\times d\mathbf{R}]](K_0-m_0)}{m(m+H)(m_0+H_0)}-\frac{2[\mathbf{n}_0\times[\mathbf{R}_0\times\mathbf{R}]](\mathbf{S}_0\cdot d\mathbf{R})}{m(m+H)(m_0+K_0)(m_0+H_0)}$$
$$=\frac{[\mathbf{n}_0\times[\mathbf{R}_0\times d\mathbf{R}]]}{m(m_0+H_0)}-\frac{[\mathbf{n}_0\times[\mathbf{R}\times d\mathbf{R}]]}{m(m+H)}-\frac{[\mathbf{n}_0\times[\mathbf{R}_0\times\mathbf{R}]](\mathbf{R}\cdot d\mathbf{R})}{mH(m+H)(m_0+H_0)}-\frac{2[\mathbf{n}_0\times\mathbf{S}_0](\mathbf{R}_0\times[\mathbf{R}\times d\mathbf{R}])}{m(m+H)(m_0+K_0)(m_0+H_0)}.$$

Now collecting the (a), (b) and (c) expressions for $d\mathbf{n}_0$ we finally get:

$$d\mathbf{n}_0=d\boldsymbol{\omega}_0+\frac{(d\boldsymbol{\omega}_0\cdot\mathbf{R})\mathbf{S}_0}{m(m_0+K_0)}+\frac{(d\boldsymbol{\omega}_0\cdot\mathbf{R})\mathbf{R}}{m(m+H)}+\frac{(d\boldsymbol{\omega}_0\cdot\mathbf{R}_0)\mathbf{S}_0(m-H)}{m(m_0+K_0)(m_0+H_0)}-\frac{(d\boldsymbol{\omega}_0\cdot\mathbf{R}_0)}{m(m_0+H_0)}\mathbf{R}+\Bigg[\frac{[\mathbf{S}_0\times\mathbf{R}]dm}{mH(m_0+H_0)}+\frac{[\mathbf{R}\times d\mathbf{S}_0]}{m(m_0+H_0)}$$
$$+\frac{[\mathbf{S}_0\times d\mathbf{S}_0](H-m)}{m(m_0+K_0)(m_0+H_0)}+\frac{[\mathbf{S}_0\times\mathbf{R}](\mathbf{S}_0\cdot d\mathbf{S}_0)}{mK_0(m_0+H_0)(m_0+K_0)}-\frac{[\mathbf{R}_0\times d\mathbf{R}]}{m(m_0+H_0)}+\frac{[\mathbf{R}\times d\mathbf{R}]}{m(m+H)}+\frac{[\mathbf{R}_0\times\mathbf{R}](\mathbf{R}\cdot d\mathbf{R})}{mH(m+H)(m_0+H_0)}$$
$$+\frac{2\mathbf{S}_0(\mathbf{R}_0\cdot[\mathbf{R}\times d\mathbf{R}])}{m(m+H)(m_0+K_0)(m_0+H_0)}\times\mathbf{n}_0\Bigg].$$

Also,

$$\Bigg(\frac{[\mathbf{S}_0\times\mathbf{R}]dm}{mH(m_0+H_0)}+\frac{[\mathbf{R}\times d\mathbf{S}_0]}{m(m_0+H_0)}+\frac{[\mathbf{S}_0\times d\mathbf{S}_0](H-m)}{m(m_0+K_0)(m_0+H_0)}+\frac{[\mathbf{S}_0\times\mathbf{R}](\mathbf{S}_0\cdot d\mathbf{S}_0)}{mK_0(m_0+H_0)(m_0+K_0)}-\frac{(\mathbf{R}_0\times d\mathbf{R})}{m(m_0+H_0)}+\frac{[\mathbf{R}\times d\mathbf{R}]}{m(m+H)}$$
$$+\frac{[\mathbf{R}_0\times\mathbf{R}](\mathbf{R}\cdot d\mathbf{R})}{mH(m+H)(m_0+H_0)}+\frac{2\mathbf{S}_0(\mathbf{R}_0\cdot[\mathbf{R}\times d\mathbf{R}])}{m(m+H)(m_0+K_0)(m_0+H_0)}\cdot\mathbf{n}_0\Bigg)$$
$$=\Bigg(\frac{[\mathbf{S}_0\times\mathbf{R}]dm}{mH(m_0+H_0)}+\frac{[\mathbf{R}\times d\mathbf{S}_0]}{m(m_0+H_0)}+\frac{[\mathbf{S}_0\times d\mathbf{S}_0](H-m)}{m(m_0+K_0)(m_0+H_0)}+\frac{[\mathbf{S}_0\times\mathbf{R}](\mathbf{S}_0\cdot dS_0)}{mK_0(m_0+H_0)(m_0+K_0)}+\frac{2\mathbf{R}(\mathbf{S}_0\cdot[\mathbf{R}\times d\mathbf{S}_0])}{m(m+H)(m_0+K_0)(m_0+H_0)}$$
$$-\frac{[\mathbf{R}_0\times d\mathbf{R}]}{m(m_0+H_0)}+\frac{[\mathbf{R}\times d\mathbf{R}]}{m(m+H)}+\frac{[\mathbf{R}_0\times\mathbf{R}](\mathbf{R}\cdot d\mathbf{R})}{mH(m+H)(m_0+H_0)}\cdot\boldsymbol{\omega}_0\Bigg).$$

Using this result we can now write the contact transformation:

$$\sum_u(\mathbf{r}_u\cdot d\mathbf{R}_u)+\sum_u(\boldsymbol{\omega}_u\cdot d\boldsymbol{\pi}_u)$$
$$=\sum_u\Bigg(d\mathbf{S}_u\cdot\mathbf{r}_u+\frac{(\mathbf{r}_u\cdot\mathbf{R})}{m(m+H)}\mathbf{R}+\frac{(\mathbf{r}_u\cdot\mathbf{R})}{mK_u}\mathbf{S}_u-\sum_v\frac{(\mathbf{r}_v\cdot\mathbf{R})H_v\mathbf{S}_v}{mHK_u}+\frac{[\boldsymbol{\omega}_u\times\mathbf{R}]}{m(m_u+H_u)}+\frac{[\boldsymbol{\omega}_u\times\mathbf{S}_u](H-m)}{m(m_u+K_u)(m_u+H_u)}$$

$$+\frac{(\boldsymbol{\omega}_u\cdot[\mathbf{S}_u+R])\mathbf{S}_u}{mK_u(m_u+H_u)(m_u+K_u)}+\frac{2(\boldsymbol{\omega}_u\cdot\mathbf{R})[\mathbf{S}_u\times\mathbf{R}]}{m(m+H)(m_u+K_u)(m_u+H_u)}+\sum_v\frac{(\boldsymbol{\omega}_v\cdot[\mathbf{S}_v\times\mathbf{R}])}{(m_v+H_v)}\frac{\mathbf{S}_u}{mHK_u}\Bigg)$$

$$+\Bigg(d\mathbf{R}\cdot\sum_u\Bigg\{\mathbf{r}_u\Bigg(\frac{H_u}{m}-\frac{(\mathbf{R}\cdot\mathbf{R}_u)}{m(m+H)}+\frac{(\mathbf{r}_u\cdot\mathbf{R})}{mH(m+H)}(H\mathbf{R}_u-\mathbf{R}H_u)-\frac{[\boldsymbol{\omega}_u\times\mathbf{R}_u]}{m(m_u+H_u)}+\frac{[\boldsymbol{\omega}_u\times\mathbf{R}]}{m(m+H)}$$

$$+\frac{([\boldsymbol{\omega}_u\times\mathbf{R}]\cdot\mathbf{R})\mathbf{R}}{mH(m+H)(m_u+H_u)}\Bigg\}\Bigg)+\sum_u\Bigg(d\boldsymbol{\vartheta}_u\cdot\boldsymbol{\omega}_u+(\boldsymbol{\omega}_u\cdot\mathbf{R})\frac{\mathbf{S}_u}{m(m_u+K_u)}+\frac{(\boldsymbol{\omega}_u\cdot\mathbf{R})\mathbf{R}}{m(m+H)}$$

$$+\frac{(\boldsymbol{\omega}_u\cdot\mathbf{R}_u)\mathbf{S}_u(m-H)}{m(m_u+K_u)(m_u+H_u)}-\frac{(\boldsymbol{\omega}_u\cdot\mathbf{R}_u)\mathbf{R}}{m(m_u+H_u)}\Bigg), \quad (1)$$

which is of the form

$$\sum_u(\mathbf{r}_u\cdot d\mathbf{R}_u)+\sum_u(\boldsymbol{\omega}_u\cdot d\boldsymbol{\pi}_u)\equiv\sum_u(\mathbf{S}_u\cdot d\mathbf{S}_u)+(\mathbf{r}\cdot d\mathbf{R})+\sum_u(\mathbf{n}_u\cdot d\boldsymbol{\theta}_u),$$

where $\sum d\mathbf{S}_u=0$. We can also write for the total angular momentum:

$$\sum_u[\mathbf{s}_u\times\mathbf{S}_u]+[\mathbf{r}\times\mathbf{R}]+\sum_u\mathbf{n}_u$$

$$=\sum_u[\mathbf{r}_u\times\mathbf{R}_u]+\sum_u\frac{[[\boldsymbol{\omega}_u\times\mathbf{R}]\times\mathbf{S}_u]}{m(m_u+H_u)}+\sum_u\frac{[[\boldsymbol{\omega}_u\times\mathbf{S}_u]\times\mathbf{S}_u](H-m)}{m(m_u+K_u)(m_u+H_u)}+\sum_u\frac{2(\boldsymbol{\omega}_u\cdot\mathbf{R})[[\mathbf{S}_u\times\mathbf{R}]\times\mathbf{S}_u]}{m(m+H)(m_u+K_u)(m_u+H_u)}$$

$$-\sum_u\frac{[[\boldsymbol{\omega}_u\times\mathbf{R}_u]\times\mathbf{R}]}{m(m_u+H_u)}+\sum_u\boldsymbol{\omega}_u+\sum_u\frac{(\boldsymbol{\omega}_u\cdot\mathbf{R})\mathbf{S}_u}{m(m_u+K_u)}+\sum_u\frac{(\boldsymbol{\omega}_u\cdot\mathbf{R})\mathbf{R}}{m(m+H)}+\sum_u\frac{(\boldsymbol{\omega}_u\cdot\mathbf{R}_u)\mathbf{S}_u(m-H)}{m(m_u+K_u)(m_u+H_u)}$$

$$-\sum_u\frac{(\boldsymbol{\omega}_0\cdot\mathbf{R}_u)\mathbf{R}}{m(m_u+H_u)}=\sum_u[\mathbf{r}_u\times\mathbf{R}_u]+\sum_u\boldsymbol{\omega}_u. \quad (2)$$

Also,

$$H\mathbf{r}-\frac{[\sum_u[\mathbf{S}_u\times\mathbf{S}_u]+\sum_u\mathbf{n}_u\times\mathbf{R}]}{H+m}=\sum_u H_u\mathbf{r}_u-\sum_u\frac{[\boldsymbol{\omega}_u\times\mathbf{R}_u]}{H_u+m_u}. \quad (3)$$

Following the same method as above, Appendix I, now:

$$\mathbf{S}_u+\boldsymbol{\lambda}=\mathbf{r}_u+(\mathbf{r}_u\cdot\mathbf{R})\left\{\frac{\mathbf{S}_u(m+H)+\mathbf{R}K_u}{m(m+H)K_u}\right\}-\sum_v(\mathbf{r}_v\cdot\mathbf{R})H_v\frac{\mathbf{S}_u}{mHK_u}+\frac{[\boldsymbol{\omega}_u\times\mathbf{R}]}{m(m_u+H_u)}+\frac{[\boldsymbol{\omega}_u\times\mathbf{S}_u](H-m)}{m(m_u+K_u)(m_u+H_u)}$$

$$+\frac{(\boldsymbol{\omega}_u\cdot[\mathbf{S}_u\times\mathbf{R}])\mathbf{S}_u}{mK_u(m_u+H_u)(m_u+K_u)}+\frac{2(\boldsymbol{\omega}_u\cdot\mathbf{R})[\mathbf{S}_u\times\mathbf{R}]}{m(m+H)(m_u+K_u)(m_u+H_u)}+\sum_v\frac{(\boldsymbol{\omega}_v\cdot[\mathbf{S}_v\times\mathbf{R}])}{m_v+H_v}\frac{\mathbf{S}_u}{mHK_u}. \quad (4)$$

$$(\mathbf{S}_u+\boldsymbol{\lambda}\cdot\mathbf{R})=\frac{H_u}{K_u}(\mathbf{r}_u\cdot\mathbf{R})-\frac{(mH_u-HK_u)}{mHK_u}\{\textstyle\sum_v H_v(\mathbf{r}_v\cdot\mathbf{R})\}$$

$$+\frac{\{[\boldsymbol{\omega}_u\times\mathbf{S}_u]\cdot\mathbf{R}\}(H_u-K_u)}{K_u(m_u+H_u)(m_u+K_u)}+\sum_v\frac{(\boldsymbol{\omega}_v\cdot[\mathbf{S}_u\times\mathbf{R}])}{(m_v+H_v)}\frac{(mH_u-HK_u)}{mHK_u},$$

$$\sum_u K_u(\mathbf{S}_u+\boldsymbol{\lambda}\cdot\mathbf{R})=\sum_u H_u(\mathbf{r}_u\cdot\mathbf{R})+\sum_u\frac{([\boldsymbol{\omega}_u\times\mathbf{S}_u]\cdot\mathbf{R})(H_u-K_u)}{(m_u+H_u)(m_u+K_u)},$$

$$(\mathbf{r}_u\cdot\mathbf{R})=\frac{K_u}{H_u}(\mathbf{s}_u+\boldsymbol{\lambda}\cdot\mathbf{R})+\frac{(mH_u-HK_u)}{mHH_u}\sum_v K_v(\mathbf{s}_v+\boldsymbol{\lambda}\cdot\mathbf{R})-\frac{\{[\boldsymbol{\omega}_u\times\mathbf{S}_u]\cdot\mathbf{R}\}(H_u-K_u)}{H_u(m_u+H_u)(m_u+K_u)}$$

$$-\frac{(mH_u-HK_u)}{mHH_u}\sum_v\frac{([\boldsymbol{\omega}_v\times\mathbf{S}_v]\cdot\mathbf{R})}{m_v+K_v},$$

$$\mathbf{r}_u=\mathbf{s}_u+\boldsymbol{\lambda}-(\mathbf{s}_u+\boldsymbol{\lambda}\cdot\mathbf{R})\left\{\frac{\mathbf{S}_u(m+H)+\mathbf{R}K_u}{m(m+H)H_u}\right\}+\left\{\sum_v K_v(\mathbf{s}_v+\boldsymbol{\lambda}\cdot\mathbf{R})-\sum_v\frac{([\boldsymbol{\omega}_v\times\mathbf{S}_v]\cdot\mathbf{R})}{m_v+K_v}\right\}$$
$$\times\left\{\frac{\mathbf{S}_u(m+H)+\mathbf{R}K_u}{m^2(m+H)H_u}-\frac{\mathbf{R}}{mH(m+H)}\right\}-\frac{(\boldsymbol{\omega}_u\cdot[\mathbf{S}_u\times\mathbf{R}])\mathbf{S}_u}{mH_u(m_u+H_u)(m_u+K_u)}$$
$$+\frac{(\boldsymbol{\omega}_u\cdot[\mathbf{S}_u\times\mathbf{R}])\mathbf{R}(H_u-K_u)}{m(m+H)H_u(m_u+H_u)(m_u+K_u)}-\frac{[\boldsymbol{\omega}_u\times\mathbf{R}]}{m(m_u+H_u)}$$
$$-\frac{[\boldsymbol{\omega}_u\times\mathbf{S}_u](H-m)}{m(m_u+K_u)(m_u+H_u)}-\frac{2(\boldsymbol{\omega}_u\cdot\mathbf{R})[\mathbf{S}_u\times\mathbf{R}]}{m(m+H)(m_u+K_u)(m_u+H_u)},$$

$$\mathbf{r}=\sum_u\left(\frac{K_u+H_u}{m+H}\right)(\mathbf{s}_u+\boldsymbol{\lambda})-\sum_u\frac{(\mathbf{s}_u+\boldsymbol{\lambda}\cdot\mathbf{R})}{m(m+H)}\mathbf{s}_u-\sum_u\frac{K_u(\mathbf{s}_u+\boldsymbol{\lambda}\cdot\mathbf{R})\mathbf{R}}{mH(m+H)}+\sum_u\frac{(\boldsymbol{\omega}_u\cdot[\mathbf{S}_u\times\mathbf{R}])\mathbf{R}}{m(m+H)H(m_u+K_u)}$$
$$-\frac{2\sum_u(\boldsymbol{\omega}_u\cdot[\mathbf{S}_u\times\mathbf{R}])\mathbf{S}_u}{m(m+H)(m_u+H_u)(m_u+K_u)}+\sum_u\left(\frac{K_u+H_u}{m+H}\right)\left\{-\frac{[\boldsymbol{\omega}_u\times\mathbf{R}]}{m(m_u+H_u)}\right.$$
$$\left.-\frac{[\boldsymbol{\omega}_u\times\mathbf{S}_u](H-m)}{m(m_u+K_u)(m_u+H_u)}-\frac{2(\boldsymbol{\omega}_u\cdot\mathbf{R})[\mathbf{S}_u\times\mathbf{R}]}{m(m+H)(m_u+K_u)(m_u+H_u)}\right\}+\sum_u\left\{\frac{[\boldsymbol{\omega}_u\times\mathbf{R}]}{m(m+H)}-\frac{[\boldsymbol{\omega}_u\times R_u]}{m(m_u+H_u)}\right\},\quad(5)$$

and, as before, $\mathbf{r}_u-\mathbf{r}$ does not contain $\boldsymbol{\lambda}$.

PHYSICAL REVIEW VOLUME 92, NUMBER 5 DECEMBER 1, 1953

Reduction of Relativistic Two-Particle Wave Equations to Approximate Forms. II*

ZENO V. CHRAPLYVY
Saint Louis University, Saint Louis, Missouri
(Received August 28, 1953)

The method of reduction of two-particle relativistic wave equations (an extension of the Foldy-Wouthuysen method), as given in Part I, was applicable only if $m_{\rm I}\neq m_{\rm II}$. Other variants of the procedure, free from this restriction, are developed now. On the basis of a discussion of properties of the matrices involved, it is found that the postulate of an "even-even" transformed Hamiltonian was too far-reaching. The less stringent requirement of a "uU separating" or an "lL separating" $\mathcal{H}_{\rm tr}$ leads to a whole class of usable transformations, which includes the transformation of Part I as a special case. Another important special case, (that of the "least change" transformation) has been calculated through in detail. Different transformations give different expressions for $\mathcal{H}_{\rm tr}$, but they coincide after (as a part of the next step of the procedure) the matrices $\beta^{\rm I}$ and $\beta^{\rm II}$ are replaced by 1 (or -1). Consequently the reduced wave equation is the same in all cases.

IN a recent paper,[1] hereafter referred to as I,† a method was developed for conversion of relativistic two-particle wave equations from the full (16-component) into an approximate (4-component) form. The procedure consists of two steps: first, a canonical transformation (strictly speaking, a sequence of canonical transformations) is performed with the help of suitable generating functions; then, twelve components of the wave equation are rejected, and only the four upper-upper or the four lower-lower components are retained, namely that quadruple which describes states with both particles possessing positive energy (the other of these two quadruples corresponds to both particles having negative energy). *The same* transformation is required to make either choice possible.

The proposed scheme was patterned after the Foldy-Wouthuysen method for one-body equations.[2] As a matter of fact, the expression for the transformed Hamiltonian in I represents a plausible, though not trivial, generalization of that obtained by Foldy and Wouthuysen. But, remarkably, our method is not

* This work was supported in part by the Office of Scientific Research, Air Research and Development Command, U. S. Air Force.

[1] Z. V. Chraplyvy, Phys. Rev. **91**, 388 (1953). We take over the terminology and notation used there.

† *Errata to* I.—In Eq. (4) the first minus sign is to be replaced by a plus sign. In Eq. (7j) the numerical coefficient is to be 1/8 (not 3/16).

[2] L. L. Foldy and S. A. Wouthuysen, Phys. Rev. **78**, 29 (1950).

applicable, if the two particles happen to have equal masses. Now, it is conceivable that more variants of the reduction procedure could be devised,[3] which, like that of I, would be extensions of the F-W method, but not restricted by the condition $m_{\rm I}\neq m_{\rm II}$. The investigation of such possibilities must be preceded by a discussion and classification of matrices.

REPRESENTATION OF MATRICES

The matrices of a two-particle wave equation consist of 256 elements each, labeled by two pairs of indices, Ω_{jkJK} $(j, k, J, K=1, 2, 3, 4)$. In order to represent them by means of two-dimensional arrays, we adopt the following convention: each such array will be subdivided into 16 submatrices; the second pair of subscripts (JK) will indicate the submatrix, the first pair (jk) the position of the element within it. Whenever a matrix can be represented as a direct product of two fourth-rank matrices,[4] our convention amounts to taking the "left" direct product[5] denoted by $\cdot\times$. Also, we consistently arrange the components ψ_{kK} of the ψ spinor in a column (rather than a square array), with K specifying one of its four subcolumns, and k the position within the subcolumn.

Examples:

$$\beta^{\rm I}=\beta\cdot\times\delta=\begin{pmatrix}\beta&0&0&0\\0&\beta&0&0\\0&0&\beta&0\\0&0&0&\beta\end{pmatrix},$$

$$\beta^{\rm II}=\delta\cdot\times\beta=\begin{pmatrix}\delta&0&0&0\\0&\delta&0&0\\0&0&-\delta&0\\0&0&0&-\delta\end{pmatrix},$$

$$\alpha_x{}^{\rm I}=\alpha_x\cdot\times\delta=\begin{pmatrix}\alpha_x&0&0&0\\0&\alpha_x&0&0\\0&0&\alpha_x&0\\0&0&0&\alpha_x\end{pmatrix},$$

$$\alpha_x{}^{\rm II}=\delta\cdot\times\alpha_x=\begin{pmatrix}0&0&\delta&0\\0&0&0&-\delta\\\delta&0&0&0\\0&-\delta&0&0\end{pmatrix},$$

$$\alpha_y{}^{\rm I}\alpha_x{}^{\rm II}=(\alpha_y\cdot\times\delta)(\delta\cdot\times\alpha_x)=\alpha_y\cdot\times\alpha_x=\begin{pmatrix}0&0&\alpha_y&0\\0&0&0&-\alpha_y\\\alpha_y&0&0&0\\0&-\alpha_y&0&0\end{pmatrix},$$

$$\alpha_y{}^{\rm II}\alpha_x{}^{\rm I}=(\delta\cdot\times\alpha_y)(\alpha_x\cdot\times\delta)=\alpha_x\cdot\times\alpha_y=\begin{pmatrix}0&0&0&-i\alpha_x\\0&0&i\alpha_x&0\\0&-i\alpha_x&0&0\\i\alpha_x&0&0&0\end{pmatrix}.$$

[3] This is quite independent of the question as to whether the original F-W method itself is unique for its purposes. A note on this subject will be published soon.

[4] This is not necessarily so in all cases, in particular following certain transformations to be introduced later.

[5] See C. C. MacDuffee, *The Theory of Matrices* (Chelsea Publishing Company, New York, 1946), p. 81.

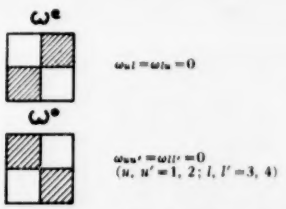

FIG. 1. The two basic types of 4×4 matrices: even and odd. At least all the shaded areas are occupied by zero elements.

($\alpha_x, \alpha_y, \alpha_z, \beta$ are the Dirac matrices and δ the fourth-rank unit matrix.)

Thus, we have fixed the manner in which matrix elements are to be arranged, and in the following classification of matrices we can often make use of convenient diagrams rather than the imperspicuous algebraic relationships accompanying them. In connection with this we have to mention the effect of the matrix multipliers $\frac{1}{2}(1+\beta^{\rm I})$, $\frac{1}{2}(1+\beta^{\rm II})$, $\frac{1}{2}(1+\beta^{\rm I}\beta^{\rm II})$, $\frac{1}{2}(1-\beta^{\rm I})$, $\frac{1}{2}(1-\beta^{\rm II})$, and $\frac{1}{2}(1-\beta^{\rm I}\beta^{\rm II})$. Since we have

$$\tfrac{1}{2}(1+\beta^{\rm I})=\begin{pmatrix}\kappa&0&0&0\\0&\kappa&0&0\\0&0&\kappa&0\\0&0&0&\kappa\end{pmatrix},\quad \tfrac{1}{2}(1+\beta^{\rm II})=\begin{pmatrix}\delta&0&0&0\\0&\delta&0&0\\0&0&0&0\\0&0&0&0\end{pmatrix},$$

$$\tfrac{1}{2}(1+\beta^{\rm I}\beta^{\rm II})=\begin{pmatrix}\kappa&0&0&0\\0&\kappa&0&0\\0&0&\lambda&0\\0&0&0&\lambda\end{pmatrix},$$

etc., with

$$\kappa=\begin{pmatrix}1&&&\\&1&&\\&&0&\\&&&0\end{pmatrix},\quad \lambda=\begin{pmatrix}0&&&\\&0&&\\&&1&\\&&&1\end{pmatrix},$$

it follows that each of these six factors, when pre-multiplied (post-multiplied) into a given matrix, produces zero elements arranged in double rows (columns) after a pattern characteristic of that factor.

CLASSIFICATION OF MATRICES

According to Foldy and Wouthuysen, any 4×4 matrix is either even, or odd, or a sum of an even and an odd matrix:

$$\omega=\omega^e+\omega^o=\tfrac{1}{2}(\omega+\beta\omega\beta)+\tfrac{1}{2}(\omega-\beta\omega\beta). \tag{1}$$

For a matrix to be even (odd), it has to commute (anticommute) with β; at least half of its elements have to be zeros, distributed as is shown in Fig. 1.

In order to obtain an analogous classification of the 16×16 matrices, we consider the following decomposition of the general matrix Ω:

$$\Omega=\Omega^{ee}+\Omega^{eo}+\Omega^{oe}+\Omega^{oo}, \tag{2}$$

with

$$\Omega^{ee}=\tfrac{1}{4}(\Omega+\beta^{\rm I}\Omega\beta^{\rm I}+\beta^{\rm II}\Omega\beta^{\rm II}+\beta^{\rm I}\beta^{\rm II}\Omega\beta^{\rm I}\beta^{\rm II}); \tag{2a}$$

$$\Omega^{eo}=\tfrac{1}{4}(\Omega+\beta^{\rm I}\Omega\beta^{\rm I}-\beta^{\rm II}\Omega\beta^{\rm II}-\beta^{\rm I}\beta^{\rm II}\Omega\beta^{\rm I}\beta^{\rm II}); \tag{2b}$$

$$\Omega^{oe}=\tfrac{1}{4}(\Omega-\beta^{\rm I}\Omega\beta^{\rm I}+\beta^{\rm II}\Omega\beta^{\rm II}-\beta^{\rm I}\beta^{\rm II}\Omega\beta^{\rm I}\beta^{\rm II}); \tag{2c}$$

$$\Omega^{oo}=\tfrac{1}{4}(\Omega-\beta^{\rm I}\Omega\beta^{\rm I}-\beta^{\rm II}\Omega\beta^{\rm II}+\beta^{\rm I}\beta^{\rm II}\Omega\beta^{\rm I}\beta^{\rm II}). \tag{2d}$$

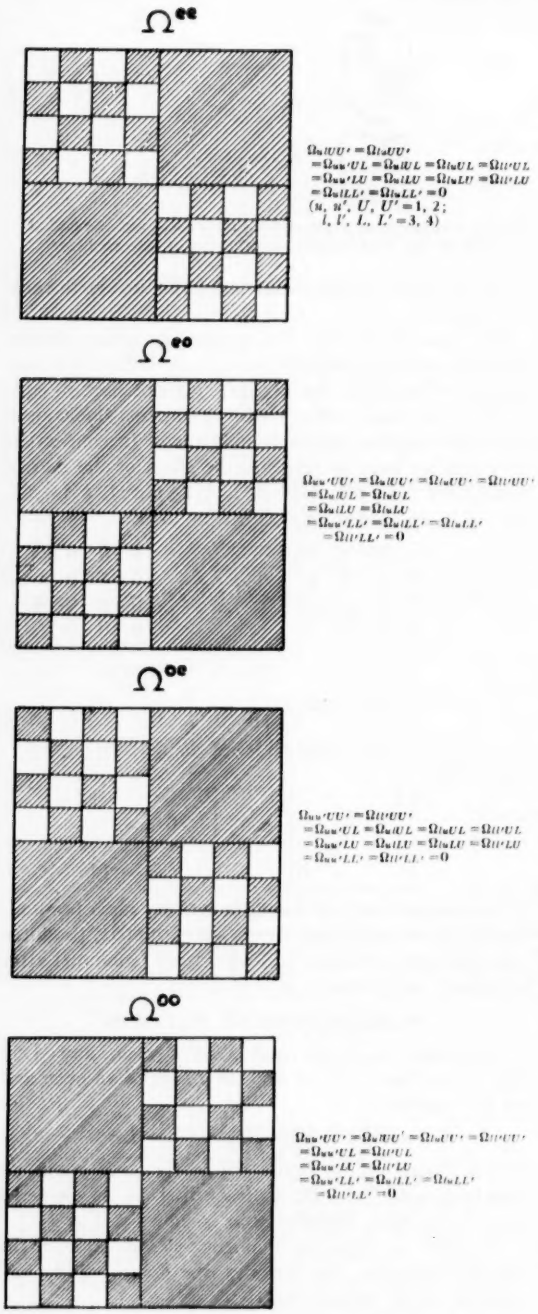

FIG. 2. The four basic types of 16×16 matrices: even-even, even-odd, odd-even, odd-odd.

Four basic types of matrices, the even-even, even-odd, odd-even, and odd-odd are defined[6] by the expressions (2a), (2b), (2c), (2d) respectively. Their commutation properties with β^{I} and β^{II} (see I, p. 389) can be deduced from the defining formulas. These formulas, when written in the form

$$\Omega^{ee} = \tfrac{1}{4}(1+\beta^{II})\Omega'(1+\beta^{II}) + \tfrac{1}{4}(1-\beta^{II})\Omega'(1-\beta^{II})$$

with

$$\Omega' = \tfrac{1}{4}(1+\beta^{I})\Omega(1+\beta^{I}) + \tfrac{1}{4}(1-\beta^{I})\Omega(1-\beta^{I}), \quad (3a)$$

etc., yield information as to which (at least) of the elements must be equal to zero, in order that the matrix be even-even, etc. Figure 2 shows the characteristic distribution of zeros in matrices of the four basic types.

An even-even matrix has the important property that it "keeps apart" the four kinds of components of the ψ spinor. This means that in the product $\Omega^{ee}\psi$, elements $(\Omega\psi)_{uU}$ are expressed entirely in terms of upper-upper components ψ_{uU}, and likewise elements $(\Omega\psi)_{uL}$, $(\Omega\psi)_{lU}$, $(\Omega\psi)_{lL}$ in terms of the ψ_{uL}, ψ_{lU}, ψ_{lL} respectively. Also in this regard the *ee* matrix appears to be a direct extension of Foldy's concept of an even matrix (see I, p. 388). However, there exists another matrix for which the same claim can be made. Its structure is shown by the first diagram of Fig. 3. The conditions imposed on it are weaker, it need not have as many zeros as an *ee* matrix; hence, its effect is smaller. When multiplied into ψ, it merely prevents the upper-upper components of ψ from mixing with components of other kinds, which means: $(\Omega\psi)_{uU}$ is expressed by the ψ_{uU} only, whereas the expressions for $(\Omega\psi)_{uL}$, $(\Omega\psi)_{lU}$, $(\Omega\psi)_{lL}$ do not

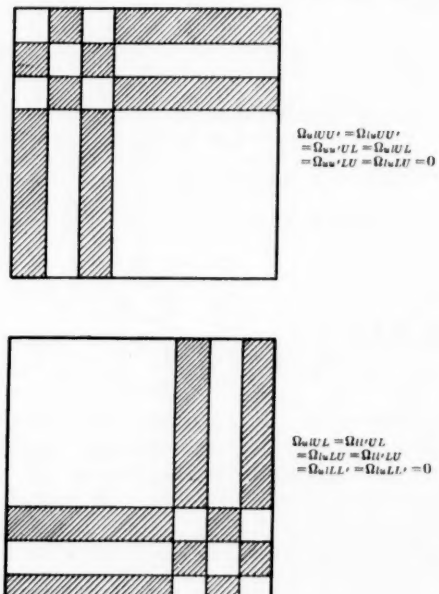
$\Omega_{uU}\Omega_{u'U'} = \Omega_{uU}\Omega_{uU'} = \Omega_{uU}\Omega_{u'U} = \Omega_{uU}\Omega_{uL} = \Omega_{uU}\Omega_{u'L} = \Omega_{uU}\Omega_{uL'} = \Omega_{uU}\Omega_{u'L'} = 0$
$\Omega_{uU}\Omega_{lU} = \Omega_{uU}\Omega_{lL} = \Omega_{uU}\Omega_{lL'} = \Omega_{uL}\Omega_{lU} = \Omega_{uL}\Omega_{lL} = \Omega_{uL}\Omega_{lL'} = \Omega_{u'L}\Omega_{lU} = \Omega_{u'L}\Omega_{lL} = \Omega_{u'L}\Omega_{lL'} = 0$

FIG. 3. Two special types of 16×16 matrices: the uU-separating and the lL-separating matrix.

[6] The definition used in I refers only to matrices representable as direct products and is, therefore, too narrow for the purposes of the present paper.

contain ψ_{uU} components. Such a matrix will be called "uU separating."

The algebraic equivalent of the diagram under consideration is found to be

$$\Omega^{us}=\Omega-\tfrac{1}{4}(1+\beta^{\mathrm{I}})(1+\beta^{\mathrm{II}})\Omega-\tfrac{1}{4}\Omega(1+\beta^{\mathrm{I}})(1+\beta^{\mathrm{II}})+\tfrac{1}{8}(1+\beta^{\mathrm{I}})(1+\beta^{\mathrm{II}})\Omega(1+\beta^{\mathrm{I}})(1+\beta^{\mathrm{II}}), \quad (4)$$

with Ω arbitrary. Every uU-separating matrix can be represented in this form. To simplify this rather unwieldy expression, we specialize it, assuming successively that Ω (and consequently also Ω^{us} itself) is even-even, even-odd, etc. If we make use of the commutation properties of β^{I} and β^{II}, we obtain the following set of rules: (1) Any even-even matrix is uU separating (but not *vice versa*). (2) An even-odd matrix is uU separating if, and only if, it can be written in the form $\frac{1}{2}(1-\beta^{\mathrm{I}})\Omega^{eo}$. Similarly, (3), (4) an odd-even matrix is rendered uU separating by the factor $\frac{1}{2}(1-\beta^{\mathrm{II}})$ in front of it, and an odd-odd matrix by the factor $\frac{1}{2}(1-\beta^{\mathrm{I}}\beta^{\mathrm{II}})$.

Rule (1) is easily verified by comparison of the corresponding diagrams. Rules (2), (3), (4) are illustrated by Fig. 4. For instance, it is seen that pre-multiplication by $\frac{1}{2}(1-\beta^{\mathrm{I}})$ provides for additional zeros in Ω^{eo}, so as to make it fit into the first scheme of Fig. 3.

The name "lL separating" is proposed for matrices possessing the property that in the elements of the product $(\Omega\psi)$ the lL components of ψ are not mixed with components of the other kinds. The most general algebraic expression for an lL-separating matrix,

$$\Omega^{ls}=\Omega-\tfrac{1}{4}(1-\beta^{\mathrm{I}})(1-\beta^{\mathrm{II}})\Omega-\tfrac{1}{4}\Omega(1-\beta^{\mathrm{I}})(1-\beta^{\mathrm{II}})+\tfrac{1}{8}(1-\beta^{\mathrm{I}})(1-\beta^{\mathrm{II}})\Omega(1-\beta^{\mathrm{I}})(1-\beta^{\mathrm{II}}) \quad (5)$$

and the corresponding distribution of zero elements (second diagram of Fig. 3) are analogous to those for uU-separating matrices. So are the four rules: (1) Any even-even matrix is lL separating. (2), (3), (4) The left multipliers, which convert a matrix into an lL-separating one, are $\frac{1}{2}(1+\beta^{\mathrm{I}})$, $\frac{1}{2}(1+\beta^{\mathrm{II}})$, and $\frac{1}{2}(1-\beta^{\mathrm{I}}\beta^{\mathrm{II}})$ for an *eo*, *oe*, *oo* matrix respectively.

Two more kinds of "separating" matrices with similar properties could be defined, but this would not lead to an exhaustive classification of matrices.

CHOICE OF GENERATING FUNCTIONS FOR CANONICAL TRANSFORMATIONS

The original wave equation $\mathfrak{H}\psi=E\psi$ (or, alternatively, $\mathfrak{H}\psi=-E\psi$) has to be transformed into $\mathfrak{H}_{\mathrm{tr}}\psi_{\mathrm{tr}}=E\psi_{\mathrm{tr}}$ (or $\mathfrak{H}_{\mathrm{tr}}\psi_{\mathrm{tr}}=-E\psi_{\mathrm{tr}}$), because we intend to separate out and to retain the only four component-equations which contain only the uU components (or the lL components) of the spinor ψ. That is, the transformed Hamiltonian $\mathfrak{H}_{\mathrm{tr}}$ is expected to be uU separating in the one case, and lL separating in the other. Any other effect of the transformation is either superfluous or irrelevant. Now the transformation proposed in I led to an even-even $\mathfrak{H}_{\mathrm{tr}}$; therefore, while satisfactory, it overshot the mark: instead of providing us with one suitable quadruple of equations, disentangled from the rest, it yielded four quadruples, not interlinked with each other.

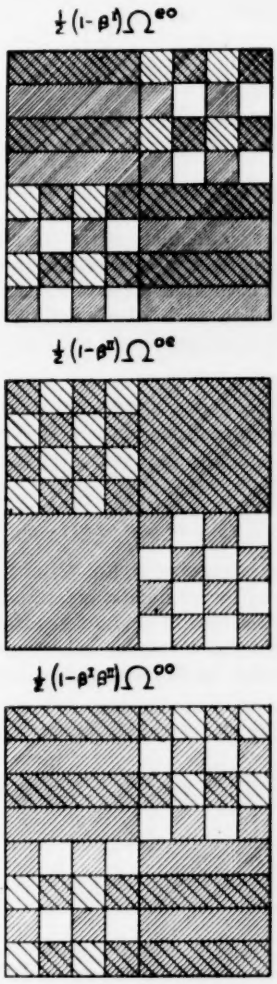

FIG. 4. The narrow-gauge shading shows the zeros due to the basic *eo*, *oe*, *oo* character of the matrix; the wide-gauge shading the zeros introduced by the respective left multiplier.

In accordance with the present more limited objective of the transformation, its generating function will now be chosen according to less stringent rules; iS will consist of expressions of the following form (rather than that given in Eq. (5a, b, c) of I]:

$$\mathfrak{S}_{eo}=\frac{\beta^{\mathrm{II}}}{2m_{\mathrm{II}}c^2}\left\{t_{eo}+\frac{1\mp\beta^{\mathrm{I}}}{2}\mathfrak{t}_{eo}\right\}, \quad (6a)$$

$$\mathfrak{S}_{oe}=\frac{\beta^{\mathrm{I}}}{2m_{\mathrm{I}}c^2}\left\{t_{oe}+\frac{1\mp\beta^{\mathrm{II}}}{2}\mathfrak{t}_{oe}\right\}; \quad (6b)$$

$$\mathfrak{S}_{oo}=\frac{1}{4c^2}\left\{\frac{\beta^{\mathrm{I}}+\beta^{\mathrm{II}}}{m_{\mathrm{I}}+m_{\mathrm{II}}}t_{oo}+\frac{\beta^{\mathrm{I}}-\beta^{\mathrm{II}}}{m_{\mathrm{I}}-m_{\mathrm{II}}}\mathrm{t}_{oe}\right\},\quad \text{if } m_{\mathrm{I}}\neq m_{\mathrm{II}};\qquad (6c)$$

$$\mathfrak{S}_{oo}'=\frac{1}{8mc^2}\{(\beta^{\mathrm{I}}+\beta^{\mathrm{II}})t_{oo}+(1-\beta^{\mathrm{I}}\beta^{\mathrm{II}})\mathrm{t}_{oo}'\}\quad \text{if } m_{\mathrm{I}}=m_{\mathrm{II}}.\ (6d)$$

Here t_{eo}, t_{oe}, t_{oo} are terms appearing in the Hamiltonian; t_{eo}, etc., is a term obtained from t_{eo}, etc., by replacing its matrix part by another matrix which is of the same (eo, etc.) type, but otherwise arbitrary. Wherever double signs occur, the upper one refers to a transformation leading to a uU-separating $\mathfrak{IC}_{\mathrm{tr}}$, whereas the lower one is to be taken, if an lL-separating $\mathfrak{IC}_{\mathrm{tr}}$ is required.

It is easily verified that

$$t_{eo}+[\mathfrak{S}_{eo},\ (\beta^{\mathrm{I}}m_{\mathrm{I}}+\beta^{\mathrm{II}}m_{\mathrm{II}})c^2]=-\tfrac{1}{2}(1\mp\beta^{\mathrm{I}})\mathrm{t}_{eo};$$
$$t_{oe}+[\mathfrak{S}_{oe},\ (\beta^{\mathrm{I}}m_{\mathrm{I}}+\beta^{\mathrm{II}}m_{\mathrm{II}})c^2]=-\tfrac{1}{2}(1\mp\beta^{\mathrm{II}})\mathrm{t}_{oe};$$
$$t_{oo}+[\mathfrak{S}_{oo},\ (\beta^{\mathrm{I}}m_{\mathrm{I}}+\beta^{\mathrm{II}}m_{\mathrm{II}})c^2]=\tfrac{1}{2}(1-\beta^{\mathrm{I}}\beta^{\mathrm{II}})(t_{oo}-\mathrm{t}_{oo});$$
$$t_{oo}+[\mathfrak{S}_{oo}',\ (\beta^{\mathrm{I}}+\beta^{\mathrm{II}})mc^2]=\tfrac{1}{2}(1-\beta^{\mathrm{I}}\beta^{\mathrm{II}})t_{oo},$$

which means: when used in Eq. (2) of I, the terms $\mathfrak{S}_{eo}$ of iS changes (by its highest-order contribution) the even-odd (undesirable) term t_{eo} of the Hamiltonian into another one, again even-odd, but acceptable, since it is uU separating (or lL separating). The undesirable terms t_{oe}, t_{oo} are affected likewise by $\mathfrak{S}_{oe}$, $\mathfrak{S}_{oo}$, (or $\mathfrak{S}_{oo}'$), respectively. In addition, each of the $\mathfrak{S}$ expressions will contribute some terms of lower order, of which the even-even and the acceptable ones will appear in the final $\mathfrak{IC}_{\mathrm{tr}}$, whereas those of undesired types must be treated in a similar manner by means of subsequent transformations.

Because of the mentioned arbitrariness in t_{eo}, etc., the expressions (6) are rather general;[7] in fact, they yield a whole class of transformations. Special cases include: for $\mathrm{t}_{eo}=\mathrm{t}_{oe}=0$, $\mathrm{t}_{oo}=t_{oo}$ ($m_{\mathrm{I}}\neq m_{\mathrm{II}}$), the "radical" transformation of I, which not only modifies, but even destroys undesirable terms; and, as the other extreme, for $\mathrm{t}_{eo}=-t_{eo}$, $\mathrm{t}_{oe}=-t_{oe}$, $\mathrm{t}_{oo}=\mathrm{t}_{oo}'=0$, the "least change" transformation, which secures the indispensable amount of modification, putting the necessary zeros in the matrices so as to make them acceptable, without causing any further "damage." It should be remarked that this is not the simplest transformation, which we rather should expect for $\mathrm{t}_{eo}=\mathrm{t}_{oe}=\mathrm{t}_{oo}=\mathrm{t}_{oo}'=0$.

THE TRANSFORMED HAMILTONIANS

By repeated application of the "least change" transformation, the following expression for the transformed Hamiltonian, approximate out to the order $(1/c)^2$, has been obtained:

$$\mathfrak{IC}_{\mathrm{tr}}=\beta^{\mathrm{I}}m_{\mathrm{I}}c^2+\beta^{\mathrm{II}}m_{\mathrm{II}}c^2+(\mathcal{E}\mathcal{E}) \qquad (7a)$$

$$+\frac{\beta^{\mathrm{I}}(1\pm\beta^{\mathrm{II}})}{4m_{\mathrm{I}}c^2}(\mathcal{O}\mathcal{E})^2+\frac{\beta^{\mathrm{II}}(1\pm\beta^{\mathrm{I}})}{4m_{\mathrm{II}}c^2}(\mathcal{E}\mathcal{O})^2 \qquad (7b)$$

$$+\frac{1\pm\beta^{\mathrm{II}}}{16m_{\mathrm{I}}^2c^4}[[(\mathcal{O}\mathcal{E}),(\mathcal{E}\mathcal{E})],(\mathcal{O}\mathcal{E})]+\frac{1\pm\beta^{\mathrm{I}}}{16m_{\mathrm{II}}^2c^4}[[(\mathcal{E}\mathcal{O}),(\mathcal{E}\mathcal{E})],(\mathcal{E}\mathcal{O})] \qquad (7c)$$

$$-\frac{\beta^{\mathrm{I}}(1\pm\beta^{\mathrm{II}})}{16m_{\mathrm{I}}^3c^6}(\mathcal{O}\mathcal{E})^4-\frac{\beta^{\mathrm{II}}(1\pm\beta^{\mathrm{I}})}{16m_{\mathrm{II}}^3c^6}(\mathcal{E}\mathcal{O})^4 \qquad (7d)$$

$$+\frac{\beta^{\mathrm{I}}\beta^{\mathrm{II}}\pm\beta^{\mathrm{I}}\pm2\beta^{\mathrm{II}}}{32m_{\mathrm{I}}m_{\mathrm{II}}c^4}[[(\mathcal{O}\mathcal{E}),(\mathcal{O}\mathcal{O})]_+,(\mathcal{E}\mathcal{O})]_+ +\frac{\beta^{\mathrm{I}}\beta^{\mathrm{II}}\pm\beta^{\mathrm{II}}\pm2\beta^{\mathrm{I}}}{32m_{\mathrm{I}}m_{\mathrm{II}}c^4}[[(\mathcal{E}\mathcal{O}),(\mathcal{O}\mathcal{O})]_+,(\mathcal{O}\mathcal{E})]_+$$
$$+\frac{1\mp\beta^{\mathrm{II}}}{32m_{\mathrm{I}}m_{\mathrm{II}}c^4}[[(\mathcal{O}\mathcal{E}),(\mathcal{O}\mathcal{O})],(\mathcal{E}\mathcal{O})]+\frac{1\mp\beta^{\mathrm{I}}}{32m_{\mathrm{I}}m_{\mathrm{II}}c^4}[[(\mathcal{E}\mathcal{O}),(\mathcal{O}\mathcal{O})],(\mathcal{O}\mathcal{E})] \qquad (7e)$$

$$+\frac{\beta^{\mathrm{I}}+\beta^{\mathrm{II}}}{4(m_{\mathrm{I}}+m_{\mathrm{II}})c^2}(\mathcal{O}\mathcal{O})^2 \qquad (7f)$$

$$+\frac{\beta^{\mathrm{I}}+\beta^{\mathrm{II}}}{16(m_{\mathrm{I}}+m_{\mathrm{II}})m_{\mathrm{I}}m_{\mathrm{II}}c^6}[(\mathcal{O}\mathcal{E}),(\mathcal{E}\mathcal{O})]^2 \qquad (7g)$$

$$-\frac{(1\pm\beta^2)(1\pm\beta^{\mathrm{II}})(\beta^{\mathrm{I}}m_{\mathrm{I}}+\beta^{\mathrm{II}}m_{\mathrm{II}})}{64m_{\mathrm{I}}^2m_{\mathrm{II}}^2c^6}[(\mathcal{O}\mathcal{E})^2,(\mathcal{E}\mathcal{O})^2]_+ \qquad (7h)$$

[7] However, they may be not the most general possible. In particular, under certain conditions t_{eo}, etc. could differ from t_{eo}, etc. not only as regards the matrix contained, but also in its other parts as well. Yet it seemed of little importance to pursue such possibilities.

$$+\frac{(1\pm\beta^{\mathrm{I}})(\beta^{\mathrm{II}}\pm 7)m_{\mathrm{I}}+(1\mp\beta^{\mathrm{II}})(5\beta_{\mathrm{I}}\mp 3)m_{\mathrm{II}}}{128m_{\mathrm{I}}{}^2m_{\mathrm{II}}{}^2c^6}(\mathcal{E}\mathcal{O})(\mathcal{O}\mathcal{E})^2(\mathcal{E}\mathcal{O})$$

$$+\frac{(1\pm\beta^{\mathrm{II}})(\beta^{\mathrm{I}}\pm 7)m_{\mathrm{II}}+(1\mp\beta^{\mathrm{I}})(5\beta^{\mathrm{II}}\mp 3)m_{\mathrm{I}}}{128m_{\mathrm{I}}{}^2m_{\mathrm{II}}{}^2c^6}(\mathcal{O}\mathcal{E})(\mathcal{E}\mathcal{O})^2(\mathcal{O}\mathcal{E}) \quad (7\mathrm{i})$$

$$+\frac{(1+\beta^{\mathrm{I}}\beta^{\mathrm{II}})(m_{\mathrm{I}}-m_{\mathrm{II}})}{16(m_{\mathrm{I}}+m_{\mathrm{II}})m_{\mathrm{I}}m_{\mathrm{II}}c^4}[[(\mathcal{E}\mathcal{O}),(\mathcal{O}\mathcal{E})],(\mathcal{O}\mathcal{O})] \quad (7\mathrm{j})$$

$$+\tfrac{1}{2}(1\mp\beta^{\mathrm{I}})\{(\mathcal{E}\mathcal{O})+\textstyle\sum\mathfrak{N}_{eo}\} \quad (7\mathrm{k})$$

$$+\tfrac{1}{2}(1\mp\beta^{\mathrm{II}})\{(\mathcal{O}\mathcal{E})+\textstyle\sum\mathfrak{N}_{oe}\} \quad (7\mathrm{l})$$

$$+\tfrac{1}{2}(1-\beta^{\mathrm{I}}\beta^{\mathrm{II}})\{(\mathcal{O}\mathcal{O})+\textstyle\sum\mathfrak{N}_{oo}\}. \quad (7\mathrm{m})$$

It contains in (7a) the (unchanged) even-even part of the original Hamiltonian; in (7k, l, m) the original even-odd, odd-even, and odd-odd part (denoted by $(\mathcal{E}\mathcal{O})$, $(\mathcal{O}\mathcal{E})$, $(\mathcal{O}\mathcal{O})$), modified in the desired manner; in (7b$\cdots$j) new even-even terms produced by the transformation, our main point of interest; and in (7k, l, m) new terms of the *eo*, *oe*, and *oo* type, numerous, but irrelevant, and for this reason not specified, but only indicated.

A comparison of this Eq. (7) with the Eq. (7) of I shows considerable differences, which is not surprising. However, it should be remembered that the transformed Hamiltonian is merely an intermediate stage. As was pointed out in I (p. 390), the next, and final step, is the replacement, now made possible, of 16×16 matrices by suitable 4×4 matrices; in particular, both β^{I} and β^{II} are to be replaced by the (fourth rank) unit or the minus unit matrix, according to whether the uU or the lL quadruple is to be retained. Now it is seen that putting $\beta^{\mathrm{I}}=\beta^{\mathrm{II}}=1$ and taking the upper signs, (or $\beta^{\mathrm{I}}=\beta^{\mathrm{II}}=-1$ with the lower signs) makes the Hamiltonians (7) and I(7) coincide. Thus, different transformations of our class finally lead to the same reduced wave equation. This fact is essential, in order that the proposed reduction procedure be sound.

Although only two special transformations have been considered in full detail, there are strong indications that the same result would ensue for all other transformations generated by (6). In order to prove this in general, it would be necessary to calculate $\mathfrak{K}_{\mathrm{tr}}$ using the full, nonspecialized expressions (6). However, in this general case the calculations, while still straightforward, become prohibitively lengthy and tedious.

The author appreciates valuable discussions on the above subject with Dr. William A. Barker.

Note on the Beta Interaction

R. FINKELSTEIN AND P. KAUS
University of California, Los Angeles, California
(Received August 17, 1953)

It is shown that the most general Lorentz invariant interaction between four mutually anticommuting fields leads to matrix elements of the form

$$(S-T+P)f_1(n,m)+(V-A)f_2(n,m)+(S-A-P)f_3(n,m).$$

In the charge-exchange order, neutron and muon decay are compatible with $f_2=f_3=0$; charged pion decay appears to correspond to $f_1=f_3=0$. It is noted that the hypothesis of the same interaction between all fermions does not imply that f_1, f_2, and f_3 are numerical constants; it is possible that they are functions of new variables (n, m) needed to characterize the associated Feynman diagrams: n indicates the number of particles produced in the reaction and m the number of particles minus antiparticles. One can make a simple choice of the f_i in such a way that the interaction is sometimes $S-T+P$, sometimes $V-A$, and never $S-A-P$.

EXPERIMENTAL evidence now appears to favor a Fermi interaction of the form $a(S \text{ or } V)+b(T)+c(P)$. Such a result is in disagreement with the Wigner-Critchfield hypothesis but is compatible with certain less restrictive symmetry principles, which have recently been proposed. These state that the matrix element is (1) antisymmetric in neutral and charged particles separately,[1] or (2) antisymmetric in particles existing before and after the reaction, again separately.[2] We show that these rules, insofar as they agree with experiment, are an elementary consequence of a Lorentz invariant interaction between four mutually anticommuting fields.

Let the interaction be

$$\mathbf{F}=\sum_{a,b,c,d} F(abcd)\mathbf{a}^*\mathbf{b}\mathbf{c}^*\mathbf{d}+\text{adjoint operator}, \quad \text{(I)}$$

where

$$F(abcd)=\sum_{\sigma=0}^{4} g_\sigma F_\sigma(abcd),$$

$$F_\sigma(abcd)=\sum_{\rho} (u_a^+\Gamma_\rho^\sigma u_b)(u_c^+\Gamma_\rho^\sigma u_d).$$

Boldface symbols indicate creation or annihilation operators. $F(abcd)$ is a linear combination of the usual five invariants, $F_\sigma(abcd)$, $\sigma=0\cdots4$. The ρ sum runs over all the components ρ of the tensor $u_a^+\Gamma_\rho^\sigma u_b$ of rank σ.

The hypothesis of the "universal interaction" is expressed by extending the *abcd* sum over all modes of all fermions: ν, e, $\mu\cdots$; and by imposing the Jordan-Wigner rules on all operators. Here this postulate is to mean the anticommutation of operators *belonging to different fermions*, as well as of operators belonging to different modes of the same fermion. (Such a premise may be motivated by supposing that the individual fermions correspond to separate modes of a single fundamental field.) The sum runs over both positive and negative energy states in the usual way, but the fields appearing in it refer to particles only (or to antiparticles only). Since there are two creation and two annihilation operators in each term of (I), the conservation of particles minus antiparticles $[n(+)-n(-)]$ is guaranteed; this feature is compatible with the experimental facts about the conservation of charge and of heavy particles.

TABLE I. General matrix elements.

O_i	O_f	Matrix element
(a) A_+^*	$B_+^*C_+^*D_-$	$2[1-P(A_+D_-)]F(B_+A_+C_+D_-)$
(b) $A_+^*B_-$	$C_+^*D_-$	$2[1-P(A_+D_-)]F(B_-A_+C_+D_-)$
(c) $A_+^*B_+^*$	$C_+^*D_+^*$	$2[1-P(A_+B_+)]F(C_+A_+D_+B_+)$

The number of particles in the initial state i plus the number in the final state f is 4: $n_i+n_f=4$. Of the possible partitions: 0+4, 1+3, 2+2 only the latter two are permitted by the conservation of energy. The possible reactions may be further classified in terms of $n(+)-n(-)$, written on the right in the following equations. Altogether it is sufficient to consider

(a) $A\rightarrow B+C+\bar{D}$ $\quad n_+-n_-=1$

(b) $A+\bar{B}\rightarrow C+\bar{D}$ $\quad n_+-n_-=0$

(c) $A+B\rightarrow C+D$ $\quad n_+-n_-=2,$

where the bar means antiparticle. (No essentially different situation is generated by applying the bar operation to these equations.) Since $n(+)-n(-)$ is conserved, the diagrams for these processes always consist of four lines, two entering and two leaving a vertex.

Let the matrix element be denoted by

$$F_{fi}=(\mathbf{F}\Psi_i, \Psi_f),$$

where the initial and final states are written as

$$\Psi_i=\mathbf{O}_i\Psi_0,$$

$$\Psi_f=\mathbf{O}_f\Psi_0.$$

[1] D. L. Pursey, Phil. Mag. **42**, 1193 (1951).
[2] E. R. Caianiello, Nuovo cimento **10**, 43 (1953).

Here Ψ_0 is the vacuum state; $\mathbf{O}_i$ and $\mathbf{O}_f$ are appropriate operators, illustrated in Table I. Then

$$F_{fi}=(\mathbf{FO}_i\Psi_0,\ \mathbf{O}_f\Psi_0)=(\mathbf{O}_f{}^*\mathbf{FO}_i\Psi_0,\ \Psi_0)$$
$$=\sum_{a,b,c,d}F(abcd)(\mathbf{O}_f{}^*(\mathbf{a}^*\mathbf{bc}^*\mathbf{d})\mathbf{O}_i\Psi_0,\ \Psi_0)+\text{adjoint part.}$$

The only contributing terms of $\mathbf{F}$ in the *abcd* sum of (I) satisfy the condition

$$\mathbf{O}_f{}^*(\mathbf{a}^*\mathbf{bc}^*\mathbf{d})\mathbf{O}_i=1,\quad\text{or}\quad\mathbf{a}^*\mathbf{bc}^*\mathbf{d}=\mathbf{O}_f\mathbf{O}_i{}^*.$$

For given initial and final states there are four terms satisfying this condition, equal in pairs and differing only in sign. The operators and the resulting matrix elements are shown in Table I for reactions (a), (b), and (c). $P(AD)$ means interchange A and D; the subscripts refer to positive and negative energy states. The following special cases are of interest (Table II). Here (a′) and (a″) represent two theories of the same reaction; later an argument excluding (a″) will be given. The diagrams are shown in Fig. 1.

TABLE II. Matrix elements for some typical reactions.

	Reaction	Matrix element
(a)	$N\to P+e+\bar{\nu}$	$2[1-P(N_+\nu_-)]F(P_+N_+e_+\nu_-)$
(a′)	$\mu\to\nu+\nu+\bar{e}$	$2[1-P(\mu_+e_-)]F(\nu_+\mu_+\nu_+e_-)$
(a″)	$\bar{\mu}\to\bar{e}+\bar{\nu}+\nu$	$2[1-P(e_-\nu_-)]F(\mu_-e_-\nu_+\nu_-)$
(b)	$P+\bar{N}\to\nu+\bar{e}$	$2[1-P(P_+e_-)]F(N_-P_+\nu_+e_-)$
(b′)	$P+\bar{N}\to\mu+\bar{\nu}$	$2[1-P(P_+\nu_-)]F(N_-P_+\mu_+\nu_-)$
(c)	$N+\mu\to P+\nu$	$2[1-P(N_+\mu_+)]F(P_+N_+\nu_+\mu_+)$

All of these matrix elements may be written

$$2[1-P(bd)]F(abcd)\qquad(1a)$$

or alternatively, since $P(ac)P(bd)=1$,

$$2[1-P(ac)]F(abcd);\qquad(1b)$$

i.e., they are antisymmetric with respect to a, c and b, d separately. In all cases except (a″) and (b′), condition (1) is equivalent to antisymmetry in charged and neutral particles separately. In cases (a″) and (b′) (which are distinguished from the others by a net charge current toward and away from the vertex) condition (1) requires that the amplitude for the charge retention decay be combined destructively with the amplitude for the charge exchange decay. In all cases the ambiguity about charge retention and charge exchange is removed. In all cases the antisymmetrization corresponds simply to the two pairings. The diagrams, which always contain two lines entering and two lines leaving a vertex, may be read as the scattering of two fermions, each with a change in type; thus $^{P}\nwarrow\!\!\swarrow^{\nu}$ may be read, according to Feynman's intuitive description, as the scattering of a fermion with change in type from ν to P. Then the two possible pairings refer to "direct and exchange scattering." From this point of view the charge symmetry condition is not an *ad hoc* rule when it is valid, but a special case of (1), which in turn follows directly from the postulated interaction (I). When the charge symmetry rule conflicts with (1), then according to the present argument only the latter is valid.

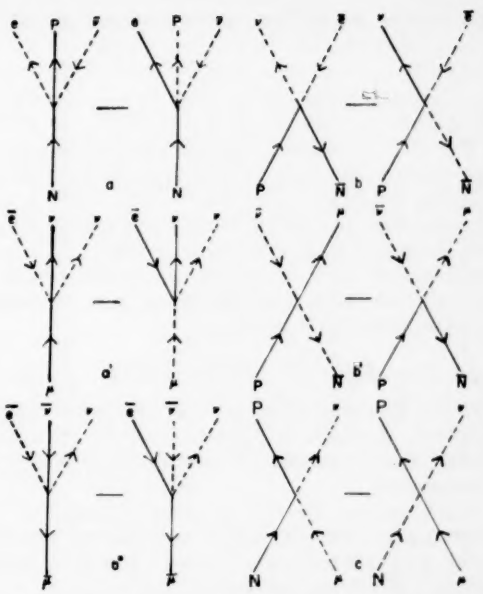

FIG. 1. Diagrams for Table II. The two figures in each diagram represent direct minus exchange scattering. The broken and unbroken lines are used to indicate the pairings. For example, the first figure in diagram (a) is read as the scattering of a ν into an e, while an N is scattered into a P

It follows that the effective part of $F(abcd)$ must have the property:

$$P_{bd}F(abcd)=-F(abcd).\qquad(2)$$

It is shown in the appendix that the general solution of this equation contains three arbitrary constants,

$$F=(f_1)(S-T+P)+(f_2)(V-A)+(f_3)(S-A-P).\quad(3)$$

According to Table (II), Eq. (3) should be written in charge exchange order, although in cases (a″) and (b′) the charge exchange and retention orders differ only in sign.[3]

It is now necessary to distinguish between (a′) and (a″), two theories of the same reaction. According to

[3] After completing this note we discovered some further remarks by D. L. Pursey [Physica **18**, 1017 (1952)] which are similar to those presented here. He also attempts to limit the interaction by use of the anticommutation rules only. However, he regards the charged fields as distinguishable; taking the charge exchange order as standard, he antisymmetrizes with respect to neutral fields only. Here there is no *a priori* distinction between charged and neutral particles, or between charge retention and charge exchange amplitudes. The main difference is that Pursey considers the operator alone, while here the proper identification of direct and exchange scattering (and the correct mixture of charge retention and charge exchange amplitudes) cannot be inferred from the operator alone, without referring to the associated diagrams describing initial and final states.

(a″) neutrino and antineutrino are produced; according to (a′), two neutrinos. In both cases a forward line is arbitrarily assigned to the negative electron; according to (a″) the positron and positive muon are similarly directed; in (a′) they are oppositely directed as shown in Fig. 1. These different physical assumptions lead to the following results. Suppose that in charge-exchange order the interaction is $S-T+P$. Then if (a″) is correct, one has $-(S-T+P)$ in charge-retention order; that interaction leads to a muon spectrum with a nonvanishing end point, in disagreement with experiment. On the other hand, if (a′) is correct, then in charge-retention order the interaction is

$$P_{bd}P_{ab}(S-T+P)=2(S+P).$$

This has a vanishing end point, in agreement with experiment. If present experimental results prove misleading, then the models (a′) and (a″) will have to be reconsidered.

The conclusion that (a′) is correct requires that the positive muon and the positron be oppositely directed. In all diagrams the neutrino, electron, positive muon, proton, and neutron are similarly directed.

Neutron decay is compatible with $f_2=f_3=0$ in Eq. (3). From the discussion just given one can say that muon decay is also compatible with the same assumption.

One would now like to know whether there are any observable effects associated with f_2 and f_3. In this connection reaction (b) is of interest; although not directly observable, it is one step in the decay of the pion:

$$\pi\rightarrow P+\bar{N}\begin{cases}\nearrow \mu+\nu & (4)\\ \searrow e+\bar{\nu}, & (4)'\end{cases}$$

according to the Yukawa theory, or the only step

$$\pi\equiv(P+\bar{N})\begin{cases}\nearrow \mu+\nu & (5)\\ \searrow e+\bar{\nu}, & (5)'\end{cases}$$

according to the composite pion picture.[4] It is known that the branching ratio $\pi e/\pi\mu$ is incorrect unless the β coupling enters here as $aV+bA$. Ordinarily one says that (a) and (b) are governed by exactly the same interaction. But there is neither experimental nor theoretical basis for this assumption. Since diagrams (a) and (b), Fig. 1, cannot be connected by a Lorentz transformation, it is quite possible to associate different interactions with them.

TABLE III. Interaction depending on n_f-n_i only.

n_i+n_f	n_f-n_i	Interaction	Typical reactions
2+2	0	$V-A$	$N+\bar{P}\rightarrow e+\bar{\nu}$ $P+e\rightarrow N+\nu$ $P+\bar{\mu}\rightarrow N+\bar{\nu}$
1+3	2	$S-T+P$	$N\rightarrow P+e+\bar{\nu}$
0+4	4	$S-A-P$	not possible

TABLE IV. Interaction depending on both n_f-n_i and n_+-n_-.

n_f-n_i	n_+-n_-	Interaction	Typical reaction
0	0	$V-A$	$N+\bar{P}\rightarrow e+\bar{\nu}$ $P+\bar{\mu}\rightarrow N+\bar{\nu}$
	2	$S-T+P$	$P+e\rightarrow N+\nu$ $N+\mu\rightarrow P+\nu$
2	1	$S-T+P$	$N\rightarrow P+e+\bar{\nu}$
4	0	$S-A-P$	not possible

More generally the Feynman diagram of a beta process is characterized by two Lorentz invariant integers: n_f-n_i the number of particles produced in the reaction, and n_+-n_- the number of particles minus the number of antiparticles, in either the initial or the final state. The three coefficients, f_1, f_2, and f_3 in Eq. (3) are at present unknown functions of n_f-n_i and n_+-n_-. [These variables are denoted by (n, m) in the abstract.]

Table III corresponds to one (*ad hoc*) choice of these unknown functions. According to this classification, in which the interaction is determined by n_f-n_i alone, neutron decay would differ from K capture—but not from positron emission.

Another classification, less simple but less at variance with the usual ideas, and also in agreement with known facts, is the following (Table IV). Here the interaction depends on n_f-n_i and n_+-n_- as well. In this case, K capture would be determined by the same interaction as positron emission.

One may assign a variable $\rho_s=+1$ or -1 depending on whether the world line is directed forwards or backwards. Then $P=\sum\rho_s=n_+-n_-$ is conserved, as permitted by the conservation of charge and of heavy particles. Such considerations lead naturally to 8-rowed spinors and a theory of the beta interaction which is invariant under the four dimensional conformal group.[5]

The functions f_i may conceivably depend not only on n_f-n_i and n_+-n_- but also on internal variables (such as type[6]). Unfortunately the conditions on the f_i are left quite arbitrary by the lack of experimental information about the elementary beta processes; at present it does not seem possible to remove any of this arbitrariness by the further assumption that all the bosons are composite.[7]

[4] It is also possible to postulate a one-step decay even if the pion is not composite;—see, for example, R. Marshak, *Meson Physics* (McGraw-Hill Book Company, Inc., New York, 1952)—but such a model must explain why the alternative mode (4)′ does not run faster. Since (4)′ needs to be cut off, this point is entirely obscure at the present time.

[5] We hope to present a discussion of a conformal theory of β decay in another journal.

[6] C. Yang and J. Tiomno, Phys. Rev. **79**, 495 (1950) and E. R. Caianiello (reference 2).

[7] R. Finkelstein, Phys. Rev. **88**, 535 (1952). The model suggested there appears compatible with the ideas of the present note. [That paper contains a misprint. In Eq. (6) the inequality is reversed, but the β interaction given there is not current anyway.]

APPENDIX

We collect here the formal results needed in the preceding discussion. By using the $F_\sigma(abcd)$ as a basis one obtains a five dimensional representation of the permutation group on $(abcd)$.[8] Thus

$$PF_\sigma(abcd)=\sum_{\sigma'} F_{\sigma'}(abcd)P_{\sigma'\sigma}.$$

The complete invariant may be regarded as a vector in this space with components g_σ,

$$F=\sum g_\sigma F_\sigma. \tag{6a}$$

Let

$$PF=\sum \bar{g}_\sigma F_\sigma. \tag{6b}$$

Then

$$\bar{g}_{\sigma'}=\sum P_{\sigma'\sigma}g_\sigma. \tag{7}$$

It is clear from the simple form of $F_\sigma(abcd)$ that this complete representation may be generated from the transposition matrices $\|P_{ab}\|$ and $\|P_{bd}\|$. For these we find (if p = number of imaginary γ_μ)

$$P_{ab}(\sigma,\sigma')=\delta(\sigma,\sigma')(-)^{\sigma(\sigma-1)/2+p(p+1)/2+\sigma p}, \tag{8}$$

$$P_{bd}(\sigma,\sigma')=u(\sigma,\sigma')w(\sigma,\sigma'), \tag{9a}$$

where

$$2^{\frac{1}{2}n}u(\sigma,\sigma')=(-)^{\frac{1}{2}(\sigma+\sigma')(\sigma+\sigma'-1)}, \tag{9b}$$

$$w(\sigma,\sigma')=\sum_{s=0}^{\min(\sigma,\sigma')} C_{n-\sigma}{}^{n-s}C_s{}^{\sigma'}(-2)^s, \tag{9c}$$

where $C_m{}^n=n!/m!(n-m)!$. These formulas are a generalization to n dimensions of results given by Fierz for 4 dimensions.[9] Here n = number of dimensions = number of generating γ_μ; 2^n = number of matrices in complete set; $n+1$ = number of F_σ = dimensionality of representation of the permutation group.

One obtains from P_{ab} and P_{bd},

$$P_{ad}=P_{ab}P_{bd}P_{ab}. \tag{10}$$

Moreover, P_{bd} and P_{ab} are related by the similarity transformation

$$P_{ad}{}^{-1}P_{bd}P_{ad}=P_{ab}. \tag{11}$$

According to this last equation the eigenvalues of P_{bd} are the diagonal elements of the diagonal matrix P_{ab} (either $+1$ or -1), and the eigenvectors of P_{bd} are the columns of P_{ad}. There are three eigenvectors belonging to -1 and the general solution of (2) is the linear combination of them shown in (3).

The representation given above is not unitary, but the following familiar method may be used to obtain a unitary representation. Define the Hermitian matrix H by

$$H=\sum_1^{24} P_iP_i{}^+,$$

where the sum extends over the whole group. Let $D=U^{-1}HU$, where D is diagonal. Then the matrices $P_i'=D^{\frac{1}{2}}U^{-1}P_iUD^{\frac{1}{2}}$ are unitary. Here H is simply $8(1+P_{ad}P_{ad}{}^+ +P_{bd}P_{bd}{}^+)$, and the unitary generating matrices P_{ab} and P_{ad} are

$$P_{ab}=\begin{Vmatrix} -1 & & & & & \\ & +1 & & & & \\ & & +1 & & & \\ & & & -1 & & \\ & & & & -1 & \end{Vmatrix},$$

$$P_{ad}=\tfrac{1}{2}\begin{Vmatrix} 1 & \sqrt{3} & 0 & 0 & 0 \\ \sqrt{3} & -1 & 0 & 0 & 0 \\ 0 & 0 & -1 & 1 & \sqrt{2} \\ 0 & 0 & 1 & -1 & \sqrt{2} \\ 0 & 0 & \sqrt{2} & \sqrt{2} & 0 \end{Vmatrix},$$

with basis functions $(\sqrt{21})(S+P)$, $-(\sqrt{7})T$, $3V$, $-3A$, $3\sqrt{2}(P-S)$. The eigenvectors of P_{bd} are the columns of P_{ad}. Those eigenvectors belonging to the eigenvalue -1 are

$$\begin{array}{ccccc} 1 & \sqrt{3} & 0 & 0 & 0 \\ 0 & 0 & 1 & -1 & \sqrt{2} \\ 0 & 0 & \sqrt{2} & \sqrt{2} & 0 \end{array} \quad \text{leading to} \quad \begin{array}{l} (\sqrt{21})(S-T+P) \\ 6(P-S)+3(V+A) \\ 3\sqrt{2}(V-A). \end{array}$$

The second line differs from the Wigner-Critchfield interaction by $V-A$. The result stated in Eq. (3) then follows. This result does not, of course, depend on the use of a unitary representation, which is merely convenient; it may be read off from Eq. (9) just as well.

[8] L. Michel, Proc. Phys. Soc. (London) **A63**, 514 (1950).
[9] M. Fierz, Z. Physik **104**, 553 (1937). The calculation of these formulas will be given in reference 5.

Letters to the Editor

PUBLICATION of brief reports of important discoveries in physics may be secured by addressing them to this department. The closing date for this department is five weeks prior to the date of issue. No proof will be sent to the authors. The Board of Editors does not hold itself responsible for the opinions expressed by the correspondents. Communications should not exceed 600 words in length and should be submitted in duplicate.

Low-Temperature Diamagnetism of Electrons in a Cylinder

R. B. DINGLE
St. John's College, Cambridge, England
(Received August 20, 1953)

IN writing his recent paper of the above title, Band[1] appears to have overlooked a number of points:

(a) As a result of the exclusion principle, all but a negligible number of available electron states correspond to extremely large quantum numbers. Now in its general mathematical form (e.g., Jeffreys[2] pp. 522–7) the WKB method becomes exact for large enough quantum numbers, and Band's objections that "the concept of localized reflected electron orbits is basic," and that "the radial equation does not have the proper boundary conditions for a rigorous application of the WKB method and one always has to add a fictitious potential $1/4r^2$ to modify the singularity at the centre of the cylinder," do not apply to it. My calculations based on such a general WKB method[3] agree with those I have obtained by other means.[4,5]

(b) In cylindrical polar coordinates the exact eigenfunctions of an electron in a magnetic field can be expressed in terms of standard confluent hypergeometric functions (e.g., Dingle[5]). Band's solution is rather complicated and inconvenient.

(c) For small magnetic fields the quantized contribution to the energy of an electron of mass M in a cylinder of radius a is

$$E=\frac{\hbar^2}{2Ma^2}x_{jm}^2+\frac{mehH}{2Mc}+\frac{e^2H^2a^2}{24Mc^2}\left\{1+\frac{2(m^2-1)}{x_{jm}^2}\right\}+O(H^4),$$

where m is an integer (positive, negative, or zero) and x_{jm} stands for the argument for which the Bessel function of order $|m|$ has its jth zero. This result may either be obtained by perturbation theory,[4,6,7] or the WKB method.[7] Band's stated approximation to the eigenvalues is not correct even to terms linear in H.

(d) Since the term, linear in H, in the eigenvalues can be of either sign, the total energy of the system contains no term linear in H, and it is, therefore, essential to retain terms in the eigenvalues quadratic in H. Band omits such quadratic terms.

(e) For large enough quantum numbers m and j, x_{jm} is given exactly by the transcendental equation (e.g., Welker,[6] Dingle[4]):

$$(x^2-m^2)^{\frac{1}{2}}-|m|\cos^{-1}(|m|/x)=(j-\tfrac{1}{4})\pi.$$

Band, however, assumes that x may be approximated by a continuum $x=\pi j$ independent of m, with a lower cutoff at $j=|m|+1.856|m|^{\frac{1}{3}}$. (Presumably πj is meant here.) But surely x is not even approximately equal to πj. As a consequence of Band's incorrect enumeration of the eigenvalues, his results are erroneous even for zero field.

[1] W. Band, Phys. Rev. **91**, 249 (1953).
[2] H. Jeffreys and B. S. Jeffreys, *Methods of Mathematical Physics* (Cambridge University Press, Cambridge, 1950), second edition.
[3] R. B. Dingle, Proc. Roy. Soc. (London) **A216**, 118 (1953).
[4] R. B. Dingle, Proc. Roy. Soc. (London) **A212**, 47 (1952).
[5] R. B. Dingle, Proc. Roy. Soc. (London) **A211**, 500 (1952).
[6] H. Welker, Sitzber. bayer Akad. Wiss. **14**, 115 (1938).
[7] R. B. Dingle, Proc. Cambridge Phil. Soc. **49**, 103 (1953).

Zone Structure of Graphite*

S. MROZOWSKI
Department of Physics, University of Buffalo, Buffalo, New York
(Received October 14, 1953)

THE Brillouin zone of graphite which contains one electron per carbon atom, as customarily stated, is bounded by six vertical planes $(1\bar{1}0,0)$ and two horizontal planes $(000,2)$; see Fig. 1(A). Wallace[1] and Coulson[2] have shown that at the six corners of the zone the energy discontinuity disappears and that consequently the occupied energy band just touches the unoccupied one, making graphite along the crystalline planes an intrinsic semiconductor with a zero energy gap. Since their work, various attempts have been made to interpret experimental results for single crystals of graphite and polycrystalline materials as well in terms of such a model. However, as the variety and accuracy of the results increase, it becomes more and more evident that this model is lacking in ability to explain and correlate a number of electronic properties of graphite. One wonders which feature of the model is responsible for these failures. It seems worth while, therefore, to look at the structure of the zone boundaries and to check if actually it is the zone Fig. 1(A) which is filled with electrons at 0°K. After all, the zone Fig. 1(A) is not the lowest zone for a perfect graphite crystal. The lowest zone is bounded by 12 inclined planes $(1\bar{1}0,1)$ in addition to the planes mentioned before and contains

$$n=1-\tfrac{3}{8}(a/c)^2[1-\tfrac{1}{4}(a/c)^2]$$

electrons per atom, where a and c are the lattice constants; see Fig. 1(B).[3] For graphite, n is about 0.96, so that there are 0.04 electron per atom located outside of the inner zone. It does not seem straightforward that these electrons should fill the volume V_1 (see Fig. 1(B)) and that the total filled zone should be that of Fig. 1(A). This would certainly occur if the energy discontinuity ΔE_i across the planes $(1\bar{1}0,1)$ should happen to be small in comparison to the discontinuity ΔE_v introduced by the $(1\bar{1}0,0)$ planes. This, however, is not the case, since the corresponding structure factor S_i is larger than the factor S_v by a factor of $\sqrt{3}$.[3] For the other limiting case, when $\Delta E_v \gg \Delta E_i$, the 0.04 electron would fill exactly the volume V_2 of Fig. 1B and the zone containing one electron per carbon atom and completely filled at 1°K would be the one given in Fig. 1(C).[4] Thermal excitation of electrons would occur over the vertical planes into the region V_3 of Fig. 1 (B),

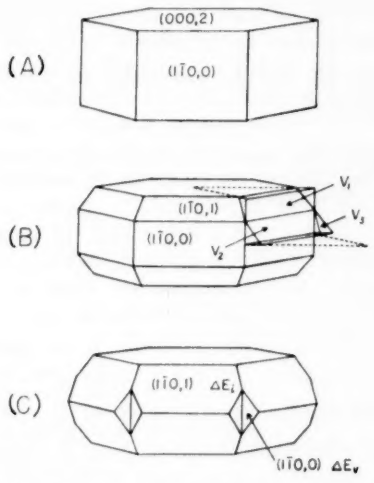

FIG. 1. (A) Zone containing 1 electron per atom filled with electrons at 0°K if $\Delta E_v \gg \Delta E_i$. Lowest zone for turbostratic crystallites. (B) Lowest zone for a graphite crystal and three adjacent zones V_1, V_2, and V_3 of which V_1 and V_3 have equal volumes. (C) Zone containing 1 electron per atom filled with electrons at 0°K if $\Delta E_v \ll \Delta E_i$.

a quite different process from the first case, where the electrons would be excited from V_1 into V_2. For energy discontinuties of comparable magnitude, the 0.04 electron might become divided between the two volumes V_1 and V_2. The author's guess is that the bulk of the electrons does occupy the volume V_1 in view of the almost cylindrical shape of the energy surfaces around the c axis (extremely large effective mass for motion in this direction), with small empty regions in the neighborhood of the six vertical corners and with the remaining electrons located close to these corners in the volume V_2. Thus a perfect graphite crystal would be in direction perpendicular to the c axis a semi-metal similar to bismuth and not a semiconductor with a zero energy gap. This is just what can be inferred from experimental evidence.[5] No definite statement can be made, however, without performing exact calculations. Irrespective of the outcome of such calculations, it is clear from the foregoing that in making predictions as to the temperature dependence of the electric resistivity, Hall constant, diamagnetic susceptibility, and so forth, no agreement with experimental data can be expected without taking the discontinuities across the planes (1$\bar{1}$0, 1) into consideration. The presence of graphite type II interspersed between the regular graphite I will be a factor complicating the comparison.

For lamellar compounds, changes in the zone structure induced by the formation of superlattice of expanded c distances might be of considerable importance. As for carbons, it should be pointed out that the zone Fig. 1(A) represents actually the lowest zone for turbostratic crystallites (absence of cross-lattice reflections). In the process of graphitization, the shifts and rotations of crystalline planes into graphitic positions will therefore bring about lareg changes in shape and distribution of the energy surfaces near the periphery of the zone Fig. 1(A).

* Supported by the U. S. Office of Naval Research.
[1] P. R. Wallace, Phys. Rev. **71**, 622 (1947).
[2] C. A. Coulson, Nature **159**, 265 (1947). See also the more recent paper by C. A. Coulson and R. Taylor, Proc. Phys. Soc. (London) **A65**, 815 (1952).
[3] N. F. Mott and H. Jones, *Theory of the Properties of Metals and Alloys* (Oxford University Press, London, 1936); see pp. 161 and 163.
[4] The polyhedron given here is an illustration of the fact that selection of the zone containing a definite number of electrons is not unique in this case.
[5] S. Mrozowski, J. Chem. Phys. **21**, 492 (1953).

Spin-Spin Interaction of Electrons and the Ionization Energy of Helium*

A. M. Sessler† and H. M. Foley
Columbia University, New York, New York
(Received September 22, 1953)

CHANDRASEKHAR, Elbert, and Herzberg[1] have recently reviewed the agreement between the theoretical and experimental values of the ionization potential of He and He-like ions. A discrepancy of 21.5 cm^{-1} for He and larger discrepancies for the He-like ions were found when all theoretical effects were presumably taken into account.

We wish to point out a term in the magnetic interaction of two electrons which seems to have been omitted in all previous calculations of the energy levels of helium. The spin-spin interaction of two classical distributions of magnetism of densities $\mu_1(\mathbf{r}_1)$, $\mu_2(\mathbf{r}_2)$ is

$$W=\int_1\int_2\left(\frac{\boldsymbol{\mu}_1\cdot\boldsymbol{\mu}_2}{r^3}-\frac{3(\boldsymbol{\mu}_1\cdot\mathbf{r})(\boldsymbol{\mu}_2\cdot\mathbf{r})}{r^5}\right)dv_1dv_2 -\int_1\int_2\frac{8}{3}\pi\boldsymbol{\mu}_1\cdot\boldsymbol{\mu}_2\delta(\mathbf{r})dv_1dv_2, \quad (1)$$

in which $\mathbf{r}=\mathbf{r}_2-\mathbf{r}_1$. The first term in Eq. (1) represents the interaction of one electron spin moment with the magnetic field due to the distant source distribution of the other electron, i.e., exclusive of a volume element cut out about the first electron. This term appears in the standard two-electron Hamiltonians in the literature. The divergence of this integral at $\mathbf{r}\to 0$ is taken care of by the conventional procedure that the integration is carried out first over $\mathbf{r}_2$, excluding the small sphere about $\mathbf{r}_1$. The second term takes into account the field produced at $\mathbf{r}_1$ by the second electron in the small sphere about $\mathbf{r}_1$. In the limit that the radius of this sphere vanishes, only the contribution of the spherically symmetric part of this moment distribution remains and yields just the delta-function result given in Eq. (1). The second term thus represents a "contact" interaction of the spin-moment densities, and is just the term which gives rise to the magnetic hyperfine interaction in atomic S states. This last term does not vanish in the ^1S ground state of helium, and the resulting magnetic energy is simply

$$W_{18}=+32\pi^2\mu_0^2\int\psi^2(r,r)r^2dr, \quad (2)$$

where $\psi^2(r,r)$ is the square of the helium electronic wave function at $\mathbf{r}_1=\mathbf{r}_2$. μ_0 is the Bohr magneton. For a hydrogenic product wave function, we obtain

$$W_{18}=+\mu_0^2Z^3/a_H^3. \quad (3)$$

With an effective $Z=1.6875$, we have $W_{18}=+14.05$ cm^{-1}. With the Hylleraas six-term function we obtain $W_{18}=+16.4$ cm^{-1}. This energy contribution is of the opposite sign to improve the agreement with experiment of the total binding energy in the case of helium. For the He-like ions the sign is in agreement with the observed discrepancy and for $Z=8$, Eq. (3) amounts to about $+1500$ cm^{-1}, or most of the discrepancy.

The Hylleraas wave function is not as well suited for the calculation of the relativistic corrections as it is for many other quantities because the behavior near the nucleus is not satisfactory. We believe that this fact raises doubts about the presently accepted relativistic calculation,[2] and we propose to employ a Hartree solution for this purpose, making corrections for the effect of electron correlation.

* Supported in part by a grant from the National Science Foundation.
† National Science Foundation Predoctoral Fellow.
[1] Chandrasekhar, Elbert, and Herzberg, Phys. Rev. **91**, 1172 (1953).
[2] H. A. S. Erikson, Z. Physik **109**, 762 (1938).

The Relativistic Correction to the Ground-State Energy of Helium*

A. M. Sessler† and H. M. Foley
Columbia University, New York, New York
(Received September 28, 1953)

CHANDRASEKHAR, Elbert, and Herzberg[1] have pointed out that the relativistic corrections to the ionization energy of the ground state of helium as calculated from hydrogenic Hartree[2] or Hylleraas[3] functions are considerably different. In view of these rather surprisingly different results for this significant quantity, we have undertaken to establish a more satisfactory value for the relativistic corrections.

The appropriate Hamiltonian terms are[3]

$$H_1=-\frac{1}{8m^3c^2}[p_1^4+p_2^4],$$

$$H_2=\frac{\pi\hbar^3Z}{2m^2c^3}[\delta(\mathbf{r}_1)+\delta(\mathbf{r}_2)],$$

$$H_3=-\frac{\pi\hbar^3}{2m^2c^3}\delta(\mathbf{r}_{12}).$$

H_1 and H_2 are one-electron operators, and thus we may evaluate them to sufficient accuracy using Hartree functions.[4] The justification for this procedure may be seen from an examination of a perturbation calculation which proceeds from hydrogenic states and includes the interelectron Coulomb term and $H_{12}=H_1+H_2$. Examination of terms linear in H_{12} shows that terms not included in the Hartree-Fock approximation first appear in the third order ($H_c^2H_{12}$), and then involve Coulomb matrix elements to doubly-

excited electron states. An estimate of these terms shows that they contribute less than ½ percent to H_{12}. In the region where H_{12} obtains most of its value, the difference between Hartree and Hartree-Fock is not significant.

H_3 is an operator which does not weight regions near the nucleus and is sensitive to the amount of electron correlation. We have therefore evaluated H_3 using the Hylleraas six-term function.

The results for a hydrogenic function with $Z=1.6875$, the Hylleraas function, and Hartree functions are given in Table I. An evaluation of H_3 with Hartree functions yields 0.59 ($\alpha^2 Ry$).

It will be noticed that our results for columns 1 and 3 disagree with those of Bethe.[2] This discrepancy seems to arise from an error of a factor of 2 in his H_3, and a numerical error in his evaluation of H_1.

TABLE I. Relativistic corrections with various wave functions, in α^2 Ry.

	Hydrogenic	Hylleraas	Present calculation
$-H_1$	20.27		26.23
$-H_2$	−19.22		−22.60
$-H_3$	0.60		0.71
Sum	+1.65	4.22	+4.34
Ion	−4.00	−4.00	−4.00
Total ($\alpha^2 Ry$)	−2.35	0.22	0.34
Total (cm^{-1})	−13.7 cm^{-1}	1.28 cm^{-1}	2.0±0.5 cm^{-1}

The hydrogenic values for H_1 and H_2 may be brought into substantial agreement with the Hartree values by using $Z=1.8$. This is reasonable in view of the weighting of the region near the nucleus by H_{12}.

Combining the interelectron magnetic interaction,[5] the mass polarization term,[2] the relativistic term, the Breit operator term,[3] and the contribution of the Lamb shift as calculated by Hakansson,[6] we obtain

$$(-16.4-5.2+2.0+0.15+1.2)\ cm^{-1}=-18.3\pm1\ cm^{-1}.$$

Using the most recent value of the electrostatic nonrelativistic eigenvalue:[1] $I=198290.9\ cm^{-1}$, and adding the above, we get $I_{corrected}=198272.7\ cm^{-1}$, $I_{observed}=198313\pm5\ cm^{-1}$. This leaves a discrepancy of 40 cm^{-1}. With the Hylleraas "eighth approximation"[1] the discrepancy is 10 cm^{-1}.

* Supported in part by a grant from the National Science Foundation.
† National Science Foundation Predoctoral Fellow.
[1] Chandrasekhar, Elbert, and Herzberg, Phys. Rev. **91**, 1172 (1953).
[2] H. A. Bethe, *Handbuch der Physik* (Springer, Berlin, 1933), Vol. 24, II, p. 384.
[3] H. A. S. Erikson, Z. Physik **109**, 762 (1938).
[4] W. S. Wilson and R. B. Lindsay, Phys. Rev. **47**, 681 (1935).
[5] A. M. Sessler and H. M. Foley, preceding Letter [Phys. Rev. **92**, 1392 (1953)].
[6] H. E. V. Hakansson, Arkiv Fysik **1**, 555 (1950).

Mobility of Impurity Ions in Germanium and Silicon

J. C. SEVERIENS* AND C. S. FULLER
Bell Telephone Laboratories, Murray Hill, New Jersey
(Received September 29, 1953)

Li and Cu have been shown to diffuse rapidly into Ge and Si and to behave as donor and acceptor elements, respectively, in these semiconductors.[1,2] It is therefore of interest to investigate the mobilities of these elements in order to secure information on their state of ionization and to provide, also, independent and more accurate measures of their diffusivities.

By diffusing hemispherical n-type regions (20 mils in diam) of Li into p-type Ge and Si, in the form of bars 0.7 in.×0.10 in.×0.05 in., and applying dc fields of 1–10 volts per cm, we have determined Li^+ mobilities in the range 150–851°C. The dc fields were obtained by passing large currents through the specimen, the current serving at the same time to heat up the specimen to the desired temperature. The electric field was measured between two tungsten probes fixed 1.0 cm apart which could be brought into contact with the specimens. Temperatures were calculated to ±5°C from the resistivities, employing data of Morin.[3] Cooling was provided by steel rods which contacted the specimens through thin mica separators. The drift times varied from 5 minutes to 3 hours and the drift distances, which were measured by means of a micrometer microscope, ranged from 3 to 25 mils. The latter were determined by measuring the distance between the centers of the circular pn junctions before and after subjection to the field. The pn junctions were made visible by means of the deposition of barium titanate on the boundaries under reverse voltages of about 40 volts.[4]

The results for Li are shown in Fig. 1. The diffusivities, D, were calculated from the Einstein relation,

$$D=\mu kT/q,$$

where μ is the ion mobility in cm^2 per volt sec and q is the ionic charge. The curves in Fig. 1 are given by

$$D=25\times10^{-4}\exp(-11\,800/RT),$$
$$D=19\times10^{-4}\exp(-14\,700/RT),$$

for Li in Ge and Si, respectively. These equations agree within experimental error with those previously published. Therefore Li follows the Einstein relation in this concentration range and migrates as a singly-charged positive ion.

The above techniques, as well as techniques using radioactive copper, Cu^{64}, have been employed to determine the drift mobility of copper ions in Ge. Radioautographs taken of Cu^{64} particles before and after diffusion for 2–3 minutes at 800–850°C in a field of about 1 volt per cm showed a drift of about 7–15 mils toward the negative electrode. However, the excess copper was not removed in these experiments so that some doubt exists whether the result was a true measure of the impurity ions in the solid. In another experiment done at 800°C, the excess copper was removed. A drift of 4 mils toward the negative electrode was observed for a field of 1 volt/cm in 45 sec. The diffusion constant calculated from

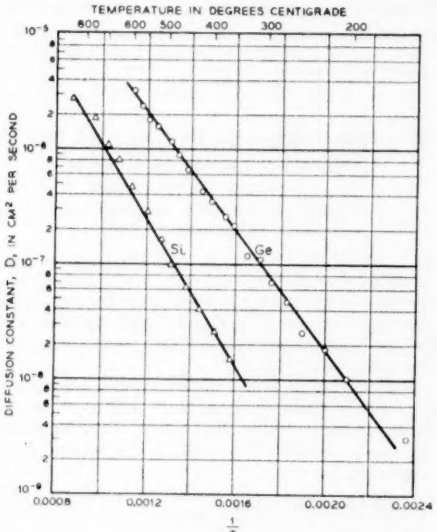

FIG. 1. Plot of the diffusivity of Li in Si and Ge against reciprocal of absolute temperature.

this mobility measurement and assuming that Cu moves as a singly-charged positive ion is 2.2×10^{-5} cm²/sec (±25 percent). This result is of the same order as that previously published.[3] Subsequent results obtained in the same manner leave no doubt that copper migrates as a positive ion at these temperatures, but more work will be required to determine definitely the magnitude of its charge.

Thanks are due to J. A. Ditzenberger for assistance with the experiment.

* Present address: Johns Hopkins University, Baltimore, Maryland.
[1] C. S. Fuller and J. A. Ditzenberger, Phys. Rev. **91**, 193 (1953).
[2] C. S. Fuller and J. D. Struthers, Phys. Rev. **87**, 526–527 (1952).
[3] F. J. Morin (to be published).
[4] G. L. Pearson (private communication).

Variations in the Decay of Phosphorescence with Frequency of Applied Electric Field*†

KEITH W. OLSON
Institute for Atomic Research and Department of Physics, Iowa State College, Ames, Iowa
(Received October 5, 1953)

DESTRIAU[1] has reported on the momentary illumination and extinguishing effects of an electric field applied to a phosphor which has a long phosphorescence decay time. The effects of varying the frequency of the applied field on the wavelength of maximum phosphorescence intensity from an ultraviolet-excited ZnS/CdS:Cu phosphor have been examined by the author. This letter discusses the qualitative features of these variations.

The samples were suspensions of the phosphor in a commercial thermo-setting plastic. The liquid suspension was poured on a polished metal plate and pressed to a thickness of about 0.005 in. with a slide of conducting glass. The thickness was controlled by Teflon spacers. Hardening was accomplished by heating to 80°C for about one hour. The samples were irradiated by near ultraviolet light for twenty seconds, and at specified times after the ultraviolet was turned off the field was applied. The emitted light was passed through a monochromator which was adjusted to transmit only the wavelength of maximum intensity, to a refrigerated photomultiplier. The current from the photomultiplier was fed through a bridge-type electrometer to a very sensitive galvanometer.

With an emf of 500 volts applied across a typical sample of RMA phosphor No. P-7 (*Y*),[2] the curves obtained at 28°C are shown in Fig. 1. Curve 1 is the ordinary phosphorescence decay curve with no field applied. Curves 2, 3, and 4 are, respectively, those for fields of 80, 800, and 5000 cps applied at 8 and 72 sec, and removed at 40 and 104 sec after the ultraviolet was turned off.

The initial momentary illumination is greatest for the 80-cps field, decreasing with increasing frequency—see *A*. Also the length of time for the decay to return to its normal scheme after the field is removed is greater for the lower-frequency fields, as can be seen in time intervals *B*–*C* and just after *D*. However, the magnitudes of the extinguishing effect after the initial increase, the increase at the first removal of the field, *B*, the extinguishing effect at *C*, and the final increase at *D* are considerably greater for the higher-frequency fields. Finally, the actual form of the decay varies appreciably with the field frequency when the field is on—shown in *C*–*D*.

All of these phenomena show strong dependence on field strength, temperature, the particular wavelength examined, and the relative amounts of ZnS and Cds. Destriau shows curves of a ZnS/Cds phosphor subjected to a 50-cps field in which the momentary increase at field removal times comparable to *B* and *D* gives an intensity considerably greater than that from the normal decay at the given time. For the phosphor discussed in this letter the intensity remained lower than the normal decay

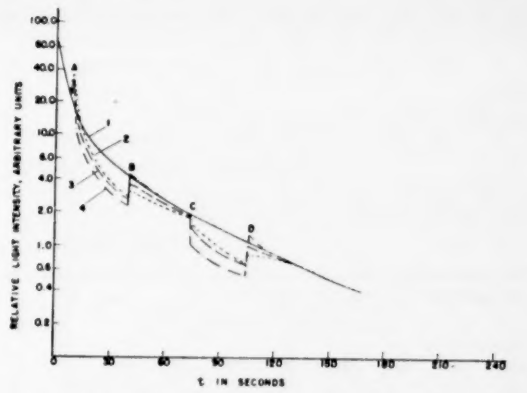

FIG. 1. Light output of ZnS/CdS:Cu phosphor *vs* time after the ultraviolet was turned off. 1. Normal phosphorescence decay curve. 2, 3, 4: Applied field frequency: 80, 800, and 5000 cps, respectively. A, C: Field on; B, D: Field off.

intensity for all the 80-cps runs and exceeded the normal intensity only for the 5000-cps field.

Work is now in progress to obtain more quantitative information on these effects as functions of temperature, field strength, and phosphor composition. Such studies may increase our understanding of trapping levels and luminescence centers in these phosphors.

* Work was performed in the Ames Laboratory of the U. S. Atomic Energy Commission.
† This work began while the author was the Sylvania Research Fellow at Iowa State College; it is presently supported by the Ames Laboratory of the U. S. Atomic Energy Commission.
[1] G. Destriau, Phil. Mag. **38**, 700, 784, 880 (1947).
[2] Kindly donated to the author by the General Electric Company, Chemical Products Works, Cleveland, Ohio.

Solution of the Wave Equation Near an Extremum of the Potential*

CHARLES J. MULLIN
University of Notre Dame, Notre Dame, Indiana
(Received October 7, 1953)

IN previous work reported in the literature,[1] solutions of the wave equation near an extremum of the potential have been obtained by expanding the potential in powers of the distance from the potential extremum y and retaining only the constant and quadratic terms. In certain problems it is desirable to have a more accurate solution which will be valid over a more extended range of the variable y. In this paper a solution is obtained which is consistent with retaining all powers through y^6 in the expansion of the potential in the vicinity of the extremum. The present work is confined to one dimension.

The wave equation is written[2]

$$(d^2\psi/dy^2)+a^2[\epsilon+P(y)]\psi=0, \tag{1}$$

with $y=0$ taken as the location of the extremum of the potential, and $P(0)=0$. The transformation

$$\psi=P^{-\frac{1}{4}}F, \quad z=\int_0^y P^{\frac{1}{2}}dy \tag{2}$$

yields the transformed wave equation

$$(d^2F/dz^2)+[a^2+(a^2\epsilon/P)-Q]F=0, \tag{3}$$

where

$$Q=-P^{-\frac{1}{4}}(d^2P^{-\frac{1}{4}}/dy^2)=P^{-\frac{1}{4}}(d^2P^{\frac{1}{4}}/dz^2).$$

Near $y=0$, $P(y)$ can be developed in a series of ascending powers of y:

$$P(y)=c_2y^2+c_3y^3+\cdots. \tag{4}$$

If z and $[(a^2\epsilon/P)-Q]$ are expanded in ascending powers of y

and the first five terms retained [this corresponds to retaining powers through y^6 in the expansion of $P(y)$], Eq. (3) becomes

$$(d^2F/dz^2)+[(3/16z^2)+(\lambda_1/z)+(\lambda_2/z^4)+\lambda_0]F=0, \quad (5)$$

where

$$\lambda_0=\{a^2+(a^2\epsilon/2c_2)[-(3c_4/2c_2)+(103c_3^2/72c_2^3)]$$
$$+(3/2c_2)[-(5c_6/3c_2)+(5c_3c_5/2c_2^2)+(109c_4^2/96c_2^2)$$
$$-(1723c_3^2c_4/576c_2^3)+(12061c_3^4/13824c_2^4)]\},$$
$$\lambda_1=(1/2c_2^{\frac{1}{2}})\{a^2\epsilon-(1/8)[(3c_4/c_2)-(7c_3^2/4c_2^2)]\},$$
$$\lambda_2=(2^{\frac{1}{2}}/c_2^{\frac{1}{2}})\{-(a^2\epsilon c_3/3c_2)+(3/10)[-(2c_5/c_2)$$
$$+(8c_3c_4/3c_2^2)-(28c_3^3/27c_2^3)]\}.$$

The independent solutions $F_{1,2}$ of (5) are expressible in terms of the parabolic cylinder functions:[3]

$$F_1=z^{\frac{1}{2}}D_n(\xi), \quad F_2=z^{\frac{1}{2}}D_{-n-1}(i\xi), \quad (6)$$

where

$$n=-(1/2)+(i/\lambda_0^{\frac{1}{2}})[\lambda_1-(\lambda_2^2/4\lambda_0)],$$
$$\xi=2\lambda_0^{\frac{1}{2}}[z^{\frac{1}{2}}+(\lambda_2/2\lambda_0)]\exp(-i\pi/4).$$

Consequently, the functions

$$\psi_1=P^{-\frac{1}{2}}z^{\frac{1}{2}}D_n(\xi),$$
$$\psi_2=P^{-\frac{1}{2}}z^{\frac{1}{2}}D_{-n-1}(i\xi) \quad (7)$$

are very good approximations to the solutions of the wave equation near $y=0$. These solutions have the advantage of being one-valued. For bound states, the parabolic cylinder function is expressible in terms of a Hermite polynomial.

The solution (7) has numerous applications. For example, a solution valid near the minimum of a potential trough yields an accurate evaluation of the energies of the low-lying levels of the potential. Also, a solution valid near the maximum of a potential barrier determines accurately the transmission coefficient of particles having energies nearly equal to the height of the barrier. The simple asymptotic form of the single-valued parabolic cylinder function readily yields the "connection" between the asymptotic solutions of (1).

* Supported in part by the U. S. Office of Naval Research.

[1] S. Goldstein, Proc. London Math. Soc. **33**, 246 (1932); R. E. Langer, Trans. Am. Math. Soc. **36**, 90 (1934); E. Guth and C. J. Mullin, Phys. Rev. **59**, 575 (1941); S. C. Miller and R. H. Good, Phys. Rev. **91**, 174 (1953).

[3] The terminology and the transformations used here are similar to those employed by I. Imai [Phys. Rev. **74**, 113 (1948) and Phys. Rev. **80**, 1112 (1950)] in obtaining an accurate solution to the wave equation near a linear turning point.

[5] E. T. Whittaker and G. N. Watson, *Modern Analysis* (Cambridge University Press, London, 1940), fourth edition, p. 347.

The Long-Wavelength Edge of Photographic Sensitivity and of the Electronic Absorption of Solids*

FRANZ URBACH
Research Laboratories, Eastman Kodak Company, Rochester, New York
(Received October 9, 1953)

IN an extensive investigation of the sensitivity spectrum of various types of photographic emulsions, it was noticed that, for the simplest unsensitized emulsions, the plot of the logarithm of sensitivity *versus* frequency approaches a straight line, as shown in Fig. 1.[1] For pure silver bromide emulsions near room temperature, the slope of this line was found to be very near to $1/kT$. If this behavior is more than a mere coincidence, it should be expected to occur over a reasonable temperature range. In the wavelength range of low sensitivity, the absorption coefficient of the halide is expected to be proportional to the sensitivity. A set of measurements carried out by F. Moser, of these laboratories, of the absorption spectrum of silver bromide crystals in the region of the absorption edge showed that the relation $d\log\epsilon/d\nu=-1/kT$ is closely approached for absorption coefficients ϵ of the order of 10^{-1} cm^{-1} for temperatures ranging at least from 200°K to 620°K (Fig. 2). The absorption spectrum behaves in this range as if, by

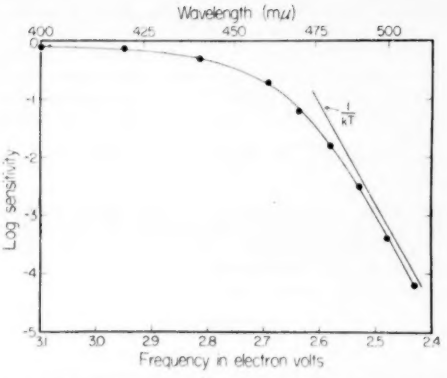

FIG. 1. Spectral sensitivity of an unfinished pure AgBr emulsion at 22°C.

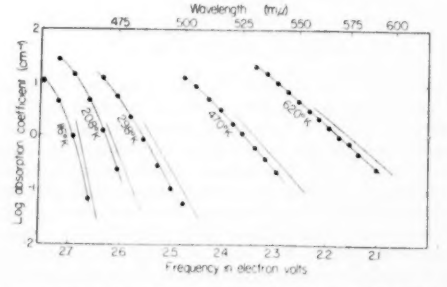

FIG. 2. Temperature dependence of absorption of an AgBr crystal. The straight lines are the $1/kT$ slopes at the corresponding temperatures.

some mechanism not known in detail, the thermal energy were contributing directly to the transitions responsible for the absorption edge. An analysis of data from various sources on materials, such as $AgCl$,[2] Ge,[3] TiO_2,[4] and CdS,[5] indicates a somewhat similar behavior, with slopes within a factor of 2 of $1/kT$, in regions of sufficiently high temperatures and low absorption constants.

Attempts to provide a more precise formulation and a definite theoretical basis for this apparent regularity have not been successful. More detailed data and some theoretical considerations will be published elsewhere.

* Communication No. 1620 from the Kodak Research Laboratories.

[1] See also the data of J. Eggert and M. Biltz, Trans. Faraday Soc. **34**, 892 (1938); J. Eggert and F. G. Kleinschrod, Z. wiss. Phot. **39**, 155 (1940), and of M. Biltz, J. Opt. Soc. Am. **39**, 994 (1949).

[2] Measurements in these laboratories and recent data by M. A. Gilleo, Phys. Rev. **91**, 534 (1953).

[3] M. Becker and H. Y. Fan, Phys. Rev. **76**, 1530 (1940).

[4] D. C. Cronemeyer, Phys. Rev. **87**, 876 (1952).

[5] C. C. Klick, Phys. Rev. **89**, 274 (1953).

Nuclear Spin of Bi^{210}

MARK FRED, FRANK S. TOMKINS, AND RAYMOND F. BARNES
Chemistry Division, Argonne National Laboratory, Lemont, Illinois
(Received September 21, 1953)

THE hyperfine structure of λ3067, the resonance line of Bi I, has been investigated for ordinary bismuth and for Bi^{210} with a large grating spectrograph. Solutions of the samples were evaporated on the ends of $\frac{1}{16}$-in. diameter silver electrodes and were then excited in a dc arc. A cylindrical lens was mounted in front of the photographic plate to shorten the astigmatic line image, giving a strong exposure in the third order of the grating (0.61A/mm) with 10^{-7} gram of bismuth. Under these conditions

the Bi^{209} line appeared as a well-resolved doublet having a separation given by the splitting of the upper state, 0.828 cm^{-1}. The close components in each member of the doublet due to the much smaller ground-state splitting could not be resolved but produced a noticeable widening.

The Bi^{210} samples were obtained as the RaE (5-day half-life) in equilibrium with 13 millicuries of RaD. The Bi^{210} was isolated by the ion exchange method of Raby and Hyde,[1] which was found to give a 98-percent yield with negligible loss of Pb. A number of separations were made at intervals of several weeks. Considerable difficulty was experienced at first with Bi^{209} contamination, so that an efficient separation process was essential. The amount of RaE isolated in each separation was determined by standard β-counting procedures and was usually about 1.5×10^{-7} gram. For Bi^{210}, λ3067 was found to be a single sharp line. An upper limit to any hfs which might possibly be present is roughly 0.1 the width of the Bi^{209} line. Since such a small splitting would lead to an unreasonably small g_I value, it seems much more probable that no splitting is present and $I=0$. Hence the 127th neutron is almost certainly in a $g_{9/2}$ state.

The isotope shift was measured by superimposing an exposure of Cs λ4593 in the second order of the grating which served as a fiducial mark. The Bi^{210} line was shifted to shorter wavelengths by 0.12 cm^{-1}. Further exposures with an improved light source are planned in order to obtain more accurate and extensive shift measurements.

[1] B. A. Raby and E. K. Hyde, University of California Radiation Laboratory Report AECD-3524, 1953 (unpublished).

Phase-Shift Calculation of High-Energy Electron Scattering by Nuclei*

D. R. YENNIE, R. N. WILSON, AND D. G. RAVENHALL
Stanford University, Stanford, California
(Received October 14, 1953)

EXPERIMENTS on the elastic scattering of high-energy electrons ($E\sim125$ Mev) by several elements have been carried out by Hofstadter, Fechter, and McIntyre.[1] The results have been analyzed by them[1] and by Schiff[2] using the Born approximation to estimate the effects of the finite nuclear size.

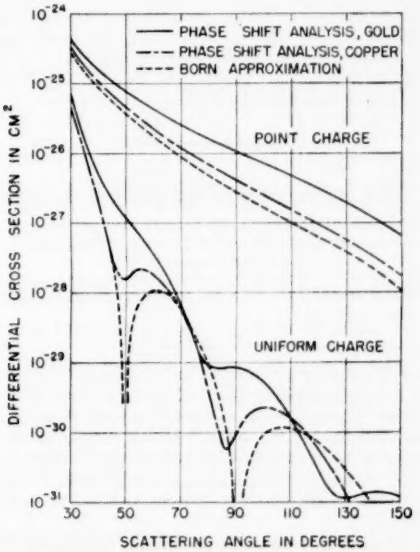

FIG. 1. Scattering from a uniform charge distribution, $kR=5.4$.

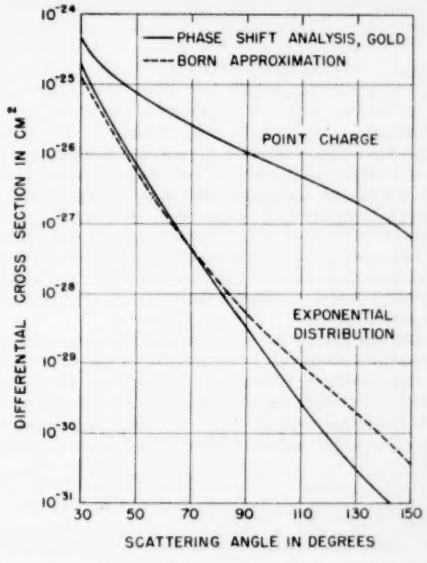

FIG. 2. Scattering from an exponential charge distribution, $ka=0.91$.

On the basis of such an analysis, the results can be fitted well by assuming an exponential distribution of the nuclear charge. Other charge distributions, such as the uniform distribution, are discriminated against because in Born approximation they predict diffraction maxima and minima in the angular distribution. In view of the fact that the Born approximation is not accurate for the heavier elements considered, we have carried out a numerical phase-shift calculation of the process. Our object in the present note is to examine the accuracy of the Born approximation, rather than to attempt to fit the experimental results. Our results are in disagreement with those of Parzen.[3]

The details of the calculation will be published later. Generally the calculation follows the methods given by Parzen[3] and Acheson,[4] with minor modifications. The phase shift relative to the Coulomb phase shift is calculated for the first nine partial waves; the last phase shift used is less than 0.003° in all cases. All the phase shifts are negative and tend monotonically to zero, in disagreement with Elton's assertion[5] that the phase shifts should tend to zero from positive values. We have found it necessary to increase the accuracy of the point scattering amplitudes given by Feshbach,[6] since at large angles this amplitude is largely canceled out by the nuclear size modifications. We estimate that the calculated cross sections given below are accurate to about 5 percent out to 110°; the major errors are contained in the first two phase shifts, which are known to only 0.01°.

The following charge distributions have been used for gold ($Z=79$):

(a) Uniform; $\rho(r)=\rho_0$, $r<R$,
$=0$, $r>R$; $kR=5.4$;

(b) Exponential; $\rho(r)=\rho_0 e^{-r/a}$; $ka=0.91$.

The cross sections given by (a) and (b) are found to decrease in approximately the same ratio between 30° and 90°, and this ratio is roughly that given by Hofstadter's experiment.

For purposes of comparison, we carried through the calculation for copper ($Z=29$) for the uniform charge distribution, with $kR=5.4$. The Born approximation to this cross section is the same, apart from a constant factor $(Z_{\text{copper}}k_{\text{gold}}/Z_{\text{gold}}k_{\text{copper}})^2$, as the Born approximation to (a).

In Fig. 1 are shown the cross sections given by the two uniform charge distributions. If we assume a nuclear radius $r_0A^{\frac{1}{3}}$, with

$r_0 = 1.22 \times 10^{-13}$ cm, the curves as shown there correspond to electron energies of 150 and 224 Mev for gold and copper, respectively. (The choice of r_0, and consequently of k, affects the cross sections by a constant factor only. For instance, if $r_0 = 1.45 \times 10^{-13}$ cm, the energies are 126 and 188 Mev, respectively.) As is expected, the cross section for copper agrees more closely with the Born approximation than does the cross section for gold. The first minimum predicted by the Born approximation appears in gold as a point of inflection only. The shift of the maxima and minima to smaller angles can be understood qualitatively as due to an increase in wave number as the electron enters the attractive potential of the nucleus. This also makes plausible the increase in slope of the cross section for the exponential distribution compared with the Born approximation, as shown in Fig. 2, and permits the experimental data to be fitted with a smaller a than is required in Born approximation.[1,2]

Further calculations are in progress with charge distributions of intermediate shape.

We wish to thank Professor L. I. Schiff for his advice and suggestions, and Professor W. E. Lamb, Jr. for interesting conversations. Discussions with Professor R. Hofstadter concerning the experiments and his analysis of them have been very stimulating.

* Supported by the Office of Scientific Research, Air Research and Development Command.

[1] Hofstadter, Fechter, and McIntyre, Phys. Rev. **92**, 978 (1953).
[2] L. I. Schiff, Phys. Rev. **92**, 988 (1953).
[3] G. Parzen, Phys. Rev. **80**, 355 (1953). Parzen (private communication to R. Hofstadter) has found an error in his work and is recomputing his results.
[4] L. K. Acheson, Jr., Phys. Rev. **82**, 488 (1951).
[5] L. R. B. Elton, Proc. Phys. Soc. (London) **A63**, 1115 (1950).
[6] H. Feshbach, Phys. Rev. **88**, 295 (1952).

Energy Levels of Be^8

R. MALM AND D. R. INGLIS
Argonne National Laboratory, Lemont, Illinois
(Received October 15, 1953)

THERE is conflicting evidence [1-10] on the spectrum of low states of Be^8, some observations suggesting rather great complexity and other investigations, by failure to observe some of the reported states, suggesting that the array is as simple as seems fitting[2] for so simple a nucleus. It is questionable whether the failure to observe the states in some cases (always with limited resolution and statistical accuracy) may arise from the reaction matrix element being small under these conditions or whether the apparent observation in the other cases arises from statistical illusions. Further observations on a variety of reactions at various angles and bombarding energies will help settle the question. The literature is summarized in Table I, the various states being indicated as (p) present in, (a) absent from, or (o) out of the observed range of, the various observations. The approximate observed width of the ground-state peak is given in Mev, as an indication of resolution. Our present results are also indicated.

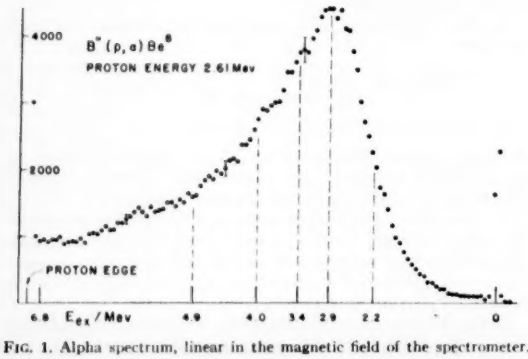

FIG. 1. Alpha spectrum, linear in the magnetic field of the spectrometer.

TABLE I. Presence (p) or absence (a) of peaks corresponding to the states of Be^8. The symbol o signifies "out of the observed range."

E_{ex}/Mev	0 (width)	2.2	2.9 (broad)	3.4	4.05	4.9	7.5 (broad)
Cambridge[a] (1939)	0.6	a	p	a	a	(p)	p
Rice[b] (1941)	0.6	(?)	p	(?)	(?)	p	p
Cambridge[c] (1949)	0.7	(?)	p	(?)	p	(p)	(p)
Zürich[d] (1953)	0.5	p	p	p	p	p	(6.8)
Hopkins[e] (1953)	0.10	a	p	(?)	o	o	o
Canberra[f] (1953)	0.3	a	p	a	a	a	(a)
Oak Ridge[g] (1953)	0.6	a	p	a	a	a	a
Copenhagen[h] (1953)	0.1	a	p	a	a	o	o
Present work	0.06	a	p	a	a	a	o

[a] See reference 3. [b] See reference 4. [c] See reference 5. [d] See reference 6. [e] See reference 7. [f] See reference 8. [g] See reference 9. [h] See reference 10.

We have observed the alpha groups from the $B^{11}(p, \alpha)Be^8$ reaction in a 16-inch, two-dimensional focusing magnetic spectrometer at 90° using a proportional counter for detection. The excitation function for the ground-state alphas is found to show resonances for proton energies of 1.98 and 2.61 Mev, corresponding to excited states of the C^{12} nucleus at 17.94 and 18.56 Mev. For each of these proton energies, the region of excitation energy E_{ex} of Be^8 from 0 to 7 Mev has been investigated and only the sharp ground-state peak and the broad 2.9-Mev state peak appear, as shown for the higher resonance in Fig. 1. In spite of the limited statistical accuracy, it is believed that any groups having a peak height greater than about 10 percent of the ground-state group would have been observed.

The statistical basis for the published observations[5,6] of the levels at 2.2, 3.4, and 4.05 Mev is not so good, but it appears at present rather likely that these states do not exist though surely more evidence on this point is desired. Evidence for the 4.9-Mev state rests mainly on an early report[4] of the gamma ray (which may be open to some doubt) and on the (n, γ) coincidence more recently reported[11] too briefly to permit critical judgement, leaving the existence of this state in sufficient doubt that it appears desirable to improve on those data and on our resolution and statistics at least in this region.

[1] F. Ajzenberg and T. Lauritsen, Revs. Modern Phys. **24**, 321 (1952).
[2] D. R. Inglis, Revs. Modern Phys. **25**, 390 (1953).
[3] C. L. Smith and E. B. M. Murrell, Proc. Cambridge Phil. Soc. **35**, 298 (1939). $B^{10}(d, \alpha)Be^8$.
[4] H. T. Richards, Phys. Rev. **59**, 796 (1941). $Li^7(d, n)Be^8$. Bennett, Bonner, Richards, and Watt, Phys. Rev. **59**, 904 (1941). $Li^7(d, n)Be^8(\gamma)Be^8$.
[5] L. L. Green and W. M. Gibson, Proc. Phys. Soc. (London) **62**, 407 (1949). $Li^7(d, n)Be^8$.
[6] Erdös, Scherrer, and Stoll, Helv. Phys. Acta **26**, 207 (1953). $B^{11}(\gamma, t)Be^8$, $B^{10}(\gamma, d)Be^8$, and $B^{11}(p, \alpha)Be^8$.
[7] R. W. Gelinas and S. S. Hanna, Phys. Rev. **89**, 483 (1953). $Be^9(d, t)Be^8$.
[8] P. B. Treacy, Phil. Mag. **44**, 326 (1953). $B^{10}(d, \alpha)Be^8$.
[9] Kunz, Moak, and Good, Phys. Rev. **91**, 676 (1953). $Li^6(He^3, p)Be^8$.
[10] Beckman, Huss, and Zupančič, Phys. Rev. **91**, 606 (1953).
[11] J. Thirion, Compt. rend. **233**, 37 (1951).

The Mechanism of Stripping Reactions

J. HOROWITZ AND A. M. L. MESSIAH
Centre d'Etudes Nucleaires de Saclay, Saclay, France
(Received October 8, 1953)

THE cross section for the reaction[1] $\mathfrak{N}_1(d, p)\mathfrak{N}_2$ is given rigorously by

$$\sigma(d \to p) = 2\pi |\langle p | V + P | \Phi \rangle|^2 \rho_E, \tag{1}$$

where V is the $n-p$ potential in the deuteron, P the interaction $p-\mathfrak{N}_1$, ρ_E the statistical factor, $\langle p|$ the product of a proton plane-wave function by the wave function $\psi_2(\mathbf{r}_n, \boldsymbol{\rho})$ of the residual nucleus, $|\Phi\rangle$ the wave function describing the whole stationary state of collision initiated by the incident deuteron; we take $\hbar = 1$ and denote by $\boldsymbol{\rho}$, $\mathbf{r}_n$, $\mathbf{r}_p$ the dynamical variables of the nucleons in $\mathfrak{N}_1$ and the neutron and proton coordinates, respectively.

The Born approximation, in the sense of Daitch and French,[2,3] consists in neglecting P throughout and replacing Φ by Φ_d,

which is the product of a deuteron plane wave and the wave function $\psi_1(\rho)$ of the initial nucleus. In the Butler theory,[4] one effectively does the same thing but for the exclusion of the range of integration $r_n \leqslant r_0$, where r_0 is the range of the interaction N between the picked-up neutron and the target nucleus.[5]

As remarked in reference 2, both approaches neglect the reaction effects of the various outgoing waves on the stripping process. In this letter, we report on calculations taking into account one of the most important of such effects, namely, the reaction of the proton outgoing wave itself. It is more convenient to consider the matrix element $I=\langle d|N+P|\Psi\rangle$ for the time-reversed process $\mathfrak{N}_2(p,d)\mathfrak{N}_1$. Both matrix elements are related in a well-known fashion. Ψ is the exact wave function for a stationary state of collision $p+\mathfrak{N}_2$. An approximate value for I is obtained by:

(a) neglecting V in the Schrödinger equation for Ψ;
(b) replacing P everywhere by a fixed average potential $\mathcal{P}$ with the effect that Ψ becomes the product of ψ_2 by a proton plane wave plus a wave elastically scattered by potential $\mathcal{P}$.

Then, using the Schrödinger equation, one gets for I an expression amenable to computation. In approximation (a), one treats the formation of the deuteron as a perturbation, as was already done in the Born approach. Approximation (b) still takes correctly into account the reaction effect of the elastically scattered wave provided $\mathcal{P}$ is properly chosen, but neglects the effect of all the other outgoing waves.

We have examined the case where $\mathcal{P}$ is a hard sphere potential with a radius r_0 equal to the range of the interaction P (and N).[6] Numerical calculations have been made with the shapes "$l=0$" and "$l=1$" for several values of the incident energy, the Q value and the parameter r_0, and the results have been compared with Butler's theory.

They are summarized as follows:

(1) The *angular distribution* predicted at low angles are much the same in both theories. For the same r_0, the peak occurs at rather smaller angles in this modified theory. This effect can be simulated by taking Butler's formula with a radius r_0 increased by about 25 percent. The reported discrepancy,[7] between the orthodox nuclear radii and the radii derived from the interpretation of stripping data through Butler's formula, is thereby explained.

(2) The *magnitude of the cross section* is much smaller. Our peak values are from 2 to 6 times smaller than those predicted by Butler's theory. Conversely, the values of the reduced widths obtained from these peak values are larger than those obtained from Butler's theory by the same factor, which explains at least qualitatively the reported discrepancy[7,8] in reduced width determination from resonance reactions and from stripping data.

(3) The stripped-off particle gets *partially polarized* provided $l>0$, in agreement with Newns' prediction.[9]

(4) In the $(d, p\gamma)$ *angular correlation*, although the over-all anisotropy remains as important as in the Butler theory, the actual shape of the distribution is completely different. In particular it does not possess any more the transferred momentum as axis of symmetry.

A fuller account of this work will be published in the *Journal de physique et le radium.*

[1] We neglect Coulomb corrections throughout. Accordingly the results on (d, p) reactions are readily extended to (d, n) by interchange of the roles of the proton and the neutron.
[2] P. B. Daitch and J. B. French, Phys. Rev. **87**, 900 (1952).
[3] Bhatia, Huang, Huby, and Newns, Phil. Mag. **43**, 485 (1952).
[4] S. T. Butler, Proc. Roy. Soc. (London) **A208**, 559 (1951).
[5] An independent proof of this point, which had been already noted by Daitch and French, (see reference 2) has been given by E. Gerjuoy, Phys. Rev. **91**, 645 (1953).
[6] The (p, d) amplitude that one gets this way could be called the amplitude for "pick-up proper," namely the amplitude that one gets when compound nucleus formation is neglected. It should fit best at energies far from the resonances of the compound nucleus $(p+\mathfrak{N}_2)$.
[7] Report of the Birmingham Conference on Nuclear Physics (Birmingham University Press, Alabama, 1953).
[8] R. G. Thomas, Phys. Rev. **91**, 453 (1953); also private communication.
[9] H. C. Newns, Proc. Roy. Soc. (London) **B66**, 477 (1953).

The Signs of the Phase Shifts for Pion-Proton Scattering

S. W. Barnes, C. E. Angell,* J. P. Perry,†
D. Miller, J. Ring, and D. Nelson
Department of Physics, University of Rochester, Rochester, New York
(Received October 5, 1953)

In principle, it is possible to determine the sign of the pion-proton nuclear interaction by measuring the effect of interference between the nuclear and Coulomb amplitudes in pion-proton scattering. Under the usual assumptions[1] that only S and P states are effective and that the charge independence hypothesis is valid, the reactions

$$\pi^+ + p \rightarrow \pi^+ + p, \tag{1}$$

$$\pi^- + p \rightarrow \pi^- + p, \tag{2}$$

$$\pi^- + p \rightarrow \pi^0 + n \tag{3}$$

are described by the six nuclear phase shifts[2] α_1, α_{11}, α_{13}, α_3, α_{31}, and α_{33}, and by the Coulomb amplitude in the manner given by Van Hove.[3] The angular distribution of reaction (1) has been investigated[4,5] at energies sufficiently low so that Coulomb effects should be detectable; however, due to the experimental uncertainties, the relative signs of the nuclear and Coulomb amplitudes could not be determined unambiguously.

Recently, Woodruff[6] has pointed out that if the phase shifts α_{11}, α_{13}, and α_{31} are taken to be negligibly small, as the evidence indicates, then the magnitudes of the other three phases α_1, α_3, and α_{33} can be determined from the total cross sections for reac-

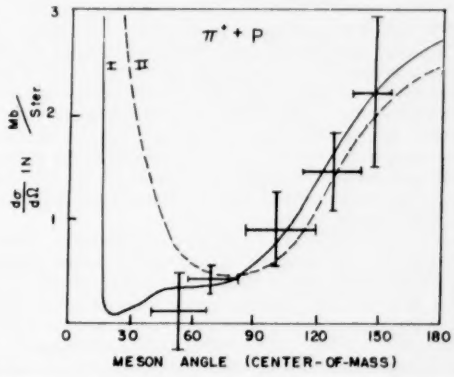

FIG. 1. Differential scattering cross section of hydrogen for π^+ mesons at 40 Mev. Curve I: $\alpha_3=-2.6°$, $\alpha_{33}=+5.7°$. Curve II: $\alpha_3=+2.6°$, $\alpha_{33}=-5.7°$.

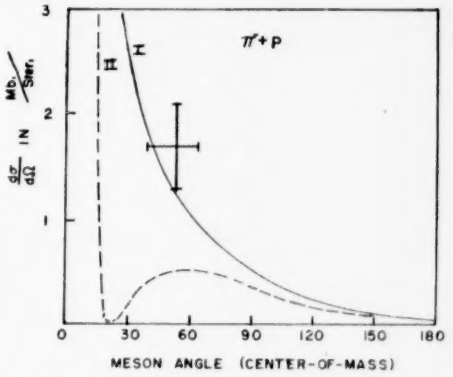

FIG. 2. Differential scattering cross section of hydrogen for π^- mesons at 40 Mev. Curve I: $\alpha_1=+9.7°$, $\alpha_3=-2.6°$, $\alpha_{33}=+5.7°$. Curve II: $\alpha_1=-9.7°$, $\alpha_3=+2.6°$, $\alpha_{33}=-5.7°$.

tions 1, 2, and 3. These have been measured at a pion energy of of about 40 Mev.[7,8] We have now obtained a value of $(1.7\pm0.4)\times10^{-27}$ cm²/sterad for the differential cross section at a laboratory angle of 45° for reaction 2 at 40 Mev. Together with the three total cross sections and the five differential points for reaction (1),[5] and under the assumption that α_{11}, α_{13}, and α_{31} are negligible, this determines the following ranges of values for the other phases:

$$\alpha_1=+9.7°\pm1.2°;\quad \alpha_2=-2.6°\pm1.4°;\quad \alpha_{33}=+5.7°\pm1.2°.$$

No solution exists with reversed signs.

The phases shifts so obtained are consistent with the strong backward maximum found recently at this energy for reaction 3.[9]

Figures 1 and 2 give the experimental points along with the curves calculated from the above three phase shifts.

* Now at General Electric Research Laboratory, Ithaca, New York.
† Now at Lincoln Project, Massachusetts Institute of Technology, Cambridge 39, Massachusetts.
[1] Anderson, Fermi, Martin, and Nagle, Phys. Rev. **91**, 155 (1953).
[2] We use the notation of reference 1.
[3] L. Van Hove, Phys. Rev. **88**, 1358 (1952).
[4] Bodansky, Sachs, and Steinberger, Phys. Rev. **90**, 996 (1953).
[5] J. P. Perry and C. E. Angell, Phys. Rev. **91**, 1289 (1953).
[6] A. E. Woodruff, Phys. Rev. **92**, 000 (1953). Rochester meeting.
[7] C. E. Angell and J. P. Perry, Phys. Rev. **92**, 835 (1953).
[8] A. Roberts and J. Tinlot, Phys. Rev. **90**, 951 (1953).
[9] J. Tinlot (private communication).

Nuclear Configurations Inferred from High-Energy Pickup-Deuteron Distributions*

W. Selove†
Harvard University, Cambridge, Massachusetts
(Received September 15, 1953)

THE production of high-energy pickup deuterons, first observed by York,[1,2] using 90-Mev neutrons, has been examined theoretically[3] as a means of determining nucleon momentum distributions inside nuclei. In experiments now in progress here, the pickup process is being studied with the improved resolution available with a proton beam—the external proton beam of the Harvard cyclotron has an energy of about 95 Mev, with an energy spread, in the work so far, of about 3 percent. Deuterons are identified by simultaneous measurement of range and specific ionization.

Some of the early results are shown in Figs. 1 and 2. Figure 1 shows the sharp energy peak obtained from carbon. Although there is some production of higher excited states of the residual nucleus, it is seen that, as was roughly indicated by the earlier work, quite predominantly only one type of neutron state in carbon enters into the pickup process. This may be regarded as rather strong evidence for an alpha-particle structure for carbon. One can readily estimate that if the six neutrons of carbon were distributed in a shell-type structure, with two in s states and four in p states, then the energy separation of these two types of levels

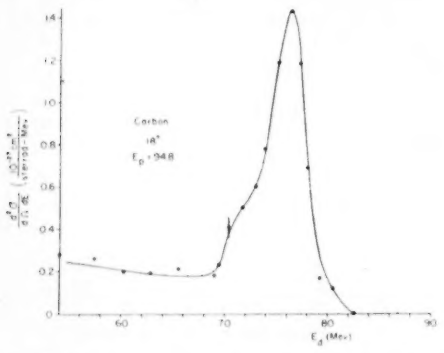

FIG. 1. Pickup-deuteron cross sections for carbon. The statistical accuracy of the points is indicated for a representative point.

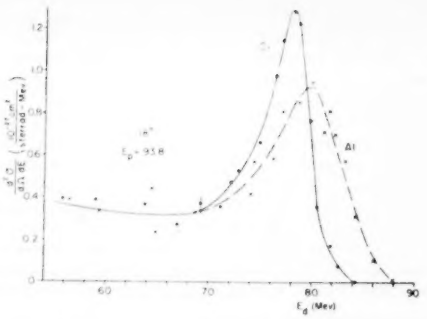

FIG. 2. Pickup-deuteron cross sections for aluminum and silicon. The accuracy of the points is indicated for a representative point.

should be of the order of 6 to 8 Mev, an easily observable separation.

The peak in carbon is still quite distinct at 60°, where the differential cross section is down by a factor of about 150 from its value in the forward direction. However, it is no longer so prominent relative to the continuum of deuterons (which presumably come from more complicated collisions), and so the separation of the "pickup" part of the cross section is uncertain to within a factor of perhaps two. Analysis of the angular distribution by the Born-approximation method of Chew and Goldberger[3] indicates a Gaussian momentum distribution for the picked up neutron.

In addition to carbon, other elements studied are beryllium, aluminum, silicon, copper, and lead; work is in process also on deuterium and helium. The heavier elements show less pronounced pickup peaks. All of the light elements show evidence of alpha-particle structure in "$4n$" nuclei. Beryllium shows the anticipated two peaks, one corresponding to a Q close to the $-16\frac{1}{2}$-Mev value found for carbon, the other to a Q near zero. Figure 2 shows the pickup deuterons from aluminum and silicon. Si^{28} (=89.6 percent of normal silicon) is expected to be a tightly bound structure on either the alpha-particle or the shell model. Al^{27} has the same number of neutrons as Si^{28}, and one proton less. Now to the extent to which the pickup process can be regarded as involving only the two nucleons concerned, with no interaction with the other nucleons in the target nucleus, the (p, d) pickup reaction samples the neutron distribution inside the target nucleus. On this basis, the results of Fig. 2 can be interpreted as showing that the neutron distribution present in the ground state of Si^{28} is considerably affected by the removal of one *proton*. This is a strong indication of alpha-particle structure in Si^{28}, particularly as compared to an individual-particle model having the neutron distribution relatively independent of the proton distribution.

* This work was supported by the joint program of the U. S. Office of Naval Research and the U. S. Atomic Energy Commission.
† Present address: Radiation Laboratory, University of California, Livermore, California.
[1] H. York, Phys. Rev. **75**, 1467 (1949).
[2] J. Hadley and H. York, Phys. Rev. **80**, 345 (1950).
[3] G. F. Chew and M. L. Goldberger, Phys. Rev. **77**, 470 (1950).

The Energy Levels of Be^{10}†

K. B. Rhodes and J. N. McGruer
University of Pittsburgh, Pittsburgh, Pennsylvania
(Received September 14, 1953)

THE proton spectrum from the reaction $Be^9(d, p)Be^{10}$ has been observed using a high-resolution magnetic spectrometer.[1] A thin (0.30 mb/cm²) Be^9 foil was bombarded by a collimated beam of 14.5-Mev deuterons. After magnetic analysis the outgoing particles were detected by a scintillating crystal and identified both by their ranges in foils and by pulse-height analysis. Observations were made at ten laboratory angles.

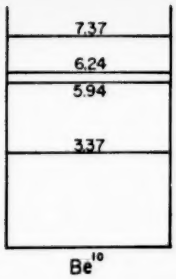

FIG. 1. Energy levels of Be^{10}.

TABLE I. Energy level values at various angles.

θ_{lab} (degrees)	Level values (Mev)	
8.9	5.94	6.24
11.8	5.94	6.24
17.2	5.95	6.25
28.0	5.94	6.24
36.3	5.95	6.25
46.8	5.94	6.24
57.7	5.95	6.24
68.1	5.93	6.24
78.4	5.93	6.23
89.9	5.88	6.18
Average	5.94 ±0.04	6.24 ±0.04

Figure 1 is an energy level diagram based upon the present work. In the energy region covered the essential difference from the previously published diagram[2] is the assignment of two levels to the region where an uncertain 6.2-Mev level was formerly reported. These two levels were clearly resolved at all angles, with Fig. 2 being a representative run. The level assignments, calculated relativistically, of 5.94 and 6.24 Mev with a standard deviation of 0.04 Mev result from an average over all angles

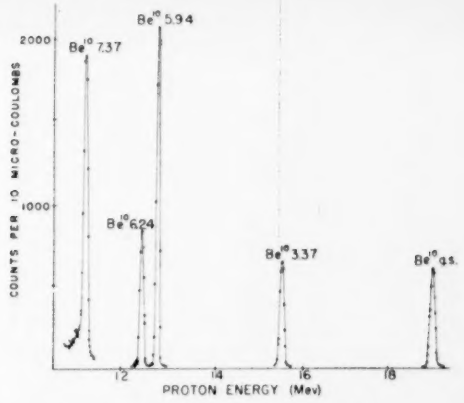

FIG. 2. Proton spectrum at $\theta_{lab} = 17.2°$.

(see Table I). The magnet was calibrated using the reported Q values for the Be^9 level at 2.429 Mev, the Be^1 ground state, and the Be^1 levels at 3.370 and 7.37 Mev.

The possibility that any of the levels shown could have been a contaminant level was ruled out by the angular dependance of the level spacing. In addition, an independent check on the identity of the target nucleus was made by placing foils of all likely contaminants in the beam and observing their spectra in the regions of interest.

† Work done in the Sarah Mellon Scaife Radiation Laboratory and assisted by the joint program of the U. S. Atomic Energy Commission and the U. S. Office of Naval Research.

[1] Bender, Reilley, Allen, Ely, Arthur, and Hausman, Rev. Sci. Instr. **23**, 542 (1952).
[2] F. Ajzenberg and T. Lauritsen, Revs. Modern Phys. **24**, 321 (1952).

CONTENTS—*Continued*

Note on the Eigh Interaction . . . . . E. Fisbeck and P. Kass 1316

Letters to the Editor:

Low-Temperature Disintegration of Electrons in a Cylinder . . . . . E. E. Dingle 1320

Zeeman Spectrum of Europium . . . . . S. Mrozowski 1320

Spin-Spin Interaction of Neutrons and the Dissociation Energy of Helium . . . . . A. M. Sessler and H. M. Foley 1321

Relativistic Correction to the Ground-State Energy of Helium . . . . . A. M. Sessler and H. M. Foley 1321

Mobility of Impurity Ions in Germanium and Silicon . . . J. C. Severiens and C. S. Fuller 1322

Variations in the Decay of Phosphorescence with Frequency of Applied Electric Field . . . . . Keith W. Olson 1323

Solution of the Wave Equation Near an Extremum of the Potential . . . Charles J. Mullin 1323

Long-Wavelength Edge of Photographic Sensitivity and of the Electronic Absorption of Solids . . . . . Franz Urbach 1324

Nuclear Spin of Sr^{87} . . . . . Mark Fred, Frank S. Tomkins, and Raymond F. Barnes 1326

Phase-Shift Calculation of High-Energy Electron Scattering by Nuclei . . . . . D. R. Yennie, R. N. Wilson, and D. G. Ravenhall 1325

Energy Levels of Be^9 . . . . . R. Malm and D. R. Inglis 1726

Mechanism of Stripping Reactions . . . . . J. Horowitz and A. M. L. Messiah 1326

Signs of the Phase Shifts for Nuclear Scattering . . . . . S. W. Barnes, C. E. Angelli, J. P. Perry, D. Miller, J. Ring, and B. Nelson 1327

Nuclear Configurations Inferred from High-Energy Proton-Deuteron Distributions . . . . . W. Selove 1328

Energy Levels of Be^9 . . . . . K. B. Rhodes and J. N. McGruer 1329

CONTENTS

THE PHYSICAL REVIEW — SECOND SERIES, VOLUME 92, NO. 5 — DECEMBER 1, 1953

Origin of the β Layer of the Ionosphere . . . Byron Boyer and Te-Yan Wu 1297
Liquid Helium II: Experiments on Compressional Waves . . . R. K. Hobbs 1306
Effect of the Exclusion and Pauli Principles on the Ionization . . . Basil S. Rice 1311
Magnetization in Weak Fields—Antiferromagnetism and Weak Ferromagnetism . . . Louis L. Hirst and Stanley J. Hutner 1320
Augmented Plane-Wave Method for the Periodic Potential Problem. II . . . M. M. Saffren and J. C. Slater 1326
Electronic Energy Bands in Cuprous Oxide . . . Thomas Wolfram and George Ellis 1344
Resonances of Isotopic Scattering Cross Sections and Their Relation to the Statistical Model . . . Richard G. Fluharty, Hanan Levine, and Ralph E. Shamu 1358
Fission Potential in the Statistical Theory of Nuclear Reactions . . . Herman J. Fong and Jay Orear 1366
Second-Order Elastic Deformation of Cubics . . . D. S. Wallace and J. L. Kelly 1369
Search for the Rest Mass of a Hypothetical Neutral Particle . . . E. W. Lamb 1380
Energy Loss of Moving Electrons by Cherenkov Emission . . . M. Frilette and R. L. Pleasonton 1382
Absolute Value of Avogadro's Number and the Dimensions of Gases . . . M. E. Strumquist 1383
Binary Recrystallization Collision . . . Raul Alcalaer 1387
Precision Measurement of 20 Mc Value of the Conversion Constant $2e$ . . . Gaston L. Rich, John K. Marsh, and Jesse W. M. DuMond 1389
Nuclear Surface Oscillations . . . A. K. Kerman 1899
Angular and Energy Distribution of Photoprotons from Aluminum and Thorium . . . M. E. Hofstad and A. G. W. Cameron 1395
Beta-Gamma Polarization Correlation . . . Donald E. Hamilton, Aaron Lazarnick, and Francis M. Fields 1402
Gamma Radiation from the Reaction $Ge^{74}(p,\gamma)As^{75}$ . . . H. H. Woodbury, R. B. Day, and A. V. Tollestrup 1408
Formation of the Long-Lived Sr^{89} Isomer . . . D. J. Hughes and H. Palevsky 1409
Mixed Configuration in Nickel . . . A. de-Shalit and M. Goldhaber 1411
Decay of $_{66}Dy^{165m}$ (1.3 min) and $_{66}Dy^{165}$ (2.3 hr) . . . W. C. Jordan, J. M. Cork, and S. B. Burson 1418
Elastic Scattering of Fast Neutrons by Bi . . . John D. Seagrave 1422
Structure of Liquid Nitrogen, Oxygen, and Argon by Neutron Diffraction . . . D. G. Henshaw, D. G. Hurst, and N. K. Pope 1426
Concentration of Uranium and Lead and the Isotopic Composition of Lead in Manganese Minerals . . . C. Patterson, H. Brown, G. Tilton, and M. Inghram 1436
Decay Scheme of Ag^{97} . . . M. L. Pitman, W. Bernstein, and R. S. Schwartz 1439
Nuclear Quadrupole Resonance of the Stable Gallium Isotopes . . . H. G. Dehmelt 1449
Directional Correlation of the Pb^{207} γ ray Cascade . . . R. Frauenfelder, J. S. Lawson, Jr., W. Jentschke, and H. DePasquali 1451
Statistical Theory of Nuclear Reactions . . . Richard L. Cohen 1456
Radioactivities of Actinide Products by Successive Bombardment of Complexions . . . E. J. Wesley and J. F. Rupert, Jr. 1460
Two-Body Scattering at Low Energy . . . Sydney Borowitz 1466
Lifetime Measurements by the Fast Beam Gates of Cl^{37} and Br^{79} from Recoil Spectra . . . Jacques Thirion and Charlotte L. Tétrault 1469
Spin of Sr^{87} and Mean Radius of the Nuclei of Isotopes . . . R. L. White and C. H. Townes 1476
Isomeric Transition of Pb^{207} as an Energy Standard in Beta Spectroscopy . . . David E. Alburger 1477
Erbium^{167} and Thulium^{167} . . . Thomas H. Handley and Elmer L. Olson 1480
Spin and Magnetic Moment of Sr^{87} and Y^{89} and the Magnetic Moment of Ge^{73} . . . C. D. Jeffries 1482
Degradation of Gamma Rays in Water . . . M. M. White and W. Bernard 1484
Scattering of 4.5-Mev Protons by Carbon and Oxygen . . . W. E. Burcham, W. M. Gibson, A. Hussain, and J. Rotblat 1485
Ionization of 10-Mev Deuterons and Oxygen . . . E. G. Fuemmeler, W. M. Gibson, D. J. Prowse, and J. Rotblat 1488
Vector Addition Coefficients Briefly . . . R. L. Gluckstern and G. B. Arfken 1490
Nuclear Spin and Quadrupole Moment of Y^{89} . . . Ralph Livingston, Ben M. Benjamin, J. T. Carr, and Walter Gordy 1491
Photoproduction of π-Mesons Pairs . . . R. D. Lawson 1492
Hypothesis Concerning the Relation among the "New Unstable Particles" . . . M. Goldhaber 1499
Semiclassical Kinship in Mixed Processes . . . Joseph A. Tilio 1502
Theory of Quantized Fields, IV . . . Julian Schwinger 1505
Relativistic Particle Dynamics. II . . . S. Schlesinger and L. H. Thomas 1507
Extension of Relativistic Two-Particle Wave Equations to Approximate Forms. II . . . Zeke V. Chraplyvy 1509

(Continued on outer flap)

LANCASTER PRESS, INC., LANCASTER, PA.